THE UNIVERSITY
of ADELAIDE

Tectonic evolution of Madagascar over three billion years of Earth's history

Sheree E. Armistead

Department of Earth Sciences
School of Physical Sciences
The University of Adelaide

May 2019

Table of Contents

Abstract

Earth's last major supercontinent, Gondwana, formed during the Neoproterozoic by convergence along the East African Orogen. Madagascar contains at least two Gondwana-forming suture zones, and hosts several suites of Neoproterozoic rocks that have been correlated with other Rodinian and Gondwanan terranes. Madagascar also hosts several Paleoproterozoic sedimentary sequences, which provide constraints on the Earth's plate configuration from the Paleoproterozoic through to the early Cambrian. These factors make Madagascar an important place to study supercontinent assembly and dispersal throughout Earth's history. In this thesis we integrate a range of isotopic, geochemical and structural datasets to decipher the timing and nature of tectonic events in these regions. A primary focus of this research is to constrain the location and timing of the controversial Betsimisaraka Suture in Madagascar and India. We have used detrital zircon U–Pb and Lu–Hf isotopes to constrain the location of this suture. We propose that the Karwar Block of western peninsular India is an extension of the western Dharwar Craton and not part of the Antananarivo Domain of Madagascar as has been suggested in some models. We also suggest that India was paleogeographically isolated from central Madagascar during the Paleoproterozoic. From northern Madagascar, we use magmatic zircon Hf and O isotopes to demonstrate that the northern component of the Bemarivo Domain is distinct from the southern part of the Bemarivo Domain. We propose that the northern terrane formed in a juvenile arc system that included the Seychelles, the Malani Igneous Suite of northwest India, Oman, and the Yangtze Belt of south China, which at the time were all outboard from continental India and south China. The final assembly of northern Madagascar and amalgamation of the northern and southern terranes occurred along the Antsaba subduction zone, with collision occurring at c. 540 Ma. In central Madagascar we have integrated remote sensing, field data and medium-temperature thermochronology (Rb–Sr mica and U–Pb apatite) to unravel complex deformation in the Ikalamavony and Itremo domains. We suggest deformation in west-central Madagascar formed in response to the c. 650 Ma collision of Azania with Africa along the Vohibory Suture in southwestern Madagascar. In eastern Madagascar, deformation is syn- to post-550 Ma, which formed in response to the final closure of the Mozambique Ocean along the Betsimisaraka Suture. A series of Paleoproterozoic sedimentary sequences overlie many of the domains in Madagascar. New U–Pb and Lu-Hf isotopes from a range of these sequences are indistinguishable from each other, and we therefore refer to these sequences as the Greater Itremo Group. We correlate these with equivalent sedimentary sequences in the Muva Supergroup in the Tanzania Craton and define an epicontinental Itremo-Muva Basin. We show that the Greater Itremo Group is distinct from Indian samples, and therefore India and Madagascar were not contiguous during the Paleoproterozoic. The integration of various isotopic datasets from Madagascar and its paleo-neighbours have provided new insights into the evolution of supercontinent assembly and dispersal during the Neoproterozoic. Although there remain some areas that require further study, this multi-disciplinary research supports a model where central Madagascar and India amalgamated during the Neoproterozoic along the Betsimisaraka Suture.

Declaration

I certify that this work contains no material which has been accepted for the award of any other degree or diploma in my name, in any university or other tertiary institution and, to the best of my knowledge and belief, contains no material previously published or written by another person, except where due reference has been made in the text. In addition, I certify that no part of this work will, in the future, be used in a submission in my name, for any other degree or diploma in any university or other tertiary institution without the prior approval of the University of Adelaide and where applicable, any partner institution responsible for the joint-award of this degree.

I acknowledge that copyright of published works contained within this thesis resides with the copyright holder(s) of those works.

I also give permission for the digital version of my thesis to be made available on the web, via the University's digital research repository, the Library Search and also through web search engines, unless permission has been granted by the University to restrict access for a period of time.

I acknowledge the support I have received for my research through the provision of an Australian Government Research Training Program Scholarship.

10/05/2019

SHEREE ARMISTEAD DATE

Acknowledgements

Thank you to my supervisors Alan Collins and John Foden, for providing me with the incredible opportunity to undertake this PhD. You have both been incredibly supportive and a source of inspiration throughout this entire journey. I am thankful for everything I have learned from you both over the past few years. I am grateful for the endless opportunities I've had to travel for field work and conferences, all of which have enriched my PhD experience.

Thank you to the PhD group at Adelaide University. Gilby, Haidee and Jack—our friendship and countless morning coffees has been a highlight of my time in Adelaide, thank you for always being supportive both academically and personally. Morgan, thank you for taking the time to teach me zircon processing when I first moved here, for being an excellent field assistant and wonderful conference buddy. Thank you to everyone else I've shared an office with, a coffee with, or a G&T with, you have all made being in this department a wonderful experience.

I have had the privilege of doing field work in some amazing places. Thank you to Shaji for assisting with field work in India and to Theodore for organising our field work in Madagascar. Auguste, thank you for being a fantastic driver and field guide for my two trips to Madagascar—I'm really glad your machete didn't end up being needed in the red zone. Renata and Raisa, I am incredibly grateful for the opportunity to do field work in Madagascar with you both and to visit Brazil, and for your continued collaboration and friendship.

I would like to thank members of the IGCP 648 and 628 projects. The conferences, field trips and friendships have been a rewarding part of my PhD and I look forward to continuing these into the future.

To all the people I've connected with on Twitter, I am truly grateful for the support, advice, opportunities and for keeping the passion for science alive. I have learnt so much about minorities in science, issues in academia and technical aspects of research that this PhD has benefited immensely from. Thank you for being a constant source of knowledge and inspiration.

Kathryn Goodenough and Peter Johnson provided very constructive reviews that have significantly improved the final version of this thesis.

Finally, thank you to my partner and best friend Adam, for your unwavering love and support. Thank you for being there for all the highs and the occasional lows of this PhD, I will be forever grateful to you.

Publications arising from this PhD research

Journal articles

Armistead, S.E., Collins, A.S., Payne, J.L., Foden, J.D., De Waele, B., Shaji, E. and Santosh, M., 2017. A re-evaluation of the Kumta Suture in western peninsular India and its extension into Madagascar. *Journal of Asian Earth Sciences*.

Armistead, S.E., Collins, A., Payne, J.L., Cox, G.M., Merdith, A.S., Foden, J.D., Razakamanana, T. and De Waele, B., 2019. Evolving marginal terranes during Neoproterozoic supercontinent reorganisation: constraints from the Bemarivo Belt in northern Madagascar. *Tectonics*.

Armistead, S.E., Collins, A.S., Redaa, A., Gilbert, S., Jepson, G., Gillespie, J., Blades, M.L., Foden, J.D. and Razakamanana, T., In Review. Structural evolution and medium-temperature thermochronology of central Madagascar: implications for Gondwana amalgamation. *Journal of the Geological Society*.

Armistead, S.E., Collins, A.S., Schmitt, R.S., Costa, R.L., De Waele, B., Foden, J.D., Razakamanana, T. and Payne, J.L., In Prep. Proterozoic basin evolution and tectonic geography of Madagascar during the Nuna Supercontinent.

Other journal articles produced during PhD

Merdith, A.S., Collins, A.S., Williams, S.E., Pisarevsky, S., Foden, J.D., Archibald, D.B., Blades, M.L., Alessio, B.L., Armistead, S. and Plavsa, D., 2017. A full-plate global reconstruction of the Neoproterozoic. *Gondwana Research*.

Armistead, S.E., Betts, P.G., Ailleres, L., Armit, R.J. and Williams, H.A., 2018. Cu-Au mineralisation in the Curnamona Province, South Australia: A hybrid stratiform genetic model for Mesoproterozoic IOCG systems in Australia. *Ore Geology Reviews*.

Costa, R.L., Schmitt, R.S., Collins, A., Armistead, S.E., Razakamanana, T. and Archibald, D., Submitted. Tectonic evolution of an Early Cryogenian synmagmatic basin in central Madagascar. *Precambrian Research*.

Conference abstracts

Armistead, S.E., Collins, A.S., Mansfield, W., Santosh, M. and Shaji, E., 2016. A re-evaluation of the Kumta Suture in southwest India and its extension into Madagascar Australian Earth Sciences Convention, Adelaide, Australia.

Armistead, S.E., Collins, A.S., Mansfield, W., Santosh, M. and Shaji, E., 2016. A re-evaluation of the Kumta Suture in southwest India and its extension into Madagascar The 35th International Geological Congress, Cape Town, South Africa.

Armistead, S.E., Collins, A. and Razakamanana, T., 2017. A structural transect through central Madagascar – constraining the Neoproterozoic tectonic evolution, Rodinia Conference, Townsville, Australia.

Armistead, S.E., Collins, A.S., Payne, J.L., De Waele, B., Shaji, E. and Santosh, M., 2017. Suturing Madagascar and India: New insights from Lu-Hf data and multi-dimensional scaling of U-Pb detrital zircon data, Rodinia Conference, Townsville, Australia.

Armistead, S.E., Collins, A.S., Foden, J.D. and Razakamanana, T., 2017. The structural evolution of central Madagascar: a tale of two orogenies, Puzzling out Gondwana, Bangkok, Thailand.

Armistead, S.E., Collins, A.S., Redaa, A., Foden, J.D. and Razakamanana, T., 2018. Deciphering key events of Neoproterozoic orogenesis in Madagascar: insights from structure and multiple thermochronometers, European Geosciences Union General Assembly, Vienna, Austria.

Armistead, S.E., Collins, A.S., Schmitt, R.S., Costa, R.L., Foden, J.D. and Razakamanana, T., 2018. Detrital provenance of the Itremo Group in central Madagascar using trace elements and Hf isotopes in zircon, European Geoscience Union General Assembly, Vienna, Austria.

Armistead, S.E., Collins, A., Payne, J.L., Cox, G.M., Merdith, A.S., Foden, J.D., Razakamanana, T. and De Waele, B., 2018. The evolution of northern Madagascar during the Neoproterozoic: implications for Rodinia and Gondwana plate reconstructions, IGCP 648 Field Symposium China.

Armistead, S.E., Collins, A.S., Payne, J.L., Foden, J.D. and De Waele, B., 2018. Tectonic evolution of the Neoproterozoic Bemarivo Belt in northern Madagascar: from Rodinia to Gondwana, Australian Geoscience Council Convention, Adelaide, Australia.

Statement of Authorship 1

Title of Paper	A re-evaluation of the Kumta Suture in western Peninsular India and its extension into Madagascar	
Publication Status	☑ Published ☐ Submitted for publication	☐ Accepted for publication ☐ Unpublished and unsubmitted, written in manuscript style
Publication Details	Armistead, S.E., Collins, A.S., Payne, J.L., Foden, J.D., De Waele, B., Shaji, E. and Santosh, M., 2017. A re-evaluation of the Kumta Suture in western peninsular India and its extension into Madagascar. *Journal of Asian Earth Sciences.* doi.org/10.1016/j.jseaes.2017.08.020	

Principal Author

Name of Principal Author (Candidate)	Sheree Armistead		
Contribution to the Paper	Conceptualisation of the work, development of ideas and conclusions, prepared samples, carried out analytical work, interpretation of the data, wrote manuscript.		
Overall percentage (%)	80%		
Certification:	This paper reports on original research I conducted during the period of my Higher Degree by Research candidature and is not subject to any obligations or contractual agreements with a third party that would constrain its inclusion in this thesis. I am the primary author of this paper.		
Signature		Date	22/04/2019

Co-Author Contributions

By signing the Statement of Authorship, each author certifies that:

i. the candidate's stated contribution to the publication is accurate (as detailed above);
ii. permission is granted for the candidate in include the publication in the thesis; and
iii. the sum of all co-author contributions is equal to 100% less the candidate's stated contribution.

Name of Co-Author	Alan Collins	Signature		Date	22/04/2019
Contribution to the Paper	Supervised work, helped with data interpretation and manuscript revision				

Name of Co-Author	Justin Payne	Signature		Date	09/05/2019
Contribution to the Paper	Assisted with collection, data processing and interpretation of Hf isotopes				

Name of Co-Author	John Foden	Signature		Date	23/04/2019
Contribution to the Paper	Co-supervised work and assisted with manuscript revisions				

Name of Co-Author	Bert De Waele	Signature		Date	30/04/2019
Contribution to the Paper	Assisted with providing samples for analysis, manuscript revisions				

Name of Co-Author	E Shaji	Signature		Date	24/04/2019
Contribution to the Paper	Organised field logistics and samples collection				

Name of Co-Author	M Santosh	Signature		Date	22/04/2019
Contribution to the Paper	Organised field logistics and sample collection, assisted with revision of the manuscript				

Statement of Authorship 2

Title of Paper	Evolving marginal terranes during Neoproterozoic supercontinent reorganisation: constraints from the Bemarivo Domain in northern Madagascar	
Publication Status	☑ Published ☐ Submitted for publication	☐ Accepted for publication ☐ Unpublished and unsubmitted, written in manuscript style
Publication Details	Armistead, S.E., Collins, A.S., Merdith, A.S., Payne, J.L., Cox, G.M., Foden, J.D., Razakamanana, T. and De Waele, B. In press. Evolving marginal terranes during Neoproterozoic supercontinent reorganisation: constraints from the Bemarivo Belt in northern Madagascar. *Tectonics*. doi.org/10.31223/osf.io/btahm	

Principal Author

Name of Principal Author (Candidate)	Sheree Armistead		
Contribution to the Paper	Conceptualisation of the work, development of ideas and conclusions, prepared samples, carried out analytical work, interpretation of the data, wrote manuscript.		
Overall percentage (%)	80%		
Certification:	This paper reports on original research I conducted during the period of my Higher Degree by Research candidature and is not subject to any obligations or contractual agreements with a third party that would constrain its inclusion in this thesis. I am the primary author of this paper.		
Signature		Date	22/04/2019

Co-Author Contributions

By signing the Statement of Authorship, each author certifies that:

i. the candidate's stated contribution to the publication is accurate (as detailed above);
ii. permission is granted for the candidate in include the publication in the thesis; and
iii. the sum of all co-author contributions is equal to 100% less the candidate's stated contribution.

Name of Co-Author	Alan Collins	Signature		Date	22/04/2019
Contribution to the Paper	Supervised work, helped with data interpretation and manuscript revision				

Name of Co-Author	Andrew Merdith	Signature		Date	22/04/2019
Contribution to the Paper	Helped with GPlates modelling, and development of manuscript				

Name of Co-Author	Justin Payne	Signature		Date	09/05/2019
Contribution to the Paper	Assisted with collection, data processing and interpretation of Hf isotopes				

Name of Co-Author	Grant Cox	Signature		Date	22/04/2019
Contribution to the Paper	Helped with interpretation of wholerock geochemistry data				

Name of Co-Author	John Foden	Signature		Date	23/04/2019
Contribution to the Paper	Helped with interpretation of wholerock and isotopic data				

Name of Co-Author	Theodore Razakamanana	Signature		Date	23/04/2019
Contribution to the Paper	Helped with the conceptualisation of the research project				

Name of Co-Author	Bert De Waele	Signature		Date	30/04/2019
Contribution to the Paper	Assisted with providing samples for analysis, manuscript revisions				

Statement of Authorship 3

Title of Paper	Structural evolution and medium-temperature thermochronology of central Madagascar: implications for Gondwana amalgamation	
Publication Status	☐ Published ☑ Submitted for publication	☐ Accepted for publication ☐ Unpublished and unsubmitted, written in manuscript style
Publication Details	Armistead, S.E., Collins, A.S., Redaa, A., Gilbert, S., Jepson, G., Gillespie, J., Blades, M.L., Foden, J.D. and Razakamanana, T., In Review. Structural evolution and medium-temperature thermochronology of central Madagascar: implications for Gondwana amalgamation. *Journal of the Geological Society*. doi.org/10.31223/osf.io/x46vc	

Principal Author

Name of Principal Author (Candidate)	Sheree Armistead		
Contribution to the Paper	Conceptualisation of the work, development of ideas and conclusions, prepared samples, carried out analytical work, interpretation of the data, wrote manuscript.		
Overall percentage (%)	80%		
Certification:	This paper reports on original research I conducted during the period of my Higher Degree by Research candidature and is not subject to any obligations or contractual agreements with a third party that would constrain its inclusion in this thesis. I am the primary author of this paper.		
Signature		Date	22/04/2019

Co-Author Contributions

By signing the Statement of Authorship, each author certifies that:

i. the candidate's stated contribution to the publication is accurate (as detailed above);
ii. permission is granted for the candidate in include the publication in the thesis; and
iii. the sum of all co-author contributions is equal to 100% less the candidate's stated contribution.

Name of Co-Author	Alan Collins	Signature		Date	22/04/2019
Contribution to the Paper	Supervised work, helped with data interpretation and manuscript revision				

Name of Co-Author	Ahmad Redaa	Signature		Date	23/04/2019
Contribution to the Paper	Lead the analysis, data processing and interpretation for the Rb–Sr section				

Name of Co-Author	Sarah Gilbert	Signature		Date	23/04/2019
Contribution to the Paper	Assisted with the analysis and data processing for all of the isotopic datasets				

Name of Co-Author	Gilby Jepson	Signature		Date	23/04/2019
Contribution to the Paper	Assisted with analysis and interpretation of U–Pb apatite				

Name of Co-Author	Jack Gillespie	Signature		Date	22/04/2019
Contribution to the Paper	Assisted with analysis and interpretation of U–Pb apatite				

Name of Co-Author	Morgan Blades	Signature		Date	22/04/2019
Contribution to the Paper	Helped with field work, sample and structural data collection				

Name of Co-Author	John Foden	Signature		Date	23/04/2019
Contribution to the Paper	Helped with field work, manuscript revisions				

Name of Co-Author	Theodore Razakamanana	Signature		Date	23/04/2019
Contribution to the Paper	Organised field work logistics, helped with field work and data/sample collection				

Statement of Authorship 4

Title of Paper	Proterozoic basin evolution and tectonic geography of Madagascar during the Nuna Supercontinent	
Publication Status	☐ Published ☐ Submitted for publication	☐ Accepted for publication ☑ Unpublished and unsubmitted, written in manuscript style
Publication Details	Armistead, S.E., Collins, A.S., Schmitt, R.S., Costa, R.L., De Waele, B., Foden, J.D., Razakamanana, T. and Payne, J.L., In prep. Proterozoic basin evolution and tectonic geography of Madagascar during the Nuna Supercontinent.	

Principal Author

Name of Principal Author (Candidate)	Sheree Armistead		
Contribution to the Paper	Conceptualisation of the work, development of ideas and conclusions, prepared samples, carried out analytical work, interpretation of the data, wrote manuscript.		
Overall percentage (%)	80%		
Certification:	This paper reports on original research I conducted during the period of my Higher Degree by Research candidature and is not subject to any obligations or contractual agreements with a third party that would constrain its inclusion in this thesis. I am the primary author of this paper.		
Signature		Date	22/04/2019

Co-Author Contributions

By signing the Statement of Authorship, each author certifies that:

i. the candidate's stated contribution to the publication is accurate (as detailed above);
ii. permission is granted for the candidate in include the publication in the thesis; and
iii. the sum of all co-author contributions is equal to 100% less the candidate's stated contribution.

Name of Co-Author	Alan Collins	Signature		Date	22/04/2019
Contribution to the Paper	Supervised work, helped with data interpretation and manuscript revision				

Name of Co-Author	Renata Schmitt	Signature		Date	25/04/2019
Contribution to the Paper	Organised field work logistics, helped with field work and data/sample collection, conceptualisation of ideas				

Name of Co-Author	Raisa Costa	Signature		Date	08/05/2019
Contribution to the Paper	Organised field work logistics, helped with field work and data/sample collection, conceptualisation of ideas				

Name of Co-Author	Bert De Waele	Signature		Date	30/04/2019
Contribution to the Paper	Assisted with providing samples for analysis, manuscript revisions				

Name of Co-Author	John Foden	Signature		Date	23/04/2019
Contribution to the Paper	Helped with field work, manuscript revisions				

Name of Co-Author	Theodore Razakamanana	Signature		Date	23/04/2019
Contribution to the Paper	Organised field work logistics, helped with field work and data/sample collection				

Name of Co-Author	Justin Payne	Signature		Date	09/05/2019
Contribution to the Paper	Assisted with collection, data processing and interpretation of Hf isotopes				

1

Introduction and background Geology

1. Introduction

Plate tectonics are critical for a range of Earth system processes, and have played an important role in the evolution of Earth over its 4.5 billion year history. The movement of Earth's tectonic plates result in periodic supercontinent formation, which in turn affects our planet in a myriad of ways. The last major supercontinent on Earth was Gondwana (Figure 1.1), and critical elements of its assembly are the focus of this PhD research. Gondwana formed during the Neoproterozoic era (1000–541 Ma), which was a dynamic period in Earth's history, with arguably the most dramatic changes to the climate, ecology and geodynamic structure of the planet (e.g. Evans, 2000; Hoffman et al., 1998; Li et al., 2013; Stern, 1994). The cyclic nature of supercontinent assembly and dispersal more broadly, has no doubt been instrumental in the evolution of life on Earth, the distribution of Earth's precious resources, and the geodynamic nature of the planet at great depths. Therefore, understanding the paleogeography of past continents and their associated mountain ranges and ocean basins, is incredibly important. However, reconstructing plate tectonics beyond ~200 million years ago is challenging because oceanic lithosphere rarely survives longer than this before being subducted and recycled. Reconstructing the Earth's tectonic geography prior to c. 200 Ma requires the use of a range of proxies for tectonic processes, such as paleomagnetic and isotopic data. Research in this thesis uses a multi-disciplinary approach that integrates isotopic data, geochemical data, and structural data to understand the timing and nature of the amalgamation of central Gondwana.

2. Geological background

Gondwana formed when the continents of eastern Gondwana including Australia, India and East Antarctica amalgamated with the Precambrian blocks of western Gondwana including Madagascar, Africa and South America (e.g. Fritz et al., 2013; Johnson et al., 2011). This thesis focuses on the largest Gondwana-forming collisional belt—the East African Orogen—and its expression into Madagascar and Madagascar's paleo-neighbours

(Figure 1.1). The East African Orogen was comparable in scale to the modern Himalaya System (>5000 km length) and formed during closure of the Mozambique Ocean that separated India, Madagascar and Africa (Collins and Pisarevsky, 2005; Fritz et al., 2013; Johnson et al., 2011; Meert, 2003; Merdith et al., 2017; Merdith et al., 2019).

The timing and duration of magmatic arc assembly along the length of the East African Orogen is still an emerging area of research. Originally, it was thought that the East African Orogen was a product of a single-stage collision between East and West Gondwana (Stern, 1994). However, with the abundance of isotopic data that now exist for the East African Orogen, we know that the age distribution does not reflect a simple single-stage collision. Considerable research has shown that smaller continental fragments came together over a protracted period of time during the Neoproterozoic and early Cambrian (e.g. Boger et al., 2015; Collins, 2006; Collins and Pisarevsky, 2005; de Wit et al., 2001; Kusky et al., 2003).

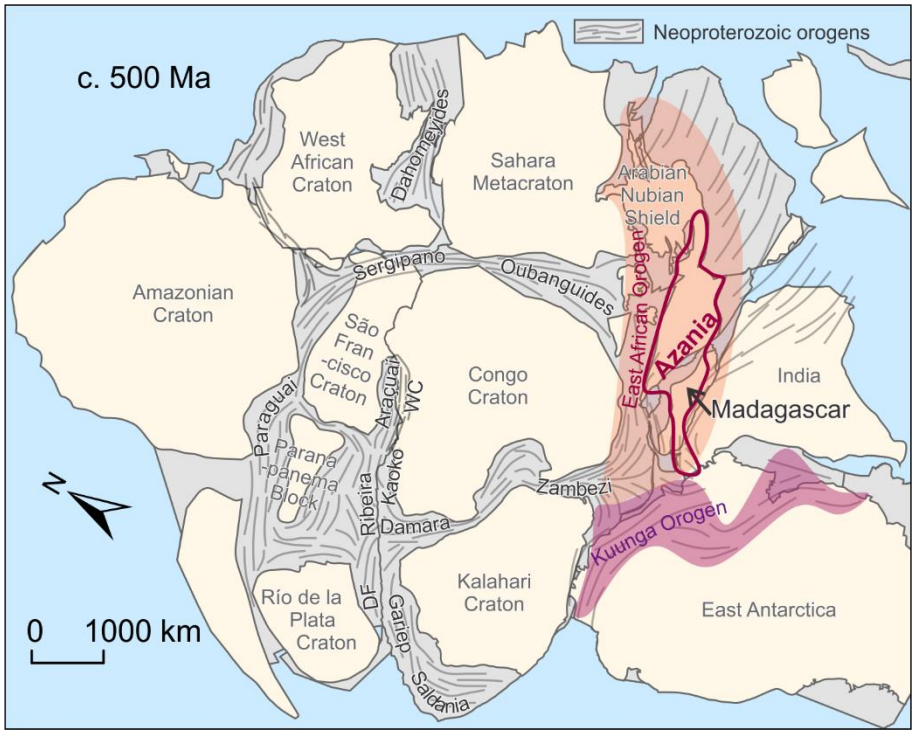

Figure 1.1 Tectonic map of Gondwana made using GPlates exported geometries from Merdith et al. (2017) in ArcGIS; projected in Hotine Oblique Mercator with Madagascar in the centre (reconstructed position, longitude=-75 and latitude=+40). DF=Dom Feliciano Belt, WC=West Congo.

The microcontinent 'Azania' was proposed by Collins and Windley (2002), which comprised fragments of Madagascar, Somalia, eastern Ethiopia and Arabia. It was suggested that Azania collided with the Congo Craton, Tanzania Craton, Bangweulu Block and the western Arabian Nubian Shield at c. 650 Ma. In Madagascar this suture is termed the Vohibory Suture, which separates the Vohibory Domain and Androyen Domain of southern Madagascar (Figure 1.2). The location of a Gondwana suture in southwestern Madagascar is contentious however. The boundary between the Androyen and Anosyen domains (Figure 1.2) has alternatively been interpreted as the major Gondwana-forming collision zone in Madagascar that sutured at c. 580–520 Ma (Boger et al., 2015; Boger et al., 2014; Boger et al., 2019).

A younger orogeny marked by the Betsimisaraka Suture in eastern Madagascar has also been proposed, which sutured Madagascar and India at c. 550 Ma (Collins and Pisarevsky, 2005). In Madagascar, this suture separates the Antananarivo Domain from the Antongil and Masora domains of Indian origin. The Betsimisaraka Suture is controversial however, with some researchers maintaining that Madagascar and India have been contiguous since c. 2500 Ma (Tucker et al., 2011; Tucker et al., 2014; Zhou et al., 2018). Other authors have suggested that the Betsimisaraka Suture is more like c. 700 Ma (Fitzsimons and Hulscher, 2005). It has also been postulated that the Betsimisaraka Suture extends into India as the "Kumta Suture", and that it is a Mesoproterozoic, rather than Neoproterozoic, suture (Ishwar-Kumar et al., 2013). Reconciling the controversies in the age and location of Gondwana collision zones in Madagascar is a focus of this thesis.

2.1. Geological domains of Madagascar

Considerable advances in the understanding of the mapped geology of Madagascar were gained through the collection of isotopic, structural and mapping data of a major World Bank Project in Madagascar (BGS-USGS-GLW, 2008). This resulted in several publications (e.g. De Waele et al., 2011; Goodenough et al., 2010; Schofield et al., 2010; Thomas et al., 2009; Tucker et al., 2014) and an updated 1:1,000,000 map for the entire country (Roig et al., 2012) that have provided a good foundation to understanding the age and composition of the major domains in Madagascar. Madagascar is made up of several domains spanning from Archean to Neoproterozoic (Figure 1.2). Central Madagascar contains the Antananarivo Domain, which is composed of magmatic gneisses of the c. 2500 Ma Betsiboka Suite (Collins and Windley, 2002; Kröner et al., 2000). In eastern Madagascar are the Antongil and Masora domains, which contain c. 3100 Ma rocks and are likely a continuation of the Dharwar Craton of India (Chapter 2/Armistead et al., 2017; Schofield et al., 2010; Tucker et al., 1999). To the southwest of, and overlying the Antananarivo Craton, is the Itremo Group, composed of quartzites, schists and marbles with a maximum depositional age of c. 1700 Ma (Chapter 5/Armistead et al., In Prep; Cox et al., 1998; Fernandez et al., 2003). To the southwest of the Itremo Group, is the Ikalamavony Group, similarly made up of quartzites, schists and marbles, but with a maximum depositional age of c. 1000 Ma. To the south of these metasedimentary

domains are the Proterozoic Anosyen, Androyen and Vohibory domains (Boger et al., 2014; Emmel et al., 2008; Jöns and Schenk, 2008). In northern Madagascar is the c. 800–700 Ma Bemarivo Domain, which likely formed as an exotic juvenile arc terrane that amalgamated with Madagascar at c. 520 Ma (Chapter 3/Armistead et al., 2019; Jöns et al., 2009; Thomas et al., 2009).

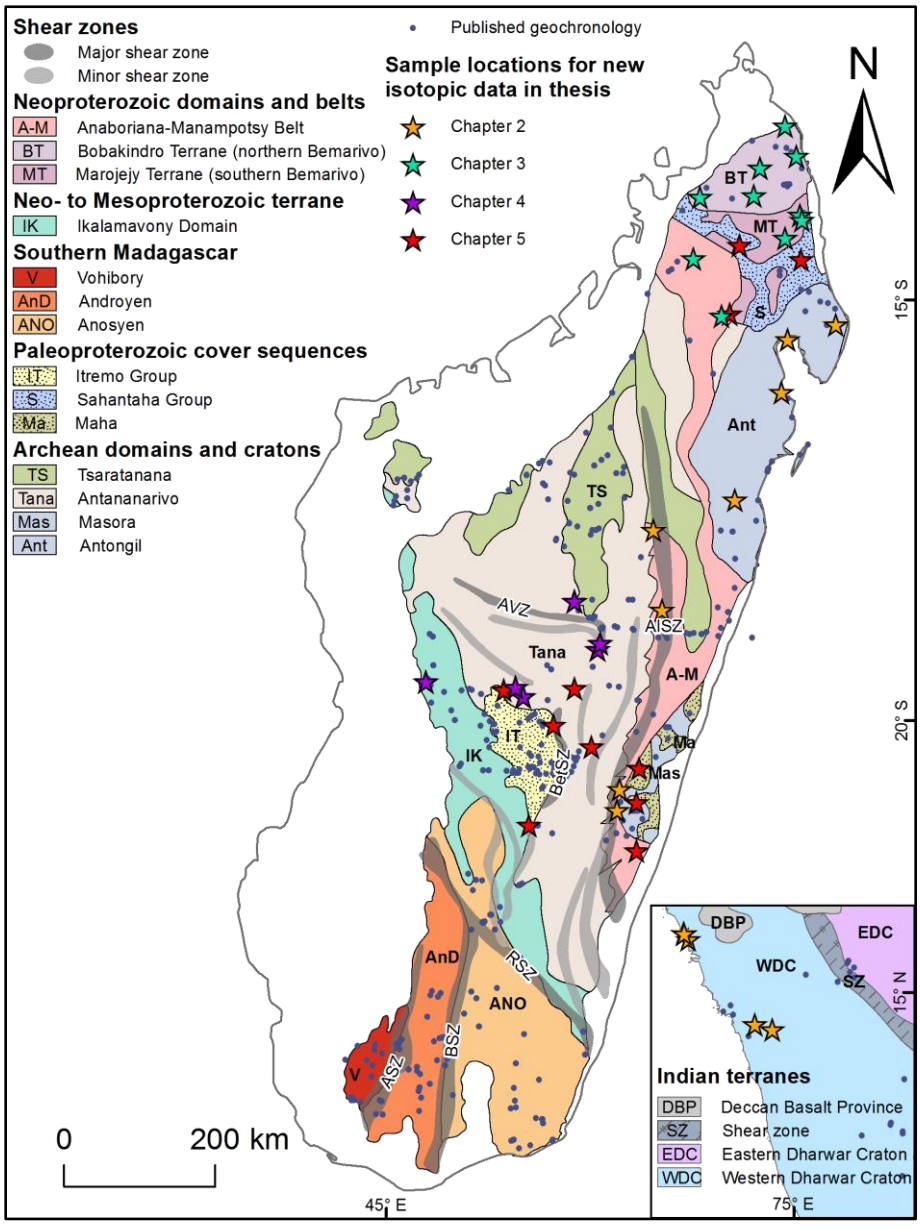

Figure 1.2 Tectonic Domains of Madagascar (De Waele et al., 2011) and western peninsular India (Rekha et al., 2014), with locations for new isotopic data collected during this PhD. Naming of the northern Neoproterozoic terranes following Chapter 3/Armistead et al. (2019). Locations for other published geochronology data also shown; updated from the compilation of Tucker et al. (2014). AISZ=Angavo-Ifanadiana shear zone, AVZ=Antananarivo virgation zone, BetSZ=Betsileo shear zone, RSZ=Ranotsara shear zone, BSZ=Beraketa shear zone, ASZ=Ampanihy shear zone.

A series of Neoproterozoic sedimentary sequences overly these major domains, and a suite of Neoproterozoic magmatic rocks intrude the domains. Overlying the Ikalamavony and Itremo domains is the Molo Group, which has a maximum depositional age of c. 620 Ma and a minimum depositional age of c. 560 Ma defined by metamorphic overgrowths (Cox et al., 2004). The c. 1000 Ma Dabolava Suite (Archibald et al., 2017) is restricted to the Ikalamavony Domain while the c. 850–750 Ma Imorona-Itsindro Suite (Archibald et al., 2016; Moine et al., 2014; Zhou et al., 2018) is widespread throughout much of central and eastern Madagascar. In the Vohibory Domain, the Linta group contains sedimentary rocks with maximum depositional ages of c. 620 Ma that closely reflect the ages of the intrusive Marasavoa and Vohitany suites.

All of these domains have been deformed and metamorphosed during the late Neoproterozoic and early Cambrian (e.g. Chapter 4/Armistead et al., In Review; Collins et al., 2003a; Collins et al., 2003b; Tucker et al., 2007) in response to the East African Orogen. Reconciling the location of suture zones responsible for this deformation in Madagascar is a focus of this PhD research.

3. Thesis outline

Madagascar records suites of rocks that formed during all of the known supercontinents that Earth has experienced. These include Gondwana (c. 0.5 Ga), Rodinia (c. 1.0 Ga), Nuna/Columbia (c. 1.8–1.3 Ga) and Kenorland (c. 2.5 Ga) (Figure 1.3). This makes Madagascar an important place to understand the evolution of its geology, its correlation with other terranes and understanding supercontinent cycles more broadly. In particular, Madagascar occupied an important place in the centre of Gondwana during the East African Orogeny. The timing and nature of how the terranes of Madagascar assembled with neighbouring blocks in Africa and India during Gondwana assembly—and indeed during other supercontinents—remains contentious and is the focus of this PhD research.

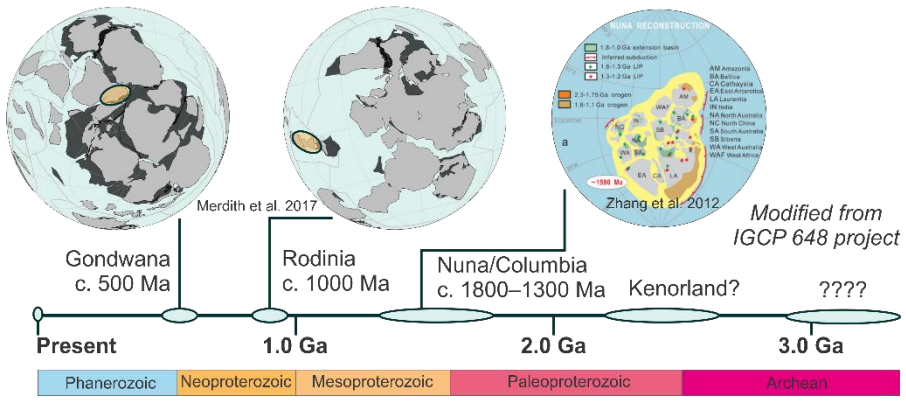

Figure 1.3 Reconstructions of Earth's major supercontinents, with Madagascar's position circled in Gondwana and Rodinia. Gondwana and Rodinia reconstructions from Merdith et al. (2017) and Nuna Reconstruction from Zhang et al. (2012).

Various fields of geoscience are currently grappling with the challenges of managing and adequately using vast quantities of data. As illustrated in Figure 1.4, the number of papers published every year using the key isotopic methods of this PhD research, is increasing exponentially. Even when considering only the papers published specifically on 'Gondwana U-Pb zircon', we can see that hundreds of datasets are being produced every year. It is no longer sufficient to compare characteristics of geological terranes using qualitative approaches alone. This PhD research explores emerging techniques for statistically comparing big isotopic datasets in addition to collecting new data in key regions. This PhD research has been driven by a multi-disciplinary and innovative approach to interpreting isotopic, geochemical and structural datasets to better understand the evolution of Madagascar and its paleo-neighbours during the Precambrian.

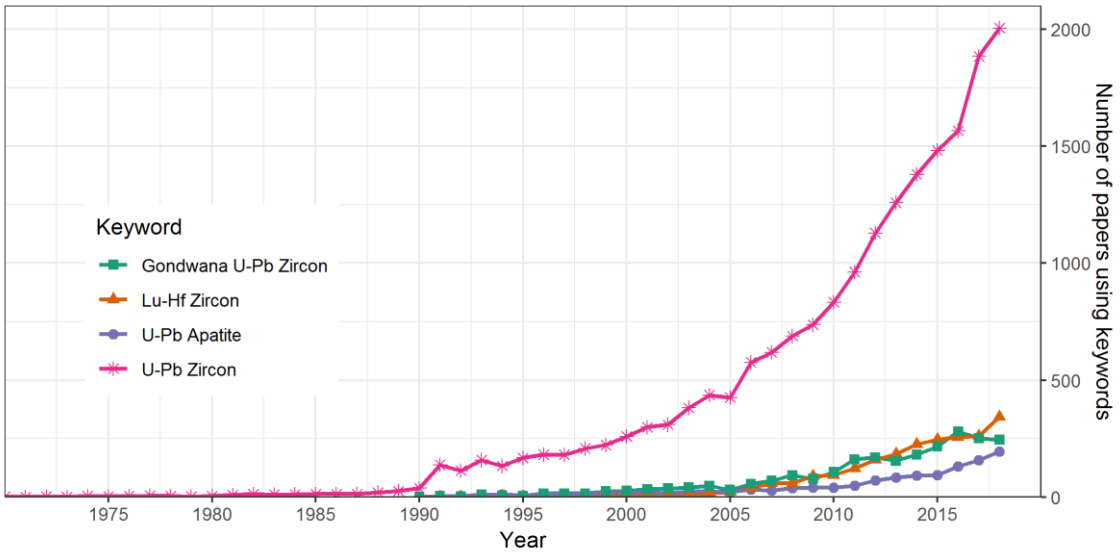

Figure 1.4 Number of publications by year using specified keywords in the Web of Science database for key isotopic methods used in this PhD research.

This PhD thesis comprises four chapters that focus on different aspects related to the tectonic evolution of Madagascar from the Archean to early Cambrian, and to ultimately constrain the timing and nature of the amalgamation of central Gondwana. The following chapters constitute either a published paper, manuscript under review, or manuscript prepared for submission. Subsequently, there is unavoidable repetition in the introduction, background geology, methodology and some components of the discussion sections of each chapter.

In Chapter 2 we compare different models for the timing and location of the Betsimisaraka Suture in eastern Madagascar and western India. We use primarily detrital and magmatic zircon U–Pb and Lu–Hf isotopes and multi-dimensional scaling methods to assess similarity of samples from different terranes in Madagascar and India. Detrital zircon geochronology is a powerful tool for identifying the provenance of source material and subsequently interpreting paleogeography.

In Chapter 3 we study the northern extent of the Betsimisaraka Suture in the Bemarivo Domain where its location is particularly ambiguous. We use primarily zircon Hf and O isotopes to understand the crustal evolution of northern Madagascar. We look at other similarly aged terranes in China, the Seychelles, and the Malani Igneous Suite of northwest India, and propose a model for an extensive juvenile arc system at c. 800–700 Ma.

In Chapter 4 we integrate structural geology and medium-temperature thermochronology to understand the evolution of central Madagascar. Central Madagascar is bound either side by the two proposed Gondwana-forming sutures—the c. 650 Ma Vohibory Suture and the c. 550 Ma Betsimisaraka Suture. Structural geology is especially useful as it provides insight into the kinematics of tectonic events, which are impossible to identify from isotopic studies alone.

In Chapter 5 we correlate Paleoproterozoic metasedimentary sequences across Madagascar and compare them to age equivalent sequences in Madagascar, Africa and India. We also address the controversy over several proposed Neoproterozoic sequences and belts in Madagascar. We use primarily detrital zircon U–Pb and Lu–Hf isotopes to quantitatively assess these correlations. This research has important implications for the tectonic geography of these regions during the entire Proterozoic eon. In particular, these correlations have important implications for addressing the likely age of the Betsimisaraka Suture as either an Archean or Neoproterozoic event.

References

Archibald, D.B., Collins, A.S., Foden, J.D., Payne, J.L., Holden, P., Razakamanana, T., De Waele, B., Thomas, R.J. and Pitfield, P.E.J., 2016. Genesis of the Tonian Imorona–Itsindro magmatic Suite in central Madagascar: Insights from U–Pb, oxygen and hafnium isotopes in zircon. Precambrian Research, 281: 312-337.

Archibald, D.B., Collins, A.S., Foden, J.D., Payne, J.L., Macey, P.H., Holden, P. and Razakamanana, T., 2017. Stenian–Tonian arc magmatism in west–central Madagascar: the genesis of the Dabolava Suite. Journal of the Geological Society: jgs2017-028.

Armistead, S.E., Collins, A., Merdith, A.S., Payne, J.L., Cox, G.M., Foden, J.D., Razakamanana, T. and De Waele, B., 2019. Evolving marginal terranes during Neoproterozoic supercontinent reorganisation: constraints from the Bemarivo Domain in northern Madagascar. Tectonics.

Armistead, S.E., Collins, A.S., Payne, J.L., Foden, J.D., De Waele, B., Shaji, E. and Santosh, M., 2017. A re-evaluation of the Kumta Suture in western peninsular India and its extension into Madagascar. Journal of Asian Earth Sciences.

Armistead, S.E., Collins, A.S., Redaa, A., Gilbert, S., Jepson, G., Gillespie, J., Blades, M.L., Foden, J.D. and Razakamanana, T., In Review. Structural evolution and medium-temperature thermochronology of central Madagascar: implications for Gondwana amalgamation. Journal of the Geological Society.

Armistead, S.E., Collins, A.S., Schmitt, R.S., Costa, R.L., De Waele, B., Foden, J.D., Razakamanana, T. and Payne, J.L., In Prep. Proterozoic basin evolution and tectonic geography of Madagascar during the Nuna Supercontinent.

BGS-USGS-GLW, 2008. Republique de Madagascar Ministère de L'engergie et des Mines (MEM/SG/DG/UCP/PGRM). British Geological Survey Research Report.

Boger, S.D., Hirdes, W., Ferreira, C.A.M., Jenett, T., Dallwig, R. and Fanning, C.M., 2015. The 580–520Ma Gondwana suture of Madagascar and its continuation into Antarctica and Africa. Gondwana Research, 28(3): 1048-1060.

Boger, S.D., Hirdes, W., Ferreira, C.A.M., Schulte, B., Jenett, T. and Fanning, C.M., 2014. From passive margin to volcano–sedimentary forearc: The Tonian to Cryogenian evolution of the Anosyen Domain of southeastern Madagascar. Precambrian Research, 247: 159-186.

Boger, S.D., Maas, R., Pastuhov, M., Macey, P.H., Hirdes, W., Schulte, B., Fanning, C.M., Ferreira, C.A.M., Jenett, T. and Dallwig, R., 2019. The tectonic domains of southern and western Madagascar. Precambrian Research.

Collins, A.S., 2006. Madagascar and the amalgamation of Central Gondwana. Gondwana Research, 9(1-2): 3-16.

Collins, A.S., Fitzsimons, I.C.W., Hulscher, B. and Razakamanana, T., 2003a. Structure of the eastern margin of the East African Orogen in central Madagascar. Precambrian Research, 123(2–4): 111-133.

Collins, A.S., Johnson, S., Fitzsimons, I.C., Powell, C.M., Hulscher, B., Abello, J. and Razakamanana, T., 2003b. Neoproterozoic deformation in central Madagascar: a structural section through part of the East African Orogen. Geological Society, London, Special Publications, 206(1): 363-379.

Collins, A.S. and Pisarevsky, S.A., 2005. Amalgamating eastern Gondwana: The evolution of the Circum-Indian Orogens. Earth-Science Reviews, 71(3-4): 229-270.

Collins, A.S. and Windley, B.F., 2002. The tectonic evolution of central and northern Madagascar and its place in the final assembly of Gondwana. The Journal of Geology, 110(3): 325-339.

Cox, R., Armstrong, R.A. and Ashwal, L.D., 1998. Sedimentology, geochronology and provenance of the Proterozoic Itremo Group, central Madagascar, and implications for pre-Gondwana palaeogeography. Journal of the Geological Society, 155(6): 1009-1024.

Cox, R., Coleman, D.S., Chokel, C.B., DeOreo, S.B., Wooden, J.L., Collins, A.S., De Waele, B. and Kröner, A., 2004. Proterozoic tectonostratigraphy and paleogeography of central Madagascar derived from detrital zircon U-Pb age populations. The Journal of geology, 112(4): 379-399.

De Waele, B., Thomas, R.J., Macey, P.H., Horstwood, M.S.A., Tucker, R.D., Pitfield, P.E.J., Schofield, D.I., Goodenough, K.M., Bauer, W., Key, R.M., Potter, C.J., Armstrong, R.A., Miller, J.A., Randriamananjara, T., Ralison, V., Rafahatelo, J.M., Rabarimanana, M. and Bejoma, M., 2011. Provenance and tectonic significance of the Palaeoproterozoic metasedimentary successions of central and northern Madagascar. Precambrian Research, 189(1-2): 18-42.

de Wit, M.J., Bowring, S.A., Ashwal, L.D., Randrianasolo, L.G., Morel, V.P.I. and Rambeloson, R.A., 2001. Age and tectonic evolution of Neoproterozoic ductile shear zones in southwestern Madagascar, with implications for Gondwana studies. Tectonics, 20(1): 1-45.

Emmel, B., Jons, N., Kroner, A., Jacobs, J., Wartho, J.A., Schenk, V., Razakamanana, T. and Austegard, A., 2008. From Closure of the Mozambique Ocean to Gondwana Breakup: New Evidence from

Geochronological Data of the Vohibory Terrane, Southwest Madagascar. The Journal of Geology, 116(1): 21-38.

Evans, D.A., 2000. Stratigraphic, geochronological, and paleomagnetic constraints upon the Neoproterozoic climatic paradox. American Journal of Science, 300(5): 347-433.

Fernandez, A., Schreurs, G., Villa, I.M., Huber, S. and Rakotondrazafy, M., 2003. Age constraints on the tectonic evolution of the Itremo region in Central Madagascar. Precambrian Research, 123(2-4): 87-110.

Fitzsimons, I.C.W. and Hulscher, B., 2005. Out of Africa: detrital zircon provenance of central Madagascar and Neoproterozoic terrane transfer across the Mozambique Ocean. Terra Nova, 17(3): 224-235.

Fritz, H., Abdelsalam, M., Ali, K.A., Bingen, B., Collins, A.S., Fowler, A.R., Ghebreab, W., Hauzenberger, C.A., Johnson, P.R., Kusky, T.M., Macey, P., Muhongo, S., Stern, R.J. and Viola, G., 2013. Orogen styles in the East African Orogen: A review of the Neoproterozoic to Cambrian tectonic evolution. Journal of African Earth Sciences, 86: 65-106.

Goodenough, K.M., Thomas, R.J., De Waele, B., Key, R.M., Schofield, D.I., Bauer, W., Tucker, R.D., Rafahatelo, J.M., Rabarimanana, M., Ralison, A.V. and Randriamananjara, T., 2010. Post-collisional magmatism in the central East African Orogen: The Maevarano Suite of north Madagascar. Lithos, 116(1-2): 18-34.

Hoffman, P.F., Kaufman, A.J., Halverson, G.P. and Schrag, D.P., 1998. A Neoproterozoic snowball earth. science, 281(5381): 1342-1346.

Ishwar-Kumar, C., Windley, B., Horie, K., Kato, T., Hokada, T., Itaya, T., Yagi, K., Gouzu, C. and Sajeev, K., 2013. A Rodinian suture in western India: New insights on India-Madagascar correlations. Precambrian Research, 236: 227-251.

Johnson, P., Andresen, A., Collins, A., Fowler, A., Fritz, H., Ghebreab, W., Kusky, T. and Stern, R., 2011. Late Cryogenian–Ediacaran history of the Arabian–Nubian Shield: a review of depositional, plutonic, structural, and tectonic events in the closing stages of the northern East African Orogen. Journal of African Earth Sciences, 61(3): 167-232.

Jöns, N., Emmel, B., Schenk, V. and Razakamanana, T., 2009. From orogenesis to passive margin—the cooling history of the Bemarivo Belt (N Madagascar), a multi-thermochronometer approach. Gondwana Research, 16(1): 72-81.

Jöns, N. and Schenk, V., 2008. Relics of the Mozambique Ocean in the central East African Orogen: evidence from the Vohibory Block of southern Madagascar. Journal of Metamorphic Geology.

Kröner, A., Hegner, E., Collins, A.S., Windley, B.F., Brewer, T.S., Razakamanana, T. and Pidgeon, R.T., 2000. Age and magmatic history of the Antananarivo Block, central Madagascar, as derived from zircon geochronology and Nd isotopic systematics. American Journal of Science, 300(4): 251-288.

Kusky, T.M., Abdelsalam, M., Tucker, R.D. and Stern, R.J., 2003. Evolution of the East African and related orogens, and the assembly of Gondwana. Precambrian Research, 123(2-4): 81-85.

Li, Z.-X., Evans, D.A.D. and Halverson, G.P., 2013. Neoproterozoic glaciations in a revised global palaeogeography from the breakup of Rodinia to the assembly of Gondwanaland. Sedimentary Geology, 294: 219-232.

Meert, J.G., 2003. A synopsis of events related to the assembly of eastern Gondwana. Tectonophysics, 362(1-4): 1-40.

Merdith, A.S., Collins, A.S., Williams, S.E., Pisarevsky, S., Foden, J.D., Archibald, D.B., Blades, M.L., Alessio, B.L., Armistead, S. and Plavsa, D., 2017. A full-plate global reconstruction of the Neoproterozoic. Gondwana Research, 50: 84-134.

Merdith, A.S., Williams, S.E., Brune, S., Collins, A.S. and Müller, R.D., 2019. Rift and plate boundary evolution across two supercontinent cycles. Global and Planetary Change, 173: 1-14.

Moine, B., Bosse, V., Paquette, J.-L. and Ortega, E., 2014. The occurrence of a Tonian–Cryogenian (~850Ma) regional metamorphic event in Central Madagascar and the geodynamic setting of the Imorona–Itsindro (~800Ma) magmatic suite. Journal of African Earth Sciences, 94: 58-73.

Rekha, S., Bhattacharya, A. and Chatterjee, N., 2014. Tectonic restoration of the Precambrian crystalline rocks along the west coast of India: Correlation with eastern Madagascar in East Gondwana. Precambrian Research, 252: 191-208.

Roig, J., Tucker, R., Delor, C., Peters, S. and Théveniaut, H., 2012. Carte géologique de la République de Madagascar à 1/1 000 000. Ministère des Mines, PGRM, Antananarivo, République de Madagascar. 1:1,000,000.

Schofield, D.I., Thomas, R.J., Goodenough, K.M., De Waele, B., Pitfield, P.E.J., Key, R.M., Bauer, W., Walsh, G.J., Lidke, D.J. and Ralison, A.V., 2010. Geological evolution of the Antongil Craton, NE Madagascar. Precambrian Research, 182(3): 187-203.

Stern, R.J., 1994. Arc-assembly and continental collision in the Neoproterozoic African orogen: implications for the consolidation of Gondwanaland. Annual Review of Earth and Planetary Sciences, 22: 319-351.

Thomas, R.J., De Waele, B., Schofield, D.I., Goodenough, K.M., Horstwood, M., Tucker, R., Bauer, W., Annells, R., Howard, K., Walsh, G., Rabarimanana, M., Rafahatelo, J.M., Ralison, A.V. and Randriamananjara, T., 2009. Geological evolution of the Neoproterozoic Bemarivo Belt, northern Madagascar. Precambrian Research, 172(3-4): 279-300.

Tucker, R., Ashwal, L., Handke, M., Hamilton, M., Le Grange, M. and Rambeloson, R., 1999. U-Pb geochronology and isotope geochemistry of the Archean and Proterozoic rocks of north-central Madagascar. The Journal of Geology, 107(2): 135-153.

Tucker, R., Roig, J.-Y., Delor, C., Amelin, Y., Goncalves, P., Rabarimanana, M., Ralison, A. and Belcher, R., 2011. Neoproterozoic extension in the Greater Dharwar Craton: a reevaluation of the "Betsimisaraka suture" in Madagascar. Canadian Journal of Earth Sciences, 48(2): 389-417.

Tucker, R.D., Kusky, T.M., Buchwaldt, R. and Handke, M.J., 2007. Neoproterozoic nappes and superposed folding of the Itremo Group, west-central Madagascar. Gondwana Research, 12(4): 356-379.

Tucker, R.D., Roig, J.Y., Moine, B., Delor, C. and Peters, S.G., 2014. A geological synthesis of the Precambrian shield in Madagascar. Journal of African Earth Sciences, 94: 9-30.

Zhang, S., Li, Z.-X., Evans, D.A., Wu, H., Li, H. and Dong, J., 2012. Pre-Rodinia supercontinent Nuna shaping up: a global synthesis with new paleomagnetic results from North China. Earth and Planetary Science Letters, 353: 145-155.

Zhou, J.-L., Li, X.-H., Tang, G.-Q., Liu, Y. and Tucker, R.D., 2018. New evidence for a continental rift tectonic setting of the Neoproterozoic Imorona-Itsindro Suite (central Madagascar). Precambrian Research, 306: 94-111.

2

A Re-Evaluation of the Kumta Suture in western Peninsular India and its extension into Madagascar

Published as:

Armistead, S.E., Collins, A.S., Payne, J.L., Foden, J.D., De Waele, B., Shaji, E. and Santosh, M., 2017. A re-evaluation of the Kumta Suture in western peninsular India and its extension into Madagascar. *Journal of Asian Earth Sciences.*

https://doi.org/10.1016/j.jseaes.2017.08.020

Abstract

It has long been recognised that Madagascar was contiguous with India until the Late Cretaceous. However, the timing and nature of the amalgamation of these two regions remain highly contentious as is the location of Madagascar against India in Gondwana. Here we address these issues with new U-Pb and Lu-Hf zircon data from five metasedimentary samples from the Karwar Block of India and new Lu-Hf data from eight previously dated igneous rocks from central Madagascar and the Antongil-Masora domains of eastern Madagascar. New U-Pb data from Karwar-region detrital zircon grains yield two dominant age peaks at c. 3100 Ma and c. 2500 Ma. The c. 3100 Ma population has relatively juvenile $\varepsilon_{Hf}(t)$ values that trend toward an evolved signature at c. 2500 Ma. The c. 2500 Ma population shows a wide range of $\varepsilon_{Hf}(t)$ values reflecting mixing of an evolved source with a juvenile source at that time. These data, and the new Lu-Hf data from Madagascar, are compared with our new compilation of over 7000 U-Pb and 1000 Lu-Hf analyses from Madagascar and India. We have used multidimensional scaling to assess similarities in these data in a statistically robust way. We propose that the Karwar Block of western peninsular India is an extension of the western Dharwar Craton and not

part of the Antananarivo Domain of Madagascar as has been suggested in some models. Based on $\varepsilon_{Hf}(t)$ signatures we also suggest that India (and the Antongil-Masora domains of Madagascar) were palaeogeographically isolated from central Madagascar (the Antananarivo Domain) during the Paleoproterozoic. This supports a model where central Madagascar and India amalgamated during the Neoproterozoic along the Betsimisaraka Suture.

1. Introduction

The assembly of central Gondwana occurred along the Neoproterozoic–Cambrian East African Orogen, which formed by at least two orogenies—the c. 650 Ma East African Orogeny and the c. 550–530 Ma Malagasy Orogeny. These events involved the amalgamation of several continental blocks along discrete orogenic belts (Collins and Pisarevsky, 2005; Fritz et al., 2013; Johnson et al., 2011; Stern, 1994). Of particular interest, and contention, is whether the amalgamation of Azania (a postulated Neoproterozoic continent that consists of central Madagascar, the Madurai Block of India, a swath of eastern Africa and a part of Yemen (Collins and Pisarevsky, 2005; Collins and Windley, 2002) and Neoproterozoic India occurred at this time, or whether this had taken place much earlier during the Archaean (e.g. Tucker et al., 2011a; Tucker et al., 2011b; Tucker et al., 2014). Several models have been proposed to account for similarities in the geology of Madagascar and India, but these models vary significantly in the timing and nature of major tectonic events that led to the amalgamation of these two regions (Boger et al., 2015; Boger et al., 2014; Collins and Pisarevsky, 2005; Collins and Windley, 2002; Ishwar-Kumar et al., 2013; Tucker et al., 2011a; Tucker et al., 2011b; Tucker et al., 2014).

Several opposing models have emerged in the literature that describe very different hypotheses for the tectonic evolution of Madagascar and India. The recognition that rocks of the Antongil-Masora domains of eastern Madagascar are similar to the Dharwar Craton (Tucker et al., 1999), and distinctly different from central Madagascar, led Collins and Windley (2002) to propose the Betsimisaraka Suture (Figure 2.1). This proposed suture zone along present day eastern Madagascar purportedly marks the site of ocean closure between the Dharwar Craton of India (at the time including the Antongil-Masora domains and a part of Neoproterozoic India) and central Madagascar (the Antananarivo Domain, a part of Azania) during the Ediacaran–Cambrian (Collins and Windley, 2002; Kröner et al., 2000). The ocean marked by the Betsimisaraka Suture would be a strand of the Neoproterozoic Mozambique Ocean that closed as India and the African continents amalgamated to form central Gondwana (Collins and Windley, 2002; Fitzsimons and Hulscher, 2005; Merdith et al., 2017).

The model of Collins and Windley (2002) was challenged by Tucker et al. (2011a) who suggested that central Madagascar and the “greater Dharwar Craton” were contiguous since at least c. 2500 Ma. In the model of Tucker et al. (2011a), much of Madagascar can be considered as two parts: the eastern part comprising the Antongil-Masora domains

that are an extension of the Dharwar Craton, and the central part comprising the Antananarivo Domain. Neoarchaean metamorphism in the Antananarivo Domain and Antongil-Masora domains was taken as evidence that these two regions amalgamated during a c. 2550–2480 Ma accretion event (Tucker et al., 2011a). This proposed amalgamation event involved emplacement of juvenile igneous rocks and high-grade metamorphism. This model dispels the existence of the Betsimisaraka Suture and instead, the site of the Betsimisaraka Suture approximately marks the site of a Neoproterozoic rift basin. This period of interpreted continental extension involved the deposition of the Manampotsy Group and the emplacement of the c. 840–760 Ma Itsindro-Imorona Suite in a rift setting (Yang et al., 2014). However, others have interpreted the Itsindro-Imorona Suite as being related to an Andean-type arc setting, rather than a rift setting (Archibald et al., 2016; Archibald et al., 2017; Boger et al., 2015). Tucker et al. (2011a) interpreted that the Manampotsy Group conceals the Neoarchaean boundary separating the Dharwar Craton (including the Antongil-Masora domains) from the Antananarivo Domain. This is broadly consistent with the interpretation of Rekha et al. (2014) who from a western Indian perspective, interpreted the Betsimisaraka Suture as a c. 2400 Ma accretion event.

Another model has recently emerged in which the Betsimisaraka Suture does exist, and extends into India in Goa and Karnataka, as the proposed Kumta and Mercara sutures (Ishwar-Kumar et al., 2016 2013; Ishwar-Kumar et al., 2013 2013). In this model, the trace of the Betsimisaraka Suture that bounds the Antongil Domain of northeast Madagascar goes offshore near Toamasina city in Madagascar and reappears as the semi-circular Kumta Suture in western peninsular India. The suture then curves back into Madagascar, joining up with the southern extension of the Betsimisaraka Suture that bounds the Masora Domain and then traces back into western peninsular India as the Mercara Suture that bounds the Coorg Block (Figure 2.1). Ishwar-Kumar et al. (2013) suggest that the Kumta Suture separates the western components—including central Madagascar, the Karwar Block around the Goa region, and the Coorg Block further to the south of western peninsular India—from the eastern component, the Dharwar Craton and Antongil-Masora domains. The authors suggest that geochronological data indicate that subduction along the Betsimisaraka-Kumta-Mercara Suture lasted for over 600 million years, beginning with ocean closure in the north at c. 1380 Ma and progressing to the south until c. 750 Ma.

The model of Ishwar-Kumar et al. (2013) involves a number of interpretations that can be tested against the geology of Madagascar and India. Firstly, the Karwar Block and western Dharwar Craton are interpreted as distinct terranes that amalgamated via the Kumta Suture. Secondly, the Karwar Block is purported to be an extension of the Antananarivo Domain and these regions should therefore have a shared geological evolution.

We have used U-Pb geochronology and Lu-Hf isotopic data to test the similarity or differences between terranes in order to assess the veracity of the various interpreted timings and locations of suturing events between Madagascar and India. This includes new U-Pb and Lu-Hf zircon data collected from the Karwar Block of western peninsular India and eastern Madagascar, and a compilation of over 8000 published U-Pb and Lu-Hf analyses from Madagascar and India. This extensive compilation allows for the use of multi-dimensional scaling (Spencer and Kirkland, 2016; Vermeesch, 2013; Vermeesch et al., 2016) to assess similarities between terranes in a more statistically robust way than traditional approaches.

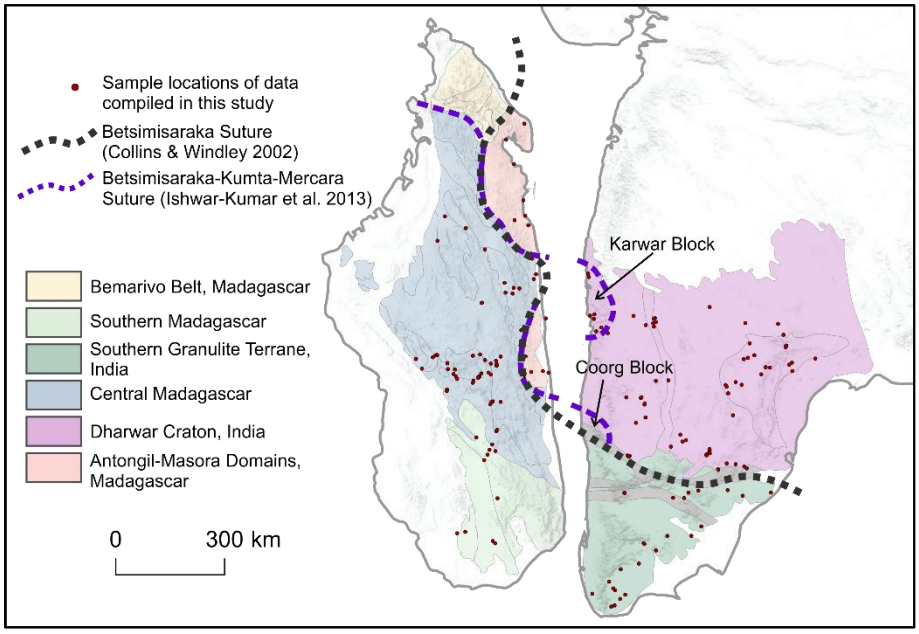

Figure 2.1 Reconstructed map of India and Madagascar in Gondwana. Further subdivision of terranes outlined in grey, modified from De Waele et al. (2011) and Geological Survey of India (1998).

1.1. Regional geology of the Karwar region, western peninsular India

The Karwar Block along the west coast of peninsular India (Figure 2.2b) has recently been the focus of a number of studies due to its contentious position in the various models for Madagascar-India correlations (Ishwar-Kumar et al., 2016; Ishwar-Kumar et al., 2013; Rekha et al., 2014; Rekha et al., 2013). Early Rb-Sr dating in the Goa region identified a gneissic basement of 3400 ± 140 Ma, granites and migmatites spanning the range c. 2650–2400 Ma, and the Goa Group metasedimentary rocks with a minimum age of c. 2600 Ma (Dhoundial et al., 1987). The Goa Group was correlated with the Chitradurga Group, which extends much further east in the western Dharwar Craton (Figure 2.2b), by Dhoundial et al. (1987), and has been further supported by more recent work (Rekha et al., 2013). Metamorphism is broadly contemporaneous (within uncertainty) of major magmatic events (Jayananda et al., 2012; Jayananda et al., 2013; Rekha et al., 2014; Rekha et al., 2013). Jayananda et al. (2013) recognised major thermal pulses at c. 3100–3000 Ma and c. 2550–2520 Ma based on chemical dating of monazite, Sm-Nd garnet-whole rock

isochrons and U-Pb zircon geochronology. The minimum depositional ages of rocks in the Dharwar Craton are poorly constrained. However, the c. 2600–2400 Ma deformation and metamorphism derived from monazite dating by Rekha et al. (2013) was interpreted to represent closure of the Goa Basin. Lithological groups of the Karwar Block have been correlated with both the western Dharwar Craton (WDC) and the Antongil-Masora domains of eastern Madagascar (Rekha et al., 2013). In the study of Rekha et al. (2013), the Goa Schist belt (Karwar) correlates with the Chitradurga Group (WDC) and Mananara Group (Madagascar); the Quepem granitoid (Karwar) correlates with the Masoala Suite (Madagascar); the Shimoga Schist Belt (Karwar) correlates with the Sagur Group (WDC) and Fenerivo Group (Madagascar); and the Peninsular gneisses (WDC) correlate with the Nosy Boraha Suite of Madagascar (Rekha et al., 2013). This is, however, contrary to the model of Ishwar-Kumar et al. (2013) who correlate the Karwar Block with the Antananarivo Domain of central Madagascar, however no detailed lithological correlations were determined by these authors.

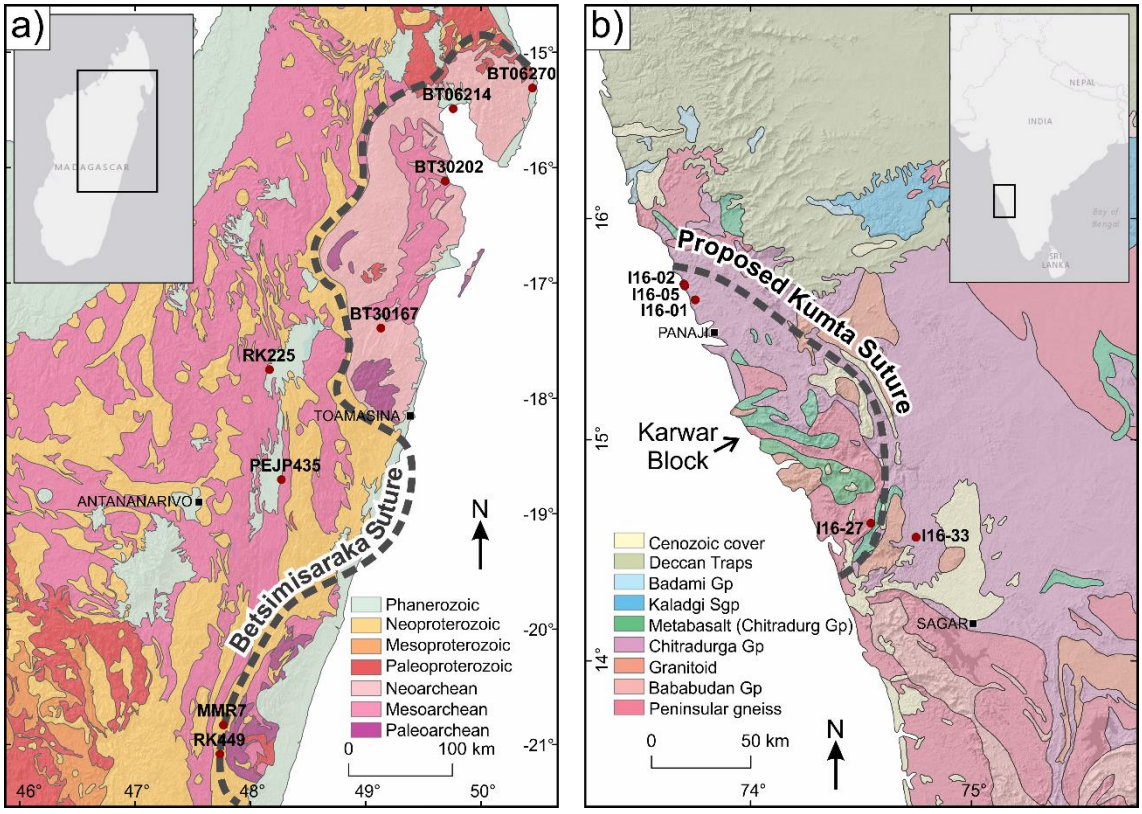

Figure 2.2 a) Geological map of north-east Madagascar overlying shaded relief map. Colours represent rock ages. Betsimisaraka Suture from Collins and Windley (2002). Samples analysed for Lu-Hf in this study shown. Modified from Roig et al. (2012); b) geological map of the Karwar Block of western Peninsular India, polygons derived from Geological Survey of India (1998), overlying shaded relief map. Samples analysed for U-Pb and Lu-Hf shown. Kumta Suture from Ishwar-Kumar et al. (2013).

2. Analytical techniques

2.1. Zircon U-Pb geochronology

Seven rock samples were crushed and the zircon fraction (sieved 79–425 μm) separated using panning and heavy liquids (LST 2.85 ± 0.02 g/mL). Five samples yielded sufficient zircon and were hand-picked and mounted in epoxy resin. The zircon mount was polished; carbon coated and imaged using a Gatan cathodoluminescence (CL) detector attached to Quanta 600 MLA Scanning Electron Microscope to identify suitable domains for analysis. Zircon U-Pb geochronology was undertaken at the University of Adelaide using an Agilent 7700 s ICP-MS with attached ASI M-50 laser ablation system. A spot size of 18 μm and frequency of 5 Hz was used. Isotopes ^{204}Pb, ^{206}Pb, ^{207}Pb, ^{208}Pb, ^{232}U and ^{238}U were measured. GEMOC GJ-1 zircon (TIMS normalising ages $^{207}Pb/^{206}Pb$ = 607.7 ± 4.3 Ma, $^{206}Pb/^{238}U$ = 600.7 ± 1.1 Ma and $^{207}Pb/^{235}U$ = 602.0 ± 1.0 Ma; Jackson et al. (2004)) was used to correct for U-Pb fractionation. The Plešovice zircon standard (ID TIMS $^{206}Pb/^{238}U$ = 337.13 ± 0.37 Ma; Sláma et al. (2008)) was used to assess accuracy over the course of the laser session; a total of 95 Plešovice standard analyses were made and yield a weighted average $^{206}Pb/^{238}U$ age of 338.27 ± 0.87 Ma (2SD, MSWD = 1.5), which is within uncertainty of the ID TIMS age of Sláma et al. (2008). Data were processed using Iolite (Paton et al., 2011).

2.2. Zircon Lu-Hf analysis

Lu-Hf isotope analyses were undertaken on the Thermo-Scientific Neptune Multi-Collector ICP-MS with an attached New Wave UP-193 ArF excimer laser at the University of Adelaide following the methods of Payne et al. (2013). A beam diameter of 50 μm or 35 μm was used depending on grain size. Typical ablation times were ~ 82 s using a 5 Hz repetition rate, a 4 ns pulse rate, and an intensity of ~4.40 J/cm^2. Zircons were ablated in a helium atmosphere that was then mixed with argon upstream of the ablation cell.

Zircon data reduction were carried out using the HfTRAX Excel macro (Payne et al., 2013). Data were normalised to $^{179}Hf/^{177}Hf$ = 0.7325 using an exponential correction for mass bias. The Yb and Lu isobaric interferences on ^{176}Hf were corrected for following the methodology of Woodhead et al. (2004).

Zircon standards were analysed before and during the analysis of unknowns to assess instrument performance and stability. The primary zircon standard Plešovice was used and yielded a mean $^{176}Hf/^{177}Hf$ ratio of 0.282468 ± 0.000022 (2SD). This is within uncertainty of the published value of 0.282482 ± 0.000013 (2SD) by Sláma et al. (2008). Values for $^{176}Hf/^{177}Hf_{CHUR(t)}$ were calculated using modern $^{176}Hf/^{177}Hf$ = 0.282785 (Bouvier et al., 2008), modern $^{176}Lu/^{177}Hf$ = 0.0336 (Bouvier et al., 2008) and ^{176}Lu decay constant of 1.865×10^{-11} year^{-1} (Scherer et al., 2001). Values for the crustal model age (T_{DMC}) were calculated using a ^{176}Lu decay constant of 1.865×10^{-11} year^{-1} (Scherer et al.,

2001), modern $^{176}Hf/^{177}Hf = 0.28325$, modern $^{176}Lu/^{177}Hf = 0.0384$ (Griffin et al., 2000), and a bulk crust value of $^{176}Lu/^{177}Hf = 0.015$ (Griffin et al., 2002). Uncertainties for $\varepsilon_{Hf}(t)$ are calculated as the $^{176}Hf/^{177}Hf_{Sample}$ uncertainty converted to epsilon notation (i.e. $((^{176}Hf/^{177}Hf_{2\sigma})/0.282785) * 10{,}000$) and are reported at the 2σ level.

3. Results

3.1. Sample descriptions

The five metasedimentary samples used for zircon U-Pb and Lu-Hf analysis are described in Table 2.1. A further eight samples from Madagascar were selected for Lu-Hf analysis from zircon mounts previously analysed for U-Pb geochronology as part of a BGS World Bank project (BGS-USGS-GLW, 2008, Schofield et al., 2010) (Table 2.1). Four of these samples (those with prefix BT) are from the Antongil Domain, which is considered to be an extension of the Dharwar Craton (Collins et al., 2003, Tucker et al., 1999). Two samples are located just outside the Masora Domain (MMR7 and RK449), approximately along the boundary between the greater Dharwar Craton and Madagascar – the Betsimisaraka Suture. The other two samples (RK225 and PEJP435) are from the area between the Antongil-Masora domains and the Antananarivo Domain.

Table 2.1 Sample descriptions, location information and maximum depositional ages. Latitudes are given as positive values if North of the equator (India samples), and negative if south of the equator (Madagascar samples).

Sample no.	Lithology	Region	Map unit	Latitude (WGS84)	Longitude (WGS84)	Elevation (m)	Youngest >10% conc. U-Pb analysis (Ma)
I16-01	Weakly metamorphosed, cross-bedded sandstone	Karwar region	Chitradurga Group	15.62926	73.74631	6	2462 ± 30
I16-02	Weakly metamorphosed, medium-grained sandstone	Karwar region	Chitradurga Group	15.70066	73.69494	0	2399 ± 39
I16-05	Fine-grained sandstone	Karwar region	Chitradurga Group	15.69217	73.69846	5	2424 ± 27
I16-27	Quartzite	Karwar region	Peninsular gneiss	14.61870	74.54080	70	3094 ± 40
I16-33	Meta-greywacke	Karwar region	Chitradurga Group	14.55550	74.74486	523	2493 ± 47
BT30167	Coarse-grained, granitic augen gneiss	Antongil Domain	Ambodiriana Group	-17.3802	49.1403	-	N/A
BT30202	Dacitic greenschist	Antongil Domain	Mananara Group	-16.1065	49.6982	-	N/A
BT06214	Granodiorite	Antongil Domain	-	-15.4786	49.7676	-	N/A
BT06270	Potassic granite	Antongil Domain	Masoala Suite	-15.2989	50.3434	-	N/A
RK255	Migmatitic gneiss	Antananarivo Domain	Anaboriana-Manampotsy	-17.7401	48.1746	-	N/A
PEJP435	Charnockitic tonalite	Antananarivo Domain	Mangoro Complex	-18.6938	48.2775	-	N/A
MMR7	Gabbro	Antananarivo Domain	Manampotsy Group	-20.8208	47.7745	-	N/A
RK449	Migmatitic biotite gneiss	Masora Domain	Masora Block	-21.0714	47.7448	-	N/A

3.2. Zircon U-Pb geochronology

Zircon descriptions are provided in Table 2.2 and U-Pb data provided in Appendix 2.1. Data are presented as concordia diagrams ($^{207}Pb/^{235}U$ v. $^{206}Pb/^{238}U$) and kernel density estimate (KDE) plots (Figure 2.3). The KDE plots were produced using the DensityPlotter java application with a bandwidth of 50 Ma. (Vermeesch, 2012).

The maximum depositional ages of samples have been calculated based on the youngest near-concordant (<10%) zircon and are listed in Table 2.1. All reported ages herein are $^{207}Pb/^{206}Pb$ calculated ages with uncertainties reported at the two sigma level. Of our five analysed samples, three have very similar detrital zircon spectra. Samples I16-01, I16-02 and I16-05 have detrital zircon spectra with dominant peaks at c. 3100 Ma and c. 2500 Ma (Figure 2.3). Samples I16-01 and I16-02 also have significant pre-3050 Ma zircon extending back to c. 3500 Ma. Sample I16-27 has only one dominant peak at c. 3100 Ma and sample I16-33 has one dominant peak at c. 2500 Ma.

Table 2.2 Zircon descriptions for analysed samples

Sample	Colour in transmitted light	Size (µm)	Aspect ratio (length:width)	Morphology	CL	Interpretation
I16-01	Pink to dark brown	~80–200	3:2–3:1, average 2:1	Euhedral to subhedral, some with preserved facets and pyramidal terminations, some rounded	Many with concentric oscillatory zoning, some banded or ill-defined zoning. Many with ill-defined cores overgrown by concentric oscillatory zoning parallel to grain margins	All zircons are interpreted as detrital zircons, many sourced locally based on preservation of crystalline grain morphology
I16-02	Translucent pale pink to pale brown, some pale yellow	~60–150	3:2–5:1, average 2:1	Mostly euhedral, many preserved with facets and pyramidal terminations, some rounded		
I16-05	Translucent pale pink to pale brown, some pale yellow	~60–140	3:2–5:1, average 2:1	Mostly euhedral, many preserved with facets and pyramidal terminations, many broken		
I16-27	Translucent colourless to pale brown	~50–190	2:1–4:1, average 3;1	Euhedral to subhedral, many preserved with facets and pyramidal terminations		
I16-33	Translucent pale pink, pale brown and pale yellow	~60–180	3:2–4:1, average 2:1	Euhedral to subhedral, many preserved with facets and pyramidal terminations		

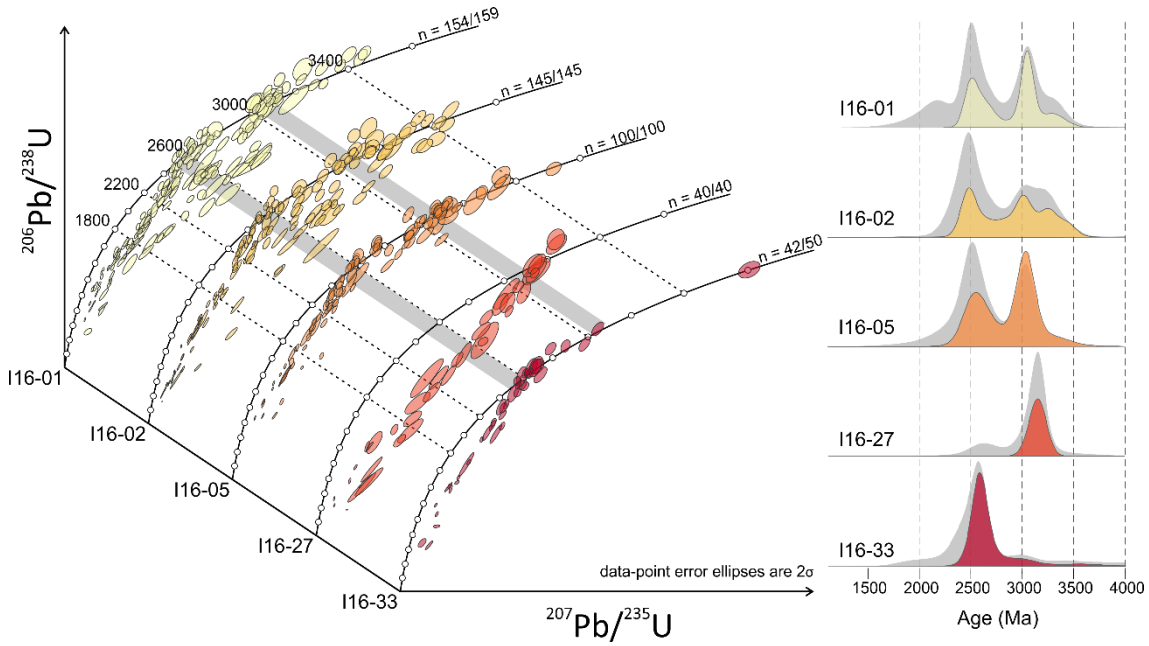

Figure 2.3 Left: Concordia diagrams for analysed samples in this study, constructed using Isoplot 4.15 (Ludwig, 2003). Grey shaded regions highlight the major age peaks in the dataset at c. 2500 Ma and c. 3100 Ma; Right: Kernel Density Estimate plots showing all data (grey) and data that is within 10% of concordance (coloured).

3.3. Multi-dimensional scaling of U-Pb data

To understand the provenance of our analysed zircon grains, it is essential to compare them to other published detrital zircon samples. We have compiled over 7000 published U-Pb zircon analyses (~5000 from detrital samples) from Madagascar and India, many of which have complex age distributions (Archibald et al., 2015; BGS-USGS-GLW, 2008; Collins et al., 2007; Collins et al., 2012; Collins et al., 2003; Collins et al., 2015; Cox et al., 1998; Cox et al., 2004; De Waele et al., 2011; Fitzsimons and Hulscher, 2005; Ishwar-Kumar et al., 2013; Lancaster et al., 2015; Li et al., 2017; Maibam et al., 2016; Maibam et al., 2011; Plavsa et al., 2014; Sarma et al., 2012; Schofield et al., 2010; Tucker et al., 2011a; Tucker et al., 2011b). Traditional techniques of visually comparing age peaks between detrital samples or regions is no longer sufficient when dealing with such large quantities of complexly distributed data.

Multi-dimensional scaling is a statistical technique that has been applied to detrital zircon data as a way of dealing with large quantities of data objectively (Vermeesch, 2013). In much the same way that traditional principal component analysis assesses dissimilarities between compositional data such as geochemistry, multi-dimensional scaling assesses dissimilarities between distributional data – in this case, detrital zircon data (Vermeesch, 2013).

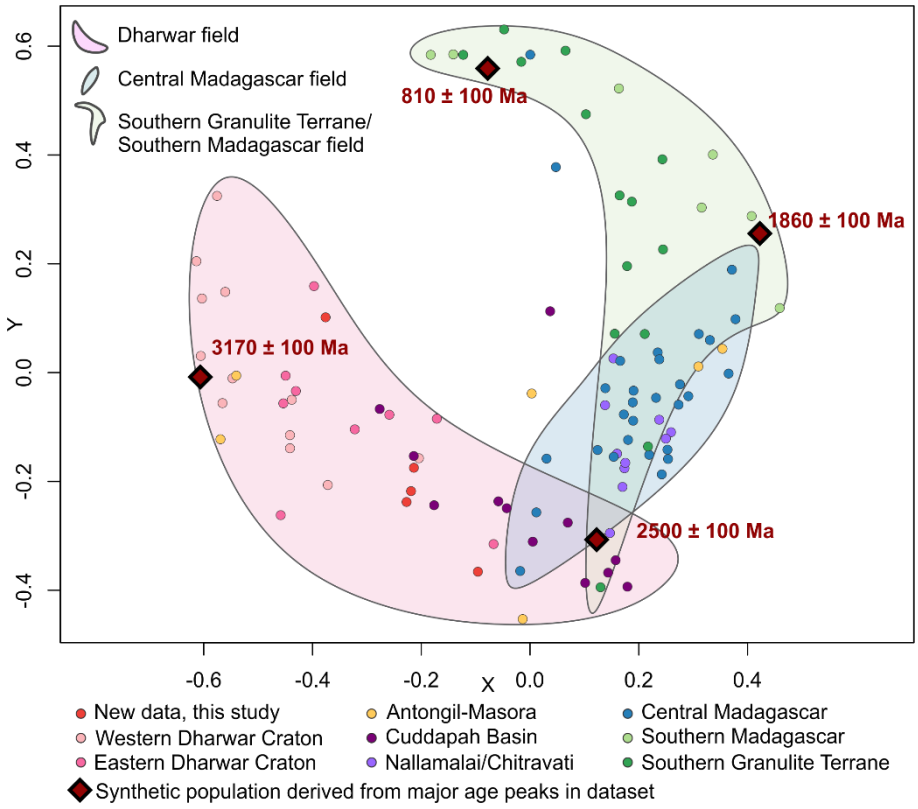

Figure 2.4 Multi-dimensional scaling plot of our new data and published detrital zircon data.

We have used the Provenance package in R (Vermeesch et al., 2016) to produce a multi-dimensional scaling plot for our new data and compiled published data (Figure 2.4). The data were filtered so that only analyses within 10% concordance were used, resulting in ~3000 analyses from 104 samples.

On a multi-dimensional scaling plot points that plot close together have less dissimilar detrital zircon spectra than points that plot further apart (Vermeesch, 2013). Similarly, points that plot further apart have detrital zircon distributions that are more dissimilar.

Multi-dimensional scaling (MDS) plots reveal the complex differences between multiple detrital samples, but it can be difficult to understand the major age peaks within each sample without having to look at the original data separately. To deal with this, we have followed the methodology of Spencer and Kirkland (2016) and added a synthetic dataset to make it easier to visualise the age peaks that are contained within each sample on the MDS plot. To achieve this, we produced a KDE of all the data in this compilation, which yielded significant age peaks at c. 3170 Ma, c. 2500 Ma, c. 1860 Ma and c. 810 Ma. The synthetic datasets were created in Microsoft Excel whereby 1000 random numbers were generated with mean age (either 3170 Ma, 2500 Ma, 1860 Ma or 810 Ma) and standard deviation of 100 Ma, as this best represents the average spread of the data. We herein refer to these synthetic datasets in quotation marks to differentiate them from descriptions of the actual sample data. These synthetic datasets aid in interpreting the

MDS plot as sample points that plot closer to any one of these ages have a more unimodal distribution of that age. In contrast, samples that plot between two synthetic ages have proportions of both of those ages. For example, many samples plot between "2500 Ma" and "1860 Ma", indicating that they contain a significant population of c. 2500 Ma zircons and c. 1860 Ma zircons.

3.3.1. New data, Karwar Block, India

Our new data from the Karwar Block of western peninsular India plot between "3170 Ma" and "2500 Ma" due to contributions from each of these age populations (Figure 2.5a). Sample I16-27 plots closer to "3170 Ma" due to it having dominantly zircons of this age. Sample I16-33 plots closer to "2500 Ma" due to it having dominantly zircons of this age. Compared to the compiled published data, our new data is least dissimilar to samples from the Dharwar Craton, some samples from the Antongil-Masora domains of Madagascar and some samples from the Cuddapah Basin of India. We have produced shaded polygons based on published data from the Dharwar Craton (Figure 2.5b) and central Madagascar (Figure 2.5e) from which we can compare our new data. Both of these polygons are underlain on the plot for easy comparison and our new data overlap with the Dharwar field, and do not overlap with the central Madagascar field.

3.3.2. Dharwar Craton, India

The Dharwar Craton samples generally plot between "3170 Ma" and "2500 Ma" (Figure 2.5b). This indicates that these samples contain varying proportions of c. 3170 Ma and c. 2500 Ma zircons. Some of the samples with prefix WD- plot further away from "3170 Ma" because they contain portions of older (c. 3370 Ma and c. 3240 Ma) zircons that are not represented by the synthetic ages. Broadly speaking there is a correlation between western Dharwar Craton samples plotting closer to "3170 Ma" and eastern Dharwar Craton samples plotting relatively closer to "2500 Ma".

3.3.3. Antongil-Masora domains, Madagascar

Samples from the Antongil-Masora domains of eastern Madagascar contain variable components of c. 3170 Ma, c. 2500 Ma and c. 1860 Ma zircons as is evident from their proximity to these synthetic ages on the plot (Figure 2.5c). Several of these samples are located toward the centre of the plot rather than between the synthetic ages. This is due to some of these samples also containing a component of c. 740 Ma zircons. Many of these samples are geographically located along the margins of the Antongil-Masora domains, which are more likely to contain complex source components. This is reflected in the MDS plot where samples are relatively dispersed compared to other groups. Four of these samples plot within the shaded area for the Dharwar Craton.

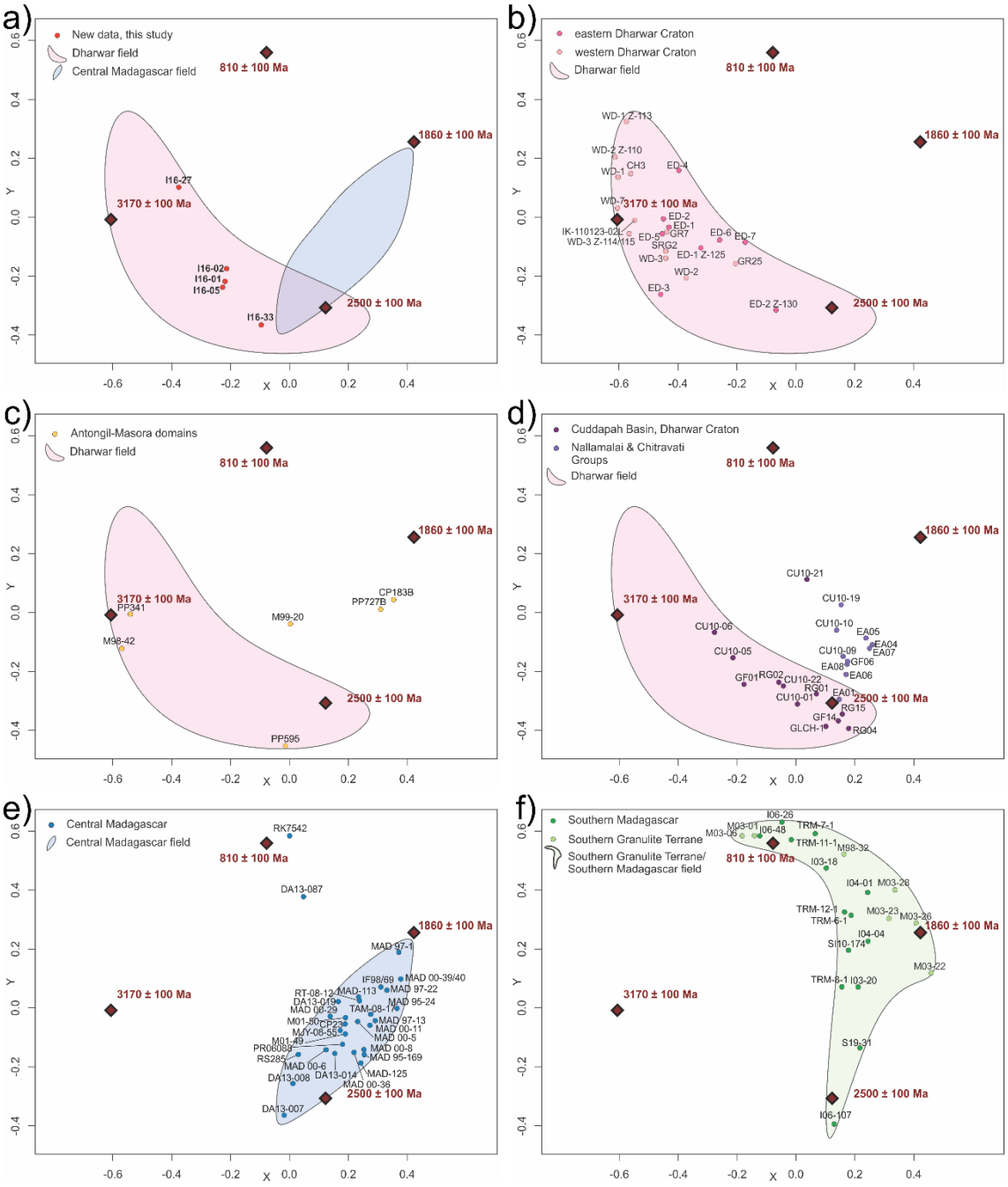

Figure 2.5 Multi-dimensional scaling plot showing only selected data-points from Figure 2.4 for each region. Plots a–d underlain by shaded area based on Dharwar Craton data, plots a and e underlain by shaded area based on central Madagascar data and plot f underlain by shaded area for southern Madagascar and the Southern Granulite Terrane.

3.3.4. Cuddapah Basin, India

We have divided samples from the Cuddapah Basin into two groups—the Cuddapah Basin proper, and the Nallamalai/Chitravati groups. Most of the Cuddapah Basin samples cluster around “2500 Ma” and trend toward “3170 Ma” implying that they have populations of zircons with these ages (Figure 2.5d). All of the Cuddapah Basin samples overlap with the ‘Dharwar trend’ shaded area. Samples from the Nallamalai and Chitravati groups plot between “2500 Ma” and “1860 Ma”, indicating components of both c.

2500 Ma and c. 1860 Ma zircons. The Nallamalai/Chitravati samples were interpreted by Collins et al. (2015) to have formed in a local foreland basin to the eastern Krishna Orogen. For this reason we do not suggest any correlation with central Madagascar, despite some similarities in the trends on the MDS plots.

3.3.5. Central Madagascar

All samples from central Madagascar plot between "2500 Ma" and "1860 Ma" (Figure 2.5e). These samples therefore contain components of c. 2500 Ma and c. 1860 Ma zircons. These samples cluster more closely together compared to other regions, which provides a reliable 'central Madagascar field' from which other samples can be compared.

3.3.6. Southern Granulite Terrane of India and southern Madagascar

Samples from the Southern Granulite Terrane of India and southern Madagascar show very similar trends with a significant spread on the MDS plot (Figure 2.5f). Most samples plot either between "1860 Ma" and "810 Ma" or between "2500 Ma" and "1860 Ma". Some of these samples are unimodal, e.g. I06-48 has only one age peak at c. 810 Ma, M03-26 has one age peak at c. 1860 Ma and I06-107 has one age peak at c. 2500 Ma. In general, the Southern Granulite Terrane samples that plot between "1860 Ma" and "810 Ma" are restricted to the south of the Southern Granulite Terrane and samples that plot between "2500 Ma" and "1860 Ma" are restricted to the north of the terrane.

3.4. Zircon Lu-Hf analysis

Sixty-nine Lu-Hf analyses were collected from five samples from the Karwar Block of India. A further 55 Lu-Hf analyses were carried out on eight samples from the BGS World Bank Project (BGS-USGS-GLW, 2008) from eastern Madagascar. Data are provided in Appendix 2.2. Analyses were obtained by overlapping pre-existing U-Pb analytical spots. We have also compiled published Lu-Hf data from Madagascar and India to compare our results. This compiled database is provided in Appendix 2.3 and includes over 1000 Lu-Hf analyses. $\varepsilon_{Hf}(t)$ values of published data were recalculated using the values listed in our analytical techniques for more accurate comparison (both recalculated values and reported values are provided in Appendix 2.3). Data that plotted above the Depleted Mantle line were excluded from the plots. Plots in Figure 2.6 were made in Matlab R2016b with point density contours calculated using the kde2d Matlab script (Botev et al., 2010).

3.4.1. Lu-Hf signature of the Karwar Block, India

This dataset contains four dominant groups based on their age and $\varepsilon_{Hf}(t)$ signature. A single analysis with U-Pb age of c. 3555 has an $\varepsilon_{Hf}(t)$ value of +3.39 and plots approximately at the Depleted Mantle evolution line. This implies that this zircon was sourced from a juvenile magma that was segregated from the mantle at approximately this time. The seven analyses with U-Pb ages of c. 3350 Ma have $\varepsilon_{Hf}(t)$ values ranging from

–2.11 to +2.15. These values are below the depleted mantle line and cluster around $\varepsilon_{Hf}(t) = 0$. This suggests that the magma from which these zircons grew contained a component of older continental crust. The 20 analyses with U-Pb ages of c. 3100 Ma also have $\varepsilon_{Hf}(t)$ values that cluster around $\varepsilon_{Hf}(t) = 0$, ranging from –3.32 to +1.86. Again, these data suggest that a component of older continental crust was involved in magma generation. The nine analyses with U-Pb ages of c. 2560 Ma have $\varepsilon_{Hf}(t)$ values ranging from –0.41 to +3.92, with an average of +2.44. This group is dominated by zircons from sample I16-33, which does not contain any age equivalent zircons with negative $\varepsilon_{Hf}(t)$ values. These moderately positive values imply that the magma from which these zircons grew contained a component of older continental crust. Twenty-six analyses with U-Pb ages of c. 2540 Ma have a wide range of $\varepsilon_{Hf}(t)$, from –11.67 to –1.00, with an average of –6.67. These data suggest an evolved source of magma that is dominantly reworked older continental crust.

Contours calculated for published data from the Dharwar Craton are underlain on the plot for new data. There is a good correlation between the other published data and our new data, with a few minor variations. The c. 2.5 Ga zircons from the Dharwar compilation show a similar range in $\varepsilon_{Hf}(t)$ to our data. However, the compilation has a higher density of points that are slightly positive whereas our dataset has a higher density of points that are quite negative. Looking more closely at the Dharwar compilation, the western Dharwar Craton, in particular, is very similar to our new data, with its c. 2.5 Ga zircons having dominantly negative $\varepsilon_{Hf}(t)$ values.

3.4.2. Lu-Hf signature of eastern Madagascar

We collected Lu-Hf analyses from eight samples from eastern Madagascar. Five analyses with U-Pb ages of c. 3140 Ma have $\varepsilon_{Hf}(t)$ values ranging from +0.21 to +2.21, with an average of +1.17. Six analyses with U-Pb ages of c. 2680 Ma have moderately positive $\varepsilon_{Hf}(t)$ values ranging from +3.39 to +5.39 with an average of +4.22. These plot very close to the line for new crust and we therefore consider these zircons to be derived from a relatively juvenile magma that was generated at approximately this time. These data overlap the age equivalent contour for the compiled Madagascar dataset very closely. The youngest group in our Madagascar data can be considered in two parts. Twenty-six analyses with U-Pb ages of c. 2520 Ma have $\varepsilon_{Hf}(t)$ values ranging from –5.40 to –2.08 with an average of –4.09. All of these samples are from the Antongil Domain and have similar $\varepsilon_{Hf}(t)$ values to our c. 2540 Ma group from the Karwar Block. Twelve analyses with U-Pb ages of c. 2480 Ma have $\varepsilon_{Hf}(t)$ ranging from –1.48 to +2.11. Of these, six cluster very close together with U-Pb ages of c. 2470 Ma and $\varepsilon_{Hf}(t)$ value of –0.53. The negative $\varepsilon_{Hf}(t)$ values of this group suggest a component of older continental crust was involved in magma generation.

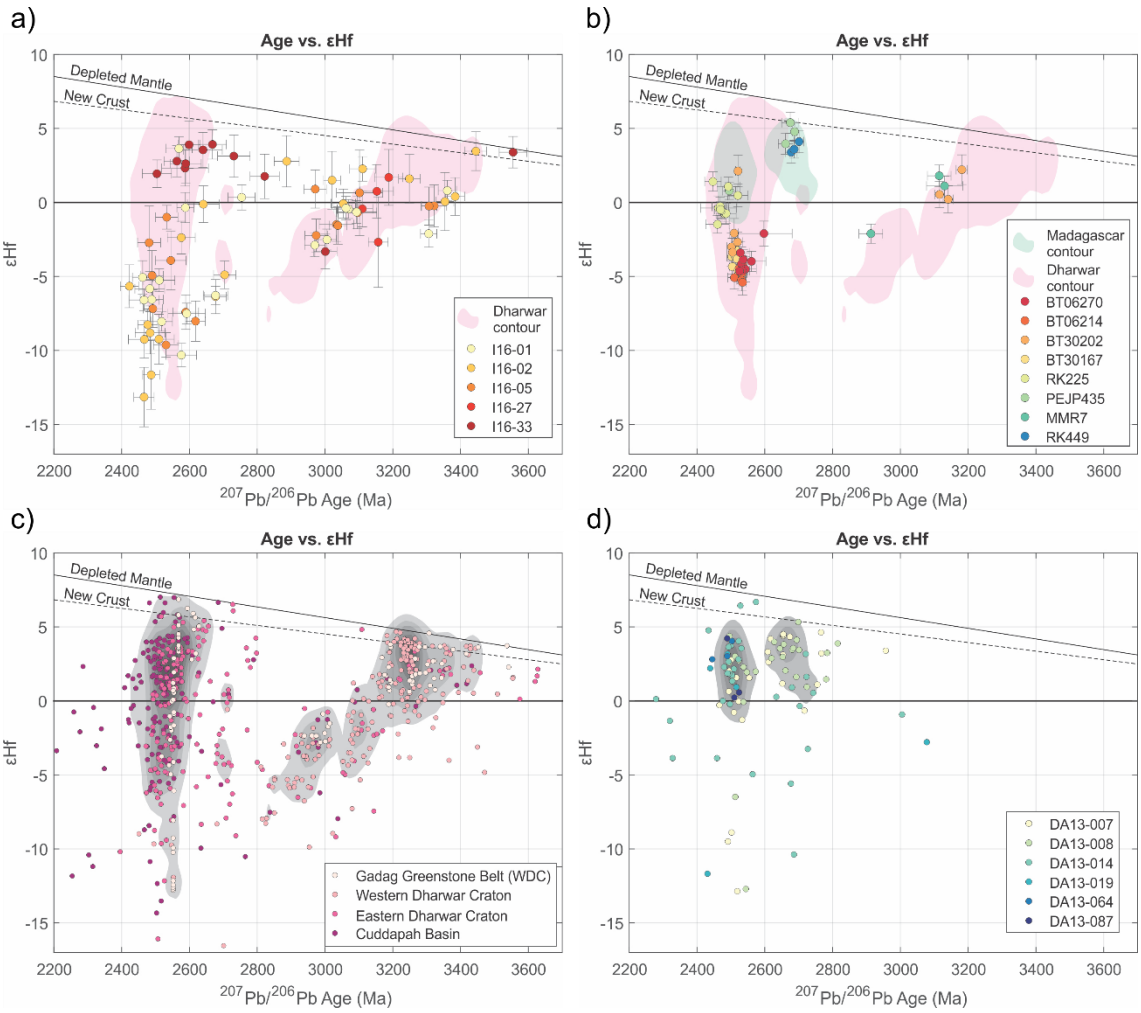

Figure 2.6 Age vs. εHf(t) plots of new and compiled data. (a) New data from the Karwar Block of western peninsular India, shaded contour calculated from data in c; (b) New data from eastern Madagascar, shaded contours calculated from data in c and d; (c) compiled data from India; and (d) compiled data from Madagascar. Contours generated using the kde2d Matlab script (Botev et al., 2010). Depleted Mantle y-intercept calculated using εHf(t) equation with values: modern 176Hf/177HfDM = 0.28325 (Griffin et al., 2000) and modern 176Hf/177HfCHUR = 0.282785 (Bouvier et al., 2008), which produces εHf(t) = 16.44 at time 0 Ma, we have assumed that εHf(t)DM = 0 at 4560 Ma. New Crust line calculated using εHf(t) = 13.2 at time 0 Ma and εHf(t) = 0 at time 4560 Ma (Dhuime et al., 2011).

3.4.3. Lu-Hf signature of compiled data from the Dharwar Craton, India

We have compiled over 700 published Lu-Hf analyses from the Dharwar Craton that we have subdivided into the Gadag Greenstone Belt, western Dharwar Craton, eastern Dharwar Craton and Cuddapah Basin (Figure 2.6c). Compiled data are sourced from: Collins et al. (2015); Glorie et al. (2014); Lancaster et al. (2015); Maibam et al. (2016); Mohan et al. (2014); Praveen et al. (2014); Sarma et al. (2012); Yang and Santosh (2015). The majority of data plot near one of two groups defined by density contours. The first of these groups is characterised by zircons with U-Pb ages of c. 3240 Ma and $\varepsilon_{Hf}(t)$ ranging from approximately –1 to +4. This group is dominated by samples from the Gadag Greenstone Belt and the western Dharwar Craton. These points plot very close to the line

for New Crust, indicating that they are sourced from relatively juvenile magmas. The group of data with U-Pb ages of c. 2550 Ma have a wide range of $\varepsilon_{Hf}(t)$, from –7 to +7, with the highest density of data points clustering around an $\varepsilon_{Hf}(t)$ value of +2. This group is dominated by samples from the Cuddapah Basin and eastern Dharwar Craton. There are data that fall along a general trend from the c. 3240 Ma 'juvenile' group to the c. 2500 Ma 'evolved' group. This trend may represent the evolution of crustal material derived from the older group.

3.4.4. Lu-Hf signature of compiled data from Madagascar

We have compiled over 300 published Lu-Hf analyses from central Madagascar. Compiled data sourced from: Archibald et al. (2016) and Archibald et al. (2015). A large portion of this dataset consists of ages spanning the range c. 900–500 Ma but since we are focusing on Archaean zircons we have restricted the plot to zircons older than c. 2200 Ma (Figure 2.6d). The majority of these data have U-Pb zircon ages spanning c. 2800–2400 Ma and positive $\varepsilon_{Hf}(t)$ values. Based on density contours, these data can be divided into two groups. The older group contains zircons with U-Pb ages of c. 2630 Ma that cluster around a $\varepsilon_{Hf}(t)$ value of +4. These values plot immediately below the line for New Crust, implying that they were sourced from relatively juvenile magmas. The younger group contains zircons with U-Pb ages of c. 2500 Ma and $\varepsilon_{Hf}(t)$ values ranging from –1 to +5. Overall these plot slightly further away from the Depleted Mantle and New Crust lines compared to the first group. There are some data that scatter within the zone for evolved crust, however, no distinct trends are apparent in here.

4. Discussion

4.1. Depositional age constraints and possible sources of the Karwar Block

Samples I16-01, I16-02, I16-05 are all sandstones and have very similar detrital zircon spectra with major density peaks at c. 3100 Ma and c. 2500 Ma. There are also lesser, but significant populations of c. 3260 Ma and c. 2670 Ma zircons within these samples. The similarity in detrital zircon age spectra of these samples is evident from the MDS plot (Figure 2.4; Figure 2.5) where these three samples plot very close together, indicating a low degree of dissimilarity. These three samples also have very similar ranges of $\varepsilon_{Hf}(t)$ values (Figure 2.6). The maximum depositional ages, based on the youngest near-concordant grain, range from c. 2460 Ma to c. 2400 Ma and are within uncertainty of each other.

Sample I16-33 has a major detrital zircon peak at c. 2600 Ma and maximum depositional age of 2493 ± 47 Ma, slightly older than the aforementioned three samples. There is a distinct absence of zircons older than c. 3000 Ma. The $\varepsilon_{Hf}(t)$ values for I16-33 are significantly more juvenile than samples I16-01, I16-02 and I16-05. Together these

factors indicate that sample I16-33 derived its source material from rocks that were slightly older and more juvenile compared to the previous three samples.

Sample I16-27 has a maximum depositional age of 3094 ± 30 Ma and is dominated by c. 3100 Ma zircons with an absence of zircons younger than c. 3000 Ma. This sample has comparable $\varepsilon_{Hf}(t)$ values to zircons of the same age from the other samples.

The majority of zircons in all samples preserve euhedral to subhedral grain morphologies, indicating that zircons were likely deposited relatively close to their source rocks. The differing proportion of c. 3100 Ma and c. 2500 Ma in these samples reflects local variation in the availability of source material of those ages.

The Archaean sedimentary successions of the western Dharwar Craton were interpreted to be deposited in a foreland basin to an accretionary arc complex to the east (Chadwick et al., 2000). Tucker et al. (2011a) suggested that central Madagascar and the Dharwar Craton were contiguous in the Neoarchaean; permitting that zircons from the new samples analysed in our study could potentially have been sourced from Madagascar. Ishwar-Kumar et al., 2013 suggested that central Madagascar and the Karwar Block were not only contiguous at this time, but actually represent the same geological terrane. However, the relatively juvenile $\varepsilon_{Hf}(t)$ of Neoarchaean zircons in central Madagascar contrast with the wide range of $\varepsilon_{Hf}(t)$ for Neoarchaean zircons in our new samples. Therefore, an appropriate source of Neoarchaean zircons with an evolved $\varepsilon_{Hf}(t)$ signature has not yet been identified in central Madagascar.

Ishwar-Kumar et al. (2013) suggested that the Karwar Block was separate from the Dharwar Craton until the Mesoproterozoic Kumta Suture amalgamated these regions. This contrasts with other models (e.g. Collins and Windley, 2002, Tucker et al., 2011a) where the Karwar Block is not identified as a separate terrane. The western and eastern Dharwar Craton are therefore possible source terranes for zircons in these new samples. Zircon age populations of c. 3100 Ma and c. 2500 Ma are widespread throughout the western Dharwar Craton (Bhaskar-Rao et al., 1991; Friend and Nutman, 1991; Lancaster et al., 2015; Maibam et al., 2016; Maibam et al., 2011; Sarma et al., 2012; Taylor et al., 1984). The c. 2600–2500 Ma Quepem, Dudhsagar and Londa granitoids in the Goa schist belt (Dhoundial et al., 1987, Rekha et al., 2013) likely represent the Neoarchaean source component of our samples. The c. 3200–3000 Ma Peninsular gneisses from the Dharwar Craton and c. 3300–3000 Ma granitoids from the Karwar Block (Ishwar-Kumar et al., 2013, Taylor et al., 1984) are likely representative of the source for the Mesoarchean component of our samples. The strong correlation between our new $\varepsilon_{Hf}(t)$ data and $\varepsilon_{Hf}(t)$ data from the western Dharwar Craton (Figure 2.6) further support this interpretation. This interpretation requires that the Karwar Block and the Dharwar Craton were contiguous at the time of deposition, interpreted here to be c. 2400 Ma.

4.2. The Karwar Block of the western Dharwar Craton

There is no recognisable difference in the age of detrital, magmatic or metamorphic rocks across the Karwar Block and the broader western Dharwar Craton. The Karwar Block contains granodiorites with reported ages of c. 3170 Ma (Ishwar-Kumar et al., 2013) comparable to granitoids elsewhere in the Dharwar Craton (e.g. Taylor et al., 1984, Bhaskar-Rao et al., 1991, Jayananda et al., 2013). Monazite dating constrains metamorphism in the Karwar Block to two phases; one at c. 3200–3100 Ma and one at c. 2600–2400 Ma (Rekha et al., 2013). This is comparable to monazite ages in the central and eastern Dharwar Craton, with two major metamorphic events recognised at c. 3200–3000 Ma and c. 2600–2400 Ma (Jayananda et al., 2013). Several schist belts and granitoids in the Karwar Block were correlated to those in the western Dharwar Craton based on published geochronological and lithological data (Dhoundial et al., 1987, Rekha et al., 2013). These published data together with new data in this study from the Karwar Block are indistinguishable from the available geochronological data from both detrital and magmatic suites in the western Dharwar Craton where populations of c. 3170 Ma and c. 2500 Ma are widespread (Lancaster et al., 2015, Maibam et al., 2016, Maibam et al., 2011, Sarma et al., 2012). The Karwar Block is therefore isotopically and lithologically indistinguishable from the western Dharwar Craton. Therefore, if the "Kumta Suture" exists, it does not separate terranes of differing origin, and we instead interpret that the Karwar Block and western Dharwar Craton have the same origin.

4.3. Correlating terranes of India and Madagascar

Several attempts have been made to correlate the geology of western peninsular India with eastern Madagascar (Collins et al., 2003, Ishwar-Kumar et al., 2013, Rekha et al., 2013, Tucker et al., 2011a). Most agree that the Antongil-Masora domains of eastern Madagascar—that contain rocks dated at c. 3100 Ma and c. 2500 Ma—were once continuous with the Dharwar Craton of India, including the Karwar Block (Collins et al., 2003, Rekha et al., 2013, Tucker et al., 2011a). The exception is a model proposed by Ishwar-Kumar et al. (2013) that correlates the Antananarivo Domain of central Madagascar with the Karwar Block of India, while supporting previous models where the Antongil-Masora domains correlate with the Dharwar Craton.

Our data support a correlation between the Antongil-Masora domains of eastern Madagascar and the western Dharwar Craton of India, including the Karwar Block. This is based on the presence of rocks with major zircon populations of c. 3100 Ma and c. 2500 Ma in both regions, which is reflected in the correlation of samples in the MDS plots (Figure 2.4). This is in contrast to the central domains of Madagascar where zircons older than c. 2700 Ma are rare. This is also evident from the MDS plots where our data from the Karwar Block do not overlap with data from central Madagascar (Figure 2.4). Further supporting this interpretation, the $\varepsilon_{Hf}(t)$ values of our samples from the Antongil-Masora domains overlap with the range of values from our Karwar samples and those from the

western Dharwar Craton. The dataset comprising the Antongil-Masora domains, Karwar Block and western Dharwar Craton is dominated by c. 3250 Ma zircons with juvenile $\varepsilon_{Hf}(t)$ signatures, which trend toward an evolved signature at c. 2500 Ma. The c. 2500 Ma component of this dataset have dominantly evolved $\varepsilon_{Hf}(t)$ signatures (below CHUR) with some data ranging to moderately juvenile, suggesting an input of juvenile magma to a relatively evolved terrane at that time. We therefore consider that the Antongil-Masora domains and the western Dharwar Craton (including the Karwar Block) were contiguous since the Archaean. These characteristics contrast with data from central Madagascar, which is dominated by zircons <c. 2800 Ma with comparatively juvenile $\varepsilon_{Hf}(t)$ signatures.

Ishwar-Kumar et al. (2013) proposed that the Karwar Block of India is analogous to the Antananarivo Domain of central Madagascar. As we have described above, there are several stark differences in the reported geology and isotope geochemistry of these terranes, and this model is therefore unsupported by available data.

4.4. Amalgamation of India and Madagascar

Our interpretation involving a correlation between the Antongil-Masora domains and western Dharwar Craton is consistent with several existing models for this region (Collins et al., 2003, Tucker et al., 2011a). However, constraining the timing of Madagascar-India collision remains contentious. Broadly speaking, there are two end-member models that have been proposed for the amalgamation of Madagascar and India, both involving a suture in approximately the same location, the "Betsimisaraka Suture". The model of Collins and Windley (2002) involves a Neoproterozoic suture that saw the closure of the Mozambique Ocean and collision between India (including the Antongil-Masora domains) and central Madagascar. Tucker et al. (2011a), contrarily proposed that the amalgamation of these regions took place in the Neoarchaean and that they formed part of the same continent—the "Greater Dharwar Craton"—from the Archaean until the breakup of Gondwana.

Although there are limited $\varepsilon_{Hf}(t)$ data from Madagascar, the available information shows distinct trends. Our c. 2700–2400 Ma data from Madagascar show a clear division between an evolved $\varepsilon_{Hf}(t)$ signature (Antongil-Masora domains) and moderately juvenile (central Madagascar). The central Madagascar component of these data overlap significantly with other $\varepsilon_{Hf}(t)$ data from Madagascar (Archibald et al., 2015, Archibald et al., 2016). These data from central Madagascar contrast with data from the Dharwar Craton and the Antongil-Masora domains where $\varepsilon_{Hf}(t)$ values show a spread to more evolved signatures. Archibald et al. (2015) demonstrate that c. 2500 Ma detrital zircons in the Ambatolampy Group (maximum depositional age c. 1836 Ma) preserve dominantly juvenile $\varepsilon_{Hf}(t)$ values, suggesting a lack of sedimentary connection to an ancient terrane (i.e. the Antongil-Masora and western Dharwar Craton) at the time of deposition. This suggests that the Antananarivo Domain was palaeogeographically isolated from the

western Dharwar Craton during the Proterozoic, supporting the 'Azania' model of Collins and Pisarevsky (2005).

5. Summary and conclusions

We have collected new detrital zircon U-Pb and Lu-Hf data from the Karwar Block of western peninsular India, and compared it with published data from Madagascar and India to constrain the tectonic evolution of these regions. We have additionally obtained Lu-Hf analyses of zircons from central Madagascar and the Antongil-Masora domains of eastern Madagascar. We summarise the key findings of this study below:

- Metasedimentary rocks in the Karwar Block have maximum depositional ages of c. 2400 Ma with significant populations of c. 3100 Ma and c. 2500 Ma zircons. These correlate well with published data from the Dharwar Craton, particularly the western Dharwar Craton.
- The c. 3100 Ma detrital zircons from the Karwar Block have relatively juvenile $\varepsilon_{Hf}(t)$ signatures and the c. 2500 Ma zircons have wide-ranging $\varepsilon_{Hf}(t)$ values. These $\varepsilon_{Hf}(t)$ values correlate well with $\varepsilon_{Hf}(t)$ values from the Dharwar Craton, with particularly good fit to the western Dharwar Craton.
- Multi-dimensional scaling of detrital zircon data from various terranes in Madagascar and India, together with $\varepsilon_{Hf}(t)$ data, indicate that the Karwar Block correlates with the western Dharwar Craton, and is not a component of the Antananarivo Domain of central Madagascar as was suggested in Ishwar-Kumar et al. (2013). Our interpretation is consistent with the correlations determined by Dhoundial et al., 1987, Rekha et al., 2013.
- The correlation between the Karwar Block and the Dharwar Craton, and the connectedness of these regions during the Neoarchaean interpreted in this study, suggests that if the Kumta Suture does exist, it does not separate provinces of different origin.
- The available $\varepsilon_{Hf}(t)$ data from Madagascar is distinctly different from the Dharwar Craton. Data from metasedimentary rocks in Madagascar deposited during the Palaeoproterozoic do not contain a significant component of 'Dharwar' zircons (i.e. those trending between juvenile c. 3100 Ma and evolved c. 2500 Ma).
- We therefore suggest that Madagascar was palaeogeographically isolated from India during the Paleoproterozoic, which supports the model of Collins and Pisarevsky (2005). Further $\varepsilon_{Hf}(t)$ data from the Antananarivo Domain and Antongil-Masora domains, from both magmatic and detrital samples, are needed to strengthen this interpretation.

References

Archibald, D.B., Collins, A.S., Foden, J.D., Payne, J.L., Holden, P., Razakamanana, T., De Waele, B., Thomas, R.J. and Pitfield, P.E.J., 2016. Genesis of the Tonian Imorona–Itsindro magmatic Suite in central Madagascar: Insights from U–Pb, oxygen and hafnium isotopes in zircon. Precambrian Research, 281: 312-337.

Archibald, D.B., Collins, A.S., Foden, J.D., Payne, J.L., Taylor, R., Holden, P., Razakamanana, T. and Clark, C., 2015. Towards unravelling the Mozambique Ocean conundrum using a triumvirate of zircon isotopic proxies on the Ambatolampy Group, central Madagascar. Tectonophysics, 662: 167-182.

Archibald, D.B., Collins, A.S., Foden, J.D. and Razakamanana, T., 2017. Tonian Arc Magmatism in Central Madagascar: The Petrogenesis of the Imorona-Itsindro Suite. The Journal of Geology, 125(3): 000-000.

BGS-USGS-GLW, 2008. Republique de Madagascar Ministère de L'engergie et des Mines (MEM/SG/DG/UCP/PGRM). British Geological Survey Research Report.

Bhaskar-Rao, Y., Naha, K., Srinivasan, R. and Gopalan, K., 1991. Geology, geochemistry and geochronology of the Archaean Peninsular gneiss around Gorur, Hassan district, Karnataka, India. Proceedings of the Indian Academy of Sciences-Earth and Planetary Sciences, 100(4): 399-412.

Boger, S.D., Hirdes, W., Ferreira, C.A.M., Jenett, T., Dallwig, R. and Fanning, C.M., 2015. The 580–520Ma Gondwana suture of Madagascar and its continuation into Antarctica and Africa. Gondwana Research, 28(3): 1048-1060.

Boger, S.D., Hirdes, W., Ferreira, C.A.M., Schulte, B., Jenett, T. and Fanning, C.M., 2014. From passive margin to volcano–sedimentary forearc: The Tonian to Cryogenian evolution of the Anosyen Domain of southeastern Madagascar. Precambrian Research, 247: 159-186.

Botev, Z.I., Grotowski, J.F. and Kroese, D.P., 2010. Kernel density estimation via diffusion. The Annals of Statistics, 38(5): 2916-2957.

Bouvier, A., Vervoort, J.D. and Patchett, P.J., 2008. The Lu–Hf and Sm–Nd isotopic composition of CHUR: constraints from unequilibrated chondrites and implications for the bulk composition of terrestrial planets. Earth and Planetary Science Letters, 273(1): 48-57.

Chadwick, B., Vasudev, V. and Hegde, G., 2000. The Dharwar craton, southern India, interpreted as the result of Late Archaean oblique convergence. Precambrian Research, 99(1): 91-111.

Collins, A.S., Clark, C., Sajeev, K., Santosh, M., Kelsey, D.E. and Hand, M., 2007. Passage through India: the Mozambique Ocean suture, high-pressure granulites and the Palghat-Cauvery shear zone system. Terra Nova, 19(2): 141-147.

Collins, A.S., Kinny, P.D. and Razakamanana, T., 2012. Depositional age, provenance and metamorphic age of metasedimentary rocks from southern Madagascar. Gondwana Research, 21(2-3): 353-361.

Collins, A.S., Kröner, A., Fitzsimons, I.C.W. and Razakamanana, T., 2003. Detrital footprint of the Mozambique ocean: U–Pb SHRIMP and Pb evaporation zircon geochronology of metasedimentary gneisses in eastern Madagascar. Tectonophysics, 375(1-4): 77-99.

Collins, A.S., Patranabis-Deb, S., Alexander, E., Bertram, C.N., Falster, G.M., Gore, R.J., Mackintosh, J., Dhang, P.C., Saha, D. and Payne, J.L., 2015. Detrital mineral age, radiogenic isotopic stratigraphy and tectonic significance of the Cuddapah Basin, India. Gondwana Research, 28(4): 1294-1309.

Collins, A.S. and Pisarevsky, S.A., 2005. Amalgamating eastern Gondwana: The evolution of the Circum-Indian Orogens. Earth-Science Reviews, 71(3-4): 229-270.

Collins, A.S. and Windley, B.F., 2002. The tectonic evolution of central and northern Madagascar and its place in the final assembly of Gondwana. The Journal of geology, 110(3): 325-339.

Cox, R., Armstrong, R.A. and Ashwal, L.D., 1998. Sedimentology, geochronology and provenance of the Proterozoic Itremo Group, central Madagascar, and implications for pre-Gondwana palaeogeography. Journal of the Geological Society, 155(6): 1009-1024.

Cox, R., Coleman, D.S., Chokel, C.B., DeOreo, S.B., Wooden, J.L., Collins, A.S., De Waele, B. and Kröner, A., 2004. Proterozoic Tectonostratigraphy and Paleogeography of Central Madagascar Derived from Detrital Zircon U-Pb Age Populations. The Journal of geology, 112(4): 379-399.

De Waele, B., Thomas, R.J., Macey, P.H., Horstwood, M.S.A., Tucker, R.D., Pitfield, P.E.J., Schofield, D.I., Goodenough, K.M., Bauer, W., Key, R.M., Potter, C.J., Armstrong, R.A., Miller, J.A., Randriamananjara, T., Ralison, V., Rafahatelo, J.M., Rabarimanana, M. and Bejoma, M., 2011. Provenance and tectonic significance of the Palaeoproterozoic metasedimentary successions of central and northern Madagascar. Precambrian Research, 189(1-2): 18-42.

Dhoundial, D., Paul, D., Sarkar, A., Trivedi, J., Gopalan, K. and Potts, P., 1987. Geochronology and geochemistry of Precambrian granitic rocks of Goa, SW India. Precambrian Research, 36(3): 287-302.

Dhuime, B., Hawkesworth, C. and Cawood, P., 2011. When continents formed. Science, 331(6014): 154-155.

Fitzsimons, I.C.W. and Hulscher, B., 2005. Out of Africa: detrital zircon provenance of central Madagascar and Neoproterozoic terrane transfer across the Mozambique Ocean. Terra Nova, 17(3): 224-235.

Friend, C. and Nutman, A., 1991. SHRIMP U-Pb geochronology of the Closepet granite and Peninsular gneiss, Karnataka, South India. Geological Society of India, 38(4): 357-368.

Fritz, H., Abdelsalam, M., Ali, K.A., Bingen, B., Collins, A.S., Fowler, A.R., Ghebreab, W., Hauzenberger, C.A., Johnson, P.R., Kusky, T.M., Macey, P., Muhongo, S., Stern, R.J. and Viola, G., 2013. Orogen styles in the East African Orogen: A review of the Neoproterozoic to Cambrian tectonic evolution. Journal of African Earth Sciences, 86: 65-106.

Geological Survey of India, 1998. Geological map of India. Geological Survey of India.

Glorie, S., De Grave, J., Singh, T., Payne, J.L. and Collins, A.S., 2014. Crustal root of the Eastern Dharwar Craton: Zircon U–Pb age and Lu–Hf isotopic evolution of the East Salem Block, southeast India. Precambrian Research, 249: 229-246.

Griffin, W., Pearson, N., Belousova, E., Jackson, S., Van Achterbergh, E., O'Reilly, S.Y. and Shee, S., 2000. The Hf isotope composition of cratonic mantle: LAM-MC-ICPMS analysis of zircon megacrysts in kimberlites. Geochimica et Cosmochimica Acta, 64(1): 133-147.

Griffin, W., Wang, X., Jackson, S., Pearson, N., O'Reilly, S.Y., Xu, X. and Zhou, X., 2002. Zircon chemistry and magma mixing, SE China: in-situ analysis of Hf isotopes, Tonglu and Pingtan igneous complexes. Lithos, 61(3): 237-269.

Ishwar-Kumar, C., Santosh, M., Wilde, S., Tsunogae, T., Itaya, T., Windley, B. and Sajeev, K., 2016. Mesoproterozoic suturing of Archean crustal blocks in western peninsular India: implications for India–Madagascar correlations. Lithos, 263: 143-160.

Ishwar-Kumar, C., Windley, B., Horie, K., Kato, T., Hokada, T., Itaya, T., Yagi, K., Gouzu, C. and Sajeev, K., 2013. A Rodinian suture in western India: New insights on India-Madagascar correlations. Precambrian Research, 236: 227-251.

Jackson, S.E., Pearson, N.J., Griffin, W.L. and Belousova, E.A., 2004. The application of laser ablation-inductively coupled plasma-mass spectrometry to in situ U–Pb zircon geochronology. Chemical Geology, 211(1): 47-69.

Jayananda, M., Banerjee, M., Pant, N., Dasgupta, S., Kano, T., Mahesha, N. and Mahabaleswar, B., 2012. 2.62 Ga high-temperature metamorphism in the central part of the Eastern Dharwar Craton: implications for late Archaean tectonothermal history. Geological Journal, 47(2-3): 213-236.

Jayananda, M., Tsutsumi, Y., Miyazaki, T., Gireesh, R., Kapfo, K.-U., Hidaka, H. and Kano, T., 2013. Geochronological constraints on Meso-and Neoarchean regional metamorphism and magmatism in the Dharwar craton, southern India. Journal of Asian Earth Sciences, 78: 18-38.

Johnson, P.R., Andresen, A., Collins, A.S., Fowler, A.R., Fritz, H., Ghebreab, W., Kusky, T. and Stern, R.J., 2011. Late Cryogenian–Ediacaran history of the Arabian–Nubian Shield: A review of depositional, plutonic, structural, and tectonic events in the closing stages of the northern East African Orogen. Journal of African Earth Sciences, 61(3): 167-232.

Kröner, A., Hegner, E., Collins, A.S., Windley, B.F., Brewer, T.S., Razakamanana, T. and Pidgeon, R.T., 2000. Age and magmatic history of the Antananarivo Block, central Madagascar, as derived from zircon geochronology and Nd isotopic systematics. American Journal of Science, 300(4): 251-288.

Lancaster, P.J., Dey, S., Storey, C.D., Mitra, A. and Bhunia, R.K., 2015. Contrasting crustal evolution processes in the Dharwar craton: insights from detrital zircon U–Pb and Hf isotopes. Gondwana Research, 28(4): 1361-1372.

Li, S.-S., Santosh, M., Indu, G., Shaji, E. and Tsunogae, T., 2017. Detrital zircon geochronology of quartzites from the southern Madurai Block, India: Implications for Gondwana reconstruction. Geoscience Frontiers, 8(4): 851-867.

Ludwig, K.R., 2003. User's manual for Isoplot 3.00: a geochronological toolkit for Microsoft Excel. Kenneth R. Ludwig.

Maibam, B., Gerdes, A. and Goswami, J., 2016. U–Pb and Hf isotope records in detrital and magmatic zircon from eastern and western Dharwar craton, southern India: Evidence for coeval Archaean crustal evolution. Precambrian Research, 275: 496-512.

Maibam, B., Goswami, J. and Srinivasan, R., 2011. Pb–Pb zircon ages of Archaean metasediments and gneisses from the Dharwar craton, southern India: implications for the antiquity of the eastern Dharwar craton. Journal of earth system science, 120(4): 643-661.

Merdith, A.S., Collins, A.S., Williams, S.E., Pisarevsky, S., Foden, J.D., Archibald, D.B., Blades, M.L., Alessio, B.L., Armistead, S. and Plavsa, D., 2017. A full-plate global reconstruction of the Neoproterozoic. Gondwana Research, 50: 84-134.

Mohan, M.R., Sarma, D.S., McNaughton, N.J., Fletcher, I.R., Wilde, S.A., Siddiqui, M.A., Rasmussen, B., Krapez, B., Gregory, C.J. and Kamo, S.L., 2014. SHRIMP zircon and titanite U-Pb ages, Lu-Hf isotope signatures and geochemical constraints for~ 2.56 Ga granitic magmatism in Western Dharwar Craton, Southern India: Evidence for short-lived Neoarchean episodic crustal growth? Precambrian Research, 243: 197-220.

Paton, C., Hellstrom, J., Paul, B., Woodhead, J. and Hergt, J., 2011. Iolite: Freeware for the visualisation and processing of mass spectrometric data. Journal of Analytical Atomic Spectrometry, 26(12): 2508-2518.

Payne, J.L., Pearson, N.J., Grant, K.J. and Halverson, G.P., 2013. Reassessment of relative oxide formation rates and molecular interferences on in situ lutetium–hafnium analysis with laser ablation MC-ICP-MS. Journal of Analytical Atomic Spectrometry, 28(7): 1068-1079.

Plavsa, D., Collins, A.S., Payne, J.L., Foden, J.D., Clark, C. and Santosh, M., 2014. Detrital zircons in basement metasedimentary protoliths unveil the origins of southern India. Geological Society of America Bulletin, 126(5-6): 791-811.

Praveen, M., Santosh, M., Yang, Q., Zhang, Z., Huang, H., Singanenjam, S. and Sajinkumar, K., 2014. Zircon U–Pb geochronology and Hf isotope of felsic volcanics from Attappadi, southern India: implications for Neoarchean convergent margin tectonics. Gondwana Research, 26(3): 907-924.

Rekha, S., Bhattacharya, A. and Chatterjee, N., 2014. Tectonic restoration of the Precambrian crystalline rocks along the west coast of India: Correlation with eastern Madagascar in East Gondwana. Precambrian Research, 252: 191-208.

Rekha, S., Viswanath, T., Bhattacharya, A. and Prabhakar, N., 2013. Meso/Neoarchean crustal domains along the north Konkan coast, western India: the Western Dharwar Craton and the Antongil-Masora Block (NE Madagascar) connection. Precambrian Research, 233: 316-336.

Roig, J., Tucker, R., Delor, C., Peters, S. and Théveniaut, H., 2012. Carte géologique de la République de Madagascar à 1/1 000 000. Ministère des Mines, PGRM, Antananarivo, République de Madagascar, 1.

Sarma, D.S., McNaughton, N.J., Belusova, E., Ram Mohan, M. and Fletcher, I.R., 2012. Detrital zircon U–Pb ages and Hf-isotope systematics from the Gadag Greenstone Belt: Archean crustal growth in the western Dharwar Craton, India. Gondwana Research, 22(3-4): 843-854.

Scherer, E., Münker, C. and Mezger, K., 2001. Calibration of the lutetium-hafnium clock. Science, 293(5530): 683-687.

Schofield, D.I., Thomas, R.J., Goodenough, K.M., De Waele, B., Pitfield, P.E.J., Key, R.M., Bauer, W., Walsh, G.J., Lidke, D.J. and Ralison, A.V., 2010. Geological evolution of the Antongil Craton, NE Madagascar. Precambrian Research, 182(3): 187-203.

Sláma, J., Košler, J., Condon, D.J., Crowley, J.L., Gerdes, A., Hanchar, J.M., Horstwood, M.S., Morris, G.A., Nasdala, L. and Norberg, N., 2008. Plešovice zircon—a new natural reference material for U–Pb and Hf isotopic microanalysis. Chemical Geology, 249(1): 1-35.

Spencer, C.J. and Kirkland, C.L., 2016. Visualizing the sedimentary response through the orogenic cycle: A multidimensional scaling approach. Lithosphere, 8(1): 29-37.

Stern, R.J., 1994. Arc-assembly and continental collision in the Neoproterozoic African orogen: implications for the consolidation of Gondwanaland. Annual Review of Earth and Planetary Sciences, 22: 319-351.

Taylor, P., Chadwick, B., Moorbath, S., Ramakrishnan, M. and Viswanatha, M., 1984. Petrography, chemistry and isotopic ages of Peninsular Gneiss, Dharwar acid volcanic rocks and the Chitradurga Granite with special reference to the late Archean evolution of the Karnataka Craton, southern India. Precambrian Research, 23(3-4): 349-375.

Tucker, R., Ashwal, L., Handke, M., Hamilton, M., Le Grange, M. and Rambeloson, R., 1999. U-Pb geochronology and isotope geochemistry of the Archean and Proterozoic rocks of north-central Madagascar. The Journal of Geology, 107(2): 135-153.

Tucker, R., Roig, J.-Y., Delor, C., Amelin, Y., Goncalves, P., Rabarimanana, M., Ralison, A. and Belcher, R., 2011a. Neoproterozoic extension in the Greater Dharwar Craton: a reevaluation of the "Betsimisaraka suture" in Madagascar. Canadian Journal of Earth Sciences, 48(2): 389-417.

Tucker, R.D., Roig, J.Y., Macey, P.H., Delor, C., Amelin, Y., Armstrong, R.A., Rabarimanana, M.H. and Ralison, A.V., 2011b. A new geological framework for south-central Madagascar, and its relevance to the "out-of-Africa" hypothesis. Precambrian Research, 185(3-4): 109-130.

Tucker, R.D., Roig, J.Y., Moine, B., Delor, C. and Peters, S.G., 2014. A geological synthesis of the Precambrian shield in Madagascar. Journal of African Earth Sciences, 94: 9-30.

Vermeesch, P., 2012. On the visualisation of detrital age distributions. Chemical Geology, 312: 190-194.

Vermeesch, P., 2013. Multi-sample comparison of detrital age distributions. Chemical Geology, 341: 140-146.

Vermeesch, P., Resentini, A. and Garzanti, E., 2016. An R package for statistical provenance analysis. Sedimentary Geology.

Woodhead, J., Hergt, J., Shelley, M., Eggins, S. and Kemp, R., 2004. Zircon Hf-isotope analysis with an excimer laser, depth profiling, ablation of complex geometries, and concomitant age estimation. Chemical Geology, 209(1–2): 121-135.

Yang, Q.-Y. and Santosh, M., 2015. Zircon U–Pb geochronology and Lu–Hf isotopes from the Kolar greenstone belt, Dharwar Craton, India: Implications for crustal evolution in an ocean-trench-continent transect. Journal of Asian Earth Sciences, 113: 797-811.

Yang, X.-A., Chen, Y.-C., Liu, S.-B., Hou, K.-J., Chen, Z.-Y. and Liu, J.-J., 2014. U–Pb zircon geochronology and geochemistry of Neoproterozoic granitoids of the Maevatanana area, Madagascar: implications for Neoproterozoic crustal extension of the Imorona–Itsindro Suite and subsequent lithospheric subduction. International Geology Review, 57(11-12): 1633-1649.

3

Evolving marginal terranes during Neoproterozoic supercontinent reorganisation: constraints from the Bemarivo Domain in northern Madagascar

Published as:

Armistead, S.E., Collins, A.S., Merdith, A.S., Payne, J.L., Cox, G.M., Foden, J.D., Razakamanana, T., and De Waele, B., 2019. Evolving marginal terranes during Neoproterozoic supercontinent reorganisation: constraints from the Bemarivo Domain in northern Madagascar. *Tectonics*.

Available as a preprint: https://eartharxiv.org/btahm/

Abstract

Madagascar is a key area for unravelling the geodynamic evolution of the transition between the Rodinia and Gondwana supercontinents as it contains several suites of c. 850–700 Ma magmatic rocks that have been postulated to correlate with other Rodinian terranes. The Bemarivo Domain of northern Madagascar contains the youngest of these units that date to c. 750–700 Ma. We present zircon Hf and O isotope data to understand northern Madagascar's place in the Neoproterozoic plate tectonic reconfiguration. We demonstrate that the northern component of the Bemarivo Domain is distinct from the southern part of the Bemarivo Domain, and have therefore assigned new names—the Bobakindro Terrane and Marojejy Terrane, respectively. Magmatic rocks of the Marojejy Terrane and Anaboriana Belt are characterised by evolved $\varepsilon_{Hf}(t)$ signatures and a range of $\delta^{18}O$ values, similar to the Imorona-Itsindro Suite of central Madagascar. These magmatic suites likely formed together in the same long-lived volcanic arc. In contrast, the Bobakindro Terrane contains juvenile $\varepsilon_{Hf}(t)$ and mantle-like $\delta^{18}O$ values, with no probable

link to the rest of Madagascar. We propose that the Bobakindro Terrane formed in a juvenile arc system that included the Seychelles, the Malani Igneous Suite of northwest India, Oman, and the Yangtze Belt of south China, which at the time were all outboard from continental India and south China. The final assembly of northern Madagascar and amalgamation of the Bobakindro Terrane and Marojejy Terrane occurred along the Antsaba subduction zone, with collision occurring at c. 540 Ma.

1. Introduction

Reconstructing the tectonic geography of the ancient Earth and building a full-plate tectonic reconstruction for the globe in deep time is critically dependent on mapping the distribution of plate tectonic sensitive rocks, including juvenile and evolved arc-related suites, through time (e.g. Merdith et al., 2017). A key goal of characterising these rocks is to better understand the supercontinent cycle, to determine whether it operates as a simple pulse (e.g. Nance et al., 2014) or as a two-stage process starting with supercontinent initiation, followed by progressive accretion (e.g. Condie, 2002). Distinguishing between differing models of the supercontinent cycle requires a detailed knowledge of the location and duration of the critical plate-margin geological events formed at either subduction zones or rifts (e.g. Mallard et al., 2016). The Neoproterozoic, in particular, is a critical period because it sees the major transition from the Nuna/Rodinia supercontinent cycle to the accretion and amalgamation of Gondwana/Pangaea (Merdith et al., 2018). Much of the evidence for this billion-year timescale plate reconfiguration is found in the East African Orogen that formed as the Mozambique Ocean closed and Neoproterozoic India collided with the Congo Craton to form central Gondwana (Armistead et al., 2017; Collins and Pisarevsky, 2005; Fritz et al., 2013). Madagascar was located in the centre of the East African Orogen and thus provides an ideal location to study how the active margins consumed the Mozambique Ocean and the eventual formation of the Gondwana Supercontinent. Of particular interest and contention, is how and when the Archean nucleus of Madagascar amalgamated with the Dharwar Craton of India to the east, and East Africa to the west, as well as with smaller continental blocks of equivocal origin. One of these blocks—the Bemarivo Domain of northern Madagascar—is composed of Neoproterozoic rocks spanning c. 750–700 Ma. Its evolution and amalgamation with the rest of Madagascar is poorly understood and is the focus of this study.

Madagascar is made up of several terranes spanning from Archean to Neoproterozoic (Figure 3.1, inset). The centre of Madagascar contains the Antananarivo Craton, which is composed of c. 2500 Ma magmatic gneisses (Collins and Windley, 2002; Kröner et al., 2000). To the east are the Antongil and Masora cratons, both of which contain rocks that are c. 3100 Ma and are likely a continuation of the Dharwar Craton of India (Armistead et al., 2017; Schofield et al., 2010; Tucker et al., 1999b). To the southwest of the Antananarivo Craton is the Itremo Group, composed of quartzites, schists and marbles

with a maximum depositional age of c. 1600 Ma (Cox et al., 1998; Fernandez et al., 2003). To the southwest of this, is the Ikalamavony Group, similarly made up of quartzites, schists and marbles, but with a maximum depositional age of c. 1000 Ma. To the south of these metasedimentary sequences are the Proterozoic Anosyen, Androyen and Vohibory terranes (Boger et al., 2014; Emmel et al., 2008; Jöns and Schenk, 2008).

North of the Antananarivo Craton is the Bemarivo Domain, made up of the Paleoproterozoic Sahantaha Group, and intruded by c. 750–700 Ma magmatic rocks with a range of geochemical compositions (Thomas et al., 2009). Separating the Antananarivo Craton from the Bemarivo Domain, is the Anaboriana-Manampotsy belt—an interpreted late Neoproterozoic sequence of gneisses that represents the suture between Madagascar and the Dharwar Craton of India (Collins and Windley, 2002).

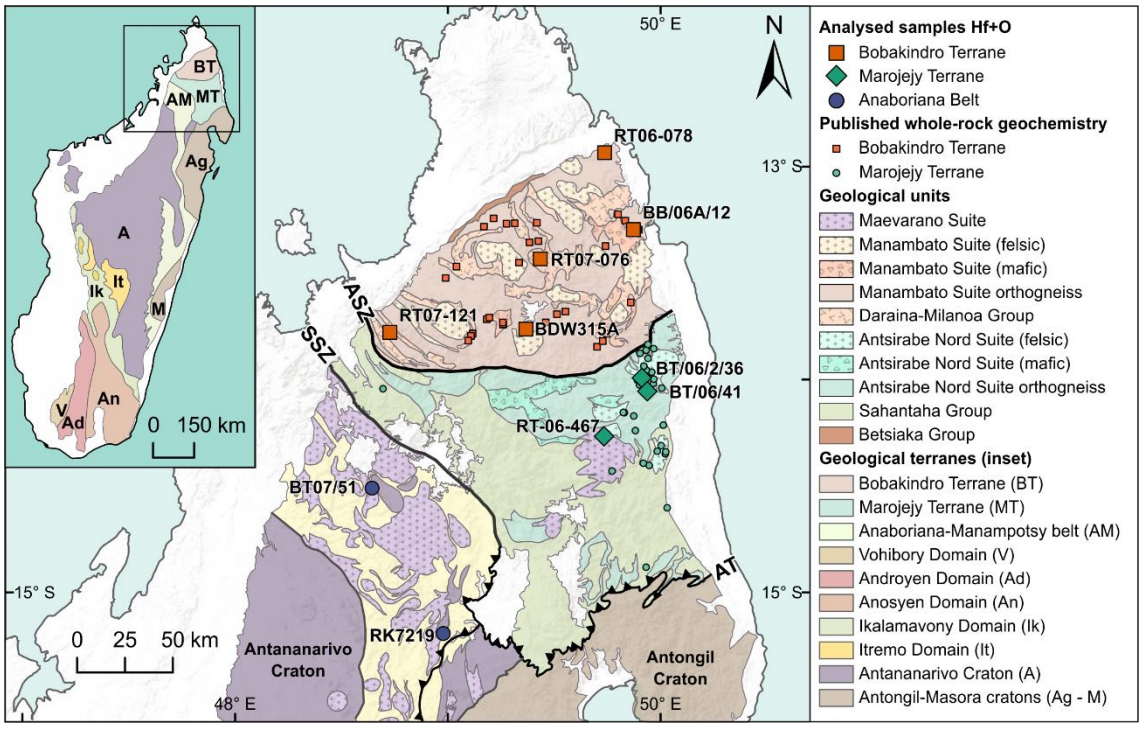

Figure 3.1 Geological map of northern Madagascar modified to reflect our interpretation of the region. ASZ=Antsaba Shear Zone, SSZ=Sandrakota Shear Zone, AT=Andaparaty Thrust. Geological map based on Roig et al. (2012) and Thomas et al. (2009), with the inset modified from De Waele et al. (2011).

Northern Madagascar comprises the c. 3100 Ma Antongil Craton, the c. 2500 Ma Antananarivo Craton and the c. 750–700 Ma Bemarivo Domain (Figure 3.1), all of which have debatable geological histories. It is well documented that the Antongil Craton of northern Madagascar shares many characteristics with the Dharwar Craton of India, and that these two terranes were probably contiguous until the breakup of Gondwana (Armistead et al., 2017; Bauer et al., 2011; Collins and Windley, 2002; Schofield et al., 2010). The Dharwar Craton and Antongil Cratons both contain abundant c. 3100 Ma and c. 2500 Ma magmatic rocks, and both cratons contain Archean metasedimentary rocks

with indistinguishable detrital zircon U–Pb and Hf isotope signatures (Armistead et al., 2017). However, the timing of collision between the Antongil-Dharwar Craton of India and the rest of Madagascar is contentious. Two end-member models are generally evaluated for the amalgamation of Madagascar; 1) the Antongil(Dharwar)-Madagascar collision occurred in the late Archean, and central Madagascar and the Dharwar Craton have existed as "the Greater Dharwar Craton" from then until the breakup of Gondwana (Tucker et al., 2011); or 2) Antongil(Dharwar) and central Madagascar were separate terranes that were sutured during the major Ediacaran–Cambrian Malagasy Orogeny, marked by the Betsimisaraka Suture (Collins and Windley, 2002). The data presented in this manuscript provides considerable support for the second model described above, although the first model cannot be ruled out entirely.

We have collected Hf and O isotope data from zircon within the Bemarivo Domain of northern Madagascar to characterise the evolution of this terrane and compare it to terranes elsewhere in Madagascar and globally. Integrating this dataset within a plate tectonic framework using GPlates reconstruction software, allows us to assess tectonic models both temporally and spatially. The results of this study are important for supercontinent reconstructions of both Rodinia and Gondwana.

1.1. Regional Geology of the Bemarivo Domain

The Bemarivo Domain has loosely been divided into two terranes separated by the ~east–west trending Antsaba Shear Zone (Figure 3.1)(Thomas et al., 2009). Following from the work of Thomas et al. (2009), in this manuscript we confirm the different origin of the northern and southern Bemarivo Domain. To avoid any confusion or implication that these terranes shared a geological history prior to their early Cambrian reworking into a mobile belt; we here refer to the northern part of the Bemarivo Domain as the Bobakindro Terrane, and the southern part of the Bemarivo Domain as the Marojejy Terrane. The Marojejy Terrane contains the Sahantaha Group, a metasedimentary sequence derived from dominantly Paleoproterozoic sources, with a Paleoproterozoic maximum depositional age. This sequence has been interpreted as the passive margin sequence to the Antananarivo Craton. The Sahantaha Group contains detrital zircons with major age peaks at c. 1750 Ma and c. 2500 Ma, similar to the Itremo Group of central Madagascar (BGS-USGS-GLW, 2008; Cox et al., 1998; Cox et al., 2004; De Waele et al., 2011; Fitzsimons and Hulscher, 2005). The Sahantaha Group is intruded by the c. 750 Ma Antsirabe Nord Suite, a plutonic suite that includes gabbros through to granites (Thomas et al., 2009). Jöns et al. (2006) analysed a magmatically zoned monazite using Electron Microprobe with four analyses producing an age of 737 ± 19 Ma, which they suggest represents the maximum depositional age of the Sahantaha Group. However, this technique is not able to distinguish lead-loss, and no other isotopic data indicate a maximum depositional age younger than c. 1730 Ma (BGS-USGS-GLW, 2008). We therefore prefer to consider the Sahantaha Group as an extension of the Itremo Group in

central Madagascar, consistent with interpretations by De Waele et al. (2011) and Boger et al. (2014).

The Bobakindro Terrane contains a component of metamorphosed Archean schist and gneiss—the c. 2477 Ma Betsiaka Group, although outcrops of these rocks are scarce and restricted to the northwest margin of the Bemarivo Domain (Thomas et al., 2009). The Betsiaka Group is in fault-contact with the Bobakindro Terrane units and possibly represents a faulted block of the Antananarivo Domain. Two volcano-sedimentary groups were deposited in the Bobakindro Terrane at c. 750–720 Ma. The high-grade, amphibolite-facies volcano-sedimentary Milanoa Group has a maximum depositional age of c. 750 Ma, and the low-grade, greenschist to lower amphibolite facies, Daraina Group has an extrusive age of c. 740–730 Ma (Thomas et al., 2009). These groups are intruded by arc-related rocks of the Manambato Suite, which comprises c. 718–705 Ma magmatic rocks (Thomas et al., 2009).

Much of northern Madagascar is intruded by the c. 530 Ma Maevarano Suite, interpreted as post-tectonic granites that formed due to orogenic collapse of the East African Orogen (Goodenough et al., 2010). This suite has been used as a maximum age constraint on the final assembly of northern Madagascar, based on the interpretation that it is exposed in all terranes of northern Madagascar (Goodenough et al., 2010; Thomas et al., 2009).

When considered as a single coherent terrane, the Bobakindro Terrane and Marojejy Terrane have for some time been interpreted as a juvenile arc terrane that accreted to the Antananarivo Craton along a Neoproterozoic–Cambrian suture (Thomas et al., 2009). Juvenile Nd data was reported in abstract only (Tucker et al., 1999a) and has been used as evidence for the juvenile nature of both the Bobakindro Terrane and Marojejy Terrane. However, sample locations were not reported and it remains unclear whether these samples were collected from the Bobakindro Terrane or Marojejy Terrane. Extensive whole-rock geochemistry data collected through the World Bank Project (BGS-USGS-GLW, 2008; Thomas et al., 2009) indicate that much of the Bemarivo Domain formed from volcanic arc processes, with the majority of rocks being interpreted as juvenile, and derived from igneous protoliths. This interpretation was based on Y-Nb tectonic discrimination diagrams, and the calc-alkaline nature of the rocks preserved in the Bemarivo Domain. However, a lack of published isotopic data beyond zircon U–Pb geochronology for this region limits our ability to fully understand the magma processes and crustal assimilation involved in the evolution of the Bemarivo Domain. Understanding the isotopic nature of these magmatic suites in terms of their crustal versus mantle components, is important for correlating them with other age-equivalent terranes. The c. 850–750 Ma Imorona-Itsindro magmatic suite is widespread in central Madagascar (Archibald et al., 2016; Archibald et al., 2017b; Zhou et al., 2018), and may be an extension of the Bemarivo Domain. Likewise, there are age-equivalent terranes in the Seychelles, the Malani Igneous Suite of northwest India, Oman and the Yangtze Belt of south China.

2. Methodology

A World Bank Project in Madagascar led to the collection of a substantial dataset of geochemical, geochronological and stratigraphic data from northern Madagascar (BGS-USGS-GLW, 2008). We were fortunate to have access to many of the zircon grain mounts analysed for U–Pb through this project, some of which we have selected for further analysis. Ten samples that cover a broad area in northern Madagascar that were analysed for U–Pb in BGS-USGS-GLW (2008) were selected for Hf and O analysis to characterise the isotopic nature of this region (Figure 3.1). Zircon U–Pb data were collected using the SHRIMP instrument at the John de Laeter Research Centre at Curtin University (BGS-USGS-GLW, 2008; Thomas et al., 2009). We have reinterpreted weighted averages from these data for consistency—which differ only slightly, if at all from the original interpreted ages—and these are summarised in Table 3.1. Isotopic data are provided in Appendix 3.1.

2.1. O isotopes

We selected near-concordant zircon grains with sufficient space for O and Hf isotopic analysis. Zircon mounts were repolished, and Aluminium coated prior to analysis using SHRIMP SI at the Research School of Earth Sciences, The Australian National University in Canberra, Australia. A 10 kV, ~3 nA Cs_+ primary ion beam and a 30 µm spot size was used for analyses. Temora was used as the zircon standard; with two standard analyses approximately every five unknown analyses. Sample $\delta^{18}O_{(zircon)}$ values were determined by difference relative to the mean $\delta^{18}O_{(zircon)}$ measured on standards following normalisation for long-term drift in its measured composition. The results of standard analyses are given in Table 3.1. CL images were used to analyse as close as possible to the U–Pb (LA-ICP-MS) analysis locations while remaining in the same CL zone. Details of the SHRIMP II method for oxygen isotope analysis are from Ickert et al. (2008).

2.2. Hf isotopes

The same grains selected for O isotopes were also analysed for Lu-Hf. Lu-Hf isotope analyses were undertaken on the Thermo-Scientific Neptune Multi-Collector ICP-MS with an attached New Wave UP-193 ArF excimer laser at the University of Adelaide following the methods of Payne et al. (2013). A beam diameter of 50 µm was used. Typical ablation times were ~82 s using a 5 Hz repetition rate, a 4 ns pulse rate, and an intensity of ~4.40 J/cm^2. Zircons were ablated in a helium atmosphere that was then mixed with argon upstream of the ablation cell. Zircon data reduction were carried out using the HfTRAX Excel macro (Payne et al., 2013). Data were normalised to $^{179}Hf/^{177}Hf$=0.7325 using an exponential correction for mass bias. The Yb and Lu isobaric interferences on ^{176}Hf were corrected for following the methodology of Woodhead et al. (2004).

Zircon standards were analysed before and during the analysis of unknowns to assess instrument performance and stability. The primary zircon standard Mud Tank was used and yielded a mean $^{176}Hf/^{177}Hf$ ratio of 0.282499 ± 0.000015 (2SD). This is within uncertainty of the published value of 0.282504 ± 0.000044 (2SD) by Woodhead and Hergt (2005). Values for $^{176}Hf/^{177}Hf_{CHUR(t)}$ were calculated using modern $^{176}Hf/^{177}Hf$=0.282785 (Bouvier et al., 2008), modern $^{176}Lu/^{177}Hf$=0.0336 (Bouvier et al., 2008) and ^{176}Lu decay constant of $1.865x10^{-11}$ $year^{-1}$ (Scherer et al., 2001). Values for the crustal model age (T_{DMC}) were calculated using a ^{176}Lu decay constant of $1.865x10^{-11}year^{-1}$ (Scherer et al., 2001), modern $^{176}Hf/^{177}Hf$=0.28325, modern $^{176}Lu/^{177}Hf$=0.0384 (Griffin et al., 2000), and a bulk crust value of $^{176}Lu/^{177}Hf$=0.015 (Griffin et al., 2002). Uncertainties for $\varepsilon_{Hf}(t)$ are calculated as the $^{176}Hf/^{177}Hf_{Sample}$ uncertainty converted to epsilon notation (i.e. $((^{176}Hf/^{177}Hf_{2\sigma})/0.282785)*10000$) and are reported at the 2σ level.

Table 3.1 Summary of samples and U–Pb zircon geochronology used in this study. All ages are interpreted as magmatic crystallisation ages, except for those indicated by * which are interpreted as maximum depositional ages, and ^ which are interpreted as metamorphic ages. Generally, for samples with lots of concordant analyses we used a cut-off of ±5% concordance.

Sample	Longitude (WGS 84)	Latitude (WGS 84)	Region	Stratigraphic unit or domain	Rock description	$^{238}U/^{206}Pb$ Age (Ma) ± 2σ	Calculation method
RK7219	48.9828	-15.1957	Anaboriana - Manampotsy belt	Groupe d'Androna-Manampotsy	Quartzofeldspathic gneiss	750 ± 4 *573 ± 13 ^514 ± 6	Weighted average of oldest near-concordant analyses: n=8, MSWD=0.80 *Youngest near-concordant (within 5%) zircon core analysis ^Metamorphic age: n=4, MSWD=0.93
BT0751	48.6479	-14.5132	Anaboriana - Manampotsy belt	Group de Bealanana, Anaboriana belt	Charnockite gneiss	768 ± 8 *561±8 ^518 ± 4	Weighted average of oldest near-concordant analyses: n= 6, MSWD=1.4 *Youngest near-concordant (within 5%) zircon core analysis ^Metamorphic age: n=7, MSWD=0.59
RT06467	49.7379	-14.2695	Marojejy Terrane	Bemarivo Domain	Granodioritic gneiss	756 ± 6	n=14, MSWD=0.60
BT0641	49.9411	-14.0582	Marojejy Terrane	Doany Arc, Bemarivo Domain	Tonalitic orthogneiss	746 ± 4	n=13, MSWD=1.5
BT0636	49.9153	-13.9953	Marojejy Terrane	Antsirabe-North Suite, Douany arc, Bemarivo Block	Diorite	754 ± 7	n=12, MSWD=0.69
RT0776	49.4385	-13.4362	Bobakindro Terrane	Bevoay Massif	Mica Granite	713 ± 6	n=5, MSWD=0.63
RT07121	48.7316	-13.7815	Bobakindro Terrane	Bemarivo Domain	Metagranodiorite gneiss	707 ± 5	n=6, MSWD=2.0
BDW315A	49.3712	-13.766	Bobakindro Terrane	Bemarivo Domain	Metagranodiorite	718 ± 7	n=6, MSWD=0.38
BB06A12	49.8762	-13.2988	Bobakindro Terrane	Daraina Group	Metarhyolite – flow banded	724 ± 7	n=9, MSWD=0.98
RT0678	49.741	-12.9375	Bobakindro Terrane	Daraina Group	Rhyolite	738 ± 7	n=5, MSWD=1.2

3. Zircon U–Pb, Hf and O isotope data

3.1. Anaboriana Belt

Two gneiss samples (BT0751 and RK7219) analysed from the Anaboriana Belt have ambiguous protoliths and it is unclear if they are derived from magmatic or sedimentary protoliths (BGS-USGS-GLW, 2008). U–Pb geochronology was unable to resolve this as there is considerable scatter on concordia plots for both samples, which could be either lead loss due to metamorphism or a detrital array. $^{176}Hf/^{177}Hf_i$ values obtained for these samples are consistent with lead loss and age resetting for the zircon grains as the values plot in a horizontal array (within uncertainty) across an age vs. $^{176}Hf/^{177}Hf_i$ plot. Although the Hf isotope data are not conclusive, a magmatic protolith is also supported by the O isotope values. Analyses from the two samples have $\delta^{18}O$ values between +1.3 ‰ and +4.4 ‰. These values are lower than those normally expected for crustal or mantle values and are typically associated with the involvement of meteoric waters and hydrothermal alteration of volcanic/sub-volcanic magma systems (e.g.Bindeman and Valley, 2001; Valley et al., 1998). It is highly unlikely that anomalous values such as these could be recorded in every single magma system that contributed detritus to a sedimentary rocks, and hence the samples are considered to have igneous protoliths—potentially volcanic or upper crustal intrusives.

Calculated magmatic crystallisation ages for samples RK7219 and BT0751 are 750 ± 4 Ma and 768 ± 8 Ma (2σ) respectively (Table 3.1). When calculated at these ages (to remove the effects of Pb-loss), $\varepsilon_{Hf}(t)$ values for magmatic zircons are in the range -3.4 to -10.1. Four U–Pb rim analyses (see CL images in Appendix 3.2) from sample RK7219 yield a calculated age of 514 ± 6 Ma and seven analyses from sample BT0751 yield an age of 518 ± 4 Ma, which we interpret as the age of metamorphism.

3.2. Marojejy Terrane

Three samples were analysed from the Marojejy Terrane. These rocks include, granodioritic gneiss, tonalitic gneiss and diorite (Table 3.1). Interpreted magmatic crystallisation ages for these rocks range from c. 756 Ma to c. 746 Ma (Figure 3.2). Lu–Hf analyses from samples BT0636, BT0641 and RT06467 have negative $\varepsilon_{Hf}(t)$ values ranging from -15.0 to -1.5 (Figure 3.3). These analyses have two-stage depleted mantle model ages spanning c. 2.6–1.7 Ga.

Oxygen isotope data from the Marojejy Terrane show a wide range of $\delta^{18}O$ values. The majority of analyses from samples BT0641 and BT0636 are between +4.8 ‰ and +5.9 ‰, overlapping with the range of values expected for mantle-derived zircons, but extending to more positive values consistent with samples that have crystallised in equilibrium with surface-derived water (Valley et al., 1998). Four analyses from sample BT0641 and two analyses from sample BT0636 have $\delta^{18}O$ values lower than what is expected for mantle

sources, ranging from +0.6 ‰ to +4.3 ‰. The majority of analyses from sample RT06467 are between +6.3 ‰ and +7.1 ‰, with two analyses of +5.8 ‰ that overlap with the mantle $\delta^{18}O$ field.

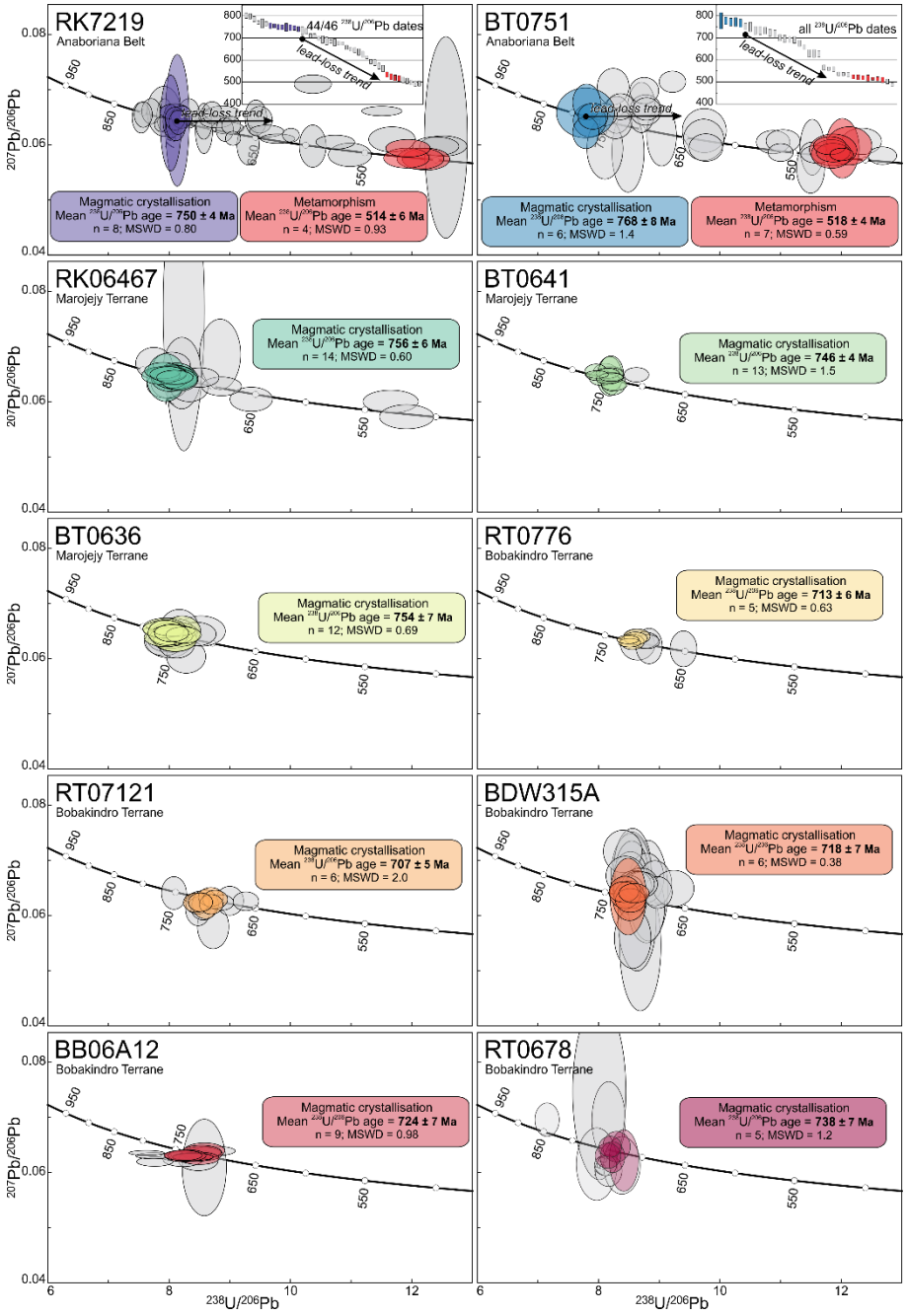

Figure 3.2 Concordia plots with reinterpreted ages using data from Thomas et al. (2009). Axes are the same range for all plots. Coloured ellipses were used to calculate the ages provided, grey ellipses show remaining data that were excluded from calculations. Several analyses were excluded from the calculated ages, as many appear to have undergone lead-loss or resetting—as indicated by the apparent shift to the right of many of the ellipses from the main population. Some samples also have analyses that appear to have undergone 'lead-gain', where analyses are negatively discordant and appear to shift to the left of the main population on the concordia plots (e.g. BB06A12 and RT0678). We therefore generally only included analyses that were within 5% concordance.

3.3. Bobakindro Terrane

Five samples from the Bobakindro Terrane were used for Hf and O isotopic analysis on zircon. These rocks include, granites, granodioritic gneisses and rhyolites (Table 3.1). Magmatic crystallisation ages for these samples are younger than for the Marojejy Terrane and range from c. 740 Ma to c. 705 Ma. Lu–Hf analyses from Bobakindro Terrane samples cluster to form a group of similar $\varepsilon_{Hf}(t)$ signature and age. These analyses have positive $\varepsilon_{Hf}(t)$ values between +4 and +11 and depleted mantle model ages spanning c. 1.4–1.0 Ga (Figure 3.3).

Samples from the Bobakindro Terrane record a restricted range of $\delta^{18}O$ values. Analyses from samples RT0776, RT07121 and BDW315A have $\delta^{18}O$ values ranging from +4.4 ‰ to +6.5 ‰ (Figure 3.3). These overlap with the range of values typical for mantle-derived zircons (5.3 ± 0.6 ‰; Valley et al. (1998)). Samples BB06A12 and RT06-78 have lower $\delta^{18}O$ values, with mean $\delta^{18}O$ values of +4.3 ‰ and +2.3 ‰ respectively.

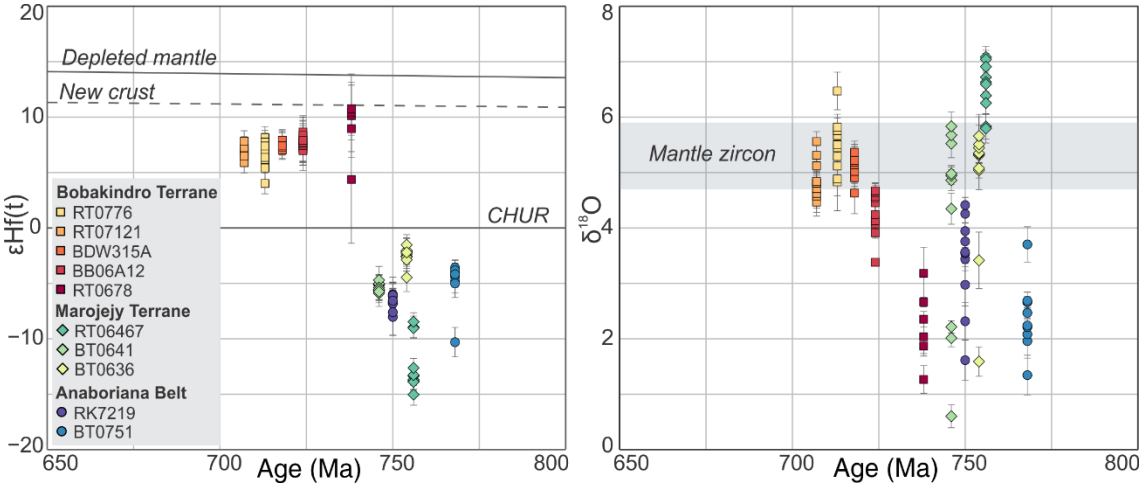

Figure 3.3 $\varepsilon_{Hf}(t)$ vs Age and $\delta^{18}O$ vs Age (calculated $^{238}U/^{206}Pb$ magmatic crystallisation ages) for samples analysed from northern Madagascar. $\varepsilon_{Hf}(t)$ for each analysis was calculated using the magmatic crystallisation age, data given in Appendix 3.1. Plots produced in R, code written to produce plots is documented in Appendix 3.3.

4. Insights from published whole-rock geochemistry data

Whole-rock geochemistry from the Bobakindro Terrane and Marojejy Terrane was published in Thomas et al. (2009). We have used these data to further compare and contrast the Bobakindro Terrane and Marojejy Terrane. We have shown that magmatic rocks from the Marojejy Terrane have evolved $\varepsilon_{Hf}(t)$ signatures, so the geochemistry is potentially reflective of the crust that's being incorporated rather than the processes that generated the mantle melts. Although there are only three samples that have both Hf isotope and whole-rock geochemistry data for the Marojejy Terrane, there does appear to be a trend between these two datasets. The more evolved sample has a ferroan signature compared to the less evolved sample, which has a magnesian signature (Figure 3.4a).

There is an increase in alkalinity for increasing $\varepsilon_{Hf}(t)$ values (Figure 3.4b). The Sr anomalies and trace elements are also higher for the evolved samples (Figure 3.4c, d). Together, this indicates that crustal assimilation was the dominant cause for changing $\varepsilon_{Hf}(t)$.

In contrast, samples from the Bobakindro Terrane are dominantly magnesian (Figure 3.4a), calc-alkalic (Figure 3.4b), and are not as enriched in trace elements (Figure 3.4d). Combined with the juvenile nature of the these rocks, they most likely formed in an arc environment, consistent with the interpretation of Thomas et al. (2009). Although there are only two samples with both Hf isotope and geochemistry data from the Bobakindro Terrane, the younger, marginally more evolved sample has a higher Sr anomaly and higher values for the majority of the trace elements (Figure 3.4c, d). Low degrees of fractionation and crustal assimilation may have been involved in the evolution of the Bobakindro Terrane, which accounts for the trend of decreasing $\varepsilon_{Hf}(t)$ values with time (Figure 3.3).

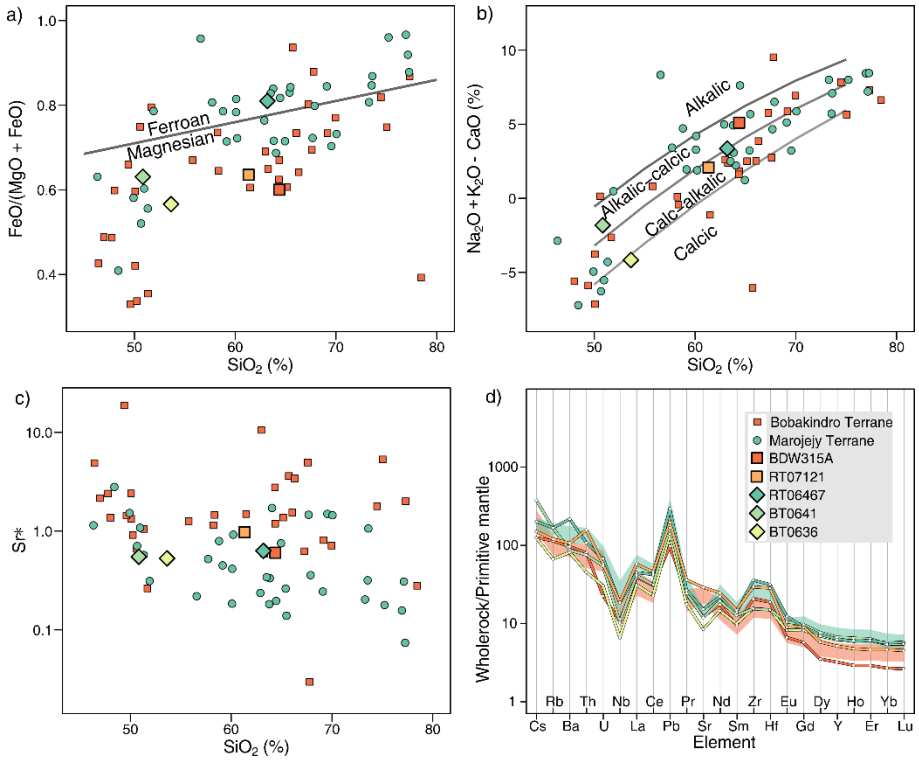

Figure 3.4 a) Fields for ferroan and magnesian rocks after Frost and Frost (2008); b) fields for alkali, alkali-calcic, calc-alkaline and calcic after Frost and Frost (2008); c) Sr anomaly (Sr*) calculated as $Sr_N/sqrt(Pr_N*Nd_N)$, where N is the chondrite normalised values after Sun and McDonough (1989); and d) Spider plot for samples with Hf and O isotope data. The shaded bands behind these lines are the bootstrapped mean and 95% confidence intervals of Primitive Mantle normalised elemental data for all samples from the Bobakindro Terrane and Marojejy Terrane; normalising values from Sun and McDonough (1989). Bootstrapping was performed with replacement for 50000 repetitions. R scripts to produce plots are provided in Appendix 3.3. Data from Thomas et al. (2009).

5. Regional evolution of the Bemarivo Domain

The Bemarivo Domain of northern Madagascar has previously been interpreted as a juvenile Neoproterozoic arc-related terrane that amalgamated with the central Madagascar craton in the late Neoproterozoic to early Cambrian (Collins, 2006; Kröner et al., 2000; Tucker et al., 1999a). Possible links between Madagascar and the Seychelles, Malani Igneous Suite of northwest India and south China have been proposed (Ashwal et al., 2002; Tucker et al., 1999a; Wang et al., 2017). Similarly, in a reconstruction presented in Cox et al. (2004), the Bemarivo Domain links up with the Seychelles and northwest India at c. 750 Ma. New Hf and O isotope data collected in this study allow us to interpret the tectonic evolution of the Bemarivo Domain and assess possible paleogeographical links. Differences between these terranes indicate that they have undergone separate tectonic histories at discrete times during the Neoproterozoic.

5.1. Anaboriana Belt

Zircons analysed from the two Anaboriana Belt samples have evolved $\varepsilon_{Hf}(t)$ signatures that overlap with values from the Marojejy Terrane samples, but are generally less evolved than those from the slightly older Imorona-Itsindro Suite (Archibald et al., 2016; Zhou et al., 2018). We interpret this evolved signature as the result of incorporation of crustal material during magma genesis. $\delta^{18}O$ values for the Anaboriana Belt samples are lower than most analyses from the Marojejy Terrane. Low $\delta^{18}O$ values are typically the result of hydrothermal cycling of meteoric water during magma generation (Bindeman and Valley, 2001; Valley et al., 1998). These are often correlated with extensional environments where rifting may have occurred that facilitated hydrothermal circulation in near-surface or volcanic settings (Bindeman and Valley, 2001; Valley et al., 1998). We therefore suggest that the Anaboriana Belt samples were generated from magmas that contained a component of older crustal material, but likely underwent hydrothermal alteration in an extensional environment.

5.2. Marojejy Terrane

The Marojejy Terrane samples contain zircons with negative $\varepsilon_{Hf}(t)$ signatures that indicate a contribution of continental crust during magma generation. $\varepsilon_{Hf}(t)$ model ages for these analyses range between c. 2.56–1.73 Ga. The majority of $\delta^{18}O$ analyses from sample BT06467 are above the mantle range, indicating that supra-crustal rock assimilation and melting were involved in magma generation. The majority of zircon analyses from samples BT0641 and BT0636 have $\delta^{18}O$ values in the mantle range. Several analyses from the aforementioned samples, as well as analyses from the Anaboriana Belt samples RK7219 and BT0751, have very low $\delta^{18}O$ values that indicate the involvement of meteoric fluids and hydrothermal alteration in a similar way to that envisaged for similar values from the Tonian Imorona-Itsindro Suite in central Madagascar by Archibald et al. (2016).

The Sahantaha Group in which these magmatic rocks intrude, have major detrital zircon components of c. 2500–1700 Ma (De Waele et al., 2011), broadly overlapping with the range of depleted mantle model ages for the analysed samples. The Antananarivo Domain, which may underlie the Sahantaha Group, is dominantly comprised of c. 2500 Ma gneisses. The data presented here support the interpretation of Thomas et al. (2009) that subduction was taking place beneath the Sahantaha Group (and underlying Antananarivo Domain) at c. 750 Ma, which produced melts that incorporated crustal material from surrounding rocks. Notably, this interpretation is consistent with previous models for the Marojejy Terrane (Thomas et al., 2009). Low $\delta^{18}O$ samples from the Anaboriana Belt likely formed in a back-arc extensional environment to the main Marojejy Terrane volcanic arc.

5.3. Bobakindro Terrane

Samples analysed from the Bobakindro Terrane are dominated by juvenile $\varepsilon_{Hf}(t)$ signatures, and $\delta^{18}O$ values that indicate a mantle source and relatively little assimilation of supra-crustal material. The majority of analyses from samples RT0776, RT07121 and BDW315A have $\delta^{18}O$ values in the mantle range, but samples BDW315A and RT0678 have $\delta^{18}O$ values that are significantly lower than those from the mantle. Given the similar $\varepsilon_{Hf}(t)$ values of these samples and the other Bobakindro Terrane samples, we propose that they were also generated from a juvenile depleted mantle source but involved hydrothermal fluids during magma generation. This relates to their generation in an extensional environment (Bindeman and Valley, 2001; Valley et al., 1998). The felsic nature of the Bobakindro Terrane indicates that the original magmas were likely to have fractionated in thickened crust. The juvenile Hf signatures of these samples, and mantle-like $\delta^{18}O$ values, imply that they formed in an arc environment, with little involvement of any significantly older, or supra-crustal material.

Our new Hf and O data from northern Madagascar indicate that the Bobakindro Terrane and the Marojejy Terrane have distinct isotopic evolutions and we therefore conclude that they were not contiguous at the time of their formation (c. 750 Ma). The Antsaba Shear Zone that marks the boundary between the Bobakindro Terrane and Marojejy Terrane (Thomas et al., 2009), also marks a boundary between samples of a juvenile signature in the north, and an evolved signature in the south. The only detailed descriptions of the Antsaba Shear Zone are presented in Thomas et al. (2009) and are summarised here. The Antasaba Shear Zone is best exposed in the western part of the Bemarivo Domain where it is ~15 km wide, and becomes less exposed toward the east where it is <1 km wide. It contains intense strike-slip deformation with zones of steeply inclined planar fabrics, with prominent shallowly plunging, strike parallel, mineral stretching lineations. Because this zone has been intensely sheared, we suspect the identification of typical suture zone rock assemblages would be difficult to identify, however further research is needed to properly characterise this structure. Given the evidence presented in our study as well as the

contrast in rock types either side of the Antsaba Shear Zone, this structure marks a major tectonic boundary in northern Madagascar and likely represents a cryptic suture zone.

6. Assembly of north Malagasy Gondwana

The terranes of northern Madagascar form a tectonically unresolved triple-junction (Figure 3.1), with the Marojejy Terrane (including the Sahantaha Group), Anaboriana Belt and Antongil Domain all in contact with each other (Figure 3.1). We have shown here that rocks from the Anaboriana Belt and Marojejy Terrane are isotopically similar, and that they were part of the same continental-margin volcanic arc system at c. 750 Ma. The relationship between these two terranes and the Antongil Domain, is less straightforward. Understanding the nature and timing of contacts between these three terranes is essential for understanding the evolution of northern Madagascar.

6.1. The amalgamation of the Dharwar Craton with Madagascar

The assembly of northern Madagascar is a contentious topic with different models proposed for the nature and timing of amalgamation (e.g. Armistead et al., 2017; Boger et al., 2014; Collins and Windley, 2002; Tucker et al., 2011). The relationship between the Sahantaha Group (maximum depositional age c. 1730 Ma, minimum depositional age c. 800 Ma) and the Antongil Craton provides clues as to the relative timing of these tectonic events. Despite the current fault contact being marked by the major Andaparaty Thrust between the Sahantaha Group and Antongil Domain (Figure 3.1), several authors have suggested that the Sahantaha Group stratigraphically overlies the Antongil Domain (Bauer et al., 2011; De Waele et al., 2011), implying that the Antongil Domain was adjacent to central Madagascar at the time of deposition. Against this interpretation are the paucity of c. 3100 Ma detrital zircons in the Sahantaha Group (De Waele et al., 2008; Thomas et al., 2009), despite the Antongil Craton being rich in zircon-bearing protoliths of this age (Tucker et al., 1999b) and the lack of any depositional contact mapped between the terranes. These observations support that the Sahantaha Group is allochthonous with respect to the Antongil Craton and that the two were juxtaposed by the major Andaparaty Thrust.

If these two terranes formed separately from one another, when did they come together? Widespread metamorphism throughout much of northern Madagascar is recorded at c. 560–510 Ma (Buchwaldt et al., 2003; Jöns et al., 2009; Jöns et al., 2006), and we propose that this time period records the amalgamation of the Antongil Craton with the rest of Madagascar (including the Sahantaha Group and Anaboriana Belt), along the Betsimisaraka Suture of Collins and Windley (2002).

6.2. What does the Anaboriana Belt represent?

The Anaboriana-Manampotsy belt (Figure 3.1) has been interpreted to mark the approximate location of the Betsimisaraka Suture that has been interpreted as the site of amalgamation of the Antananarivo Craton with the Dharwar Craton (at the time including the Antongil-Masora domains) during the Ediacaran to early Cambrian (Armistead et al., 2017; Collins et al., 2003; Collins and Windley, 2002). The Anaboriana Belt is the northern part of this extensive belt and separates the Sahantaha Group from the Antananarivo Craton. Above, we have argued that the Sahantaha Group formed stratigraphically above the Antananarivo Craton, which implies that the Anaboriana Belt is not a suture, or at least would only have been a minor marginal Neoproterozoic ocean basin suture. An alternative interpretation for the Anaboriana-Manampotsy belt is that it does not represent a suture zone but was an elongated sedimentary basin that formed due to Tonian rifting (Tucker et al., 2011).

As we have described in our interpretation of samples from the Anaboriana Belt, due to pervasive high-grade metamorphism, it can be difficult to recognise sample protoliths as either sedimentary or magmatic in origin. It is therefore unclear whether the Anaboriana Belt represents a sedimentary sequence at all, or whether it should really be considered as a zone of major high-strain shearing (or both). To date, samples from the entire length of the Anaboriana Belt have been interpreted with protolith ages ranging from c. 850 Ma to c. 750 Ma, with metamorphism interpreted from zircon rims at c. 550–520 Ma. The Anaboriana-Manampotsy Belt is therefore best considered as a forearc basin that formed in response to subduction at c. 750 Ma. At c. 550 Ma this belt was significantly reworked during the Betsimisaraka Suture event, and approximately marks the location of the Gondwana suture in Madagascar. As it trends north, the suture is represented by the Andaparaty Thrust, which separates the Antongil Craton from the Marojejy Terrane (Figure 3.1).The Betsimisaraka Suture then strikes north-easterly into sea, and continues back on land as the east-west striking Antsaba Shear Zone (Figure 3.1; Figure 3.5).

6.3. Final assembly of northern Madagascar

Two stages of metamorphism have been identified in the Bemarivo Domain that represent collision of the Bemarivo Domain with the rest of Madagascar (Jöns et al., 2006). M1 monazite cores range from c. 563 Ma to c. 532 Ma, which represent the collisional event; and M2 monazite rims represent peak metamorphic temperatures and record ages of c. 521 to c. 513 Ma (Jöns et al., 2006). These authors concluded that collision led to the burial of much of the Marojejy Terrane to a depth of > 25 km, and approximately 25–30 Ma later, the terrane underwent magmatic underplating and ultrahigh temperature metamorphism. They suggested that the northern part of the Bemarivo Domain (the Bobakindro Terrane) was also affected by this event, but was buried to lower depths and therefore metamorphosed to lower grades. We propose this is why c. 560–510 Ma metamorphic evidence is much more apparent in the Marojejy Terrane compared to the

Bobakindro Terrane in the north. Jöns et al. (2006) suggested these metamorphic events represent the entire Bemarivo Domain docking with the rest of Madagascar. In light of new evidence presented in our study whereby the two terranes of the Bemarivo Domain are separate, and that the Marojejy Terrane was likely contiguous with the Antananarivo Craton—we instead propose that these metamorphic events represent the suturing the Bobakindro and Marjojejy terranes along the Antsaba Shear Zone to form the Bemarivo mobile belt. This accounts for the different metamorphic assemblages and conditions described in either terrane by Jöns et al. (2006). The c. 537–522 Ma post-tectonic Maevarano Suite that crops out in the Marojejy Terrane, Anaboriana Belt and the Antananarivo Craton also provides a constraint on the final assembly of northern Madagascar (Goodenough et al., 2010). This magmatic suite is the likely driver of the age-equivalent ultrahigh temperatures recorded in the Marojejy Terrane by Jöns et al. (2006) .

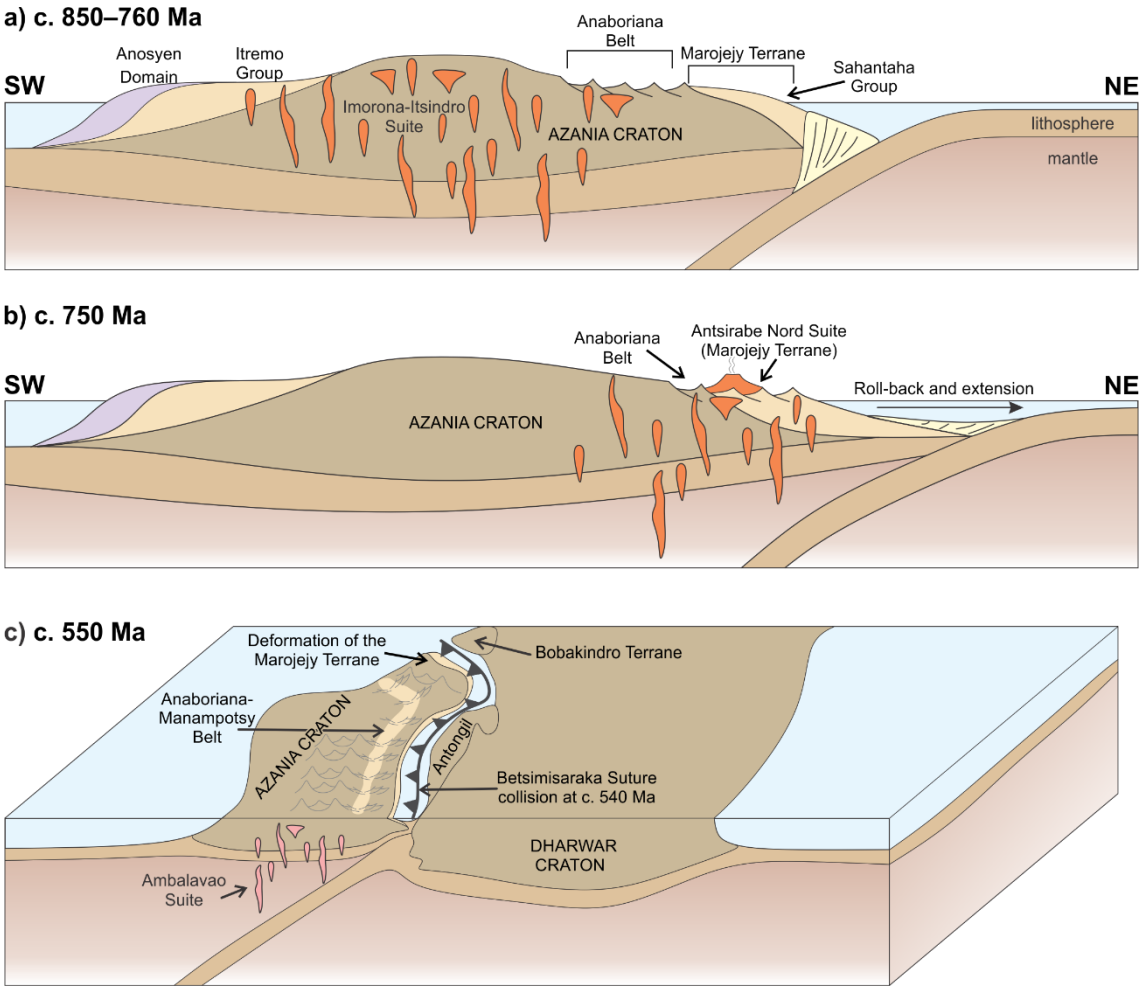

Figure 3.5 Schematic diagram of the Neoproterozoic arc evolution of Madagascar; a) Intrusion of the Imorona-Itsindro Suite in central Madagascar at c. 850–750 Ma; b) roll-back and extension of the subduction zone and subsequent intrusive and extrusive rocks associated with the Antsirabe Nord Suite; and c) collision of the Dharwar Craton and Bobakindro Terrane with the Azania Craton.

7. Links to Rodinia

In an attempt to link the Bobakindro Terrane with other potential c. 720 Ma arc terranes, we have compared our new isotopic data with several regions containing age equivalent rocks. We compared the Bobakindro Terrane with South China, northwest India, central Madagascar, the Seychelles, Oman and the Arabian Nubian Shield (Figure 3.6). We also integrated this dataset with the *GPlates* (www.gplates.org) Neoproterozoic tectonic model (Merdith et al., 2017) to assess correlations temporally and spatially.

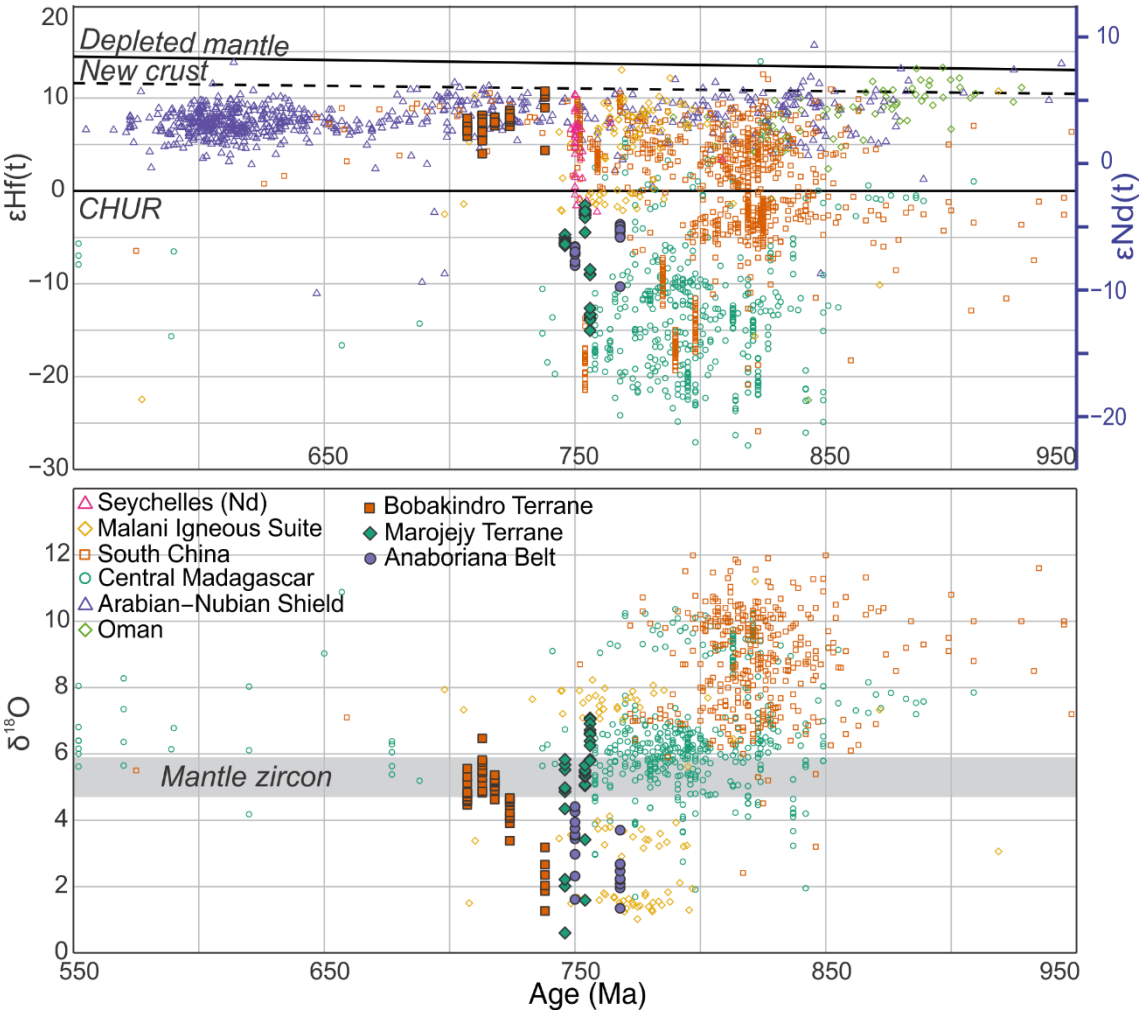

Figure 3.6 $\varepsilon_{Hf}(t)$ vs age and $\delta^{18}O$ vs age for other regions compared to northern Madagascar; Seychelles data is converted from $\varepsilon_{Nd}(t)$ to $\varepsilon_{Hf}(t)$ using the equation $\varepsilon_{Hf}(t) = 1.34\varepsilon Nd(t) + 2.95$ for 'terrestrial array' (Vervoort et al., 1999) and scale is shown to the right of the plot. R scripts to produce plots are provided in Appendix 3.3. Data sourced from: Alessio et al. (2018); Archibald et al. (2016); Ashwal et al. (2002); Blades et al. (2015); Huang et al. (2008); Long et al. (2011); Morag et al. (2011); Qi et al. (2012); Robinson et al. (2014); Wang et al. (2017); Wang et al. (2013); Zhao et al. (2013); Zheng et al. (2008); Zheng et al. (2007); Zhou et al. (2018).

We have used a revised version of the Merdith et al. (2017) full-plate model of the Neoproterozoic, which provides a kinematic framework that models plate boundaries and the evolution of continental crust from 1000 to 520 Ma. Using such a model allows us to account for paleogeographic and paleotectonic constraints from other regions, as the model integrates key datasets such as paleomagnetism, geochronology and geophysics to form a full-plate tectonic framework. We calculated an average age and average $\varepsilon_{Hf}(t)$ for each sample compiled in our database. This dataset was then added to GPlates as a shapefile and a start and end time for each data point was assigned ± 30 Ma (i.e. each point will show up 30 Ma before the average age and disappear 30 Ma after). Data points are coloured according to their average $\varepsilon_{Hf}(t)$ value.

It has been suggested that the Imorona-Itsindro Suite of central Madagascar is analogous to the Seychelles and the Malani Igneous Suite granitoids based on age correlations (Tucker et al., 2001; Tucker et al., 2014). Tectonic models by Wang et al. (2017) and Ashwal et al. (2013) proposed a continuous juvenile Andean-type arc between south China, the Malani Igneous Suite of northwest India and Seychelles. Wang et al. (2017) further included the Imorona-Itsindro suite along with this magmatic arc. However, available $\varepsilon_{Hf}(t)$ data from the Imorona-Itsindro Suite of central Madagascar (Archibald et al., 2016; Zhou et al., 2018) is predominantly evolved (Figure 3.6), implying that it does not correlate with this juvenile arc system. Oman has also been interpreted as a series of arcs that accreted to Rajasthan in northwest India (which includes the Malani Igneous Suite) during the period c. 850–720 Ma (Blades et al., in review). We have shown here that age-equivalent rocks from the Bobakindro Terrane, have juvenile $\varepsilon_{Hf}(t)$ signatures, which correlate well with $\varepsilon_{Hf}(t)$ data from the proposed south China–Malani–Seychelles arc system of Wang et al. (2017) as well as new data from Oman (Blades et al., in review) (Figure 3.6). These correlations are highlighted in the full-plate tectonic model in GPlates, where juvenile analyses (data points with shades of red; Figure 3.7) all form an elongated 'arc' along the western (reconstructed orientation) margin of India and China.

The period of magmatism in this proposed arc was long-lived, beginning at around c. 850 Ma and ending at around c. 700 Ma. There is a general southward younging trend (reconstructed orientation; Figure 3.7), with the oldest record coming from China, and progressing to younger rocks through Oman, Malani, Seychelles and the Bobakindro Terrane. It is possible that this period of juvenile arc magmatism represents a single long-lived arc, however, we argue that a complex history of accretionary terranes that formed along the edge of Rodinia, is more likely.

Samples analysed from the Bobakindro Terrane are slightly younger than rocks from south China and Malani, although they have similar juvenile $\varepsilon_{Hf}(t)$ signatures. The Bobakindro Terrane therefore formed during the late stages of this juvenile arc system. The whole-rock geochemistry data (Figure 3.4) indicate that the Bobakindro Terrane underwent a degree of crustal assimilation and fractionation (see section 4). However, the $\varepsilon_{Hf}(t)$ data show that the Bobakindro Terrane is dominantly juvenile, with little input of significantly older crustal material. Together this implies that the crustal assimilate incorporated into

magmatic rocks of the Bobakindro Terrane was not significantly older than c. 720 Ma. This supports a model where the Bobakindro Terrane formed on a rolled-back crustal remnant of slightly older crust, possibly from south China, Malani or Oman (Alessio et al., 2018).

The integration of $\varepsilon_{Hf}(t)$ data with the full-plate tectonic model of (Merdith et al., 2017) broadly supports the south China–Malani–Seychelles linkage proposed by Wang et al. (2017) and Ashwal et al. (2013), and the links between Oman and northwest India proposed by Blades et al. (in review). We further extend this model to include the Bobakindro Terrane of northern Madagascar as a younger, more outboard component of this arc system. There is no significant overlap between the highly evolved data from the Imorona-Itsindro Suite and that of this proposed juvenile Neoproterozoic arc system. The lack of juvenile Hf data from the Imorona-Itsindro Suite indicates that this terrane was not part of the south China–Malani–Seychelles–Bemarivo arc.

Our proposal to link these previously discrete volcanic arcs into a long-lived subduction zone would elucidate long term trends in plate boundary length and, when compared to the connectedness of continental lithosphere, assist with quantitatively understanding the supercontinent cycle for pre-Pangea supercontinents (e.g. Merdith et al., 2019).

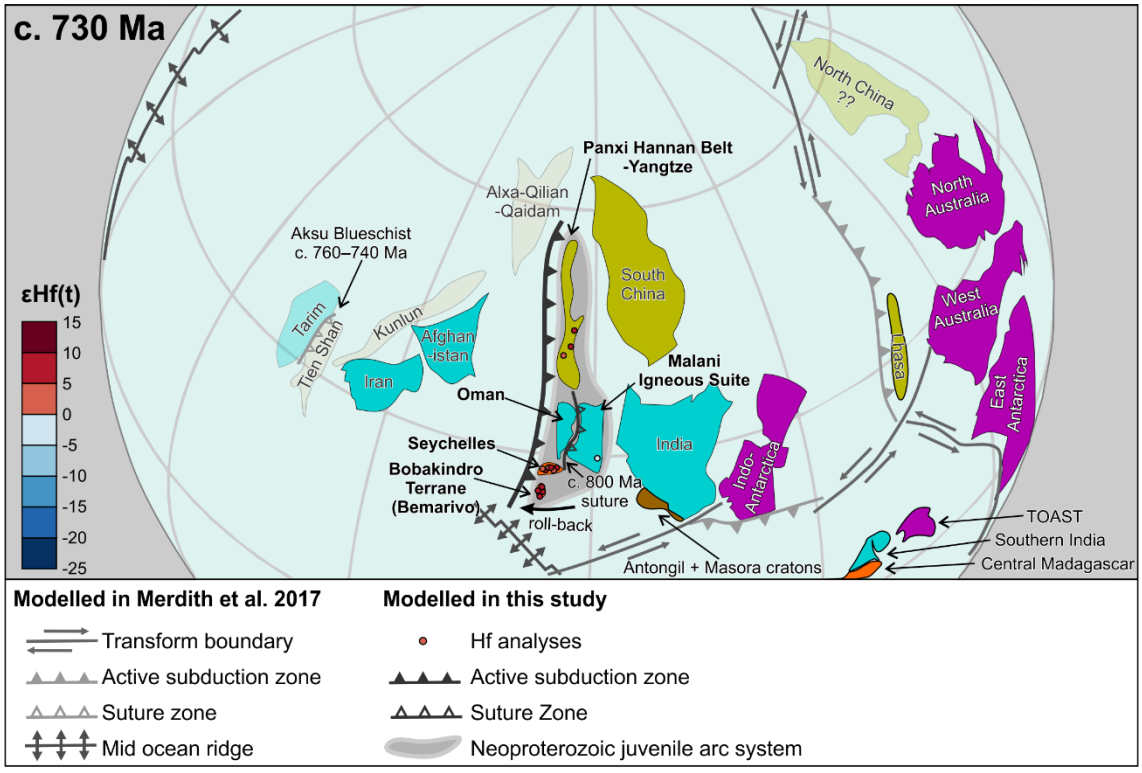

Figure 3.7 GPlates reconstruction at 730 Ma showing the location of compiled Hf and Nd isotope data (see Figure 3.6 for the conversion calculation used). Transparent polygons are uncertain in the model but are included as suggestions based on their positions post-Gondwana amalgamation. Lhasa is linked to Australia after Zhu et al. (2011), addition of the TOAST terrane to Azania after Jacobs et al. (2015) and Archibald et al. (2017a).

Distinguishing between different arc systems for India-south China as we have in this study, suggest a far more nuanced and intricate subduction system than has previously been captured in tectonic models for the Neoproterozoic (e.g. Li et al., 2008; Merdith et al., 2017). Plate modelling necessitates some simplifications in the geometrical representation of real-world tectonic systems (e.g. rifts, arcs), however, this should result in more conservative estimates of their lengths (Merdith et al., 2019). Consequently, plate modelling can reveal pertinent implications in understanding whole earth systems such as the supercontinent cycle.

Here, our preferred tectonic reconstruction at 730 Ma suggests nearly 4000 km of continuous subduction occurring from the Panxi-Hanaan belt in south China (Cawood et al., 2018) through to southern India occurring over 250 million years. The size and longevity of this subduction system, in addition to the size of the combined south China-India continent (Figure 3.7), suggest a considerable portion of continental lithosphere (roughly equivalent to present-day Australia) with an active subduction zone was removed from Rodinia. This raises questions about the nature of the supercontinent cycle and what classifies as a 'supercontinent', beyond that of whether all continental crust must be present for a supercontinent to exist (e.g. Pastor-Galán et al., 2018). In particular, we highlight that processes typically associated with supercontinents such as slab roll-back leading to intracratonic rifting (e.g. Nanhua rift system in south China; Wang and Li (2003)) and the continental amalgamation of juvenile crust and evolved continental ribbons to continental masses occurred away from the established Rodinian supercontinent. This is not irreconcilable with some geodynamic modelling, which suggests that the sizable separate pieces of continental crust can also induce changes in mantle flow and structure (e.g. Flament et al., 2017). Further study could analyse the impact of such a subduction system as described here on mantle flow and the surface expression of the flow.

8. Conclusions

We have presented new zircon Hf and O isotope data that help unravel the subduction history of the Mozambique Ocean during the critical time of supercontinent cycle transition—from the Nuna/Rodinia cycle to the amalgamation of Gondwana. We have compared these Madagascar data to other age-equivalent terranes globally. The key outcomes of this research are:

1. The Bobakindro Terrane and Marojejy Terrane in the Bemarivo Domain of northern Madagascar are different terranes that have separate tectonic evolutions until the Cambrian, based on zircon $\varepsilon_{Hf}(t)$ and $\delta^{18}O$ data.
2. The c. 750 Ma Marojejy Terrane and Anaboriana Belt are isotopically evolved terranes that likely represent a younger component of the retreating volcanic arc represented in central Madagascar by the Imorona-Itsindro Suite.

3. The c. 720 Ma Bobakindro Terrane is a juvenile terrane that likely formed in a juvenile arc environment related to the Seychelles, the Malani Igneous Suite of northwest India, Oman and the Yangtze Belt of South China. The Bobakindro Terrane is interpreted as forming above an aging, retreating, subduction zone.
4. The Bobakindro Terrane collided with Madagascar at c. 540 Ma along the Antsaba Shear Zone/Betsimisaraka Suture, which marks final closure of the Mozambique Ocean and assembly of supercontinent Gondwana.

References

Alessio, B.L., Blades, M.L., Murray, G., Thorpe, B., Collins, A.S., Kelsey, D.E., Foden, J., Payne, J., Al-Khirbash, S., Jourdan, F., 2018. Origin and tectonic evolution of the NE basement of Oman: a window into the Neoproterozoic accretionary growth of India? Geological Magazine 155, 1150-1174.

Archibald, D.B., Collins, A.S., Foden, J.D., Payne, J.L., Holden, P., Razakamanana, T., De Waele, B., Thomas, R.J., Pitfield, P.E.J., 2016. Genesis of the Tonian Imorona–Itsindro magmatic Suite in central Madagascar: Insights from U–Pb, oxygen and hafnium isotopes in zircon. Precambrian Research 281, 312-337.

Archibald, D.B., Collins, A.S., Foden, J.D., Payne, J.L., Macey, P.H., Holden, P., Razakamanana, T., 2017a. Stenian–Tonian arc magmatism in west–central Madagascar: the genesis of the Dabolava Suite. Journal of the Geological Society, jgs2017-2028.

Archibald, D.B., Collins, A.S., Foden, J.D., Razakamanana, T., 2017b. Tonian Arc Magmatism in Central Madagascar: The Petrogenesis of the Imorona-Itsindro Suite. The Journal of Geology 125, 000-000.

Armistead, S.E., Collins, A.S., Payne, J.L., Foden, J.D., De Waele, B., Shaji, E., Santosh, M., 2017. A re-evaluation of the Kumta Suture in western peninsular India and its extension into Madagascar. Journal of Asian Earth Sciences.

Ashwal, L., Demaiffe, D., Torsvik, T., 2002. Petrogenesis of Neoproterozoic granitoids and related rocks from the Seychelles: the case for an Andean-type arc origin. Journal of Petrology 43, 45-83.

Ashwal, L.D., Solanki, A.M., Pandit, M.K., Corfu, F., Hendriks, B.W.H., Burke, K., Torsvik, T.H., 2013. Geochronology and geochemistry of Neoproterozoic Mt. Abu granitoids, NW India: Regional correlation and implications for Rodinia paleogeography. Precambrian Research 236, 265-281.

Bauer, W., Walsh, G.J., de Waele, B., Thomas, R.J., Horstwood, M.S.A., Bracciali, L., Schofield, D.I., Wollenberg, U., Lidke, D.J., Rasaona, I.T., Rabarimanana, M.H., 2011. Cover sequences at the northern margin of the Antongil Craton, NE Madagascar. Precambrian Research 189, 292-312.

BGS-USGS-GLW, 2008. Republique de Madagascar Ministère de L'engergie et des Mines (MEM/SG/DG/UCP/PGRM). British Geological Survey Research Report.

Bindeman, I.N., Valley, J.W., 2001. Low-δ18O rhyolites from Yellowstone: Magmatic evolution based on analyses of zircons and individual phenocrysts. Journal of Petrology 42, 1491-1517.

Blades, M.L., Collins, A.S., Foden, J., Payne, J.L., Xu, X., Alemu, T., Woldetinsae, G., Clark, C., Taylor, R.J.M., 2015. Age and hafnium isotopic evolution of the Didesa and Kemashi Domains, western Ethiopia. Precambrian Research 270, 267-284.

Boger, S.D., Hirdes, W., Ferreira, C.A.M., Schulte, B., Jenett, T., Fanning, C.M., 2014. From passive margin to volcano–sedimentary forearc: The Tonian to Cryogenian evolution of the Anosyen Domain of southeastern Madagascar. Precambrian Research 247, 159-186.

Bouvier, A., Vervoort, J.D., Patchett, P.J., 2008. The Lu–Hf and Sm–Nd isotopic composition of CHUR: constraints from unequilibrated chondrites and implications for the bulk composition of terrestrial planets. Earth and Planetary Science Letters 273, 48-57.

Buchwaldt, R., Tucker, R.D., Dymek, R.F., 2003. Geothermobarometry and U-Pb Geochronology of metapelitic granulites and pelitic migmatites from the Lokoho region, Northern Madagascar. American Mineralogist 88, 1753-1768.

Cawood, P.A., Zhao, G., Yao, J., Wang, W., Xu, Y., Wang, Y., 2018. Reconstructing South China in phanerozoic and precambrian supercontinents. Earth-Science Reviews 186, 173-194.

Collins, A.S., 2006. Madagascar and the amalgamation of Central Gondwana. Gondwana Research 9, 3-16.

Collins, A.S., Fitzsimons, I.C.W., Hulscher, B., Razakamanana, T., 2003. Structure of the eastern margin of the East African Orogen in central Madagascar. Precambrian Research 123, 111-133.

Collins, A.S., Pisarevsky, S.A., 2005. Amalgamating eastern Gondwana: The evolution of the Circum-Indian Orogens. Earth-Science Reviews 71, 229-270.

Collins, A.S., Windley, B.F., 2002. The tectonic evolution of central and northern Madagascar and its place in the final assembly of Gondwana. The Journal of Geology 110, 325-339.

Condie, K.C., 2002. Breakup of a Paleoproterozoic supercontinent. Gondwana Research 5, 41-43.

Cox, R., Armstrong, R.A., Ashwal, L.D., 1998. Sedimentology, geochronology and provenance of the Proterozoic Itremo Group, central Madagascar, and implications for pre-Gondwana palaeogeography. Journal of the Geological Society 155, 1009-1024.

Cox, R., Coleman, D.S., Chokel, C.B., DeOreo, S.B., Wooden, J.L., Collins, A.S., De Waele, B., Kröner, A., 2004. Proterozoic tectonostratigraphy and paleogeography of central Madagascar derived from detrital zircon U-Pb age populations. The Journal of geology 112, 379-399.

De Waele, B., Thomas, R.J., Horstwood, M., Pitfield, P., Tucker, R., Potter, C., Key, R., Smith, R., Bauer, W., Randriamananjara, T., 2008. U-Pb detrital zircon geochronological provenance patterns of supracrustal successions in central and northern Madagascar.

De Waele, B., Thomas, R.J., Macey, P.H., Horstwood, M.S.A., Tucker, R.D., Pitfield, P.E.J., Schofield, D.I., Goodenough, K.M., Bauer, W., Key, R.M., Potter, C.J., Armstrong, R.A., Miller, J.A., Randriamananjara, T., Ralison, V., Rafahatelo, J.M., Rabarimanana, M., Bejoma, M., 2011. Provenance and tectonic significance of the Palaeoproterozoic metasedimentary successions of central and northern Madagascar. Precambrian Research 189, 18-42.

Emmel, B., Jons, N., Kroner, A., Jacobs, J., Wartho, J.A., Schenk, V., Razakamanana, T., Austegard, A., 2008. From Closure of the Mozambique Ocean to Gondwana Breakup: New Evidence from Geochronological Data of the Vohibory Terrane, Southwest Madagascar. The Journal of Geology 116, 21-38.

Fernandez, A., Schreurs, G., Villa, I.M., Huber, S., Rakotondrazafy, M., 2003. Age constraints on the tectonic evolution of the Itremo region in Central Madagascar. Precambrian Research 123, 87-110.

Fitzsimons, I.C.W., Hulscher, B., 2005. Out of Africa: detrital zircon provenance of central Madagascar and Neoproterozoic terrane transfer across the Mozambique Ocean. Terra Nova 17, 224-235.

Flament, N., Williams, S., Müller, R., Gurnis, M., Bower, D.J., 2017. Origin and evolution of the deep thermochemical structure beneath Eurasia. Nature communications 8, 14164.

Fritz, H., Abdelsalam, M., Ali, K.A., Bingen, B., Collins, A.S., Fowler, A.R., Ghebreab, W., Hauzenberger, C.A., Johnson, P.R., Kusky, T.M., Macey, P., Muhongo, S., Stern, R.J., Viola, G., 2013. Orogen styles in the East African Orogen: A review of the Neoproterozoic to Cambrian tectonic evolution. Journal of African Earth Sciences 86, 65-106.

Frost, B.R., Frost, C.D., 2008. A geochemical classification for feldspathic igneous rocks. Journal of Petrology 49, 1955-1969.

Goodenough, K.M., Thomas, R.J., De Waele, B., Key, R.M., Schofield, D.I., Bauer, W., Tucker, R.D., Rafahatelo, J.M., Rabarimanana, M., Ralison, A.V., Randriamananjara, T., 2010. Post-collisional magmatism in the central East African Orogen: The Maevarano Suite of north Madagascar. Lithos 116, 18-34.

Griffin, W., Pearson, N., Belousova, E., Jackson, S., Van Achterbergh, E., O'Reilly, S.Y., Shee, S., 2000. The Hf isotope composition of cratonic mantle: LAM-MC-ICPMS analysis of zircon megacrysts in kimberlites. Geochimica et Cosmochimica Acta 64, 133-147.

Griffin, W., Wang, X., Jackson, S., Pearson, N., O'Reilly, S.Y., Xu, X., Zhou, X., 2002. Zircon chemistry and magma mixing, SE China: in-situ analysis of Hf isotopes, Tonglu and Pingtan igneous complexes. Lithos 61, 237-269.

Huang, X.-L., Xu, Y.-G., Li, X.-H., Li, W.-X., Lan, J.-B., Zhang, H.-H., Liu, Y.-S., Wang, Y.-B., Li, H.-Y., Luo, Z.-Y., 2008. Petrogenesis and tectonic implications of Neoproterozoic, highly fractionated A-type granites from Mianning, South China. Precambrian Research 165, 190-204.

Ickert, R., Hiess, J., Williams, I., Holden, P., Ireland, T., Lanc, P., Schram, N., Foster, J., Clement, S., 2008. Determining high precision, in situ, oxygen isotope ratios with a SHRIMP II: Analyses of MPI-DING silicate-glass reference materials and zircon from contrasting granites. Chemical Geology 257, 114-128.

Jacobs, J., Elburg, M., Läufer, A., Kleinhanns, I.C., Henjes-Kunst, F., Estrada, S., Ruppel, A.S., Damaske, D., Montero, P., Bea, F., 2015. Two distinct late Mesoproterozoic/early Neoproterozoic basement provinces in central/eastern Dronning Maud Land, East Antarctica: The missing link, 15–21 E. Precambrian Research 265, 249-272.

Jöns, N., Emmel, B., Schenk, V., Razakamanana, T., 2009. From orogenesis to passive margin—the cooling history of the Bemarivo Belt (N Madagascar), a multi-thermochronometer approach. Gondwana Research 16, 72-81.

Jöns, N., Schenk, V., 2008. Relics of the Mozambique Ocean in the central East African Orogen: evidence from the Vohibory Block of southern Madagascar. Journal of Metamorphic Geology 0.

Jöns, N., Schenk, V., Appel, P., Razakamanana, T., 2006. Two-stage metamorphic evolution of the Bemarivo Belt of northern Madagascar: constraints from reaction textures and in situ monazite dating. Journal of Metamorphic Geology 24, 329-347.

Kröner, A., Hegner, E., Collins, A.S., Windley, B.F., Brewer, T.S., Razakamanana, T., Pidgeon, R.T., 2000. Age and magmatic history of the Antananarivo Block, central Madagascar, as derived from zircon geochronology and Nd isotopic systematics. American Journal of Science 300, 251-288.

Li, Z.X., Bogdanova, S.V., Collins, A.S., Davidson, A., De Waele, B., Ernst, R.E., Fitzsimons, I.C.W., Fuck, R.A., Gladkochub, D.P., Jacobs, J., Karlstrom, K.E., Lu, S., Natapov, L.M., Pease, V., Pisarevsky, S.A., Thrane, K., Vernikovsky, V., 2008. Assembly, configuration, and break-up history of Rodinia: A synthesis. Precambrian Research 160, 179-210.

Long, X., Yuan, C., Sun, M., Kröner, A., Zhao, G., Wilde, S., Hu, A., 2011. Reworking of the Tarim Craton by underplating of mantle plume-derived magmas: evidence from Neoproterozoic granitoids in the Kuluketage area, NW China. Precambrian Research 187, 1-14.

Mallard, C., Coltice, N., Seton, M., Müller, R.D., Tackley, P.J., 2016. Subduction controls the distribution and fragmentation of Earth's tectonic plates. Nature 535, 140.

Merdith, A.S., Collins, A.S., Williams, S.E., Pisarevsky, S., Foden, J.D., Archibald, D.B., Blades, M.L., Alessio, B.L., Armistead, S., Plavsa, D., 2017. A full-plate global reconstruction of the Neoproterozoic. Gondwana Research 50, 84-134.

Merdith, A.S., Williams, S.E., Brune, S., Collins, A.S., Müller, R.D., 2019. Rift and plate boundary evolution across two supercontinent cycles. Global and Planetary Change 173, 1-14.

Morag, N., Avigad, D., Gerdes, A., Belousova, E., Harlavan, Y., 2011. Crustal evolution and recycling in the northern Arabian-Nubian Shield: New perspectives from zircon Lu–Hf and U–Pb systematics. Precambrian Research 186, 101-116.

Nance, R.D., Murphy, J.B., Santosh, M., 2014. The supercontinent cycle: a retrospective essay. Gondwana Research 25, 4-29.

Pastor-Galán, D., Nance, R.D., Murphy, J.B., Spencer, C.J., 2018. Supercontinents: myths, mysteries, and milestones. Geological Society, London, Special Publications 470, SP470. 416.

Payne, J.L., Pearson, N.J., Grant, K.J., Halverson, G.P., 2013. Reassessment of relative oxide formation rates and molecular interferences on in situ lutetium–hafnium analysis with laser ablation MC-ICP-MS. Journal of Analytical Atomic Spectrometry 28, 1068-1079.

Qi, X., Zeng, L., Zhu, L., Hu, Z., Hou, K., 2012. Zircon U–Pb and Lu–Hf isotopic systematics of the Daping plutonic rocks: implications for the Neoproterozoic tectonic evolution of the northeastern margin of the Indochina block, Southwest China. Gondwana Research 21, 180-193.

Robinson, F.A., Foden, J.D., Collins, A.S., Payne, J.L., 2014. Arabian Shield magmatic cycles and their relationship with Gondwana assembly: Insights from zircon U–Pb and Hf isotopes. Earth and Planetary Science Letters 408, 207-225.

Roig, J., Tucker, R., Delor, C., Peters, S., Théveniaut, H., 2012. Carte géologique de la République de Madagascar à 1/1 000 000. Ministère des Mines, PGRM, Antananarivo, République de Madagascar 1.

Scherer, E., Münker, C., Mezger, K., 2001. Calibration of the lutetium-hafnium clock. Science 293, 683-687.

Schofield, D.I., Thomas, R.J., Goodenough, K.M., De Waele, B., Pitfield, P.E.J., Key, R.M., Bauer, W., Walsh, G.J., Lidke, D.J., Ralison, A.V., 2010. Geological evolution of the Antongil Craton, NE Madagascar. Precambrian Research 182, 187-203.

Sun, S.-S., McDonough, W.-S., 1989. Chemical and isotopic systematics of oceanic basalts: implications for mantle composition and processes. Geological Society, London, Special Publications 42, 313-345.

Thomas, R.J., De Waele, B., Schofield, D.I., Goodenough, K.M., Horstwood, M., Tucker, R., Bauer, W., Annells, R., Howard, K., Walsh, G., Rabarimanana, M., Rafahatelo, J.M., Ralison, A.V., Randriamananjara, T., 2009. Geological evolution of the Neoproterozoic Bemarivo Belt, northern Madagascar. Precambrian Research 172, 279-300.

Tucker, R., Ashwal, L., Hamilton, M., Torsvik, T., Carter, L., 1999a. Neoproterozoic silicic magmatism of northern Madagascar, Seychelles, and NW India: clues to Rodinia's assembly and dispersal, Geological Society of America, Abstracts with Programs, p. 317.

Tucker, R., Ashwal, L., Handke, M., Hamilton, M., Le Grange, M., Rambeloson, R., 1999b. U-Pb geochronology and isotope geochemistry of the Archean and Proterozoic rocks of north-central Madagascar. The Journal of Geology 107, 135-153.

Tucker, R., Ashwal, L., Torsvik, T., 2001. U–Pb geochronology of Seychelles granitoids: a Neoproterozoic continental arc fragment. Earth and Planetary Science Letters 187, 27-38.

Tucker, R., Roig, J.-Y., Delor, C., Amelin, Y., Goncalves, P., Rabarimanana, M., Ralison, A., Belcher, R., 2011. Neoproterozoic extension in the Greater Dharwar Craton: a reevaluation of the "Betsimisaraka suture" in Madagascar. Canadian Journal of Earth Sciences 48, 389-417.

Tucker, R.D., Roig, J.Y., Moine, B., Delor, C., Peters, S.G., 2014. A geological synthesis of the Precambrian shield in Madagascar. Journal of African Earth Sciences 94, 9-30.

Valley, J.W., Kinny, P.D., Schulze, D.J., Spicuzza, M.J., 1998. Zircon megacrysts from kimberlite: oxygen isotope variability among mantle melts. Contributions to mineralogy and petrology 133, 1-11.

Vervoort, J.D., Patchett, P.J., Blichert-Toft, J., Albarède, F., 1999. Relationships between Lu–Hf and Sm–Nd isotopic systems in the global sedimentary system. Earth and Planetary Science Letters 168, 79-99.

Wang, J., Li, Z.-X., 2003. History of Neoproterozoic rift basins in South China: implications for Rodinia break-up. Precambrian Research 122, 141-158.

Wang, W., Cawood, P.A., Zhou, M.F., Pandit, M.K., Xia, X.P., Zhao, J.H., 2017. Low-δ18O Rhyolites From the Malani Igneous Suite: A Positive Test for South China and NW India Linkage in Rodinia. Geophysical Research Letters 44.

Wang, Y., Zhang, A., Cawood, P.A., Fan, W., Xu, J., Zhang, G., Zhang, Y., 2013. Geochronological, geochemical and Nd–Hf–Os isotopic fingerprinting of an early Neoproterozoic arc–back-arc system in South China and its accretionary assembly along the margin of Rodinia. Precambrian Research 231, 343-371.

Woodhead, J., Hergt, J., Shelley, M., Eggins, S., Kemp, R., 2004. Zircon Hf-isotope analysis with an excimer laser, depth profiling, ablation of complex geometries, and concomitant age estimation. Chemical Geology 209, 121-135.

Woodhead, J.D., Hergt, J.M., 2005. A preliminary appraisal of seven natural zircon reference materials for in situ Hf isotope determination. Geostandards and Geoanalytical Research 29, 183-195.

Zhao, J.-H., Zhou, M.-F., Zheng, J.-P., 2013. Constraints from zircon U–Pb ages, O and Hf isotopic compositions on the origin of Neoproterozoic peraluminous granitoids from the Jiangnan Fold Belt, South China. Contributions to Mineralogy and Petrology 166, 1505-1519.

Zheng, Y.-F., Wu, R.-X., Wu, Y.-B., Zhang, S.-B., Yuan, H., Wu, F.-Y., 2008. Rift melting of juvenile arc-derived crust: geochemical evidence from Neoproterozoic volcanic and granitic rocks in the Jiangnan Orogen, South China. Precambrian Research 163, 351-383.

Zheng, Y.-F., Zhang, S.-B., Zhao, Z.-F., Wu, Y.-B., Li, X., Li, Z., Wu, F.-Y., 2007. Contrasting zircon Hf and O isotopes in the two episodes of Neoproterozoic granitoids in South China: implications for growth and reworking of continental crust. Lithos 96, 127-150.

Zhou, J.-L., Li, X.-H., Tang, G.-Q., Liu, Y., Tucker, R.D., 2018. New evidence for a continental rift tectonic setting of the Neoproterozoic Imorona-Itsindro Suite (central Madagascar). Precambrian Research 306, 94-111.

Zhu, D.-C., Zhao, Z.-D., Niu, Y., Dilek, Y., Mo, X.-X., 2011. Lhasa terrane in southern Tibet came from Australia. Geology 39, 727-730.

4

Structural evolution and medium-temperature thermochronology of central Madagascar: implications for Gondwana amalgamation

Under review as:

Armistead, S.E., Collins, A.S., Redaa, A., Gilbert, S., Jepson, G., Gillespie, J., Blades, M.L., Foden, J.D. and Razakamanana, T., In Review. Structural evolution and medium-temperature thermochronology of central Madagascar: implications for Gondwana amalgamation. *Journal of the Geological Society.*

Available as a preprint: https://eartharxiv.org/x46vc/

Abstract

Madagascar occupied an important place in the amalgamation of Gondwana, and preserves a record of several Neoproterozoic events that can be linked to orogenesis of the East African Orogen. We integrate remote sensing and field data to unravel complex deformation in the Ikalamavony and Itremo domains of central Madagascar. The deformation sequence comprises a gneissic foliation (S1), followed by south to south-west directed, tight to isoclinal, recumbent folding (D2). These are overprinted by north-trending upright folds that formed during a ~E–W shortening event. Together these produced type 1 and type 2 fold interference patterns throughout the Itremo and Ikalamavony domains. Apatite U–Pb and muscovite and biotite Rb–Sr thermochronometers indicate that much of central Madagascar was thermally reset to at least ~500°C at c. 500 Ma. Deformation in west-central Madagascar occurred between c. 750 Ma and c. 550 Ma, and we suggest this deformation formed in response to the c. 650 Ma collision of Azania with Africa along the Vohibory Suture in southwestern Madagascar.

In eastern Madagascar, deformation is syn- to post-550 Ma, which formed in response to the final closure of the Mozambique Ocean along the Betsimisaraka Suture that amalgamated Madagascar with the Dharwar Craton of India.

1. Introduction

The amalgamation of central Gondwana occurred through convergence at several discrete subduction and collisional zones; collectively forming the East African Orogen. Madagascar was located in the centre of Gondwana and provides an ideal natural laboratory to study how this supercontinent coalesced (Collins, 2006; Collins and Windley, 2002; Tucker et al., 1999). Of particular interest and contention, is how and when the Archaean nucleus of Madagascar amalgamated with the Dharwar Craton of India to the east, and East Africa to the west, as well as smaller continental blocks of equivocal origin. Reconciling this tectonic history has major implications for global plate tectonic models during the Neoproterozoic (e.g. Merdith et al., 2017).

Madagascar is made up of several domains ranging in age from Archaean to Neoproterozoic (Figure 4.1b). The centre of Madagascar is made up of the Antananarivo Domain, which has a basement of c. 2500 Ma magmatic gneisses (Collins and Windley, 2002; Kröner et al., 2000; Tucker et al., 1999), known as the Betsiboka Suite (Roig et al., 2012), interleaved with the Ambatolampy Group granulite- and amphibolite-facies metasedimentary rocks (Archibald et al., 2015). To the east of the Antananarivo Domain is the Antongil-Masora Domain, which contains gneisses that are c. 3100 Ma and c. 2500 Ma, and are interpreted as a continuation of the Dharwar Craton of India (Armistead et al., 2017; Schofield et al., 2010; Tucker et al., 1999).

Overlying the Antananarivo Domain is the Itremo Group (Figure 4.1). Classified as a sub-domain of the Antananarivo Domain by Roig et al. (2012), the Itremo Group is comprised of quartzites, schists and marbles with maximum depositional age of c. 1600 Ma (Costa et al., Submitted; Cox et al., 1998; Fernandez et al., 2003). The Itremo Group is interpreted as a continental margin sequence that was deposited on the Antananarivo Domain basement (Cox et al., 1998; 2004). To the southwest, thrust over the Itremo Group, is the Ikalamavony Group within the Ikalamavony Domain, similarly made up of quartzites, schists and marbles but with a maximum depositional age of c. 1000 Ma (Archibald et al., 2017a; Tucker et al., 2014). In places the Ikalamavony Domain is in tectonic contact directly with the Antananarivo Domain basement, with no Itremo Group rocks separating them (Figure 4.1b; Figure 4.2). To the south of these metasedimentary terranes are the Proterozoic Anosyen, Androyen and Vohibory domains (Boger et al., 2014; Emmel et al., 2008; Jöns and Schenk, 2008). In northern Madagascar is the c. 800–700 Ma Bemarivo Belt, which formed as an exotic juvenile arc terrane that amalgamated with Madagascar at c. 520 Ma (Armistead et al., 2019; Jöns et al., 2009; Thomas et al., 2009).

The central Madagascan terranes discussed in this paper are bounded by two major sutures; the eastern Betsimisaraka Suture and the western Vohibory Suture (mapped as the Ampanihy shear zone in Figure 4.1). These resulted from at least two distinct major orogenic events that amalgamated central Madagascar, the Dharwar Craton of India and Africa within Gondwana (Figure 4.1). However, the timing, location, and direction of subduction leading to these orogenic events remain contentious. Two end-member models are generally evaluated for the amalgamation of Madagascar; 1) that the Dharwar–central Madagascar collision (eastern suture) occurred in the late Archaean, and that central Madagascar and the Dharwar craton existed as the "Greater Dharwar Craton" through the entire Proterozoic eon (Tucker et al., 2011), and that widespread Neoproterozoic–Cambrian magmatism and metamorphism in Madagascar resulted from Madagascar–Africa collision (western suture); or 2) that the Dharwar Craton and central Madagascar were separate terranes that were sutured during a major Ediacaran–Cambrian East African orogenic event (the Malagasy Orogeny of Collins and Pisarevsky 2005), marked by the Betsimisaraka Suture in eastern Madagascar (Figure 4.1b). In this model, the central Madagascar–Africa collision occurred at c. 650–630 Ma (Collins and Pisarevsky, 2005; Collins and Windley, 2002; Emmel et al., 2008; Jöns and Schenk, 2011) as the East African Orogeny. Other authors have suggested a c. 750–650 Ma age for the eastern suture (Fitzsimons and Hulscher, 2005), or a c. 850–750 Ma age for the western suture (Moine et al., 2014). The proximity of these two suture zones makes it difficult to unravel the timing of events, as more recent events have the potential to overprint and obliterate the record of earlier events, such as through high temperature resetting of key minerals used for thermochronology and metamorphism.

The cross-cutting relationships and deformation history of the terranes that make up Madagascar can provide clues as to the timing of major orogenic events in Madagascar. Here we use structural geology to understand the deformation history of a part of central Madagascar, which lies between the two hypothesised suture zones. We have also collected U–Pb zircon, U–Pb apatite, Rb–Sr muscovite and Rb–Sr biotite thermochronology data to provide some absolute timing constraints on deformation in the region.

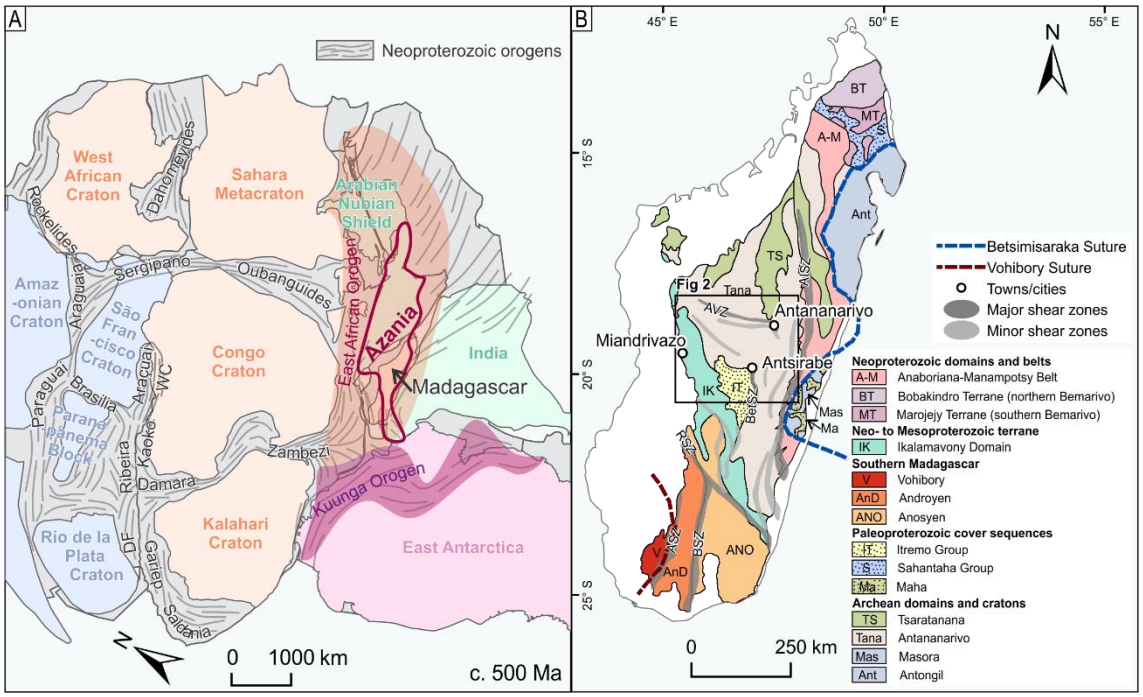

Figure 4.1 a) Tectonic map of Gondwana made using GPlates exported geometries from Merdith et al. (2017) in ArcGIS; projected in Hotine Oblique Mercator with Madagascar in the centre (reconstructed position, longitude=-75 and latitude=+40). DF=Dom Feliciano Belt, WC=West Congo; b) Present day map of the geological domains of Madagascar after (De Waele et al., 2011). AISZ=Angavo-Ifanadiana shear zone, AVZ=Antananarivo virgation zone, BetSZ=Betsileo shear zone, RSZ=Ranotsara shear zone, BSZ=Beraketa shear zone, ASZ=Ampanihy shear zone.

1.1. Regional structural and geochronological framework for central Madagascar

This study focuses on central Madagascar including parts of the Ikalamavony, and Antananarivo domains and the Itremo sub-domain (Figure 4.1b, Figure 4.2). Structural geology and various geochronological methods are used to define and distinguish deformation events in central Madagascar. Collins et al. (2003b) and Tucker et al. (2007) undertook comprehensive studies of the structure of the Itremo Group in central Madagascar. This area contains spectacularly folded sequences visible from satellite imagery. Collins et al. (2003b) interpreted a D1 event that produced 10 km scale recumbent, isoclinal folding predating c. 800–780 Ma intrusive rocks of the Imorona-Itsindro Suite. D2 was interpreted as a local deformation event that occurred synchronously with c. 800–780 Ma intrusions. D3 was interpreted as an east-west shortening event with thrusting and at least two phases of upright folding. D4 is expressed as post-550 Ma normal shearing and locally marks the boundary between the least metamorphosed parts of the Itremo Group and the granulite-facies Betsiboka Suite and Ambatolampy Group of the Antananarivo Domain (Betsileo Shear Zone; Collins et al. 2000). Tucker et al. (2007) interpreted a similar history for the Itremo Group with km-scale fold and thrust nappes, and east-directed vergence. This resulted in inversion and repetition of the Archaean Antananarivo Domain gneisses and the Proterozoic Itremo

Group, with high-grade (old) rocks being thrust over low-grade (young) rocks. The inversion was followed by east-west shortening that resulted in upright folding of nappes to produce km-scale fold interference patterns. This event occurred within a sinistral transpressive regime and was interpreted as being associated with the Ranotsara Shear Zone in southern Madagascar (Tucker et al., 2007). These two models for the Itremo Group differ in that Tucker et al. (2007) interpreted the timing of deformation as occurring after c. 720 Ma, whereas Collins et al. (2003b) interpreted the early nappes as forming before 800–780 Ma, and the upright folding having occurred after the c. 780 Ma intrusive rocks.

The region between the eastern-most part of our study area and the east coast of Madagascar was studied from a structural perspective in Collins et al. (2003a); Martelat et al. (2000); Nédélec et al. (2000); Raharimahefa and Kusky (2006, 2009); Raharimahefa et al. (2013). Interpretations of this region generally include a D1 event characterised by N-S striking foliations that dip to the west, with a top to the east sense of movement (Collins et al., 2003a; Nédélec et al., 2000). These rocks are reworked by D2 shear zones such as the Angavo Shear Zone and the Antananarivo virgation zone (Figure 4.1b) that underwent low-pressure, granulite conditions (Nédélec et al., 2000; Paquette and Nédélec, 1998). D3 is characterised by >20 km wide mylonitic high-strain zones and smaller discrete shear zones (Collins et al., 2003a). These dip gently to the west, with a top to the east sense of movement. D4 is characterised by poorly preserved late stage folding (Collins et al., 2003a). Raharimahefa and Kusky (2006, 2009) interpreted three folding events associated with ~N-S striking shear zones along the northeastern and southeastern margins of the Betsimisaraka Suture. A syn-kinematic granite within the Angavo Shear Zone constrains deformation here to c. 550 Ma (Raharimahefa and Kusky, 2010).

Precise dating of deformation in Madagascar is difficult due to resetting from successive overlapping tectono-thermal events. Latest metamorphism in the Anosyen and Androyen domains to the south of our study area is constrained to c. 580–520 Ma (Collins et al., 2012; de Wit et al., 2001; Martelat et al., 2000; Paquette et al., 1994) and attributed to high-strain shearing along the Ampanihy and Beraketa shear zones (Figure 4.1b) (Boger et al., 2015; Boger et al., 2014). Jöns and Schenk (2011) demonstrated that in southern Madagascar, high-grade metamorphism yielded ages of c. 650–600 Ma in the west, but recorded ages of c. 560–530 Ma in the east. In central Madagascar, U–Pb dating of zircon rims and titanite have been used to constrain latest metamorphism in the Itremo Group to c. 550–500 Ma (Tucker et al., 2007). Further east, between the eastern-most part of the study area and the east coast of Madagascar, metamorphism has been dated to c. 560–520 Ma (BGS-USGS-GLW, 2008; Collins et al., 2003c; Kröner et al., 2000). From this, it is clear that whatever event was taking place at c. 580–520 Ma, its effects were widespread and resulted in metamorphism throughout most of Madagascar, sparing, perhaps, the far southwest.

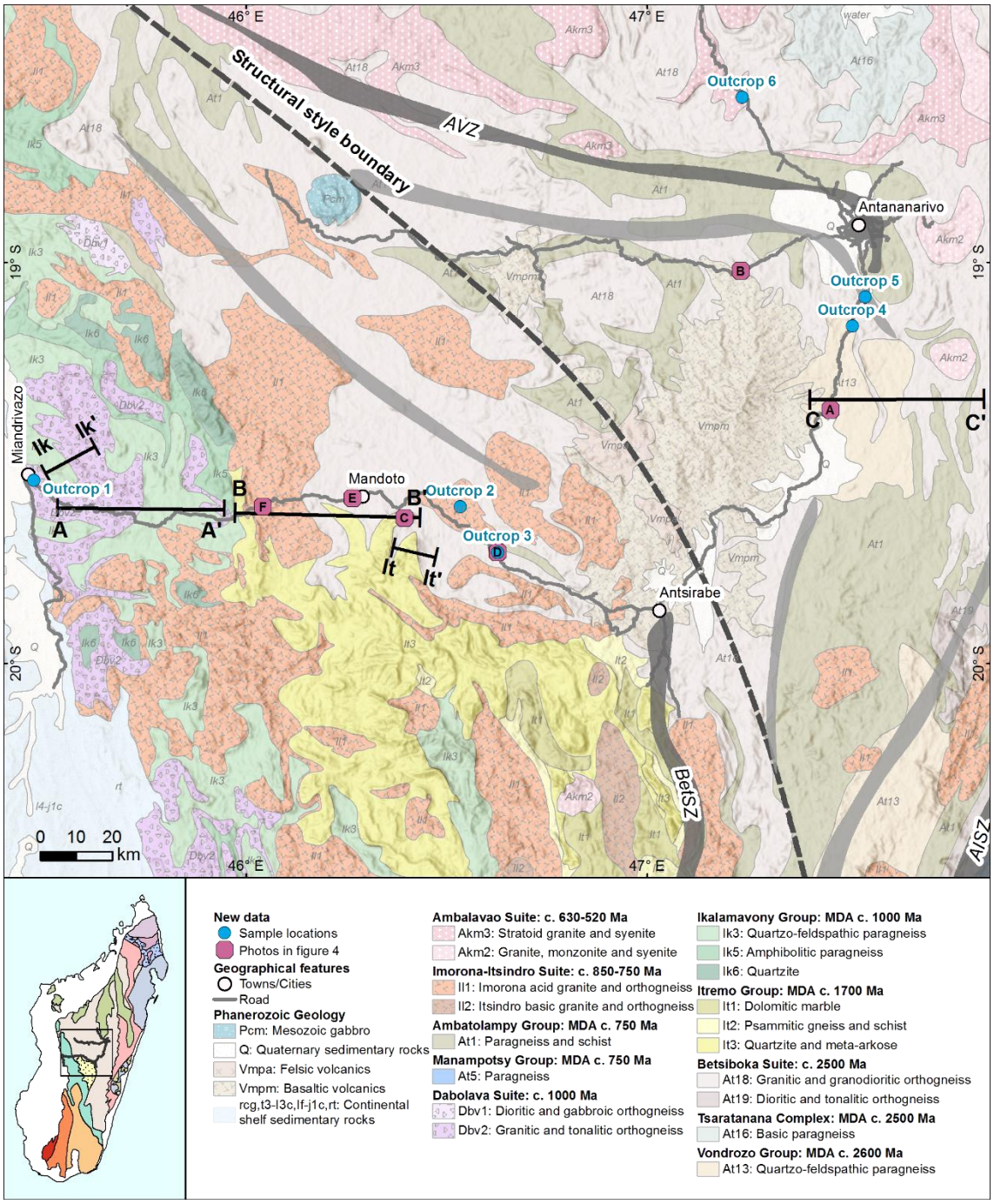

Figure 4.2 Geological map of central Madagascar (Roig et al., 2012) with sample locations, photo locations from Figure 4.4. Our remote sensing interpretation, new structural measurements and structural measurements from Macey et al. (2009); Moine (1968); Service Géologique de Madagascar (1962, 1963a, 1963b), and published geochronology are provided in a detailed PDF copy of this map where layers can be turned on and off in a pdf viewer (Appendix 4.1).

In this study we attempt to link up previous structural studies and further extend these interpretations to cover the entire central Madagascar region. We have used remotely sensed data such as satellite imagery and Landsat to interpret the structural framework of central Madagascar, and integrated existing geochronological and structural data

(Appendix 4.1). We have ground-truthed this interpretation by collecting structural data and key rock samples for U–Pb zircon, U–Pb apatite, Rb–Sr muscovite and Rb–Sr biotite analysis. These systems span a wide range of closure temperatures from which we can reconstruct the temporal and thermal evolution of this region.

2. Thermochronology

A range of magmatic and orthogneiss samples were collected with the aim of having a representative sample set of the major magmatic suites of central Madagascar. This is important for determining overprinting relationships of key structural events, and determining relative and absolute timing constraints on these events. We used four geochronology/thermochronology techniques: zircon U–Pb (closure temperature ~900–1000°C), apatite U–Pb (closure temperature ~350–550°C), muscovite Rb–Sr (closure temperature ~500–600°C) and biotite Rb–Sr (closure temperature ~300–400°C). Detailed methodologies for these techniques are provided in Appendix 4.2. Due to the abundance of samples (41 in total), detailed results for each sample and outcrop are also provided in Appendix 4.2. Sample descriptions, location and age data are summarised in Table 2. Isotopic data are given in Appendix 4.3.

2.1. Zircon U–Pb data

Thirteen magmatic samples from six key localities were analysed for U–Pb zircon geochronology. Concordia plots are shown for each locality in Appendix 4.2; Figure A.7.2 and age data is summarised in Table 1 of the manuscript. Samples were generally very discordant and difficult to interpret magmatic crystallisation ages. This is not surprising given all samples have been thermally reset during a younger event, as revealed by both the apatite U–Pb and mica Rb–Sr results. If samples contained sufficient concordant data, we used a weigthed average to calculate the magmatic crystallisation age (e.g. M16-45). However, as most data were discordant we generally calculated upper intercept ages of discordia lines of those data that appeared to form a linear trend away from the concordia curve. Data points that were very discordant and did not plot along a linear trend with other data ellipses, were generally excluded from age calculations. Many of these points may represent inherited zircons that have become discordant, or zircons that have undergone a complex history of multi-stage lead-loss. However, without several analyses forming a trend, it is impossible to interpret these 'outliers' with confidence.

2.2. Apatite U–Pb data

Apatite has a U–Pb closure temperature of ~450–550°C (Chamberlain and Bowring, 2001; Schoene and Bowring, 2007), which makes it a potentially useful system for understanding the thermal evolution of orogenic events. Coupled with other minerals

with different closure temperatures, we can reconstruct the thermal and tectonic evolution of central Madagascar.

Of the thirteen samples separated for heavy mineral analysis, ten yielded sufficient apatite for U–Pb analysis. Appendix 4.2; Figure A.7.3 shows Concordia plots for all samples analysed, and grouped by locality. Discordia lines were calculated for each sample. Some analyses in each sample plotted significantly off the discordia lines, and were excluded from the calculated intercept ages (higher transparency ellipses in Appendix 4.2; Figure A.7.3). Some of these analyses appear to form a distinct trend, and so we calculated an intercept age based on these analyses for each locality, as indicated by the red discordia lines and red outlined ellipses in Appendix 4.2; Figure A.7.3.

2.3. Biotite and muscovite Rb–Sr data

Muscovite and biotite have closure temperatures of ~500–600°C (Armstrong et al., 1966) and ~300–400°C (Del Moro et al., 1982; Jenkin et al., 2001; Verschure et al., 1980) respectively, which makes them useful for understanding medium-temperature geological events. Appendix 4.2; Figure A.7.4 and Figure A.7.5 show isochron plots for all samples that produced reasonable age calculations, and are grouped by locality. Isochron lines were calculated for each sample. Some analyses in each sample plotted significantly off the isochron lines, and were excluded from the calculated intercept ages (higher transparency ellipses in Appendix 4.2; Figure A.7.4 and Figure A.7.5).

Table 2 Summary of sample descriptions, outcrop and cross-cutting relationships, and age data. Letters given for each outcrop are the interpreted order of formation/intrusion, based on cross-cutting relationships. All zircon ages are interpreted as magmatic crystallisation ages except for metamorphic ages indicated by (*) and lower intercept ages indicated by (#).

Sample ID	Transect	Outcrop	Sample description	Magmatic Suite	Latitude	Longitude	Elevation (m)	Zircon U–Pb age (Ma)	Apatite U–Pb age (Ma)	Muscovite Rb–Sr age (Ma)	Biotite Rb–Sr age (Ma)
M16-24	West	1	K-spar granite	Ambalavao	-19.5443	45.47028	182	576 ± 24	–	519 ± 69	505 ± 59
M16-32	West	2/A	Coarse-grained gneiss	Betsiboka	-19.6107	46.53399	989	2553 ± 24	519 ± 11	446 ± 161	502 ± 20
M16-33	West	2/D	Microgranodioritic dyke-undeformed	Imorona-Itsindro	-19.6107	46.53399	989	798 ± 24	–	–	–
M16-34	West	2/C	Thin dyke intruding M16-32	Betsiboka	-19.6107	46.53399	989	2511 ± 14	515 ± 7	–	–
M16-35	West	2/B	k-spar rich deformed dyke	Betsiboka	-19.6107	46.53399	989	2583 ± 26 2494 ± 14 (*)	502 ± 6	–	513 ± 18
M16-15	West	3/A	Orthogneiss	Betsiboka	-19.7239	46.62736	1067	2456 ± 17	492 ± 5	624 ± 152	528 ± 18
M16-16	West	3/B	Granite	Imorona-Itsindro	-19.7239	46.62736	1067	795 ± 24	498 ± 7	506 ± 82	499 ± 68
M16-17	West	3/C	Pegmatite veins, k-spar rich	Imorona-Itsindro	-19.7239	46.62736	1067	–	494 ± 7	526 ± 39	492 ± 51
M16-46	East	4/A	Orthogneiss	Betsiboka	-19.1599	47.51211	1351	2522 ± 8 543 ± 27 (#)	497 ± 15	604 ± 211	512 ± 24

M16-47	East	4/B	Undeformed cross-cutting granite	Imorona-Itsindro	-19.1599	47.51211	1351	798 ± 48 532 ± 44 (#)	–	657 ± 98	–
M16-45	East	5	Fine-grained granite	Ambalavao	-19.0869	47.54429	1312	543 ± 18	507 ± 35	–	512 ± 16
M16-52	East	6/A	Grey granite, very weakly foliated	Ambalavao	-18.589	47.23721	1359	568 ± 16	484 ± 14	527 ± 51	511 ± 16
M16-53	East	6/B	Cross-cutting pink granite	Ambalavao	-18.589	47.23721	1359	c. 568	500 ± 10	537 ± 35	521 ± 18

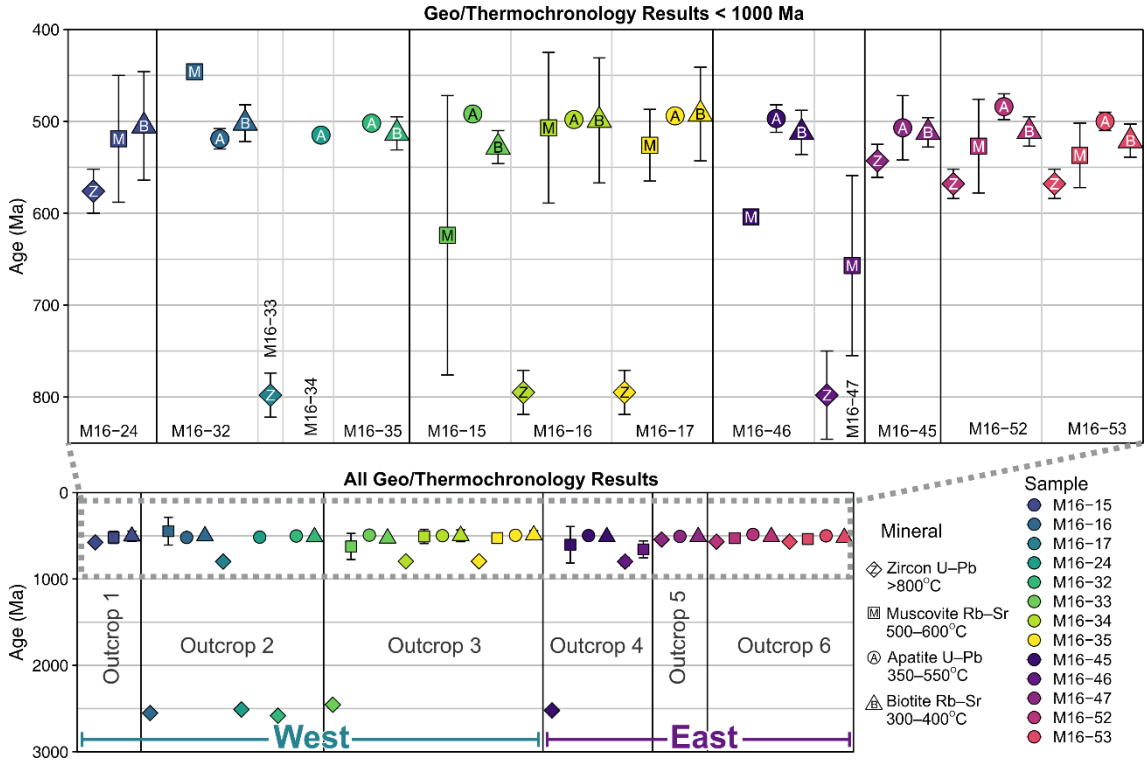

Figure 4.3 Summary of geo/thermochronology data for each sample and outcrop collected in this study. Error bars are 2σ. Sample locations shown in Figure 4.2. The bottom figure shows all of the sample data collected, and the top image zooms in on all data that are younger than 1000 Ma.

3. Structural geology methods

3.1. Remote sensing methods

We used high resolution aerial imagery and Landsat 8 data to define the structural framework for the study area (Figure 4.5). Structural trends and lithological boundaries were delineated from the ESRI world imagery basemap and Landsat 8 data in ArcGIS. Examples of Landsat images and bands used as well as our structural interpretation are documented in Appendix 4.4. Structures in the Itremo Group are easily identifiable due to relatively low vegetation cover and a strong contrast between quartzites and other rock types. Faults were defined by small offsets in lithologies or as large linear features. Lithologies were identified by similar signals in Landsat data and aerial imagery and

boundaries were determined accordingly. Following the identification of major rock packages, lithological trends (S1, S2 etc.) and faults, we were able to identify fold interference patterns and interpret the major deformation events responsible for producing these poly-deformed folds.

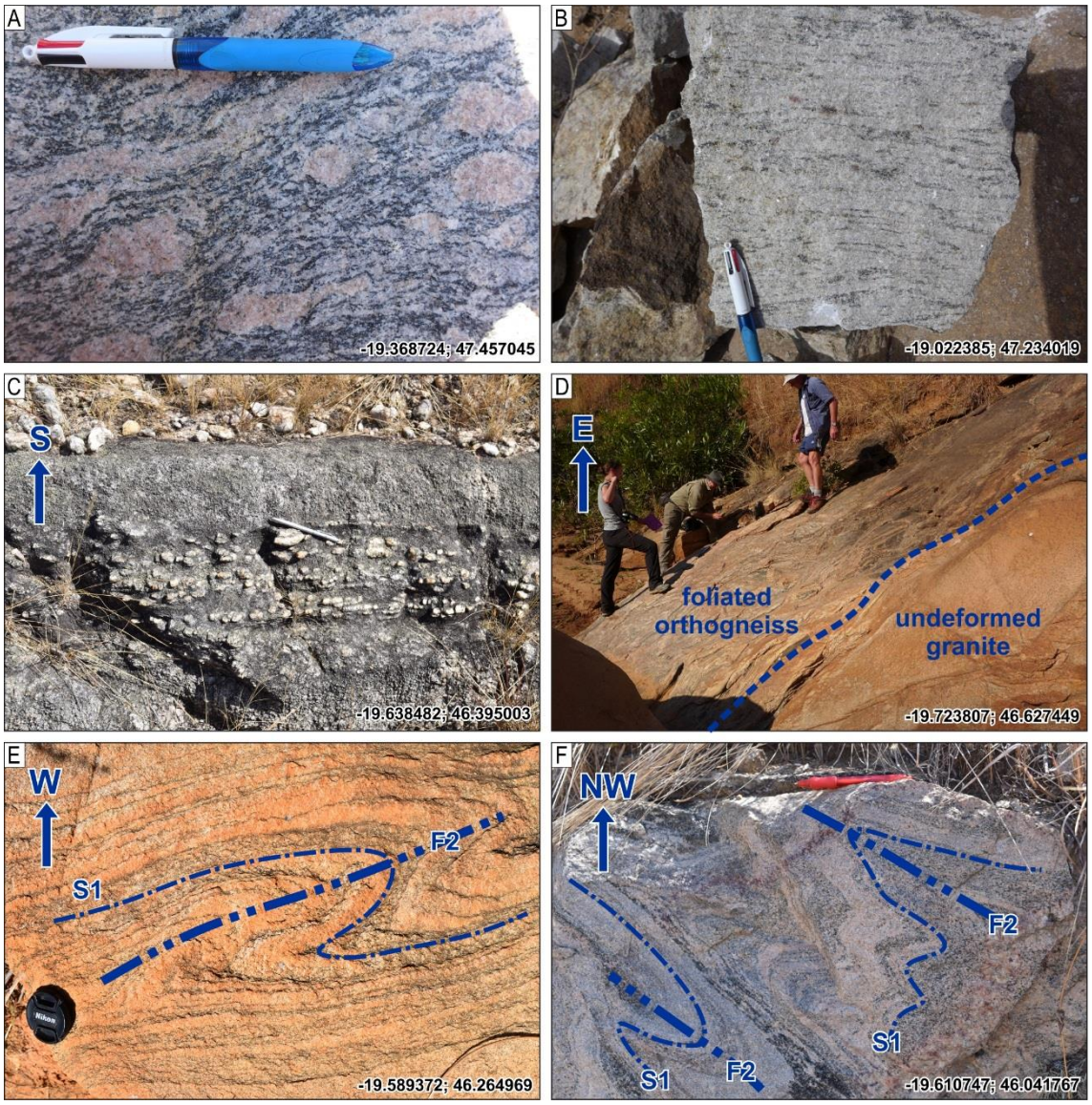

Figure 4.4 Examples of samples and field outcrops; latitude and longitude given in lower right corner and shown in Figure 4.2; a) S1 foliation in a sample of augen gneiss of the Betsiboka Suite in the Antananarivo Domain, b) S1 foliation in a sample of gneiss from the Antananarivo Domain, west of Antananarivo, c) flattened conglomerate where S1 is parallel to S0 in the Itremo Group of the Itremo Domain, d) outcrop of foliated gneiss (left) intruded by undeformed granite (right), e) S1 foliation folded around an F2 fold in the Itremo Domain, and f) S1 foliation folding around F2 folds in the Itremo Domain. Locations of field photos shown in Figure 4.2.

3.2. Field methods

Several hundred structural measurements were taken from over 70 localities. Data collected by the Council for Geoscience during the World Bank project in Madagascar were also used, which contains measurements for bedding and foliation (Macey et al., 2009). We additionally georeferenced geological maps (Moine, 1968; Service Géologique de Madagascar, 1962, 1963a, b) and extracted structural readings. Based on broad lithological and structural styles across the region, we have divided the study area into three sections. The Ikalamavony transect was conducted along the ~east–west road between Miandrivazo and the boundary of the Ikalamavony Domain (Figure 4.5), the Itremo section was conducted along the same road from the Ikalamavony-Itremo boundary toward the east approximately 50 km. The strike of S1 fabrics interpreted from remotely sensed data very closely match those measured at outcrops, we can therefore be confident that our interpretation of S1 structures from remotely sensed data is reliable.

4. Structure of central Madagascar

Large-scale structures, fold interference patterns, faults and shear zones are recognisable in remotely sensed data in the region west of Antsirabe (Figure 4.2). East of Antsirabe, polydeformed folds are no longer observed and the structural style changes significantly. We have delineated this as a 'structural style boundary' in Figure 4.2. The Itremo Nappes in the Itremo Domain have been investigated extensively due to their prominence in remotely sensed data and availability of outcrops (Collins et al., 2003b; Tucker et al., 2007). Here we further extend these interpretations to the Ikalamavony Domain, where identification of lithostratigraphy from remotely sensed data is more difficult, and interpretation is less straightforward. We have integrated our new interpretation from remotely sensed data with new 1:100,000 mapping and available structural data (Macey et al., 2009), to interpret the deformation history of the Ikalamavony, Itremo and Antananarivo (sub)domains.

We have constructed several cross-sections of the three central Madagascan domains and key type 2 fold interference patterns (Figure 4.5, Figure 4.6, Figure 4.7, Figure 4.8). We used the QGIS qProf plugin to construct cross-sections. Structural data within ~2 km of the section were included and projected onto the profile. The Africa Digital Elevation Model (30 m resolution) was used to construct the topographic profile.

4.1. Ikalamavony Domain

The Ikalamavony Domain contains metasedimentary rocks of the Ikalamavony Group, which are dominated by paragneiss, schist, quartzite and amphibolite. Generally these are finer grained than the Itremo Group. We observe many of the gneisses with bands of mylonite, indicating a high strain environment. Unique to the Ikalamavony Domain is the

Dabolava Suite, which is composed of granitic to gabbroic orthogneiss (Archibald et al., 2017a). The Dabolava Suite and the age-equivalent Ikalamavony Group have been interpreted as an oceanic arc terrane (Archibald et al., 2017a). The terrane must have accreted prior to the intrusion of the c. 850–750 Ma Imorona-Itsindro Suite, which intrudes the Ikalamavony, Itremo and Antananarivo domains—placing a minimum age on the juxtaposition of the three central Madagascan domains.

4.1.1. D1 Deformation

The first recognisable deformation event at the outcrop scale is defined by a pervasive foliation observed in orthogneisses, paragneisses and metasedimentary rocks. In orthogneisses and paragneisses, the foliation is typically defined by the elongation and alignment of biotite, feldspar and quartz. In metasedimentary rocks such as schist and paragneiss, the foliation is commonly defined by the orientation of biotite crystals and biotite rich layers. Primary sedimentary features such as bedding were difficult to recognise due to significant metamorphism and recrystallisation.

In remotely sensed data, linear or curvilinear trends such as ridges, are interpreted as being representative of the S1 foliation. Quartzite units in particular, which are less common than in the Itremo Domain, are easy to recognise in remotely sensed data due to the large contrast in different Landsat bands (e.g. Figure 4.7). In the Ikalamavony Domain the orientation of measured S1 foliations is dominantly northwest trending, and lineations and fold axes plunge moderately toward the west.

4.1.2. D2 Deformation

D2 deformation is most easily identifiable from remotely sensed data due to the large scale (>1 km) wavelength of folds. F2 antiforms and synforms are identifiable by the repetition of mapped geological units and constrained by structural measurements. D2 is defined by tight to isoclinal folds with axial traces approximately parallel to S1 in fold limbs. At the outcrop scale we observe these as decimetre- to metre-scale asymmetric, tight to isoclinal folds. F2 folds are similar-type folds, with thickened hinge zones and thinned limbs. An axial planar foliation is difficult to recognise in outcrops, but sometimes occurs as the alignment of biotite in hinge zones. Due to the isoclinal nature of folding, F2 axial traces are approximately parallel to S1 at the regional scale. F2 folds have been subsequently deformed during D3 and D4, however their original orientation would have been preserved with ~east-west striking axial traces.

4.1.3. D3 Deformation and associated fold interference patterns

We do not observe evidence for a third generation deformation event at the outcrop scale, however D3 folds are recognisable in remotely sensed data. The folding of F2 folds during D3 has produced a series of fold interference patterns similar to those in the Itremo Domain. Type 1 and type 2 fold interference patterns are observed in remotely sensed data (Figure 4.7). Type 1 folds occur when an upright folding event is overprinted by an orthogonal upright folding event (Grasemann et al., 2004). Type 2 fold interference

patterns occur when a recumbent folding event is orthogonally overprinted by an upright folding event (Grasemann et al., 2004) and is expressed in Figure 4.7. We therefore interpret D3 as the result of ~northeast-southwest shortening (present day orientation). Cross-section Ik–Ik' (Figure 4.7) has F2 folds that are very tight to isoclinal, with axial traces approximately parallel to F3 in F3 fold limbs. This formed by ~southeast-directed recumbent folding that was overprinted by a north to northwest trending F3 fold.

4.1.4. D4 Deformation

The axial traces of F3 folds vary across the Ikalamavony Domain, indicating a fourth generation of deformation. For example the F3 fold axes vary from northwest-trending in the west near Miandrivazo (e.g. the cross-section in Figure 4.7c), and curve to become north- to northeast-trending in the eastern side of Figure 4.7. We suggest this is caused by large wavelength (~30–50 km), F4 open folding with approximately east-west shortening. This event may have occurred in the late stages of folding and thrusting of the Itremo sub-domain and Ikalamavony Domain, or may be related to far-field deformation associated with orogenesis in eastern Madagascar (Collins et al., 2003a).

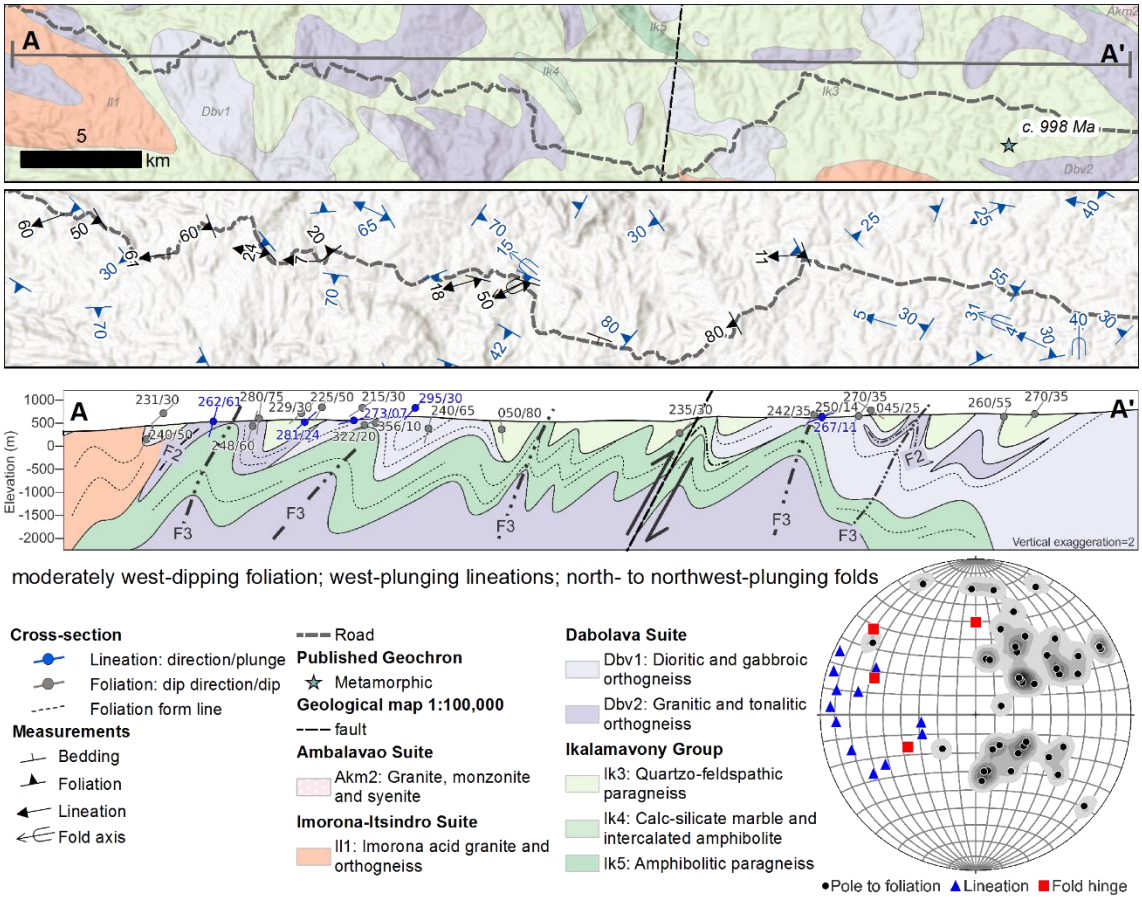

Figure 4.5 Geological map, structural data and cross-section through the Ikalamavony Domain. In this transect foliations are moderately west-dipping; lineations are west-plunging, and folds plunge toward north to northwest.

4.2. Itremo-Antananarivo Domain

The Itremo Group is a continental marginal sequence deposited on basement rocks of the Antananarivo Domain (e.g. Cox et al., 1998; 2004). Therefore, we consider these 'domains' together. Transect B–B' (Figure 4.6) contains metasedimentary rocks of the Itremo Group, which are dominantly quartzites, marbles and schists, with minor conglomerates. The majority of quartzites that we observe are strongly recrystallised and it is often difficult to recognise primary sedimentary features. The Itremo Group overlies the Archean Betsiboka Suite and was intruded by the c. 850–750 Ma Imorona-Itsindro Suite, after early deformation (Collins et al., 2003b). Together, these suites of rocks underwent a complex deformation history that must post-date the intrusion of the Imorona-Itsindro Suite.

4.2.1. D1 Deformation

In remotely sensed data, D1 structures are prominent features. Quartzite units in particular are easy to recognise in remotely sensed data due to the large contrast in different Landsat bands (e.g. Figure 4.7). The orientation of S1 is variable in the Itremo sub-domain due to the abundance of poly-deformed folds. Similar to the Ikalamavony Domain, foliations trend dominantly north-northwest, with lineations and fold axes plunging moderately toward the west.

Like the Ikalamavony Domain, the first generation foliation at the outcrop scale is typically defined by the elongation and alignment of biotite, feldspar and quartz in orthogneisses and paragneisses. In metasedimentary rocks such as quartzites and marbles, the foliation is sometimes defined by the orientation of biotite crystals and biotite rich layers, but is often difficult to recognise due to significant recrystallisation of quartz and a lack of other minerals. Primary sedimentary features such as bedding were difficult to recognise in quartzites due to significant recrystallisation. Within the quartzite packages, there are several conglomerate units with large (up to ~5 cm) pebbles (Figure 4.4c). Here we observe S0 as the interbedded pebble layers, and S1 as the flattening of pebbles.

4.2.2. D2 Deformation

Identical to the Ikalamavony Domain, D2 is defined by tight to isoclinal folds with axial traces approximately parallel to S1 in fold limbs. At the outcrop scale we observe these as decimetre- to metre-scale asymmetric, tight to isoclinal folds (Figure 4.4e,f). F2 folds are similar-type folds, with thickened hinge zones and thinned limbs. F2 axial traces are approximately parallel to S1 at the regional scale. F2 folds are recognisable in remotely sensed data as ~500–1000 m wavelength, tight to isoclinal folds.

F2 folds have been subsequently deformed during D3 and D4, however their original orientation would have been preserved with ~east-west striking axial traces. Further south where structures are more north-south trending, Tucker et al. (2007) interpreted east or

south-east directed vergence from these fold trends. We suggest both the east to south-east vergence outlined in Tucker et al. (2007), as well as the ~south to southwest-directed vergence identified in this study, developed as a result of ~northeast-southwest shortening (present day orientation).

4.2.3. D3 Deformation and associated fold interference patterns

Similar to the Ikalamavony Domain, we do not observe evidence for a third generation deformation event at the outcrop scale, however D3 folds are recognisable in remotely sensed data. The majority of F3 fold axial traces are ~north-south striking, and orthogonally overprint F2 folds. We therefore interpret D3 as a ~east-west shortening event. The folding of F2 folds during D3 has produced a series of fold interference patterns. Type 2 fold interference patterns are observed in remotely sensed data in the Itremo Domain (Figure 4.7). Type 2 fold interference patterns occur when a recumbent folding event is orthogonally overprinted by an upright folding event (Grasemann et al., 2004) and is expressed in both examples in Figure 4.7.

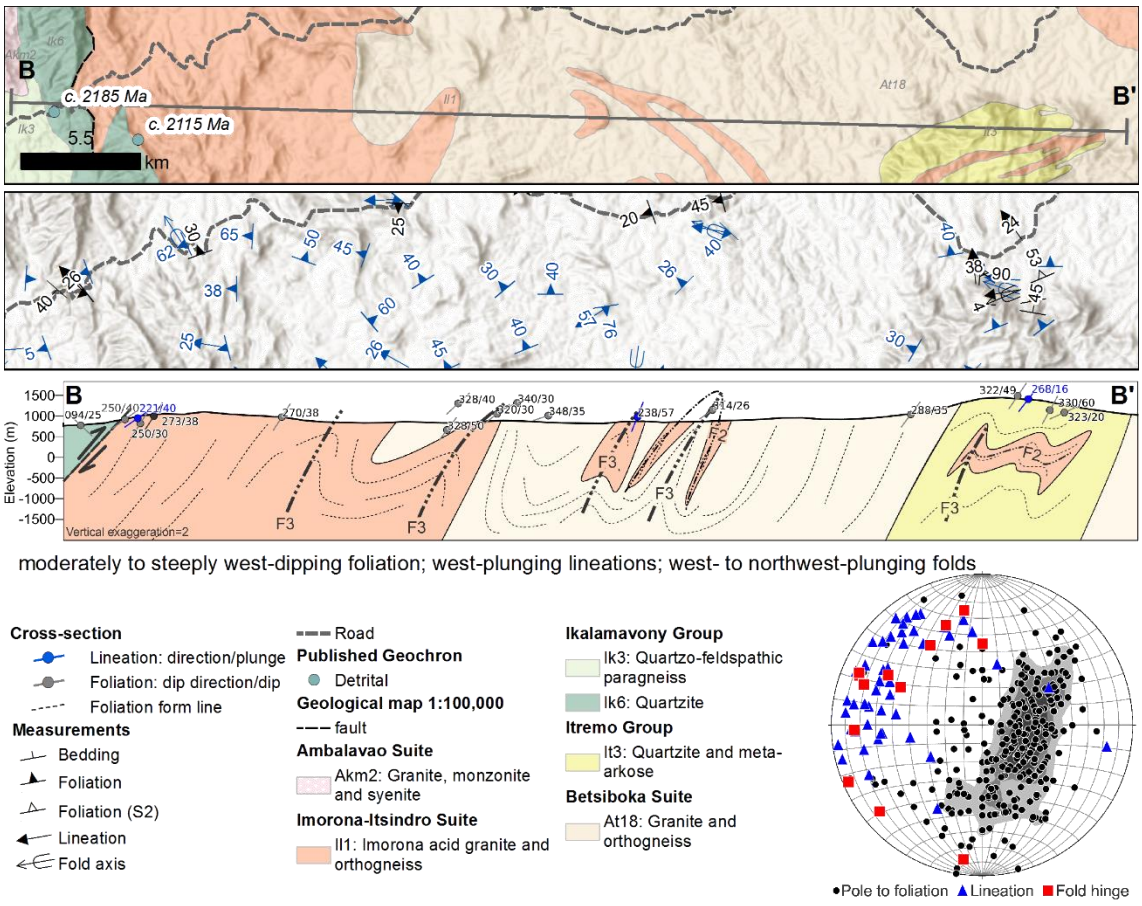

Figure 4.6 Geological map, structural data and cross-section through the Itremo-Antananarivo domain. Similar to the Ikalamavony transect, the Itremo transect contains moderately to steeply west-dipping foliations, west-plunging lineations and west to northwest-plunging folds.

Cross-section It–It' in Figure 4.7 represents a type 2 fold interference pattern. Armistead et al. (2018) modelled a structure of very similar geometry and orientation, and showed that this type of feature formed from south-directed, tight, recumbent folding that was orthogonally overprinted by third generation upright folding. In our example from the Itremo Group, the F2 recumbent folding formed during south to slightly south-west directed folding that locally formed by ~north-south shortening. The overprinting F3 upright fold formed during ~east-west shortening that resulted in a north to north-east trending axial trace. These interpreted kinematics are consistent with previous interpretations for deformation in the Itremo Group (Collins et al., 2003b; Tucker et al., 2007).

Adding to the complexity of the structure in It–It' is the juxtaposition of older units (the Archaean Betsiboka Suite) structurally above younger units (Paleoproterozoic Itremo Group). Tucker et al. (2007) observed that the km-scale fold and thrust nappes (our interpreted D2), resulted in the inversion and repetition of Archaean and Proterozoic rocks. This interpretation accounts for why the It–It' section contains older units that appear structurally above younger units.

4.2.4. D4 Deformation

The axial traces of F3 folds vary across the Ikalamavony, Itremo and Antananarivo regions, as we have shown in the examples of It–It' and Ik–Ik' above. The trend of structures vary from the northwest of central Madagascar near Miandrivazo, to the southeast of the study area along the eastern margin of the Itremo Group (Figure 4.2). Near Miandrivazo (e.g. Figure 4.5), D3 axial traces generally trend northwest-southeast. In the Itremo Group and further to the south, these structures are generally north-south trending. This trend broadly follows the curve of our transect boundary line between the western and eastern transects delineated in Figure 4.2. This regional variation may relate to D4 deformation or may relate to orogenic bending as orogenesis progressed.

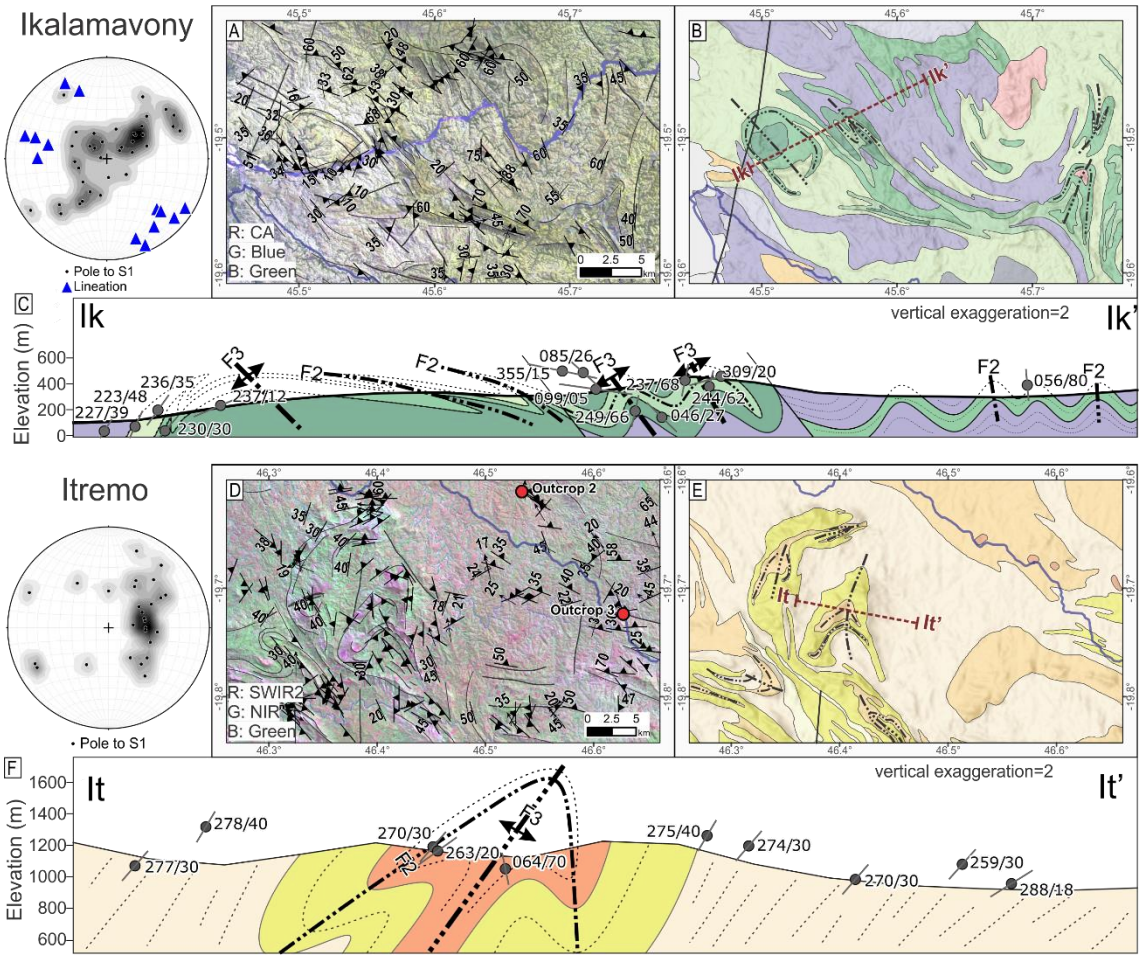

Figure 4.7 Examples of poly-deformed folds in the Ikalamavony and Itremo domains. Ik–Ik': an example of type 2 fold interference patterns with north-west trending third generation upright folds. It–It': an example of a type 2 fold interference pattern with D2 south-directed recumbent folding overprinted by a F3 north to north-east trending upright fold. Geological polygons from Council for Geosciences 1:100000 mapsheets (Macey et al., 2010). Sections generated using QProf plugin in QGIS. Structural measurements (dip direction/dip) within ~2km of the section are projected along the profile. Topographic profile derived from 30 arc-second DEM of Africa (USGS). Legend for geological units is the same as Figure 4.5 and Figure 4.6.

4.3. Antananarivo Domain

Precambrian outcrop near Antsirabe is scarce due to the widespread coverage of the Ankaratra Volcanics. Generally, deformation in this area is much less intense than the Ikalamavony Domain and Itremo sub-domain, and we observe fewer deformation events. Here we only identify a primary foliation (S1), with no later deformation events recognised. Deformation becomes more intense further east, along the road west of Antananarivo where Collins et al. (2003a) have described at least four phases of deformation.

4.3.1. D1 Deformation

Much like the western transect, at the outcrop scale we observe a pervasive foliation within the Betsiboka Suite, which we interpret as an S1 foliation. The foliation is commonly preserved by the alignment of biotite, feldspar and quartz in orthogneisses. Structural measurements from Service Géologique de Madagascar (1963a) and Service Géologique de Madagascar (1963b) indicate that S1 foliations between Antsirabe and Antananarivo dominantly strike ~north-northeast, with dips moderately to the west (Figure 4.8). North of Antananarivo, S1 is more variable, and folded following the Antananarivo virgation zone (e.g. Nédélec et al., 2000).

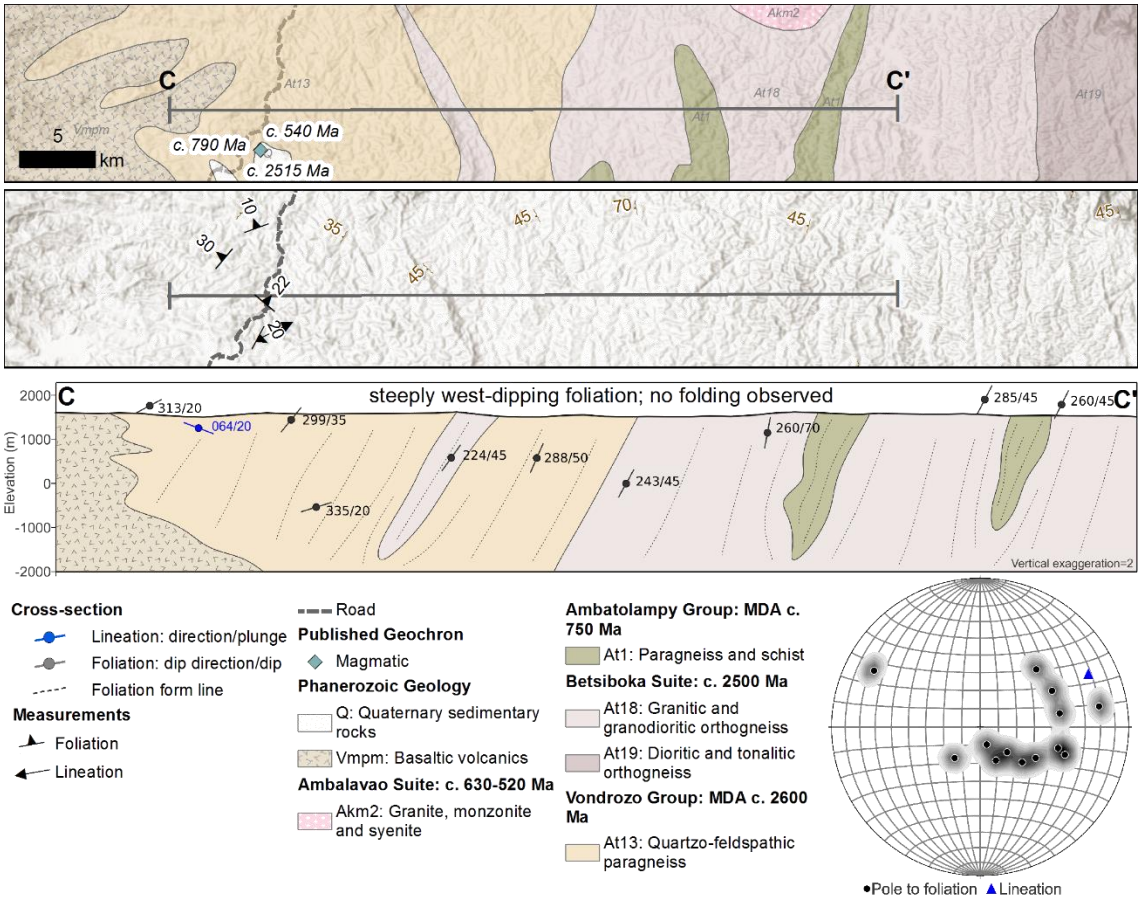

Figure 4.8 Geological map, structural data and cross-section through the Antananarivo Domain. This transect does not contain the complex folding that we observe in the Ikalamavony and Itremo domains. Here, foliations are steeply west-dipping.

4.4. Regional variation in deformation

Complex fold interference patterns are widespread throughout the Ikalamavony Domain and Itremo sub-domain (incorporating parts of the Betsiboka Suite). Tucker et al. (2007) proposed that complex folds in the Itremo sub-domain can be broadly considered in two groups; “high-grade, internal nappes” and “low-grade, external nappes.” These were

considered to be separated by a west-dipping thrust fault, although the exact location of this boundary is ambiguous from the highly schematic diagrams presented in that study. We broadly agree that metamorphic grade and deformation intensity appears to increase toward the west, however a sharp tectonic boundary hasn't been observed in this study within the Itremo Group. We do however see a major tectonic boundary between the Ikalamavony Domain and the Itremo/Antananarivo Domain. This boundary may more accurately reflect the boundary between the internal and external nappes proposed by Tucker et al. (2007).

Deformation intensity appears to weaken toward the east of the Itremo sub-domain, with an absence of complex fold interference patterns between Antsirabe and Antananarivo. The Imorona-Itsindro Suite in particular becomes progressively less deformed to the east. In the west, the Imorona-Itsindro Suite is folded into fold interference patterns, whereas in the east it only appears to be folded into weakly-defined F3 folds. This is consistent with our sampling of c. 850–750 Ma rocks along this weakly deformed margin (along the main road in Figure 4.2), where rock samples appear undeformed or very weakly deformed. Other authors have interpreted these rocks as strongly deformed further to the south (e.g. Archibald et al., 2016), where we and others have interpreted poly-deformed folds. Together with the observation that deformation and metamorphic grade increases toward the west in the Ikalamavony Domain, this implies that the tectonic event responsible for complex deformation in central Madagascar is focussed west of the study area, and its effects become less intense toward the east.

Constraining the timing of deformation within the Imorona-Itsindro Suite is particularly important due to its age (c. 850–750 Ma). Due to an intrusive contact between the Imorona-Itsindro Suite and surrounding rocks, it is difficult to determine whether the Imorona-Itsindro Suite underwent all phases of deformation, or whether it was intruded after the earliest D1 phase.

To the east of the Antananarivo–Antsirabe road (Figure 4.2; Figure 4.8), there is a distinct change in structural trend. In the Ikalamavony and Itremo Domains, structures dominantly trend northwest. North of Antananarivo, structures trend ~west (near samples M16-52 and M16-53), and between Antananarivo and Antsirabe (Figure 4.8) structures trend north or north-east. These structures were studied in detail in Collins et al. (2003a); Nédélec et al. (2000); Raharimahefa and Kusky (2006, 2009); Raharimahefa et al. (2013). The intensity of these structures increases toward the east, with at least four phases of deformation recognised resulting from the Betsimisaraka Suture in eastern Madagascar.

5. Discussion

5.1. Structural evolution of central Madagascar

The structural style of the Ikalamavony and Itremo domains are indistinguishable, and we suggest that they were deformed together in the same orogenic system. Type 1 and Type 2 fold interference patterns are common in fold-and-thrust belts, and more commonly form during progressive deformation rather than discrete deformation events. A myriad of complex processes ranging from rheological contrasts to progressive rotation during deformation, can cause fold structures with trends that are oblique to the transport direction of the overall fold-and-thrust belt (e.g. Poblet and Lisle, 2011). Therefore, we suggest that D2 and D3 in the Ikalamavony Domain and Itremo sub-domain formed during the same orogenic event, through progressive deformation, consistent with the interpretation based on metamorphism in this region by Moine et al. (2014).

As pointed out in Tucker et al. (2007), nappes in the southern Itremo Domain are east-verging and were likely produced within a zone of west-dipping subduction (present day direction). We interpret structures in our study areas of the Ikalamavony and Itremo Domains to be dominantly north-west trending, with northeast directed vergence. We propose that a subduction zone southwest of the Ikalamavony Domain and Itremo sub-domain was ~southwest-dipping, and was responsible for deformation in central Madagascar. Direct evidence for a suture in this region (e.g. obducted ophiolite sequences) has not been observed, however this zone separates terranes that have distinct geological histories and so a suture is a reasonable interpretation.

The boundaries between the major domains in southern Madagascar represent possible suture zones responsible for deformation in the Ikalamavony Domain and Itremo sub-domain. Boger et al. (2014); (2019) suggested that the Beraketa high strain zone that separates the Anosyen and Androyen domains represents a c. 580–520 Ma suture. The west-dipping c. 650 Ma Vohibory Suture (Figure 4.11), which separates the Vohibory Domain from the Androyen Domain, is also a possible suture responsible for deformation. Based on our observation that the c. 580–520 Ma Ambalavao Suite is undeformed in central Madagascar, the orogenic event must pre-date these magmatic rocks—therefore we suggest that the c. 650 Ma Vohibory Suture was responsible for complex deformation in the Ikalamavony and Itremo domains.

In the eastern part of the study area, east of the 'structural style boundary' in Figure 4.2, the deformation style changes in orientation and intensity. Our transect C–C' is less deformed than the Ikalamavony and Itremo transects, and we do not observe any complex folding here. The orientation of structures also change, and become more north to north-east trending. Further east of our C–C' transect is the dextral Angavo Shear Zone, which was active at c. 550 Ma (Raharimahefa and Kusky, 2010). Collins et al. (2003a) constructed a cross-section from Antananarivo eastwards to Brickaville along the east

coast of Madagascar. This transect region contains a deformation sequence distinct from the Ikalamavony and Itremo domains and was therefore caused by a different tectonic event. Although controversial, there is significant metamorphic and structural evidence that the sequence of deformation described by Collins et al. (2003a) can be attributed to the c. 550 Ma Betsimisaraka Suture that amalgamated Madagascar with the Dharwar Craton of India.

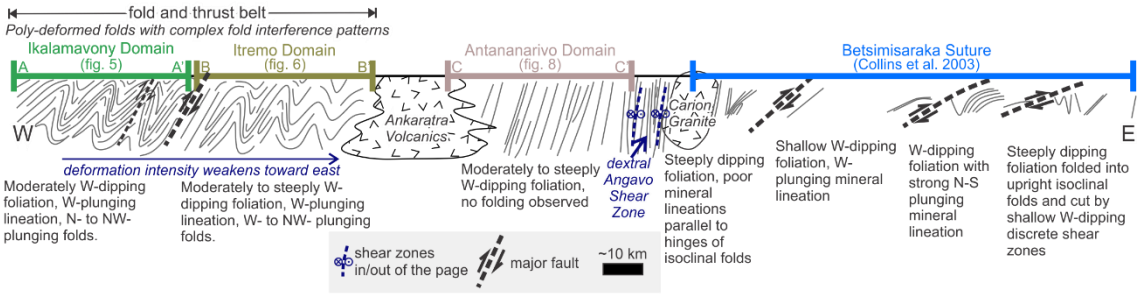

Figure 4.9 Schematic cross-section through central Madagascar from Miandrivazo to Brickaville, combining our new structural study with that of Collins et al. (2003a). The Ikalamavony and Itremo domains preserve the same structural styles and kinematics. A change in structural style occurs east of these sections, with the Antananarivo Domain section containing no complex fold interference patterns. Further east, Collins et al. (2003a) interpret intense deformation associated with the Neoproterozoic–Cambrian Betsimisaraka Suture.

5.2. Temporal constraints on deformation

5.2.1. Relative timing of deformation

Understanding the ages of geological units that are deformed and undeformed can help constrain the timing of deformation. At the regional scale in the western transect, the c. 850–750 Ma Imorona-Itsindro Suite is poly-deformed, and therefore was intruded prior to the onset of at least D2 and D3. In the eastern transect and in the region studied by Collins et al. (2003a); Nédélec et al. (2000); Raharimahefa and Kusky (2006, 2009), the Imorona-Itsindro Suite is not poly-deformed into complex fold interference patterns but instead is elongated along the length of the c. 550 Ma Angavo shear zone (Figure 4.2). This suggests that different structural regimes are responsible for deformation in the west and east of Madagascar.

In the Ikalamavony Domain and Itremo sub-domain, the c. 550 Ma Ambalavao Suite is undeformed and, therefore, provides a minimum age constraint on deformation here. In the east, the Ambalavao Suite is represented by both deformed and undeformed rocks. We therefore suggest that deformation in the Ikalamavony Domain and Itremo sub-domain occurred between c. 750 and c. 550 Ma, which is consistent with interpretations by Tucker et al. (2007). Deformation in eastern Madagascar likely occurred later at c. 550 Ma, which is consistent with age determinations for the Angavo Shear Zone and Antananarivo virgation zone (Meert et al., 2003; Nédélec et al., 2000; Paquette and Nédélec, 1998; Raharimahefa and Kusky, 2010).

5.2.2. Thermochronology

We have used minerals that record a range of temperatures in an attempt to capture different stages of the tectonic evolution of Madagascar. Our sampling included the major magmatic suites of Madagascar, including the c. 2500 Ma Betsiboka Suite, the c. 850–750 Ma Imorona-Itsindro Suite, and the c. 550 Ma Ambalavao Suite (Figure 4.3). Interestingly, apatite U–Pb ages—which record the age the minerals were cooled through ~350–550°C (Chamberlain and Bowring, 2001; Schoene and Bowring, 2007)—are all c. 500 Ma regardless of their magmatic crystallisation age. Muscovite and biotite, which have Rb–Sr closure temperatures of ~500–600°C (Armstrong et al., 1966) and ~300–400°C (Del Moro et al., 1982; Jenkin et al., 2001; Verschure et al., 1980), respectively, also record ages of c. 500 Ma. This implies that the final stages of orogenesis in Madagascar, regardless of whether this was in the west or east, affected the entire central region of the island, where rocks were heated to at least ~500°C.

Multiple thermochronometers have provided insights into the medium-temperature thermo-tectonic evolution across the western and eastern part of Madagascar. As we have shown here, the more recent c. 550–500 Ma thermo-tectonic event affected the entire island such that it cooled synchronously through ~500–300°C at c. 500 Ma. The c. 550–500 Ma regional thermal perturbation would have overprinted prior events, obscuring any evidence of a pre-existing thermo-tectonic evolution. Using thermochronometers that record temperatures higher than ~600°C (e.g. monazite U–Pb) in future research may be able to provide further constraints on the timing of orogenesis, particularly in the distal regions, where temperatures during the c. 550 Ma event may not have been hot enough to cause complete reset. Without direct dating of the structures observed, we need to look further afield for evidence of subduction and collision that resulted in deformation of central Madagascar.

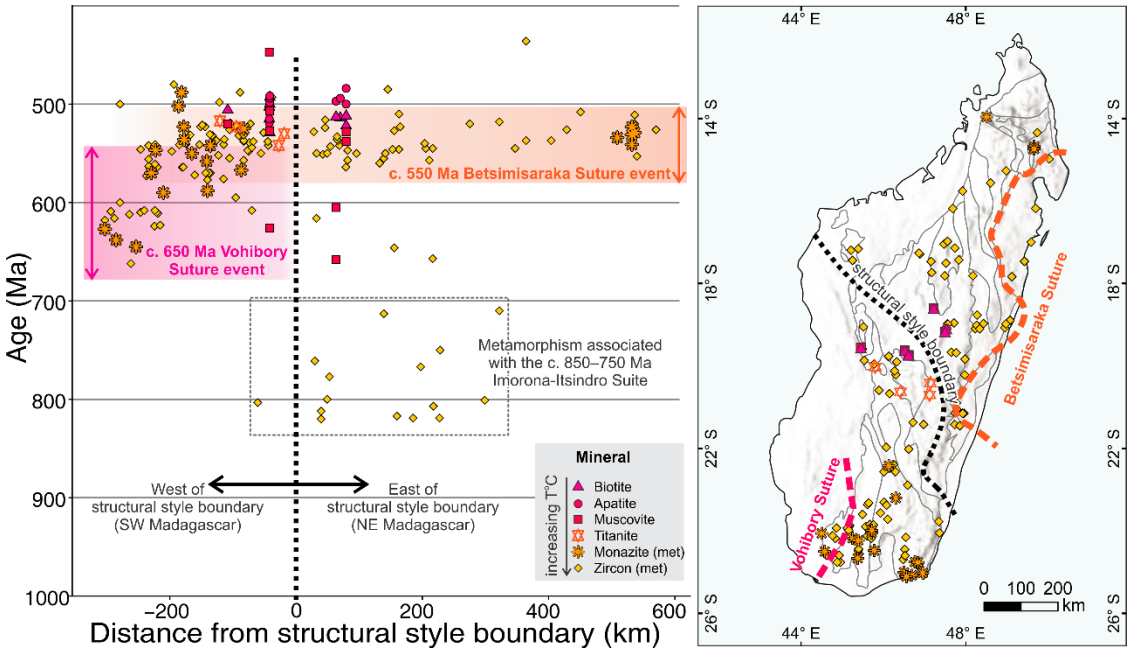

Figure 4.10 Summary of new thermochronology data and published metamorphic data. Biotite, apatite and muscovite are from this study. Metamorphic minerals zircon, monazite and titanite are from the compilation of Tucker et al. (2014). Locations of data points shown in the map to the right, terranes are the same as those from Figure 4.1b.

5.3. Tectonic model for the evolution of central Madagascar

Prior to the juxtaposition of the Itremo sub-domain and Ikalamavony Domain, we agree with previous interpretations that the Itremo Group was deposited on the Antananarivo Domain basement (Cox et al., 1998; 2004) and that the Ikalamavony Domain evolved as an exotic island arc terrane (Archibald et al., 2017a). The presence of the Imorona-Itsindro Suite in the Ikalamavony Domain suggests that it must have accreted to central Madagascar before c. 850 Ma (Figure 4.11c). A large west-dipping thrust fault separating the Ikalamavony Domain from the Itremo sub-domain (Figure 4.6), possibly represents this suture zone (schematic thrust in Figure 4.11c). This implies west-dipping subduction, which is consistent with previous models for the accretion of the Ikalamavony Domain to central Madagascar (e.g. Boger et al., 2019).

Based on the interpreted kinematics and overprinting relationships, deformation of the Ikalamavony Domain and Itremo sub-domain was the result of west-dipping subduction. Increasing deformation intensity in the Ikalamavony Domain and the orientation of structures imply that this subduction zone must have lain southwest of these domains. Based on cross-cutting relationships, the timing of deformation is constrained between c. 750 and c. 550 Ma. We suggest this was in response to the Vohibory Suture (Figure 4.11e).

A change in deformation style and kinematics toward the east of Madagascar and younger geochronological constraints, indicate that complex folding in eastern Madagascar

formed in response to a different event than that in the west (Figure 4.11g). Based on structural kinematics, this event was west-dipping, and was likely related to the c. 550 Ma Betsimisaraka Suture (Collins et al., 2003a).

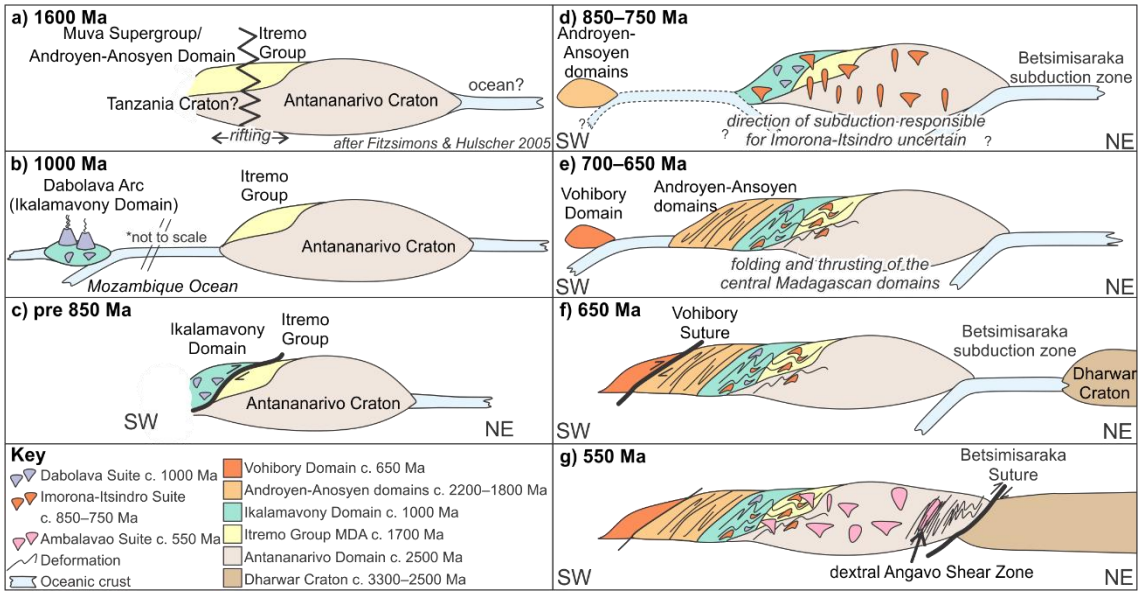

Figure 4.11 Schematic diagram showing our interpretation of the evolution of central Madagascar. a) Sometime after the deposition of the Itremo Group/Muva Supergroup onto the Antananarivo Craton/Tanzania Craton, these regions begin to rift (Cox et al., 2004; Fitzsimons and Hulscher, 2005); b) at c. 1000 Ma the Dabolava Arc forms as an oceanic island arc outboard from the Antananarivo Domain (Archibald et al., 2017a); c) prior to the intrusion of the c. 850–750 Ma Imorona-Itsindro Suite, the Ikalamavony Domain is thrust over the Antananarivo/Itremo Domain; d) the intrusion of the Imorona-Itsindro Suite resulting from Andean-type subduction, with polarity uncertain (Archibald et al., 2017b); e) west-dipping subduction beneath the Vohibory Domain, resulting in complex deformation that we have interpreted in central Madagascar; f) closure of the Mozambique ocean along the Vohibory Suture; and g) final amalgamation of central Gondwana along the c. 550 Ma Betsimisaraka Suture.

6. Conclusions

We have integrated structural analysis with medium-temperature thermochronology to constrain the timing of orogenic events in Madagascar. We observe complex fold interference patterns in both the Ikalamavony Domain and Itremo sub-domain. We suggest these formed in response to ~southwest-dipping subduction beneath the Vohibory Domain at c. 650 Ma. North-south trending structures in eastern Madagascar formed in response to the ~west-dipping c. 550 Ma Betsimisaraka Suture, which resulted in the emplacement of widespread granitic rocks and the resetting of medium-temperature minerals throughout much of central Madagascar. We have shown the importance of using medium-temperature thermochronometers such as U–Pb apatite to date the cooling stages post orogenesis, as well as the potential for Rb–Sr mica dating to provide useful thermochronological constraints.

References

Archibald, D.B., Collins, A.S., Foden, J.D., Payne, J.L., Holden, P., Razakamanana, T., De Waele, B., Thomas, R.J. and Pitfield, P.E.J., 2016. Genesis of the Tonian Imorona–Itsindro magmatic Suite in central Madagascar: Insights from U–Pb, oxygen and hafnium isotopes in zircon. Precambrian Research, 281: 312-337.

Archibald, D.B., Collins, A.S., Foden, J.D., Payne, J.L., Macey, P.H., Holden, P. and Razakamanana, T., 2017a. Stenian–Tonian arc magmatism in west–central Madagascar: the genesis of the Dabolava Suite. Journal of the Geological Society: jgs2017-028.

Archibald, D.B., Collins, A.S., Foden, J.D., Payne, J.L., Taylor, R., Holden, P., Razakamanana, T. and Clark, C., 2015. Towards unravelling the Mozambique Ocean conundrum using a triumvirate of zircon isotopic proxies on the Ambatolampy Group, central Madagascar. Tectonophysics, 662: 167-182.

Archibald, D.B., Collins, A.S., Foden, J.D. and Razakamanana, T., 2017b. Tonian Arc Magmatism in Central Madagascar: The Petrogenesis of the Imorona-Itsindro Suite. The Journal of Geology, 125(3): 000-000.

Armistead, S.E., Betts, P.G., Ailleres, L., Armit, R.J. and Williams, H.A., 2018. Cu-Au mineralisation in the Curnamona Province, South Australia: A hybrid stratiform genetic model for Mesoproterozoic IOCG systems in Australia. Ore Geology Reviews, 94: 104-117.

Armistead, S.E., Collins, A., Merdith, A.S., Payne, J.L., Cox, G.M., Foden, J.D., Razakamanana, T. and De Waele, B., 2019. Evolving marginal terranes during Neoproterozoic supercontinent reorganisation: constraints from the Bemarivo Domain in northern Madagascar. Tectonics.

Armistead, S.E., Collins, A.S., Payne, J.L., Foden, J.D., De Waele, B., Shaji, E. and Santosh, M., 2017. A re-evaluation of the Kumta Suture in western peninsular India and its extension into Madagascar. Journal of Asian Earth Sciences.

Armstrong, R.L., Jäger, E. and Eberhardt, P., 1966. A comparison of K-Ar and Rb-Sr ages on Alpine biotites. Earth and Planetary Science Letters, 1(1): 13-19.

BGS-USGS-GLW, 2008. Republique de Madagascar Ministère de L'engergie et des Mines (MEM/SG/DG/UCP/PGRM). British Geological Survey Research Report.

Boger, S.D., Hirdes, W., Ferreira, C.A.M., Jenett, T., Dallwig, R. and Fanning, C.M., 2015. The 580–520Ma Gondwana suture of Madagascar and its continuation into Antarctica and Africa. Gondwana Research, 28(3): 1048-1060.

Boger, S.D., Hirdes, W., Ferreira, C.A.M., Schulte, B., Jenett, T. and Fanning, C.M., 2014. From passive margin to volcano–sedimentary forearc: The Tonian to Cryogenian evolution of the Anosyen Domain of southeastern Madagascar. Precambrian Research, 247: 159-186.

Boger, S.D., Maas, R., Pastuhov, M., Macey, P.H., Hirdes, W., Schulte, B., Fanning, C.M., Ferreira, C.A.M., Jenett, T. and Dallwig, R., 2019. The tectonic domains of southern and western Madagascar. Precambrian Research.

Chamberlain, K.R. and Bowring, S.A., 2001. Apatite–feldspar U–Pb thermochronometer: a reliable, mid-range (~450°C), diffusion-controlled system. Chemical Geology, 172(1): 173-200.

Collins, A.S., 2006. Madagascar and the amalgamation of Central Gondwana. Gondwana Research, 9(1-2): 3-16.

Collins, A.S., Fitzsimons, I.C.W., Hulscher, B. and Razakamanana, T., 2003a. Structure of the eastern margin of the East African Orogen in central Madagascar. Precambrian Research, 123(2–4): 111-133.

Collins, A.S., Johnson, S., Fitzsimons, I.C., Powell, C.M., Hulscher, B., Abello, J. and Razakamanana, T., 2003b. Neoproterozoic deformation in central Madagascar: a structural section through part of the East African Orogen. Geological Society, London, Special Publications, 206(1): 363-379.

Collins, A.S., Kinny, P.D. and Razakamanana, T., 2012. Depositional age, provenance and metamorphic age of metasedimentary rocks from southern Madagascar. Gondwana Research, 21(2-3): 353-361.

Collins, A.S., Kröner, A., Fitzsimons, I.C.W. and Razakamanana, T., 2003c. Detrital footprint of the Mozambique ocean: U–Pb SHRIMP and Pb evaporation zircon geochronology of metasedimentary gneisses in eastern Madagascar. Tectonophysics, 375(1-4): 77-99.

Collins, A.S. and Pisarevsky, S.A., 2005. Amalgamating eastern Gondwana: The evolution of the Circum-Indian Orogens. Earth-Science Reviews, 71(3-4): 229-270.

Collins, A.S., Razakamanana, T. and Windley, B.F., 2000. Neoproterozoic extensional detachment in central Madagascar: implications for the collapse of the East African Orogen. Geological Magazine, 137(1): 39-51.

Collins, A.S. and Windley, B.F., 2002. The tectonic evolution of central and northern Madagascar and its place in the final assembly of Gondwana. The Journal of Geology, 110(3): 325-339.

Costa, R.L., Schmitt, R.S., Collins, A., Armistead, S.E., Razakamanana, T. and Archibald, D., Submitted. Tectonic evolution of an Early Cryogenian synmagmatic basin in central Madagascar. Precambrian Research.

Cox, R., Armstrong, R.A. and Ashwal, L.D., 1998. Sedimentology, geochronology and provenance of the Proterozoic Itremo Group, central Madagascar, and implications for pre-Gondwana palaeogeography. Journal of the Geological Society, 155(6): 1009-1024.

Cox, R., Coleman, D.S., Chokel, C.B., DeOreo, S.B., Wooden, J.L., Collins, A.S., De Waele, B. and Kröner, A., 2004. Proterozoic tectonostratigraphy and paleogeography of central Madagascar derived from detrital zircon U-Pb age populations. The Journal of geology, 112(4): 379-399.

De Waele, B., Thomas, R.J., Macey, P.H., Horstwood, M.S.A., Tucker, R.D., Pitfield, P.E.J., Schofield, D.I., Goodenough, K.M., Bauer, W., Key, R.M., Potter, C.J., Armstrong, R.A., Miller, J.A., Randriamananjara, T., Ralison, V., Rafahatelo, J.M., Rabarimanana, M. and Bejoma, M., 2011. Provenance and tectonic significance of the Palaeoproterozoic metasedimentary successions of central and northern Madagascar. Precambrian Research, 189(1-2): 18-42.

de Wit, M.J., Bowring, S.A., Ashwal, L.D., Randrianasolo, L.G., Morel, V.P.I. and Rambeloson, R.A., 2001. Age and tectonic evolution of Neoproterozoic ductile shear zones in southwestern Madagascar, with implications for Gondwana studies. Tectonics, 20(1): 1-45.

Del Moro, A., Puxeddu, M., di Brozolo, F.R. and Villa, I.M., 1982. Rb-Sr and K-Ar ages on minerals at temperatures of 300°–400° C from deep wells in the Larderello geothermal field (Italy). Contributions to Mineralogy and Petrology, 81(4): 340-349.

Emmel, B., Jons, N., Kroner, A., Jacobs, J., Wartho, J.A., Schenk, V., Razakamanana, T. and Austegard, A., 2008. From Closure of the Mozambique Ocean to Gondwana Breakup: New Evidence from Geochronological Data of the Vohibory Terrane, Southwest Madagascar. The Journal of Geology, 116(1): 21-38.

Fernandez, A., Schreurs, G., Villa, I.M., Huber, S. and Rakotondrazafy, M., 2003. Age constraints on the tectonic evolution of the Itremo region in Central Madagascar. Precambrian Research, 123(2-4): 87-110.

Fitzsimons, I.C.W. and Hulscher, B., 2005. Out of Africa: detrital zircon provenance of central Madagascar and Neoproterozoic terrane transfer across the Mozambique Ocean. Terra Nova, 17(3): 224-235.

Grasemann, B., Wiesmayr, G., Draganits, E. and Fusseis, F., 2004. Classification of refold structures. The Journal of geology, 112(1): 119–125.

Jenkin, G.R.T., Ellam, R.M., Rogers, G. and Stuart, F.M., 2001. An investigation of closure temperature of the biotite Rb-Sr system: The importance of cation exchange. Geochimica et Cosmochimica Acta, 65(7): 1141-1160.

Jöns, N., Emmel, B., Schenk, V. and Razakamanana, T., 2009. From orogenesis to passive margin—the cooling history of the Bemarivo Belt (N Madagascar), a multi-thermochronometer approach. Gondwana Research, 16(1): 72-81.

Jöns, N. and Schenk, V., 2008. Relics of the Mozambique Ocean in the central East African Orogen: evidence from the Vohibory Block of southern Madagascar. Journal of Metamorphic Geology.

Jöns, N. and Schenk, V., 2011. The ultrahigh temperature granulites of southern Madagascar in a polymetamorphic context: implications for the amalgamation of the Gondwana supercontinent. European Journal of Mineralogy, 23(2): 127-156.

Kröner, A., Hegner, E., Collins, A.S., Windley, B.F., Brewer, T.S., Razakamanana, T. and Pidgeon, R.T., 2000. Age and magmatic history of the Antananarivo Block, central Madagascar, as derived from zircon geochronology and Nd isotopic systematics. American Journal of Science, 300(4): 251-288.

Macey, P.H., Bisnath, A., Yibas, B., Robson, L. and Andriamanantsoa, E., 2009. Carte Geologique de Madagascar. Council for Geoscience, Pretoria, Afrique du Sud. 1:100,000.

Macey, P.H., Thomas, R.J., Grantham, G.H., Ingram, B.A., Jacobs, J., Armstrong, R.A., Roberts, M.P., Bingen, B., Hollick, L., de Kock, G.S., Viola, G., Bauer, W., Gonzales, E., Bjerkgård, T., Henderson, I.H.C., Sandstad, J.S., Cronwright, M.S., Harley, S., Solli, A., Nordgulen, Ø., Motuza, G., Daudi, E. and Manhiça, V., 2010. Mesoproterozoic geology of the Nampula Block, northern Mozambique: Tracing fragments of Mesoproterozoic crust in the heart of Gondwana. Precambrian Research, 182(1-2): 124-148.

Martelat, J.-E., Lardeaux, J.-M., Nicollet, C. and Rakotondrazafy, R., 2000. Strain pattern and late Precambrian deformation history in southern Madagascar. Precambrian research, 102(1-2): 1-20.

Meert, J.G., Nédélec, A. and Hall, C., 2003. The stratoid granites of central Madagascar: paleomagnetism and further age constraints on neoproterozoic deformation. Precambrian Research, 120(1-2): 101-129.

Merdith, A.S., Collins, A.S., Williams, S.E., Pisarevsky, S., Foden, J.D., Archibald, D.B., Blades, M.L., Alessio, B.L., Armistead, S. and Plavsa, D., 2017. A full-plate global reconstruction of the Neoproterozoic. Gondwana Research, 50: 84-134.

Moine, B., 1968. Massif Schisto-Quartzo-Dolomitique: Reion d'Ambatofinandrahana centre-ouest du socle cristallin precambrien de Madagascar 1:200 000.

Moine, B., Bosse, V., Paquette, J.-L. and Ortega, E., 2014. The occurrence of a Tonian–Cryogenian (~850Ma) regional metamorphic event in Central Madagascar and the geodynamic setting of the Imorona–Itsindro (~800Ma) magmatic suite. Journal of African Earth Sciences, 94: 58-73.

Nédélec, A., Ralison, B., Bouchez, J.L. and Grégoire, V., 2000. Structure and metamorphism of the granitic basement around Antananarivo: A key to the Pan-African history of central Madagascar and its Gondwana connections. Tectonics, 19(5): 997-1020.

Paquette, J.-L. and Nédélec, A., 1998. A new insight into Pan-African tectonics in the East–West Gondwana collision zone by U–Pb zircon dating of granites from central Madagascar. Earth and Planetary Science Letters, 155(1-2): 45-56.

Paquette, J.-L., Nédélec, A., Moine, B. and Rakotondrazafy, M., 1994. U-Pb, single zircon Pb-evaporation, and Sm-Nd isotopic study of a granulite domain in SE Madagascar. The Journal of Geology, 102(5): 523-538.

Poblet, J. and Lisle, R.J., 2011. Kinematic evolution and structural styles of fold-and-thrust belts. Geological Society, London, Special Publications, 349(1): 1-24.

Raharimahefa, T. and Kusky, T.M., 2006. Structural and remote sensing studies of the southern Betsimisaraka Suture, Madagascar. Gondwana Research, 10(1-2): 186-197.

Raharimahefa, T. and Kusky, T.M., 2009. Structural and remote sensing analysis of the Betsimisaraka Suture in northeastern Madagascar. Gondwana Research, 15(1): 14-27.

Raharimahefa, T. and Kusky, T.M., 2010. Temporal evolution of the Angavo and related shear zones in Gondwana: Constraints from LA-MC-ICP-MS U–Pb zircon ages of granitoids and gneiss from central Madagascar. Precambrian Research, 182(1-2): 30-42.

Raharimahefa, T., Kusky, T.M., Toraman, E., Rasoazanamparany, C. and Rasaonina, I., 2013. Geometry and kinematics of the late Proterozoic Angavo Shear Zone, Central Madagascar: Implications for Gondwana Assembly. Tectonophysics, 592: 113-129.

Roig, J., Tucker, R., Delor, C., Peters, S. and Théveniaut, H., 2012. Carte géologique de la République de Madagascar à 1/1 000 000. Ministère des Mines, PGRM, Antananarivo, République de Madagascar. 1:1,000,000.

Schoene, B. and Bowring, S.A., 2007. Determining accurate temperature–time paths from U–Pb thermochronology: An example from the Kaapvaal craton, southern Africa. Geochimica et Cosmochimica Acta, 71(1): 165-185.

Schofield, D.I., Thomas, R.J., Goodenough, K.M., De Waele, B., Pitfield, P.E.J., Key, R.M., Bauer, W., Walsh, G.J., Lidke, D.J. and Ralison, A.V., 2010. Geological evolution of the Antongil Craton, NE Madagascar. Precambrian Research, 182(3): 187-203.

Service Géologique de Madagascar, T., 1962. Moramanga-Brickaville. 1:200,000.

Service Géologique de Madagascar, T., 1963a. Antsirabe-Ampatolampy 1:200,000.

Service Géologique de Madagascar, T., 1963b. Miarinarivo-Tanarive. 1:200,000.

Thomas, R.J., De Waele, B., Schofield, D.I., Goodenough, K.M., Horstwood, M., Tucker, R., Bauer, W., Annells, R., Howard, K., Walsh, G., Rabarimanana, M., Rafahatelo, J.M., Ralison, A.V. and Randriamananjara, T., 2009. Geological evolution of the Neoproterozoic Bemarivo Belt, northern Madagascar. Precambrian Research, 172(3-4): 279-300.

Tucker, R., Ashwal, L., Handke, M., Hamilton, M., Le Grange, M. and Rambeloson, R., 1999. U-Pb geochronology and isotope geochemistry of the Archean and Proterozoic rocks of north-central Madagascar. The Journal of Geology, 107(2): 135-153.

Tucker, R., Roig, J.-Y., Delor, C., Amelin, Y., Goncalves, P., Rabarimanana, M., Ralison, A. and Belcher, R., 2011. Neoproterozoic extension in the Greater Dharwar Craton: a reevaluation of the "Betsimisaraka suture" in Madagascar. Canadian Journal of Earth Sciences, 48(2): 389-417.

Tucker, R.D., Kusky, T.M., Buchwaldt, R. and Handke, M.J., 2007. Neoproterozoic nappes and superposed folding of the Itremo Group, west-central Madagascar. Gondwana Research, 12(4): 356-379.

Tucker, R.D., Roig, J.Y., Moine, B., Delor, C. and Peters, S.G., 2014. A geological synthesis of the Precambrian shield in Madagascar. Journal of African Earth Sciences, 94: 9-30.

Verschure, R.H., Andriessen, P.A.M., Boelrijk, N.A.I.M., Hebeda, E.H., Maijer, C., Priem, H.N.A. and Verdurmen, E.A.T., 1980. On the thermal stability of Rb-Sr and K-Ar biotite systems: Evidence from coexisting Sveconorwegian (ca 870 Ma) and Caledonian (ca 400 Ma) biotites in SW Norway. Contributions to Mineralogy and Petrology, 74(3): 245-252.

5

Proterozoic basin evolution and tectonic geography of Madagascar during the Nuna Supercontinent

In preparation as:

Armistead, S.E., Collins, A.S., Schmitt, R.S., Costa, R.L., De Waele, B., Foden, J.D., Razakamanana, T. and Payne, J.L., In Prep. Proterozoic basin evolution and tectonic geography of Madagascar during the Nuna Supercontinent. *Precambrian Research.*

Abstract

Madagascar hosts several Paleoproterozoic sedimentary sequences that are key to unravelling the geodynamic evolution of past supercontinents on Earth. We use new detrital zircon U–Pb geochronology and Hf isotopes, and a substantial database of magmatic and detrital data to compare and contrast sedimentary sequences in Madagascar, Africa and India. We show that the Itremo Group in central Madagascar, the Sahantaha Group in northern Madagascar, the Maha Group in eastern Madagascar, and the Ambatolampy group in central Madagascar have indistinguishable age and isotopic characteristics. These samples have maximum depositional ages > c.1700 Ma, with major zircon age peaks at c. 2500 Ma, c. 2000 Ma and c. 1850 Ma. We name this the Greater Itremo Basin, which covered a vast area of Madagascar in the late Paleoproterozoic. We further assess the correlation of these samples against those in the Tanzania and Congo cratons of Africa, and the Dharwar Craton and Southern Granulite Terrane of India. We show that the Greater Itremo Basin and sedimentary sequences in the Tanzania Craton of Africa are likely correlatives. We also tentatively correlate these with the Southern Granulite Terrane of India, which together formed a major intra-Nuna/Columbia sedimentary basin that we name the Itremo-Muva-Pandyan Basin. We propose a plate tectonic configuration for the Paleoproterozoic where central Madagascar is contiguous

with the Tanzania Craton to the west and the Southern Granulite Terrane to the east. This model strongly supports an ancient Proterozoic origin for central Madagascar against the Tanzania Craton of East Africa. It also supports the isolation of central Madagascar as the late Mesoproterozoic microcontinent Azania that collided back with East Africa and India in the Neoproterozoic–Cambrian.

1. Introduction

The amalgamation of central Gondwana occurred along several discrete subduction zones that collectively formed the East African Orogen. This orogen resulted from the collision of Africa, Madagascar and India (Collins and Pisarevsky, 2005; Fritz et al., 2013; Johnson et al., 2011; Merdith et al., 2017; Schmitt et al., 2018). Madagascar records two Neoproterozoic sutures that closed the Mozambique Ocean during this time, which makes it an ideal location to study the nature and timing of Gondwana amalgamation. Although there is general agreement over the final configuration of the Gondwana supercontinent (see Schmitt et al., 2018), the timing of the collisional belts remains contentious. In particular, the timing of the amalgamation of Madagascar with the Dharwar Craton is controversial and has important implications for how we interpret the Proterozoic evolution of Madagascar. Two end-member models are generally considered for the amalgamation of Madagascar with India; 1) the Antongil(Dharwar)-Madagascar collision occurred in the late Archean, and central Madagascar and the Dharwar Craton are best considered as "the Greater Dharwar Craton" from the Archean to the breakup of Gondwana (Tucker et al., 2011a); or 2) Antongil(Dharwar) and central Madagascar were separate terranes that collided during the major Ediacaran–Cambrian Malagasy Orogeny, marked by the Betsimisaraka Suture (Collins, 2006; Collins and Windley, 2002).

Reconstructing the terranes of eastern Africa, Madagascar and India prior to the Neoproterozoic is even more challenging due to a scarcity of Mesoproterozoic rocks in some of these regions, limiting assessment of their correlation. Similarities in Paleoproterozoic sedimentary rocks of the Itremo Group in central Madagascar and the Muva Supergroup in the Tanzania Craton in Africa have been recognised for some time (Alessio et al., 2019; Cox et al., 1998; Cox et al., 2004; Fitzsimons and Hulscher, 2005). Similarities between the Itremo Group and the Cuddapah Basin of eastern India have also been recognised (Tucker et al., 2011a) as have similarities between the Itremo Group and the Southern Granulite Terrane (Collins et al., 2012; Collins et al., 2007b; Plavsa et al., 2014). These potential correlations provide vital supercontinental links, sedimentary piercing points, and they provide important constraints on paleogeographic reconstructions of the Earth during the period of Nuna supercontinent formation.

Not only is the correlation of the Itremo Group with other continents a topic of interest and importance, but the correlation of the Itremo Group with other sedimentary groups in Madagascar is also unresolved. De Waele et al. (2011) proposed that the Itremo, Maha and Sahantaha groups in Madagascar are equivalent sedimentary sequences. Boger et al.

(2014); Boger et al. (2019) linked the Anosyen Domain of southern Madagascar to the Itremo Group. The validity of these correlations, and likelihood that these represent contiguous Paleoproterozoic–Mesoproterozoic depositional systems, governs the paleogeographic reconstruction of this extensive part of Nuna and its tectonic geographic interpretation.

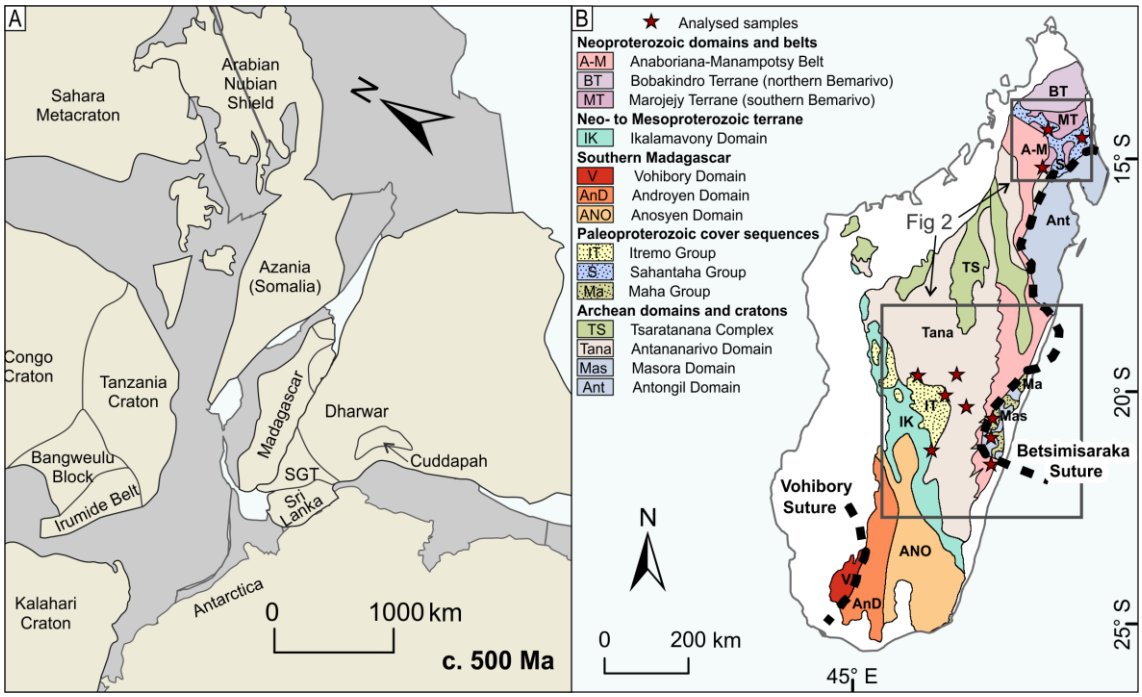

Figure 5.1 a) Tectonic map of central Gondwana made using GPlates exported geometries from Merdith et al. (2017) in ArcGIS; projected in Hotine Oblique Mercator with Madagascar in the centre (reconstructed position, longitude=-75 and latitude=+40).; b) Present day map of the geological domains of Madagascar after (De Waele et al., 2011).

1.1. Regional geology

Madagascar is made up of several domains that contain rocks dated from Archean to Neoproterozoic (Figure 5.1b). Central Madagascar consists of the Antananarivo Domain, which is composed of c. 2500 Ma magmatic gneisses (Collins and Windley, 2002; Kröner et al., 2000) and amphibolite–granulite facies metasedimentary rocks of the Ambatolampy Group (Archibald et al., 2015). To the east are the Antongil and Masora Domains, which contain c. 3100 Ma rocks and are likely a continuation of the Dharwar Craton of India (Armistead et al., 2017; Schofield et al., 2010; Tucker et al., 1999). To the southwest of the Antananarivo Domain, and locally unconformable on it (Cox et al., 1998), is the Itremo Group, composed of quartzites, schists and marbles with a maximum depositional age of c. 1600 Ma (Cox et al., 1998; Cox et al., 2004; Fernandez et al., 2003). To the southwest of the Itremo Group, is the Ikalamavony Domain that contains the

Ikalamavony Group, similarly made up of quartzites, schists and marbles, but with notable volcanic and volcanoclastic horizons and a maximum depositional age of c. 1000 Ma (Tucker et al., 2011b).

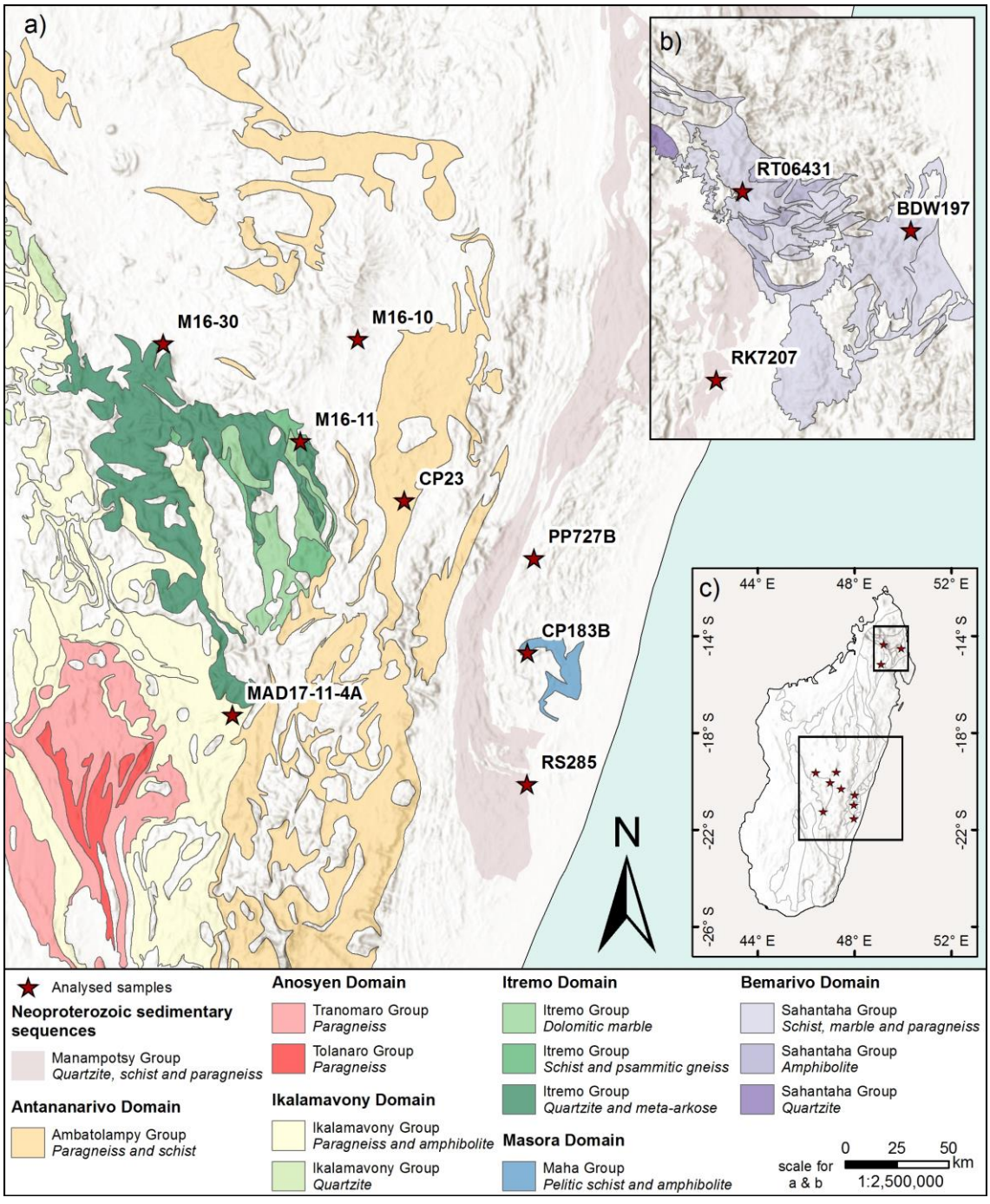

Figure 5.2 Geological map of Madagascar modified after Roig et al. (2012); a) central Madagascar showing major Proterozoic sedimentary groups; b) geological map of northern Madagascar including the Sahantaha Group; c) geological terranes of Madagascar showing insets for maps a and c.

To the south of these metasedimentary domains are the Proterozoic Anosyen, Androyen and Vohibory terranes (Boger et al., 2014; Emmel et al., 2008; Jöns and Schenk, 2008). The Anosyen and Androyen domains contain the Tranomaro, Tolanaro and Mangoky groups, that like the Itremo Group, also have c. 1700 Ma maximum depositional ages (Boger et al., 2014).

A series of Neoproterozoic sedimentary sequences overly these major domains, and a suite of Neoproterozoic magmatic rocks intrude the domains. Overlying the Ikalamavony and Itremo domains is the Molo Group, which has a maximum depositional age of c. 620 Ma and a minimum depositional age of c. 560 Ma defined by metamorphic overgrowths (Cox et al., 2004). The c. 1080–980 Ma Dabolava Suite (Archibald et al., 2017a) is restricted to the Ikalamavony Domain while the c. 850–750 Ma Imorona-Itsindro Suite (Archibald et al., 2016) is widespread throughout much of central and eastern Madagascar. In the Vohibory Domain, the Linta Group contains sedimentary rocks with maximum depositional ages of c. 620 Ma that closely reflect the ages of the intrusive Marasavoa and Vohitany suites.

Because it is difficult to put absolute age constraints on sedimentary sequences, there is some ambiguity over the nomenclature of Neoproterozoic sedimentary rocks within the Antananarivo Domain. The Ambatolampy Group and Manampotsy Group were interpreted as Cryogenian sequences in the most recent mapping of Roig et al. (2012). However, in light of new published data (Archibald et al., 2015) and what we will show in this manuscript, these two groups have very different detrital zircon spectra and ages; and should therefore be considered separately. Thomas et al. (2009) and BGS-USGS-GLW (2008) defined a new terrane—the Anaboriana Belt—which defines the boundary between the Antongil/Masora/Bemarivo domains and the Antananarivo Domain, and approximately represents the Betsimisaraka Suture (Collins and Windley, 2002). This belt occupies most of what has traditionally been mapped as the Manampotsy Group (e.g. in Roig et al., 2012). We therefore refer to this as the Anaboriana-Manampotsy Belt herein and treat the Ambatolampy Group separately.

1.1.1. Sedimentology and depositional environment of the Itremo Group in central Madagascar

The Itremo Group contains well-sorted quartzite, psammitic schist and gneiss, and dolomitic marbles. A detailed sedimentological study of the Itremo Group is given in Cox et al. (1998) and is summarised below. The Itremo Group quartzites contains well-sorted quartz arenites with flat lamination, wave ripples, cross-laminations, dune cross-bedding and rare hummocky cross stratification (Cox et al., 1998). These sedimentary structures indicate deposition under shallow, subaqueous, conditions and are consistent with a shallow subtidal depositional setting (Cox et al., 1998). Pelitic rocks of the Itremo Group are finely laminated siltstone and mudstone, with interbedded sandstones. They contain flat and cross-laminations, which indicate currents were periodically active (Cox et al., 1998). They were likely deposited in deeper water compared to the quartzites, with some

deposited in a subtidal shelf environment (Cox et al., 1998). Carbonate rocks, which occur at the top of Itremo Group, consist of dolomitic marble with stromatolites, and sandy marble. Some desiccation features indicate subaerial exposure in an intertidal setting for the carbonates, while the sandy marbles were likely deposited in a marginal marine environment (Cox et al., 1998). Overall, the Itremo Group is interpreted as a passive margin sequence, deposited on a shallow continental shelf or continental platform, with continental or cratonic sources (Cox et al., 1998; De Waele et al., 2011).

The Itremo Group is intruded by the c. 850–750 Ma Imorona-Itsindro Suite, which provides a minimum age of its deposition. The Itremo Group along with the Imorona-Itsindro Suite has been folded into polydeformed folds sometime between c. 750 Ma and c. 550 Ma (Armistead et al., In Review; Collins et al., 2003a; Tucker et al., 2007). This deformation likely occurred at c. 650 Ma in response to west-dipping subduction (present day direction) beneath the Vohibory Domain, that led to the amalgamation of Madagascar with Africa (Armistead et al., In Review).

Pioneering detrital zircon U–Pb studies instigated the 'out-of-Africa' model for the Itremo Group of central Madagascar (e.g. Cox et al., 1998; Cox et al., 2004; Fitzsimons and Hulscher, 2005). The age distribution of the Itremo Group closely matches the Tanzanian Craton but has little resemblance to sedimentary rocks in the dominantly Archean Dharwar Craton (see Collins et al., 2015). In subsequent years, this has been challenged and other datasets complimentary to U–Pb ages, such as Hf isotopes, have been collected on possible comparable sequences and source regions. This has left the Itremo Group as a relatively poorly known group. Here we compare detrital zircon spectra and their Hf isotope compositions for a range of sedimentary sequences in Madagascar, Africa and India.

2. Analytical methods

2.1. Zircon U–Pb

Rock samples were crushed and the zircon fraction (sieved 79–425 μm) was separated by panning. Zircons were hand-picked and mounted in epoxy resin. The zircon mount was polished; carbon coated and imaged using a Gatan cathodoluminescence (CL) detector attached to Quanta 600 MLA Scanning Electron Microscope to identify suitable domains for analysis. Zircon U–Pb and REE/trace element geochronology was undertaken at the University of Adelaide using an Agilent 7900x ICP-MS with attached ASI Resolution excimer 193nm laser ablation system. A spot size of 29 μm and frequency of 5 Hz was used. Isotopes ^{90}Zr, ^{201}Hg, ^{204}Pb, ^{206}Pb, ^{207}Pb, ^{208}Pb, ^{232}Th and ^{238}U were measured. Each analysis comprised a 20s background and 30s ablation. GEMOC GJ-1 zircon (TIMS normalising ages ^{207}Pb/^{206}Pb = 607.7 ± 4.3 Ma, ^{206}Pb/^{238}U = 600.7 ± 1.1 Ma and ^{207}Pb/^{235}U = 602.0 ± 1.0 Ma; Jackson et al. 2004) was used to correct for U–Pb

fractionation. The Plešovice zircon standard (ID TIMS $^{206}Pb/^{238}U$ = 337.13 ± 0.37 Ma; Sláma et al. (2008)) was used to assess accuracy over the course of the laser session; 58 Plešovice standard analyses were made and yield a weighted average $^{206}Pb/^{238}U$ age of 339.4 ± 1.5 Ma (95% confidence limits) which closely matches the ID TIMS age. Data were processed using Iolite (Paton et al., 2011). U–Pb data are provided in Appendix 5.1, REE data are provided in Appendix 5.2 and example CL images provided in Appendix 5.3.

2.2. Zircon Lu–Hf

Near concordant U–Pb spots were additionally analysed for Hf isotopes. Lu–Hf isotope analyses were undertaken on the Thermo-Scientific Neptune Multi-Collector ICP-MS with an attached New Wave UP-193 ArF excimer laser at the University of Adelaide following the methods of Payne et al. (2013). A beam diameter of 50 µm was used. Typical ablation times were ~82 s using a 5 Hz repetition rate, a 4 ns pulse rate, and an intensity of ~4.40 J/cm^2. Zircons were ablated in a helium atmosphere that was then mixed with argon upstream of the ablation cell.

Zircon data reduction were carried out using the HfTRAX Excel macro (Payne et al., 2013). Data were normalised to $^{179}Hf/^{177}Hf$=0.7325 using an exponential correction for mass bias. The Yb and Lu isobaric interferences on ^{176}Hf were corrected for following the methodology of Woodhead et al. (2004).

Zircon standards were analysed before and during the analysis of unknowns to assess instrument performance and stability. The primary zircon standard Mud Tank was used and yielded a mean $^{176}Hf/^{177}Hf$ ratio of 0.282499 ± 0.000015 (2SD). This is within uncertainty of the published value of 0.282504 ± 0.000044 (2SD) by Woodhead and Hergt (2005). Values for $^{176}Hf/^{177}Hf_{CHUR(t)}$ were calculated using modern $^{176}Hf/^{177}Hf$=0.282785 (Bouvier et al., 2008), modern $^{176}Lu/^{177}Hf$=0.0336 (Bouvier et al., 2008) and ^{176}Lu decay constant of $1.865x10^{-11}$ year^{-1} (Scherer et al., 2001). Values for the crustal model age (T_{DMC}) were calculated using a ^{176}Lu decay constant of $1.865x10^{-11}$year^{-1} (Scherer et al., 2001), modern $^{176}Hf/^{177}Hf$=0.28325, modern $^{176}Lu/^{177}Hf$=0.0384 (Griffin et al., 2000), and a bulk crust value of $^{176}Lu/^{177}Hf$=0.015 (Griffin et al., 2002). Uncertainties for $\varepsilon_{Hf}(t)$ are calculated as the $^{176}Hf/^{177}Hf_{Sample}$ uncertainty converted to epsilon notation (i.e. $((^{176}Hf/^{177}Hf_{2\sigma})/0.282785)*10000$) and are reported at the 2σ level. Isotopic data are provided in Appendix 5.4.

3. Results

3.1. Sample descriptions

Three quartzite samples from the Itremo Group and one sample from the Ambatolampy Group (Figure 5.2) were collected and analysed for U–Pb, trace element geochemistry and

Hf isotopes. The aim was to have a range of quartzite samples from a broad geographical region that are representative of the major metasedimentary groups in Madagascar, most notably the Itremo Group. A further three samples from the Anaboriana-Manampotsy Belt, two samples from the Maha Group and two samples from the Sahantaha Group (Figure 5.2) that were dated for U–Pb geochronology in BGS-USGS-GLW (2008) and De Waele et al. (2011) were analysed for Hf isotopes in this study. Sample descriptions and location information are summarised in Table 5.1. Together, this collection of samples represents the main quartzite groups across the major geological domains of Madagascar, with the exception of the Anosyen, Androyen and Vohibory domains of southern Madagascar (Figure 5.1).

Table 5.1 Summary of sample descriptions and maximum depositional ages (calculated as the youngest near-concordant $^{207}Pb/^{206}Pb$ date) for samples analysed in this study. Age uncertainties are 2σ.

Sample ID	Lithology	Geological unit	Latitude	Longitude	Maximum depositional age	U–Pb data source
M16-10	Quartzite	Ambatolampy Group	-19.62080	47.23781	1835 ± 86 Ma	This study
M16-11	Quartzite	Itremo Group	-20.06404	46.98979	1774 ± 90 Ma	This study
M16-30	Quartzite	Itremo Group	-19.64042	46.39433	1827 ± 91 Ma	This study
MAD-17-11-4A	Quartzite	Itremo Group	-21.21432	46.66460	1727 ± 89 Ma	This study
RK7207	Quartzite	Anaboriana-Manampotsy	-15.17330	49.08520	636 ± 35 Ma	BGS et al. 2008
RS285	Quartzite	Anaboriana-Manampotsy	-21.55100	47.97240	762 ± 75 Ma	BGS et al. 2008
CP23	Quartzite	Anaboriana-Manampotsy	-20.32070	47.44030	1001 ± 44 Ma	BGS et al. 2008
PP727B	Quartzite	Maha Group	-20.57110	48.00350	1742 ± 19 Ma	De Waele et al. 2011
CP183B	Quartzite	Maha Group	-20.98050	47.97490	1801 ± 18 Ma	De Waele et al. 2011
BDW197	Quartzite	Sahantaha Group	-14.52460	49.93010	1733 ± 18 Ma	BGS et al. 2008
RT06431	Quartzite	Sahantaha Group	-14.35410	49.19930	1771 ± 18 Ma	BGS et al. 2008

3.2. Zircon U–Pb and trace element geochemistry

We analysed zircons for U–Pb and trace elements. The aim of analysing for trace elements was that it might distinguish different populations of zircons. Unfortunately, the trace element signatures were not distinct for different age populations, so their usefulness for distinguishing different populations is limited. The trace element profiles were strongly correlated with discordance, which adds additional uncertainty to their meaning. Trace element profiles are provided in Appendix 5.5 for completeness, however we do not consider these data any further.

Three quartzite samples analysed from the Itremo Group and one sample from the Ambatolampy Group contain near-concordant (<10%) detrital zircons ranging from c. 3485 to c. 1727 Ma (Figure 5.3). They contain similar age spectra with dominant peaks at c. 2500 Ma, c. 2200 Ma and c. 1800 Ma. Their maximum depositional ages are given in Table 5.2.

3.3. Zircon Lu–Hf analysis

Itremo Group and Ambatolampy Group samples with zircon dates of c. 2500 Ma are dominantly juvenile to moderately evolved; with $\varepsilon_{Hf}(t)$ values of ranging from +5 to -14 (Figure 5.3). Zircon dates of c. 2200–1800 Ma are moderately evolved; with $\varepsilon_{Hf}(t)$ values ranging from +5 to -10. Zircon analyses with dates of c. 1800–1700 Ma cluster with $\varepsilon_{Hf}(t)$ ranging from 0 to -14.

Age equivalent analyses from the Maha Group have $\varepsilon_{Hf}(t)$ values ranging from +5 to -11 for c. 2500 Ma zircons, and +4 to -6 for c. 2200–1800 Ma zircons, and +2 to -10 for c. 1800–1700 Ma zircons (Figure 5.3). Age equivalent analyses from the Sahantaha Group have $\varepsilon_{Hf}(t)$ values ranging from +6 to -10 for c. 2500 Ma zircons, 0 to -4 for c. 2200–1800 Ma zircons, and -2 to -10 for c. 1800–1700 Ma zircons.

From the Anaboriana-Manampotsy Belt, sample RK7207 has a unimodal zircon peak at c. 780 Ma, with $\varepsilon_{Hf}(t)$ values ranging from -10 to -15. Sample RS285 contains zircons with dates of c. 3400–3000 Ma that have $\varepsilon_{Hf}(t)$ values ranging from +3 to -3. Zircons from this sample with dates of c. 2500 Ma have $\varepsilon_{Hf}(t)$ values ranging from +2 to -13. A single c. 1809 Ma zircon has an $\varepsilon_{Hf}(t)$ values of -2. Sample CP23 has c. 2500 Ma zircons with $\varepsilon_{Hf}(t)$ values ranging from +6 to -8; c. 2200–1800 Ma zircons with $\varepsilon_{Hf}(t)$ values ranging from -4 to -9; and c. 1100 Ma zircons with $\varepsilon_{Hf}(t)$ values ranging from +3 to -8.

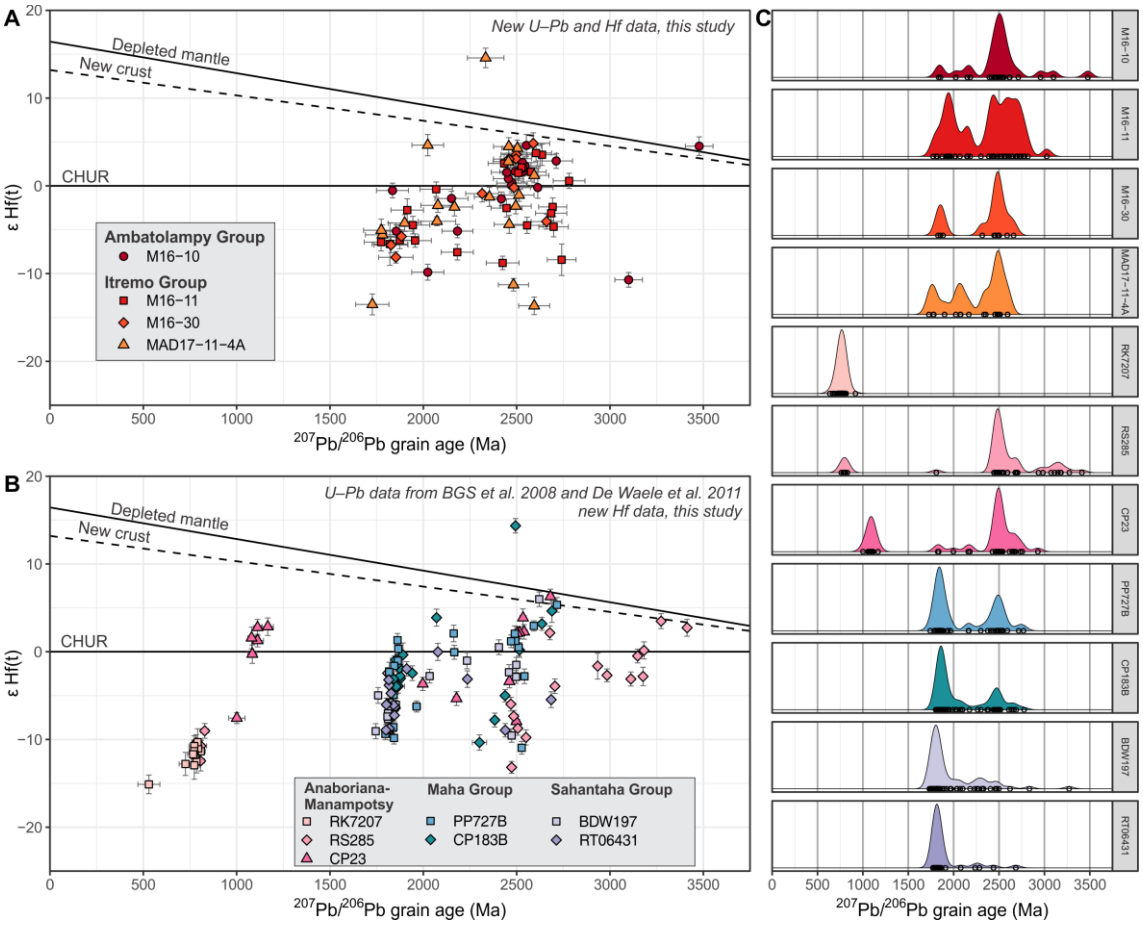

Figure 5.3 New zircon U–Pb and Lu–Hf isotope data for metasedimentary units in Madagascar. Plots made in R, kernel density estimate plots include data that are within 10% concordance and have bandwidth of 50 Ma. U–Pb data for the Maha Group and Sahantaha Group are from De Waele et al. (2011); U–Pb data for the Anaboriana-Manampotsy samples are from BGS-USGS-GLW (2008).

4. Discussion

We have compiled an extensive database of published data from Madagascar, India and Africa (Appendix 5.6) that builds on the database of Armistead et al. (2017). Since we are focusing primarily on Paleoproterozoic samples and correlations of zircons within the Greater Itremo Basin, we do not consider the substantial set of Neoproterozoic data in detail. However, some supplementary figures showing these data are given in Appendix 5.7. References for the data used tabulated below in Table 5.2.

Table 5.2 References for data used in the compilation, data provided in Appendix 5.6.

Type	Continent	References
Detrital	Madagascar	Archibald et al. (2015); BGS-USGS-GLW (2008); Boger et al. (2014); Collins et al. (2012); Collins et al. (2003b); Costa et al. (Submitted); Cox et al. (1998); Cox et al. (2004); De Waele et al. (2011); Fitzsimons and Hulscher (2005); Tucker et al. (2011a); Tucker et al. (2011b).
Detrital	Africa	Alessio et al. (2019); Alessio et al. (2018); Batumike et al. (2009); Batumike et al. (2007); De Waele and Fitzsimons (2007); Foster et al. (2015); Kazimoto et al. (2014); Koegelenberg et al. (2015); Konopásek et al. (2014); Linol et al. (2016); Thomas et al. (2016)

Detrital	India	Armistead et al. (2017); Collins et al. (2007a); Collins et al. (2015); Henderson et al. (2014); Ishwar-Kumar et al. (2013); Joy et al. (2015); Kooijman et al. (2011); Lancaster et al. (2015); Li et al. (2017); Maibam et al. (2016); Maibam et al. (2011); Plavsa et al. (2014); Prakash and Sharma (2011); Raith et al. (2010); Sarma et al. (2012); Teale et al. (2011); Upadhyay et al. (2009);
Magmatic	Madagascar	Archibald et al. (2016); Armistead et al. (2017); Bauer et al. (2011); BGS-USGS-GLW (2008); Buchwaldt et al. (2003); Collins et al. (2012); Collins et al. (2003b); de Wit et al. (2001); Goodenough et al. (2010); Handke et al. (1999); Kabete et al. (2006); Kröner et al. (2000); Paquette et al. (2004); Paquette and Nédélec (1998); Paquette et al. (1994); Schofield et al. (2010); Tucker et al. (1999); Tucker et al. (2011a); Tucker et al. (2007); Tucker et al. (2011b);
Magmatic	Africa	Alessio (2019); Alessio et al. (2019); Ali et al. (2014); Blades et al. (2015); Bulambo et al. (2004); Cox et al. (2002); Daly (1986); De Waele et al. (2006); Dodson et al. (1975); Hanson et al. (1988); John (2001); Katongo et al. (2004); Key et al. (2001); Morag et al. (2011); Ngoyi et al. (1991); Nutman et al. (2013); Rainaud et al. (2005); Ring et al. (1999); Ring et al. (1997); Schenk and Appel (2001); Thomas et al. (2016); Vrána et al. (2004)
Magmatic	India	Clark et al. (In review); Clark et al. (2009); Ghosh et al. (2004); Glorie et al. (2014); Ishwar-Kumar et al. (2013); Jayananda et al. (2015); Kröner et al. (2012); Kumar et al. (2017); Maibam et al. (2011); Mohan et al. (2014); Pavan (Unpublished); Plavsa et al. (2015); Plavsa et al. (2012); Praveen et al. (2014); Yang and Santosh (2015)

4.1. Correlation of sedimentary sequences in Madagascar

4.1.1. Archean sequences

Detrital samples with Archean maximum depositional ages (here we include samples with MDAs down to c. 2450 Ma) are restricted to the Antongil-Masora domains and Anaboriana-Manampotsy Belt. The > 3000 Ma samples from the Masora Domain have unimodal peaks at c. 3150 Ma. The c. 2500 Ma sample from the Antongil Domain also comprises a restricted spectrum of detrital zircon dates, with the majority between c. 2680 Ma and c. 2500 Ma. In contrast, the Anaboriana-Manampotsy belt samples have two distinct zircon peaks at c. 2650 Ma and c. 2500 Ma. These ages closely reflect the ages of magmatic gneisses in the Antananarivo Domain, which are likely the source of these grains (Archibald et al., 2015; Armistead et al., 2017). Although the Anaboriana-Manampotsy samples have similar maximum depositional ages to the Antongil Domain sample, their provenance suggests that they were deposited in a different paleogeographic setting. The detrital zircons of the Antongil-Masora domains are of similar age and Hf isotope composition as rocks exposed within the Dharwar Craton (Armistead et al., 2017; Pavan, Unpublished).

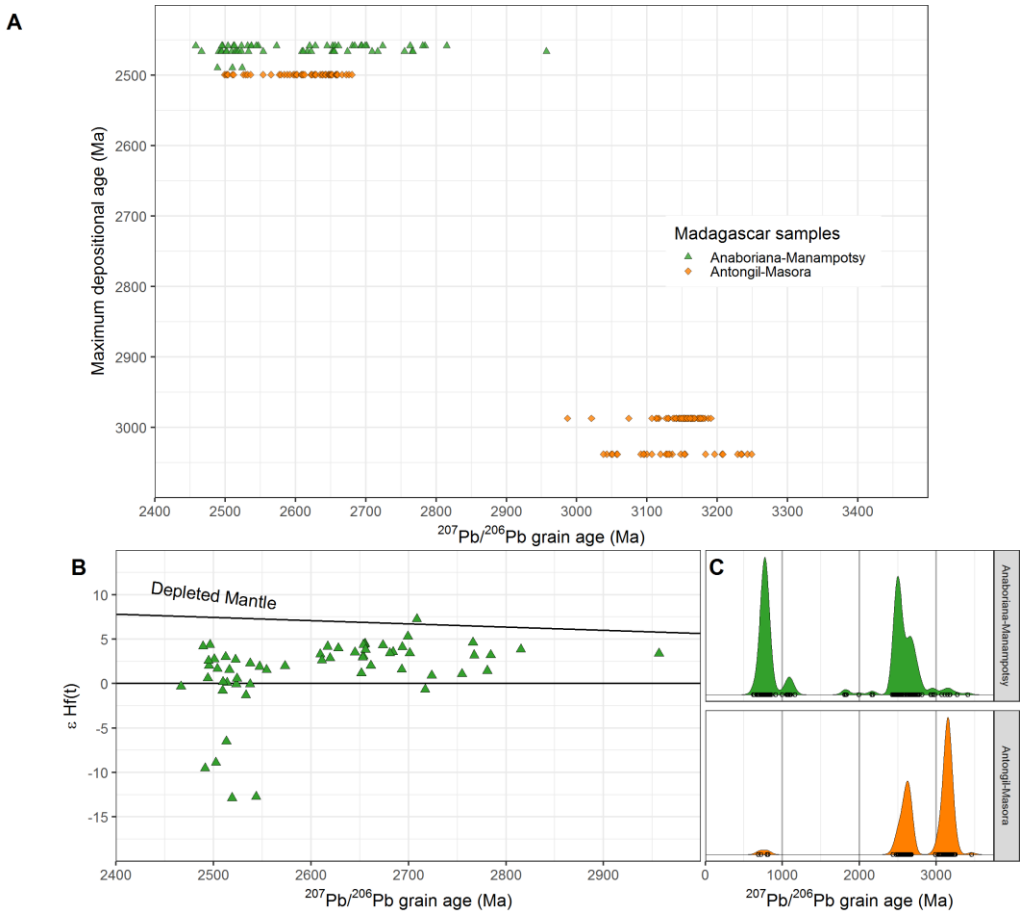

Figure 5.4 Comparison of Archean detrital zircon samples from Madagascar, symbolised by Group/Region a) Maximum depositional age vs. grain age; b) εHf(t) vs. grain age for samples from Madagascar; c) Kernel Density Estimate (KDE) plots of Archean samples, bandwidth=50. Dataset includes new data from Figure 5.3 as well as data from Appendix 5.6.

4.1.2. Paleoproterozoic sequences

With the addition of new Hf isotope data to conventional U–Pb zircon data, we confirm the interpretations of De Waele et al. (2011) that the Itremo, Sahantaha and Maha groups formed together as continental margin successions deposited no earlier than c. 1700 Ma. We further include the Ambatolampy Group and southern Madagascar in this interpretation. Samples from the Itremo Group, Maha Group, Sahantaha Group, Ambatolampy Group and southern Madagascar have similar detrital zircon age spectra, maximum depositional ages within uncertainty of each other and similar $\varepsilon_{Hf}(t)$ values (Figure 5.5). There are subtle differences in the relative zircon age peak heights. For example, the Itremo Group has a stronger c. 2500 Ma peak compared to the younger peaks; the Maha Group has a smaller c. 2500 Ma peak and higher c. 1800 Ma peak; and the Sahantaha Group has a dominant c. 1800 Ma peak with minor older peaks (Figure 5.3). We suggest these subtle differences reflect the proximity of these sample locations to particular sources across this broad region. Despite these minor differences, the major zircon components are present in all samples, maximum depositional ages are within uncertainty of each other and $\varepsilon_{Hf}(t)$ values are similar. We propose, therefore, that these

samples were deposited within the same sedimentary system and sourced their detritus from similar sources, consistent with interpretations by Boger et al. (2014) and De Waele et al. (2011).

These samples are geographically widespread across Madagascar, with samples in the Sahantaha Group of northern Madagascar, the Itremo Group and Ambatolampy Group in central Madagascar, the Maha Group of eastern Madagascar and the Mangoky and Tolanaro groups of southern Madagascar. Published samples from southern Madagascar (Boger et al., 2014; Collins et al., 2012) that have similar detrital zircon age spectra, but no available Hf isotope data, are also likely part of this extensive sedimentary system. This suggests that a large basin existed over much of Madagascar at some point during or after the Paleoproterozoic—we herein refer to this as the 'Greater Itremo Basin'.

The majority of samples deposited within the Greater Itremo Basin have maximum depositional ages between c. 1875 Ma and c. 1700 Ma (Figure 5.4). However, two samples—one from the Itremo Group and one from southern Madagascar—have maximum depositional ages of 1592 ± 320 Ma and 1593 ± 68 Ma (2σ), respectively. There are only three zircon grains from the entire database for the Greater Itremo Basin that have dates less than c. 1700 Ma and these have large uncertainties. The youngest significant cluster of dates is at c. 1700 Ma, which we propose as the maximum age for the existence of the Greater Itremo Basin.

Unfortunately, the minimum age constraint on the Greater Itremo Basin—the cross-cutting c. 850–750 Ma Imorona-Itsindro Suite—is almost a billion years younger than the maximum depositional ages. This leaves the age of deposition of sediments within the Greater Itremo Basin open to various interpretations. Based on the maximum depositional ages and lack of any younger detrital zircons, the simplest interpretation is that the Greater Itremo Basin was a late Paleoproterozoic basin. An alternative interpretation to this, is that the Greater Itremo Basin existed in the Mesoproterozoic and possibly even through to the early Neoproterozoic (e.g. Boger et al., 2014; Boger et al., 2019). However, for this to have occurred, sediments within the basin would have exclusively sourced zircons that formed hundreds of millions of years earlier than when they were deposited, with no near-contemporaneous sources. This is despite the exotic Ikalamavony Domain being thrust over the Itremo Domain in the Tonian and the early stages of the Imorona-Itsindro Suite being intruded at this time. In addition, stromatolite morphology and carbon isotope data from carbonates in the Itremo Group are consistent with them being deposited in the Paleoproterozoic (Cox et al., 2004). Based on these factors, we prefer the model whereby the Greater Itremo Basin was deposited shortly after their maximum depositional ages, during the late Paleoproterozoic.

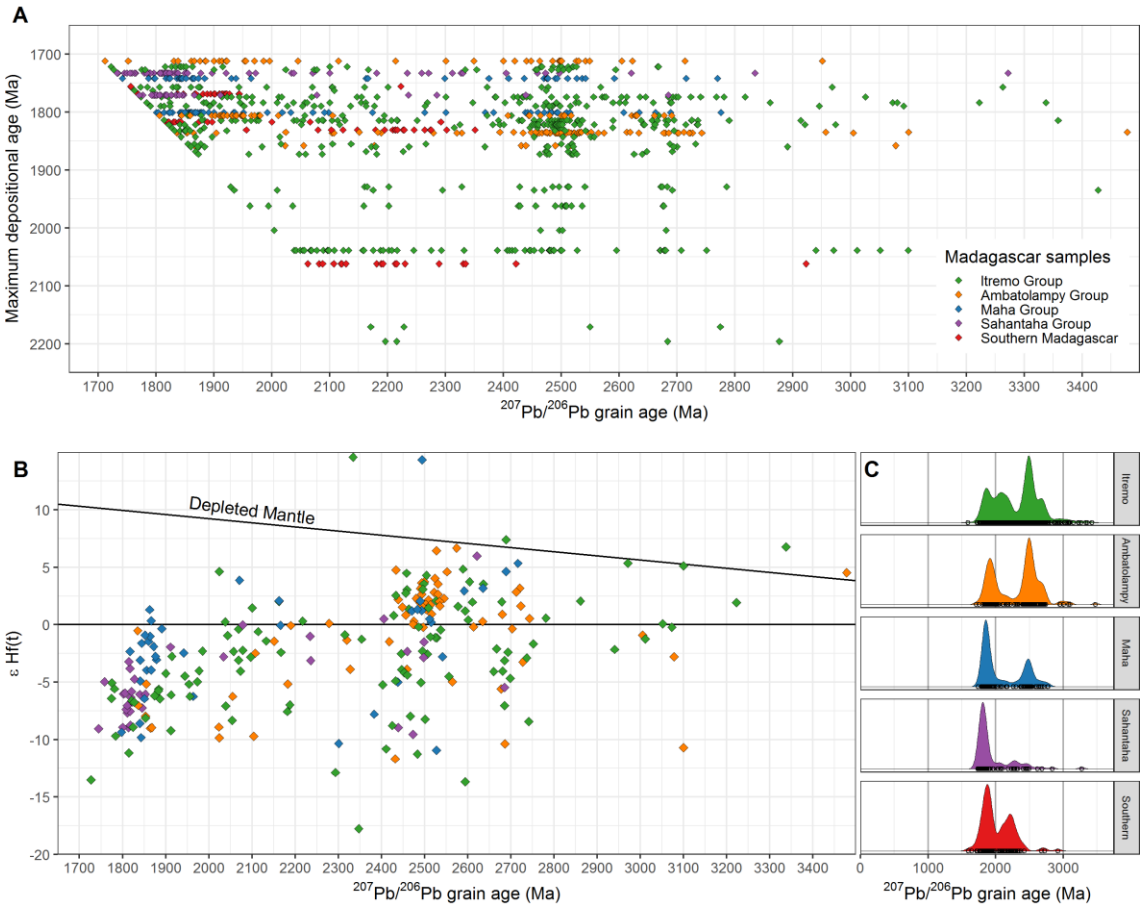

Figure 5.5 Comparison of Paleoproterozoic detrital zircon samples from Madagascar, symbolised by Group/Region a) Maximum depositional age vs. grain age; b) εHf(t) vs. grain age for samples from Madagascar; c) Kernel Density Estimate (KDE) plots of Paleoproterozoic samples, bandwidth=50. Dataset includes new data from Figure 5.3 as well as data from Appendix 5.6.

4.1.3. Neoproterozoic sequences

Several sedimentary groups have Neoproterozoic maximum depositional ages (Figure 5.5). These are located within the Anaboriana-Manampotsy Belt, the Molo Group and the Vohibory Domain, with one sample tentatively from the Antongil Domain. The Antongil-Masora Domain sample in Figure 5.5 is from Collins et al. (2003b); where they interpreted it as being from the Betsimisaraka Suture zone. However since its location is within the Antongil Domain based on more recent maps (e.g. Roig et al. (2012)), we have included it in this domain to be consistent with the way we have classified sample locations elsewhere. The majority of samples from these interpreted Neoproterozoic sequences have maximum depositional ages between c. 790 Ma and c. 625 Ma. Of these, the Anaboriana-Manampotsy Belt and Molo Group samples contain detrital zircons of similar age and Hf signature to the Greater Itremo Basin samples, with the addition of Neoproterozoic detritus. Therefore, these samples have likely sourced a significant proportion of their detritus either from the same sources as the sediments within the Greater Itremo Basin, or from recycling the sedimentary rocks within the Itremo Group and its equivalents. The c. 850–750 Ma Imorona-Itsindro Group, which has relatively evolved $\varepsilon_{Hf}(t)$ values ranging from approximately 0 to -30 (Archibald et al., 2015), is a

likely candidate for some of the younger detritus within these sequences. The c. 750 Ma southern Bemarivo Belt, which has evolved $\varepsilon_{Hf}(t)$ values ranging from approximately 0 to -15 (Armistead et al., 2019), is also a likely candidate for some of this younger detritus, particularly those samples located in northern Madagascar. Constraints on the minimum depositional age are given by zircon rim analyses that span c. 660–560 Ma for both the Molo Group and the Anaboriana-Manampotsy Belt. The deposition of these groups therefore occurred during the Neoproterozoic, between c. 700 Ma and c. 600 Ma.

The Linta Group in the Vohibory Domain has detrital zircon dates between c. 1068 and c. 555 Ma. These closely match ages from the Marasavoa Suite (c. 660–610 Ma) and the Vohitany Suite (c. 850 Ma), which are also in the Vohibory Domain (BGS-USGS-GLW, 2008). The sedimentary rocks in the Vohibory Domain appear to have exclusively derived material from local sources.

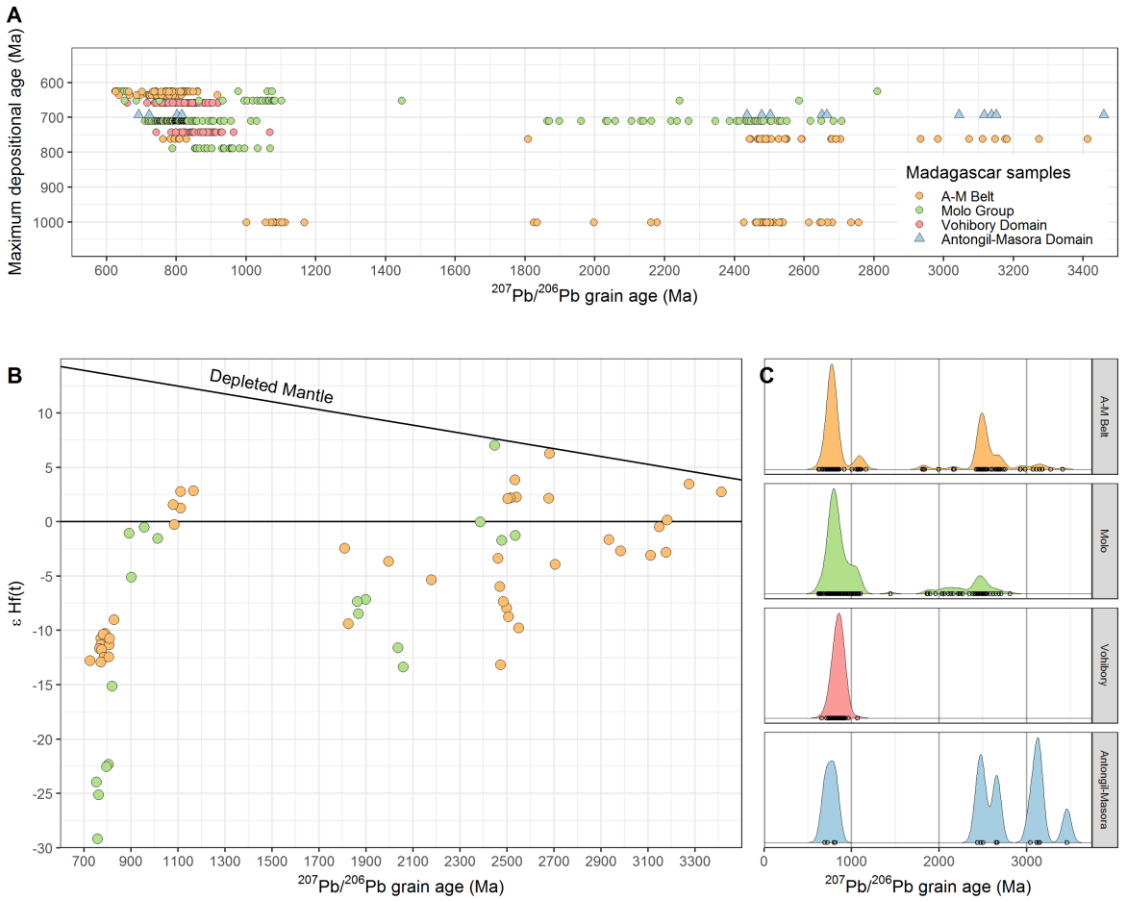

Figure 5.6 Comparison of Neoproterozoic detrital zircon samples from Madagascar, symbolised by Group/Region a) Maximum depositional age vs. grain age; b) εHf(t) vs. grain age for samples from Madagascar; c) Kernel Density Estimate (KDE) plots of Neoproterozoic samples, bandwidth=50. Dataset includes new data from Figure 5.3 as well as data from Appendix 5.6.

4.2. Correlation of the Greater Itremo Basin formations with other regions

The Greater Itremo Basin contains formations with detrital zircon spectra that are broadly similar to those in the Tanzania Craton, Cuddapah Basin of eastern India and the Southern Granulite Terrane of southern India (Figure 5.6, Figure 5.7). To assess these similarities, we have calculated kernel density contours for each of these regions to provide some quantitative constraints on these correlations (Figure 5.6). We have also produced a multi-dimensional scaling plot for detrital data with maximum depositional ages >1500 Ma (Figure 5.7). From Figure 5.6 it is clear that the Greater Itremo Basin and the Tanzania Craton both have detrital zircons that span the same ranges. Most notably, both regions have many samples with maximum depositional ages between c. 1850–1750 Ma. Within these, the Tanzania Craton has major grain age peaks at c. 2020 Ma and c. 1875 Ma. The formations within the Greater Itremo Basin have major zircon age peaks at c. 2675 Ma, c. 2500 Ma and c. 1850 Ma. These differences likely reflect the proximity of the depositional environment to the source rocks. For example, c. 2500 Ma magmatic rocks in Madagascar are likely a major source for c. 2500 Ma detrital zircons in the Greater Itremo Basin, given similarities in their age and Hf isotope signature. This accounts for why the Greater Itremo Basin contains abundant c. 2500 Ma zircons. The abundance of c. 2020 Ma detrital zircons in the Tanzania Craton indicates that it was closer to the sources of age-equivalent protoliths. However, we are wary of over interpreting the relative peaks of detrital zircon age spectra. The similarity in $\varepsilon_{Hf}(t)$ signatures of the Greater Itremo Basin formations and the Tanzania Craton zircons (Figure 5.6c) also suggests that these samples sourced their detritus from similar protoliths.

The majority of Southern Granulite Terrane samples have maximum depositional ages greater that c. 1900 Ma; older than those zircons in the Itremo Group and Tanzania Craton. These contain dominant zircon age peaks at c. 2650 Ma, c. 2075 Ma and 2425 Ma, which overlap with analyses from the Greater Itremo Basin and the Tanzania Craton, and may be derived from similar sources. If these are related, the Southern Granulite Terrane may represent an older depocenter, or separate basin, sourcing similar regions to the Greater Itremo Basin. The multi-dimensional scaling plot also indicates that samples from the Greater Itremo Basin, Tanzania Craton and Southern Granulite Terrane are similar (Figure 5.7).

The Cuddapah Basin samples are predominantly younger than c. 1700 Ma, with the majority of maximum depositional ages and zircon grain ages between c. 1750 and 1550 Ma. The main peaks as indicated by the KDE contours in Figure 5.6, do not overlap with the other regions assessed, although there are more sporadic zircons that range in similar age to the older age concentrations in the Greater Itremo Basin, Tanzania Craton and Southern Granulite Terrane. It is therefore likely that the Cuddapah Basin did not form together with the Greater Itremo Basin or the sedimentary rocks of the Tanzania Craton. The Cuddapah Basin samples also have $\varepsilon_{Hf}(t)$ that extend to more negative values compared to the other terranes. This indicates that the Cuddapah Basin is not related to the Greater Itremo Basin. Collins et al. (2015) suggested that sources for the Cuddapah Basin were identifiable within the SE Indian Krishna Orogen and the eastern Dharwar Craton.

4.3. Provenance of the Greater Itremo Basin

Establishing the sources of detrital zircons far back in time is problematic for a myriad of reasons. The sources may no longer be exposed at the surface, and therefore our current databases might not reflect the actual source rocks being eroded at the time. Source protoliths may not be magmatic in nature, indeed the maturity of the quartzites in the Greater Itremo Basin lend support to a multi-phase sedimentary cycle for their final deposition, and many of the sources may be sedimentary rocks. Also, the Earth's tectonic plate configuration (especially in a full-plate sense) beyond the Neoproterozoic is poorly constrained, making it difficult to determine proximal terranes and therefore, potential sources.

Despite these substantial limitations to establishing sources of detrital zircons, we have attempted to provide some preliminary assessment of potential source regions. To do this, we have only looked at magmatic protoliths, and used the magmatic crystallisation ages to compare with our detrital zircon dataset (Figure 5.6). Detrital zircon source regions for the Itremo Group outside of Madagascar have been proposed in east Africa (Cox et al., 1998; Cox et al., 2004; Fitzsimons and Hulscher, 2005) and India (Tucker et al., 2011a). We address these proposals in light of currently available data below.

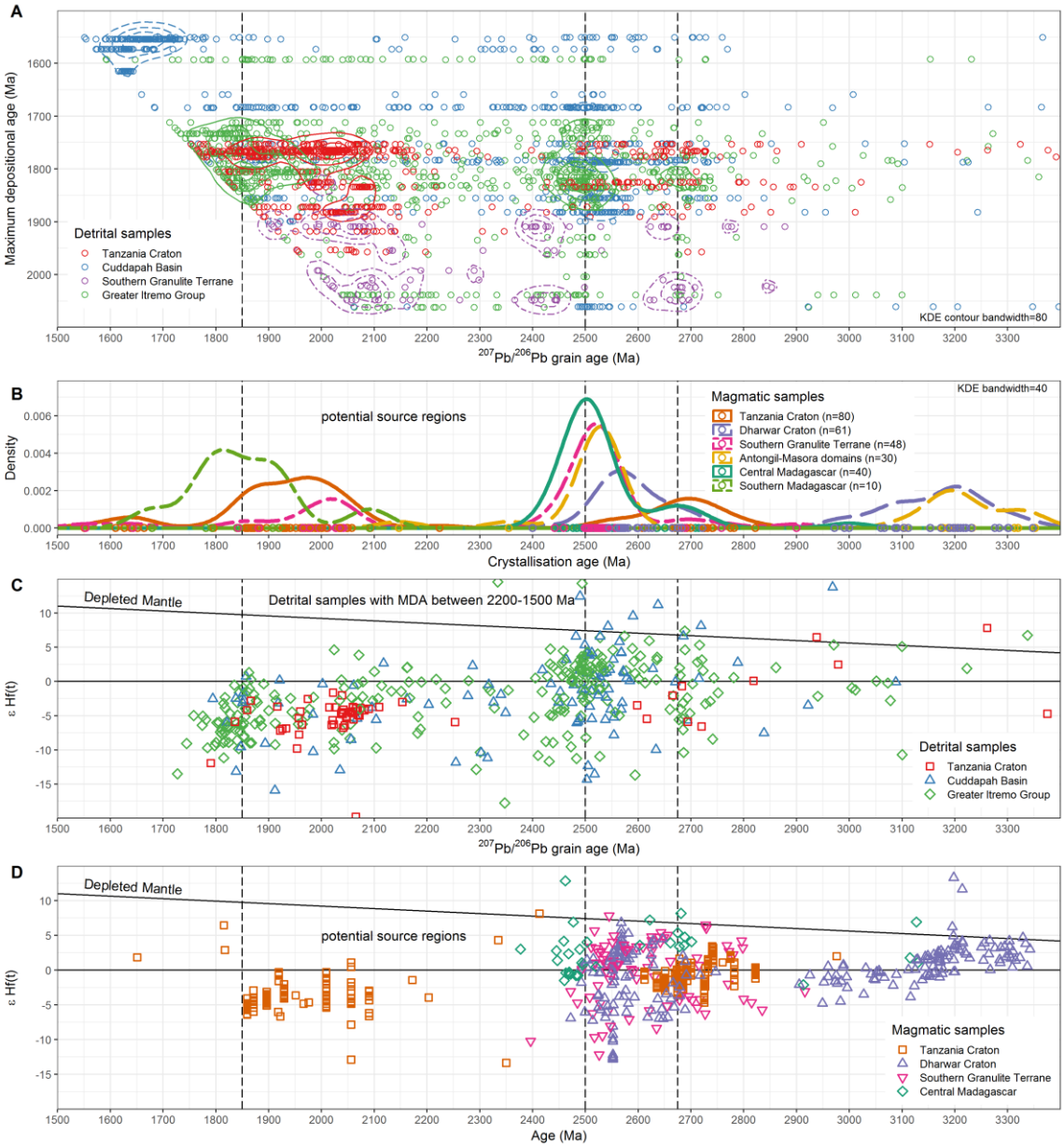

Figure 5.7 Comparison of detrital zircon data with magmatic crystallisation ages for different regions in Africa, Madagascar and India a) Detrital samples from the Tanzania Craton, Cuddapah Basin, Southern Granulite Terrane and Greater Itremo Basin plotted and contoured using KDE (bandwidth=80). Only data within 10% concordance is plotted; b) KDE plots (bandwidth=40) of magmatic crystallisation ages for potential source regions. X-axis scales are the same for both plots; c) Hf isotopes for detrital samples with maximum depositional ages between 2200 and 1500 Ma; and d) Hf isotopes for magmatic samples.

The c. 2650 Ma peak in the Greater Itremo Basin data closely matches magmatic data from central Madagascar, the Southern Granulite Terrane and the Tanzania Craton. This age is less common in the Dharwar Craton. Given that the Itremo Group overlies the Archean orthogneisses of central Madagascar, this source is unsurprising. The more significant detrital zircon age peak at c. 2500 Ma is indistinguishable from the central Madagascar peak (Figure 5.6). It's worth noting here that the Dharwar Craton, Southern Granulite Terrane and Antongil-Masora peaks are slightly older. These observations

support a local, central Madagascan origin for the majority of Archean detrital zircons in the Greater Itremo Basin.

The c. 2000–1750 Ma peak for the Greater Itremo Basin correlates with magmatic data from southern Madagascar, the Tanzania Craton and the Southern Granulite Terrane. Magmatic sources for these zircons are unknown in the Dharwar Craton India. The age similarities in both sedimentary and magmatic rocks in Madagascar and the Tanzania Craton suggest that these regions were juxtaposed during the Paleoproterozoic/early Mesoproterozoic. The abundant c. 2500 Ma detritus in the Tanzania Craton sedimentary rocks, with lack of age equivalent magmatic rocks nearby, suggests that central Madagascar was a likely source for this component.

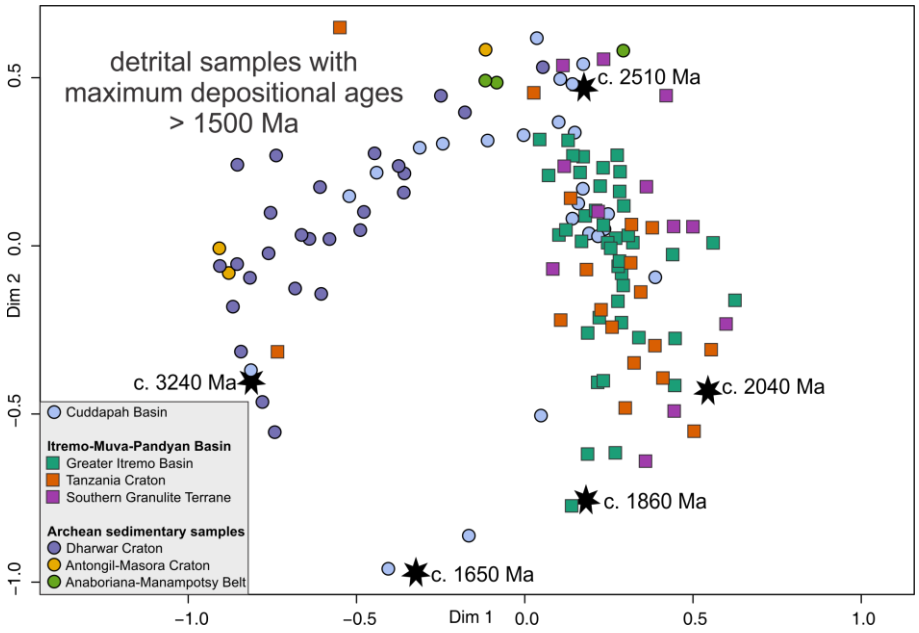

Figure 5.8 Multi-dimensional scaling plot using Provenance package in R (Vermeesch et al., 2016) of detrital samples with maximum depositional ages > 1500 Ma. Synthetic ages indicated by the black stars, calculated as 200 randomly generated, normally distributed, numbers with mean as per the label and standard deviation of 50.

The Southern Granulite Terrane, although with maximum depositional ages that are slightly older, has a significant c. 2100–1900 Ma component of detrital zircons. Magmatic rocks of this age are also found in the Southern Granulite Terrane (e.g. Clark et al., In review; Ghosh et al., 2004; Kumar et al., 2017). However, rocks of this age are not found in the adjacent Dharwar Craton. Given the similarities in both magmatic and detrital zircon data, it is likely that the Southern Granulite Terrane was contiguous with Madagascar at the time of deposition during the Paleoproterozoic. The c. 2700 Ma and c. 2400 Ma detrital zircon peaks for the Southern Granulite Terrane also broadly correlate with age

equivalent magmatic rocks from central Madagascar. Although detrital samples with Paleoproterozoic maximum depositional ages are limited (n=12), it is curious that the main magmatic peak at c. 2530 Ma for the Southern Granulite Terrane is not expressed in the detrital zircon record for this region. This may be related to the high-grade reworking of the Southern Granulite Terrane, resulting in c. 2.5 Ga zircons becoming discordant or reset by metamorphism.

4.4. Implications for Proterozoic paleogeography

The Greater Itremo Basin sequences are comparable to sedimentary sequences in the Tanzania Craton and we suggest that they sourced detritus from the Archean basement rocks of Madagascar and the magmatic rocks of the Tanzania Craton and southern Madagascar. This implies that the Tanzania Craton was contiguous with central Madagascar at the time of deposition, which we have interpreted here as latest Paleoproterozoic to early Mesoproterozoic. This broadly supports the tectonic model of Cox et al. (2004) and Fitzsimons and Hulscher (2005). The connection with the Southern Granulite Terrane is less clear; some data correlate with the main grain age peaks of the Itremo/Tanzania data, however, the Southern Granulite Terrane samples have older maximum depositional ages. We suggest that these terranes were contiguous, and that sedimentary sequences of the Southern Granulite Terrane represent either an older part of the basin, or a separate, older basin sourcing the same regions. Further Hf isotope studies on Paleoproterozoic detrital zircons from the Southern Granulite Terrane would provide further evidence either for or against this model.

To test this model, we have incorporated our database into a continental reconstruction, and interpolated the age data (Figure 5.8). We modified the model and used the plate geometries of the Merdith et al. (2017) *GPlates* model; reconstructing the model based on our interpretation at c. 1700 Ma. Our georeferenced age database was reconstructed according to this modification and exported to ArcGIS where we then interpolated the data. We used natural neighbour interpolation of age data with a consistent legend for both plots for easy comparison.

Maximum depositional ages for Africa, Madagascar and the Southern Granulite Terrane are shown in Figure 5.8a, and the magmatic ages for these terranes are shown in Figure 5.8b. It's an assumption that the magmatic samples collected today are representative of the rocks exposed at c. 1700 Ma, and that these represent source regions available at the time. Despite this limitation, the reconstruction is supported by the maximum depositional ages in the detrital zircon data, which closely reflect the ages of these source regions. This suggests that the sediments in the Greater Itremo Basin and coeval sediments deposited in this part of Nuna/Columbia were sourced from reasonably proximal regions, even when these sources are now in dispersed parts of the world.

The magmatic age data are very consistent across the boundaries of the Tanzania Craton and Central Madagascar Craton in the reconstruction (Figure 5.8a). Notably, the progression from older Archean rocks in the north (reconstructed position) to Paleoproterozoic rocks in the south is consistent across both the Tanzania and Central Madagascar cratons. This shows spatially, our interpreted link between the Irumide Belt, the Usagaran-Ubendian belts, and southern Madagascar. Similar aged Archean rocks of the Tanzania Craton and Central Madagascar Craton also suggest a link. The Paleoproterozoic zone in the south of the map (yellow) as well as the Archean zone in the north of the map (pink-purple) represent the two major source regions for detritus in the sedimentary rocks of the Tanzania Craton, Madagascar and the Southern Granulite Terrane.

The correlation of samples with Paleoproterozoic maximum depositional ages is highlighted by the broad yellow zone in Figure 5.8. Although further detrital zircon data from Africa would make this interpolation more robust. This highlights the broad geographical area that these Paleoproterozoic rocks were deposited in and crudely outlines the reconstructed, but presently exposed, margins of a wider late Paleoproterozoic to early Mesoproterozoic basin. We suggest this basin be called the Itremo-Muva-Pandyan Basin after two of the most extensive sedimentary systems and the name for the 'mobile belt' that encompasses the Southern Granulite Belt of India.

The correlation of both basement terranes and sedimentary basins between central Madagascar and the Tanzania Craton (as well as the Southern Granulite Terrane), and the dissimilarity of these systems with the Dharwar Craton, supports the 'Out of Africa' model of central Madagascar's origin (Collins, 2006; Collins and Pisarevsky, 2005; Collins and Windley, 2002; Cox et al., 2004; Fitzsimons and Hulscher, 2005). These correlations refute the Greater Dharwar model (Tucker et al., 2011a; Tucker et al., 2011b) for the Paleoproterozoic and Mesoproterozoic. Furthermore, to evolve from Nuna/Columbia to Gondwana, central Madagascar would have to rift off the Tanzania Craton to form an isolated late Mesoproterozoic–Neoproterozoic continent (named Azania by Collins and Pisarevsky, 2005) to later collide back against East Africa with Stenian–Cryogenian arc terranes marking the suture (Archibald et al., 2017a; Archibald et al., 2017b; Jöns and Schenk, 2008) and India in the Ediacaran–Cambrian (Collins, 2006; Fritz et al., 2013; Merdith et al., 2017).

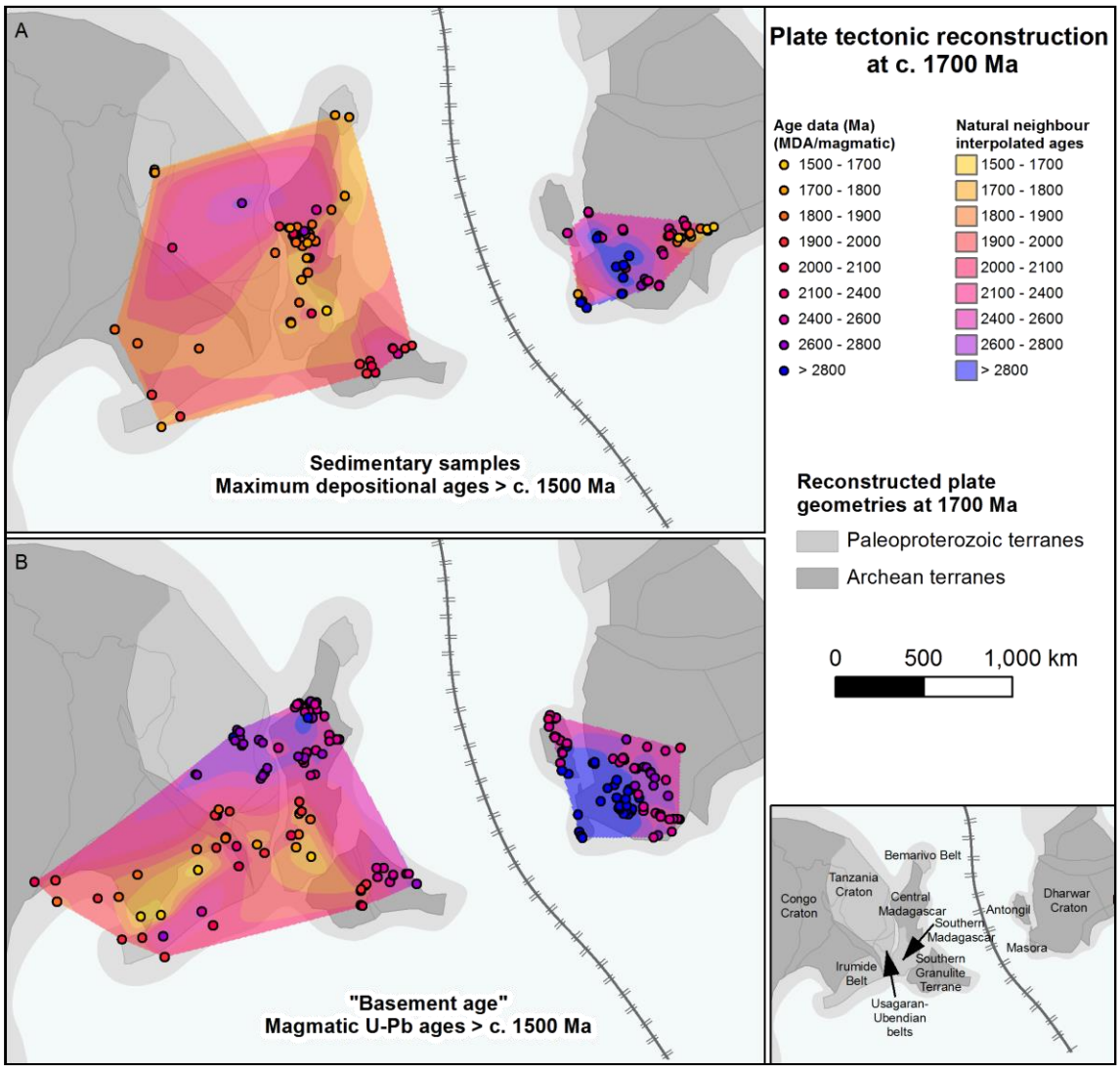

Figure 5.9 Reconstruction at 1700 Ma, with our U–Pb zircon magmatic and detrital database mapped and interpolated. All detrital samples with maximum depositional ages > c. 1500 Ma and magmatic samples with zircon U–Pb ages > c. 1500 Ma are included. The boundary separating the Africa-Madagascar-Southern India data and the Dharwar-Antongil-Masora data is arbitrary and simply indicates that we interpret these regions to be separate at this time.

The modelling highlights some regions where further data collection would be beneficial to increase the confidence of this reconstruction. More data from the Southern Granulite Terrane would be useful, particularly given the maximum depositional age differences. Further detrital studies of the Tanzania Craton, Usagaran-Ubendian belts and the Irumide Belt would also be useful for increasing the resolution of the interpolation in this region. Figure 5.6 also highlights regions where there is limited or no Hf isotope data. To our knowledge, there are no published Hf isotope data for detrital samples with c. 2000–1600 Ma maximum depositional ages in the Southern Granulite Terrane, southern Madagascar, and very few data for the Tanzania Craton (Figure 5.6). Likewise, there are no Hf isotope data for c. 2000–1600 Ma magmatic samples from southern Madagascar, and very few Hf isotope data for magmatic rocks in the Tanzania Craton and Dharwar Craton for all of the

major age peaks presented in Figure 5.6. Further data collection will enable a more robust test of some of the ideas and the reconstruction we've presented in this manuscript.

5. Conclusions

New U–Pb and Lu–Hf zircon data together with a substantial database of magmatic and detrital U–Pb and Lu–Hf data, have been used to show the similarities and differences of terranes in Africa, Madagascar and India. The Itremo Group, which has traditionally been mapped as a relatively localised sedimentary package, is here correlated with other sedimentary rocks in Madagascar, including the Maha Group, Sahantaha Group, southern Madagascar, and the Ambatolampy Group. These are also correlated with Paleoproterozoic sedimentary rocks of the Tanzania Craton in Africa and tentatively with metasedimentary rocks in the Southern Granulite Terrane of India to form a major intra-Nuna/Columbia sedimentary basin that we name the Itremo-Muva-Pandyan Basin. We propose a plate tectonic configuration for the Paleoproterozoic where central Madagascar is contiguous with the Tanzania Craton to the west and the Southern Granulite Terrane to the east. This model strongly supports an ancient Proterozoic origin for central Madagascar against the Tanzania Craton of East Africa, and the isolation of central Madagascar as the late Mesoproterozoic microcontinent Azania that collided back with East Africa and India in the Neoproterozoic–Cambrian. This work suggests that the Greater Dharwar model is incorrect for the Paleoproterozoic to Mesoproterozoic.

References

Alessio, B.L., 2019. The tectonic evolution of the southern Congo Craton. PhD Thesis.

Alessio, B.L., Collins, A.S., Clark, C., Glorie, S., Siegfried, P.R. and Taylor, R., 2019. Age, origin and palaeogeography of the Southern Irumide Belt, Zambia. Journal of the Geological Society: jgs2018-174.

Alessio, B.L., Collins, A.S., Siegfried, P., Glorie, S., De Waele, B., Payne, J. and Archibald, D.B., 2018. Neoproterozoic tectonic geography of the south-east Congo Craton in Zambia as deduced from the age and composition of detrital zircons. Geoscience Frontiers.

Ali, K.A., Jeon, H., Andresen, A., Li, S.-Q., Harbi, H.M. and Hegner, E., 2014. U–Pb zircon geochronology and Nd–Hf–O isotopic systematics of the Neoproterozoic Hadb adh Dayheen ring complex, Central Arabian Shield, Saudi Arabia. Lithos, 206-207: 348-360.

Archibald, D.B., Collins, A.S., Foden, J.D., Payne, J.L., Holden, P., Razakamanana, T., De Waele, B., Thomas, R.J. and Pitfield, P.E.J., 2016. Genesis of the Tonian Imorona–Itsindro magmatic Suite in central Madagascar: Insights from U–Pb, oxygen and hafnium isotopes in zircon. Precambrian Research, 281: 312-337.

Archibald, D.B., Collins, A.S., Foden, J.D., Payne, J.L., Macey, P.H., Holden, P. and Razakamanana, T., 2017a. Stenian–Tonian arc magmatism in west–central Madagascar: the genesis of the Dabolava Suite. Journal of the Geological Society: jgs2017-028.

Archibald, D.B., Collins, A.S., Foden, J.D., Payne, J.L., Taylor, R., Holden, P., Razakamanana, T. and Clark, C., 2015. Towards unravelling the Mozambique Ocean conundrum using a triumvirate of zircon isotopic proxies on the Ambatolampy Group, central Madagascar. Tectonophysics, 662: 167-182.

Archibald, D.B., Collins, A.S., Foden, J.D. and Razakamanana, T., 2017b. Tonian Arc Magmatism in Central Madagascar: The Petrogenesis of the Imorona-Itsindro Suite. The Journal of Geology, 125(3): 000-000.

Armistead, S.E., Collins, A., Merdith, A.S., Payne, J.L., Cox, G.M., Foden, J.D., Razakamanana, T. and De Waele, B., 2019. Evolving marginal terranes during Neoproterozoic supercontinent reorganisation: constraints from the Bemarivo Domain in northern Madagascar. Tectonics.

Armistead, S.E., Collins, A.S., Payne, J.L., Foden, J.D., De Waele, B., Shaji, E. and Santosh, M., 2017. A re-evaluation of the Kumta Suture in western peninsular India and its extension into Madagascar. Journal of Asian Earth Sciences.

Armistead, S.E., Collins, A.S., Redaa, A., Gilbert, S., Jepson, G., Gillespie, J., Blades, M.L., Foden, J.D. and Razakamanana, T., In Review. Structural evolution and medium-temperature thermochronology of central Madagascar: implications for Gondwana amalgamation. Journal of the Geological Society.

Batumike, J.M., Griffin, W.L., O'Reilly, S.Y., Belousova, E.A. and Pawlitschek, M., 2009. Crustal evolution in the central Congo-Kasai Craton, Luebo, D.R. Congo: Insights from zircon U–Pb ages, Hf-isotope and trace-element data. Precambrian Research, 170(1-2): 107-115.

Batumike, J.M., O'Reilly, S.Y., Griffin, W.L. and Belousova, E.A., 2007. U–Pb and Hf-isotope analyses of zircon from the Kundelungu Kimberlites, D.R. Congo: Implications for crustal evolution. Precambrian Research, 156(3-4): 195-225.

Bauer, W., Walsh, G.J., de Waele, B., Thomas, R.J., Horstwood, M.S.A., Bracciali, L., Schofield, D.I., Wollenberg, U., Lidke, D.J., Rasaona, I.T. and Rabarimanana, M.H., 2011. Cover sequences at the northern margin of the Antongil Craton, NE Madagascar. Precambrian Research, 189(3-4): 292-312.

BGS-USGS-GLW, 2008. Republique de Madagascar Ministère de L'engergie et des Mines (MEM/SG/DG/UCP/PGRM). British Geological Survey Research Report.

Blades, M.L., Collins, A.S., Foden, J., Payne, J.L., Xu, X., Alemu, T., Woldetinsae, G., Clark, C. and Taylor, R.J.M., 2015. Age and hafnium isotopic evolution of the Didesa and Kemashi Domains, western Ethiopia. Precambrian Research, 270: 267-284.

Boger, S.D., Hirdes, W., Ferreira, C.A.M., Schulte, B., Jenett, T. and Fanning, C.M., 2014. From passive margin to volcano–sedimentary forearc: The Tonian to Cryogenian evolution of the Anosyen Domain of southeastern Madagascar. Precambrian Research, 247: 159-186.

Boger, S.D., Maas, R., Pastuhov, M., Macey, P.H., Hirdes, W., Schulte, B., Fanning, C.M., Ferreira, C.A.M., Jenett, T. and Dallwig, R., 2019. The tectonic domains of southern and western Madagascar. Precambrian Research.

Bouvier, A., Vervoort, J.D. and Patchett, P.J., 2008. The Lu–Hf and Sm–Nd isotopic composition of CHUR: constraints from unequilibrated chondrites and implications for the bulk composition of terrestrial planets. Earth and Planetary Science Letters, 273(1): 48-57.

Buchwaldt, R., Tucker, R.D. and Dymek, R.F., 2003. Geothermobarometry and U-Pb Geochronology of metapelitic granulites and pelitic migmatites from the Lokoho region, Northern Madagascar. American Mineralogist, 88(11-12): 1753-1768.

Bulambo, M., De Waele, B., Kampunzu, A. and Tembo, F., 2004. SHRIMP U–Pb geochronology of the Choma–Kalomo block (Zambia) and geological implications, 20th Colloquium of African Geology, Orléans, France, pp. 96.

Clark, C., Collins, A., Taylor, R. and Hand, M., In review. An African origin for the tip of India.

Clark, C., Collins, A.S., Timms, N.E., Kinny, P.D., Chetty, T. and Santosh, M., 2009. SHRIMP U–Pb age constraints on magmatism and high-grade metamorphism in the Salem Block, southern India. Gondwana Research, 16(1): 27-36.

Collins, A.S., 2006. Madagascar and the amalgamation of Central Gondwana. Gondwana Research, 9(1-2): 3-16.

Collins, A.S., Clark, C., Sajeev, K., Santosh, M., Kelsey, D.E. and Hand, M., 2007a. Passage through India: the Mozambique Ocean suture, high-pressure granulites and the Palghat-Cauvery shear zone system. Terra Nova, 19(2): 141-147.

Collins, A.S., Johnson, S., Fitzsimons, I.C., Powell, C.M., Hulscher, B., Abello, J. and Razakamanana, T., 2003a. Neoproterozoic deformation in central Madagascar: a structural section through part of the East African Orogen. Geological Society, London, Special Publications, 206(1): 363-379.

Collins, A.S., Kinny, P.D. and Razakamanana, T., 2012. Depositional age, provenance and metamorphic age of metasedimentary rocks from southern Madagascar. Gondwana Research, 21(2-3): 353-361.

Collins, A.S., Kröner, A., Fitzsimons, I.C.W. and Razakamanana, T., 2003b. Detrital footprint of the Mozambique ocean: U–Pb SHRIMP and Pb evaporation zircon geochronology of metasedimentary gneisses in eastern Madagascar. Tectonophysics, 375(1-4): 77-99.

Collins, A.S., Patranabis-Deb, S., Alexander, E., Bertram, C.N., Falster, G.M., Gore, R.J., Mackintosh, J., Dhang, P.C., Saha, D. and Payne, J.L., 2015. Detrital mineral age, radiogenic isotopic stratigraphy and tectonic significance of the Cuddapah Basin, India. Gondwana Research, 28(4): 1294-1309.

Collins, A.S. and Pisarevsky, S.A., 2005. Amalgamating eastern Gondwana: The evolution of the Circum-Indian Orogens. Earth-Science Reviews, 71(3-4): 229-270.

Collins, A.S., Santosh, M., Braun, I. and Clark, C., 2007b. Age and sedimentary provenance of the Southern Granulites, South India: U-Th-Pb SHRIMP secondary ion mass spectrometry. Precambrian Research, 155(1-2): 125-138.

Collins, A.S. and Windley, B.F., 2002. The tectonic evolution of central and northern Madagascar and its place in the final assembly of Gondwana. The Journal of Geology, 110(3): 325-339.

Costa, R.L., Schmitt, R.S., Collins, A., Armistead, S.E., Razakamanana, T. and Archibald, D., Submitted. Tectonic evolution of an Early Cryogenian synmagmatic basin in central Madagascar. Precambrian Research.

Cox, R., Armstrong, R.A. and Ashwal, L.D., 1998. Sedimentology, geochronology and provenance of the Proterozoic Itremo Group, central Madagascar, and implications for pre-Gondwana palaeogeography. Journal of the Geological Society, 155(6): 1009-1024.

Cox, R., Coleman, D.S., Chokel, C.B., DeOreo, S.B., Wooden, J.L., Collins, A.S., De Waele, B. and Kröner, A., 2004. Proterozoic tectonostratigraphy and paleogeography of central Madagascar derived from detrital zircon U-Pb age populations. The Journal of geology, 112(4): 379-399.

Cox, R., Rivers, T., Mapani, B., Tembo, D. and De Waele, B., 2002. New U-Pb data for the Irumide belt: LAM-ICP-MS results for Luangwa Terrane, Abstracts, 11th IAGOD Quadrennial Symposium and Geocongress Windhoek.

Daly, M., 1986. The tectonic and thermal evolution of the Irumide belt, Zambia, University of Leeds.

De Waele, B. and Fitzsimons, I.C.W., 2007. The nature and timing of Palaeoproterozoic sedimentation at the southeastern margin of the Congo Craton; zircon U–Pb geochronology of plutonic, volcanic and clastic units in northern Zambia. Precambrian Research, 159(1-2): 95-116.

De Waele, B., Liégeois, J.-P., Nemchin, A.A. and Tembo, F., 2006. Isotopic and geochemical evidence of proterozoic episodic crustal reworking within the irumide belt of south-central Africa, the southern metacratonic boundary of an Archaean Bangweulu Craton. Precambrian Research, 148(3-4): 225-256.

De Waele, B., Thomas, R.J., Macey, P.H., Horstwood, M.S.A., Tucker, R.D., Pitfield, P.E.J., Schofield, D.I., Goodenough, K.M., Bauer, W., Key, R.M., Potter, C.J., Armstrong, R.A., Miller, J.A., Randriamananjara, T., Ralison, V., Rafahatelo, J.M., Rabarimanana, M. and Bejoma, M., 2011. Provenance and tectonic significance of the Palaeoproterozoic metasedimentary successions of central and northern Madagascar. Precambrian Research, 189(1-2): 18-42.

de Wit, M.J., Bowring, S.A., Ashwal, L.D., Randrianasolo, L.G., Morel, V.P.I. and Rambeloson, R.A., 2001. Age and tectonic evolution of Neoproterozoic ductile shear zones in southwestern Madagascar, with implications for Gondwana studies. Tectonics, 20(1): 1-45.

Dodson, M., Cavanagh, B., Thatcher, E. and Aftalion, M., 1975. Age limits for the Ubendian metamorphic episode in northern Malawi. Geological Magazine, 112(4): 403-410.

Emmel, B., Jons, N., Kroner, A., Jacobs, J., Wartho, J.A., Schenk, V., Razakamanana, T. and Austegard, A., 2008. From Closure of the Mozambique Ocean to Gondwana Breakup: New Evidence from Geochronological Data of the Vohibory Terrane, Southwest Madagascar. The Journal of Geology, 116(1): 21-38.

Fernandez, A., Schreurs, G., Villa, I.M., Huber, S. and Rakotondrazafy, M., 2003. Age constraints on the tectonic evolution of the Itremo region in Central Madagascar. Precambrian Research, 123(2-4): 87-110.

Fitzsimons, I.C.W. and Hulscher, B., 2005. Out of Africa: detrital zircon provenance of central Madagascar and Neoproterozoic terrane transfer across the Mozambique Ocean. Terra Nova, 17(3): 224-235.

Foster, D.A., Goscombe, B.D., Newstead, B., Mapani, B., Mueller, P.A., Gregory, L.C. and Muvangua, E., 2015. U–Pb age and Lu–Hf isotopic data of detrital zircons from the Neoproterozoic Damara Sequence: implications for Congo and Kalahari before Gondwana. Gondwana Research, 28(1): 179-190.

Fritz, H., Abdelsalam, M., Ali, K.A., Bingen, B., Collins, A.S., Fowler, A.R., Ghebreab, W., Hauzenberger, C.A., Johnson, P.R., Kusky, T.M., Macey, P., Muhongo, S., Stern, R.J. and Viola, G., 2013. Orogen styles in the East African Orogen: A review of the Neoproterozoic to Cambrian tectonic evolution. Journal of African Earth Sciences, 86: 65-106.

Ghosh, J.G., de Wit, M.J. and Zartman, R., 2004. Age and tectonic evolution of Neoproterozoic ductile shear zones in the Southern Granulite Terrain of India, with implications for Gondwana studies. Tectonics, 23(3).

Glorie, S., De Grave, J., Singh, T., Payne, J.L. and Collins, A.S., 2014. Crustal root of the Eastern Dharwar Craton: Zircon U–Pb age and Lu–Hf isotopic evolution of the East Salem Block, southeast India. Precambrian Research, 249: 229-246.

Goodenough, K.M., Thomas, R.J., De Waele, B., Key, R.M., Schofield, D.I., Bauer, W., Tucker, R.D., Rafahatelo, J.M., Rabarimanana, M., Ralison, A.V. and Randriamananjara, T., 2010. Post-collisional magmatism in the central East African Orogen: The Maevarano Suite of north Madagascar. Lithos, 116(1-2): 18-34.

Griffin, W., Pearson, N., Belousova, E., Jackson, S., Van Achterbergh, E., O'Reilly, S.Y. and Shee, S., 2000. The Hf isotope composition of cratonic mantle: LAM-MC-ICPMS analysis of zircon megacrysts in kimberlites. Geochimica et Cosmochimica Acta, 64(1): 133-147.

Griffin, W., Wang, X., Jackson, S., Pearson, N., O'Reilly, S.Y., Xu, X. and Zhou, X., 2002. Zircon chemistry and magma mixing, SE China: in-situ analysis of Hf isotopes, Tonglu and Pingtan igneous complexes. Lithos, 61(3): 237-269.

Handke, M.J., Tucker, R.D. and Ashwal, L.D., 1999. Neoproterozoic continental arc magmatism in west-central Madagascar. Geology, 27(4): 351-354.

Hanson, R.E., Wilson, T.J., Brueckner, H.K., Onstott, T.C., Wardlaw, M.S., Johns, C.C. and Hardcastle, K.C., 1988. Reconnaissance geochronology, tectonothermal evolution, and regional significance of the Middle Proterozoic Choma-Kalomo block, southern Zambia. Precambrian Research, 42(1-2): 39-61.

Henderson, B., Collins, A.S., Payne, J., Forbes, C. and Saha, D., 2014. Geologically constraining India in Columbia: The age, isotopic provenance and geochemistry of the protoliths of the Ongole Domain, Southern Eastern Ghats, India. Gondwana Research, 26(3-4): 888-906.

Ishwar-Kumar, C., Windley, B., Horie, K., Kato, T., Hokada, T., Itaya, T., Yagi, K., Gouzu, C. and Sajeev, K., 2013. A Rodinian suture in western India: New insights on India-Madagascar correlations. Precambrian Research, 236: 227-251.

Jayananda, M., Chardon, D., Peucat, J.-J. and Fanning, C.M., 2015. Paleo-to Mesoarchean TTG accretion and continental growth in the western Dharwar craton, Southern India: Constraints from SHRIMP U–Pb zircon geochronology, whole-rock geochemistry and Nd–Sr isotopes. Precambrian Research, 268: 295-322.

John, T., 2001. Subduction and continental collision in the Lufilian Arc-Zambesi Belt orogen: A petrological, geochemical, and geochronological study of eclogites and whiteschists (Zambia), Christian-Albrechts Universität Kiel.

Johnson, P.R., Andresen, A., Collins, A.S., Fowler, A.R., Fritz, H., Ghebreab, W., Kusky, T. and Stern, R.J., 2011. Late Cryogenian–Ediacaran history of the Arabian–Nubian Shield: A review of depositional, plutonic, structural, and tectonic events in the closing stages of the northern East African Orogen. Journal of African Earth Sciences, 61(3): 167-232.

Jöns, N. and Schenk, V., 2008. Relics of the Mozambique Ocean in the central East African Orogen: evidence from the Vohibory Block of southern Madagascar. Journal of Metamorphic Geology.

Joy, S., Jelsma, H., Tappe, S. and Armstrong, R., 2015. SHRIMP U–Pb zircon provenance of the Sullavai Group of Pranhita–Godavari Basin and Bairenkonda Quartzite of Cuddapah Basin, with implications for the Southern Indian Proterozoic tectonic architecture. Journal of Asian Earth Sciences, 111: 827-839.

Kabete, J., Groves, D., McNaughton, N. and Dunphy, J., 2006. The geology, SHRIMP U–Pb geochronology and metallogenic significance of the Ankisatra-Besakay District, Andriamena belt, northern Madagascar. Journal of African Earth Sciences, 45(1): 87-122.

Katongo, C., Koller, F., Kloetzli, U., Koeberl, C., Tembo, F. and De Waele, B., 2004. Petrography, geochemistry, and geochronology of granitoid rocks in the Neoproterozoic-Paleozoic Lufilian–Zambezi belt, Zambia: Implications for tectonic setting and regional correlation. Journal of African Earth Sciences, 40(5): 219-244.

Kazimoto, E.O., Schenk, V. and Berndt, J., 2014. Neoarchean and Paleoproterozoic crust formation in the Ubendian Belt of Tanzania: insights from zircon geochronology and geochemistry. Precambrian Research, 252: 119-144.

Key, R., Liyungu, A., Njamu, F.M., Somwe, V., Banda, J., Mosley, P. and Armstrong, R., 2001. The western arm of the Lufilian Arc in NW Zambia and its potential for copper mineralization. Journal of African Earth Sciences, 33(3-4): 503-528.

Koegelenberg, C., Kisters, A., Kramers, J. and Frei, D., 2015. U–Pb detrital zircon and 39Ar–40Ar muscovite ages from the eastern parts of the Karagwe-Ankole Belt: Tracking Paleoproterozoic basin formation and Mesoproterozoic crustal amalgamation along the western margin of the Tanzania Craton. Precambrian Research, 269: 147-161.

Konopásek, J., Košler, J., Sláma, J. and Janoušek, V., 2014. Timing and sources of pre-collisional Neoproterozoic sedimentation along the SW margin of the Congo Craton (Kaoko Belt, NW Namibia). Gondwana Research, 26(1): 386-401.

Kooijman, E., Upadhyay, D., Mezger, K., Raith, M.M., Berndt, J. and Srikantappa, C., 2011. Response of the U–Pb chronometer and trace elements in zircon to ultrahigh-temperature metamorphism: The Kadavur anorthosite complex, southern India. Chemical Geology, 290(3-4): 177-188.

Kröner, A., Hegner, E., Collins, A.S., Windley, B.F., Brewer, T.S., Razakamanana, T. and Pidgeon, R.T., 2000. Age and magmatic history of the Antananarivo Block, central Madagascar, as derived from zircon geochronology and Nd isotopic systematics. American Journal of Science, 300(4): 251-288.

Kröner, A., Santosh, M. and Wong, J., 2012. Zircon ages and Hf isotopic systematics reveal vestiges of Mesoproterozoic to Archaean crust within the late Neoproterozoic–Cambrian high-grade terrain of southernmost India. Gondwana Research, 21(4): 876-886.

Kumar, T.V., Rao, Y.B., Plavsa, D., Collins, A.S., Tomson, J., Gopal, B.V. and Babu, E., 2017. Zircon U-Pb ages and Hf isotopic systematics of charnockite gneisses from the Ediacaran–Cambrian high-grade metamorphic terranes, southern India: Constraints on crust formation, recycling, and Gondwana correlations. Bulletin, 129(5-6): 625-648.

Lancaster, P.J., Dey, S., Storey, C.D., Mitra, A. and Bhunia, R.K., 2015. Contrasting crustal evolution processes in the Dharwar craton: insights from detrital zircon U–Pb and Hf isotopes. Gondwana Research, 28(4): 1361-1372.

Li, S.-S., Santosh, M., Indu, G., Shaji, E. and Tsunogae, T., 2017. Detrital zircon geochronology of quartzites from the southern Madurai Block, India: Implications for Gondwana reconstruction. Geoscience Frontiers, 8(4): 851-867.

Linol, B., de Wit, M.J., Barton, E., de Wit, M.M.J. and Guillocheau, F., 2016. U–Pb detrital zircon dates and source provenance analysis of Phanerozoic sequences of the Congo Basin, central Gondwana. Gondwana Research, 29(1): 208-219.

Maibam, B., Gerdes, A. and Goswami, J., 2016. U–Pb and Hf isotope records in detrital and magmatic zircon from eastern and western Dharwar craton, southern India: Evidence for coeval Archaean crustal evolution. Precambrian Research, 275: 496-512.

Maibam, B., Goswami, J. and Srinivasan, R., 2011. Pb–Pb zircon ages of Archaean metasediments and gneisses from the Dharwar craton, southern India: implications for the antiquity of the eastern Dharwar craton. Journal of earth system science, 120(4): 643-661.

Merdith, A.S., Collins, A.S., Williams, S.E., Pisarevsky, S., Foden, J.D., Archibald, D.B., Blades, M.L., Alessio, B.L., Armistead, S. and Plavsa, D., 2017. A full-plate global reconstruction of the Neoproterozoic. Gondwana Research, 50: 84-134.

Mohan, M.R., Sarma, D.S., McNaughton, N.J., Fletcher, I.R., Wilde, S.A., Siddiqui, M.A., Rasmussen, B., Krapez, B., Gregory, C.J. and Kamo, S.L., 2014. SHRIMP zircon and titanite U-Pb ages, Lu-Hf isotope signatures and geochemical constraints for~ 2.56 Ga granitic magmatism in Western Dharwar Craton, Southern India: Evidence for short-lived Neoarchean episodic crustal growth? Precambrian Research, 243: 197-220.

Morag, N., Avigad, D., Gerdes, A., Belousova, E. and Harlavan, Y., 2011. Crustal evolution and recycling in the northern Arabian-Nubian Shield: New perspectives from zircon Lu–Hf and U–Pb systematics. Precambrian Research, 186(1-4): 101-116.

Ngoyi, L.K.K., Liégeois, J.-P., Demaiffe, D. and Dumont, P., 1991. Age tardi-ubendien (Protérozoïque inférieur) des dômes granitiques de l'arc cuprifère zaïro-zambien. Comptes rendus de l'Académie des sciences. Série 2, Mécanique, physique, chimie, sciences de l'univers, sciences de la terre, 313(1): 83-89.

Nutman, A.P., Mohajjel, M., Bennett, V.C. and Fergusson, C.L., 2013. Gondwanan Eoarchean–Neoproterozoic ancient crustal material in Iran and Turkey: zircon U–Pb–Hf isotopic evidence. Canadian Journal of Earth Sciences, 51(3): 272-285.

Paquette, J.-L., Goncalves, P., Devouard, B. and Nicollet, C., 2004. Micro-drilling ID-TIMS U-Pb dating of single monazites: A new method to unravel complex poly-metamorphic evolutions. Application to the UHT granulites of Andriamena (North-Central Madagascar). Contributions to Mineralogy and Petrology, 147(1): 110-122.

Paquette, J.-L. and Nédélec, A., 1998. A new insight into Pan-African tectonics in the East–West Gondwana collision zone by U–Pb zircon dating of granites from central Madagascar. Earth and Planetary Science Letters, 155(1-2): 45-56.

Paquette, J.-L., Nédélec, A., Moine, B. and Rakotondrazafy, M., 1994. U-Pb, single zircon Pb-evaporation, and Sm-Nd isotopic study of a granulite domain in SE Madagascar. The Journal of Geology, 102(5): 523-538.

Paton, C., Hellstrom, J., Paul, B., Woodhead, J. and Hergt, J., 2011. Iolite: Freeware for the visualisation and processing of mass spectrometric data. Journal of Analytical Atomic Spectrometry, 26(12): 2508-2518.

Pavan, Unpublished. Unpublished zircon data from the Dharwar Craton.

Payne, J.L., Pearson, N.J., Grant, K.J. and Halverson, G.P., 2013. Reassessment of relative oxide formation rates and molecular interferences on in situ lutetium–hafnium analysis with laser ablation MC-ICP-MS. Journal of Analytical Atomic Spectrometry, 28(7): 1068-1079.

Plavsa, D., Collins, A.S., Foden, J.D. and Clark, C., 2015. The evolution of a Gondwanan collisional orogen: A structural and geochronological appraisal from the Southern Granulite Terrane, South India. Tectonics, 34(5): 820-857.

Plavsa, D., Collins, A.S., Foden, J.F., Kropinski, L., Santosh, M., Chetty, T.R.K. and Clark, C., 2012. Delineating crustal domains in Peninsular India: Age and chemistry of orthopyroxene-bearing felsic gneisses in the Madurai Block. Precambrian Research, 198-199: 77-93.

Plavsa, D., Collins, A.S., Payne, J.L., Foden, J.D., Clark, C. and Santosh, M., 2014. Detrital zircons in basement metasedimentary protoliths unveil the origins of southern India. Geological Society of America Bulletin, 126(5-6): 791-811.

Prakash, D. and Sharma, I., 2011. Metamorphic evolution of the Karimnagar granulite terrane, Eastern Dharwar Craton, south India. Geological Magazine, 148(1): 112-132.

Praveen, M., Santosh, M., Yang, Q., Zhang, Z., Huang, H., Singanenjam, S. and Sajinkumar, K., 2014. Zircon U–Pb geochronology and Hf isotope of felsic volcanics from Attappadi, southern India: implications for Neoarchean convergent margin tectonics. Gondwana Research, 26(3): 907-924.

Rainaud, C., Master, S., Armstrong, R. and Robb, L., 2005. Geochronology and nature of the Palaeoproterozoic basement in the Central African Copperbelt (Zambia and the Democratic Republic of Congo), with regional implications. Journal of African Earth Sciences, 42(1-5): 1-31.

Raith, M.M., Sengupta, P., Kooijman, E., Upadhyay, D. and Srikantappa, C., 2010. Corundum–leucosome-bearing aluminous gneiss from Ayyarmalai, Southern Granulite Terrain, India: A textbook example of vapor phase-absent muscovite-melting in silica-undersaturated aluminous rocks. American Mineralogist, 95(7): 897-907.

Ring, U., Kröner, A., Layer, P., Buchwaldt, R. and Toulkeridis, T., 1999. Deformed A-type granites in northern Malawi, east-central Africa: pre-or syntectonic? Journal of the Geological Society, 156(4): 695-714.

Ring, U., Kröner, A. and Toulkeridis, T., 1997. Palaeoproterozoic granulite-facies metamorphism and granitoid intrusions in the Ubendian-Usagaran Orogen of northern Malawi, east-central Africa. Precambrian Research, 85(1-2): 27-51.

Roig, J., Tucker, R., Delor, C., Peters, S. and Théveniaut, H., 2012. Carte géologique de la République de Madagascar à 1/1 000 000, Ministère des Mines, PGRM, Antananarivo, République de Madagascar.

Sarma, D.S., McNaughton, N.J., Belusova, E., Ram Mohan, M. and Fletcher, I.R., 2012. Detrital zircon U–Pb ages and Hf-isotope systematics from the Gadag Greenstone Belt: Archean crustal growth in the western Dharwar Craton, India. Gondwana Research, 22(3-4): 843-854.

Schenk, V. and Appel, P., 2001. Anti-clockwise P–T path during ultrahigh-temperature (UHT) metamorphism at ca. 1050 Ma in the Irumide Belt of Eastern Zambia. Berichte der Deutschen Mineralogischen Gesellschaft, Beihefte zum European Journal of Mineralogy, 13(161): 99-121.

Scherer, E., Münker, C. and Mezger, K., 2001. Calibration of the lutetium-hafnium clock. Science, 293(5530): 683-687.

Schmitt, R.S., de Araújo Fragoso, R. and Collins, A.S., 2018. Suturing Gondwana in the Cambrian: the orogenic events of the final amalgamation, Geology of Southwest Gondwana. Springer, pp. 411-432.

Schofield, D.I., Thomas, R.J., Goodenough, K.M., De Waele, B., Pitfield, P.E.J., Key, R.M., Bauer, W., Walsh, G.J., Lidke, D.J. and Ralison, A.V., 2010. Geological evolution of the Antongil Craton, NE Madagascar. Precambrian Research, 182(3): 187-203.

Sláma, J., Košler, J., Condon, D.J., Crowley, J.L., Gerdes, A., Hanchar, J.M., Horstwood, M.S., Morris, G.A., Nasdala, L. and Norberg, N., 2008. Plešovice zircon—a new natural reference material for U–Pb and Hf isotopic microanalysis. Chemical Geology, 249(1): 1-35.

Teale, W., Collins, A.S., Foden, J., Payne, J.L., Plavsa, D., Chetty, T.R.K., Santosh, M. and Fanning, M., 2011. Cryogenian (~830Ma) mafic magmatism and metamorphism in the northern Madurai Block, southern India: A magmatic link between Sri Lanka and Madagascar? Journal of Asian Earth Sciences, 42(3): 223-233.

Thomas, R.J., De Waele, B., Schofield, D.I., Goodenough, K.M., Horstwood, M., Tucker, R., Bauer, W., Annells, R., Howard, K., Walsh, G., Rabarimanana, M., Rafahatelo, J.M., Ralison, A.V. and Randriamananjara, T., 2009. Geological evolution of the Neoproterozoic Bemarivo Belt, northern Madagascar. Precambrian Research, 172(3-4): 279-300.

Thomas, R.J., Spencer, C., Bushi, A.M., Baglow, N., Boniface, N., de Kock, G., Horstwood, M.S., Hollick, L., Jacobs, J. and Kajara, S., 2016. Geochronology of the central Tanzania Craton and its southern and eastern orogenic margins. Precambrian Research, 277: 47-67.

Tucker, R., Ashwal, L., Handke, M., Hamilton, M., Le Grange, M. and Rambeloson, R., 1999. U-Pb geochronology and isotope geochemistry of the Archean and Proterozoic rocks of north-central Madagascar. The Journal of Geology, 107(2): 135-153.

Tucker, R., Roig, J.-Y., Delor, C., Amelin, Y., Goncalves, P., Rabarimanana, M., Ralison, A. and Belcher, R., 2011a. Neoproterozoic extension in the Greater Dharwar Craton: a reevaluation of the "Betsimisaraka suture" in Madagascar. Canadian Journal of Earth Sciences, 48(2): 389-417.

Tucker, R.D., Kusky, T.M., Buchwaldt, R. and Handke, M.J., 2007. Neoproterozoic nappes and superposed folding of the Itremo Group, west-central Madagascar. Gondwana Research, 12(4): 356-379.

Tucker, R.D., Roig, J.Y., Macey, P.H., Delor, C., Amelin, Y., Armstrong, R.A., Rabarimanana, M.H. and Ralison, A.V., 2011b. A new geological framework for south-central Madagascar, and its relevance to the "out-of-Africa" hypothesis. Precambrian Research, 185(3-4): 109-130.

Upadhyay, D., Gerdes, A. and Raith, M.M., 2009. Unraveling sedimentary provenance and tectonothermal history of high-temperature metapelites, using zircon and monazite chemistry: a case study from the Eastern Ghats Belt, India. The Journal of Geology, 117(6): 665-683.

Vermeesch, P., Resentini, A. and Garzanti, E., 2016. An R package for statistical provenance analysis. Sedimentary Geology.

Vrána, S., Kachlık, V., Kröner, A., Marheine, D., Seifert, A., Žáček, V. and Babůrek, J., 2004. Ubendian basement and its late Mesoproterozoic and early Neoproterozoic structural and metamorphic overprint in northeastern Zambia. Journal of African Earth Sciences, 38(1): 1-21.

Woodhead, J., Hergt, J., Shelley, M., Eggins, S. and Kemp, R., 2004. Zircon Hf-isotope analysis with an excimer laser, depth profiling, ablation of complex geometries, and concomitant age estimation. Chemical Geology, 209(1–2): 121-135.

Woodhead, J.D. and Hergt, J.M., 2005. A preliminary appraisal of seven natural zircon reference materials for in situ Hf isotope determination. Geostandards and Geoanalytical Research, 29(2): 183-195.

Yang, Q.-Y. and Santosh, M., 2015. Zircon U–Pb geochronology and Lu–Hf isotopes from the Kolar greenstone belt, Dharwar Craton, India: Implications for crustal evolution in an ocean-trench-continent transect. Journal of Asian Earth Sciences, 113: 797-811.

6

Key outcomes and conclusions of the thesis

Through this multidisciplinary PhD research, significant progress has been made toward understanding the evolution of Madagascar and surrounding geological terranes during the Precambrian. The primary aims of this research were:

1. To investigate the timing and location of the controversial Betsimisaraka Suture in eastern Madagascar and the Dharwar Craton of India.
2. To determine the evolution of northern Madagascar, assess linkages with other age-equivalent terranes, and model its tectonic evolution during the Neoproterozoic.
3. To study the structural evolution and medium-temperature thermochronology of central Madagascar as a way of determining the timing and locations of Gondwana-forming sutures.
4. To examine the poorly-understood Itremo Group, its correlation with other Proterozoic cover sequences in Madagascar, and link it to other continents during the Paleoproterozoic.

1. Betsimisaraka Suture

All of the chapters of this thesis go some way to addressing the first aim of this thesis. In Chapter 1 we assessed the correlation of detrital samples across Madagascar and India, to constrain the location of a boundary—the Betsimisaraka Suture—that separates distinct terranes. We showed that the boundary between the Antongil-Masora domains and the Antananarivo Domain is supported by differences in detrital zircon data. A previously proposed boundary in the western Dharwar Craton, was shown here to not be supported by available data, and therefore the Betsimisaraka Suture does not extend into India as the Kumta Suture.

In Chapter 2, we concluded that the Bemarivo Domain in northern Madagascar amalgamated with the Antananarivo Craton at c. 540 Ma, which is the approximate timing of the Betsimisaraka Suture. In Chapter 3, we showed that the structural style in central Madagascar was caused by orogenesis in southwest Madagascar between c. 750–550 Ma. In contrast, eastern Madagascar was deformed syn- to post-550 Ma. In Chapter 4 we looked at Paleoproterozoic sedimentary rocks in Madagascar and assessed their correlation with Africa and India. We show that these Madagascan rocks correlate with Africa, but not India. Although not conclusive, this does broadly support the idea that Madagascar and India were not connected during the Paleoproterozoic.

Although we cannot use the absence of evidence, as evidence for absence, the lack of any known shared geological units between Madagascar and the Dharwar Craton of India during the Proterozoic, are more supportive of a model where these cratons were not contiguous until the late Neoproterozoic to early Cambrian. We therefore conclude that the most likely model for the assembly of central Gondwana, is one where Madagascar and the Dharwar Craton amalgamated along the Betsimisaraka Suture at c. 550–500 Ma. This closed the final strand of the Mozambique Ocean that lay between Madagascar and India.

2. Northern Madagascar

In Chapter 2 we used new Hf and O isotope data to characterise the geological terranes in northern Madagascar. We showed that the northern and southern Bemarivo domains (newly named in our research as the Bobakindro Terrane and Marojejy Terrane, respectively) have different isotopic evolutions. The Betsimisaraka Suture had previously been mapped as the approximate location of the Sandrakota Shear Zone, which separates the Bemarivo Domain from the Antananarivo Domain. However our new data suggest the boundary is more likely to be the Antsaba Shear Zone. Further evidence of this is given in Chapter 4 where we assess detrital zircon data from the Sahantaha Group, and show that it is indistinguishable from the Itremo Group. In these two chapters we show that the Sahantaha Group most likely overlies Antananarivo basement, and that the Marojejy Terrane igneous rocks are likely associated with the Imorona-Itsindro Suite.

In Chapter 2 we present a data compilation of c. 800–700 Ma Hf and O isotope data from other regions, and propose that the Bobakindro Terrane in the northern Bemarivo Domain was likely part of a long-lived magmatic arc. This included parts of south China, the Malani Igneous Suite of northwest India, the Seychelles and Oman. Final accretion of the Bobakindro Terrane to the rest of Madagascar occurred at c. 540 Ma, along the Antasaba Shear Zone, which we interpret as an extension of the Betsimisaraka Suture.

3. Deformation of central Madagascar

In Chapter 3 we undertook a detailed structural study of central Madagascar, which included the Antananarivo, Itremo and Ikalamavony domains. We showed for the first time that the Ikalamavony and Itremo domains were deformed together. This study built on previous structural studies of the Itremo Domain, and confirmed that deformation formed in response to a west-dipping structure in southwestern Madagascar. Overprinting relationships of magmatic rocks indicate that deformation occurred between c. 750 and c. 550 Ma. We suggest that this is most likely the c. 650 Ma Vohibory Suture, however we cannot rule out other timings and locations for the major Gondwana-forming suture in southwestern Madagascar. We also show that the structural style changes in eastern Madagascar. Based on overprinting relationships and published metamorphic data, we show that deformation in eastern Madagascar is younger and most likely formed in response to the c. 550–500 Ma Betsimisaraka Suture.

4. Proterozoic cover sequences

We collected new detrital zircon U–Pb and Hf isotope data from a range of Paleoproterozoic sedimentary sequences, including the Itremo Group, Sahantaha Group, Maha Group and Ambatolampy Group. We show that sedimentary samples with maximum depositional ages of c. 1700 Ma have comparable age distributions, and likely formed as part of the same large sedimentary basin at c. 1700 Ma. This basin covered much of Madagascar and the Tanzania Craton of Africa. This study provides important constraints on the paleogeography of Africa and Madagascar during the Paleoproterozoic, when the Nuna supercontinent was being formed.

5. Implications for plate reconstructions and the evolution of central Gondwana

Overall, the research produced during this PhD strongly support:

1. That the Tanzania Craton of Africa and the Antananarivo Domain of Madagascar were contiguous at c. 1700 Ma, and were likely separate from the Dharwar Craton of India until the late Neoproterozoic to early Cambrian.
2. A long-lived c. 800–750 Ma juvenile magmatic arc that involved the Bobakindro Terrane of northern Madagascar existed outboard from continental India and China. This arc included parts of south China, the Malani Igneous Suite of northwest India, Oman and the Seychelles.
3. The Mozambique Ocean between Africa and Madagascar most likely closed along the Vohibory Suture at c. 650 Ma, resulting in complex deformation in central Madagascar. The Ikalamavony and Itremo domains preserve the same structural styles and deformation history.

4. Final closure of the Mozambique Ocean occurred between Madagascar and India at c. 550–500 Ma, along the Betsimisaraka Suture. The northern extent of the Betsimisaraka Suture is marked by the Antsaba Shear Zone that sutured the Bobakindro Terrane with the Antananarivo Domain at c. 540 Ma. The Betsimisaraka Suture resulted in complex deformation and shear zone activity in eastern Madagascar. The final assembly of central Gondwana resulted in prolonged thermal activity in central Madagascar, with final cooling below 500°C occurring at c. 500 Ma.

7

Appendices

Chapter 2

Appendix 2.1 The Kumta Suture of western Peninsular India: U–Pb zircon data
Appendix 2.2 The Kumta Suture of western Peninsular India: Hf isotope data
Appendix 2.3 The Kumta Suture of western Peninsular India: Isotopic database
doi.org/10.1016/j.jseaes.2017.08.020

Chapter 3

Appendix 3.1 The Bemarivo Domain of northern Madagascar: Hf and O data
Appendix 3.2 The Bemarivo Domain of northern Madagascar: CL images
doi.org/10.25909/5cd273ecdbd07
Appendix 3.3 The Bemarivo Domain of northern Madagascar: R codes
doi.org/10.25909/5cd273b507ab5

Chapter 4

Appendix 4.1 Structure and thermochronology of Madagascar: Geological map of central Madagascar doi.org/10.25909/5cd2738a3b036
Appendix 4.2 Structure and thermochronology of Madagascar: Analytical methods and detailed results
Appendix 4.3 Structure and thermochronology of Madagascar: isotopic data for geo/thermochronology
Appendix 4.4 Structure and thermochronology of Madagascar: Landsat images and structural interpretation examples

Chapter 5

Appendix 5.1 Proterozoic basin evolution during Nuna: U–Pb zircon data
Appendix 5.2 Proterozoic basin evolution during Nuna: REE zircon data
Appendix 5.3 Proterozoic basin evolution during Nuna: CL images
Appendix 5.4 Proterozoic basin evolution during Nuna: Hf isotope data
Appendix 5.5 Proterozoic basin evolution during Nuna: Itremo Group REE plots
Appendix 5.6 Proterozoic basin evolution during Nuna: Detrital zircon database
doi.org/10.25909/5cd27304e5cf9
Appendix 5.7 Proterozoic basin evolution during Nuna: Detrital zircon U–Pb and Hf plots for all data

Appendix 2.1 The Kumta Suture of western Peninsular India: U–Pb zircon data

Sample No.	Sample - spot	Pb (PPM)	Th (PPM)	U (PPM)	U/Th	$^{207}Pb/^{206}Pb$	± 2SE	$^{207}Pb/^{235}U$	± 2SE	$^{206}Pb/^{238}U$	± 2SE	Error Correlation 6/38 vs 7/35	Age $^{207}Pb/^{235}U$	± 2SE	Age $^{206}Pb/^{238}U$	± 2SE	Age $^{207}Pb/^{206}Pb$	± 2SE	Concordance 7/6 vs 6/38	Concordance 6/38 vs 7/35
I16-01	I1601 - 001	2393	282	409	1.412	0.1732	0.0025	12.19	0.21	0.5048	0.0079	0.59031	2614	17	2631	34	2588	25	102	101
I16-01	I1601 - 002	626	58.4	137	2.17	0.214	0.0056	18.26	0.55	0.618	0.014	0.50322	2999	29	3096	56	2922	42	106	103
I16-01	I1601 - 003	1564	136.2	243.8	1.708	0.2271	0.0032	19.72	0.33	0.6268	0.0093	0.51421	3075	17	3133	37	3025	23	104	102
I16-01	I1601 - 004	2560	660	3460	6.6	0.1261	0.0031	1.973	0.066	0.1119	0.0039	0.74782	1101	22	683	22	2029	44	34	62
I16-01	I1601 - 005	4460	637	1035	2.13	0.1874	0.0074	6.32	0.58	0.241	0.019	0.84863	1948	81	1368	95	2703	68	51	70
I16-01	I1601 - 007	1180	123.8	198.8	1.56	0.2244	0.0038	18.56	0.32	0.6037	0.0097	0.55757	3014	17	3041	39	3006	27	101	101
I16-01	I1601 - 008	121	12.1	218.2	26.6	0.1757	0.0034	13.08	0.23	0.5434	0.009	0.36884	2681	17	2794	38	2603	33	107	104
I16-01	I1601 - 009	1.06E+04	5090	4960	0.96	0.197	0.02	2.27	0.31	0.0835	0.0063	0.56101	1149	92	516	37	2690	170	19	45
I16-01	I1601 - 010	3200	311	224	0.686	0.1821	0.0033	13.62	0.24	0.5503	0.0087	0.40127	2723	17	2823	36	2672	29	106	104
I16-01	I1601 - 011	8620	747	244.9	0.319	0.2504	0.0036	22.9	0.43	0.671	0.011	0.68095	3218	19	3307	44	3182	23	104	103
I16-01	I1601 - 012	4410	546	588	1.56	0.2168	0.0064	13.84	0.85	0.456	0.018	0.9323	2675	63	2406	81	2929	49	82	90
I16-01	I1601 - 013	3670	983	1467	1.404	0.1111	0.0019	2.831	0.065	0.1879	0.0032	0.68488	1359	17	1109	17	1810	32	61	82
I16-01	I1601 - 014	558	83.2	126	1.327	0.2061	0.0061	13.63	0.87	0.476	0.025	0.88713	2654	66	2480	110	2852	49	87	93
I16-01	I1601 - 015	1510	113.3	220	1.84	0.2355	0.0037	20.69	0.36	0.641	0.011	0.54877	3121	17	3193	42	3085	26	104	102
I16-01	I1601 - 016	824	353	276	0.782	0.2276	0.0041	10.09	0.36	0.3178	0.0098	0.82514	2425	32	1772	47	3032	31	58	73
I16-01	I1601 - 017	1623	158.4	280.7	1.8	0.184	0.0035	12.12	0.25	0.4733	0.0091	0.54017	2609	19	2494	40	2676	32	93	96
I16-01	I1601 - 018	1001	177	575.5	3.61	0.1648	0.0026	8.02	0.32	0.347	0.013	0.90527	2209	37	1909	63	2503	26	76	86
I16-01	I1601 - 019	1.77E+04	805	1100	1.723	0.2777	0.008	15.82	0.97	0.403	0.021	0.82697	2812	58	2157	95	3332	43	65	77
I16-01	I1601 - 020	1862	404	369	1.224	0.1841	0.0029	10.57	0.35	0.409	0.012	0.88173	2473	32	2201	53	2684	27	82	89
I16-01	I1601 - 021	1239	220.2	539	2.69	0.1659	0.0029	7.35	0.17	0.3172	0.0055	0.599	2150	20	1777	28	2513	28	71	83
I16-01	I1601 - 022	5930	442	429	0.958	0.261	0.014	17.9	1.7	0.472	0.024	0.88049	2900	93	2470	100	3202	84	77	85
I16-01	I1601 - 023	1052	114	471	3.87	0.2713	0.0041	25.06	0.37	0.661	0.01	0.47213	3310	15	3267	39	3306	24	99	99
I16-01	I1601 - 024	5130	598	580	0.828	0.1735	0.0037	10.79	0.57	0.432	0.018	0.93547	2450	59	2294	83	2579	38	89	94
I16-01	I1601 - 025	304	144	469	5.95	0.2076	0.0034	15.29	0.5	0.521	0.014	0.86484	2816	33	2696	60	2882	28	94	96
I16-01	I1601 - 026	2670	191	129.9	0.685	0.2578	0.0049	24.92	0.55	0.698	0.015	0.6287	3305	22	3406	57	3225	31	106	103
I16-01	I1601 - 027	3450	259.2	261	0.993	0.2612	0.004	24.12	0.45	0.658	0.011	0.64378	3267	18	3253	43	3246	24	100	100
I16-01	I1601 - 028	712	79.3	119.4	1.448	0.2301	0.0053	17.21	0.38	0.536	0.012	0.49323	2946	22	2767	48	3039	38	91	94
I16-01	I1601 - 029	668	183	1095	6.57	0.1301	0.0017	4.204	0.072	0.2295	0.003	0.63381	1671	14	1331	16	2092	24	64	80

Sample No.	Sample - spot	Pb (PPM)	Th (PPM)	U (PPM)	U/Th	$^{207}Pb/^{206}Pb$	± 2SE	$^{207}Pb/^{235}U$	± 2SE	$^{206}Pb/^{238}U$	± 2SE	Error Correlation 6/38 vs 7/35	Age $^{207}Pb/^{235}U$	± 2SE	Age $^{206}Pb/^{238}U$	± 2SE	Age $^{207}Pb/^{206}Pb$	± 2SE	Concordance 7/6 vs 6/38	Concordance 6/38 vs 7/35
I16-01	I1601 - 030	455	36.9	793	22.5	0.1606	0.0037	7.35	0.37	0.321	0.011	0.92121	2119	44	1786	54	2442	40	73	84
I16-01	I1601 - 031	2380	518	806	1.439	0.1439	0.0041	5.84	0.29	0.2853	0.0085	0.86692	1914	47	1613	43	2255	51	72	84
I16-01	I1601 - 032	1982	395	785	2.3	0.1456	0.0029	5.95	0.23	0.2917	0.0083	0.85594	1948	32	1645	41	2280	34	72	84
I16-01	I1601 - 033	1076	129.3	259.4	1.994	0.178	0.0048	9.31	0.31	0.3861	0.0098	0.74032	2361	33	2104	47	2611	43	81	89
I16-01	I1601 - 034	2051	371	443	1.323	0.1685	0.0025	9.42	0.41	0.404	0.017	0.93151	2348	42	2168	79	2541	25	85	92
I16-01	I1601 - 035	2850	284.6	499	1.784	0.2229	0.0036	16.73	0.46	0.544	0.012	0.79111	2912	26	2793	50	3001	27	93	96
I16-01	I1601 - 036	933	77.3	232	3.08	0.2296	0.0065	17.82	0.77	0.568	0.019	0.73981	2977	40	2906	75	3033	46	96	98
I16-01	I1601 - 037	5730	2350	4560	2.3	0.1308	0.0017	3.09	0.11	0.1718	0.0059	0.92814	1421	27	1020	32	2104	23	48	72
I16-01	I1601 - 038	3550	528	595	1.179	0.1675	0.003	8.21	0.17	0.3624	0.0059	0.55957	2252	19	1991	28	2525	31	79	88
I16-01	I1601 - 039	1640	203.6	519.6	2.65	0.2635	0.0043	15.71	0.32	0.436	0.0091	0.66926	2855	19	2330	41	3262	26	71	82
I16-01	I1601 - 040	3590	449	496	1.208	0.2774	0.0051	18.93	0.9	0.496	0.022	0.93932	2990	55	2569	96	3345	28	77	86
I16-01	I1601 - 041	1875	420	768	1.85	0.1648	0.003	5.83	0.15	0.2594	0.0052	0.69844	1944	22	1485	27	2497	31	59	76
I16-01	I1601 - 042	2540	273	258.2	1.05	0.1725	0.0034	11.16	0.2	0.476	0.008	0.35181	2532	17	2511	34	2577	33	97	99
I16-01	I1601 - 043	1786	400.9	690	1.745	0.1652	0.0027	6.92	0.14	0.3072	0.0049	0.65776	2097	18	1725	24	2500	27	69	82
I16-01	I1601 - 044	1.85E+04	9.50E+03	7730	1.11	0.1381	0.0027	2.87	0.11	0.1517	0.004	0.90196	1363	29	909	22	2189	34	42	67
I16-01	I1601 - 045	1720	443	911	2.32	0.1351	0.0027	4.28	0.12	0.2325	0.0052	0.72921	1686	24	1345	27	2150	35	63	80
I16-01	I1601 - 046	4940	427	1057	2.99	0.1576	0.0049	5.56	0.37	0.249	0.011	0.8921	1870	53	1427	55	2398	49	60	76
I16-01	I1601 - 047	4080	829	917	1.109	0.1462	0.0031	4.65	0.13	0.2331	0.0056	0.68479	1754	23	1349	29	2290	35	59	77
I16-01	I1601 - 048	1163	75	188.2	2.53	0.2383	0.0091	19.4	0.64	0.605	0.022	0.44174	3056	32	3043	88	3093	60	98	100
I16-01	I1601 - 049	4120	712	1222	1.725	0.1187	0.002	3.586	0.072	0.2211	0.0038	0.57443	1542	16	1287	20	1925	30	67	83
I16-01	I1601 - 050	1294	170.6	534	3.18	0.1612	0.0028	8.79	0.17	0.398	0.0067	0.64519	2313	18	2157	31	2461	29	88	93
I16-01	I1601 - 051	3930	839	957	1.18	0.161	0.003	4.43	0.13	0.2007	0.0056	0.77517	1711	24	1177	30	2461	32	48	69
I16-01	I1601 - 052	5060	1340	811	0.756	0.1464	0.0023	5.23	0.14	0.2642	0.0065	0.79958	1849	25	1508	33	2295	27	66	82
I16-01	I1601 - 053	2285	196.2	249.9	1.289	0.1624	0.0032	11.07	0.22	0.5006	0.0081	0.41673	2525	18	2613	35	2466	34	106	103
I16-01	I1601 - 054	1361	199	279.1	1.464	0.1567	0.0037	7.59	0.22	0.3537	0.0069	0.60716	2174	26	1950	33	2411	39	81	90
I16-01	I1601 - 055	3370	311	1487	6.03	0.1636	0.0043	4.32	0.17	0.1934	0.0066	0.79083	1676	35	1136	35	2468	45	46	68
I16-01	I1601 - 056	2190	699	2200	3.134	0.1193	0.0025	2.455	0.081	0.1493	0.0041	0.78868	1250	24	899	24	1936	37	46	72
I16-01	I1601 - 057	1360	127.2	825	7.94	0.2012	0.0032	12.02	0.51	0.434	0.016	0.92207	2577	40	2306	73	2827	26	82	89
I16-01	I1601 - 058	7.90E+04	673	4440	6.46	0.32	0.016	11.89	0.95	0.257	0.01	0.9086	2487	79	1468	51	3481	86	42	59
I16-01	I1601 - 059	3070	659	1284	1.972	0.1241	0.0032	3.6	0.11	0.2122	0.0055	0.53409	1546	24	1239	29	2008	47	62	80

Sample No.	Sample - spot	Pb (PPM)	Th (PPM)	U (PPM)	U/Th	$^{207}Pb/^{206}Pb$	± 2SE	$^{207}Pb/^{235}U$	± 2SE	$^{206}Pb/^{238}U$	± 2SE	Error Correlation 6/38 vs 7/35	Age $^{207}Pb/^{235}U$	± 2SE	Age $^{206}Pb/^{238}U$	± 2SE	Age $^{207}Pb/^{206}Pb$	± 2SE	Concordance 7/6 vs 6/38	Concordance 6/38 vs 7/35
I16-01	I1601 - 060	611	48.6	110.6	2.2	0.1732	0.0046	12.4	0.38	0.515	0.011	0.47844	2624	28	2678	47	2576	45	104	102
I16-01	I1601 - 061	1993	380	652	1.76	0.1683	0.0028	6.59	0.14	0.2814	0.0047	0.64029	2052	19	1600	24	2538	29	63	78
I16-01	I1601 - 062	1695	141	142.4	1.001	0.1922	0.0044	14.05	0.31	0.529	0.011	0.38235	2747	22	2748	44	2754	40	100	100
I16-01	I1601 - 063	2850	346	565	1.586	0.2641	0.0043	18.1	0.54	0.492	0.013	0.77918	2987	28	2576	53	3268	24	79	86
I16-01	I1601 - 064	1229	134	423	3.071	0.2505	0.0042	16.38	0.64	0.471	0.017	0.9004	2886	37	2478	73	3183	26	78	86
I16-01	I1601 - 065	571	109	1795	15.83	0.1061	0.0028	2.689	0.091	0.182	0.0049	0.61709	1319	25	1077	27	1726	52	62	82
I16-01	I1601 - 066	1430	127	242	1.726	0.177	0.006	12.43	0.78	0.497	0.019	0.86709	2579	62	2582	84	2592	55	100	100
I16-01	I1601 - 067	892	63.2	141.3	2.104	0.2316	0.0049	20.5	0.5	0.631	0.012	0.52236	3105	24	3147	48	3052	35	103	101
I16-01	I1601 - 068	1120	75.4	196.4	2.46	0.234	0.01	19.77	0.84	0.617	0.027	0.53261	3071	42	3090	110	3062	69	101	101
I16-01	I1601 - 069	713	61.5	1098	17.53	0.1277	0.0035	3.33	0.11	0.1842	0.0039	0.58642	1482	27	1090	21	2054	49	53	74
I16-01	I1601 - 070	1203	406	1860	5	0.1486	0.004	3.81	0.37	0.171	0.012	0.91994	1541	67	1008	65	2314	45	44	65
I16-01	I1601 - 071	958	338	251	0.842	0.1676	0.0042	7.74	0.32	0.33	0.013	0.7948	2177	36	1825	61	2510	43	73	84
I16-01	I1601 - 072	6.10E+04	368	3130	8.15	0.323	0.016	14.4	1.7	0.275	0.023	0.97229	2530	120	1570	120	3494	87	45	62
I16-01	I1601 - 073	2277	147.2	159.4	1.043	0.2695	0.0048	27.51	0.59	0.729	0.015	0.5384	3396	22	3521	54	3297	27	107	104
I16-01	I1601 - 074	3070	544	849	1.469	0.1397	0.0026	5.09	0.11	0.2563	0.0043	0.4862	1830	19	1469	22	2220	32	66	80
I16-01	I1601 - 075	2380	262	491	1.819	0.1625	0.0043	10.36	0.23	0.456	0.011	0.3458	2466	21	2416	50	2466	45	98	98
I16-01	I1601 - 076	1377	274	823	2.99	0.1348	0.0026	5	0.14	0.263	0.0056	0.74177	1810	24	1503	28	2150	33	70	83
I16-01	I1601 - 077	1048	99.7	159	1.443	0.1676	0.0046	12.21	0.31	0.52	0.011	0.27504	2612	23	2693	47	2511	46	107	103
I16-01	I1601 - 078	245	103.3	1294	14	0.1145	0.0039	3.01	0.17	0.1885	0.009	0.82896	1402	49	1110	48	1846	62	60	79
I16-01	I1601 - 079	1305	153.4	139.9	0.878	0.1646	0.0044	10.76	0.28	0.4663	0.0094	0.34345	2494	24	2463	41	2483	44	99	99
I16-01	I1601 - 080	1781	140.5	213	1.44	0.2195	0.0039	19.66	0.35	0.644	0.012	0.55548	3075	17	3197	48	2970	30	108	104
I16-01	I1601 - 081	1541	132.9	227.6	1.659	0.2304	0.0044	19.24	0.43	0.601	0.014	0.56833	3049	22	3026	57	3046	31	99	99
I16-01	I1601 - 082	3.67E+04	1574	5070	3.22	0.2419	0.0079	9.18	0.71	0.258	0.011	0.95801	2278	63	1470	56	3112	51	47	65
I16-01	I1601 - 083	850	301	149.2	0.5	0.2731	0.0073	13.79	0.63	0.373	0.018	0.84167	2714	43	2023	84	3307	40	61	75
I16-01	I1601 - 084	2029	214	355	1.61	0.1617	0.0029	10.45	0.23	0.4644	0.0095	0.65115	2468	20	2454	42	2462	30	100	99
I16-01	I1601 - 085	3440	330	688	1.94	0.1636	0.0021	11.87	0.25	0.5268	0.009	0.72365	2593	19	2724	38	2490	22	109	105
I16-01	I1601 - 086	418	57.6	878	14.73	0.158	0.0034	6.16	0.12	0.2813	0.005	0.46383	1995	17	1597	25	2428	35	66	80
I16-01	I1601 - 087	751	129.6	1204	10.75	0.1187	0.0025	3.764	0.081	0.2291	0.0032	0.45776	1582	18	1329	17	1924	37	69	84
I16-01	I1601 - 088	2025	144.3	154.9	1.058	0.2405	0.0068	23.03	0.76	0.695	0.021	0.41926	3221	32	3395	78	3114	45	109	105
I16-01	I1601 - 089	500	310	419	1.129	0.2067	0.0073	7.9	0.58	0.269	0.014	0.90126	2150	72	1525	72	2847	57	54	71

Sample No.	Sample - spot	Pb (PPM)	Th (PPM)	U (PPM)	U/Th	$^{207}Pb/^{206}Pb$	± 2SE	$^{207}Pb/^{235}U$	± 2SE	$^{206}Pb/^{238}U$	± 2SE	Error Correlation 6/38 vs 7/35	Age $^{207}Pb/^{235}U$	± 2SE	Age $^{206}Pb/^{238}U$	± 2SE	Age $^{207}Pb/^{206}Pb$	± 2SE	Concordance 7/6 vs 6/38	Concordance 6/38 vs 7/35
I16-01	I1601 - 090	1862	194	324	1.679	0.2264	0.0033	19.03	0.44	0.609	0.013	0.7595	3034	23	3057	54	3020	23	101	101
I16-01	I1601 - 091	1499	167.4	938	5.42	0.1626	0.0034	7.96	0.31	0.342	0.01	0.79926	2213	33	1892	50	2471	36	77	85
I16-01	I1601 - 092	1232	130.9	482	3.627	0.1852	0.0027	12.8	0.24	0.4906	0.008	0.71665	2665	17	2570	35	2692	24	95	96
I16-01	I1601 - 093	687	119.3	668	5.68	0.2118	0.0034	13.53	0.29	0.45	0.0067	0.65325	2715	19	2393	30	2915	25	82	88
I16-01	I1601 - 094	1312	101.8	182.4	1.79	0.2344	0.0047	20.67	0.43	0.621	0.011	0.56403	3118	21	3109	43	3069	33	101	100
I16-01	I1601 - 095	905	106.8	1129	10.79	0.1452	0.0071	6.58	0.92	0.279	0.024	0.98891	1840	100	1550	110	2206	80	70	84
I16-01	I1601 - 096	1.29E+04	2520	2850	1.085	0.1815	0.0082	3.73	0.37	0.1424	0.0078	0.95319	1545	66	856	43	2642	70	32	55
I16-01	I1601 - 097	3220	234	358	1.445	0.229	0.004	20.3	0.36	0.627	0.012	0.62608	3103	17	3130	48	3039	28	103	101
I16-01	I1601 - 098	2770	333	381	1.006	0.2287	0.0042	17.9	0.35	0.559	0.01	0.55084	2981	19	2864	40	3036	28	94	96
I16-01	I1601 - 099	2430	1460	976	1.39	0.2166	0.0043	9.26	0.27	0.3016	0.0095	0.78458	2360	26	1695	48	2953	33	57	72
I16-01	I1601 - 100	802	241	411	2.13	0.2605	0.005	17.4	1	0.469	0.023	0.96129	2889	66	2450	100	3241	31	76	85
I16-01	I1601 - 101	1505	213.6	852	3.94	0.1864	0.0034	9.9	0.35	0.3776	0.009	0.86948	2410	33	2060	42	2699	31	76	85
I16-01	I1601 - 102	1373	127.1	315	2.37	0.2292	0.0036	19.95	0.36	0.62	0.01	0.62137	3086	18	3110	39	3042	25	102	101
I16-01	I1601 - 103	2620	438	857	2.046	0.1696	0.0036	6.97	0.26	0.294	0.0066	0.83442	2091	34	1667	31	2537	36	66	80
I16-01	I1601 - 104	1600	224	767	5.72	0.1713	0.0029	7.93	0.23	0.3324	0.0062	0.78729	2215	25	1848	30	2564	29	72	83
I16-01	I1601 - 105	2016	201.3	296.6	1.41	0.1642	0.0033	11.32	0.21	0.4997	0.0086	0.40429	2549	18	2608	37	2489	34	105	102
I16-01	I1601 - 106	1860	269	229	0.918	0.2792	0.005	19.04	0.84	0.49	0.023	0.91478	3019	41	2559	98	3356	26	76	85
I16-01	I1601 - 107	2485	183.1	213.1	1.132	0.2837	0.0047	29.03	0.51	0.733	0.013	0.47715	3449	17	3546	48	3382	26	105	103
I16-01	I1601 - 108	1541	110.4	192	1.704	0.2878	0.0056	28.64	0.54	0.722	0.016	0.60509	3439	20	3493	59	3393	31	103	102
I16-01	I1601 - 109	2239	273	486	1.669	0.2149	0.0062	14.13	0.9	0.454	0.024	0.93416	2665	79	2390	110	2932	47	82	90
I16-01	I1601 - 110	661	114	155	1.346	0.2362	0.0066	11.66	0.31	0.3539	0.0092	0.42218	2575	26	1950	44	3086	47	63	76
I16-01	I1601 - 111	875	125.7	191.6	1.513	0.1677	0.0045	9.67	0.25	0.411	0.01	0.44015	2407	24	2217	46	2528	47	88	92
I16-01	I1601 - 112	3180	377	403.7	1.053	0.168	0.0031	10.63	0.2	0.4501	0.0082	0.56863	2493	18	2397	36	2530	31	95	96
I16-01	I1601 - 114	4040	1184	3176	2.656	0.1278	0.0031	2.55	0.18	0.1377	0.0074	0.96706	1249	53	828	42	2058	43	40	66
I16-01	I1601 - 115	6240	831	2290	2.64	0.1904	0.0063	3.61	0.28	0.134	0.011	0.90561	1498	53	800	56	2707	56	30	53
I16-01	I1601 - 116	2450	248	358	1.364	0.1673	0.0031	11.59	0.22	0.4909	0.0082	0.58178	2569	17	2576	37	2518	32	102	100
I16-01	I1601 - 117	2700	680	849	1.198	0.1505	0.003	4.56	0.23	0.213	0.011	0.92763	1712	40	1237	56	2337	33	53	72
I16-01	I1601 - 118	4390	1120	965	0.874	0.215	0.0077	9.72	0.82	0.313	0.018	0.9081	2351	74	1742	89	2919	57	60	74
I16-01	I1601 - 119	1359	206.6	269.8	1.287	0.2285	0.0046	14.53	0.3	0.4506	0.0086	0.5919	2781	20	2394	38	3036	33	79	86
I16-01	I1601 - 120	1540	147.2	216.2	1.44	0.2315	0.0041	17.87	0.53	0.549	0.015	0.81867	2975	29	2819	63	3056	29	92	95
I16-01	I1601 - 121	1420	172	255	1.432	0.1798	0.0051	10.76	0.36	0.429	0.013	0.54682	2497	32	2297	60	2649	48	87	92

Sample No.	Sample - spot	Pb (PPM)	Th (PPM)	U (PPM)	U/Th	$^{207}Pb/^{206}Pb$	± 2SE	$^{207}Pb/^{235}U$	± 2SE	$^{206}Pb/^{238}U$	± 2SE	Error Correlation 6/38 vs 7/35	Age $^{207}Pb/^{235}U$	± 2SE	Age $^{206}Pb/^{238}U$	± 2SE	Age $^{207}Pb/^{206}Pb$	± 2SE	Concordance 7/6 vs 6/38	Concordance 6/38 vs 7/35
I16-01	I1601 - 122	810	75.3	136.3	1.732	0.1844	0.0039	13.6	0.36	0.533	0.012	0.62067	2714	25	2748	51	2677	36	103	101
I16-01	I1601 - 123	1226	243	350	1.516	0.1753	0.0031	10.5	0.67	0.431	0.027	0.95364	2408	66	2270	120	2601	31	87	94
I16-01	I1601 - 124	397	29.7	77.4	2.381	0.215	0.0071	18.28	0.65	0.617	0.019	0.52887	2995	34	3090	73	2938	50	105	103
I16-01	I1601 - 125	2.74E+04	121.7	2700	18.91	0.2809	0.0049	10.76	0.34	0.2789	0.0065	0.82124	2491	29	1587	32	3369	27	47	64
I16-01	I1601 - 126	3850	313	310	0.903	0.28	0.0047	26.68	0.42	0.703	0.012	0.52074	3370	15	3432	46	3361	27	102	102
I16-01	I1601 - 127	2530	329.4	677	1.924	0.164	0.0041	9.33	0.24	0.4224	0.0089	0.57446	2365	24	2269	40	2490	44	91	96
I16-01	I1601 - 128	3680	768	632	0.749	0.1762	0.0061	8.69	0.29	0.367	0.014	0.50959	2298	31	2010	66	2608	63	77	87
I16-01	I1601 - 129	1462	113.6	167.5	1.327	0.2353	0.0051	20.79	0.43	0.671	0.013	0.43686	3127	20	3301	48	3073	35	107	106
I16-01	I1601 - 130	1850	170	195	1.256	0.2676	0.0074	22.2	1.2	0.624	0.028	0.85516	3145	55	3090	110	3276	44	94	98
I16-01	I1601 - 131	2099	267.5	289.2	1.008	0.2725	0.0056	18.47	0.44	0.515	0.011	0.65185	3013	23	2674	48	3309	32	81	89
I16-01	I1601 - 132	1725	168.6	239.1	1.376	0.1664	0.0032	10.7	0.24	0.49	0.01	0.63576	2494	21	2564	44	2516	33	102	103
I16-01	I1601 - 133	859	204	334	1.655	0.1669	0.0041	6.36	0.21	0.2922	0.008	0.6066	2022	30	1648	40	2505	42	66	82
I16-01	I1601 - 134	2170	287	691	2.344	0.234	0.0035	12.19	0.27	0.3925	0.0071	0.681	2614	20	2132	33	3072	24	69	82
I16-01	I1601 - 135	263	121.2	74.7	0.594	0.2205	0.007	13.07	0.46	0.445	0.014	0.53219	2669	33	2363	64	2962	54	80	89
I16-01	I1601 - 136	400	79.6	1162	33	0.1386	0.0048	4.95	0.36	0.2479	0.0094	0.94961	1757	56	1421	48	2166	59	66	81
I16-01	I1601 - 137	2056	144.2	282	1.862	0.2382	0.0046	21.44	0.33	0.653	0.011	0.24266	3155	15	3233	42	3100	30	104	102
I16-01	I1601 - 138	2360	310	1800	5.39	0.1843	0.0027	13.59	0.83	0.516	0.026	0.96265	2671	50	2680	110	2687	24	100	100
I16-01	I1601 - 139	3690	422	790	2.08	0.2111	0.0069	13.12	0.9	0.443	0.025	0.88798	2640	69	2340	110	2893	52	81	89
I16-01	I1601 - 140	1597	189.3	389	2.027	0.2364	0.0036	18.72	0.4	0.573	0.013	0.7642	3019	21	2913	53	3088	24	94	96
I16-01	I1601 - 141	471	54	830	12.9	0.163	0.0062	9.49	0.92	0.391	0.028	0.96609	2250	100	2090	130	2442	67	86	93
I16-01	I1601 - 142	609	101.7	1391	14.51	0.1248	0.0026	3.416	0.09	0.1951	0.004	0.67496	1504	20	1148	21	2017	37	57	76
I16-01	I1601 - 143	2560	235	465	2.18	0.1633	0.0027	9.85	0.28	0.4283	0.009	0.74754	2415	26	2293	41	2488	28	92	95
I16-01	I1601 - 144	702	56.4	137	2.38	0.2226	0.006	14.19	0.5	0.455	0.012	0.61714	2748	36	2417	50	2985	47	81	88
I16-01	I1601 - 145	5340	749	531	0.961	0.2419	0.006	14.51	0.96	0.421	0.024	0.91315	2716	65	2230	110	3118	39	72	82
I16-01	I1601 - 146	175	22.35	860	38.9	0.1371	0.0019	5.287	0.087	0.2729	0.0032	0.53567	1866	15	1555	16	2186	24	71	83
I16-01	I1601 - 147	546	82.1	1243	15.07	0.1338	0.0045	4.99	0.2	0.267	0.012	0.56961	1819	35	1524	58	2133	63	71	84
I16-01	I1601 - 148	495	75.6	895	12.14	0.1588	0.0027	7.54	0.24	0.338	0.01	0.82106	2164	28	1868	47	2441	28	77	86
I16-01	I1601 - 149	2740	350	353	1.024	0.1653	0.003	9.85	0.29	0.426	0.011	0.71532	2414	27	2280	51	2498	31	91	94
I16-01	I1601 - 150	840	202	171	1.047	0.1692	0.0051	7.73	0.54	0.324	0.02	0.89126	2115	72	1780	100	2524	51	71	84
I16-01	I1601 - 151	674	70.2	144.7	2.025	0.1726	0.0039	12.37	0.3	0.5092	0.0099	0.50298	2623	23	2648	42	2569	39	103	101
I16-01	I1601 - 152	165	15.49	31.6	2.014	0.1894	0.0089	14.54	0.63	0.552	0.017	0.24253	2768	41	2823	71	2678	79	105	102

Sample No.	Sample - spot	Pb (PPM)	Th (PPM)	U (PPM)	U/Th	$^{207}Pb/^{206}Pb$	± 2SE	$^{207}Pb/^{235}U$	± 2SE	$^{206}Pb/^{238}U$	± 2SE	Error Correlation 6/38 vs 7/35	Age $^{207}Pb/^{235}U$	± 2SE	Age $^{206}Pb/^{238}U$	± 2SE	Age $^{207}Pb/^{206}Pb$	± 2SE	Concordance 7/6 vs 6/38	Concordance 6/38 vs 7/35
I16-01	I1601 - 153	1230	193.9	835	4.218	0.161	0.0039	6.33	0.26	0.2771	0.0092	0.81273	2014	38	1575	47	2458	42	64	78
I16-01	I1601 - 154	536	189	251	1.405	0.2051	0.0054	8.25	0.59	0.288	0.019	0.90845	2194	63	1606	94	2843	43	56	73
I16-01	I1601 - 155	339	60.8	1125	17.87	0.1397	0.0025	4.83	0.12	0.2471	0.0055	0.65075	1785	21	1422	28	2215	31	64	80
I16-01	I1601 - 156	1771	314.1	1067	3.28	0.1404	0.0046	5.2	0.16	0.2663	0.009	0.50937	1846	27	1519	46	2221	55	68	82
I16-01	I1601 - 157	304	76.1	75.2	0.968	0.2396	0.0076	13.29	0.37	0.4026	0.0097	0.29819	2692	25	2175	45	3090	49	70	81
I16-01	I1601 - 158	1353	98.4	161.6	1.614	0.229	0.01	18.67	0.68	0.606	0.028	0.44956	3016	36	3040	110	3019	73	101	101
I16-01	I1601 - 159	1973	149.6	271.7	1.749	0.2375	0.0036	20.64	0.38	0.627	0.01	0.57117	3119	18	3135	40	3099	25	101	101
I16-01	I1601 - 160	3320	577	390	0.637	0.1579	0.0033	7.11	0.16	0.3285	0.0067	0.58295	2120	21	1828	32	2426	34	75	86
I16-01	I1601 - 6	3.50E+03	45	75	0.074	0.256	0.017	8.6	1	0.228	0.014	0.97205	2180	110	1316	75	3140	110	42	60
I16-02	I1602 - 001	97	5.11	66.1	13.14	0.3013	0.0077	27.87	0.71	0.663	0.014	0.45094	3404	26	3272	55	3463	38	94	96
I16-02	I1602 - 002	6840	629	784	1.299	0.2622	0.0033	18.4	0.45	0.498	0.011	0.81856	3001	24	2599	45	3254	20	80	87
I16-02	I1602 - 003	941	59.5	109.1	1.744	0.2415	0.0058	21.47	0.45	0.632	0.011	0.34411	3153	21	3160	46	3111	38	102	100
I16-02	I1602 - 005	7400	655	932	1.367	0.2473	0.0035	12.56	0.33	0.3563	0.0081	0.84538	2636	25	1966	37	3167	22	62	75
I16-02	I1602 - 006	2014	100.9	144.2	1.407	0.2327	0.0053	19.94	0.41	0.607	0.011	0.38576	3085	19	3051	45	3054	36	100	99
I16-02	I1602 - 007	13290	1249	1723	1.392	0.1244	0.0021	3.169	0.055	0.1799	0.0034	0.61877	1447	14	1066	19	2012	30	53	74
I16-02	I1602 - 011	14050	601	657	1.09	0.1918	0.0044	11.44	0.3	0.42	0.011	0.6914	2555	25	2260	51	2750	37	82	88
I16-02	I1602 - 012	2730	116.1	166	1.468	0.181	0.0052	12.67	0.33	0.502	0.012	0.39623	2648	25	2619	50	2641	47	99	99
I16-02	I1602 - 013	1650	74.7	173	2.29	0.1746	0.0054	11.41	0.36	0.468	0.014	0.47961	2549	30	2469	60	2584	53	96	97
I16-02	I1602 - 014	3950	168.4	367.7	2.178	0.2328	0.0044	16	0.74	0.489	0.02	0.91485	2851	46	2553	88	3068	29	83	90
I16-02	I1602 - 015	11600	3980	3990	1.109	0.167	0.0033	2.253	0.075	0.0971	0.0034	0.83316	1192	24	596	20	2518	33	24	50
I16-02	I1602 - 016	6040	606	3300	5.46	0.1491	0.002	2.517	0.049	0.1223	0.0023	0.73866	1276	14	743	13	2328	23	32	58
I16-02	I1602 - 017	6550	1056	4910	4.58	0.1846	0.0027	1.315	0.022	0.05135	0.00092	0.69603	850.8	9.7	322.7	5.6	2694	26	12	38
I16-02	I1602 - 018	1053	96.6	129.2	1.342	0.1627	0.0044	12.16	0.32	0.542	0.01	0.29946	2610	25	2787	43	2467	47	113	107
I16-02	I1602 - 019	1810	196	266	1.73	0.162	0.0035	10.06	0.25	0.4489	0.0095	0.52389	2431	23	2386	42	2470	36	97	98
I16-02	I1602 - 020	2560	359	609	1.79	0.1725	0.0032	7.44	0.25	0.3088	0.0072	0.84304	2154	29	1732	35	2572	30	67	80
I16-02	I1602 - 021	2490	182.5	318	1.675	0.1866	0.0037	13.04	0.45	0.505	0.017	0.80978	2671	34	2626	73	2704	33	97	98
I16-02	I1602 - 022	1457	101.3	233	2.31	0.2051	0.0046	15.2	0.57	0.532	0.016	0.78063	2808	36	2739	67	2857	37	96	98
I16-02	I1602 - 023	4010	391	555	1.445	0.2533	0.0038	16.62	0.44	0.473	0.011	0.81692	2910	25	2492	47	3205	23	78	86
I16-02	I1602 - 025	3280	238	1830	26.4	0.1433	0.0023	3.98	0.18	0.1994	0.009	0.93144	1607	40	1166	49	2267	29	51	73
I16-02	I1602 - 026	11380	1720	1402	0.822	0.1468	0.0023	4.98	0.15	0.2452	0.0082	0.87207	1807	27	1410	43	2301	28	61	78

Sample No.	Sample - spot	Pb (PPM)	Th (PPM)	U (PPM)	U/Th	$^{207}Pb/^{206}Pb$	± 2SE	$^{207}Pb/^{235}U$	± 2SE	$^{206}Pb/^{238}U$	± 2SE	Error Correlation 6/38 vs 7/35	Age $^{207}Pb/^{235}U$	± 2SE	Age $^{206}Pb/^{238}U$	± 2SE	Age $^{207}Pb/^{206}Pb$	± 2SE	Concordance 7/6 vs 6/38	Concordance 6/38 vs 7/35
I16-02	I1602 - 027	6070	607	546	0.946	0.1556	0.0036	9.08	0.35	0.42	0.015	0.81947	2337	34	2257	66	2399	39	94	97
I16-02	I1602 - 028	641	43.1	90.1	2.055	0.2227	0.0058	18.53	0.5	0.598	0.015	0.42751	3006	27	3013	60	2986	43	101	100
I16-02	I1602 - 029	368	20.9	52.1	2.77	0.2249	0.0074	21.28	0.68	0.688	0.02	0.43655	3138	31	3364	75	2995	53	112	107
I16-02	I1602 - 030	1253	83	168.7	1.974	0.2261	0.005	19.81	0.39	0.629	0.01	0.25309	3076	19	3142	40	3009	35	104	102
I16-02	I1602 - 031	2488	27.9	1655	62.6	0.1501	0.0022	4.67	0.11	0.2234	0.0051	0.77746	1755	21	1298	27	2339	25	55	74
I16-02	I1602 - 032	3870	1190	2510	2.28	0.1566	0.0032	2.44	0.1	0.1121	0.0049	0.87166	1244	29	683	28	2415	36	28	55
I16-02	I1602 - 033	4310	660	1450	2.125	0.1475	0.0024	4.04	0.22	0.196	0.011	0.95015	1617	45	1148	58	2310	28	50	71
I16-02	I1602 - 034	8.90E+03	1090	1383	1.47	0.1642	0.0036	7.04	0.21	0.3058	0.0075	0.66425	2108	26	1717	37	2499	34	69	81
I16-02	I1602 - 035	1517	99.2	213	1.963	0.2957	0.0056	28.88	0.6	0.696	0.013	0.60646	3443	20	3409	48	3437	30	99	99
I16-02	I1602 - 036	1927	160.4	253.1	1.518	0.2086	0.0046	14.41	0.44	0.494	0.012	0.67296	2770	28	2581	53	2887	37	89	93
I16-02	I1602 - 037	1341	98.8	187.1	1.772	0.2109	0.0046	16.34	0.41	0.552	0.011	0.5281	2891	24	2833	49	2902	36	98	98
I16-02	I1602 - 038	2040	123.2	700	5.96	0.1771	0.0029	9.9	0.56	0.399	0.022	0.93969	2380	56	2140	100	2617	27	82	90
I16-02	I1602 - 039	5.14E+04	5840	3176	0.5076	0.1746	0.0017	10.19	0.12	0.4191	0.0055	0.70099	2450	11	2255	25	2599	16	87	92
I16-02	I1602 - 04	4260	314	553	1.797	0.272	0.0032	21.28	0.52	0.552	0.012	0.87046	3143	24	2828	49	3313	18	85	90
I16-02	I1602 - 040	2951	254.5	530.4	1.955	0.1769	0.0027	10.24	0.24	0.4152	0.0087	0.81676	2452	21	2240	40	2616	25	86	91
I16-02	I1602 - 041	2660	172	303	1.868	0.243	0.0053	17.2	0.4	0.509	0.01	0.51959	2937	23	2648	44	3128	35	85	90
I16-02	I1602 - 042	5090	613	510	0.795	0.1662	0.0031	8.41	0.19	0.3662	0.0078	0.6582	2273	20	2008	37	2508	31	80	88
I16-02	I1602 - 043	2129	173.5	377.4	2.081	0.1839	0.0039	11.34	0.3	0.445	0.011	0.63059	2543	25	2366	48	2676	35	88	93
I16-02	I1602 - 044	705	42.5	81.5	1.851	0.2454	0.0064	21.37	0.55	0.632	0.013	0.45754	3149	26	3152	53	3135	42	101	100
I16-02	I1602 - 045	2800	206.8	550	2.532	0.2525	0.0045	17.98	0.26	0.5109	0.0085	0.45039	2986	14	2662	37	3191	29	83	89
I16-02	I1602 - 046	9030	1041	2001	1.82	0.1757	0.0026	4.2	0.15	0.1724	0.006	0.90152	1658	29	1023	33	2608	25	39	62
I16-02	I1602 - 047	2120	137.7	505	3.466	0.2289	0.0042	13.54	0.83	0.415	0.019	0.94936	2670	51	2221	82	3037	30	73	83
I16-02	I1602 - 048	1012	65.7	94.1	1.35	0.2253	0.0051	18.98	0.47	0.613	0.014	0.49967	3031	24	3073	54	3007	36	102	101
I16-02	I1602 - 049	3300	63.7	2090	32.7	0.1569	0.0032	2.54	0.11	0.117	0.0048	0.84898	1266	32	711	28	2411	36	29	56
I16-02	I1602 - 050	2.03E+04	4040	2080	0.511	0.1567	0.0029	4.74	0.45	0.221	0.021	0.97043	1682	83	1260	110	2415	30	52	75
I16-02	I1602 - 051	2220	49.8	2070	39.4	0.1529	0.0027	3.29	0.11	0.1561	0.0057	0.87959	1467	25	933	32	2367	30	39	64
I16-02	I1602 - 052	2728	74.4	1550	20.25	0.1493	0.0023	4.28	0.13	0.2056	0.0062	0.85033	1683	26	1203	33	2334	27	52	71
I16-02	I1602 - 053	4740	1277	4270	3.19	0.146	0.0029	1.629	0.096	0.0807	0.0049	0.93727	964	36	499	29	2288	35	22	52
I16-02	I1602 - 054	946	104.7	186	1.71	0.1683	0.0037	11.71	0.27	0.496	0.0085	0.44273	2573	21	2593	37	2523	37	103	101
I16-02	I1602 - 055	4360	504	1780	3.23	0.1539	0.0022	4.57	0.22	0.212	0.01	0.95696	1715	41	1233	54	2382	24	52	72

Sample No.	Sample - spot	Pb (PPM)	Th (PPM)	U (PPM)	U/Th	$^{207}Pb/^{206}Pb$	± 2SE	$^{207}Pb/^{235}U$	± 2SE	$^{206}Pb/^{238}U$	± 2SE	Error Correlation 6/38 vs 7/35	Age $^{207}Pb/^{235}U$	± 2SE	Age $^{206}Pb/^{238}U$	± 2SE	Age $^{207}Pb/^{206}Pb$	± 2SE	Concordance 7/6 vs 6/38	Concordance 6/38 vs 7/35
I16-02	I1602 - 056	1704	163	363	2.133	0.2175	0.0032	14.07	0.31	0.4608	0.0088	0.75147	2747	22	2439	39	2954	24	83	89
I16-02	I1602 - 057	1547	186	270	1.481	0.1687	0.0037	8.47	0.46	0.359	0.019	0.91356	2238	52	1955	92	2532	37	77	87
I16-02	I1602 - 058	1899	235	893	3.71	0.1549	0.0025	6.45	0.16	0.2971	0.0079	0.80994	2035	22	1674	39	2393	27	70	82
I16-02	I1602 - 059	2400	72.2	1630	20.9	0.147	0.0025	4.88	0.26	0.234	0.011	0.9565	1762	47	1346	58	2300	29	59	76
I16-02	I1602 - 060	4060	374	5580	14.8	0.144	0.0028	1.41	0.2	0.071	0.01	0.98651	826	72	432	60	2271	34	19	52
I16-02	I1602 - 061	1037	83.7	145.1	2.08	0.2092	0.0051	16.86	0.47	0.576	0.014	0.55429	2915	27	2924	56	2885	42	101	100
I16-02	I1602 - 062	1106	82.4	144.9	1.714	0.2215	0.0048	18.5	0.43	0.597	0.013	0.5357	3008	23	3011	52	2981	34	101	100
I16-02	I1602 - 063	2407	205.8	366	1.756	0.19	0.0031	14.36	0.34	0.541	0.011	0.73839	2765	23	2782	47	2733	27	102	101
I16-02	I1602 - 064	1860	129.3	454	3.67	0.225	0.0032	19.78	0.29	0.6329	0.0086	0.55072	3080	14	3158	34	3017	22	105	103
I16-02	I1602 - 065	4480	286.6	336.7	1.175	0.2631	0.0065	23.53	0.85	0.641	0.022	0.71327	3242	36	3193	90	3260	38	98	98
I16-02	I1602 - 066	5300	343.3	423	1.233	0.2267	0.0036	19.33	0.31	0.6144	0.0087	0.47535	3057	15	3085	35	3021	25	102	101
I16-02	I1602 - 067	1483	74.5	155.5	2.08	0.2856	0.0051	29.2	0.67	0.73	0.017	0.73471	3452	23	3523	64	3384	28	104	102
I16-02	I1602 - 068	11430	829	456	0.553	0.1619	0.003	10.06	0.2	0.4464	0.0076	0.58657	2441	18	2376	34	2463	32	96	97
I16-02	I1602 - 069	8580	580	416	0.783	0.164	0.0026	9.47	0.15	0.4158	0.0057	0.42156	2383	15	2240	26	2487	27	90	94
I16-02	I1602 - 070	2250	102	485	7.5	0.2564	0.0081	17.52	0.83	0.486	0.02	0.68056	2950	47	2545	89	3213	50	79	86
I16-02	I1602 - 071	2918	119.4	262.2	2.262	0.2227	0.0042	16.58	0.38	0.532	0.012	0.66578	2903	22	2744	50	2989	30	92	95
I16-02	I1602 - 072	7900	351	448	1.236	0.1836	0.0035	11.92	0.57	0.461	0.018	0.91189	2568	47	2428	81	2677	32	91	95
I16-02	I1602 - 073	2470	88.7	114.5	1.258	0.2074	0.0054	17.62	0.48	0.613	0.014	0.45168	2957	27	3073	57	2863	43	107	104
I16-02	I1602 - 074	2770	135.8	181.9	1.42	0.1717	0.0035	11.73	0.24	0.4892	0.0093	0.50254	2577	19	2563	40	2559	35	100	99
I16-02	I1602 - 075	5740	457	590	1.251	0.1688	0.0029	6.4	0.14	0.2724	0.0056	0.70627	2028	20	1551	28	2536	28	61	76
I16-02	I1602 - 076	1591	100.9	150.5	1.472	0.1644	0.0041	10.8	0.28	0.4757	0.0082	0.34879	2496	24	2505	36	2484	44	101	100
I16-02	I1602 - 077	3680	158.8	182.1	1.182	0.264	0.0045	24.5	0.73	0.669	0.018	0.82481	3277	30	3289	70	3265	26	101	100
I16-02	I1602 - 078	4840	378	1493	4.17	0.1537	0.0024	3.29	0.13	0.1546	0.0064	0.89893	1463	31	923	35	2385	28	39	63
I16-02	I1602 - 079	3290	228	494	2.31	0.1569	0.0036	5.34	0.33	0.245	0.016	0.92828	1839	51	1399	80	2414	40	58	76
I16-02	I1602 - 080	3710	212	392	1.957	0.1614	0.0029	10.03	0.25	0.445	0.01	0.73231	2428	25	2366	45	2466	30	96	97
I16-02	I1602 - 082	6910	747	2740	4.13	0.1505	0.0028	2.034	0.071	0.0967	0.0035	0.86086	1122	23	594	20	2344	32	25	53
I16-02	I1602 - 083	2410	165	546	3.524	0.1638	0.0025	10.82	0.2	0.4746	0.0084	0.64898	2505	17	2505	36	2487	25	101	100
I16-02	I1602 - 084	1136	58.7	94.1	1.638	0.2246	0.0057	19.97	0.54	0.638	0.014	0.41463	3081	27	3175	54	3004	42	106	103
I16-02	I1602 - 085	5140	543	1098	2.3	0.1441	0.0023	4.9	0.11	0.2447	0.0051	0.73238	1796	19	1409	27	2268	28	62	78
I16-02	I1602 - 086	8.70E+03	1060	5740	5.18	0.186	0.0037	2.71	0.52	0.104	0.02	0.99153	1200	110	620	110	2700	32	23	52
I16-02	I1602 - 087	6490	670	551	1.025	0.1577	0.0025	10.19	0.35	0.462	0.015	0.87827	2437	34	2438	66	2423	27	101	100

Sample No.	Sample - spot	Pb (PPM)	Th (PPM)	U (PPM)	U/Th	$^{207}Pb/^{206}Pb$	± 2SE	$^{207}Pb/^{235}U$	± 2SE	$^{206}Pb/^{238}U$	± 2SE	Error Correlation 6/38 vs 7/35	Age $^{207}Pb/^{235}U$	± 2SE	Age $^{206}Pb/^{238}U$	± 2SE	Age $^{207}Pb/^{206}Pb$	± 2SE	Concordance 7/6 vs 6/38	Concordance 6/38 vs 7/35
I16-02	I1602 - 088	2271	169.6	256	1.513	0.1604	0.0037	10.66	0.21	0.4772	0.0075	0.20227	2489	19	2512	33	2442	40	103	101
I16-02	I1602 - 089	3460	401	1171	2.928	0.1486	0.0022	4.61	0.2	0.222	0.01	0.94116	1739	38	1295	54	2322	25	56	74
I16-02	I1602 - 090	1748	137.8	216.5	1.655	0.1583	0.0033	10.62	0.23	0.482	0.01	0.51692	2486	20	2535	43	2428	35	104	102
I16-02	I1602 - 091	3440	233	285	1.481	0.2798	0.0046	26.99	0.52	0.706	0.013	0.64146	3383	18	3445	51	3354	26	103	102
I16-02	I1602 - 092	4010	393.2	545	1.319	0.1742	0.0028	11.53	0.2	0.4853	0.0078	0.59179	2563	16	2547	34	2589	27	98	99
I16-02	I1602 - 093	1305	29.67	1218	39.7	0.1719	0.0023	6.559	0.095	0.2787	0.0033	0.44622	2052	13	1584	16	2571	22	62	77
I16-02	I1602 - 094	5340	556	2370	5.01	0.1947	0.004	3.32	0.13	0.1264	0.0059	0.87459	1475	32	765	34	2773	33	28	52
I16-02	I1602 - 095	2060	151	246	1.678	0.2229	0.0044	18.21	0.38	0.602	0.01	0.48957	2999	21	3033	41	2996	31	101	101
I16-02	I1602 - 096	9910	1896	4270	2.223	0.1673	0.0034	2.323	0.071	0.1029	0.0037	0.77566	1215	21	630	22	2522	33	25	52
I16-02	I1602 - 097	3050	309.1	488	1.544	0.1621	0.0042	8.38	0.24	0.377	0.011	0.64712	2266	26	2059	55	2469	45	83	91
I16-02	I1602 - 098	1502	119.3	425	3.45	0.1576	0.0027	9	0.2	0.4182	0.0083	0.63628	2332	20	2255	39	2421	30	93	97
I16-02	I1602 - 099	672	45.2	81.9	1.785	0.2176	0.0056	19.88	0.48	0.671	0.013	0.28953	3076	24	3303	51	2953	42	112	107
I16-02	I1602 - 100	3170	239	406	1.7	0.1626	0.0034	8.71	0.3	0.396	0.014	0.84099	2299	32	2150	62	2467	36	87	94
I16-02	I1602 - 101	7820	1120	527	0.494	0.238	0.0042	14.7	0.58	0.447	0.014	0.90582	2774	38	2371	63	3097	28	77	85
I16-02	I1602 - 102	3160	216	389	2.02	0.2502	0.0042	18.14	0.58	0.528	0.016	0.84463	2985	31	2721	67	3180	27	86	91
I16-02	I1602 - 103	4080	315	374	1.155	0.163	0.0028	11.38	0.2	0.5067	0.0077	0.48663	2553	16	2640	33	2477	29	107	103
I16-02	I1602 - 104	3827	329.2	666	1.997	0.2108	0.0036	12.71	0.64	0.432	0.019	0.95071	2624	51	2300	86	2904	28	79	88
I16-02	I1602 - 105	3590	293	448	1.535	0.2142	0.0033	14.12	0.33	0.4743	0.0092	0.72007	2750	22	2499	40	2930	25	85	91
I16-02	I1602 - 106	2631	274	203.5	0.784	0.2808	0.0054	20.44	0.54	0.525	0.012	0.72843	3103	25	2721	52	3361	31	81	88
I16-02	I1602 - 107	3490	191	198	1.057	0.2925	0.005	26.21	0.62	0.647	0.014	0.70529	3354	23	3210	55	3425	27	94	96
I16-02	I1602 - 108	4990	336	334	1.009	0.2807	0.0044	22.97	0.53	0.587	0.013	0.72273	3217	23	2970	52	3365	26	88	92
I16-02	I1602 - 109	3970	289	627	2.43	0.2573	0.0039	12.67	0.44	0.356	0.012	0.89896	2640	32	1954	58	3223	24	61	74
I16-02	I1602 - 110	4270	469	906	2.027	0.1699	0.0026	5.55	0.24	0.235	0.01	0.92704	1886	39	1352	53	2556	27	53	72
I16-02	I1602 - 111	2740	281	567	2.122	0.1732	0.0036	7.26	0.26	0.3021	0.0091	0.80653	2133	33	1698	46	2578	35	66	80
I16-02	I1602 - 112	5220	348	393	1.172	0.2615	0.0054	22.92	0.61	0.632	0.015	0.67317	3218	27	3155	58	3249	32	97	98
I16-02	I1602 - 113	2046	129.5	353	2.734	0.2574	0.0068	23.36	0.53	0.657	0.015	0.31301	3242	21	3250	58	3221	42	101	100
I16-02	I1602 - 114	2060	132.6	149.9	1.202	0.2974	0.0062	26.75	0.63	0.647	0.013	0.57551	3367	23	3220	53	3445	32	93	96
I16-02	I1602 - 115	3490	289	182	0.68	0.1724	0.004	12.25	0.29	0.5105	0.0089	0.37582	2619	23	2656	38	2576	41	103	101
I16-02	I1602 - 116	1247	103	225.9	2.24	0.2876	0.0066	16.7	1.4	0.414	0.033	0.95939	2821	96	2190	160	3399	34	64	78
I16-02	I1602 - 117	5050	632	669	1.12	0.1617	0.0026	7.11	0.17	0.3167	0.0075	0.76412	2118	21	1770	37	2465	27	72	84
I16-02	I1602 - 118	2290	240	335	1.158	0.1608	0.0045	9.27	0.61	0.414	0.024	0.85747	2323	64	2210	110	2459	46	90	95
I16-02	I1602 - 119	2330	231.6	332.1	1.39	0.1676	0.0039	8.4	0.23	0.3612	0.0077	0.59674	2265	25	1984	37	2515	39	79	88

Sample No.	Sample - spot	Pb (PPM)	Th (PPM)	U (PPM)	U/Th	$^{207}Pb/^{206}Pb$	± 2SE	$^{207}Pb/^{235}U$	± 2SE	$^{206}Pb/^{238}U$	± 2SE	Error Correlation 6/38 vs 7/35	Age $^{207}Pb/^{235}U$	± 2SE	Age $^{206}Pb/^{238}U$	± 2SE	Age $^{207}Pb/^{206}Pb$	± 2SE	Concordance 7/6 vs 6/38	Concordance 6/38 vs 7/35
I16-02	I1602 - 120	747	49.5	114.6	2.222	0.2374	0.0063	20.64	0.56	0.635	0.016	0.59809	3118	27	3161	62	3085	42	102	101
I16-02	I1602 - 121	2350	137.3	213	1.485	0.2911	0.0047	28.11	0.56	0.7	0.013	0.61641	3420	19	3423	47	3416	25	100	100
I16-02	I1602 - 122	136	5.49	529	119	0.2027	0.004	14.54	0.46	0.518	0.013	0.7624	2779	30	2689	55	2842	33	95	97
I16-02	I1602 - 123	2000	274	866	4.89	0.2242	0.0035	8.61	0.52	0.276	0.016	0.95742	2261	52	1560	78	3005	25	52	69
I16-02	I1602 - 124	2400	182	201	1.179	0.1814	0.0052	9.89	0.41	0.395	0.015	0.76634	2410	39	2148	71	2643	48	81	89
I16-02	I1602 - 125	1430	75.5	370	4.78	0.2071	0.0044	14.24	0.38	0.498	0.013	0.724	2757	26	2597	57	2871	35	90	94
I16-02	I1602 - 126	1310	16.11	1124	71.3	0.1623	0.0031	6.99	0.17	0.3106	0.0049	0.55801	2105	21	1742	24	2475	34	70	83
I16-02	I1602 - 127	3450	264.8	841	3.2	0.2731	0.0054	8.02	0.48	0.209	0.012	0.92147	2196	56	1224	68	3319	32	37	56
I16-02	I1602 - 128	2060	142	544	3.91	0.1796	0.004	11.07	0.42	0.442	0.015	0.80975	2518	35	2354	66	2640	36	89	93
I16-02	I1602 - 129	1350	91	373	6.91	0.2458	0.0046	16.8	1	0.488	0.027	0.93847	2867	60	2520	120	3155	30	80	88
I16-02	I1602 - 130	3430	220	216	1.016	0.2647	0.0049	26.12	0.58	0.711	0.015	0.6583	3350	22	3454	58	3269	30	106	103
I16-02	I1602 - 131	2570	170.4	257	1.486	0.2608	0.0047	22.12	0.73	0.606	0.017	0.83063	3175	32	3043	68	3243	29	94	96
I16-02	I1602 - 132	4830	453.5	426	0.93	0.2347	0.0044	15.69	0.35	0.478	0.01	0.64583	2854	21	2517	44	3077	30	82	88
I16-02	I1602 - 133	4120	336	1476	4.99	0.2608	0.005	4.78	0.28	0.1307	0.0072	0.94413	1746	54	788	42	3242	31	24	45
I16-02	I1602 - 134	3560	239	317	1.332	0.2638	0.0059	25.1	0.68	0.683	0.016	0.58339	3306	26	3352	62	3261	35	103	101
I16-02	I1602 - 135	5660	1256	3840	3.01	0.1378	0.0031	1.767	0.081	0.0914	0.0038	0.85219	1026	29	563	23	2197	37	26	55
I16-02	I1602 - 136	5110	529	1270	2.207	0.166	0.0028	6.58	0.19	0.2898	0.0091	0.85416	2046	26	1635	46	2508	29	65	80
I16-02	I1602 - 137	945	93.9	156.1	1.669	0.1669	0.0045	11.81	0.31	0.517	0.011	0.39607	2582	25	2683	48	2510	45	107	104
I16-02	I1602 - 138	3138	398.2	595	1.418	0.1589	0.0027	8.61	0.15	0.3959	0.0052	0.42861	2295	16	2149	24	2438	28	88	94
I16-02	I1602 - 139	396	34.7	67.2	1.84	0.2402	0.0078	21.88	0.74	0.663	0.017	0.4212	3164	33	3271	65	3102	54	105	103
I16-02	I1602 - 140	4690	1513	3270	2.047	0.1535	0.0036	1.887	0.056	0.0897	0.0028	0.65442	1073	19	554	16	2374	40	23	52
I16-02	I1602 - 141	3900	709	1062	1.393	0.1516	0.0025	5.78	0.16	0.2786	0.0069	0.80713	1937	24	1581	35	2357	29	67	82
I16-02	I1602 - 142	107	10.06	39.6	3.9	0.1958	0.0082	14.59	0.59	0.547	0.017	0.35428	2774	39	2821	76	2747	75	103	102
I16-02	I1602 - 143	795	68.8	92.8	1.299	0.2468	0.0078	21.65	0.57	0.644	0.014	0.21246	3161	25	3206	59	3144	49	102	101
I16-02	I1602 - 144	320	33.7	303	8.67	0.1866	0.0037	12.84	0.23	0.5039	0.0083	0.39336	2663	17	2633	35	2700	33	98	99
I16-02	I1602 - 145	2700	353	421	1.175	0.1675	0.0031	9.81	0.22	0.4287	0.0091	0.63931	2411	21	2296	41	2523	32	91	95
I16-02	I1602 - 146	3970	365	2670	7.69	0.163	0.0028	2.95	0.15	0.1326	0.0069	0.94086	1373	37	799	39	2477	28	32	58
I16-02	I1602 - 147	2930	349	579	1.661	0.1909	0.0034	11.75	0.26	0.4496	0.0091	0.70171	2579	21	2390	40	2741	29	87	93
I16-02	I1602 - 148	712	57.3	154	2.72	0.2349	0.0051	18.01	0.45	0.552	0.012	0.59828	2982	24	2828	48	3082	34	92	95
I16-02	I1602 - 149	662	46.1	347	7.06	0.263	0.0046	22.86	0.63	0.634	0.017	0.74812	3215	26	3158	66	3256	28	97	98
I16-02	I1602 - 150	652	44	767	17.16	0.1858	0.0039	9.86	0.31	0.3829	0.0093	0.71918	2414	29	2087	43	2702	37	77	86
I16-05	I1605 - 006	43.6	2.68	483	247	0.2167	0.0037	17.12	0.36	0.569	0.01	0.57626	2934	21	2897	43	2949	29	98	99

Sample No.	Sample - spot	Pb (PPM)	Th (PPM)	U (PPM)	U/Th	$^{207}Pb/^{206}Pb$	± 2SE	$^{207}Pb/^{235}U$	± 2SE	$^{206}Pb/^{238}U$	± 2SE	Error Correlation 6/38 vs 7/35	Age $^{207}Pb/^{235}U$	± 2SE	Age $^{206}Pb/^{238}U$	± 2SE	Age $^{207}Pb/^{206}Pb$	± 2SE	Concordance 7/6 vs 6/38	Concordance 6/38 vs 7/35
I16-05	I1605 - 007	2327	178.7	320	1.689	0.2469	0.0039	21.75	0.41	0.634	0.01	0.64224	3167	18	3162	40	3160	26	100	100
I16-05	I1605 - 008	342	25.78	48	1.802	0.2322	0.0074	20.11	0.6	0.627	0.014	0.27439	3085	30	3130	55	3034	51	103	101
I16-05	I1605 - 009	2500	263	383	1.56	0.1654	0.0064	8.03	0.46	0.36	0.021	0.79445	2215	56	1970	100	2491	67	79	89
I16-05	I1605 - 010	1490	131	272	2.44	0.2199	0.0044	17.42	0.62	0.574	0.016	0.8019	2941	35	2913	68	2974	33	98	99
I16-05	I1605 - 011	888	78.9	162.5	1.945	0.2251	0.0052	17.15	0.42	0.554	0.012	0.53191	2933	24	2834	49	3001	37	94	97
I16-05	I1605 - 012	2830	168	1790	12.23	0.154	0.0042	7.24	0.52	0.336	0.02	0.91401	2096	63	1852	93	2381	47	78	88
I16-05	I1605 - 013	4590	759	2100	2.88	0.1533	0.0035	5	0.26	0.236	0.01	0.88878	1799	45	1359	53	2372	40	57	76
I16-05	I1605 - 014	4450	456	870	1.83	0.1893	0.0025	11.66	0.22	0.4479	0.008	0.75602	2573	17	2389	37	2734	23	87	93
I16-05	I1605 - 015	1590	117	236.7	1.943	0.2624	0.0062	24.14	0.46	0.669	0.013	0.26866	3269	19	3297	49	3247	37	102	101
I16-05	I1605 - 016	1714	123.6	167.4	1.309	0.2222	0.0054	19.62	0.44	0.634	0.014	0.4475	3075	21	3161	57	2992	37	106	103
I16-05	I1605 - 017	308	24.05	571	23.7	0.2184	0.003	18.46	0.29	0.6066	0.0089	0.62445	3015	14	3068	34	2969	21	103	102
I16-05	I1605 - 018	875	68	118.2	1.694	0.2333	0.0078	19.49	0.48	0.607	0.017	0.38579	3060	24	3051	69	3051	53	100	100
I16-05	I1605 - 019	1820	217	364	1.74	0.1713	0.0042	10.35	0.26	0.437	0.01	0.47024	2461	23	2333	45	2558	41	91	95
I16-05	I1605 - 020	750	59	297	4.92	0.2201	0.0046	18.11	0.42	0.6	0.012	0.56936	2996	22	3027	48	2971	33	102	101
I16-05	I1605 - 021	2609	76.5	2069	26.2	0.1361	0.0019	4.643	0.088	0.2445	0.0037	0.72538	1753	16	1412	18	2175	23	65	81
I16-05	I1605 - 022	7910	866	1624	1.846	0.1475	0.0028	6.25	0.19	0.3069	0.0073	0.77765	2007	27	1723	36	2308	32	75	86
I16-05	I1605 - 023	429	34.3	63	1.759	0.2338	0.0065	20.14	0.52	0.628	0.014	0.36662	3090	26	3133	56	3053	45	103	101
I16-05	I1605 - 024	4300	615	569	0.907	0.1728	0.0035	8.87	0.26	0.3645	0.0083	0.77621	2319	25	2001	39	2578	33	78	86
I16-05	I1605 - 025	4371	477	980	2.18	0.1583	0.0028	8.37	0.27	0.379	0.01	0.86572	2259	32	2063	48	2430	29	85	91
I16-05	I1605 - 026	1293	100.1	200	1.9	0.231	0.0038	20.32	0.48	0.634	0.013	0.71048	3100	23	3164	48	3061	27	103	102
I16-05	I1605 - 027	1086	92.2	261	2.68	0.1839	0.0037	14.03	0.3	0.553	0.01	0.56481	2745	20	2834	44	2675	33	106	103
I16-05	I1605 - 028	992	71.5	103.3	1.403	0.2286	0.0062	19.86	0.5	0.63	0.012	0.28744	3076	25	3147	50	3018	44	104	102
I16-05	I1605 - 029	9950	930	1114	1.154	0.1607	0.0023	9.19	0.13	0.4094	0.005	0.57557	2354	13	2211	23	2460	23	90	94
I16-05	I1605 - 030	3900	449	303	0.685	0.1642	0.0033	10.34	0.24	0.4526	0.0079	0.53118	2458	21	2403	35	2490	33	97	98
I16-05	I1605 - 031	1482	114.1	200.4	1.723	0.2344	0.0051	20.25	0.39	0.619	0.011	0.33892	3097	19	3103	43	3071	36	101	100
I16-05	I1605 - 032	16320	6200	6570	1.037	0.1405	0.0018	2.95	0.11	0.1488	0.0053	0.93227	1383	29	892	30	2231	21	40	64
I16-05	I1605 - 033	4860	560	1080	4.71	0.1682	0.0028	9.14	0.38	0.391	0.012	0.89405	2336	38	2125	54	2534	28	84	91
I16-05	I1605 - 034	1462	123.9	182	1.41	0.1852	0.0041	14.08	0.35	0.546	0.012	0.53881	2745	24	2800	49	2683	37	104	102
I16-05	I1605 - 035	2763	336.7	501	1.464	0.168	0.003	9.44	0.21	0.4028	0.0087	0.70446	2375	20	2177	40	2530	31	86	92
I16-05	I1605 - 036	3920	354	671	1.84	0.2576	0.0035	20.23	0.53	0.559	0.012	0.83133	3095	25	2857	49	3228	21	89	92
I16-05	I1605 - 037	2008	34.5	923	35.1	0.1776	0.0026	9.88	0.21	0.3965	0.0078	0.74491	2419	21	2151	36	2626	24	82	89
I16-05	I1605 - 038	5090	1390	1173	0.885	0.1457	0.0026	5.06	0.43	0.243	0.018	0.97833	1748	65	1382	88	2292	29	60	79

Sample No.	Sample - spot	Pb (PPM)	Th (PPM)	U (PPM)	U/Th	$^{207}Pb/^{206}Pb$	± 2SE	$^{207}Pb/^{235}U$	± 2SE	$^{206}Pb/^{238}U$	± 2SE	Error Correlation 6/38 vs 7/35	Age $^{207}Pb/^{235}U$	± 2SE	Age $^{206}Pb/^{238}U$	± 2SE	Age $^{207}Pb/^{206}Pb$	± 2SE	Concordance 7/6 vs 6/38	Concordance 6/38 vs 7/35
I16-05	I1605 - 039	929	79.1	98.7	1.235	0.1816	0.005	13.95	0.41	0.553	0.013	0.45249	2736	28	2837	57	2652	48	107	104
I16-05	I1605 - 040	4230	633	1150	1.94	0.1438	0.003	5.8	0.33	0.293	0.014	0.91871	1918	43	1641	67	2259	34	73	86
I16-05	I1605 - 041	691	65.2	417	6.24	0.2034	0.0048	15.14	0.34	0.534	0.011	0.4508	2821	21	2755	46	2847	38	97	98
I16-05	I1605 - 042	1065	81.2	159	1.857	0.2299	0.0048	19.89	0.37	0.624	0.013	0.47278	3080	18	3126	53	3037	34	103	101
I16-05	I1605 - 043	3220	297	163.7	0.525	0.1706	0.0046	11.93	0.27	0.509	0.01	0.30394	2596	22	2646	45	2545	45	104	102
I16-05	I1605 - 044	3830	1050	2823	3.33	0.1237	0.0025	3	0.14	0.1775	0.0085	0.87642	1401	37	1050	46	2008	34	52	75
I16-05	I1605 - 045	814	59.4	203	3.53	0.2104	0.0047	17.29	0.56	0.578	0.015	0.65694	2940	31	2934	59	2898	36	101	100
I16-05	I1605 - 046	13530	2127	1130	0.515	0.1618	0.0038	7.37	0.18	0.3315	0.0072	0.51477	2153	22	1844	35	2466	40	75	86
I16-05	I1605 - 047	4640	352.1	472	1.276	0.2326	0.0037	20.57	0.31	0.637	0.01	0.5717	3117	15	3180	39	3061	26	104	102
I16-05	I1605 - 048	1520	127.2	201.4	1.476	0.1844	0.0037	13.69	0.32	0.5364	0.0099	0.5927	2726	21	2764	42	2684	33	103	101
I16-05	I1605 - 049	6290	1028	1393	1.293	0.1582	0.0024	5.84	0.17	0.2656	0.0067	0.82264	1945	25	1515	34	2428	26	62	78
I16-05	I1605 - 050	1707	285.9	544	1.875	0.1926	0.0049	4.78	0.15	0.1816	0.0063	0.67684	1778	26	1073	34	2744	42	39	60
I16-05	I1605 - 051	486	40.1	67	1.626	0.1679	0.0059	12.2	0.41	0.523	0.012	0.24844	2610	31	2705	49	2517	59	107	104
I16-05	I1605 - 052	2255	233.2	1283	5.38	0.1637	0.0033	7.01	0.18	0.3075	0.005	0.77357	2103	23	1727	24	2484	34	70	82
I16-05	I1605 - 053	4960	354.4	345	0.936	0.2707	0.004	25.93	0.45	0.693	0.011	0.66769	3341	18	3390	41	3307	23	103	101
I16-05	I1605 - 054	1490	107.3	190	1.8	0.2684	0.0094	23.45	0.89	0.649	0.026	0.63586	3243	40	3210	100	3281	54	98	99
I16-05	I1605 - 055	1635	142.6	302.4	2.153	0.1841	0.0031	13.95	0.25	0.5417	0.0079	0.46865	2742	17	2788	33	2686	27	104	102
I16-05	I1605 - 056	7690	860	651	0.732	0.1762	0.0039	10.62	0.28	0.4383	0.0099	0.59336	2484	25	2340	45	2613	39	90	94
I16-05	I1605 - 057	6280	854	2013	2.232	0.1843	0.0024	6.74	0.1	0.2607	0.0033	0.59744	2077	13	1492	17	2687	21	56	72
I16-05	I1605 - 058	4320	312	516	1.67	0.2379	0.0089	19.81	0.62	0.599	0.023	0.41342	3076	31	3017	91	3102	68	97	98
I16-05	I1605 - 059	668	46.1	66.7	1.399	0.2662	0.0068	25.98	0.73	0.709	0.017	0.47802	3332	28	3442	65	3263	40	105	103
I16-05	I1605 - 060	1.47E+04	3670	2800	0.909	0.1524	0.0023	4.1	0.21	0.1491	0.0068	0.93517	1624	40	892	38	2368	27	38	55
I16-05	I1605 - 061	1954	147	264	1.701	0.2288	0.0039	20.76	0.41	0.647	0.011	0.57879	3121	19	3210	44	3041	28	106	103
I16-05	I1605 - 062	3850	649	1685	2.75	0.154	0.0052	5.72	0.19	0.2748	0.0071	0.43244	1929	29	1564	36	2390	53	65	81
I16-05	I1605 - 063	3660	359	890	2.75	0.1679	0.0036	9.78	0.56	0.409	0.018	0.95793	2355	61	2188	84	2530	36	86	93
I16-05	I1605 - 064	3720	339	812	2.29	0.1647	0.0038	9.64	0.25	0.4294	0.0096	0.58048	2399	22	2300	43	2494	38	92	96
I16-05	I1605 - 065	3860	203	2580	12.81	0.1295	0.0021	4	0.083	0.2247	0.0046	0.7303	1636	17	1306	24	2088	30	63	80
I16-05	I1605 - 066	6740	890	1330	1.485	0.1576	0.0026	9.54	0.39	0.432	0.016	0.90417	2365	39	2301	70	2424	27	95	97
I16-05	I1605 - 067	4450	486	1062	2.139	0.1612	0.0036	9.02	0.2	0.4054	0.0094	0.5529	2339	19	2199	45	2471	37	89	94
I16-05	I1605 - 068	7000	2040	2320	1.205	0.1437	0.0029	5.07	0.49	0.241	0.02	0.984	1699	88	1360	100	2257	36	60	80
I16-05	I1605 - 069	4980	491	630	1.206	0.1637	0.0027	10.66	0.17	0.4681	0.0068	0.44419	2490	15	2478	31	2492	28	99	100

Sample No.	Sample - spot	Pb (PPM)	Th (PPM)	U (PPM)	U/Th	$^{207}Pb/^{206}Pb$	± 2SE	$^{207}Pb/^{235}U$	± 2SE	$^{206}Pb/^{238}U$	± 2SE	Error Correlation 6/38 vs 7/35	Age $^{207}Pb/^{235}U$	± 2SE	Age $^{206}Pb/^{238}U$	± 2SE	Age $^{207}Pb/^{206}Pb$	± 2SE	Concordance 7/6 vs 6/38	Concordance 6/38 vs 7/35
I16-05	I1605 - 070	7020	934	2790	2.872	0.1392	0.0025	5.105	0.099	0.2641	0.0049	0.66287	1834	17	1510	25	2215	29	68	82
I16-05	I1605 - 071	1235	109.9	234.1	2.17	0.1638	0.0033	11.23	0.23	0.4918	0.0092	0.50936	2536	19	2585	40	2481	34	104	102
I16-05	I1605 - 072	2380	195	763	4.7	0.219	0.0031	16.07	0.31	0.525	0.01	0.71736	2875	19	2713	43	2973	24	91	94
I16-05	I1605 - 073	3610	324.5	409	1.193	0.1772	0.0031	12.65	0.22	0.5105	0.007	0.45063	2649	17	2656	30	2618	29	101	100
I16-05	I1605 - 074	6250	476	5750	11.73	0.1086	0.0015	2.179	0.072	0.1431	0.0045	0.83676	1168	22	860	25	1780	25	48	74
I16-05	I1605 - 075	1920	205	436.2	2.26	0.1531	0.0031	7.92	0.17	0.3683	0.0063	0.50442	2217	20	2020	30	2370	35	85	91
I16-05	I1605 - 076	9740	816	520	0.619	0.1665	0.0053	10.31	0.41	0.452	0.02	0.68487	2457	38	2398	91	2527	58	95	98
I16-05	I1605 - 077	1506	139.5	341.6	2.41	0.168	0.0038	11.52	0.27	0.5	0.01	0.55221	2563	23	2609	44	2531	37	103	102
I16-05	I1605 - 078	2450	318	380	1.203	0.1749	0.0033	10	0.22	0.4111	0.0073	0.5886	2427	21	2217	33	2597	31	85	91
I16-05	I1605 - 079	769	69.2	135.9	1.918	0.1693	0.0052	11.93	0.32	0.51	0.014	0.41834	2596	26	2673	58	2538	51	105	103
I16-05	I1605 - 080	2744	246	1897	7.71	0.1319	0.002	3.896	0.06	0.2116	0.0032	0.62055	1614	12	1236	17	2118	26	58	77
I16-05	I1605 - 081	1216	108.5	236	2.13	0.2147	0.004	17.07	0.41	0.568	0.011	0.57823	2929	23	2893	47	2938	31	98	99
I16-05	I1605 - 082	2770	204	300	1.507	0.2288	0.0036	20	0.39	0.627	0.011	0.63315	3090	18	3139	42	3038	26	103	102
I16-05	I1605 - 083	4180	389	213.7	0.544	0.1677	0.0041	11.52	0.27	0.498	0.011	0.42793	2562	22	2601	46	2524	43	103	102
I16-05	I1605 - 084	7810	881	873	0.945	0.1651	0.0047	9.54	0.23	0.428	0.014	0.34413	2388	22	2293	61	2496	48	92	96
I16-05	I1605 - 085	3990	321	447	1.437	0.2292	0.004	18.99	0.35	0.597	0.011	0.49134	3045	19	3011	46	3049	28	99	99
I16-05	I1605 - 086	880	68.5	1007	14.9	0.1839	0.0056	12.2	0.81	0.477	0.023	0.8919	2586	63	2500	100	2672	52	94	97
I16-05	I1605 - 087	1618	119.2	205.9	1.626	0.2293	0.0045	19.92	0.36	0.628	0.01	0.34551	3082	17	3136	40	3035	31	103	102
I16-05	I1605 - 088	2420	157	243.3	1.58	0.2729	0.0069	25.82	0.91	0.681	0.024	0.75468	3330	35	3336	93	3322	37	100	100
I16-05	I1605 - 089	1890	130.8	171.6	1.45	0.3057	0.0051	31.07	0.6	0.724	0.013	0.42231	3518	19	3502	50	3503	25	100	100
I16-05	I1605 - 090	2400	237	363	1.528	0.1741	0.0038	11.58	0.42	0.481	0.017	0.77302	2568	35	2517	74	2589	38	97	98
I16-05	I1605 - 091	5330	465	842	1.7	0.2206	0.0027	16.81	0.34	0.5474	0.0089	0.8261	2920	19	2811	37	2983	19	94	96
I16-05	I1605 - 092	1100	81.9	140.9	1.669	0.2299	0.0049	20.84	0.43	0.642	0.011	0.32524	3127	20	3193	44	3046	35	105	102
I16-05	I1605 - 093	4290	513	819	1.506	0.1563	0.0028	7.69	0.21	0.3547	0.0088	0.77579	2183	26	1958	41	2416	28	81	90
I16-05	I1605 - 094	1906	126.9	766	5.89	0.2112	0.0035	14.99	0.52	0.498	0.013	0.86359	2806	32	2602	56	2911	27	89	93
I16-05	I1605 - 095	740	55.1	225	3.86	0.1978	0.0044	17.03	0.44	0.617	0.015	0.63941	2929	27	3095	59	2790	38	111	106
I16-05	I1605 - 096	1393	117.6	135.8	1.091	0.1901	0.0049	13.98	0.35	0.533	0.011	0.41774	2738	24	2746	46	2720	43	101	100
I16-05	I1605 - 097	645	38.8	77.9	1.971	0.2389	0.0085	20.86	0.82	0.615	0.017	0.42634	3122	37	3086	66	3096	57	100	99
I16-05	I1605 - 098	11600	1219	586	0.68	0.168	0.0031	8.63	0.17	0.2882	0.0064	0.60472	2296	19	1634	31	2538	31	64	71
I16-05	I1605 - 099	4980	578	969	1.643	0.1595	0.0035	7.82	0.22	0.3554	0.0088	0.66684	2214	25	1958	42	2442	36	80	88
I16-05	I1605 - 100	383	28	58.2	2.009	0.2379	0.0082	20.94	0.7	0.634	0.019	0.35391	3126	31	3159	73	3081	58	103	101
I16-05	I1605 - 101	2750	185	594	3.99	0.2325	0.0047	18.66	0.67	0.57	0.017	0.82635	3002	35	2896	68	3060	33	95	96

Sample No.	Sample - spot	Pb (PPM)	Th (PPM)	U (PPM)	U/Th	$^{207}Pb/^{206}Pb$	± 2SE	$^{207}Pb/^{235}U$	± 2SE	$^{206}Pb/^{238}U$	± 2SE	Error Correlation 6/38 vs 7/35	Age $^{207}Pb/^{235}U$	± 2SE	Age $^{206}Pb/^{238}U$	± 2SE	Age $^{207}Pb/^{206}Pb$	± 2SE	Concordance 7/6 vs 6/38	Concordance 6/38 vs 7/35
I16-05	I1605 - 102	3920	347	461	1.38	0.1784	0.0038	11.33	0.58	0.454	0.023	0.90744	2497	58	2380	110	2640	35	90	95
I16-05	I1605 - 103	2176	200.7	318	1.53	0.1684	0.0034	12.03	0.21	0.5062	0.0082	0.30975	2604	17	2639	35	2533	33	104	101
I16-05	I1605 - 104	3077	231.1	347	1.443	0.23	0.0039	20	0.34	0.622	0.01	0.51597	3091	16	3119	39	3047	26	102	101
I16-05	I1605 - 105	5990	1700	3450	2.87	0.1165	0.0019	2.98	0.13	0.1807	0.0061	0.90446	1383	32	1068	33	1900	31	56	77
I16-27	I1627 - 01	820	69.4	152	2.077	0.254	0.0061	16.13	0.41	0.4519	0.0082	0.43501	2876	24	2400	36	3194	38	75	83
I16-27	I1627 - 02	2370	208	428	2.058	0.2369	0.0062	18.4	1	0.563	0.03	0.86795	2975	63	2880	130	3094	40	93	97
I16-27	I1627 - 03	410	27.3	49	1.776	0.2469	0.009	23.19	0.69	0.69	0.02	0.26003	3224	29	3371	77	3135	58	108	105
I16-27	I1627 - 04	1890	208	516	2.5	0.218	0.011	9.8	1	0.309	0.021	0.78274	2384	93	1730	100	2945	88	59	73
I16-27	I1627 - 05	1570	149	440	2.86	0.228	0.012	9.31	0.72	0.272	0.015	0.74863	2320	79	1545	78	2998	82	52	67
I16-27	I1627 - 06	5010	608	1590	2.447	0.223	0.0078	5.36	0.84	0.154	0.024	0.96929	1690	130	890	130	2997	59	30	53
I16-27	I1627 - 07	2260	136.8	379	2.72	0.2536	0.0068	14.26	0.62	0.421	0.024	0.84013	2757	43	2250	110	3195	43	70	82
I16-27	I1627 - 08	4450	423	746	1.71	0.2277	0.0095	8.06	0.48	0.221	0.012	0.72311	2225	51	1287	61	3039	71	42	58
I16-27	I1627 - 09	5750	1520	3620	2.35	0.1501	0.0059	1.725	0.062	0.0859	0.0041	0.59205	1015	23	530	25	2331	66	23	52
I16-27	I1627 - 10	2440	187	398	2.1	0.253	0.0093	21.3	1.1	0.615	0.025	0.73696	3143	50	3084	99	3193	59	97	98
I16-27	I1627 - 11	8150	1590	2669	1.619	0.1883	0.0058	3.23	0.1	0.1273	0.0054	0.62538	1460	24	772	31	2730	46	28	53
I16-27	I1627 - 12	2630	252	730	2.82	0.239	0.012	9.1	1	0.244	0.023	0.87469	2260	120	1390	120	3079	83	45	62
I16-27	I1627 - 13	3190	357	587	1.635	0.2312	0.0057	11.83	0.78	0.368	0.023	0.89996	2544	67	2000	110	3061	42	65	79
I16-27	I1627 - 14	4550	1318	3170	2.327	0.1823	0.0056	1.744	0.069	0.0705	0.0033	0.75824	1023	26	439	20	2657	51	17	43
I16-27	I1627 - 15	2130	241	1035	4.68	0.191	0.013	5.63	0.62	0.217	0.021	0.75978	1904	94	1260	110	2730	110	46	66
I16-27	I1627 - 16	2160	121.8	268	2.099	0.2484	0.0066	21.33	0.68	0.633	0.019	0.64892	3145	31	3152	76	3163	43	100	100
I16-27	I1627 - 17	1890	159	426	2.558	0.2446	0.0068	11.18	0.68	0.334	0.019	0.82109	2519	55	1848	90	3152	41	59	73
I16-27	I1627 - 18	1710	91.1	211	2.247	0.2589	0.0089	20.08	0.55	0.565	0.02	0.57978	3095	28	2879	83	3226	52	89	93
I16-27	I1627 - 19	2390	202	443	2.45	0.2516	0.0071	12.8	0.6	0.374	0.02	0.88116	2644	47	2035	95	3188	45	64	77
I16-27	I1627 - 20	6.40E+03	810	3.60E+03	4.36	0.279	0.012	4.4	1.1	0.112	0.028	0.96462	1490	170	660	150	3352	70	20	44
I16-27	I1627 - 21	5.10E+03	780	3.50E+03	4.9	0.294	0.013	5.1	1.1	0.125	0.027	0.95769	1570	180	730	150	3438	70	21	46
I16-27	I1627 - 22	3360	287	432	1.523	0.2418	0.0069	15.94	0.73	0.476	0.017	0.78122	2850	45	2512	78	3114	45	81	88
I16-27	I1627 - 23	1541	122.9	268	2.09	0.2399	0.0046	19.54	0.45	0.579	0.011	0.59066	3063	22	2941	45	3110	31	95	96
I16-27	I1627 - 24	14930	3181	3928	1.189	0.359	0.0089	2.982	0.077	0.0606	0.001	0.47927	1400	20	379.4	6.3	3737	38	10	27
I16-27	I1627 - 25	7170	1972	1868	0.921	0.2651	0.0045	4.236	0.079	0.1137	0.0019	0.62149	1677	15	695	10	3271	28	21	41
I16-27	I1627 - 26	5930	1053	1227	1.155	0.1739	0.0033	5.16	0.28	0.2078	0.0084	0.93929	1809	47	1212	45	2584	31	47	67

Sample No.	Sample - spot	Pb (PPM)	Th (PPM)	U (PPM)	U/Th	$^{207}Pb/^{206}Pb$	± 2SE	$^{207}Pb/^{235}U$	± 2SE	$^{206}Pb/^{238}U$	± 2SE	Error Correlation 6/38 vs 7/35	Age $^{207}Pb/^{235}U$	± 2SE	Age $^{206}Pb/^{238}U$	± 2SE	Age $^{207}Pb/^{206}Pb$	± 2SE	Concordance 7/6 vs 6/38	Concordance 6/38 vs 7/35
I16-27	I1627 - 27	6860	1532	1524	0.963	0.1703	0.0035	3.79	0.14	0.1593	0.005	0.79271	1578	30	951	28	2558	37	37	60
I16-27	I1627 - 28	3240	378	987	2.53	0.2313	0.0093	7.56	0.29	0.247	0.01	0.55987	2188	40	1420	53	3052	63	47	65
I16-27	I1627 - 29	6370	1413	1257	0.853	0.1762	0.0052	4.92	0.19	0.207	0.01	0.73469	1800	32	1210	53	2610	50	46	67
I16-27	I1627 - 30	2910	190.8	262.9	1.336	0.251	0.0071	23.24	0.81	0.679	0.019	0.63884	3227	34	3348	70	3188	42	105	104
I16-27	I1627 - 31	5450	283	621	2.092	0.264	0.012	16.3	1.1	0.455	0.035	0.77666	2876	66	2400	160	3256	71	74	83
I16-27	I1627 - 32	2650	171	257	1.441	0.2429	0.0074	17.8	0.64	0.539	0.021	0.65352	2974	36	2786	83	3132	50	89	94
I16-27	I1627 - 33	2400	198	328	1.659	0.2457	0.0076	20.92	0.77	0.629	0.022	0.58921	3124	37	3137	88	3152	51	100	100
I16-27	I1627 - 34	1798	192.9	284.6	1.437	0.2344	0.0053	16.46	0.52	0.508	0.014	0.70265	2898	29	2643	60	3083	34	86	91
I16-27	I1627 - 35	1055	77	184.2	2.301	0.2509	0.0076	18.52	0.6	0.543	0.019	0.55602	3014	33	2789	79	3184	50	88	93
I16-27	I1627 - 36	1590	177	492	2.84	0.218	0.011	10.7	1.3	0.367	0.037	0.91844	2480	120	2010	180	2957	83	68	81
I16-27	I1627 - 37	7730	582	465	0.773	0.2467	0.0045	21.13	0.35	0.612	0.01	0.37167	3142	16	3077	40	3157	29	97	98
I16-27	I1627 - 38	3080	211	291	1.391	0.2549	0.0043	18.64	0.33	0.523	0.011	0.6025	3021	18	2705	46	3207	27	84	90
I16-27	I1627 - 39	2410	204.4	448	2.123	0.2426	0.0058	13.63	0.46	0.41	0.014	0.74267	2714	31	2207	62	3125	39	71	81
I16-27	I1627 - 40	1086	86	143	1.728	0.2468	0.0078	21.29	0.82	0.619	0.024	0.71977	3136	42	3110	100	3153	49	99	99
I16-33	I1633 - 01	3930	1270	785	0.645	0.165	0.012	3.52	0.27	0.1522	0.0027	0.30763	1513	56	913	15	2420	110	38	60
I16-33	I1633 - 02	3190	354	423	1.126	0.1714	0.0032	9.9	0.3	0.4112	0.0089	0.76871	2411	29	2216	41	2560	30	87	92
I16-33	I1633 - 03	1320	101.2	293	2.78	0.179	0.007	12.68	0.48	0.52	0.019	0.49391	2647	37	2691	82	2624	64	103	102
I16-33	I1633 - 04	4480	220	1371	6.3	0.2284	0.0086	8.5	0.54	0.273	0.011	0.74545	2279	52	1553	56	3048	59	51	68
I16-33	I1633 - 05	2151	268	519	1.873	0.165	0.0033	9.03	0.22	0.3943	0.0077	0.54597	2334	23	2140	36	2497	34	86	92
I16-33	I1633 - 06	1046	83.4	130.5	1.656	0.2009	0.0051	16	0.38	0.572	0.012	0.35968	2871	23	2911	51	2822	43	103	101
I16-33	I1633 - 07	1050	43.4	316	8.23	0.29	0.013	18.2	2.3	0.466	0.056	0.94469	2940	120	2430	240	3401	70	71	83
I16-33	I1633 - 08	2900	336	472	1.575	0.165	0.003	8.92	0.25	0.3868	0.0099	0.76653	2317	27	2102	46	2499	32	84	91
I16-33	I1633 - 09	1890	174	283	1.611	0.1739	0.0042	11.86	0.32	0.4818	0.0094	0.49443	2586	25	2532	41	2583	40	98	98
I16-33	I1633 - 10	2500	221	190.7	0.901	0.1796	0.0041	12.08	0.3	0.4783	0.0083	0.43734	2604	24	2516	36	2636	39	95	97
I16-33	I1633 - 11	5680	1550	1223	0.87	0.155	0.005	2.79	0.31	0.108	0.0087	0.92115	1288	66	662	51	2387	58	28	51
I16-33	I1633 - 12	5530	1560	1270	0.81	0.1436	0.004	3.54	0.13	0.1803	0.0051	0.70439	1534	31	1068	27	2257	48	47	70
I16-33	I1633 - 13	2110	208	527	2.49	0.1649	0.0046	9.76	0.37	0.43	0.015	0.71204	2407	35	2298	66	2493	47	92	95
I16-33	I1633 - 14	639	56.1	73.8	1.295	0.1806	0.0065	13.33	0.48	0.525	0.014	0.40202	2690	35	2716	58	2640	57	103	101
I16-33	I1633 - 15	636	46.2	116.3	2.45	0.1814	0.0075	13.15	0.54	0.527	0.017	0.47725	2678	39	2753	72	2637	68	104	103
I16-33	I1633 - 16	4560	875	878	0.957	0.1478	0.0033	4.88	0.14	0.2387	0.008	0.74362	1790	23	1380	42	2308	38	60	77
I16-33	I1633 - 17	1664	140.9	219.3	1.515	0.1737	0.0066	11.74	0.42	0.501	0.019	0.45839	2583	32	2609	83	2587	69	101	101
I16-33	I1633 - 18	4290	730	885	1.186	0.154	0.0043	5.49	0.18	0.2541	0.0038	0.52581	1892	27	1459	19	2375	47	61	77

Sample No.	Sample - spot	Pb (PPM)	Th (PPM)	U (PPM)	U/Th	$^{207}Pb/^{206}Pb$	± 2SE	$^{207}Pb/^{235}U$	± 2SE	$^{206}Pb/^{238}U$	± 2SE	Error Correlation 6/38 vs 7/35	Age $^{207}Pb/^{235}U$	± 2SE	Age $^{206}Pb/^{238}U$	± 2SE	Age $^{207}Pb/^{206}Pb$	± 2SE	Concordance 7/6 vs 6/38	Concordance 6/38 vs 7/35
I16-33	I1633 - 19	2.43E+04	982	3410	3.38	0.279	0.015	7.42	0.54	0.1907	0.0073	0.68187	2140	68	1123	39	3343	87	34	52
I16-33	I1633 - 20	3750	645	910	1.303	0.1559	0.0048	6.41	0.6	0.296	0.023	0.95292	1990	84	1660	110	2400	52	69	83
I16-33	I1633 - 21	2034	190.9	310	1.533	0.1647	0.004	11.29	0.25	0.4909	0.0086	0.24212	2541	21	2572	37	2504	43	103	101
I16-33	I1633 - 22	2050	200	271	1.43	0.1724	0.0059	10.96	0.46	0.463	0.018	0.64306	2517	38	2446	78	2565	57	95	97
I16-33	I1633 - 23	1593	130	245.6	1.91	0.1851	0.0066	13.07	0.47	0.521	0.017	0.47653	2686	31	2714	65	2696	56	101	101
I16-33	I1633 - 24	4450	612	483	0.76	0.1595	0.0025	7.88	0.13	0.3543	0.0055	0.45628	2216	16	1954	26	2450	28	80	88
I16-33	I1633 - 25	3170	598	533	0.854	0.1517	0.0028	5.64	0.12	0.2662	0.0047	0.61921	1917	18	1520	24	2353	31	65	79
I16-33	I1633 - 26	887	68.7	125.5	1.906	0.1921	0.0056	13.57	0.52	0.505	0.015	0.68341	2706	36	2633	64	2731	48	96	97
I16-33	I1633 - 27	4.36E+04	5.10E+03	2010	0.726	0.432	0.019	17.89	0.95	0.309	0.014	0.65461	2943	51	1733	67	3963	70	44	59
I16-33	I1633 - 28	2894	525	987	1.804	0.1393	0.0032	4.75	0.12	0.2456	0.0045	0.54005	1770	20	1415	23	2210	38	64	80
I16-33	I1633 - 29	5260	553	316.2	0.592	0.1692	0.0033	10.28	0.22	0.4367	0.0095	0.5709	2456	19	2331	43	2540	33	92	95
I16-33	I1633 - 30	3960	472	786	1.612	0.1649	0.0039	8.42	0.39	0.37	0.015	0.86055	2258	44	2022	71	2495	40	81	90
I16-33	I1633 - 31	3050	584	1115	1.814	0.1329	0.0035	4.67	0.3	0.2434	0.0089	0.9444	1717	49	1399	46	2110	46	66	81
I16-33	I1633 - 32	2113	200.3	503	2.38	0.1701	0.0025	11.45	0.22	0.4805	0.0071	0.58298	2558	17	2531	30	2554	25	99	99
I16-33	I1633 - 33	1115	70.6	79.9	1.093	0.318	0.0081	33.78	0.86	0.75	0.016	0.40847	3597	25	3600	61	3555	41	101	100
I16-33	I1633 - 34	3.12E+05	364	644	2.15	0.62	0.048	1260	250	11	2.1	0.99458	5370	440	1.09E+04	1.40E+03	4240	200	257	203
I16-33	I1633 - 35	7.86E+04	3970	3160	0.913	0.603	0.012	20.3	1.3	0.234	0.012	0.91966	3046	57	1346	60	4506	30	30	44
I16-33	I1633 - 36	3.93E+04	4860	3320	0.71	0.402	0.025	11.4	1.5	0.176	0.015	0.92959	2300	130	1039	84	3800	100	27	45
I16-33	I1633 - 37	2500	490	2000	4.36	0.123	0.012	2.12	0.32	0.1132	0.0085	0.63627	1110	100	689	49	1910	170	36	62
I16-33	I1633 - 38	1776	157.9	238	1.459	0.1755	0.0035	12.49	0.29	0.5092	0.0087	0.60757	2635	22	2650	37	2599	33	102	101
I16-33	I1633 - 39	2632	241.5	225	0.909	0.1719	0.0039	12.12	0.26	0.5089	0.009	0.40482	2610	20	2648	39	2563	38	103	101
I16-33	I1633 - 40	3360	737	1061	1.393	0.1205	0.0027	3.44	0.11	0.2017	0.0039	0.71648	1505	25	1183	21	1947	40	61	79
I16-33	I1633 - 41	4580	344	224	0.652	0.2243	0.0046	19.11	0.47	0.612	0.013	0.59328	3041	23	3069	53	3001	34	102	101
I16-33	I1633 - 42	1.07E+04	661	894	1.359	0.242	0.023	12.4	2.3	0.33	0.027	0.95174	2390	140	1880	140	2890	130	65	79
I16-33	I1633 - 43	4080	520	725	1.461	0.1811	0.004	9.25	0.47	0.367	0.018	0.91253	2322	49	1995	87	2651	36	75	86
I16-33	I1633 - 44	3190	353	508	1.396	0.1808	0.0032	9.86	0.22	0.3855	0.0076	0.58211	2414	21	2099	35	2649	29	79	87
I16-33	I1633 - 45	775	57.5	102.5	1.73	0.1834	0.0046	14.54	0.43	0.566	0.012	0.52068	2775	28	2889	48	2668	41	108	104
I16-33	I1633 - 46	4700	703	604	0.828	0.1571	0.0033	6.65	0.16	0.3013	0.0055	0.60629	2058	21	1699	28	2409	35	71	83

Sample No.	Sample - spot	Pb (PPM)	Th (PPM)	U (PPM)	U/Th	$^{207}Pb/^{206}Pb$	± 2SE	$^{207}Pb/^{235}U$	± 2SE	$^{206}Pb/^{238}U$	± 2SE	Error Correlation 6/38 vs 7/35	Age $^{207}Pb/^{235}U$	± 2SE	Age $^{206}Pb/^{238}U$	± 2SE	Age $^{207}Pb/^{206}Pb$	± 2SE	Concordance 7/6 vs 6/38	Concordance 6/38 vs 7/35
I16-33	I1633 - 47	4620	451	436	0.913	0.1681	0.0045	9.98	0.3	0.4284	0.0099	0.50081	2423	28	2294	45	2520	46	91	95
I16-33	I1633 - 48	471	64.5	155.5	2.38	0.1756	0.0048	11.35	0.3	0.464	0.0087	0.34152	2549	26	2454	38	2589	46	95	96
I16-33	I1633 - 49	1061	66.3	353	5.1	0.2246	0.0054	17.84	0.45	0.577	0.014	0.6259	2976	24	2931	57	3004	38	98	98
I16-33	I1633 - 50	2780	234	290	1.155	0.1723	0.0034	12.3	0.24	0.511	0.0081	0.40551	2624	18	2662	36	2579	33	103	101

Appendix 2.2 The Kumta Suture of western Peninsular India: Hf isotope data

Sample N	Analysis N	$^{176}Hf/^{177}Hf$	2 S.E.	$^{176}Lu/^{177}Hf$	U/Pb AGE	2 S.E.	Hf Chur (t)	Hf DM (t)	Hf NC(t)	Hf_i	eHf	2SE	TDMc	TNCc	Above DM line?
I16-01	SA I16-01-151	0.281295808	2.27528E-05	0.001173802	2569	39	0.281136	0.281365	0.281303	0.281238	3.64	0.804596896	2.84	2.705913329	No
I16-01	SA I16-01-126	0.280688829	1.99162E-05	0.000848066	3361	27	0.280611	0.280766	0.280713	0.280634	0.80	0.704287236	3.63	3.523967992	No
I16-01	SA I16-01-061	0.28107041	2.4286E-05	0.000888161	2754	40	0.281014	0.281226	0.281166	0.281024	0.34	0.858816075	3.18	3.053041362	No
I16-01	SA I16-01-001	0.28117814	2.91114E-05	0.001306026	2588	25	0.281123	0.281351	0.281289	0.281114	-0.35	1.029454244	3.09	2.958116319	No
I16-01	SA I16-01-067	0.280835984	2.28543E-05	0.000623419	3062	35	0.280810	0.280993	0.280937	0.280799	-0.39	0.808184984	3.47	3.347987795	No
I16-01	SA I16-01-094	0.280838916	1.8269E-05	0.000779245	3069	33	0.280806	0.280988	0.280931	0.280793	-0.45	0.64603734	3.47	3.357230056	No
I16-01	SA I16-01-048	0.280824103	2.17404E-05	0.000884004	3093	60	0.280790	0.280970	0.280913	0.280772	-0.65	0.768796598	3.51	3.388261247	No
I16-01	SA I16-01-023	0.280729687	2.60483E-05	0.002213739	3306	24	0.280648	0.280808	0.280754	0.280589	-2.11	0.921135464	3.76	3.647515597	No
I16-01	SA I16-01-007	0.280824389	2.02025E-05	0.000822738	3006	27	0.280848	0.281036	0.280978	0.280777	-2.51	0.714410746	3.55	3.425918629	No
I16-01	SA I16-01-080	0.280849089	2.26814E-05	0.001027155	2970	30	0.280871	0.281063	0.281005	0.280791	-2.88	0.802071121	3.54	3.417785081	No
I16-01	SA I16-01-084	0.281104035	3.20659E-05	0.000853438	2462	30	0.281206	0.281446	0.281382	0.281064	-5.06	1.133932002	3.27	3.134204899	No
I16-01	SA I16-01-077	0.281079888	2.20475E-05	0.001122564	2511	46	0.281174	0.281409	0.281346	0.281026	-5.26	0.779657484	3.32	3.185764198	No
I16-01	SA I16-01-079	0.281112332	3.33194E-05	0.001768262	2483	44	0.281192	0.281430	0.281366	0.281029	-5.83	1.178260766	3.33	3.196572948	No
I16-01	SA I16-01-122	0.280932997	1.74708E-05	0.000872054	2677	36	0.281065	0.281284	0.281223	0.280888	-6.28	0.617810522	3.51	3.379535467	No
I16-01	SA I16-01-105	0.281045736	1.8862E-05	0.000874352	2489	34	0.281189	0.281425	0.281362	0.281004	-6.56	0.667009028	3.38	3.24417155	No
I16-01	SA I16-01-075	0.281053633	2.05198E-05	0.000753367	2466	45	0.281204	0.281443	0.281379	0.281018	-6.59	0.72563086	3.36	3.227969739	No
I16-01	SA I16-01-066	0.280955072	2.005E-05	0.00091816	2592	55	0.281121	0.281348	0.281286	0.280910	-7.51	0.709019112	3.51	3.383437858	No
I16-01	SA I16-01-116	0.280979765	1.85706E-05	0.000761616	2518	32	0.281169	0.281404	0.281341	0.280943	-8.05	0.656702706	3.49	3.355441532	No
I16-01	SA I16-01-060	0.280886017	2.24261E-05	0.000902492	2576	45	0.281131	0.281360	0.281298	0.280842	-10.31	0.793043192	3.66	3.534332174	No
I16-02	SA I16-02-114	0.280722273	3.74163E-05	0.001052025	3445	32	0.280555	0.280702	0.280650	0.280652	3.46	1.323134978	3.55	3.439212906	No
I16-02	SA I16-02-036	0.28108847	4.95374E-05	0.001517697	2887	37	0.280926	0.281126	0.281067	0.281005	2.78	1.751768441	3.14	3.018030506	No
I16-02	SA I16-02-003	0.280919261	2.38179E-05	0.001300981	3111	38	0.280778	0.280956	0.280900	0.280842	2.27	0.842262962	3.35	3.232777392	No
I16-02	SA I16-02-112	0.280836454	4.70127E-05	0.001688637	3249	32	0.280686	0.280851	0.280797	0.280731	1.60	1.662490119	3.50	3.385512697	No
I16-02	SA I16-02-066	0.281015966	5.57757E-05	0.002350216	3021	25	0.280838	0.281024	0.280967	0.280880	1.50	1.972372869	3.32	3.203559376	No
I16-02	SA I16-02-067	0.280697411	3.66285E-05	0.001381221	3384	28	0.280596	0.280748	0.280695	0.280607	0.40	1.295277886	3.68	3.565989167	No
I16-02	SA I16-02-091	0.280701071	5.6052E-05	0.001290979	3354	26	0.280616	0.280771	0.280718	0.280618	0.06	1.982142643	3.67	3.561361958	No
I16-02	SA I16-02-006	0.280874803	2.80304E-05	0.001047895	3054	36	0.280816	0.280999	0.280943	0.280813	-0.08	0.991227826	3.44	3.323276327	No
I16-02	SA I16-02-012	0.281132037	3.54693E-05	0.000925524	2641	47	0.281089	0.281311	0.281250	0.281085	-0.12	1.254283325	3.12	2.987448977	No
I16-02	SA I16-02-115	0.281114403	3.16113E-05	0.001012126	2576	41	0.281131	0.281360	0.281298	0.281065	-2.38	1.117854866	3.20	3.067903561	No
I16-02	SA I16-02-021	0.280971641	2.68094E-05	0.001198137	2704	33	0.281047	0.281264	0.281203	0.280910	-4.89	0.948049917	3.45	3.31974855	No

Sample N	Analysis N	$^{176}Hf/^{177}Hf$	2 S.E.	$^{176}Lu/^{177}Hf$	U/Pb AGE	2 S.E.	Hf Chur (t)	Hf DM (t)	Hf NC(t)	Hf_i	eHf	2SE	TDMc	TNCc	Above DM line?
I16-02	SA I16-02-087	0.281132997	4.13638E-05	0.001306387	2423	27	0.281232	0.281475	0.281411	0.281073	-5.66	1.462728038	3.27	3.138241065	No
I16-02	SA I16-02-072	0.280953545	3.29859E-05	0.00131642	2677	32	0.281065	0.281284	0.281223	0.280886	-6.36	1.166466959	3.51	3.384127595	No
I16-02	SA I16-02-103	0.281024733	3.02718E-05	0.001279766	2477	29	0.281196	0.281434	0.281371	0.280964	-8.26	1.070487601	3.47	3.334714264	No
I16-02	SA I16-02-076	0.281032518	4.09155E-05	0.00186374	2484	44	0.281192	0.281429	0.281366	0.280944	-8.81	1.44687777	3.51	3.372728641	No
I16-02	SA I16-02-137	0.280983792	4.80561E-05	0.001439234	2510	45	0.281175	0.281410	0.281346	0.280915	-9.24	1.699386155	3.55	3.419198295	No
I16-02	SA I16-02-018	0.280996331	3.60079E-05	0.0011362	2467	47	0.281203	0.281442	0.281378	0.280943	-9.25	1.273330627	3.52	3.385167621	No
I16-02	SA I16-02-083	0.281021122	6.64547E-05	0.003348926	2487	25	0.281190	0.281427	0.281363	0.280862	-11.65	2.350008777	3.67	3.542240152	No
I16-02	SA I16-02-080	0.280896582	5.74035E-05	0.001330803	2466	30	0.281204	0.281443	0.281379	0.280834	-13.15	2.029934659	3.75	3.61293372	No
I16-05	SA I16-05-020	0.280946026	3.6751E-05	0.000877277	2971	33	0.280871	0.281062	0.281004	0.280896	0.90	1.299608449	3.32	3.197623219	No
I16-05	SA I16-05-058	0.280920644	8.22997E-05	0.001990478	3102	68	0.280784	0.280963	0.280907	0.280802	0.65	2.910327655	3.44	3.319888453	No
I16-05	SA I16-05-088	0.280745242	4.0496E-05	0.001785346	3322	37	0.280637	0.280796	0.280742	0.280631	-0.23	1.432041058	3.66	3.55148165	No
I16-05	SA I16-05-053	0.280730487	3.66899E-05	0.001415577	3307	23	0.280647	0.280807	0.280753	0.280640	-0.25	1.297450137	3.65	3.540608321	No
I16-05	SA I16-05-097	0.280825763	3.10359E-05	0.000962858	3096	57	0.280788	0.280968	0.280911	0.280769	-0.69	1.097508916	3.51	3.392977026	No
I16-05	SA I16-05-103	0.281171681	2.30274E-05	0.000832183	2533	33	0.281160	0.281392	0.281329	0.281131	-1.00	0.814308041	3.08	2.951770301	No
I16-05	SA I16-05-008	0.280861943	3.24985E-05	0.00128361	3034	51	0.280829	0.281015	0.280957	0.280787	-1.49	1.149230686	3.51	3.388882634	No
I16-05	SA I16-05-082	0.280834289	3.5974E-05	0.000888416	3038	26	0.280826	0.281011	0.280954	0.280782	-1.56	1.272134086	3.51	3.396443388	No
I16-05	SA I16-05-010	0.280853828	3.16305E-05	0.000837636	2974	33	0.280869	0.281060	0.281002	0.280806	-2.23	1.118533783	3.50	3.383388674	No
I16-05	SA I16-05-071	0.281291977	7.06785E-05	0.003687682	2481	34	0.281194	0.281431	0.281368	0.281117	-2.72	2.499373	3.14	3.011061158	No
I16-05	SA I16-05-043	0.281102567	5.69327E-05	0.001253536	2545	45	0.281152	0.281383	0.281321	0.281042	-3.92	2.013284957	3.27	3.133742318	No
I16-05	SA I16-05-030	0.281137088	4.82169E-05	0.001856091	2490	33	0.281188	0.281425	0.281361	0.281049	-4.94	1.70507259	3.28	3.149895412	No
I16-05	SA I16-05-069	0.281061593	3.63211E-05	0.001616706	2492	28	0.281187	0.281423	0.281360	0.280985	-7.18	1.284405365	3.42	3.28333786	No
I16-05	SA I16-05-090	0.28098874	3.32525E-05	0.001501506	2589	38	0.281123	0.281350	0.281288	0.280914	-7.41	1.175892959	3.50	3.374987094	No
I16-05	SA I16-05-073	0.28095897	3.8837E-05	0.001609691	2618	29	0.281104	0.281329	0.281267	0.280878	-8.02	1.373374772	3.56	3.433719499	No
I16-05	SA I16-05-077	0.280926308	2.37371E-05	0.0007458	2531	37	0.281161	0.281394	0.281331	0.280890	-9.63	0.839404823	3.59	3.458505228	No
I16-27	SA I16-27-30	0.280883644	5.39821E-05	0.001785496	3188	42	0.280727	0.280898	0.280842	0.280774	1.69	1.908944674	3.44	3.32967483	No
I16-27	SA I16-27-40	0.280856636	5.16324E-05	0.001414664	3153	49	0.280750	0.280924	0.280869	0.280771	0.75	1.825853043	3.47	3.356084482	No
I16-27	SA I16-27-23	0.280826936	3.50237E-05	0.001014319	3110	31	0.280779	0.280957	0.280901	0.280766	-0.43	1.238526584	3.51	3.389644486	No
I16-27	SA I16-27-37	0.280804763	8.73356E-05	0.002189419	3157	29	0.280747	0.280921	0.280866	0.280672	-2.68	3.088411321	3.67	3.558959065	No
I16-33	SA I16-33-45	0.281235034	2.83246E-05	0.001057851	2668	41	0.281071	0.281291	0.281230	0.281181	3.92	1.001629816	2.90	2.770439144	No
I16-33	SA I16-33-38	0.281371247	4.57635E-05	0.002925821	2599	33	0.281116	0.281343	0.281281	0.281226	3.90	1.618313832	2.85	2.714805884	No
I16-33	SA I16-33-14	0.281220573	3.38761E-05	0.000626519	2640	57	0.281089	0.281312	0.281250	0.281189	3.55	1.197945402	2.90	2.769664069	No
I16-33	SA I16-33-33	0.280650427	3.03293E-05	0.001074435	3555	41	0.280482	0.280618	0.280567	0.280577	3.39	1.07252124	3.64	3.534621358	No
I16-33	SA I16-33-26	0.281166574	4.08581E-05	0.000943325	2731	48	0.281029	0.281244	0.281183	0.281117	3.13	1.444846913	3.00	2.869205562	No

Sample N	Analysis N	$^{176}Hf/^{177}Hf$	2 S.E.	$^{176}Lu/^{177}Hf$	U/Pb AGE	2 S.E.	Hf Chur (t)	Hf DM (t)	Hf NC(t)	Hf_i	eHf	2SE	TDMc	TNCc	Above DM line?
I16-33	SA I16-33-39	0.281277242	3.03348E-05	0.00120251	2563	38	0.281140	0.281370	0.281307	0.281218	2.79	1.072715957	2.88	2.751260071	No
I16-33	SA I16-33-47	0.281287058	3.70677E-05	0.001833749	2589	46	0.281123	0.281350	0.281288	0.281196	2.62	1.310809237	2.91	2.783010965	No
I16-33	SA I16-33-17	0.281216864	3.47063E-05	0.000559206	2587	69	0.281124	0.281352	0.281290	0.281189	2.32	1.227303839	2.93	2.799182002	No
I16-33	SA I16-33-21	0.281280077	2.66826E-05	0.000977908	2504	43	0.281179	0.281414	0.281351	0.281233	1.94	0.943564379	2.89	2.753206723	No
I16-33	SA I16-33-06	0.281101331	4.29129E-05	0.001527268	2822	43	0.280969	0.281175	0.281115	0.281019	1.76	1.517509604	3.15	3.024715095	No
I16-33	SA I16-33-41	0.280838569	3.3598E-05	0.001406574	3001	34	0.280851	0.281040	0.280982	0.280758	-3.32	1.188110501	3.59	3.468894744	No
BT06214	SA_BT06214-02	0.282464977	1.58672E-05	0.000100234	2514.9	18.3	0.281171	0.281406	0.281343	0.282460	45.83	0.56110576	0.23	0.087501528	Yes
BT06214	SA_BT06214-07	0.281067989	1.7319E-05	0.000556724	2533.9	14	0.281159	0.281392	0.281329	0.281041	-4.20	0.612442808	3.27	3.141290688	No
BT06214	SA_BT06214-24	0.281083055	2.08223E-05	0.000923112	2529.8	14.7	0.281162	0.281395	0.281332	0.281038	-4.38	0.736328501	3.28	3.149044265	No
BT06214	SA_BT06214-15	0.281071455	2.13178E-05	0.000648939	2524.6	12.9	0.281165	0.281399	0.281336	0.281040	-4.45	0.753851443	3.28	3.148453315	No
BT06214	SA_BT06214-18	0.281058224	1.88934E-05	0.00049913	2526.6	22.9	0.281164	0.281397	0.281334	0.281034	-4.61	0.668117371	3.29	3.15994731	No
BT06214	SA_BT06214-09	0.281050938	1.95423E-05	0.000524712	2532.7	14.3	0.281160	0.281393	0.281330	0.281026	-4.77	0.691065407	3.31	3.174454561	No
BT06214	SA_BT06214-19	0.281050576	1.95993E-05	0.000502999	2531.0	13.5	0.281161	0.281394	0.281331	0.281026	-4.79	0.693080326	3.31	3.173971698	No
BT06214	SA_BT06214-23	0.281062155	2.20958E-05	0.000636392	2510.2	19.1	0.281175	0.281410	0.281346	0.281032	-5.08	0.781363859	3.31	3.174497532	No
BT06214	SA_BT06214-04	0.281046743	2.16276E-05	0.000687858	2531.5	14.1	0.281161	0.281394	0.281331	0.281013	-5.23	0.764806245	3.33	3.20047609	No
BT06214	SA_BT06214-08	0.281058589	2.44699E-05	0.001069164	2534.3	11.3	0.281159	0.281391	0.281329	0.281007	-5.40	0.86531969	3.34	3.212826839	No
BT06270	SA_BT06270-11	0.281124775	2.39314E-05	0.001343467	2597.5	83.2	0.281117	0.281344	0.281282	0.281058	-2.10	0.846276744	3.20	3.069346335	No
BT06270	SA_BT06270-18	0.281103292	2.19236E-05	0.000743777	2528.0	26	0.281163	0.281396	0.281333	0.281067	-3.40	0.775276093	3.22	3.089364559	No
BT06270	SA_BT06270-02	0.281095888	1.95027E-05	0.000965874	2536.3	5.8	0.281157	0.281390	0.281327	0.281049	-3.85	0.689664254	3.25	3.122990125	No
BT06270	SA_BT06270-13	0.281071647	1.95367E-05	0.000859552	2560.7	42.6	0.281141	0.281372	0.281309	0.281030	-3.98	0.690869175	3.28	3.150074977	No
BT06270	SA_BT06270-23	0.281127403	3.28361E-05	0.001717981	2531.0	12.8	0.281161	0.281394	0.281331	0.281044	-4.15	1.16116918	3.27	3.135987894	No
BT06270	SA_BT06270-08	0.281144937	2.4764E-05	0.002440009	2542.6	32.3	0.281153	0.281385	0.281322	0.281026	-4.51	0.875717836	3.30	3.166973949	No
BT06270	SA_BT06270-04	0.281091735	2.28912E-05	0.001283299	2533.4	21.2	0.281159	0.281392	0.281329	0.281030	-4.61	0.809492295	3.30	3.165491238	No
BT06270	SA_BT06270-03	0.281073777	2.04008E-05	0.000822172	2525.4	7.8	0.281165	0.281398	0.281335	0.281034	-4.64	0.721425972	3.29	3.160625756	No
BT30167	SA_BT30167-02	0.28111493	1.57576E-05	0.000697491	2514.8	8.4	0.281172	0.281406	0.281343	0.281081	-3.21	0.557227298	3.20	3.067322746	No
BT30167	SA_BT30167-25	0.28109751	1.59703E-05	0.000550448	2512.2	10.3	0.281173	0.281408	0.281345	0.281071	-3.63	0.564750621	3.22	3.090497439	No
BT30167	SA_BT30167-20	0.281132513	1.88735E-05	0.001163559	2502.4	13.9	0.281180	0.281415	0.281352	0.281077	-3.66	0.667414365	3.22	3.083891562	No
BT30167	SA_BT30167-29	0.281087148	1.60596E-05	0.000515299	2517.8	8.5	0.281170	0.281404	0.281341	0.281062	-3.81	0.567907309	3.24	3.10564978	No
BT30167	SA_BT30167-26	0.281085645	1.47047E-05	0.000611682	2504.3	9.1	0.281178	0.281414	0.281351	0.281056	-4.34	0.519997286	3.26	3.12591452	No
BT30167	SA_BT30167-03	0.281067405	1.62181E-05	0.000610196	2521.1	6.9	0.281167	0.281401	0.281338	0.281038	-4.60	0.573514239	3.29	3.154927531	No
BT30202	SA_BT30202-17	0.280925542	2.87125E-05	0.002162191	3181.2	16.6	0.280731	0.280903	0.280848	0.280793	2.21	1.015346225	3.41	3.29377572	No
BT30202	SA_BT30202-08	0.281292462	3.04801E-05	0.00135699	2520.8	6.9	0.281168	0.281402	0.281338	0.281227	2.12	1.077853398	2.89	2.756697651	No
BT30202	SA_BT30202-34	0.28084751	2.52875E-05	0.000961343	3115.6	14.4	0.280775	0.280953	0.280897	0.280790	0.54	0.894228902	3.45	3.337455957	No

Sample N	Analysis N	$^{176}Hf/^{177}Hf$	2 S.E.	$^{176}Lu/^{177}Hf$	U/Pb AGE	2 S.E.	Hf Chur (t)	Hf DM (t)	Hf NC(t)	Hf_i	eHf	2SE	TDMc	TNCc	Above DM line?
BT30202	SA_BT30202-25	0.280829622	2.60658E-05	0.001093479	3141.1	14.8	0.280758	0.280933	0.280878	0.280764	0.21	0.921754914	3.49	3.377917884	No
BT30202	SA_BT30202-18	0.281160787	2.84202E-05	0.000925088	2509.6	12.6	0.281175	0.281410	0.281347	0.281116	-2.08	1.005011537	3.13	2.996619345	No
BT30202	SA_BT30202-30	0.281113725	1.95208E-05	0.000424676	2519.3	16.2	0.281169	0.281403	0.281340	0.281093	-2.68	0.690306501	3.17	3.039823815	No
BT30202	SA_BT30202-16	0.281155882	2.74684E-05	0.001265906	2502.0	13.9	0.281180	0.281416	0.281352	0.281095	-3.01	0.971354217	3.18	3.045228207	No
BT30202	SA_BT30202-23	0.281144289	2.71751E-05	0.001268896	2504.6	9.1	0.281178	0.281414	0.281350	0.281084	-3.37	0.960981201	3.20	3.068585045	No
MMR7	SA_MMR7-02	0.280846064	2.07816E-05	0.000337408	3114.8	34.8	0.280775	0.280953	0.280897	0.280826	1.80	0.734891893	3.38	3.263258622	No
MMR7	SA_MMR7-10	0.280812044	1.89495E-05	0.000263005	3130.4	53.3	0.280765	0.280941	0.280885	0.280796	1.11	0.670101848	3.43	3.316189784	No
MMR7	SA_MMR7-19	0.280864714	1.84575E-05	0.000265025	2913.0	35.1	0.280909	0.281106	0.281048	0.280850	-2.11	0.652706077	3.45	3.326391205	No
MMR7	SA_MMR7-03	0.280980221	2.0881E-05	0.000300081	3127.0	30.2	0.280767	0.280944	0.280888	0.280962	6.94	0.738406479	3.09	2.972049918	Yes
PEJP435	SA_PEJP435-43	0.281270786	2.02768E-05	0.001043721	2675.3	25.4	0.281066	0.281285	0.281224	0.281217	5.39	0.717039636	2.82	2.689595921	No
PEJP435	SA_PEJP435-46	0.281219989	1.80772E-05	0.000543472	2688.0	7.4	0.281058	0.281276	0.281215	0.281192	4.78	0.639255172	2.86	2.7358981	No
PEJP435	SA_PEJP435-50	0.281237666	2.00484E-05	0.001003104	2661.3	21.6	0.281075	0.281296	0.281235	0.281187	3.96	0.708962649	2.89	2.762528631	No
PEJP435	SA_PEJP435-11	0.281225354	1.68034E-05	0.00038973	2495.0	19.1	0.281185	0.281421	0.281358	0.281207	0.79	0.594211459	2.95	2.814441915	No
RK225	SA_RK225-26	0.281268707	1.8566E-05	0.000279104	2446.9	24.4	0.281216	0.281457	0.281393	0.281256	1.41	0.656542666	2.87	2.738462868	No
RK225	SA_RK225-27	0.281227969	1.81215E-05	0.000242716	2492.5	33.7	0.281186	0.281423	0.281359	0.281216	1.07	0.640821952	2.93	2.795499485	No
RK225	SA_RK225-09	0.281204826	2.19912E-05	0.000494042	2520.4	29.4	0.281168	0.281402	0.281339	0.281181	0.47	0.777666281	2.99	2.85430654	No
RK225	SA_RK225-11	0.281219989	1.80772E-05	0.000543472	2468.5	24.2	0.281202	0.281441	0.281377	0.281194	-0.27	0.639255172	2.99	2.855734055	No
RK225	SA_RK225-14	0.281220528	2.35316E-05	0.000547066	2463.3	52.9	0.281205	0.281445	0.281381	0.281195	-0.38	0.832138936	2.99	2.857781664	No
RK225	SA_RK225-18	0.281196575	1.63559E-05	0.000190027	2469.3	16.8	0.281201	0.281440	0.281377	0.281188	-0.49	0.578385916	3.00	2.869579043	No
RK225	SA_RK225-07	0.281192224	1.58806E-05	0.000168544	2472.1	21.5	0.281200	0.281438	0.281374	0.281184	-0.55	0.561577226	3.01	2.875043583	No
RK225	SA_RK225-16	0.28118653	1.92965E-05	0.00035932	2485.8	29.5	0.281191	0.281428	0.281364	0.281169	-0.75	0.682372214	3.03	2.898428074	No
RK225	SA_RK225-20	0.281186874	1.61701E-05	0.000314444	2481.7	15.1	0.281193	0.281431	0.281367	0.281172	-0.76	0.571815039	3.03	2.895528891	No
RK225	SA_RK225-05	0.281181308	1.71311E-05	0.000334551	2460.4	34.6	0.281207	0.281447	0.281383	0.281166	-1.48	0.605797856	3.06	2.921095681	No
RK449	SA_RK449-25	0.281224916	2.16645E-05	0.001166336	2701.0	14.6	0.281049	0.281266	0.281205	0.281165	4.11	0.766110565	2.91	2.786357606	No
RK449	SA_RK449-17	0.281184763	1.72506E-05	0.00049245	2686.6	14.2	0.281059	0.281277	0.281216	0.281159	3.59	0.610024561	2.93	2.80549072	No
RK449	SA_RK449-37	0.281201607	2.10505E-05	0.0008199	2677.7	17.6	0.281064	0.281284	0.281222	0.281160	3.39	0.74439986	2.94	2.810185744	No
RK449	SA_RK449-21	0.281562482	2.45066E-05	0.00062917	2667.4	15.6	0.281071	0.281291	0.281230	0.281530	16.34	0.866615142	2.16	2.028457927	Yes
RK449	SA_RK449-28	0.281576149	2.20204E-05	0.000474323	2672.6	21.8	0.281068	0.281287	0.281226	0.281552	17.22	0.778697936	2.11	1.97944062	Yes

Appendix 3.1 The Bemarivo Domain of northern Madagascar: Hf and O data

					Calculations using grain age ($^{238}U/^{206}Pb$)											*Calculations using magmatic crystallisation age*												
Sample No	**N.**	**$^{176}Hf/^{177}Hf$**	**2 S.E.**	**$^{176}Lu/^{177}Hf$**	**Grain age**	**2σ**	**Hf Chur(t)**	**Hf DM (t)**	**Hf NC(t)**	**Hf_i**	**eHf**	**2SE**	**TD Mc**	**TNCc**	**DM line**	**Rock age**	**2σ**	**Hf Chur(t)**	**Hf DM (t)**	**Hf NC(t)**	**Hf_i**	**eHf**	**2SE**	**TD Mc**	**TNCc**	**DM line**	**$\delta^{18}O$**	**95 %**
BB06A12	13	0.2826	0.0001	0.0041	710	22	0.2823	0.2827	0.2827	0.2826	7.68	2.0531	1.12	0.9347	No	724	7	0.2823	0.2827	0.2826	0.2826	7.95	2.0531	1.12	0.9289	No	4.24	0.26
BB06A12	19	0.2826	0.0000	0.0022	713	21	0.2823	0.2827	0.2827	0.2825	7.10	1.3949	1.16	0.9736	No	724	7	0.2823	0.2827	0.2826	0.2825	7.32	1.3949	1.15	0.9681	No	3.38	0.06
BB06A12	12	0.2826	0.0000	0.0022	714	21	0.2823	0.2827	0.2827	0.2826	8.45	1.4912	1.08	0.8892	No	724	7	0.2823	0.2827	0.2826	0.2826	8.65	1.4912	1.07	0.8843	No	4.13	0.16
BB06A12	15	0.2826	0.0001	0.0035	717	22	0.2823	0.2827	0.2826	0.2825	6.82	1.7973	1.18	0.9942	No	724	7	0.2823	0.2827	0.2826	0.2825	6.96	1.7973	1.18	0.9912	No	4.07	0.14
BB06A12	3	0.2826	0.0001	0.0035	726	22	0.2823	0.2827	0.2826	0.2826	7.91	1.8331	1.12	0.9321	No	724	7	0.2823	0.2827	0.2826	0.2826	7.88	1.8331	1.12	0.9328	No	4.67	0.09
BB06A12	6	0.2826	0.0000	0.0026	726	22	0.2823	0.2827	0.2826	0.2825	7.72	1.7371	1.13	0.9451	No	724	7	0.2823	0.2827	0.2826	0.2825	7.67	1.7371	1.13	0.9461	No	4.64	0.16
BB06A12	16	0.2826	0.0000	0.0028	734	22	0.2823	0.2827	0.2826	0.2825	7.30	1.4413	1.16	0.9772	No	724	7	0.2823	0.2827	0.2826	0.2825	7.10	1.4413	1.17	0.9819	No	3.91	0.10
BB06A12	4	0.2826	0.0001	0.0028	737	23	0.2823	0.2827	0.2826	0.2825	7.71	1.7756	1.14	0.9539	No	724	7	0.2823	0.2827	0.2826	0.2825	7.45	1.7756	1.15	0.9601	No	4.45	0.21
BB06A12	11	0.2826	0.0000	0.0026	739	22	0.2823	0.2827	0.2826	0.2826	8.66	1.6378	1.08	0.8965	No	724	7	0.2823	0.2827	0.2826	0.2826	8.34	1.6378	1.09	0.9040	No	4.57	0.11
BB06A12	20	0.2826	0.0001	0.0030	794	23	0.2823	0.2827	0.2826	0.2825	9.23	1.8382	1.09	0.9050	No	724	7	0.2823	0.2827	0.2826	0.2825	7.80	1.8382	1.12	0.9381	No	4.54	0.27
BDW315A	26	0.2826	0.0000	0.0004	695	18	0.2823	0.2827	0.2827	0.2825	7.05	1.0111	1.15	0.9613	No	718	7	0.2823	0.2827	0.2826	0.2825	7.57	1.0111	1.13	0.9477	No	5.02	0.20
BDW315A	24	0.2826	0.0000	0.0004	710	16	0.2823	0.2827	0.2827	0.2826	7.74	0.8263	1.12	0.9304	No	718	7	0.2823	0.2827	0.2826	0.2826	7.92	0.8263	1.11	0.9258	No	4.91	0.16
BDW315A	5	0.2825	0.0000	0.0004	715	18	0.2823	0.2827	0.2827	0.2825	7.32	0.8068	1.15	0.9605	No	718	7	0.2823	0.2827	0.2826	0.2825	7.40	0.8068	1.15	0.9586	No	5.36	0.14
BDW315A	25	0.2825	0.0000	0.0004	715	16	0.2823	0.2827	0.2827	0.2825	7.36	0.6527	1.15	0.9582	No	718	7	0.2823	0.2827	0.2826	0.2825	7.43	0.6527	1.14	0.9565	No	5.14	0.23
BDW315A	4	0.2826	0.0000	0.0015	716	17	0.2823	0.2827	0.2826	0.2825	7.40	1.1697	1.14	0.9570	No	718	7	0.2823	0.2827	0.2826	0.2825	7.44	1.1697	1.14	0.9561	No	4.63	0.37
BDW315A	1	0.2826	0.0000	0.0004	718	20	0.2823	0.2827	0.2826	0.2826	7.90	0.9644	1.11	0.9271	No	718	7	0.2823	0.2827	0.2826	0.2826	7.90	0.9644	1.11	0.9271	No	5.22	0.24
BDW315A	15	0.2825	0.0000	0.0005	722	17	0.2823	0.2827	0.2826	0.2825	7.13	0.8532	1.17	0.9790	No	718	7	0.2823	0.2827	0.2826	0.2825	7.03	0.8532	1.17	0.9815	No	5.02	0.12
BDW315A	14	0.2825	0.0000	0.0005	724	16	0.2823	0.2827	0.2826	0.2825	7.43	0.7149	1.15	0.9611	No	718	7	0.2823	0.2827	0.2826	0.2825	7.30	0.7149	1.15	0.9645	No	5.18	0.38
BT0636	6	0.2822	0.0000	0.0015	739	20	0.2823	0.2827	0.2826	0.2822	-4.80	1.2779	1.92	1.7382	No	754	7	0.2823	0.2827	0.2826	0.2822	-4.47	1.2779	1.91	1.7299	No	5.08	0.10
BT0636	22	0.2822	0.0000	0.0009	750	25	0.2823	0.2827	0.2826	0.2822	-2.96	1.0189	1.82	1.6330	No	754	7	0.2823	0.2827	0.2826	0.2822	-2.88	1.0189	1.81	1.6308	No	5.51	0.35
BT0636	20	0.2822	0.0000	0.0006	751	26	0.2823	0.2827	0.2826	0.2822	-2.63	1.0832	1.80	1.6132	No	754	7	0.2823	0.2827	0.2826	0.2822	-2.57	1.0832	1.80	1.6114	No	5.33	0.26
BT0636	19	0.2823	0.0000	0.0010	752	27	0.2823	0.2827	0.2826	0.2823	-1.58	0.9223	1.73	1.5480	No	754	7	0.2823	0.2827	0.2826	0.2823	-1.53	0.9223	1.73	1.5467	No	5.44	0.27
BT0636	14	0.2823	0.0000	0.0021	752	25	0.2823	0.2827	0.2826	0.2823	-2.09	1.1403	1.76	1.5799	No	754	7	0.2823	0.2827	0.2826	0.2823	-2.04	1.1403	1.76	1.5787	No	3.41	0.51
BT0636	7	0.2822	0.0000	0.0010	756	20	0.2823	0.2827	0.2826	0.2822	-2.59	0.8940	1.80	1.6144	No	754	7	0.2823	0.2827	0.2826	0.2822	-2.63	0.8940	1.80	1.6153	No	5.35	0.66
BT0636	15	0.2823	0.0000	0.0008	756	25	0.2823	0.2827	0.2826	0.2822	-2.17	0.8736	1.77	1.5882	No	754	7	0.2823	0.2827	0.2826	0.2822	-2.21	0.8736	1.77	1.5894	No	5.66	0.39
BT0636	8	0.2822	0.0000	0.0007	764	22	0.2823	0.2827	0.2826	0.2822	-2.32	0.7789	1.79	1.6042	No	754	7	0.2823	0.2827	0.2826	0.2822	-2.54	0.7789	1.79	1.6099	No	5.04	0.14
BT0636	13	0.2823	0.0000	0.0016	767	26	0.2823	0.2827	0.2826	0.2822	-1.86	1.1666	1.76	1.5779	No	754	7	0.2823	0.2827	0.2826	0.2822	-2.14	1.1666	1.77	1.5847	No	1.59	0.27
BT0636	16	0.2823	0.0000	0.0011	767	26	0.2823	0.2827	0.2826	0.2822	-2.06	0.8467	1.77	1.5906	No	754	7	0.2823	0.2827	0.2826	0.2822	-2.35	0.8467	1.78	1.5980	No	5.31	0.30
BT0641	14	0.2822	0.0000	0.0022	737	15	0.2823	0.2827	0.2826	0.2822	-5.35	0.9753	1.95	1.7707	No	746	4	0.2823	0.2827	0.2826	0.2822	-5.16	0.9753	1.95	1.7659	No	0.60	0.21

					Calculations using grain age ($^{238}U/^{206}Pb$)											*Calculations using magmatic crystallisation age*											
Sample No	**N.**	**$^{176}Hf/^{177}Hf$**	**2 S.E.**	**$^{176}Lu/^{177}Hf$**	**Grain age**	**2σ**	**Hf Chur(t)**	**Hf DM (t)**	**Hf NC(t)**	**Hf_i**	**eHf**	**2SE**	**TD Mc**	**TNCc**	**DM line**	**Rock age**	**2σ**	**Hf Chur(t)**	**Hf DM (t)**	**Hf NC(t)**	**Hf_i**	**eHf**	**2SE**	**TD Mc**	**TNCc**	**DM line**	**$\delta^{18}O$**	**95 %**
BT0641	13	0.2822	0.0000	0.0014	738	14	0.2823	0.2827	0.2826	0.2822	-5.20	0.8264	1.95	1.7625	No	746	4	0.2823	0.2827	0.2826	0.2822	-5.03	0.8264	1.94	1.7581	No	4.86	0.19
BT0641	7	0.2822	0.0000	0.0016	741	14	0.2823	0.2827	0.2826	0.2822	-5.67	0.9895	1.98	1.7937	No	746	4	0.2823	0.2827	0.2826	0.2822	-5.56	0.9895	1.97	1.7909	No	5.67	0.12
BT0641	9	0.2822	0.0000	0.0022	741	13	0.2823	0.2827	0.2826	0.2822	-5.76	1.1058	1.98	1.7992	No	746	4	0.2823	0.2827	0.2826	0.2822	-5.65	1.1058	1.98	1.7966	No	2.01	0.16
BT0641	1	0.2822	0.0000	0.0012	743	14	0.2823	0.2827	0.2826	0.2822	-5.67	0.8828	1.98	1.7961	No	746	4	0.2823	0.2827	0.2826	0.2822	-5.62	0.8828	1.98	1.7947	No	4.94	0.16
BT0641	3	0.2822	0.0000	0.0008	744	14	0.2823	0.2827	0.2826	0.2822	-5.79	0.7875	1.99	1.8038	No	746	4	0.2823	0.2827	0.2826	0.2822	-5.75	0.7875	1.99	1.8027	No	5.83	0.26
BT0641	2	0.2822	0.0000	0.0017	746	13	0.2823	0.2827	0.2826	0.2822	-5.40	1.0727	1.96	1.7808	No	746	4	0.2823	0.2827	0.2826	0.2822	-5.39	1.0727	1.96	1.7807	No	5.52	0.26
BT0641	11	0.2822	0.0000	0.0017	746	13	0.2823	0.2827	0.2826	0.2821	-5.89	1.1877	2.00	1.8120	No	746	4	0.2823	0.2827	0.2826	0.2821	-5.90	1.1877	2.00	1.8121	No	2.22	0.11
BT0641	10	0.2822	0.0000	0.0009	755	14	0.2823	0.2827	0.2826	0.2822	-4.91	0.8386	1.94	1.7583	No	746	4	0.2823	0.2827	0.2826	0.2822	-5.12	0.8386	1.95	1.7637	No	4.35	0.28
BT0641	5	0.2822	0.0000	0.0020	762	14	0.2823	0.2827	0.2826	0.2822	-4.38	1.2377	1.91	1.7300	No	746	4	0.2823	0.2827	0.2826	0.2822	-4.71	1.2377	1.92	1.7381	No	4.98	0.15
BT0751	1	0.2822	0.0000	0.0007	561	8	0.2824	0.2828	0.2828	0.2822	-7.95	0.7011	1.98	1.7928	No	768	8	0.2823	0.2827	0.2826	0.2822	-3.39	0.7011	1.86	1.6740	No	2.08	0.15
BT0751	11	0.2822	0.0000	0.0011	630	17	0.2824	0.2828	0.2827	0.2822	-6.81	0.8487	1.96	1.7770	No	768	8	0.2823	0.2827	0.2826	0.2822	-3.82	0.8487	1.88	1.7005	No	2.21	0.14
BT0751	6	0.2822	0.0000	0.0012	676	14	0.2824	0.2828	0.2827	0.2822	-6.18	0.9536	1.96	1.7745	No	768	8	0.2823	0.2827	0.2826	0.2822	-4.20	0.9536	1.91	1.7239	No	1.96	0.31
BT0751	29	0.2822	0.0000	0.0015	692	15	0.2823	0.2828	0.2827	0.2822	-5.62	1.0105	1.94	1.7519	No	768	8	0.2823	0.2827	0.2826	0.2822	-3.99	1.0105	1.89	1.7109	No	2.69	0.16
BT0751	28	0.2822	0.0000	0.0012	724	16	0.2823	0.2827	0.2826	0.2822	-5.06	0.9998	1.93	1.7426	No	768	8	0.2823	0.2827	0.2826	0.2822	-4.11	0.9998	1.90	1.7184	No	1.34	0.36
BT0751	30	0.2822	0.0000	0.0012	735	18	0.2823	0.2827	0.2826	0.2822	-4.35	0.8951	1.89	1.7072	No	768	8	0.2823	0.2827	0.2826	0.2822	-3.63	0.8951	1.87	1.6888	No	2.24	0.26
BT0751	7	0.2822	0.0000	0.0014	768	18	0.2823	0.2827	0.2826	0.2822	-4.83	1.2697	1.95	1.7628	No	768	8	0.2823	0.2827	0.2826	0.2822	-4.82	1.2697	1.95	1.7626	No	3.70	0.32
BT0751	12	0.2820	0.0000	0.0010	773	20	0.2823	0.2827	0.2826	0.2820	-10.02	1.3309	2.27	2.0877	No	768	8	0.2823	0.2827	0.2826	0.2820	-10.12	1.3309	2.27	2.0903	No	2.66	0.10
BT0751	8	0.2822	0.0000	0.0016	779	37	0.2823	0.2827	0.2826	0.2822	-4.37	1.0521	1.93	1.7436	No	768	8	0.2823	0.2827	0.2826	0.2822	-4.61	1.0521	1.93	1.7494	No	2.47	0.09
RK7219	7	0.2822	0.0000	0.0022	626	14	0.2824	0.2828	0.2827	0.2821	-8.60	1.5468	2.07	1.8851	No	750	4	0.2823	0.2827	0.2826	0.2821	-6.01	1.5468	2.01	1.8219	No	1.61	0.36
RK7219	3	0.2821	0.0000	0.0016	685	8	0.2824	0.2828	0.2827	0.2821	-8.21	1.3161	2.09	1.9068	No	750	4	0.2823	0.2827	0.2826	0.2821	-6.82	1.3161	2.06	1.8722	No	2.97	0.38
RK7219	9	0.2821	0.0000	0.0018	746	11	0.2823	0.2827	0.2826	0.2821	-8.14	1.6403	2.13	1.9511	No	750	4	0.2823	0.2827	0.2826	0.2821	-8.06	1.6403	2.13	1.9492	No	3.44	0.21
RK7219	4	0.2821	0.0001	0.0023	748	14	0.2823	0.2827	0.2826	0.2821	-7.68	2.0861	2.11	1.9236	No	750	4	0.2823	0.2827	0.2826	0.2821	-7.63	2.0861	2.11	1.9224	No	3.94	0.15
RK7219	6	0.2821	0.0000	0.0014	749	18	0.2823	0.2827	0.2826	0.2821	-6.65	1.5737	2.04	1.8615	No	750	4	0.2823	0.2827	0.2826	0.2821	-6.64	1.5737	2.04	1.8612	No	2.32	0.34
RK7219	8	0.2821	0.0000	0.0016	751	12	0.2823	0.2827	0.2826	0.2821	-6.82	1.3600	2.06	1.8726	No	750	4	0.2823	0.2827	0.2826	0.2821	-6.83	1.3600	2.06	1.8730	No	4.25	0.16
RK7219	1	0.2822	0.0000	0.0016	756	10	0.2823	0.2827	0.2826	0.2821	-6.07	1.1991	2.01	1.8309	No	750	4	0.2823	0.2827	0.2826	0.2821	-6.21	1.1991	2.02	1.8342	No	3.54	0.24
RK7219	2	0.2822	0.0000	0.0023	757	13	0.2823	0.2827	0.2826	0.2821	-6.43	1.6419	2.04	1.8538	No	750	4	0.2823	0.2827	0.2826	0.2821	-6.58	1.6419	2.04	1.8573	No	4.41	0.14
RK7219	5	0.2821	0.0000	0.0011	766	10	0.2823	0.2827	0.2826	0.2821	-6.47	1.1680	2.05	1.8634	No	750	4	0.2823	0.2827	0.2826	0.2821	-6.82	1.1680	2.06	1.8723	No	3.56	0.20
RK7219	10	0.2822	0.0000	0.0011	799	12	0.2823	0.2827	0.2826	0.2821	-5.01	1.1733	1.98	1.7992	No	750	4	0.2823	0.2827	0.2826	0.2821	-6.08	1.1733	2.01	1.8265	No	3.76	0.23
RT06467	23	0.2819	0.0000	0.0011	689	20	0.2824	0.2828	0.2827	0.2819	-15.34	0.7148	2.53	2.3499	No	756	6	0.2823	0.2827	0.2826	0.2819	-13.89	0.7148	2.49	2.3127	No	6.39	0.56
RT06467	15	0.2821	0.0000	0.0012	744	21	0.2823	0.2827	0.2826	0.2821	-9.22	0.9983	2.20	2.0156	No	756	6	0.2823	0.2827	0.2826	0.2821	-8.95	0.9983	2.19	2.0089	No	7.04	0.23
RT06467	12	0.2819	0.0000	0.0009	745	22	0.2823	0.2827	0.2826	0.2819	-14.03	0.9304	2.49	2.3133	No	756	6	0.2823	0.2827	0.2826	0.2819	-13.80	0.9304	2.49	2.3072	No	7.08	0.12
RT06467	14	0.2819	0.0000	0.0008	747	23	0.2823	0.2827	0.2826	0.2819	-15.24	0.9551	2.57	2.3889	No	756	6	0.2823	0.2827	0.2826	0.2819	-15.04	0.9551	2.56	2.3838	No	6.72	0.28

					Calculations using grain age ($^{238}U/^{206}Pb$)											*Calculations using magmatic crystallisation age*											
Sample No	**N.**	**$^{176}Hf/^{177}Hf$**	**2 S.E.**	**$^{176}Lu/^{177}Hf$**	**Grain age**	**2σ**	**Hf Chur(t)**	**Hf DM (t)**	**Hf NC(t)**	**Hf_i**	**eHf**	**2SE**	**TD Mc**	**TNCc**	**DM line**	**Rock age**	**2σ**	**Hf Chur(t)**	**Hf DM (t)**	**Hf NC(t)**	**Hf_i**	**eHf**	**2SE**	**TD Mc**	**TNCc**	**DM line**	**$\delta^{18}O$**	**95 %**
RT06467	22	0.2819	0.0000	0.0011	751	21	0.2823	0.2827	0.2826	0.2819	-13.80	0.8798	2.48	2.3035	No	756	6	0.2823	0.2827	0.2826	0.2819	-13.69	0.8798	2.48	2.3006	No	6.91	0.24
RT06467	8	0.2821	0.0000	0.0008	752	23	0.2823	0.2827	0.2826	0.2821	-9.12	0.8327	2.20	2.0164	No	756	6	0.2823	0.2827	0.2826	0.2821	-9.04	0.8327	2.20	2.0142	No	6.59	0.22
RT06467	26	0.2819	0.0000	0.0007	757	22	0.2823	0.2827	0.2826	0.2819	-13.26	0.7898	2.46	2.2746	No	756	6	0.2823	0.2827	0.2826	0.2819	-13.27	0.7898	2.46	2.2751	No	5.83	0.23
RT06467	27	0.2821	0.0000	0.0005	758	22	0.2823	0.2827	0.2826	0.2821	-8.43	0.8185	2.16	1.9780	No	756	6	0.2823	0.2827	0.2826	0.2821	-8.47	0.8185	2.16	1.9792	No	6.25	0.21
RT06467	13	0.2819	0.0000	0.0006	764	24	0.2823	0.2827	0.2826	0.2819	-13.20	0.8354	2.46	2.2766	No	756	6	0.2823	0.2827	0.2826	0.2819	-13.37	0.8354	2.46	2.2812	No	6.63	0.21
RT06467	5	0.2820	0.0000	0.0006	772	24	0.2823	0.2827	0.2826	0.2820	-12.28	0.8518	2.41	2.2266	No	756	6	0.2823	0.2827	0.2826	0.2820	-12.63	0.8518	2.42	2.2357	No	5.79	0.26
RT0678	3	0.2826	0.0001	0.0020	724	16	0.2823	0.2827	0.2826	0.2826	10.05	2.4693	0.98	0.7960	No	738	7	0.2823	0.2827	0.2826	0.2826	10.35	2.4693	0.98	0.7887	No	1.87	0.14
RT0678	5	0.2829	0.0002	0.0020	734	15	0.2823	0.2827	0.2826	0.2829	20.31	7.1790	0.34	0.1518	Yes	738	7	0.2823	0.2827	0.2826	0.2829	20.40	7.1790	0.34	0.1496	Yes	2.35	0.14
RT0678	4	0.2825	0.0002	0.0033	739	14	0.2823	0.2827	0.2826	0.2824	4.33	5.7540	1.35	1.1687	No	738	7	0.2823	0.2827	0.2826	0.2824	4.30	5.7540	1.35	1.1693	No	2.03	0.35
RT0678	1	0.2827	0.0001	0.0029	742	13	0.2823	0.2827	0.2826	0.2826	10.77	2.3922	0.95	0.7654	No	738	7	0.2823	0.2827	0.2826	0.2826	10.68	2.3922	0.95	0.7675	No	3.18	0.47
RT0678	2	0.2826	0.0001	0.0021	746	15	0.2823	0.2827	0.2826	0.2826	9.05	2.0745	1.06	0.8770	No	738	7	0.2823	0.2827	0.2826	0.2826	8.89	2.0745	1.07	0.8809	No	2.66	0.09
RT0678	6	0.2826	0.0001	0.0013	844	18	0.2823	0.2826	0.2826	0.2826	12.36	3.7543	0.93	0.7488	No	738	7	0.2823	0.2827	0.2826	0.2826	10.07	3.7543	0.99	0.8063	No	1.27	0.25
RT07121	4	0.2825	0.0000	0.0008	661	12	0.2824	0.2828	0.2827	0.2825	5.72	1.0923	1.21	1.0175	No	707	5	0.2823	0.2827	0.2827	0.2825	6.74	1.0923	1.18	0.9912	No	4.58	0.22
RT07121	5	0.2825	0.0000	0.0008	679	13	0.2824	0.2828	0.2827	0.2825	6.41	0.9270	1.18	0.9891	No	707	5	0.2823	0.2827	0.2827	0.2825	7.02	0.9270	1.16	0.9732	No	4.47	0.18
RT07121	13	0.2826	0.0000	0.0010	689	12	0.2824	0.2828	0.2827	0.2826	7.43	0.9406	1.12	0.9329	No	707	5	0.2823	0.2827	0.2827	0.2826	7.82	0.9406	1.11	0.9228	No	5.56	0.18
RT07121	11	0.2825	0.0000	0.0008	697	13	0.2823	0.2827	0.2827	0.2825	6.26	0.9387	1.20	1.0127	No	707	5	0.2823	0.2827	0.2827	0.2825	6.49	0.9387	1.19	1.0069	No	5.31	0.28
RT07121	1	0.2826	0.0000	0.0009	702	12	0.2823	0.2827	0.2827	0.2825	7.05	0.9404	1.15	0.9672	No	707	5	0.2823	0.2827	0.2827	0.2825	7.16	0.9404	1.15	0.9643	No	4.71	0.24
RT07121	15	0.2825	0.0000	0.0007	702	13	0.2823	0.2827	0.2827	0.2825	5.79	0.9269	1.23	1.0471	No	707	5	0.2823	0.2827	0.2827	0.2825	5.89	0.9269	1.23	1.0444	No	4.84	0.19
RT07121	6	0.2826	0.0000	0.0008	709	14	0.2823	0.2827	0.2827	0.2825	7.28	1.0378	1.15	0.9590	No	707	5	0.2823	0.2827	0.2827	0.2825	7.23	1.0378	1.15	0.9603	No	5.12	0.13
RT07121	3	0.2825	0.0000	0.0011	715	13	0.2823	0.2827	0.2827	0.2825	7.04	1.2441	1.17	0.9788	No	707	5	0.2823	0.2827	0.2827	0.2825	6.86	1.2441	1.17	0.9835	No	4.62	0.41
RT07121	2	0.2825	0.0000	0.0009	721	14	0.2823	0.2827	0.2826	0.2825	7.23	1.2619	1.16	0.9716	No	707	5	0.2823	0.2827	0.2827	0.2825	6.92	1.2619	1.17	0.9795	No	4.81	0.19
RT07121	14	0.2825	0.0000	0.0008	752	15	0.2823	0.2827	0.2826	0.2825	7.50	0.8136	1.17	0.9800	No	707	5	0.2823	0.2827	0.2827	0.2825	6.51	0.8136	1.19	1.0056	No	4.80	0.18
RT0776	3	0.2826	0.0000	0.0016	652	12	0.2824	0.2828	0.2827	0.2825	5.73	1.1497	1.20	1.0092	No	713	6	0.2823	0.2827	0.2827	0.2825	7.05	1.1497	1.16	0.9765	No	4.83	0.52
RT0776	1	0.2826	0.0000	0.0011	691	13	0.2823	0.2828	0.2827	0.2826	7.67	0.9971	1.11	0.9198	No	713	6	0.2823	0.2827	0.2827	0.2826	8.14	0.9971	1.09	0.9077	No	4.88	0.31
RT0776	7	0.2825	0.0000	0.0027	693	12	0.2823	0.2828	0.2827	0.2825	5.00	1.3310	1.28	1.0892	No	713	6	0.2823	0.2827	0.2827	0.2825	5.41	1.3310	1.27	1.0796	No	5.76	0.10
RT0776	4	0.2825	0.0000	0.0017	698	15	0.2823	0.2827	0.2827	0.2825	5.86	1.0960	1.23	1.0387	No	713	6	0.2823	0.2827	0.2827	0.2825	6.19	1.0960	1.22	1.0305	No	5.29	0.19
RT0776	8	0.2825	0.0000	0.0007	706	18	0.2823	0.2827	0.2827	0.2824	3.84	0.9330	1.36	1.1720	No	713	6	0.2823	0.2827	0.2827	0.2824	4.01	0.9330	1.35	1.1677	No	6.47	0.34
RT0776	10	0.2826	0.0000	0.0031	707	14	0.2823	0.2827	0.2827	0.2825	6.73	1.7168	1.18	0.9911	No	713	6	0.2823	0.2827	0.2827	0.2825	6.86	1.7168	1.18	0.9881	No	5.50	0.36
RT0776	6	0.2826	0.0000	0.0011	708	12	0.2823	0.2827	0.2827	0.2825	7.29	1.0634	1.14	0.9577	No	713	6	0.2823	0.2827	0.2827	0.2825	7.39	1.0634	1.14	0.9551	No	5.82	0.23
RT0776	5	0.2826	0.0000	0.0017	712	13	0.2823	0.2827	0.2827	0.2826	7.72	1.0524	1.12	0.9334	No	713	6	0.2823	0.2827	0.2827	0.2826	7.74	1.0524	1.12	0.9331	No	5.45	0.17
RT0776	9	0.2825	0.0000	0.0008	716	12	0.2823	0.2827	0.2826	0.2825	6.42	0.8027	1.21	1.0183	No	713	6	0.2823	0.2827	0.2827	0.2825	6.36	0.8027	1.21	1.0200	No	5.67	0.31
RT0776	2	0.2825	0.0000	0.0020	718	12	0.2823	0.2827	0.2826	0.2825	5.66	1.2403	1.25	1.0684	No	713	6	0.2823	0.2827	0.2827	0.2825	5.54	1.2403	1.26	1.0712	No	5.12	0.17

Appendix 4.2 Structure and thermochronology of Madagascar: Analytical methods and detailed results

Analytical methods

Zircon U–Pb

Thirteen rock samples were crushed and the zircon fraction (sieved 79–425 μm) was separated by panning. Zircons were hand-picked and mounted in epoxy resin. The zircon mount was polished; carbon coated and imaged using a Gatan cathodoluminescence (CL) detector attached to Quanta 600 MLA Scanning Electron Microscope to identify suitable domains for analysis. Zircon U–Pb geochronology was undertaken at the University of Adelaide using an Agilent 7900x ICP-MS with attached ASI Resolution excimer 193nm laser ablation system. A spot size of 29 μm and frequency of 5 Hz was used. Isotopes ^{90}Zr, ^{201}Hg, ^{204}Pb, ^{206}Pb, ^{207}Pb, ^{208}Pb, ^{232}Th and ^{238}U were measured. Each analysis comprised a 20s background and 30s ablation. GEMOC GJ-1 zircon (TIMS normalising ages ^{207}Pb/^{206}Pb = 607.7 ± 4.3 Ma, ^{206}Pb/^{238}U = 600.7 ± 1.1 Ma and ^{207}Pb/^{235}U = 602.0 ± 1.0 Ma; Jackson et al. 2004) was used to correct for U–Pb fractionation. The Plešovice zircon standard (ID TIMS ^{206}Pb/^{238}U = 337.13 ± 0.37 Ma; Sláma et al. (2008)) was used to assess accuracy over the course of the laser session; a total of 52 Plešovice standard analyses were made and yield a weighted average ^{206}Pb/^{238}U age of 338.41± 0.69 Ma (95% confidence limits) which closely matches the ID TIMS age. Data were processed using Iolite (Paton et al., 2011).

Apatite U–Pb

Apatite grains were picked from the zircon fraction (see previous section) for 13 samples and mounted in epoxy resin. Prior to analysis, samples were chemically etched in a 5 M HNO3 solution for 20s at 20°C to identify whether apatite was present in the sample (Hasebe et al., 2009). Ten of these samples yielded sufficient apatite to be analysed. Apatite U–Pb thermochronology was undertaken at the University of Adelaide using an Agilent 7900x ICP-MS with attached ASI Resolution excimer 193nm laser ablation system. A spot size of 29 μm and frequency of 5 Hz was used. Isotopes ^{43}Ca, ^{201}Hg, ^{204}Pb, ^{206}Pb, ^{207}Pb, ^{208}Pb, ^{232}Th and ^{238}U were measured. Each analysis comprised a 30s background and 30s ablation. McClure Mountain syenite apatite was used as the primary standard (Schoene and Bowring, 2006), and the Madagascar apatite (Thomson et al., 2012) was used as a secondary standard. Data reduction was performed using the "VisualAge_UcomPbine" DRS (Chew et al., 2014) in the Iolite software package (Paton et al., 2011). This data reduction scheme can account for variable common Pb in the standards and unknowns, and was used to apply baseline, downhole fractionation, and long-term drift corrections. The Madagascar apatite standard yielded a ^{207}Pb-corrected age of 468 ± 5 Ma (n=70), which closely matches the published value of 474.25 ± 0.41

(Thomson et al., 2012). Concordia diagrams were made using the isoplot plugin in Microsoft Excel (Ludwig, 2003).

Mica Rb–Sr

Muscovite and biotite grains were picked from the coarse fraction (>425 µm) of the same 13 samples used for zircon and apatite U–Pb geochronology and mounted in epoxy resin. Of these, nine samples yielded sufficient muscovite and 12 samples yielded sufficient biotite for analysis (although one of these did not yield data that formed a reasonable isochron age). Mica Rb–Sr geochronology was undertaken at the University of Adelaide using an Agilent 8900x ICP-MS/MS with attached ASI Resolution excimer 193nm laser ablation system. The CRPG reference material Mica-Mg (Govindaraju et al., 1994) prepared as a pressed power pellet was used as the primary standard (Hogmalm et al., 2017), and a mineral phlogopite (MDC) sourced from the same quarry in the Bekily area of Madagascar as Mica-Mg and assumed to be of the same age, was used as a secondary standard. We also analysed standards NIST612, NIST610, and BCR-2G; as well as biotite samples of known age, KW and LP6. We used a Rb decay constant of 1.393 x10^{-11} (Nebel et al., 2011). The Isoplot add-in in excel was used to calculate isochron ages (Ludwig, 2003). The mineral standard MDC was tied to $^{87}Rb/^{86}Sr$ = 0.00001±0.00001 and $^{87}Sr/^{86}Sr$ = 0.72607±0.00363 initial ratios and yielded an isochron age of 535 ± 11 Ma (MSWD=2.8). While this is within uncertainty of the published value (519.4 ± 6.5 Ma; Hogmalm et al. (2017)), it is at the very limits of this range. To be conservative we have incorporated additional uncertainty into our calculated age uncertainties, based on the difference between the expected and measured age values. Using this approach, the accuracy of this technique within our setup is out by 3.68%. This adds further uncertainty to any ages calculated from this dataset, and we have added an uncertainty of 3.68% in quadrature to all calculated isochron age uncertainties.

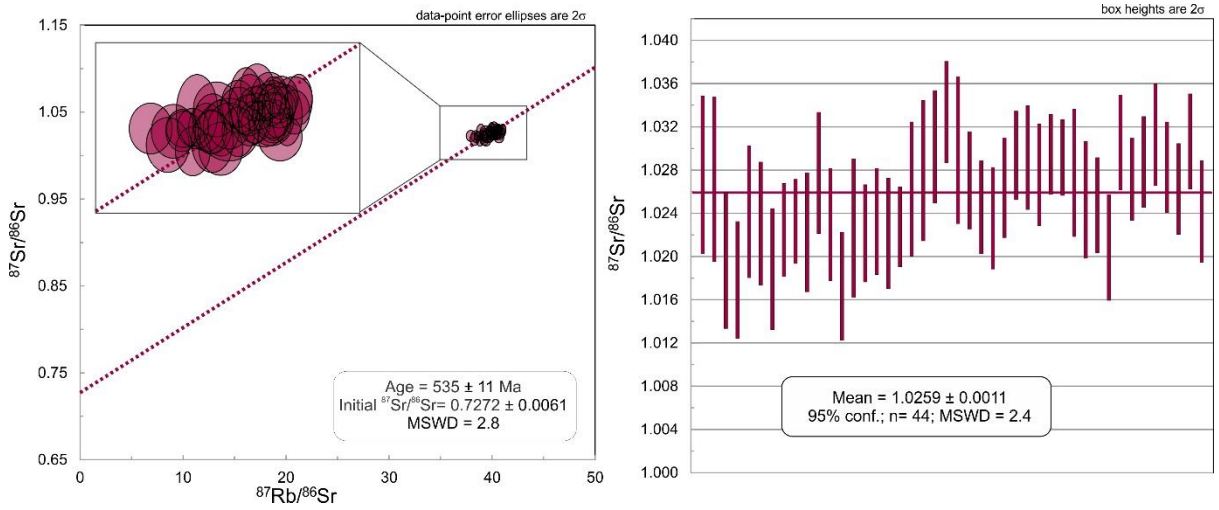

Figure A.7.1 $^{87}Sr/^{86}Sr$ vs $^{87}Rb/^{86}Sr$ plot and weighted average plot of $^{87}Sr/^{86}Sr$ for Mica mineral standard.

Detailed thermochronology results

Zircon U–Pb data

Key locality 1 (western transect)

Three samples from locality one were analysed for U–Pb zircon geochronology. Several analyses in sample M16-15 form a discordia trend with upper intercept age of 2456 ± 17 Ma, which we interpret as the crystallisation age of this orthogneiss. Sample M16-16 comprises several analyses that together form a discordia line with an upper intercept age of 795 ± 24 Ma. Sample M16-17 contained analyses that were very scattered on concordia plots with no distinct trends. Two data points plot near the cluster of points at c. 795 Ma for sample M16-16 and field relationships suggest that M16-17 pegmatite cross-cuts the M16-16 granite – suggesting that they are either coeval or that M16-17 post-dates the main granite. Based on so few data, the age of this sample is inconclusive.

Key locality 2 (western transect)

M16-24 was the only sample analysed from locality two and contains analyses that have undergone a degree of lead-loss, as indicated by their slip down the concordia. We therefore calculated an upper intercept age of the analyses that cluster on the concordia, and those that appear to form a lead-loss trend with these analyses. The upper intercept age of these analyses is 576 ± 24 Ma.

Key locality 3 (western transect)

Four samples were analysed from locality three. Twenty-one analyses from sample M16-32 were used to calculate an upper intercept age of 2553 ± 24 Ma. Sample M16-33 is comprised of mostly discordant data. Five analyses form a discordia trend with an upper intercept age of 798 ± 24 Ma. Several older discordant analyses from this sample may represent c. 815 Ma inherited zircons. M16-34 contains thirteen analyses that form a discordia trend with an upper intercept age of 2511 ± 14 Ma. Sample M16-35 contains analyses that appear to form two distinct populations. The first population has an upper intercept age of 2583 ± 26 Ma (MSWD=2.8, n=13), which we interpret as the magmatic crystallisation age. A second population of mostly zircon rims identified from CL images, forms a discordia trend with upper intercept age of 2494 ± 14 Ma (MSWD=1.5, n=10), which we interpret as a metamorphic age.

Key locality 4 (eastern transect)

The majority of analyses from M16-45 plot as part of a cluster on the concordia line. A weighted average of all of these analyses does not yield a reasonable MSWD (6.0), and show a decrease trend more than expected for normal variability in a magmatic

population. We suggest the younger analyses in this group are the result of lead-loss following Spencer et al. (2016). Seventeen near-concordant analyses yield a $^{206}Pb/^{238}U$ weighted average of 543 ± 18 Ma (MSWD=0.68), which we interpret as the magmatic crystallisation age of this granite.

Key locality 5 (eastern transect)

Analyses in sample M16-46 form a discordia trend with upper intercept age of 2522 ± 8 Ma and lower intercept age of 543 ± 27 Ma (Figure A.7.2). We suggest 2522 ± 8 Ma is the magmatic crystallisation age of this orthogneiss and that the isotopic system was disturbed during an event at c. 543 Ma. Analyses from sample M16-47 show significant scatter along the concordia line, which makes the identification of a lead-loss trend difficult. Given that Sample M16-46 from the same outcrop has a lower intercept age of c. 543 Ma that we interpret as isotopic disturbance, it is probable that sample M16-47 has also been disturbed at this time. If this is the case, the majority of analyses intersect a line between c. 800 Ma and c. 543 Ma, and potentially represent a coherent population that was disturbed at c. 543 Ma. Analyses that form along this general trend produce a discordia line with upper intercept age of 798 ± 48 Ma and lower intercept age of 532 ± 44 Ma (MSWD=1.4, n=18). We therefore suggest that the magmatic crystallisation age of this granite is 798 ± 48 Ma, and that isotopic disturbance occurred at 532 ± 44 Ma.

Key locality 6 (eastern transect)

The majority of analyses in sample M16-52 plot near the concordia line at c. 570 Ma. A calculated upper intercept age for these analyses is 568 ± 16 Ma (MSWD=2.2, n=18), which we interpret as the magmatic crystallisation age of this granite. Sample M16-53 contains very scattered data, with only one analysis intersecting the concordia line. This analysis clusters with three other analyses near c. 570 Ma, however these do not form a statistically robust weighted average or a concordia age. From field relationships, this sample cross-cuts sample M16-52 and therefore cannot be older than c. 568 Ma. We suggest this sample is most likely c. 568 Ma that formed during a magmatic event contemporaneously with M16-52.

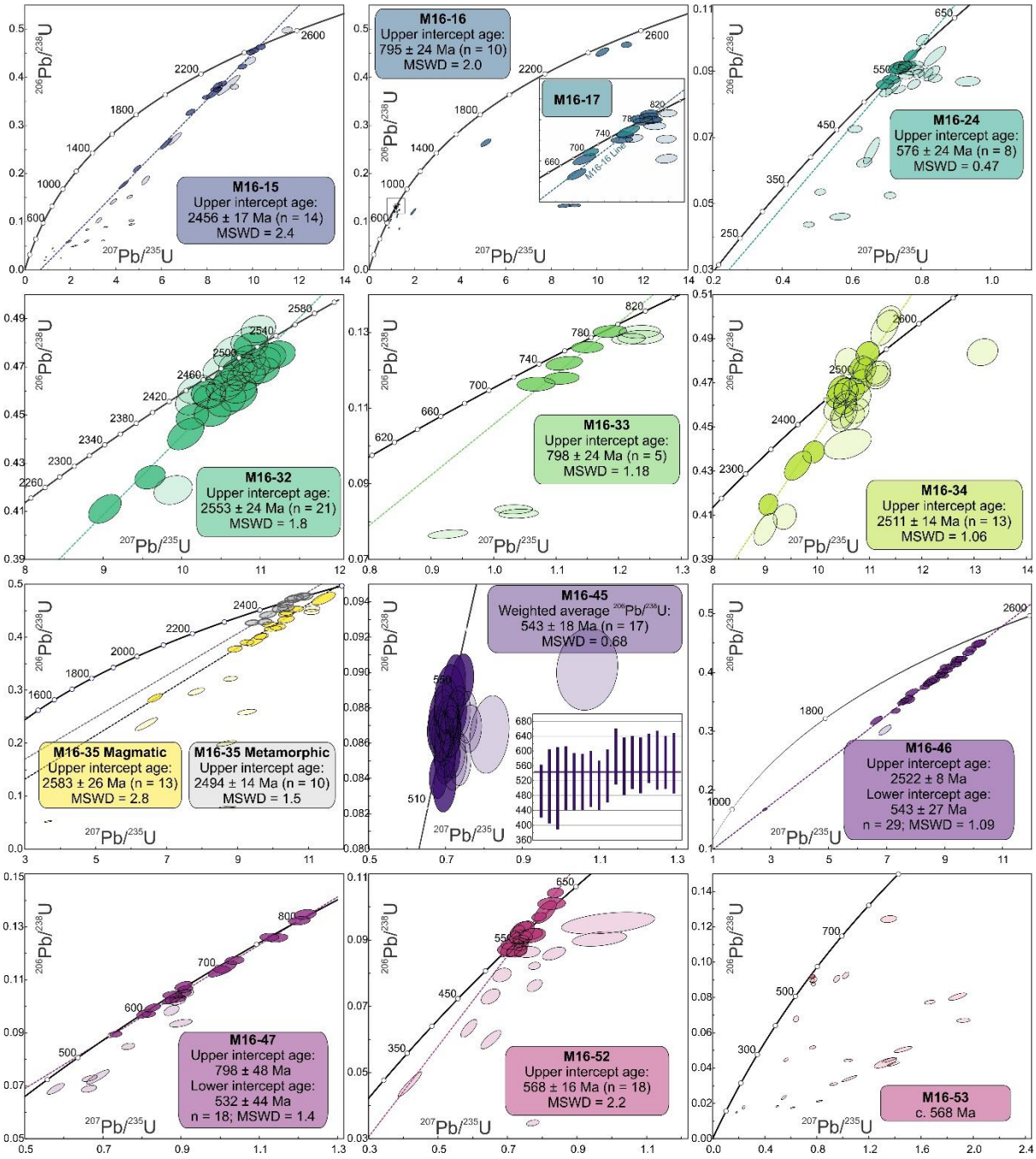

Figure A.7.2 Zircon U–Pb concordia plots for each sample, locations indicated on the map in Figure 2. X and Y axes are the same on all plots. Ellipses with higher transparency were not used to calculate ages.

Apatite U–Pb data

Key locality 1 (western transect)

Magmatic crystallisation ages interpreted from U–Pb zircon data for samples M16-15, M16-16 and M16-17 are c. 2500 Ma, c. 795 Ma and c. 787 Ma respectively. All three samples have very similar apatite U–Pb ages that are within uncertainty of each other, suggesting that they were thermally reset during a later event, and cooled below ~450–

550°C at c. 495 Ma. Sample ages, the number of analyses and MSWDs are given in (Figure A.7.3). Several analyses from locality 1 fall off the regression lines. A calculated regression line through the analyses of all three samples combined produced an age of 493 ± 19 Ma, which is indistinguishable from the ages calculated for the main analysis populations in these samples.

Key locality 3 (western transect)

Magmatic crystallisation ages interpreted from U–Pb zircon data for samples M16-32, M16-34 and M16-35 are all c. 2500 Ma. All samples have been reset during a later event and cooled through ~450–550°C at c. 510 Ma. Several analyses fall off these discordia lines and were excluded from the sample age calculations. Together these four 'discordant' analyses produce a regression line and lower intercept age of c. 613 ± 25 Ma. These analyses potentially record an earlier event that post-dates magmatic emplacement, and pre-dates the main phase of thermal resetting of the majority of analyses.

Key locality 4/5 (eastern transect)

We have grouped samples M16-45 and M16-46 together due to the geographic proximity and similarity in apatite U–Pb age. The magmatic ages calculated from U–Pb zircon data are c. 543 Ma and c. 2500 Ma for samples M16-45 and M16-46 respectively. Apatite U–Pb data reveals that these samples have been thermally reset during a later event, and cooled through ~450–550°C at c. 500 Ma. Several analyses do not overlap the regression lines and together produce an age of 559 ± 89 Ma. Although this apatite U–Pb age is older than the main sample population ages, it is still within uncertainty. These analyses either represent partial lead diffusion during reheating or record an age closer to the magmatic crystallisation age of M16-45 at c. 543 Ma.

Key locality 6 (eastern transect)

Samples M16-52 and M16-53 have zircon U–Pb magmatic crystallisation ages of c. 565 Ma. Apatite U–Pb ages for these samples are 484 ± 14 Ma and 500 ± 10 Ma respectively. This suggests that these rocks either slowly cooled from the time of magmatic crystallisation to ~450–550°C over a protracted period of c. 60 Ma, or that these magmatic rocks were thermally reset during a younger event. Several analyses do not overlap the apatite U–Pb regression lines, and together produce an intercept age of 547 ± 25 Ma. Unlike key locality 4/5, this age is not within uncertainty of the main apatite U–Pb population, and more closely matches the age of zircon crystallisation. We therefore suggest that the U–Pb system closed in these grains earlier than the majority of grains analysed.

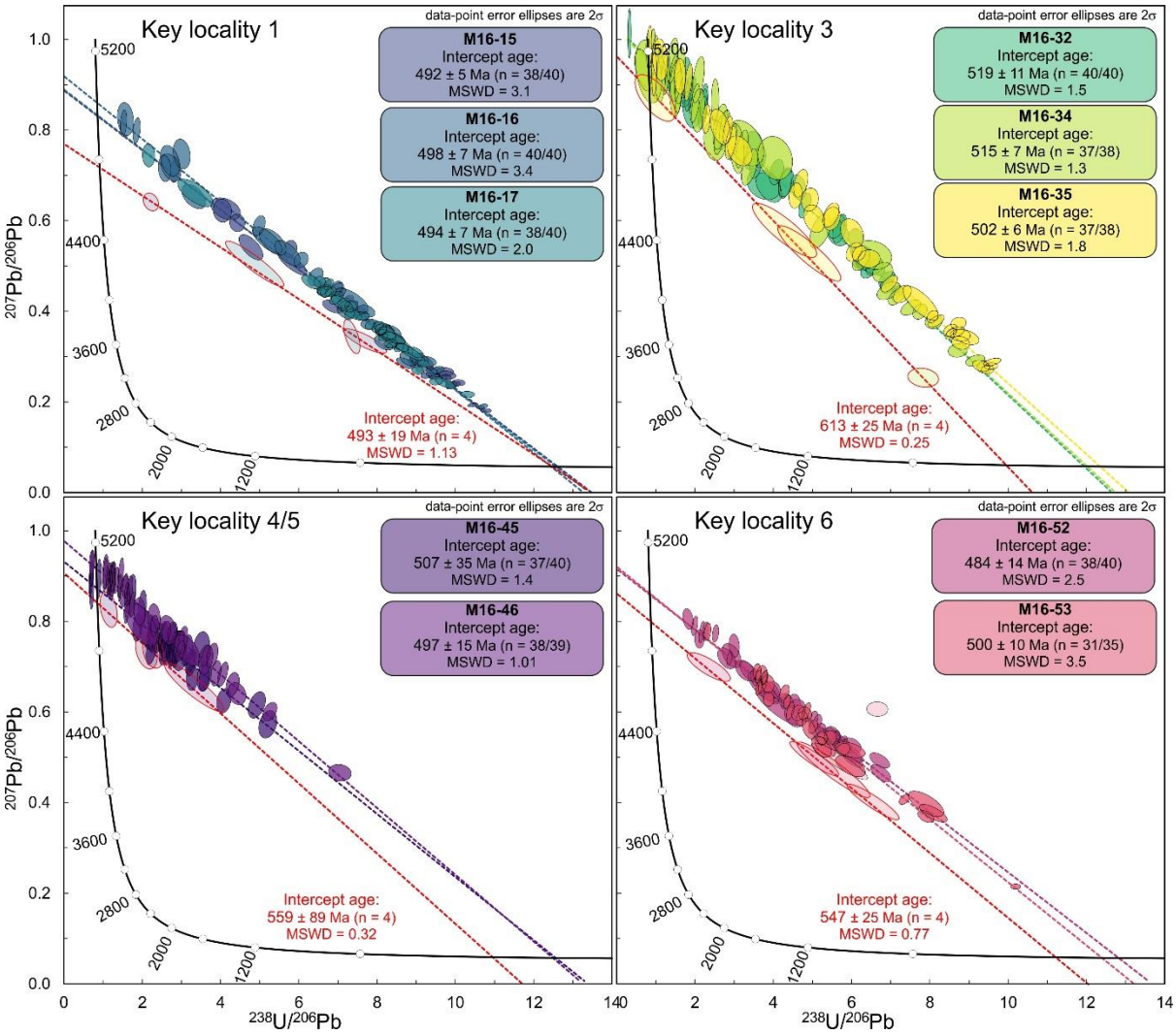

Figure A.7.3 Apatite U–Pb concordia plots of data analysed from key localities indicated on the map in Figure 2 of the manuscript. X and Y axes are the same on all plots. Ellipses with higher transparency were not used to calculate the intercept age.

Biotite and muscovite Rb–Sr data

Key locality 1

All three samples from key locality one were analysed for biotite and muscovite Rb–Sr dating. Biotite isochron ages for samples M16-15, M16-16 and M16-17 are 528 ± 18 Ma, 499 ± 68 Ma and 492 ± 51 Ma (2σ) respectively. Muscovite isochron ages for samples M16-15, M16-16 and M16-17 are 624 ± 152 Ma, 506 ± 82 Ma and 526 ± 39 Ma (2σ) respectively. Taking into account the uncertainties on these ages, we suggest that both muscovite and biotite cooled through their closure temperatures at c. 500 Ma.

Key locality 2

Sample M16-24 yielded a biotite isochron age of 505 ± 59 Ma and a muscovite age of 519 ± 69 Ma. These ages are within uncertainty of each other, so we suggest this sample was heated to at least ~300–600°C at this time. These are broadly consistent with ages obtained from key locality 1, suggesting that thermal activity was regionally widespread.

Key locality 3

Samples M16-32 and M16-35 yielded biotite ages of 502 ± 20 Ma and 513 ± 18 Ma respectively. Sample M16-32 yielded a muscovite isochron age of 446 ± 161 Ma. Given the large uncertainty for the muscovite age, we suggest that these samples underwent temperatures of ~300–600°C at c. 500 Ma, based on the biotite age.

Key locality 4/5

Sample M16-45 has a biotite age of 512 ± 16 Ma. Sample M16-46 has a biotite age of 512 ± 24 Ma, and a muscovite age of 604 ± 211 Ma. Sample M16-47 has a muscovite age of 657 ± 98 Ma. Given the uncertainties of these ages, we cannot reconcile whether there is an older c. 650–600 Ma event recorded here, or if these ages represent an event similar to other samples at c. 500 Ma.

Key locality 6

Samples M16-52 and M16-53 have biotite ages of 511 ± 16 Ma and 521 ± 18 Ma respectively. These samples have muscovite ages of 527 ± 51 Ma and 537 ± 35 Ma. The muscovite samples are slightly older, although still within uncertainty, of the biotite ages. We therefore suggest these samples cooled through ~300–600°C at c. 530–510 Ma.

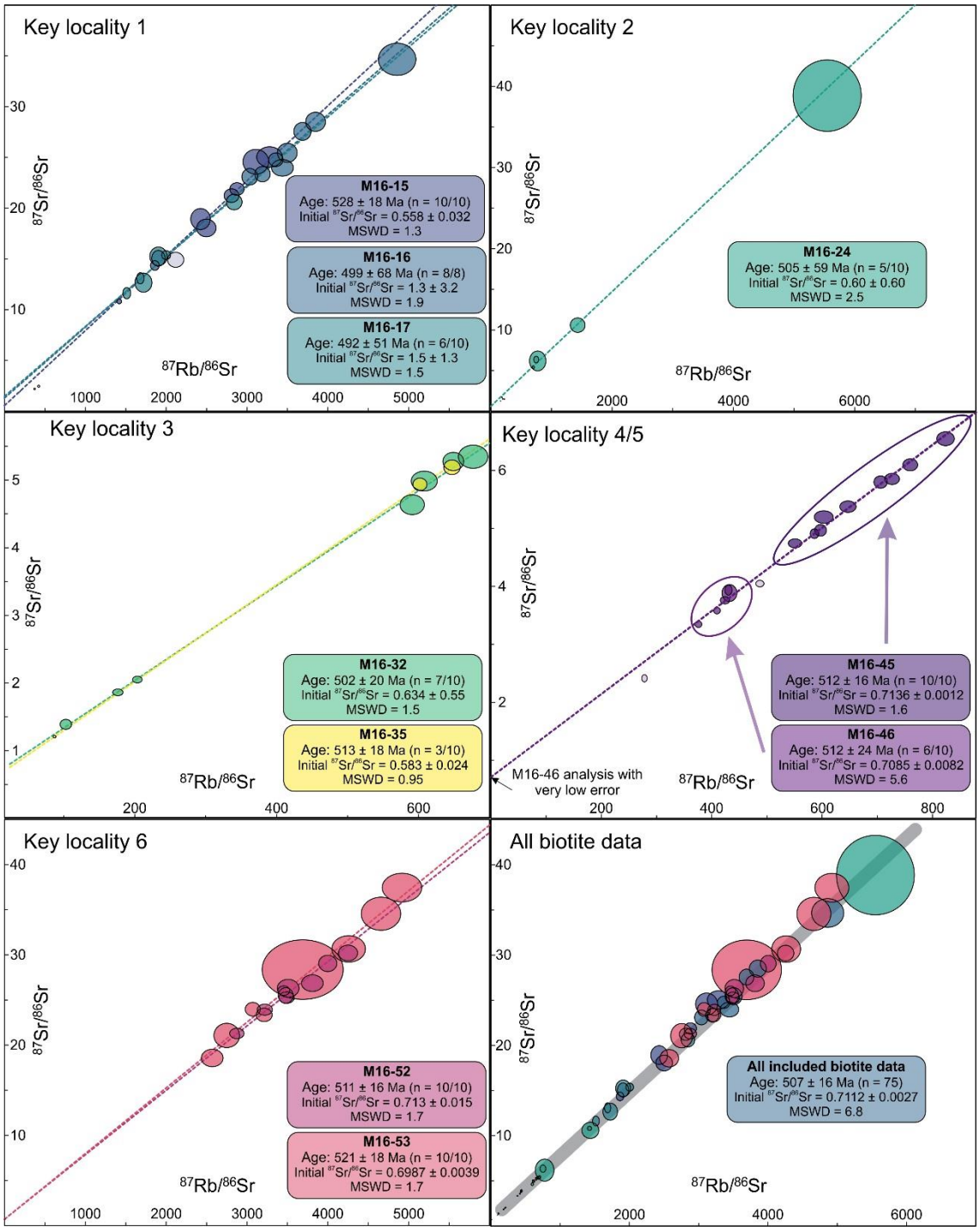

Figure A.7.4 Biotite Rb–Sr data plotted for each locality and coloured by sample. Isochrons calculated for each sample. High transparency ellipses were excluded from age calculations. Due to some very low values and associated low errors, not all data is visible on the plots, see supplementary B for isotopic data. Data-point error ellipses are 2σ.

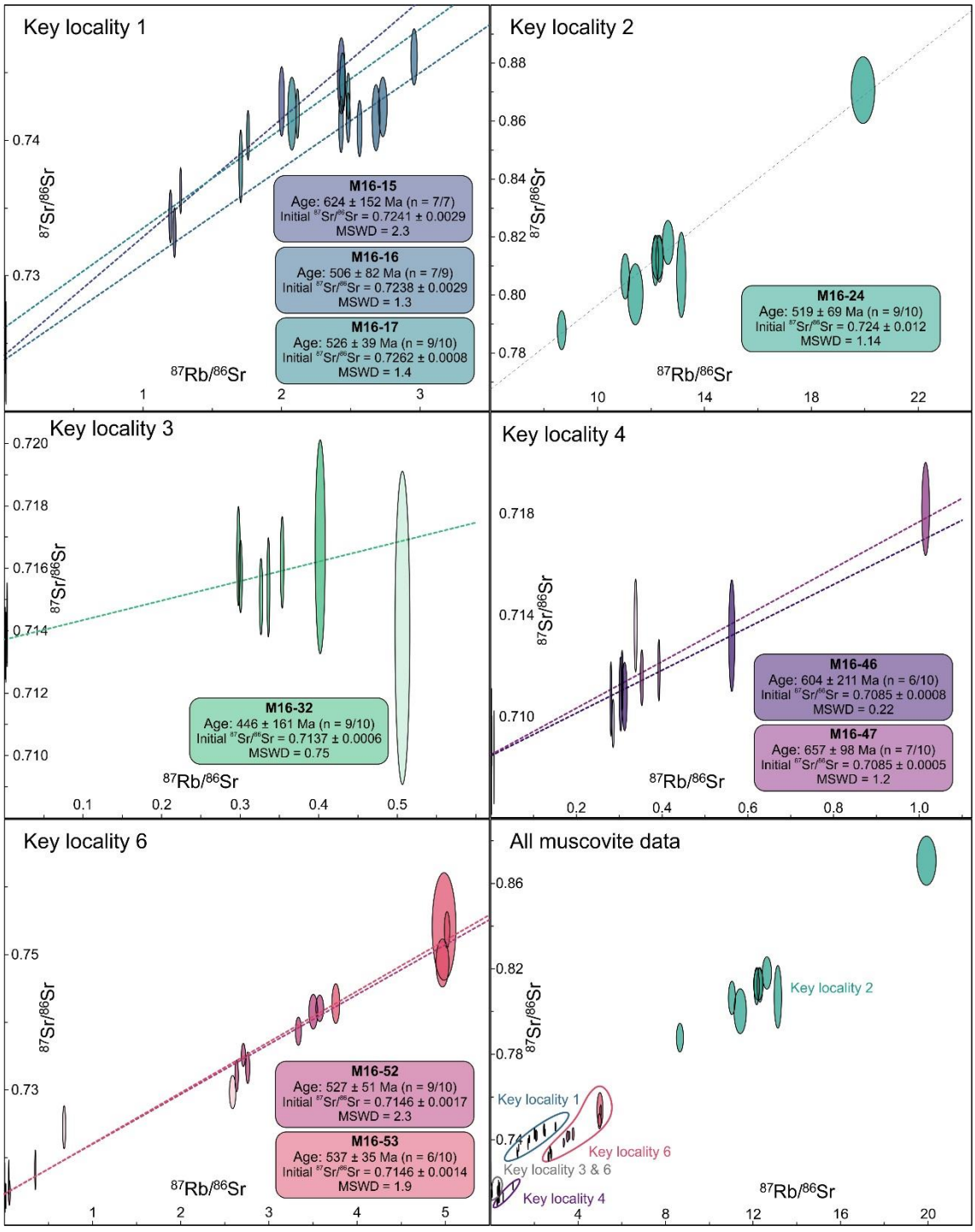

Figure A.7.5 Muscovite Rb–Sr data plotted for each locality and coloured by sample. Isochrons calculated for each sample. High transparency ellipses were excluded from age calculations. Due to some very low values and associated low errors, not all data is visible on the plots, see supplementary B for isotopic data. Data-point error ellipses are 2σ.

References

Armstrong, R.L., Jäger, E. and Eberhardt, P., 1966. A comparison of K-Ar and Rb-Sr ages on Alpine biotites. Earth and Planetary Science Letters, 1(1): 13-19.

Chamberlain, K.R. and Bowring, S.A., 2001. Apatite–feldspar U–Pb thermochronometer: a reliable, mid-range (~450°C), diffusion-controlled system. Chemical Geology, 172(1): 173-200.

Chew, D., Petrus, J. and Kamber, B., 2014. U–Pb LA–ICPMS dating using accessory mineral standards with variable common Pb. Chemical Geology, 363: 185-199.

Del Moro, A., Puxeddu, M., di Brozolo, F.R. and Villa, I.M., 1982. Rb-Sr and K-Ar ages on minerals at temperatures of 300°–400° C from deep wells in the Larderello geothermal field (Italy). Contributions to Mineralogy and Petrology, 81(4): 340-349.

Govindaraju, K., RUBESKA, I. and PAUKERT, T., 1994. 1994 Report on Zinnwaldite ZW-C analysed by ninety-two GIT-IWG member-laboratories. Geostandards Newsletter, 18(1): 1-42.

Hasebe, N., Carter, A., Hurford, A.J. and Arai, S., 2009. The effect of chemical etching on LA–ICP-MS analysis in determining uranium concentration for fission-track chronometry. Geological Society, London, Special Publications, 324(1): 37-46.

Hogmalm, K.J., Zack, T., Karlsson, A.K.-O., Sjöqvist, A.S. and Garbe-Schönberg, D., 2017. In situ Rb–Sr and K–Ca dating by LA-ICP-MS/MS: an evaluation of N 2 O and SF 6 as reaction gases. Journal of Analytical Atomic Spectrometry, 32(2): 305-313.

Jenkin, G.R.T., Ellam, R.M., Rogers, G. and Stuart, F.M., 2001. An investigation of closure temperature of the biotite Rb-Sr system: The importance of cation exchange. Geochimica et Cosmochimica Acta, 65(7): 1141-1160.

Ludwig, K.R., 2003. User's manual for Isoplot 3.00: a geochronological toolkit for Microsoft Excel. Kenneth R. Ludwig.

Nebel, O., Scherer, E.E. and Mezger, K., 2011. Evaluation of the 87Rb decay constant by age comparison against the U–Pb system. Earth and Planetary Science Letters, 301(1-2): 1-8.

Paton, C., Hellstrom, J., Paul, B., Woodhead, J. and Hergt, J., 2011. Iolite: Freeware for the visualisation and processing of mass spectrometric data. Journal of Analytical Atomic Spectrometry, 26(12): 2508-2518.

Schoene, B. and Bowring, S.A., 2006. U–Pb systematics of the McClure Mountain syenite: thermochronological constraints on the age of the 40 Ar/39 Ar standard MMhb. Contributions to Mineralogy and Petrology, 151(5): 615.

Schoene, B. and Bowring, S.A., 2007. Determining accurate temperature–time paths from U–Pb thermochronology: An example from the Kaapvaal craton, southern Africa. Geochimica et Cosmochimica Acta, 71(1): 165-185.

Sláma, J., Košler, J., Condon, D.J., Crowley, J.L., Gerdes, A., Hanchar, J.M., Horstwood, M.S., Morris, G.A., Nasdala, L. and Norberg, N., 2008. Plešovice zircon—a new natural reference material for U–Pb and Hf isotopic microanalysis. Chemical Geology, 249(1): 1-35.

Spencer, C.J., Kirkland, C.L. and Taylor, R.J., 2016. Strategies towards statistically robust interpretations of in situ U–Pb zircon geochronology. Geoscience Frontiers, 7(4): 581-589.

Thomson, S.N., Gehrels, G.E., Ruiz, J. and Buchwaldt, R., 2012. Routine low-damage apatite U-Pb dating using laser ablation–multicollector–ICPMS. Geochemistry, Geophysics, Geosystems, 13(2).

Verschure, R.H., Andriessen, P.A.M., Boelrijk, N.A.I.M., Hebeda, E.H., Maijer, C., Priem, H.N.A. and Verdurmen, E.A.T., 1980. On the thermal stability of Rb-Sr and K-Ar biotite systems: Evidence from coexisting Sveconorwegian (ca 870 Ma) and Caledonian (ca 400 Ma) biotites in SW Norway. Contributions to Mineralogy and Petrology, 74(3): 245-252.

Appendix 4.3 Structure and thermochronology of Madagascar: isotopic data for geo/thermochronology

Zircon U–Pb geochronology

Sample No.	Sample - spot	$^{207}Pb/^{206}Pb$	± 2SE	$^{207}Pb/^{235}U$	± 2SE	$^{206}Pb/^{238}U$	± 2SE	Error Correlation 6/38 vs 7/35	Age $^{207}Pb/^{235}U$	± 2SE	Age $^{206}Pb/^{238}U$	± 2SE	Age $^{207}Pb/^{206}Pb$	± 2SE	Concordance 7/6 vs 6/38	Pb (PPM)	Th (PPM)	U (PPM)	U/Th
M16-15	M16-15 - 1	0.16295	0.0029	8.467	0.15	0.3753	0.0044	0.86928	2282.2	16	2054	21	2485.9	30	82.63	2831	418	417	1.026
M16-15	M16-15 - 10	0.15839	0.0028	9.923	0.16	0.452	0.0041	0.63187	2427.4	15	2403.9	18	2438.1	29	98.60	2825	252.7	411.4	1.644
M16-15	M16-15 - 11	0.16454	0.0029	9.89	0.2	0.4341	0.0067	0.93062	2424	18	2323	30	2502.6	30	92.82	4750	270	529.5	2.08
M16-15	M16-15 - 12	0.2395	0.0044	1.297	0.025	0.039	0.00065	0.91065	844	11	246.6	4	3117	30	7.91	11290	2408	4760	1.999
M16-15	M16-15 - 13	0.16021	0.0028	7.27	0.16	0.3278	0.0055	0.96015	2144	19	1826	27	2458.1	30	74.29	3169	332	616	1.8715
M16-15	M16-15 - 14	0.1973	0.0037	1.227	0.032	0.045	0.0011	0.95171	812	15	283.8	6.7	2802	31	10.13	5570	757	4230	5.497
M16-15	M16-15 - 15	0.15988	0.0028	7.954	0.13	0.3588	0.0035	0.72456	2225.5	15	1977.1	16	2454.6	29	80.55	2991	278.1	521	1.895
M16-15	M16-15 - 16	0.16792	0.0029	11.512	0.19	0.4985	0.0051	0.87313	2566.4	16	2607	22	2536.7	29	102.77	11810	982	1003	1.012
M16-15	M16-15 - 17	0.2204	0.004	4.605	0.1	0.1518	0.0031	0.93365	1749	18	911	17	2983	29	30.54	12430	1122	1815	1.65
M16-15	M16-15 - 18	0.16999	0.003	8.95	0.4	0.384	0.017	0.99588	2316	43	2082	80	2557.8	29	81.40	11710	937	861	0.923
M16-15	M16-15 - 19	0.1763	0.0032	6.57	0.25	0.272	0.011	0.99339	2043	34	1548	55	2617.6	30	59.14	3550	849	1313	1.8
M16-15	M16-15 - 2	0.2414	0.0045	1.965	0.07	0.0592	0.0024	0.99172	1097	23	370	14	3128	30	11.83	17510	1338	4380	3.364
M16-15	M16-15 - 20	0.3162	0.008	2.18	0.12	0.0498	0.0019	0.97432	1165	38	313	11	3547	39	8.82	14050	13220	2590	0.1955
M16-15	M16-15 - 21	0.2013	0.0037	3.89	0.12	0.1421	0.0046	0.97941	1604	26	855	26	2835	30	30.16	13590	6720	2180	0.319
M16-15	M16-15 - 22	0.16393	0.0029	10.35	0.17	0.4632	0.0046	0.79957	2466.1	15	2454	20	2496.1	29	98.31	2058	189	360	1.896
M16-15	M16-15 - 23	0.2137	0.0056	5.3	0.14	0.1863	0.0074	0.96357	1865	22	1097	40	2922	42	37.54	11450	2710	2128	0.822
M16-15	M16-15 - 24	0.2614	0.0055	0.933	0.024	0.02654	0.00089	0.98126	668.7	13	168.8	5.6	3251	33	5.19	10700	3540	6080	1.679
M16-15	M16-15 - 25	0.1646	0.0029	8.685	0.15	0.3872	0.0043	0.81839	2305.9	15	2111	21	2503	30	84.34	3345	316.5	544.8	1.693
M16-15	M16-15 - 26	0.4802	0.0084	1.587	0.031	0.02427	0.00035	0.94003	964.3	12	154.6	2.2	4182.3	26	3.70	3.91E+04	3910	9880	2.547
M16-15	M16-15 - 27	0.2914	0.0053	3.554	0.068	0.08926	0.0011	0.82918	1538.6	15	551.8	6.5	3424.3	28	16.11	27060	22820	3830	0.1671
M16-15	M16-15 - 28	0.3648	0.0065	4.698	0.1	0.095	0.0016	0.93015	1766	18	584.8	9.6	3771.4	27	15.51	2.38E+04	2.63E+04	2230	0.09
M16-15	M16-15 - 29	0.18	0.0032	4.34	0.17	0.1773	0.007	0.99486	1700	32	1050	39	2654.2	30	39.56	3650	129.6	1630	12.03
M16-15	M16-15 - 3	0.3305	0.0092	4.677	0.091	0.1029	0.0019	-0.10432	1762	16	631	11	3608	44	17.49	28030	34240	3112	0.0907
M16-15	M16-15 - 30	0.17299	0.003	6.21	0.22	0.2624	0.0096	0.9942	2001	31	1502	49	2586.2	29	58.08	8690	608	2009	4.13
M16-15	M16-15 - 31	0.3269	0.0072	2.719	0.088	0.06	0.0024	0.97085	1330	24	375	14	3601	34	10.41	3.05E+04	2660	5000	1.846
M16-15	M16-15 - 32	0.16044	0.0028	8.29	0.26	0.3675	0.0096	0.99173	2255	29	2013	45	2459.8	30	81.84	17430	1519	2840	1.99
M16-15	M16-15 - 33	0.1724	0.0033	9.193	0.15	0.3808	0.0045	0.33842	2357.6	15	2081	21	2581	32	80.63	3300	455	563.1	1.31
M16-15	M16-15 - 34	0.16048	0.0028	9.551	0.16	0.4226	0.0044	0.79095	2392.1	15	2272	20	2460.2	29	92.35	2721	254.2	420.8	1.684

Zircon U–Pb geochronology

Sample No.	Sample - spot	$^{207}Pb/^{206}Pb$	± 2SE	$^{207}Pb/^{235}U$	± 2SE	$^{206}Pb/^{238}U$	± 2SE	Error Correlation 6/38 vs 7/35	Age $^{207}Pb/^{235}U$	± 2SE	Age $^{206}Pb/^{238}U$	± 2SE	Age $^{207}Pb/^{206}Pb$	± 2SE	Concordance 7/6 vs 6/38	Pb (PPM)	Th (PPM)	U (PPM)	U/Th
M16-15	M16-15 - 35	0.1683	0.0033	4.93	0.14	0.2106	0.0056	0.9457	1808	23	1231	30	2544	32	48.39	3720	1210	696	0.542
M16-15	M16-15 - 36	0.3104	0.0058	0.879	0.033	0.01996	0.00058	0.98273	639	18	127.4	3.6	3522	29	3.62	11040	2500	5600	2.243
M16-15	M16-15 - 37	0.15789	0.0028	8.33	0.14	0.3752	0.0039	0.85373	2267	16	2054	19	2433.3	30	84.41	2865	283.6	487.7	1.7259
M16-15	M16-15 - 4	0.16031	0.0028	8.459	0.16	0.3824	0.0059	0.94304	2282.9	17	2086	27	2459.2	29	84.82	2904	1140	525	0.556
M16-15	M16-15 - 5	0.2393	0.0044	2.75	0.067	0.0841	0.0017	0.93803	1345	17	520.1	10	3114	29	16.70	14650	1414	2870	1.991
M16-15	M16-15 - 6	0.15968	0.0028	10.066	0.17	0.4559	0.0043	0.81357	2440.6	15	2421	19	2451.9	30	98.74	3319	306.5	478.3	1.5633
M16-15	M16-15 - 7	0.2254	0.0073	3.256	0.11	0.1033	0.0052	0.83178	1467	25	638	31	2994	56	21.31	7770	1360	1956	1.854
M16-15	M16-15 - 8	0.2317	0.0044	1.87	0.046	0.0584	0.0013	0.95013	1069	16	365.6	8	3062	30	11.94	16570	4000	4050	1.011
M16-15	M16-15 - 9	0.4106	0.009	3.447	0.062	0.06077	0.00093	0.2364	1514.7	14	380.3	5.6	3945	33	9.64	41040	33350	5169	0.1569
M16-16	M16-16 - 1	0.0645	0.0015	1.171	0.025	0.12921	0.0014	0.07658	786.1	12	783.3	8	757	52	103.47	416	115.4	119.1	1.0393
M16-16	M16-16 - 10	0.487	0.014	9.05	0.21	0.1341	0.0025	0.19619	2346	22	812	14	4205	42	19.31	277.1	24.04	15.17	0.6304
M16-16	M16-16 - 11	0.074	0.0017	0.895	0.019	0.088	0.0013	0.38178	648.8	10	543.5	7.9	1050	48	51.76	402	96.3	357	3.698
M16-16	M16-16 - 12	0.1403	0.0035	5.14	0.19	0.2645	0.0066	0.82342	1835	33	1510	34	2237	45	67.50	101.9	12.35	28.8	2.299
M16-16	M16-16 - 13	0.11574	0.0022	1.95	0.1	0.121	0.0058	0.98864	1079	36	733	33	1891	33	38.76	1503	384	574	1.6
M16-16	M16-16 - 14	0.1753	0.0032	11.306	0.19	0.4679	0.0047	0.48574	2549.7	16	2474	21	2609	31	94.83	621	53.7	128.8	2.531
M16-16	M16-16 - 15	0.06627	0.0014	1.199	0.024	0.13006	0.0013	0.1937	799.5	11	788.2	7.5	812	46	97.07	990	268	143.2	0.559
M16-16	M16-16 - 16	0.0679	0.0013	1.249	0.022	0.13304	0.0014	0.45485	822.4	10	805.1	7.7	863	39	93.29	1405	380	590	1.5
M16-16	M16-16 - 17	0.698	0.027	28.9	3.4	0.275	0.027	0.94603	3300	110	1530	130	4732	63	32.33	194.1	7.8	4.73	0.649
M16-16	M16-16 - 18	no value	NAN	no value	NAN	no value	NAN	NaN	no value	NAN	no value	NAN	no value	NAN	#VALUE!	79.4	0.009	0.00038	no value
M16-16	M16-16 - 19	0.0803	0.0019	1.244	0.027	0.1111	0.0018	0.27889	820.8	12	679.2	10	1207	47	56.27	1820	499	485	1.083
M16-16	M16-16 - 2	0.06412	0.0013	1.191	0.023	0.13299	0.0014	0.1236	796	11	805.3	7.8	748	43	107.66	889	245	231.5	0.965
M16-16	M16-16 - 20	0.0663	0.0017	1.196	0.029	0.12985	0.0014	0.17626	798	13	787.5	8	818	52	96.27	615	173.7	104.9	0.638
M16-16	M16-16 - 21	0.06737	0.0012	0.965	0.024	0.1035	0.0022	0.93207	684.6	12	634	13	849	38	74.68	397.2	85.9	890	10.56
M16-16	M16-16 - 22	0.0701	0.0017	1.326	0.031	0.13606	0.0014	0.11153	858.5	13	822.3	8.1	921	51	89.28	617	166.3	129.1	0.782
M16-16	M16-16 - 23	0.1145	0.0039	1.347	0.03	0.0858	0.0015	-0.53915	865.7	13	530.4	8.7	1842	60	28.79	3680	1261	842	0.676
M16-16	M16-16 - 24	0.06863	0.0013	1.144	0.022	0.1209	0.0015	0.67193	775.1	11	735.9	8.6	885	39	83.15	1930	589	575	1.077
M16-16	M16-16 - 25	0.06559	0.0014	1.189	0.024	0.13177	0.0013	0.047629	794.8	11	797.9	7.5	793	46	100.62	243.8	71.6	186	2.581
M16-16	M16-16 - 26	0.06582	0.0014	1.115	0.022	0.12261	0.0013	0.35749	760.8	10	746.1	7.4	809	43	92.22	1015	323.9	370.7	1.128
M16-16	M16-16 - 27	0.0667	0.0017	1.105	0.028	0.12023	0.0012	0.08339	756	14	731.9	6.9	824	53	88.82	863	236	482.3	2.054
M16-16	M16-16 - 28	0.0651	0.0016	1.165	0.028	0.1305	0.0016	0.097684	783.9	13	790.4	9	773	54	102.25	372	105.7	106.4	1.0041

Zircon U–Pb geochronology

Sample No.	Sample - spot	$^{207}Pb/^{206}Pb$	± 2SE	$^{207}Pb/^{235}U$	± 2SE	$^{206}Pb/^{238}U$	± 2SE	Error Correlation 6/38 vs 7/35	Age $^{207}Pb/^{235}U$	± 2SE	Age $^{206}Pb/^{238}U$	± 2SE	Age $^{207}Pb/^{206}Pb$	± 2SE	Concordance 7/6 vs 6/38	Pb (PPM)	Th (PPM)	U (PPM)	U/Th
M16-16	M16-16 - 29	0.0809	0.0018	1.28	0.028	0.11563	0.0013	0.21158	836.1	12	705.3	7.3	1212	45	58.19	910	307.3	299.6	0.95
M16-16	M16-16 - 3	0.461	0.014	8.58	0.24	0.1336	0.003	0.46255	2290	25	808	17	4119	43	19.62	255.1	21.87	15.73	0.7207
M16-16	M16-16 - 4	0.783	0.029	52.9	2.7	0.483	0.023	0.75879	4056	53	2527	98	4929	66	51.27	199.2	2.44	2.24	0.962
M16-16	M16-16 - 5	0.16254	0.0028	10.25	0.23	0.4528	0.0072	0.96388	2454	21	2406	32	2481.7	30	96.95	6600	566.1	550.9	0.9771
M16-16	M16-16 - 6	0.0741	0.0017	1.243	0.025	0.1206	0.0016	0.038198	819.8	11	734	9.1	1042	49	70.44	1118	296.9	228.5	0.78
M16-16	M16-16 - 7	0.0684	0.0018	1.208	0.028	0.127	0.0015	0.091113	803.8	13	770.6	8.8	872	55	88.37	380	154.5	219.5	1.439
M16-16	M16-16 - 8	0.0642	0.0014	0.989	0.029	0.1109	0.0023	0.86704	700	14	677	13	749	46	90.39	869	248	358	2.21
M16-16	M16-16 - 9	0.07788	0.0014	1.333	0.025	0.1241	0.0015	0.76952	859.9	11	754	8.7	1142	36	66.02	7422	2071	1152	0.5549
M16-17	M16-17 - 1	0.101	0.0025	1.307	0.024	0.0948	0.0013	-0.22369	849.7	11	583.9	7.9	1646	46	35.47	1518	1934	489	0.2585
M16-17	M16-17 - 10	0.0807	0.0018	1.34	0.026	0.1187	0.0016	0.23814	864.1	12	722.8	9.1	1219	43	59.29	2249	635	531	0.841
M16-17	M16-17 - 11	0.0913	0.0029	0.964	0.029	0.07542	0.00088	-0.13179	685	15	468.7	5.2	1453	62	32.26	1444	774	1354	1.79
M16-17	M16-17 - 12	0.5713	0.013	7.76	0.49	0.097	0.0048	0.98495	2170	65	596	28	4433	35	13.44	2.24E+04	6330	1557	0.266
M16-17	M16-17 - 13	0.481	0.013	7.78	0.32	0.1147	0.0022	0.96245	2186	39	700	13	4170	42	16.79	2.55E+04	1653	1796	1.129
M16-17	M16-17 - 14	0.3848	0.0071	4.802	0.095	0.089	0.0014	0.80904	1785	17	549.5	8.4	3852	29	14.27	14570	2064	1610	0.785
M16-17	M16-17 - 15	0.5832	0.012	7.92	0.23	0.0968	0.0017	0.95756	2217	27	595.6	10	4465	30	13.34	2.40E+04	1281	1694	1.326
M16-17	M16-17 - 16	0.183	0.013	2.47	0.23	0.0945	0.0052	0.64763	1194	66	580	31	2550	110	22.75	3.12E+04	9580	11810	1.36
M16-17	M16-17 - 17	0.2082	0.0041	2.683	0.058	0.09237	0.001	0.70596	1323	16	569.5	6.2	2890	32	19.71	7436	75.4	2043	27.56
M16-17	M16-17 - 18	0.2817	0.01	2.623	0.061	0.0661	0.0021	0.23585	1306	17	413	13	3364	56	12.28	7580	2823	1198	0.424
M16-17	M16-17 - 19	0.4786	0.0092	2.923	0.068	0.04424	0.00083	0.87113	1386	18	279	5.1	4175	29	6.68	14220	5150	2870	0.5712
M16-17	M16-17 - 2	0.08461	0.0017	0.9791	0.018	0.08359	0.00084	0.11995	693.3	9	517.5	5	1307	37	39.59	919	158.8	943	5.912
M16-17	M16-17 - 20	0.07025	0.0013	0.7957	0.015	0.08119	0.00078	0.53708	594.1	8.2	503.2	4.6	936	38	53.76	655	162.4	966	5.972
M16-17	M16-17 - 21	0.2303	0.0091	2.154	0.084	0.0668	0.0012	0.30919	1163	27	417	7.1	3016	65	13.83	9080	3230	1950	0.627
M16-17	M16-17 - 22	0.4442	0.0096	1.864	0.064	0.03014	0.00061	0.95134	1062	23	191.4	3.8	4061	33	4.71	1.50E+04	1132	4520	3.81
M16-17	M16-17 - 23	0.5529	0.01	6.926	0.14	0.08899	0.0012	0.83724	2100	18	549.5	7	4390	27	12.52	21430	921	1711	1.858
M16-17	M16-17 - 24	0.1645	0.0039	1.362	0.024	0.0594	0.0013	0.42182	872.7	10	371.8	7.7	2500	40	14.87	2923	672	1570	2.339
M16-17	M16-17 - 25	0.06551	0.0013	1.125	0.029	0.1244	0.0023	0.90206	767	14	755	13	787	40	95.93	1289	354	566	1.69
M16-17	M16-17 - 26	0.4718	0.0089	1.564	0.044	0.02414	0.00061	0.93546	953	17	153.7	3.8	4155	28	3.70	2.70E+04	7390	8200	1.08
M16-17	M16-17 - 27	0.3456	0.0072	5.099	0.11	0.1069	0.0017	0.68851	1835	18	654.8	9.9	3690	31	17.75	6270	526	504	0.941
M16-17	M16-17 - 28	0.3308	0.0066	3.334	0.057	0.0737	0.0011	0.4322	1488.7	13	458.4	6.7	3619	31	12.67	12740	1700	1806	1.061
M16-17	M16-17 - 29	0.6154	0.011	5.16	0.21	0.061	0.0023	0.99415	1830	35	381	14	4545.2	25	8.38	4.37E+04	6090	4250	0.713
M16-17	M16-17 - 3	0.5312	0.0092	2.943	0.097	0.0403	0.0013	0.99259	1385	26	255.3	8	4330.4	25	5.90	2.97E+04	7380	5360	0.707

Zircon U–Pb geochronology

Sample No.	Sample - spot	$^{207}Pb/^{206}Pb$	± 2SE	$^{207}Pb/^{235}U$	± 2SE	$^{206}Pb/^{238}U$	± 2SE	Error Correlation 6/38 vs 7/35	Age $^{207}Pb/^{235}U$	± 2SE	Age $^{206}Pb/^{238}U$	± 2SE	Age $^{207}Pb/^{206}Pb$	± 2SE	Concordance 7/6 vs 6/38	Pb (PPM)	Th (PPM)	U (PPM)	U/Th
M16-17	M16-17 - 30	0.5083	0.0094	4.752	0.12	0.0681	0.0014	0.94094	1778	21	424.4	8.3	4264.7	27	9.95	2.95E+04	391	3200	8.07
M16-17	M16-17 - 4	0.2073	0.0038	1.94	0.04	0.06853	0.00099	0.81239	1095	14	427.2	6	2884	30	14.81	6810	4150	1172	0.295
M16-17	M16-17 - 5	0.06095	0.0012	0.7523	0.014	0.08995	0.0011	0.39033	569.3	7.8	555.2	6.2	639	42	86.89	449	152.3	1036	6.843
M16-17	M16-17 - 6	0.07338	0.0014	0.855	0.023	0.0853	0.0017	0.92775	627	13	527.8	10	1023	38	51.59	945	116.3	1838	16.07
M16-17	M16-17 - 7	0.06531	0.0014	0.8036	0.015	0.08914	0.0011	0.16387	598.7	8.6	550.4	6.2	787	46	69.94	504	98.4	1411	14.91
M16-17	M16-17 - 8	0.06401	0.0012	1.009	0.02	0.1143	0.0015	0.88326	708.6	10	697.4	8.6	740	38	94.24	1020	290	2637	9.12
M16-17	M16-17 - 9	0.2315	0.0053	1.229	0.039	0.039	0.0016	0.94187	812	18	246.8	9.8	3059	36	8.07	5380	3620	1508	0.43
M16-24	M16-24 - 1	0.06582	0.0012	0.7798	0.015	0.08612	0.0012	0.87348	585.5	8.9	532.5	6.9	802	38	66.40	5290	2704	2392	0.869
M16-24	M16-24 - 10	0.1338	0.0096	1.678	0.065	0.0949	0.0038	-0.59872	992	24	586	22	2030	130	28.87	1840	736	409	0.551
M16-24	M16-24 - 11	0.06532	0.0013	0.814	0.018	0.0895	0.0013	0.62749	604.1	10	553.2	7.8	786	45	70.38	858	366	474	1.311
M16-24	M16-24 - 12	0.0743	0.0021	0.637	0.018	0.0625	0.0012	0.48606	500.8	11	390.9	7.4	1035	55	37.77	209.1	84.75	147.4	1.79
M16-24	M16-24 - 13	0.0601	0.0018	0.61	0.017	0.0726	0.0009	0.019605	483.3	11	451.7	5.4	602	65	75.03	163.8	72.7	107.8	1.519
M16-24	M16-24 - 14	0.06369	0.0012	0.737	0.016	0.08451	0.001	0.79608	561.6	9.1	522.9	6.2	733	42	71.34	1723	698.8	669.1	0.981
M16-24	M16-24 - 15	0.05846	0.001	0.8047	0.015	0.0995	0.0014	0.91234	599.6	8.7	611.5	7.9	548	39	111.59	4812	1802	2829	1.621
M16-24	M16-24 - 16	0.069	0.0019	0.51	0.013	0.05358	0.00079	0.1782	418.2	8.8	336.4	4.8	886	58	37.97	190.1	100.7	161.4	1.617
M16-24	M16-24 - 17	0.05955	0.0012	0.75	0.016	0.09093	0.0011	0.47477	567.5	9.1	561	6.6	592	46	94.76	1005	407	363	0.9123
M16-24	M16-24 - 18	0.0614	0.0022	0.771	0.029	0.0916	0.0013	0.28373	579	16	564.7	7.8	646	76	87.41	173.8	76	96.6	1.28
M16-24	M16-24 - 19	0.0742	0.0024	0.658	0.019	0.066	0.0033	0.96512	512.2	12	412	20	1028	66	40.08	6280	3810	2854	0.768
M16-24	M16-24 - 2	0.0894	0.0038	0.567	0.024	0.04613	0.00083	0.15857	455	16	290.7	5.1	1397	81	20.81	276	146.3	207	1.396
M16-24	M16-24 - 20	0.0594	0.0018	0.715	0.02	0.08757	0.0011	0.074313	548	12	541.1	6.4	560	68	96.63	162.2	64.52	90.7	1.405
M16-24	M16-24 - 21	0.05903	0.001	0.77	0.016	0.0948	0.0014	0.91251	579.4	9.1	583.8	8.4	567	39	102.96	7010	2790	2710	0.9893
M16-24	M16-24 - 22	0.06773	0.0013	0.831	0.019	0.0894	0.0019	0.86988	614.2	10	552	11	860	40	64.19	2870	4910	1754	0.45
M16-24	M16-24 - 23	0.0575	0.0027	0.74	0.028	0.0912	0.0016	-0.04961	561	17	562.3	9.6	512	100	109.82	172.7	74.8	89.8	1.199
M16-24	M16-24 - 24	0.06883	0.0014	0.841	0.016	0.08792	0.00098	0.45631	620	8.9	543.2	5.8	893	42	60.83	1670	876	1900	2.073
M16-24	M16-24 - 25	0.0773	0.0025	0.935	0.029	0.087	0.0012	0.18213	669	15	537.5	7.4	1147	63	46.86	182	61.3	80.8	1.297
M16-24	M16-24 - 26	0.0995	0.0025	0.7114	0.014	0.0525	0.00081	0.01336	545.2	8.5	329.8	5	1604	50	20.56	2166	1958	1172	0.598
M16-24	M16-24 - 27	0.06147	0.0011	0.72	0.018	0.0854	0.002	0.97158	549.4	11	528	12	658	39	80.24	7270	3340	3230	0.96
M16-24	M16-24 - 28	0.0594	0.0018	0.747	0.022	0.09171	0.0011	0.060045	565	13	565.6	6.7	564	67	100.28	190.7	69.9	88.6	1.2548
M16-24	M16-24 - 29	0.0584	0.0018	0.697	0.021	0.0861	0.0012	0.23727	536	12	532.7	7.3	533	66	99.94	173.9	66.8	83.9	1.24
M16-24	M16-24 - 3	0.06128	0.0013	0.699	0.015	0.08366	0.0011	0.58739	538.2	9.1	518.3	6.7	651	44	79.62	1023	407.7	383.3	0.9251
M16-24	M16-24 - 30	0.0587	0.0018	0.739	0.02	0.09063	0.0012	-0.04407	562	12	559.8	7	545	65	102.72	207.7	80.4	98.6	1.2223

Zircon U–Pb geochronology

Sample No.	Sample - spot	$^{207}Pb/^{206}Pb$	± 2SE	$^{207}Pb/^{235}U$	± 2SE	$^{206}Pb/^{238}U$	± 2SE	Error Correlation 6/38 vs 7/35	Age $^{207}Pb/^{235}U$	± 2SE	Age $^{206}Pb/^{238}U$	± 2SE	Age $^{207}Pb/^{206}Pb$	± 2SE	Concordance 7/6 vs 6/38	Pb (PPM)	Th (PPM)	U (PPM)	U/Th
M16-24	M16-24 - 4	0.06444	0.0012	0.7922	0.014	0.08937	0.001	0.50342	592.3	7.8	551.8	6	755	40	73.09	10980	5790	3430	0.59
M16-24	M16-24 - 5	0.0787	0.0024	0.477	0.013	0.04373	0.00066	0.18874	395.4	8.9	275.9	4.1	1177	59	23.44	305.4	178.2	251.3	1.393
M16-24	M16-24 - 6	0.0618	0.0019	0.778	0.024	0.0904	0.0012	0.21571	582	14	558	7.3	665	66	83.91	155.4	61.8	81.3	1.2917
M16-24	M16-24 - 7	0.0598	0.0017	0.761	0.021	0.09191	0.001	0.044621	574	12	566.8	6.1	599	62	94.62	172.6	71	89.2	1.2321
M16-24	M16-24 - 8	0.0618	0.0016	0.757	0.018	0.0889	0.001	0.071223	572.4	11	549	6.2	685	57	80.15	271.6	112	130.7	1.1597
M16-24	M16-24 - 9	0.06343	0.0012	0.84	0.026	0.0946	0.0025	0.96023	618	15	582	15	722	39	80.61	4575	1657	1428	0.86
M16-32	M16-32 - 1	0.16568	0.0029	10.879	0.18	0.479	0.0044	0.58114	2513	16	2522.7	19	2514.5	30	100.33	3613	296.9	215.5	0.7294
M16-32	M16-32 - 10	0.1685	0.003	11.01	0.19	0.4685	0.0044	0.38891	2523.4	16	2477	19	2544	30	97.37	2831	244.7	155.3	0.6285
M16-32	M16-32 - 11	0.1671	0.0031	10.887	0.19	0.4692	0.0048	0.39347	2513.5	16	2480	21	2527	31	98.14	1063	94.6	65.8	0.6904
M16-32	M16-32 - 12	0.1679	0.003	10.727	0.19	0.4581	0.0053	0.70884	2498.9	16	2432	23	2539	30	95.79	1367	116.6	177.1	1.488
M16-32	M16-32 - 13	no value	NAN	no value	NAN	no value	NAN	NaN	no value	NAN	no value	NAN	no value	NAN	#VALUE!	Below LOD	Below LOD	Below LOD	no value
M16-32	M16-32 - 14	0.167	0.0033	10.57	0.2	0.456	0.0054	0.4077	2485	17	2421	24	2526	34	95.84	726	63.8	50.7	0.788
M16-32	M16-32 - 15	0.1651	0.003	10.602	0.18	0.4631	0.0044	0.418	2489	16	2453	19	2508	30	97.81	1089	95.5	101.7	1.0532
M16-32	M16-32 - 16	0.1675	0.0032	10.72	0.19	0.4608	0.0047	0.44503	2498.4	17	2443	21	2531	32	96.52	857	74.5	57.1	0.7572
M16-32	M16-32 - 17	0.1671	0.0032	10.82	0.2	0.4662	0.0049	0.38049	2507.7	17	2466	22	2528	32	97.55	792	68.7	59.2	0.87
M16-32	M16-32 - 18	0.1704	0.0031	11.216	0.19	0.4752	0.0046	0.41972	2541.3	16	2506	20	2560	31	97.89	1981	167	114.2	0.677
M16-32	M16-32 - 19	0.1647	0.0031	10.544	0.19	0.4614	0.0046	0.46584	2484.4	16	2447	20	2505	31	97.68	744	66.1	73.52	1.109
M16-32	M16-32 - 2	0.1633	0.0032	10.65	0.2	0.4761	0.0056	0.4764	2491.8	17	2510	24	2489	33	100.84	567	45.16	38.19	0.8399
M16-32	M16-32 - 20	0.16557	0.003	10.85	0.18	0.4734	0.0046	0.51185	2510.4	16	2498	20	2514.2	30	99.36	1682	139	154.9	1.235
M16-32	M16-32 - 21	0.1602	0.0029	10.14	0.18	0.4563	0.005	0.57484	2448.3	17	2423	22	2456	31	98.66	1214	105.3	92.5	0.8807
M16-32	M16-32 - 22	0.1629	0.0032	10.341	0.18	0.4592	0.0048	0.2372	2464.8	16	2436	21	2487	33	97.95	979	84.7	60.7	0.7158
M16-32	M16-32 - 23	0.15816	0.0028	9.02	0.17	0.4111	0.0049	0.82035	2340.6	17	2219	22	2436	30	91.09	1116	106.4	224.8	2.107
M16-32	M16-32 - 24	0.1631	0.0029	10.05	0.19	0.4422	0.0054	0.80609	2439	18	2361	24	2487	30	94.93	1598	135.1	127.9	0.932
M16-32	M16-32 - 25	0.1659	0.0033	10.39	0.19	0.451	0.0046	0.28355	2469.9	17	2399	21	2515	33	95.39	944	79	57.4	0.7157
M16-32	M16-32 - 26	0.16229	0.0028	9.596	0.16	0.4242	0.004	0.58285	2396.5	15	2279.2	18	2479.7	30	91.91	777	64.44	276.5	4.207
M16-32	M16-32 - 27	0.1641	0.003	10.643	0.19	0.4655	0.0046	0.36085	2491.6	16	2464	20	2501	32	98.52	891	73	62.7	0.846
M16-32	M16-32 - 28	0.1692	0.0036	9.89	0.2	0.4189	0.0049	0.41847	2423	19	2255	22	2551	35	88.40	1303	109	97.9	0.8888
M16-32	M16-32 - 29	0.1672	0.0032	11.014	0.2	0.4725	0.0048	0.34308	2523.4	17	2494	21	2528	32	98.66	683	55.5	74	1.3103
M16-32	M16-32 - 3	0.16462	0.0029	10.976	0.18	0.4858	0.0046	0.49385	2521.2	16	2552	20	2502.8	30	101.97	4610	371	185	0.504
M16-32	M16-32 - 30	0.16738	0.003	11.106	0.18	0.4744	0.0045	0.49009	2531.7	15	2503	20	2530.7	30	98.91	2550	202.1	139.7	0.682

Zircon U–Pb geochronology

Sample No.	Sample - spot	$^{207}Pb/^{206}Pb$	± 2SE	$^{207}Pb/^{235}U$	± 2SE	$^{206}Pb/^{238}U$	± 2SE	Error Correlation 6/38 vs 7/35	Age $^{207}Pb/^{235}U$	± 2SE	Age $^{206}Pb/^{238}U$	± 2SE	Age $^{207}Pb/^{206}Pb$	± 2SE	Concordance 7/6 vs 6/38	Pb (PPM)	Th (PPM)	U (PPM)	U/Th
M16-32	M16-32 - 31	0.1646	0.0031	10.73	0.19	0.4682	0.0047	0.42015	2500.7	17	2475	21	2506	32	98.76	939	75.5	55.2	0.7161
M16-32	M16-32 - 4	0.1624	0.0031	10.18	0.19	0.4608	0.0048	0.52647	2451.3	17	2442	21	2482	33	98.39	814	65.1	59.07	0.922
M16-32	M16-32 - 5	0.1643	0.003	10.858	0.19	0.481	0.0048	0.38681	2511	16	2531	21	2502	32	101.16	1630	127	91.1	0.7305
M16-32	M16-32 - 6	0.1632	0.0031	10.501	0.19	0.4691	0.005	0.34874	2479.8	17	2479	22	2490	31	99.56	859	70.7	52.1	0.7435
M16-32	M16-32 - 7	0.1642	0.0031	10.702	0.19	0.4706	0.0049	0.31756	2498.2	17	2486	21	2500	32	99.44	837	68.6	61	0.894
M16-32	M16-32 - 8	0.16449	0.0029	10.356	0.17	0.4579	0.0041	0.63275	2466.9	15	2430	18	2502	29	97.12	11300	971	496	0.5143
M16-32	M16-32 - 9	0.16387	0.0029	10.134	0.17	0.4494	0.0044	0.51886	2446.5	16	2392	20	2496	31	95.83	967	81.83	143.3	1.745
M16-33	M16-33 - 1	0.06799	0.0013	1.216	0.022	0.12836	0.0012	0.33199	807.5	10	778.5	6.8	867	39	89.79	1839	494	391.7	0.7887
M16-33	M16-33 - 10	0.0904	0.0024	1.032	0.025	0.08328	0.00099	0.096475	722.4	13	515.6	5.9	1431	49	36.03	336	117.7	151.1	1.298
M16-33	M16-33 - 11	0.0696	0.0018	1.235	0.03	0.1288	0.0015	0.14107	817	13	781.4	8.5	910	51	85.87	314	86	126	1.441
M16-33	M16-33 - 12	0.0914	0.0024	1.04	0.026	0.08213	0.001	0.31301	724	13	508.8	6.1	1452	52	35.04	238	74	142.3	1.882
M16-33	M16-33 - 13	0.0876	0.0023	0.927	0.026	0.07671	0.00096	0.30815	666	13	476.4	5.7	1374	54	34.67	252.1	87.4	171.3	1.959
M16-33	M16-33 - 2	0.59	0.059	88	11	1.002	0.099	0.73478	4500	130	4450	340	4420	170	100.68	56.5	0.041	0.288	-216
M16-33	M16-33 - 3	no value	NAN	no value	NAN	no value	NAN	NaN	no value	NAN	no value	NAN	no value	NAN	#VALUE!	Below LOD	Below LOD	Below LOD	no value
M16-33	M16-33 - 4	0.0682	0.0016	1.234	0.027	0.13024	0.0014	0.23959	815.1	12	789.2	8.2	867	48	91.03	591	157.2	124.9	0.774
M16-33	M16-33 - 5	0.06742	0.0015	1.109	0.023	0.11795	0.0013	0.23138	757.7	11	718.7	7.6	851	46	84.45	660	190	182	0.992
M16-33	M16-33 - 6	0.06557	0.0013	1.15	0.021	0.12615	0.0012	0.33073	777.7	10	765.8	7.1	792	42	96.69	1362	388	331.6	0.868
M16-33	M16-33 - 7	0.06626	0.0014	1.113	0.024	0.1219	0.0015	0.63122	759.7	11	741.6	8.8	824	44	90.00	617	173.4	247.6	1.413
M16-33	M16-33 - 8	0.0655	0.0017	1.068	0.025	0.1164	0.0015	0.14941	737	12	710.6	8.4	798	58	89.05	463	152	172	1.208
M16-33	M16-33 - 9	0.06603	0.0013	1.186	0.022	0.13033	0.0013	0.21336	794.5	10	789.7	7.2	807	43	97.86	1880	574	401	0.726
M16-34	M16-34 - 1	0.1683	0.003	10.52	0.2	0.4554	0.0061	0.81439	2482	18	2418	27	2540	30	95.20	2256	205.1	154	0.7455
M16-34	M16-34 - 10	0.1672	0.0034	10.78	0.2	0.4637	0.005	0.21119	2503.1	17	2455	22	2530	35	97.04	482.1	43.11	36.8	0.8461
M16-34	M16-34 - 11	0.1642	0.0029	10.837	0.18	0.4769	0.0044	0.53989	2508.9	15	2514.6	19	2498.7	30	100.64	6870	557	315.9	0.5786
M16-34	M16-34 - 12	0.16483	0.0029	11.371	0.19	0.4991	0.0048	0.6718	2554.7	16	2610	21	2506	30	104.15	4560	334	258.9	0.8002
M16-34	M16-34 - 13	0.16365	0.0029	10.962	0.18	0.4834	0.0044	0.52039	2519.7	15	2541.9	19	2493.9	29	101.92	4075	322.3	233.9	0.7377
M16-34	M16-34 - 14	0.162	0.0029	10.394	0.18	0.4643	0.0046	0.46226	2470.5	16	2458	20	2477	31	99.23	991	80.8	112.7	1.43
M16-34	M16-34 - 15	0.1614	0.0031	10.434	0.19	0.4671	0.005	0.46497	2475.6	17	2470	22	2468	32	100.08	792	64.1	65.4	1.043
M16-34	M16-34 - 16	0.16324	0.0028	10.332	0.17	0.4582	0.0042	0.52325	2465.1	15	2431.2	18	2489.1	29	97.67	3845	300.7	265.3	0.9111
M16-34	M16-34 - 17	0.1629	0.0031	10.543	0.18	0.4668	0.0046	0.36414	2482.9	16	2469	20	2488	32	99.24	806	62.6	77.6	1.259
M16-34	M16-34 - 18	0.15776	0.0028	9.063	0.15	0.4149	0.0039	0.53216	2344.5	15	2237	18	2431.3	30	92.01	1328	118.4	322.3	2.756

Zircon U–Pb geochronology

Sample No.	Sample - spot	$^{207}Pb/^{206}Pb$	± 2SE	$^{207}Pb/^{235}U$	± 2SE	$^{206}Pb/^{238}U$	± 2SE	Error Correlation 6/38 vs 7/35	Age $^{207}Pb/^{235}U$	± 2SE	Age $^{206}Pb/^{238}U$	± 2SE	Age $^{207}Pb/^{206}Pb$	± 2SE	Concordance 7/6 vs 6/38	Pb (PPM)	Th (PPM)	U (PPM)	U/Th
M16-34	M16-34 - 19	0.1598	0.0032	10.57	0.19	0.4798	0.005	0.29736	2485.8	17	2526	22	2453	33	102.98	676	52.2	51.5	1.0101
M16-34	M16-34 - 2	0.1738	0.0057	10.58	0.37	0.4423	0.0056	0.043779	2476	19	2360	25	2568	35	91.90	535	48.56	41.05	0.839
M16-34	M16-34 - 20	0.16568	0.0029	10.902	0.18	0.476	0.0045	0.53774	2514.5	15	2510	20	2514.6	29	99.82	3335	256.3	213.1	0.8479
M16-34	M16-34 - 21	0.164	0.0033	10.55	0.19	0.4661	0.005	0.20192	2484.2	17	2466	22	2496	34	98.80	636	49.4	50	1.0279
M16-34	M16-34 - 22	0.16615	0.003	10.531	0.18	0.4598	0.0044	0.58544	2482.1	16	2438	20	2519.3	30	96.77	2629	205	190.7	0.9453
M16-34	M16-34 - 23	0.16621	0.0029	10.83	0.18	0.4705	0.0046	0.62943	2508.3	15	2486	20	2520.1	29	98.65	4827	371.7	246.7	0.6748
M16-34	M16-34 - 24	0.1973	0.0039	13.16	0.24	0.484	0.005	0.34426	2693	18	2544	22	2801	32	90.82	1119	65.3	55.38	0.8627
M16-34	M16-34 - 25	0.16368	0.003	9.928	0.17	0.4387	0.0041	0.51914	2427.5	16	2344.8	18	2495	30	93.98	1452	115	171.4	1.509
M16-34	M16-34 - 26	0.1648	0.003	11.29	0.22	0.495	0.0066	0.80725	2545	18	2591	28	2506	31	103.39	2950	186	128.7	0.724
M16-34	M16-34 - 27	0.1615	0.0029	9.01	0.18	0.4037	0.0059	0.8426	2341	18	2185	27	2472	30	88.39	1192	97.3	133	1.46
M16-34	M16-34 - 28	0.16404	0.0029	10.531	0.18	0.4613	0.0044	0.56939	2482.1	16	2445	19	2497.7	30	97.89	1565	127.2	207.6	1.614
M16-34	M16-34 - 29	0.16476	0.003	10.685	0.18	0.4668	0.0044	0.48453	2496.2	15	2469	19	2505.9	30	98.53	3050	245.5	200.5	0.8082
M16-34	M16-34 - 3	0.1705	0.0031	10.759	0.19	0.4573	0.0046	0.5268	2501.8	16	2427	20	2561	31	94.77	1592	145	119.6	0.8402
M16-34	M16-34 - 30	0.1612	0.0031	9.63	0.21	0.4326	0.0054	0.7432	2401	20	2317	24	2465	33	94.00	982	83.2	89.15	1.052
M16-34	M16-34 - 4	0.17017	0.003	11.127	0.18	0.4748	0.0043	0.4705	2534.5	15	2504.3	19	2558.5	30	97.88	3101	281.4	202.6	0.7171
M16-34	M16-34 - 5	0.1667	0.0031	10.472	0.18	0.4552	0.0046	0.45097	2477.5	16	2418	20	2524	31	95.80	1495	135	105.5	0.7759
M16-34	M16-34 - 6	0.17039	0.003	11.169	0.19	0.4744	0.0047	0.53672	2537.5	16	2503	21	2561.7	30	97.71	2156	186.2	152.3	0.805
M16-34	M16-34 - 7	0.1664	0.0035	9.38	0.18	0.4094	0.0047	0.32473	2377	18	2212	22	2519	35	87.81	522	44.3	51.4	1.173
M16-34	M16-34 - 8	0.17087	0.003	11.163	0.19	0.4727	0.0044	0.57231	2537.5	16	2495.4	19	2565.4	30	97.27	3627	314.6	266.9	0.8466
M16-34	M16-34 - 9	0.1688	0.0031	10.673	0.19	0.4546	0.0047	0.61265	2495.8	16	2415	21	2548	31	94.78	1128	102.4	135.5	1.3216
M16-35	M16-35 - 1	0.189	0.0035	7.84	0.19	0.2976	0.0056	0.91955	2213	21	1679	28	2732	31	61.46	3960	375	500	1.278
M16-35	M16-35 - 10	0.16512	0.0029	10.899	0.19	0.477	0.0054	0.93892	2515.1	16	2515	23	2508.6	29	100.26	19090	1605	1722	1.0658
M16-35	M16-35 - 11	0.1695	0.0031	9.896	0.17	0.4246	0.0041	0.46384	2425.8	15	2281	19	2554	31	89.31	1085	104.1	126.5	1.2267
M16-35	M16-35 - 12	0.17751	0.0031	11.108	0.18	0.4544	0.0042	0.68545	2531.8	15	2414.5	19	2629.9	29	91.81	4725	363.3	479.3	1.336
M16-35	M16-35 - 13	0.1691	0.0031	10.644	0.18	0.4534	0.0046	0.45496	2491.8	16	2410	21	2551	31	94.47	943	80.2	81.7	1.014
M16-35	M16-35 - 14	0.1713	0.0034	8.93	0.17	0.3782	0.0049	0.64489	2329	18	2067	23	2571	33	80.40	830	70.3	67.16	0.963
M16-35	M16-35 - 15	0.16864	0.003	10.391	0.17	0.4474	0.0043	0.48918	2470.4	16	2385	19	2543.3	30	93.78	1575	135.3	142.7	1.079
M16-35	M16-35 - 16	0.16897	0.003	10.367	0.17	0.4439	0.0043	0.62063	2468.3	16	2368	19	2547.5	30	92.95	1503	132.1	143.8	1.1041
M16-35	M16-35 - 17	0.175	0.0033	10.147	0.18	0.4197	0.0046	0.35579	2448.3	16	2259	21	2606	31	86.68	901	80.4	95.2	1.202
M16-35	M16-35 - 18	0.1743	0.0032	11.43	0.27	0.4733	0.0098	0.92977	2558	22	2498	43	2599	31	96.11	2450	164	151.9	1.061
M16-35	M16-35 - 19	0.1717	0.0033	9.267	0.16	0.3906	0.0042	0.23867	2363.9	16	2125	19	2575	33	82.52	673	65.55	74.7	1.15

Zircon U–Pb geochronology

Sample No.	Sample - spot	$^{207}Pb/^{206}Pb$	± 2SE	$^{207}Pb/^{235}U$	± 2SE	$^{206}Pb/^{238}U$	± 2SE	Error Correlation 6/38 vs 7/35	Age $^{207}Pb/^{235}U$	± 2SE	Age $^{206}Pb/^{238}U$	± 2SE	Age $^{207}Pb/^{206}Pb$	± 2SE	Concordance 7/6 vs 6/38	Pb (PPM)	Th (PPM)	U (PPM)	U/Th
M16-35	M16-35 - 2	0.1966	0.0036	8.805	0.16	0.3221	0.0038	0.68756	2316.7	17	1800	18	2798	31	64.33	1684	116.4	126.5	1.086
M16-35	M16-35 - 20	0.2612	0.0055	9.26	0.22	0.2589	0.0045	0.72623	2364	22	1483	23	3251	33	45.62	2069	89.2	179.2	2.006
M16-35	M16-35 - 21	0.3139	0.0062	8.69	0.23	0.2	0.0046	0.92006	2302	25	1175	25	3539	30	33.20	1797	71.1	134.5	1.936
M16-35	M16-35 - 22	0.5084	0.0094	3.662	0.09	0.0524	0.0011	0.92551	1561	19	329.4	6.8	4266	27	7.72	7340	1373	1167	0.8496
M16-35	M16-35 - 23	0.1731	0.0033	10.37	0.19	0.4341	0.0056	0.58713	2468.8	17	2323	25	2587	32	89.80	923	85.1	68.6	0.8123
M16-35	M16-35 - 24	0.1744	0.0031	9.54	0.23	0.3955	0.01	0.98767	2388	23	2143	47	2600	29	82.42	9990	854	1294	1.534
M16-35	M16-35 - 25	0.1703	0.0032	6.67	0.17	0.2854	0.0066	0.92236	2069	23	1616	33	2560	31	63.13	1322	123	165.1	1.344
M16-35	M16-35 - 26	0.1617	0.0031	10.569	0.19	0.4722	0.0051	0.39215	2486	17	2493	22	2473	33	100.81	891	73.2	54.1	0.737
M16-35	M16-35 - 27	0.16066	0.0029	9.86	0.19	0.4429	0.0052	0.88477	2420	18	2363	24	2462	30	95.98	1865	165.4	165.8	0.9951
M16-35	M16-35 - 28	0.16323	0.0028	10.818	0.18	0.4777	0.0052	0.91317	2507.1	16	2518	23	2489.2	29	101.16	29190	2408	2231	0.9273
M16-35	M16-35 - 29	0.15933	0.0028	9.416	0.16	0.4278	0.0042	0.62208	2378.9	15	2296	19	2448.6	30	93.77	2059	188	191.8	1.02
M16-35	M16-35 - 3	0.161	0.003	10.631	0.19	0.4748	0.0047	0.35941	2491.3	16	2506	20	2466	31	101.62	1013	80.9	62.28	0.7541
M16-35	M16-35 - 30	0.7912	0.014	8.72	0.19	0.07946	0.0012	0.95722	2308	20	492.8	6.9	4943	31	9.97	28820	2430	1892	0.79
M16-35	M16-35 - 31	0.1729	0.0035	10	0.2	0.4166	0.0043	0.43443	2431	17	2245	19	2588	31	86.75	1251	97.6	118.4	1.2156
M16-35	M16-35 - 32	0.1982	0.0041	6.43	0.26	0.236	0.01	0.96688	2038	36	1371	54	2809	34	48.81	1404	120.5	138.9	1.147
M16-35	M16-35 - 4	0.1778	0.0032	11.09	0.18	0.4483	0.0043	0.41879	2530.4	15	2388	19	2632	29	90.73	2680	194.6	206.5	1.0521
M16-35	M16-35 - 5	0.1636	0.0032	10.367	0.19	0.4561	0.005	0.29707	2468.6	16	2422	22	2495	33	97.07	701	57.05	64.8	1.118
M16-35	M16-35 - 6	0.1621	0.0029	10.205	0.18	0.455	0.0056	0.79262	2452.4	17	2417	25	2477	31	97.58	1776	151.6	168.3	1.104
M16-35	M16-35 - 7	0.17354	0.003	9.673	0.17	0.4022	0.0048	0.9137	2403.4	16	2178	22	2591.7	29	84.04	10710	946	1327	1.409
M16-35	M16-35 - 8	0.16111	0.0029	10.349	0.19	0.4632	0.0053	0.75991	2465.4	17	2458	24	2466.4	30	99.66	945	80.2	112.9	1.384
M16-35	M16-35 - 9	0.1645	0.003	9.766	0.17	0.4294	0.0043	0.44883	2414.3	16	2303	19	2501	31	92.08	1047	87.8	97.9	1.0953
M16-45	M16-45 - 1	0.664	0.021	25.6	1.2	0.279	0.012	0.78211	3323	47	1578	58	4659	49	33.87	435	126.3	4.48	0.03641
M16-45	M16-45 - 10	0.0609	0.0023	0.721	0.024	0.08549	0.0012	-0.05476	550	14	529.4	7.2	613	77	86.36	506.1	207.4	65.7	0.3105
M16-45	M16-45 - 11	0.0574	0.0019	0.695	0.021	0.08757	0.0012	-0.12483	537	12	541.1	7.2	489	74	110.65	270	109.1	66.8	0.6041
M16-45	M16-45 - 12	0.0582	0.0021	0.703	0.023	0.08734	0.0011	-0.10394	538	14	539.7	6.5	518	77	104.19	979	402	97.7	0.2398
M16-45	M16-45 - 13	0.0579	0.0021	0.693	0.024	0.08647	0.0011	-0.02339	533	14	534.6	6.5	517	75	103.40	550	243	72.4	0.397
M16-45	M16-45 - 14	0.0573	0.0027	0.694	0.032	0.0874	0.0016	0.13152	533	19	540.1	9.5	500	110	108.02	242	107.4	68.6	0.624
M16-45	M16-45 - 15	0.0572	0.0018	0.676	0.02	0.08675	0.0011	0.19922	524	13	536.2	6.7	492	71	108.98	527	223.6	70.8	0.3102
M16-45	M16-45 - 16	0.922	0.045	110.2	8.6	0.933	0.075	0.84642	4744	83	4130	250	5236	100	78.88	149.2	15.4	0.65	0.0415
M16-45	M16-45 - 17	0.0628	0.002	0.725	0.024	0.0847	0.0011	0.22429	554	14	524.1	6.6	679	69	77.19	427	174.6	63.6	0.347
M16-45	M16-45 - 18	0.0648	0.0022	0.762	0.025	0.08683	0.0011	0.10769	577	15	536.7	6.6	761	70	70.53	949	394.1	121	0.3052

Zircon U–Pb geochronology

Sample No.	Sample - spot	$^{207}Pb/^{206}Pb$	± 2SE	$^{207}Pb/^{235}U$	± 2SE	$^{206}Pb/^{238}U$	± 2SE	Error Correlation 6/38 vs 7/35	Age $^{207}Pb/^{235}U$	± 2SE	Age $^{206}Pb/^{238}U$	± 2SE	Age $^{207}Pb/^{206}Pb$	± 2SE	Concordance 7/6 vs 6/38	Pb (PPM)	Th (PPM)	U (PPM)	U/Th
M16-45	M16-45 - 19	0.063	0.0022	0.736	0.024	0.08507	0.0012	0.039857	559	14	526.2	7.1	707	73	74.43	240	99.6	60.68	0.658
M16-45	M16-45 - 2	0.0573	0.0023	0.7	0.025	0.0882	0.0012	0.093438	541	15	544.5	7.3	478	85	113.91	438	177.6	65.5	0.3758
M16-45	M16-45 - 20	0.0597	0.0021	0.696	0.023	0.08541	0.0011	0.054709	538	14	528.9	6.8	562	75	94.11	235	93	72.8	0.79
M16-45	M16-45 - 21	0.0689	0.0036	0.813	0.042	0.0865	0.0018	0.035303	605	24	536.8	10	880	110	61.00	232	80.6	34.92	0.4259
M16-45	M16-45 - 22	0.06	0.0022	0.711	0.023	0.08667	0.0012	-0.09907	544	14	536.3	7	576	79	93.11	210.4	83	64.4	0.764
M16-45	M16-45 - 23	0.0624	0.002	0.755	0.021	0.08748	0.0012	0.014308	571	13	540.5	6.9	662	69	81.65	469	186.4	76.1	0.4031
M16-45	M16-45 - 24	0.0586	0.002	0.709	0.023	0.08721	0.0011	-0.02711	542	13	539	6.5	525	75	102.67	272.7	98.1	80.5	0.8416
M16-45	M16-45 - 25	0.0594	0.002	0.71	0.022	0.08539	0.0011	0.043444	544	13	528.2	6.4	570	71	92.67	336	123.7	84.9	0.7046
M16-45	M16-45 - 26	0.0593	0.0019	0.713	0.021	0.08656	0.0011	-0.00044	545	13	535.6	6.7	569	71	94.13	770	270	85	0.3313
M16-45	M16-45 - 27	0.0578	0.0018	0.68	0.019	0.0841	0.001	-0.03567	527.4	12	520.5	6.1	508	66	102.46	386	146.2	93.6	0.6611
M16-45	M16-45 - 28	0.0585	0.0019	0.695	0.02	0.0862	0.0012	0.13798	534	12	533	7.4	533	71	100.00	318	113.9	72.3	0.665
M16-45	M16-45 - 29	0.0596	0.0021	0.697	0.024	0.08357	0.0012	0.060479	536	14	517.3	7.1	567	81	91.23	183	67.6	63.8	1.013
M16-45	M16-45 - 3	0.0593	0.0019	0.726	0.023	0.08764	0.0011	0.16758	556	14	541.5	6.5	580	66	93.36	904	357	89.7	0.2512
M16-45	M16-45 - 30	0.0575	0.002	0.685	0.022	0.08642	0.0012	0.017881	531	13	534.2	6.9	480	76	111.29	239.3	83.3	75.4	0.9295
M16-45	M16-45 - 4	0.0585	0.0024	0.721	0.025	0.0892	0.0015	-0.01855	551	15	550.4	8.8	527	86	104.44	440	176.5	61.95	0.3583
M16-45	M16-45 - 5	0.0861	0.0054	1.067	0.065	0.0902	0.0019	0.13661	731	32	556	11	1360	110	40.88	212	69	27.53	0.4067
M16-45	M16-45 - 6	0.0599	0.002	0.743	0.024	0.0896	0.0012	0.072509	563	14	553.1	7.3	585	75	94.55	359	140.7	57.3	0.4102
M16-45	M16-45 - 7	0.0573	0.0027	0.709	0.032	0.0885	0.0016	-0.124	543	19	546.8	9.4	505	100	108.28	187.1	73.7	28.4	0.395
M16-45	M16-45 - 8	0.0612	0.0022	0.733	0.025	0.08776	0.0012	0.078882	559	14	542.2	7	629	75	86.20	249.6	93.5	61	0.661
M16-45	M16-45 - 9	0.0594	0.0021	0.698	0.022	0.08516	0.0012	-0.00852	538	13	527.3	7	559	77	94.33	442	186	72.4	0.381
M16-46	M16-46 - 1	0.16269	0.0028	9.545	0.16	0.4229	0.0042	0.75427	2391.3	16	2273	19	2483.4	29	91.53	4230	364	534	1.4838
M16-46	M16-46 - 10	0.155	0.0028	7.87	0.18	0.3665	0.0052	0.95079	2214	21	2012	25	2401	31	83.80	3237	348.3	703.4	2.003
M16-46	M16-46 - 11	0.15591	0.0027	7.529	0.13	0.3487	0.0034	0.83488	2177	15	1928	16	2411.4	29	79.95	4630	539	774	1.405
M16-46	M16-46 - 12	0.15987	0.0029	8.55	0.22	0.3871	0.0079	0.95797	2291	23	2108	37	2454	30	85.90	3991	443	669	1.477
M16-46	M16-46 - 13	0.15971	0.0028	8.315	0.14	0.3761	0.0037	0.70558	2265.5	15	2058	17	2452	30	83.93	2640	382.2	476.7	1.2291
M16-46	M16-46 - 14	0.15065	0.0027	6.65	0.17	0.3188	0.006	0.96525	2063	23	1783	29	2353.8	30	75.75	4382	527	842	1.573
M16-46	M16-46 - 15	0.1216	0.0024	2.815	0.069	0.1678	0.0022	0.91323	1364	19	999.6	12	1978	35	50.54	1705	273	996	3.676
M16-46	M16-46 - 16	0.16565	0.0029	6.95	0.18	0.3025	0.0069	0.97315	2101	23	1701	34	2513.7	29	67.67	4820	913	807	0.895
M16-46	M16-46 - 17	0.16339	0.0028	9.909	0.16	0.4398	0.004	0.64897	2426.8	15	2349.7	18	2491.2	29	94.32	4394	428	552	1.281
M16-46	M16-46 - 18	0.16082	0.0028	8.868	0.15	0.3973	0.0039	0.77889	2324.5	15	2156	18	2464.5	29	87.48	3469	467.1	602.8	1.325
M16-46	M16-46 - 19	0.15649	0.0028	7.68	0.19	0.3541	0.0067	0.97297	2191	23	1952	32	2417.4	30	80.75	3726	453.7	695	1.524

Zircon U–Pb geochronology

Sample No.	Sample - spot	$^{207}Pb/^{206}Pb$	± 2SE	$^{207}Pb/^{235}U$	± 2SE	$^{206}Pb/^{238}U$	± 2SE	Error Correlation 6/38 vs 7/35	Age $^{207}Pb/^{235}U$	± 2SE	Age $^{206}Pb/^{238}U$	± 2SE	Age $^{207}Pb/^{206}Pb$	± 2SE	Concordance 7/6 vs 6/38	Pb (PPM)	Th (PPM)	U (PPM)	U/Th
M16-46	M16-46 - 2	0.16313	0.0029	9.394	0.15	0.4145	0.004	0.65698	2377.4	15	2235.3	18	2489.3	29	89.80	4010	325	460	1.534
M16-46	M16-46 - 20	0.1608	0.0028	8.647	0.15	0.3869	0.004	0.80972	2300.8	16	2108	19	2463.5	30	85.57	4200	450	629	1.421
M16-46	M16-46 - 21	0.1635	0.0028	9.816	0.16	0.434	0.004	0.65808	2417.8	15	2323.4	18	2491.8	29	93.24	6650	654	868	1.3261
M16-46	M16-46 - 22	0.16243	0.0029	9.392	0.16	0.4178	0.0039	0.54917	2376.4	16	2250.1	18	2481	30	90.69	1086	110.7	198.1	1.7946
M16-46	M16-46 - 23	0.15799	0.0028	7.318	0.13	0.335	0.0037	0.86058	2150.3	15	1862	18	2435.1	30	76.47	4060	639	758	1.1919
M16-46	M16-46 - 24	0.15996	0.0028	7.791	0.15	0.3531	0.005	0.92807	2208	18	1949	24	2455.9	29	79.36	9900	1402	938	0.6778
M16-46	M16-46 - 25	0.16116	0.0028	9.437	0.16	0.4226	0.0045	0.86168	2381.4	16	2272	20	2467.4	29	92.08	3647	311.4	559.4	1.813
M16-46	M16-46 - 26	0.1613	0.003	8.543	0.15	0.3846	0.0038	0.40901	2290.5	16	2097	18	2468	31	84.97	819	102.7	146.5	1.453
M16-46	M16-46 - 27	0.16163	0.0028	9.2	0.15	0.411	0.004	0.79306	2358.2	15	2219	18	2473	30	89.73	3290	288	620	2.082
M16-46	M16-46 - 28	0.15618	0.0027	7.618	0.12	0.3528	0.0033	0.56649	2186.8	14	1947.8	16	2414.1	30	80.68	3199	324.9	495	1.558
M16-46	M16-46 - 29	0.1604	0.0028	8.93	0.15	0.4023	0.004	0.82971	2332.7	15	2179	18	2459.4	29	88.60	5680	512	702	1.402
M16-46	M16-46 - 3	0.1641	0.0029	10.218	0.18	0.4504	0.0051	0.85598	2454.6	16	2396	23	2498.6	29	95.89	5100	401	545	1.428
M16-46	M16-46 - 30	0.16012	0.0028	8.42	0.14	0.3809	0.0035	0.70221	2278.4	15	2080.3	16	2457.1	30	84.66	4353	428.7	628.6	1.53
M16-46	M16-46 - 4	0.16369	0.0029	8.955	0.15	0.3948	0.0038	0.63822	2333.6	15	2145	18	2493.6	29	86.02	5390	500	677	1.387
M16-46	M16-46 - 5	0.16273	0.0028	9.097	0.15	0.4045	0.004	0.82436	2347.8	15	2190	18	2485	29	88.13	5839	516	759	1.5042
M16-46	M16-46 - 6	0.16371	0.0028	9.574	0.17	0.423	0.0045	0.85784	2393.9	16	2276	20	2493.9	29	91.26	4080	348	595	1.763
M16-46	M16-46 - 7	0.16203	0.0028	8.846	0.14	0.3957	0.0036	0.67366	2322.4	15	2149.1	17	2476.5	29	86.78	5643	520.1	741	1.438
M16-46	M16-46 - 8	0.16357	0.0029	10.15	0.19	0.449	0.0057	0.91086	2448.3	17	2390	25	2493.2	29	95.86	5880	505	580	1.208
M16-46	M16-46 - 9	0.1589	0.0028	9.022	0.15	0.4096	0.0038	0.76622	2339.9	15	2212.9	17	2443.4	30	90.57	6220	656	818	1.2188
M16-47	M16-47 - 1	0.06043	0.0011	0.827	0.017	0.0995	0.0013	0.90286	612	9.3	611.5	7.9	620	40	98.63	6790	1410	2175	3.33
M16-47	M16-47 - 10	0.06134	0.0011	0.8173	0.014	0.09709	0.00097	0.73446	606.7	8	597.3	5.7	650	38	91.89	803	185.9	2870	15.41
M16-47	M16-47 - 11	0.06363	0.0011	0.9127	0.016	0.10494	0.0012	0.84074	658.2	8.7	643.2	7	730	38	88.11	1480	420	2360	5.676
M16-47	M16-47 - 12	0.06245	0.0011	0.881	0.018	0.1031	0.0016	0.9182	641	9.9	632.6	9.6	689	38	91.81	1591	393	3430	8.611
M16-47	M16-47 - 13	0.06244	0.0012	0.892	0.017	0.10293	0.0011	0.63343	647.5	9.1	631.5	6.7	692	42	91.26	547	53.3	1527	28.44
M16-47	M16-47 - 14	0.06383	0.0013	1.006	0.03	0.1141	0.0024	0.92062	704	15	696	14	743	42	93.67	785	237	512.2	3.09
M16-47	M16-47 - 15	0.0695	0.0016	0.899	0.024	0.0937	0.0012	0.76429	651	13	577.3	6.9	913	45	63.23	829	248	1000	4.41
M16-47	M16-47 - 16	0.0612	0.0012	0.579	0.018	0.0689	0.0017	0.95404	463.8	11	429.4	10	644	41	66.68	4260	7.60E+03	2990	0.71
M16-47	M16-47 - 17	0.06466	0.0012	0.8755	0.016	0.0985	0.0016	0.84042	638.7	8.8	605.4	9.5	764	39	79.24	868	203	1794	8.98
M16-47	M16-47 - 18	0.06588	0.0013	1.147	0.022	0.12587	0.0013	0.52817	776.6	10	764.2	7.5	801	40	95.41	932	276.1	482	1.725
M16-47	M16-47 - 19	0.06395	0.0013	1.0047	0.018	0.11396	0.0011	0.20491	705.9	9.3	695.7	6.5	735	42	94.65	741	229.5	436.5	1.902
M16-47	M16-47 - 2	0.06802	0.0012	0.687	0.024	0.0734	0.0022	0.97304	530	14	456	13	871	38	52.35	1.94E+04	1.37E+04	3820	0.313

Zircon U–Pb geochronology

Sample No.	Sample - spot	$^{207}Pb/^{206}Pb$	± 2SE	$^{207}Pb/^{235}U$	± 2SE	$^{206}Pb/^{238}U$	± 2SE	Error Correlation 6/38 vs 7/35	Age $^{207}Pb/^{235}U$	± 2SE	Age $^{206}Pb/^{238}U$	± 2SE	Age $^{207}Pb/^{206}Pb$	± 2SE	Concordance 7/6 vs 6/38	Pb (PPM)	Th (PPM)	U (PPM)	U/Th
M16-47	M16-47 - 20	0.0594	0.0011	0.7327	0.013	0.08956	0.00089	0.4721	558.3	7.6	552.9	5.3	582	40	95.00	292	106	966	9.36
M16-47	M16-47 - 21	0.06519	0.0012	0.7644	0.014	0.08493	0.001	0.7733	576.2	8.4	525.4	6	780	38	67.36	806	151	1992	13.14
M16-47	M16-47 - 22	0.06349	0.0011	0.891	0.016	0.10194	0.0011	0.68945	646.6	8.4	625.7	6.6	723	38	86.54	1398	358	2250	6.33
M16-47	M16-47 - 23	0.06584	0.0013	1.203	0.023	0.13241	0.0013	0.19941	801.2	11	801.6	7.3	799	42	100.33	837	230.2	357.3	1.567
M16-47	M16-47 - 24	0.06419	0.0013	1.126	0.02	0.1262	0.0012	0.19421	765.5	9.7	766.1	7	750	42	102.15	1109	296.6	516	1.7323
M16-47	M16-47 - 25	0.06557	0.0013	1.218	0.023	0.1348	0.0015	0.43156	808.5	11	815.1	8.8	788	42	103.44	1346	322	455	1.423
M16-47	M16-47 - 26	0.06059	0.0014	0.877	0.02	0.1044	0.0011	0.36161	639.9	11	640.5	6.7	621	49	103.14	199	49.2	261.9	6.9
M16-47	M16-47 - 27	0.06389	0.0013	1.037	0.02	0.1174	0.0012	0.42493	721.8	9.8	715.6	7.1	733	42	97.63	867	237.9	359.2	1.493
M16-47	M16-47 - 3	0.06017	0.0011	0.805	0.016	0.0972	0.0014	0.8959	599.8	9.1	600	8.5	611	39	98.20	4070	1550	2320	2.75
M16-47	M16-47 - 4	0.07	0.0016	0.664	0.016	0.0689	0.0011	0.61376	516.8	9.7	429.5	6.6	931	48	46.13	522	71.5	1289	18.48
M16-47	M16-47 - 5	0.06216	0.0011	0.9111	0.016	0.10656	0.0011	0.66511	657.8	8.8	652.7	6.5	679	39	96.13	1830	345	1472	5.17
M16-47	M16-47 - 6	0.06219	0.0011	0.8713	0.016	0.10224	0.0011	0.86162	636	8.5	627.5	6.7	679	39	92.42	7750	2700	2468	1.89
M16-47	M16-47 - 7	0.06115	0.0011	0.906	0.018	0.1078	0.0014	0.79713	655.4	9.6	659.6	8	644	40	102.42	594	153.9	905	6.37
M16-47	M16-47 - 8	0.06262	0.0011	0.9064	0.016	0.10502	0.0011	0.60486	654.9	8.6	643.7	6.5	698	39	92.22	1108	310	1161	4.062
M16-47	M16-47 - 9	0.06618	0.0013	0.666	0.016	0.07285	0.001	0.8596	518.3	9.9	453.2	6.1	812	42	55.81	877	216	1348	6.47
M16-52	M16-52 - 1	0.731	0.019	31.2	1.2	0.3052	0.0093	0.79336	3510	38	1716	46	4807	43	35.70	456	9.33	7.57	0.807
M16-52	M16-52 - 10	0.1626	0.0038	0.7729	0.015	0.0348	0.00074	0.67465	582.1	8.4	220.5	4.6	2478	39	8.90	3660	2180	1870	0.872
M16-52	M16-52 - 11	0.0653	0.0015	0.419	0.028	0.0465	0.0031	0.96691	349	20	292	19	783	49	37.29	344	114.4	475	4.3
M16-52	M16-52 - 12	0.0601	0.0016	0.809	0.026	0.0986	0.0028	0.73584	602	14	606	17	613	56	98.86	169	63.1	426	8.2
M16-52	M16-52 - 13	0.0585	0.0026	0.737	0.029	0.091	0.0017	0.070577	560	18	561.2	9.9	503	94	111.57	191.8	76.4	38	0.4947
M16-52	M16-52 - 14	0.0625	0.0021	0.684	0.022	0.0795	0.0017	0.29506	530	14	493.2	10	698	69	70.66	219	85.9	112	1.46
M16-52	M16-52 - 15	0.0597	0.0031	0.714	0.035	0.0872	0.0017	0.065077	545	21	538.7	10	570	110	94.51	321	141	65.3	0.455
M16-52	M16-52 - 16	0.0649	0.0027	0.757	0.03	0.0865	0.0014	0.18267	574	18	534.6	8.1	720	91	74.25	333	137.1	57.7	0.422
M16-52	M16-52 - 17	0.06864	0.0013	0.7774	0.014	0.08227	0.00091	0.33687	584.5	7.9	509.6	5.4	886	39	57.52	5515	2312	1035	0.4487
M16-52	M16-52 - 18	0.0683	0.0017	0.589	0.019	0.0634	0.0022	0.81942	471	13	396	13	876	50	45.21	492	184	427	2.85
M16-52	M16-52 - 19	0.0578	0.0022	0.714	0.027	0.0888	0.0013	0.0767	548	16	548.1	7.7	524	85	104.60	335.4	136.8	56.6	0.4085
M16-52	M16-52 - 2	0.05852	0.0013	0.791	0.017	0.09712	0.0011	0.23266	590.9	9.7	597.5	6.6	548	51	109.03	275	103.7	219	2.1
M16-52	M16-52 - 20	0.06025	0.0013	0.721	0.02	0.0872	0.0018	0.71835	550.5	11	539.1	11	607	46	88.81	480	212	840	4.55
M16-52	M16-52 - 21	0.0744	0.0017	0.778	0.018	0.0763	0.0015	0.64402	583.8	10	473.7	9.1	1059	46	44.73	499	105.7	497	4.55
M16-52	M16-52 - 22	0.0606	0.0025	0.827	0.033	0.1011	0.0015	0.21952	614	18	621.1	8.5	603	91	103.00	289	122.2	92.8	0.749
M16-52	M16-52 - 23	0.0601	0.0015	0.737	0.018	0.08928	0.0011	0.38342	560.5	10	551.3	6.2	615	55	89.64	459	202	188	1.07

Zircon U–Pb geochronology

Sample No.	Sample - spot	$^{207}Pb/^{206}Pb$	± 2SE	$^{207}Pb/^{235}U$	± 2SE	$^{206}Pb/^{238}U$	± 2SE	Error Correlation 6/38 vs 7/35	Age $^{207}Pb/^{235}U$	± 2SE	Age $^{206}Pb/^{238}U$	± 2SE	Age $^{207}Pb/^{206}Pb$	± 2SE	Concordance 7/6 vs 6/38	Pb (PPM)	Th (PPM)	U (PPM)	U/Th
M16-52	M16-52 - 24	0.0613	0.0021	0.727	0.024	0.0867	0.0015	0.21115	555	15	535.9	8.7	624	74	85.88	318	132.7	92	0.79
M16-52	M16-52 - 25	0.0585	0.0014	0.838	0.019	0.10439	0.0012	0.17449	618.1	11	640	7.1	544	53	117.65	280	123	191.8	2.02
M16-52	M16-52 - 26	0.0607	0.0022	0.742	0.029	0.0923	0.0029	0.55312	564	18	569	17	613	75	92.82	794	318	200	0.63
M16-52	M16-52 - 27	0.0601	0.0025	0.771	0.032	0.0915	0.0018	0.29657	582	19	564	11	604	92	93.38	91.4	34.4	32.1	0.962
M16-52	M16-52 - 28	0.0576	0.0016	0.743	0.022	0.094	0.0014	0.51468	564	12	578.8	8.2	500	63	115.76	1190	480	149	0.391
M16-52	M16-52 - 29	0.0799	0.002	0.652	0.024	0.06	0.0023	0.94736	508	15	376	14	1186	49	31.70	987	99.4	1346	14.8
M16-52	M16-52 - 3	0.05915	0.0013	0.708	0.024	0.0887	0.0031	0.82127	541	14	547	18	581	49	94.15	670	240	481	3.02
M16-52	M16-52 - 30	0.0754	0.0047	0.965	0.064	0.0904	0.0018	0.15755	670	33	557.6	11	1030	130	54.14	112.7	38.4	23.4	0.629
M16-52	M16-52 - 31	0.0652	0.0021	0.651	0.022	0.073	0.0019	0.53237	510	14	454	12	767	65	59.19	183.9	56.2	140	2.77
M16-52	M16-52 - 32	0.0759	0.0078	0.99	0.11	0.0952	0.0027	0.4422	683	56	586	16	1040	230	56.35	339	131	54.9	0.4289
M16-52	M16-52 - 4	0.172	0.0045	2.162	0.056	0.0911	0.0013	0.38821	1172	18	562	7.9	2576	42	21.82	1020	169.6	98.8	0.5806
M16-52	M16-52 - 5	0.0701	0.002	0.834	0.027	0.086	0.0016	0.63374	619	14	531.5	9.6	923	56	57.58	383	115	139.5	1.35
M16-52	M16-52 - 6	0.06037	0.0014	0.74	0.017	0.08827	0.0012	0.44429	562.7	10	545.2	7.1	618	48	88.22	321	112	260	2.84
M16-52	M16-52 - 7	0.0599	0.0021	0.768	0.027	0.0919	0.0014	0.33316	580	16	566.6	8	629	77	90.08	165.3	63.4	102	1.68
M16-52	M16-52 - 8	0.0588	0.0017	0.739	0.019	0.09022	0.0011	0.024976	561.2	11	556.8	6.2	560	62	99.43	317.6	113.2	145.3	1.251
M16-52	M16-52 - 9	0.05739	0.0013	0.728	0.017	0.0927	0.0015	0.56664	555.8	10	571.2	9	509	54	112.22	569	217.3	421.8	1.894
M16-53	M16-53 - 1	0.2239	0.0041	1.05	0.047	0.0341	0.0014	0.98536	723	24	216	8.9	3009	30	7.18	10170	11010	3780	0.338
M16-53	M16-53 - 10	0.2053	0.0051	1.463	0.056	0.0506	0.0014	0.83352	908	23	318.7	8.8	2863	40	11.13	7770	4120	2020	0.69
M16-53	M16-53 - 11	0.0796	0.0029	1.353	0.05	0.1245	0.0016	0.20101	872	22	756.1	9.3	1156	76	65.41	338	92.9	75.7	0.8196
M16-53	M16-53 - 12	0.2103	0.0049	1.927	0.042	0.06709	0.00095	0.45653	1090	15	418.6	5.8	2904	38	14.41	10260	3002	1667	0.5545
M16-53	M16-53 - 13	0.0677	0.002	0.641	0.017	0.0679	0.0014	0.51135	502.3	10	423.6	8.5	853	62	49.66	2439	923	374	0.4085
M16-53	M16-53 - 14	0.07617	0.0015	0.954	0.02	0.0907	0.0016	0.81691	679.5	10	559.7	9.7	1096	39	51.07	12020	4800	3670	0.843
M16-53	M16-53 - 15	0.1563	0.0029	1.668	0.033	0.07741	0.00098	0.78087	997.7	13	480.6	5.9	2416	32	19.89	8700	2836	1327	0.4734
M16-53	M16-53 - 16	0.1072	0.0026	0.767	0.02	0.05178	0.00075	0.61956	576.9	12	325.4	4.6	1753	44	18.56	710	138.7	388	2.909
M16-53	M16-53 - 17	0.2245	0.0056	0.929	0.024	0.03103	0.00068	0.81121	667	13	197	4.2	3007	40	6.55	8450	2980	3430	1.231
M16-53	M16-53 - 18	0.2201	0.004	1.357	0.044	0.0447	0.0012	0.97247	871	19	281.5	7.5	2980	30	9.45	1.32E+04	8.00E+03	3820	0.616
M16-53	M16-53 - 19	0.17	0.0035	1.882	0.056	0.0806	0.0017	0.91986	1077	20	499.8	10	2560	36	19.52	7630	2690	1690	0.628
M16-53	M16-53 - 2	0.06029	0.0013	0.767	0.016	0.09204	0.00093	0.16193	578.1	9.3	567.6	5.5	623	49	91.11	2349	879	322.4	0.3713
M16-53	M16-53 - 20	0.1958	0.0037	0.4959	0.01	0.01847	0.00032	0.86119	408.6	7	118	2	2794	30	4.22	6420	3560	4180	1.167
M16-53	M16-53 - 21	0.06135	0.0014	0.763	0.017	0.0898	0.00092	0.14798	575.2	9.5	554.3	5.5	649	49	85.41	2250	924	370	0.401
M16-53	M16-53 - 22	0.08048	0.0015	1.021	0.021	0.0926	0.0015	0.84058	713.6	11	570.6	9	1210	36	47.16	11310	3600	4180	1.186

Zircon U–Pb geochronology

Sample No.	Sample - spot	$^{207}Pb/^{206}Pb$	± 2SE	$^{207}Pb/^{235}U$	± 2SE	$^{206}Pb/^{238}U$	± 2SE	Error Correlation 6/38 vs 7/35	Age $^{207}Pb/^{235}U$	± 2SE	Age $^{206}Pb/^{238}U$	± 2SE	Age $^{207}Pb/^{206}Pb$	± 2SE	Concordance 7/6 vs 6/38	Pb (PPM)	Th (PPM)	U (PPM)	U/Th
M16-53	M16-53 - 23	0.1696	0.0045	0.547	0.016	0.02344	0.00099	0.88786	442.6	10	149.3	6.3	2553	44	5.85	4250	1738	2045	1.172
M16-53	M16-53 - 24	0.2782	0.005	0.819	0.02	0.0214	0.00039	0.94433	607	11	136.5	2.5	3353.8	29	4.07	8900	9170	4000	0.429
M16-53	M16-53 - 25	0.228	0.0096	1.327	0.07	0.043	0.0024	0.48098	844	30	271	15	3036	68	8.93	1.25E+04	12190	3750	0.294
M16-53	M16-53 - 26	0.2511	0.0045	0.614	0.014	0.01766	0.00034	0.94421	486.1	9.2	112.8	2.1	3190.7	29	3.54	8250	4080	5150	1.267
M16-53	M16-53 - 3	0.0888	0.0021	0.1836	0.0065	0.01506	0.00054	0.8849	171.6	5.7	96.3	3.4	1398	45	6.89	827	199	3110	16.01
M16-53	M16-53 - 4	0.1678	0.0046	1.04	0.027	0.04442	0.00064	0.29035	723	13	280.8	3.9	2527	46	11.11	6570	2760	1639	0.6099
M16-53	M16-53 - 5	0.0628	0.0015	0.777	0.02	0.09	0.0014	0.66597	583.8	12	555.6	8.3	693	50	80.17	2212	820	337.4	0.4147
M16-53	M16-53 - 6	0.091	0.002	0.564	0.015	0.04483	0.00083	0.75363	453.2	9.4	282.7	5.1	1452	41	19.47	2380	554	914	1.642
M16-53	M16-53 - 7	0.2362	0.0042	1.39	0.039	0.04247	0.001	0.97282	882	16	268.1	6.4	3094.6	28	8.66	9370	244.5	2260	9.26
M16-53	M16-53 - 8	0.0984	0.0049	0.2396	0.0084	0.01796	0.00093	0.4829	217.8	6.9	114.7	5.9	1576	96	7.28	507	172	371.4	2.19
M16-53	M16-53 - 9	0.06411	0.0013	0.7736	0.014	0.08769	0.00082	-0.15583	581.6	7.8	541.9	4.9	742	43	73.03	6180	2434	1440	0.5936

Apatite U–Pb thermochronology

Sample No.	Sample - spot	$^{207}Pb/^{206}Pb$	± 2SE	$^{207}Pb/^{235}U$	± 2SE	$^{206}Pb/^{238}U$	± 2SE	ErrorCorrelation 6/38 vs 7/35	Th (PPM)	U (PPM)	U/Th
M16-15	M16-15 - 1	0.2854	0.0073	4.46	0.11	0.1112	0.0099	0.29863	113	136.8	1.27
M16-15	M16-15 - 10	0.627	0.02	21.8	1.9	0.243	0.028	0.9223	2.98	14.61	5.38
M16-15	M16-15 - 11	0.2391	0.0055	3.387	0.084	0.1008	0.009	0.45082	116.2	141.2	1.278
M16-15	M16-15 - 12	0.189	0.0034	2.497	0.044	0.09419	0.0083	0.23559	424	244.1	0.6035
M16-15	M16-15 - 13	0.3982	0.0099	7.47	0.24	0.1335	0.012	0.64191	60.3	61.66	1.075
M16-15	M16-15 - 14	0.3001	0.0069	4.69	0.11	0.1107	0.0098	0.19449	96.1	111.8	1.226
M16-15	M16-15 - 15	0.538	0.016	13.1	0.47	0.1735	0.016	0.58016	12.55	26.57	2.285
M16-15	M16-15 - 16	0.411	0.012	8.52	0.49	0.1458	0.014	0.94677	84.1	64.6	0.87
M16-15	M16-15 - 17	0.2903	0.0067	4.57	0.11	0.1122	0.0099	0.47725	100.5	109.2	1.156
M16-15	M16-15 - 18	0.2669	0.0077	3.84	0.13	0.1029	0.0092	0.61355	127.2	120.2	1.004
M16-15	M16-15 - 19	0.335	0.022	6.35	0.88	0.1303	0.015	0.95775	84	102	1.383
M16-15	M16-15 - 2	0.181	0.0039	2.364	0.053	0.09289	0.0082	0.34206	284	265.8	0.983
M16-15	M16-15 - 20	0.596	0.016	19.01	0.87	0.2266	0.021	0.80638	15.37	24.78	1.712
M16-15	M16-15 - 21	0.2988	0.0076	4.66	0.13	0.1111	0.0099	0.44366	109.3	89.6	0.8689
M16-15	M16-15 - 22	0.447	0.013	9.4	0.26	0.1493	0.013	0.26811	44.4	52.2	1.244
M16-15	M16-15 - 23	0.2429	0.0056	3.398	0.093	0.0994	0.0088	0.52458	124.8	141	1.2
M16-15	M16-15 - 24	0.2685	0.0062	3.972	0.084	0.1054	0.0093	0.20563	112.4	127	1.198
M16-15	M16-15 - 25	0.623	0.021	22	1.3	0.248	0.024	0.80675	11.4	19.2	1.893
M16-15	M16-15 - 26	0.423	0.011	8.19	0.2	0.1382	0.012	0.26787	62.8	58.2	0.984
M16-15	M16-15 - 27	0.29	0.013	4.47	0.25	0.1088	0.0098	0.79528	164	137	0.932
M16-15	M16-15 - 28	0.2385	0.005	3.409	0.078	0.1012	0.0089	0.37016	141.2	151	1.14
M16-15	M16-15 - 29	0.411	0.011	7.87	0.22	0.1365	0.012	0.41189	33.8	47.8	1.515
M16-15	M16-15 - 3	0.542	0.023	16.3	1.3	0.21	0.021	0.91368	27.2	39.6	1.649
M16-15	M16-15 - 30	0.2868	0.0059	4.419	0.094	0.1096	0.0097	0.34503	165.4	124.7	0.802
M16-15	M16-15 - 31	0.1938	0.0034	2.614	0.044	0.09591	0.0084	0.13799	385	222.8	0.6175
M16-15	M16-15 - 32	0.2588	0.0057	3.86	0.1	0.106	0.0094	0.5336	158.9	144.9	0.9754
M16-15	M16-15 - 33	0.332	0.012	5.55	0.3	0.1179	0.011	0.8473	100.2	91.5	0.989
M16-15	M16-15 - 34	0.256	0.0052	3.805	0.075	0.1058	0.0093	0.22871	198.7	140.5	0.7558
M16-15	M16-15 - 35	0.2889	0.006	4.543	0.094	0.1115	0.0099	0.23675	108.5	103	1.0125
M16-15	M16-15 - 36	0.507	0.022	12.6	1.1	0.1718	0.017	0.95166	35.5	44.8	1.419
M16-15	M16-15 - 37	0.34	0.012	5.7	0.29	0.1183	0.011	0.78601	73.4	81.4	1.199
M16-15	M16-15 - 38	0.642	0.016	41.7	3.2	0.453	0.05	0.94036	47.3	14.38	0.341

Apatite U–Pb thermochronology

Sample No.	Sample - spot	$^{207}Pb/^{206}Pb$	± 2SE	$^{207}Pb/^{235}U$	± 2SE	$^{206}Pb/^{238}U$	± 2SE	ErrorCorrelation 6/38 vs 7/35	Th (PPM)	U (PPM)	U/Th
M16-15	M16-15 - 39	0.406	0.013	7.83	0.36	0.1362	0.012	0.7445	37.4	62.7	1.796
M16-15	M16-15 - 4	0.2601	0.0072	3.75	0.14	0.1023	0.0091	0.67393	126.8	143.4	1.196
M16-15	M16-15 - 40	0.713	0.023	35.5	1.6	0.354	0.034	0.65033	8.97	12.78	1.557
M16-15	M16-15 - 5	0.2531	0.0068	3.63	0.1	0.1026	0.009	0.48306	287	155.1	0.568
M16-15	M16-15 - 6	0.2699	0.0067	4.05	0.12	0.1067	0.0094	0.52626	136.7	145	1.115
M16-15	M16-15 - 7	0.2591	0.0056	3.929	0.086	0.1083	0.0096	0.40735	123.5	126.3	1.077
M16-15	M16-15 - 8	0.2346	0.0045	3.358	0.066	0.10145	0.0089	0.1474	175.2	183.8	1.1007
M16-15	M16-15 - 9	0.3275	0.0098	5.43	0.22	0.1176	0.011	0.72362	82.5	80.9	1.034
M16-16	M16-16 - 1	0.451	0.011	9.65	0.23	0.1518	0.014	0.32049	61.2	43.8	0.766
M16-16	M16-16 - 10	0.2948	0.0099	4.59	0.2	0.1104	0.0099	0.70012	194	99.7	0.5585
M16-16	M16-16 - 11	0.558	0.024	15.6	1.6	0.193	0.021	0.95321	44.3	28.4	0.7
M16-16	M16-16 - 12	0.296	0.013	4.71	0.25	0.114	0.01	0.67305	174	98.2	0.6093
M16-16	M16-16 - 13	0.2714	0.0066	4	0.1	0.1049	0.0093	0.32208	198	113.3	0.6178
M16-16	M16-16 - 14	0.716	0.024	39.6	2.2	0.391	0.038	0.81607	15	9.32	0.683
M16-16	M16-16 - 15	0.45	0.011	9.15	0.24	0.1436	0.013	0.38141	74.3	44.33	0.6467
M16-16	M16-16 - 16	0.354	0.013	5.99	0.3	0.1197	0.011	0.72751	81.7	61.4	0.816
M16-16	M16-16 - 17	0.529	0.023	13.3	1.2	0.1755	0.018	0.91627	45.7	23.2	0.577
M16-16	M16-16 - 18	0.286	0.01	4.65	0.24	0.1148	0.01	0.83676	167	97.6	0.6387
M16-16	M16-16 - 19	0.3716	0.0096	6.73	0.25	0.128	0.012	0.69102	103.5	63	0.665
M16-16	M16-16 - 2	0.3902	0.0083	7.21	0.21	0.1313	0.012	0.67835	95.1	61.11	0.6887
M16-16	M16-16 - 20	0.8	0.023	61.3	2.7	0.543	0.052	0.77566	5.91	6.1	1.14
M16-16	M16-16 - 21	0.477	0.016	10.43	0.35	0.156	0.014	0.33942	52.6	29.27	0.6031
M16-16	M16-16 - 22	0.4412	0.0094	8.82	0.18	0.1426	0.013	0.40931	68.7	43.1	0.6833
M16-16	M16-16 - 23	0.2647	0.0061	3.973	0.09	0.1066	0.0094	0.23893	208.8	117.7	0.6131
M16-16	M16-16 - 24	0.455	0.0099	9.18	0.22	0.1436	0.013	0.50672	68.2	44.27	0.708
M16-16	M16-16 - 25	0.425	0.022	8.37	0.7	0.1364	0.013	0.89736	101.8	52.1	0.569
M16-16	M16-16 - 26	0.3533	0.009	5.99	0.16	0.1208	0.011	0.33268	126.1	67.8	0.5854
M16-16	M16-16 - 27	0.331	0.013	5.75	0.3	0.1226	0.011	0.77986	145	75.1	0.5754
M16-16	M16-16 - 28	0.2731	0.0061	4.191	0.093	0.1097	0.0097	0.37337	217.7	101.3	0.5074
M16-16	M16-16 - 29	0.554	0.024	14.7	1.2	0.188	0.019	0.91952	44.8	27	0.659
M16-16	M16-16 - 3	0.748	0.027	34.7	2.8	0.334	0.037	0.90449	12.81	9.62	0.834
M16-16	M16-16 - 30	0.718	0.025	37.7	3.5	0.368	0.043	0.93136	18.2	11.9	0.753

Apatite U–Pb thermochronology

Sample No.	Sample - spot	$^{207}Pb/^{206}Pb$	± 2SE	$^{207}Pb/^{235}U$	± 2SE	$^{206}Pb/^{238}U$	± 2SE	ErrorCorrelation 6/38 vs 7/35	Th (PPM)	U (PPM)	U/Th
M16-16	M16-16 - 31	0.733	0.028	39.2	3.4	0.371	0.041	0.89148	11.9	10.13	0.977
M16-16	M16-16 - 32	0.4115	0.0093	7.83	0.16	0.1356	0.012	0.21329	80.6	51.7	0.703
M16-16	M16-16 - 33	0.3575	0.009	6.11	0.16	0.1216	0.011	0.27653	136.4	70.7	0.5667
M16-16	M16-16 - 34	0.2902	0.0092	4.42	0.2	0.1081	0.0098	0.68077	144.2	97.6	0.748
M16-16	M16-16 - 35	0.816	0.024	75.6	3.4	0.662	0.064	0.73371	4.46	4.64	1.157
M16-16	M16-16 - 36	0.401	0.011	7.35	0.3	0.1297	0.012	0.77994	93.8	53.4	0.6244
M16-16	M16-16 - 37	0.2912	0.0084	4.53	0.14	0.1106	0.0098	0.31428	163.6	91.7	0.6128
M16-16	M16-16 - 38	0.3622	0.0091	6.27	0.17	0.1228	0.011	0.47755	105.1	64.06	0.6692
M16-16	M16-16 - 39	0.433	0.01	8.75	0.23	0.1437	0.013	0.53699	66.9	44.15	0.723
M16-16	M16-16 - 4	0.654	0.022	28.4	2.5	0.303	0.034	0.93957	19.9	13.67	0.763
M16-16	M16-16 - 40	0.59	0.018	16.51	0.49	0.2013	0.018	0.48513	36.46	23.04	0.695
M16-16	M16-16 - 5	0.402	0.014	7.96	0.37	0.139	0.013	0.64355	86.5	54.4	0.685
M16-16	M16-16 - 6	0.46	0.012	9.76	0.28	0.1506	0.013	0.45683	70.7	39.21	0.5979
M16-16	M16-16 - 7	0.825	0.03	75	6.4	0.642	0.074	0.91158	5.48	4.21	0.952
M16-16	M16-16 - 8	0.1908	0.0042	2.508	0.053	0.09354	0.0082	0.10686	295.4	215.3	0.7862
M16-16	M16-16 - 9	0.514	0.014	11.93	0.38	0.1655	0.015	0.5566	59.2	31	0.565
M16-17	M16-17 - 1	0.3864	0.0066	7.12	0.14	0.1307	0.012	0.496	72.4	75.4	1.145
M16-17	M16-17 - 10	0.34	0.011	5.72	0.31	0.1185	0.011	0.87586	129.9	92.7	0.797
M16-17	M16-17 - 11	0.351	0.015	6.07	0.42	0.1216	0.011	0.79002	133.2	92.8	0.7703
M16-17	M16-17 - 12	0.3644	0.0096	6.35	0.15	0.1246	0.011	0.18939	47.5	68.1	1.585
M16-17	M16-17 - 13	0.4167	0.0097	8.24	0.22	0.1397	0.012	0.45257	71.3	70.1	1.092
M16-17	M16-17 - 14	0.343	0.031	6.73	0.7	0.1358	0.012	0.72258	251	113	0.605
M16-17	M16-17 - 15	0.415	0.015	8.3	0.52	0.1404	0.013	0.91075	56.5	69.9	1.375
M16-17	M16-17 - 16	0.396	0.013	7.68	0.48	0.1361	0.013	0.92477	83	77.4	1.151
M16-17	M16-17 - 17	0.3413	0.0067	5.88	0.11	0.1225	0.011	0.29273	78.1	95.9	1.359
M16-17	M16-17 - 18	0.2827	0.0061	4.32	0.11	0.1087	0.0096	0.58257	151.9	128.4	0.931
M16-17	M16-17 - 19	0.3179	0.0074	5.21	0.12	0.1167	0.01	0.15937	95.6	103.4	1.209
M16-17	M16-17 - 2	0.308	0.01	4.87	0.24	0.1112	0.0099	0.80939	134.2	112.2	0.919
M16-17	M16-17 - 20	0.41	0.01	7.91	0.26	0.1363	0.012	0.52243	74.02	64.47	0.967
M16-17	M16-17 - 21	0.504	0.041	16.7	3.2	0.205	0.032	0.98408	66	50.6	0.934
M16-17	M16-17 - 22	0.444	0.011	9.36	0.33	0.1496	0.014	0.694	59.16	49.06	0.921
M16-17	M16-17 - 23	0.4444	0.0079	9.48	0.18	0.1508	0.013	0.31922	57.6	48.5	0.937

Apatite U–Pb thermochronology

Sample No.	Sample - spot	$^{207}Pb/^{206}Pb$	± 2SE	$^{207}Pb/^{235}U$	± 2SE	$^{206}Pb/^{238}U$	± 2SE	ErrorCorrelation 6/38 vs 7/35	Th (PPM)	U (PPM)	U/Th
M16-17	M16-17 - 24	0.2393	0.0093	3.48	0.19	0.1025	0.0092	0.82676	294	177.5	0.6707
M16-17	M16-17 - 25	0.359	0.01	6.23	0.19	0.1233	0.011	0.3655	94.3	77.4	0.9129
M16-17	M16-17 - 26	0.3916	0.0099	7.54	0.19	0.137	0.012	0.33058	86.7	76.9	0.994
M16-17	M16-17 - 27	0.2446	0.0076	3.62	0.12	0.105	0.0093	0.36726	83.9	89.7	1.22
M16-17	M16-17 - 28	0.2681	0.0072	4.2	0.14	0.1105	0.0098	0.51282	143	152.9	1.236
M16-17	M16-17 - 29	0.464	0.013	10.4	0.55	0.1581	0.015	0.89029	58.4	54.2	1.039
M16-17	M16-17 - 3	0.357	0.016	6.2	0.4	0.122	0.011	0.85122	146.4	95	0.7131
M16-17	M16-17 - 30	0.3233	0.0056	5.44	0.1	0.1193	0.011	0.3883	131.4	110.6	0.9392
M16-17	M16-17 - 31	0.332	0.022	5.72	0.63	0.1177	0.012	0.94381	221	91.5	0.501
M16-17	M16-17 - 32	0.3551	0.0079	6.12	0.13	0.1228	0.011	0.27199	86	96.9	1.258
M16-17	M16-17 - 33	0.3688	0.0079	6.62	0.14	0.1278	0.011	0.2452	73.8	83.9	1.268
M16-17	M16-17 - 34	0.442	0.0095	9.26	0.23	0.1491	0.013	0.48173	68.2	57.3	0.939
M16-17	M16-17 - 35	0.458	0.01	9.45	0.2	0.1476	0.013	0.29148	78.3	53.81	0.773
M16-17	M16-17 - 36	0.661	0.025	29	4	0.298	0.042	0.97668	24.3	19.2	0.949
M16-17	M16-17 - 37	0.4109	0.0091	8.06	0.17	0.1398	0.012	0.28799	80.1	68.5	0.959
M16-17	M16-17 - 38	0.2148	0.0058	2.928	0.087	0.0969	0.0086	0.47397	211.1	189.5	1.01
M16-17	M16-17 - 39	0.3194	0.0076	5.21	0.17	0.1156	0.01	0.73702	61.8	94.5	1.718
M16-17	M16-17 - 4	0.744	0.021	48.5	3.5	0.462	0.05	0.92231	8.95	11.14	1.391
M16-17	M16-17 - 40	0.355	0.0078	6.16	0.13	0.1232	0.011	0.23683	80.6	84	1.169
M16-17	M16-17 - 5	0.4252	0.0089	8.55	0.17	0.144	0.013	0.40894	96.5	55.5	0.6312
M16-17	M16-17 - 6	0.464	0.01	9.98	0.28	0.1529	0.014	0.62745	40.42	50.59	1.383
M16-17	M16-17 - 7	0.3274	0.0073	5.5	0.14	0.1196	0.011	0.50827	69.33	90.3	1.43
M16-17	M16-17 - 8	0.31	0.016	5.07	0.43	0.1133	0.011	0.93418	136	112.9	0.949
M16-17	M16-17 - 9	0.442	0.0091	9.1	0.21	0.1465	0.013	0.41939	74.6	60.5	0.892
M16-32	M16-32 - 1	0.707	0.023	24.33	0.81	0.2446	0.023	0.61331	3.05	8.68	3.26
M16-32	M16-32 - 10	0.919	0.029	130.6	7	1.017	0.1	0.82902	0.786	1.85	2.82
M16-32	M16-32 - 11	0.44	0.013	8.62	0.23	0.1397	0.012	0.18607	19.02	31.1	1.853
M16-32	M16-32 - 12	0.582	0.026	14.25	0.57	0.1754	0.016	0.15338	4.24	15.85	4.33
M16-32	M16-32 - 13	0.916	0.037	73.7	6.2	0.565	0.063	0.90634	1.276	3.61	3.42
M16-32	M16-32 - 14	0.881	0.032	66.5	2.9	0.541	0.054	0.65303	0.393	3.74	12.3
M16-32	M16-32 - 15	0.799	0.036	40.7	1.7	0.366	0.034	0.37158	2.89	4.95	1.99
M16-32	M16-32 - 16	1.014	0.045	436	44	3.09	0.41	0.92715	0.272	0.453	2.36

Apatite U–Pb thermochronology

Sample No.	Sample - spot	$^{207}Pb/^{206}Pb$	± 2SE	$^{207}Pb/^{235}U$	± 2SE	$^{206}Pb/^{238}U$	± 2SE	ErrorCorrelation 6/38 vs 7/35	Th (PPM)	U (PPM)	U/Th
M16-32	M16-32 - 17	0.673	0.023	20.26	0.98	0.2152	0.02	0.85238	3.41	12.14	4.22
M16-32	M16-32 - 18	0.781	0.029	42.4	1.7	0.384	0.035	0.49274	0.852	6.12	8.88
M16-32	M16-32 - 19	0.633	0.023	18.36	0.6	0.2079	0.019	0.2662	6.24	13.69	2.53
M16-32	M16-32 - 2	0.86	0.035	53.6	2.2	0.448	0.043	0.51612	2.25	3.72	2.01
M16-32	M16-32 - 20	0.507	0.015	11.34	0.39	0.1584	0.014	0.53782	68.3	26.6	0.44
M16-32	M16-32 - 21	0.683	0.025	22.21	0.92	0.2311	0.022	0.57778	6.18	12.35	2.295
M16-32	M16-32 - 22	0.572	0.023	14.34	0.94	0.1769	0.017	0.81381	24.4	22.6	1.1
M16-32	M16-32 - 23	0.517	0.016	11.58	0.38	0.1589	0.014	0.30893	29.58	26.6	1.018
M16-32	M16-32 - 24	0.497	0.015	10.61	0.32	0.1516	0.014	0.38339	34.5	25.27	0.841
M16-32	M16-32 - 25	0.673	0.027	25.1	2.4	0.257	0.028	0.91032	14.7	10.65	0.879
M16-32	M16-32 - 26	0.515	0.014	11.54	0.37	0.1589	0.014	0.50167	16.33	22.27	1.562
M16-32	M16-32 - 27	0.489	0.014	10.69	0.32	0.1557	0.014	0.46723	31.2	25.85	0.949
M16-32	M16-32 - 28	0.946	0.034	117.5	5.9	0.906	0.095	0.8044	0.482	2.26	6.17
M16-32	M16-32 - 29	0.679	0.027	25.8	2.5	0.266	0.032	0.90923	4.76	9.8	2.38
M16-32	M16-32 - 3	0.838	0.03	53	2.2	0.455	0.045	0.66465	1.51	4.19	3.45
M16-32	M16-32 - 30	0.586	0.021	14.55	0.55	0.1778	0.017	0.46796	7.52	16.38	2.515
M16-32	M16-32 - 31	0.683	0.028	22.28	0.94	0.232	0.021	0.45595	5.1	9.06	2.059
M16-32	M16-32 - 32	0.513	0.028	11.6	1.1	0.1558	0.016	0.87848	40.2	27.2	0.808
M16-32	M16-32 - 33	0.455	0.013	9.26	0.29	0.1448	0.013	0.46066	18.58	29.41	1.82
M16-32	M16-32 - 34	0.98	0.03	173.3	8.8	1.265	0.13	0.84208	0.332	1.5	6.8
M16-32	M16-32 - 35	0.859	0.026	54.3	2.1	0.449	0.042	0.61354	0.816	4.83	7.13
M16-32	M16-32 - 36	0.739	0.019	28.3	1.1	0.2727	0.026	0.683	2.07	7.59	4.5
M16-32	M16-32 - 37	0.755	0.035	30.7	2.2	0.289	0.031	0.76204	4.28	7.87	2.42
M16-32	M16-32 - 38	0.846	0.034	62.6	6.2	0.521	0.063	0.90773	2.05	4.54	3.02
M16-32	M16-32 - 39	0.728	0.029	28.2	1.1	0.28	0.027	0.47802	4.05	7.37	2.16
M16-32	M16-32 - 4	0.561	0.017	12.92	0.51	0.1636	0.015	0.63897	49.97	21.26	0.4786
M16-32	M16-32 - 40	0.919	0.032	101.6	4.7	0.791	0.081	0.79106	0.918	1.932	2.51
M16-32	M16-32 - 5	0.878	0.034	63.8	3	0.517	0.05	0.59212	0.818	3.55	5.31
M16-32	M16-32 - 6	0.899	0.039	84	12	0.64	0.098	0.94426	1.62	3.33	2.21
M16-32	M16-32 - 7	0.763	0.024	36.3	1.4	0.339	0.032	0.56766	1.46	7.46	5.9
M16-32	M16-32 - 8	0.513	0.015	11.58	0.36	0.161	0.015	0.42505	108.1	25.8	0.268
M16-32	M16-32 - 9	0.469	0.015	9.48	0.27	0.1447	0.013	0.3339	36.29	32.7	1.023

Apatite U–Pb thermochronology

Sample No.	Sample - spot	$^{207}Pb/^{206}Pb$	± 2SE	$^{207}Pb/^{235}U$	± 2SE	$^{206}Pb/^{238}U$	± 2SE	ErrorCorrelation 6/38 vs 7/35	Th (PPM)	U (PPM)	U/Th
M16-34	M16-34 - 1	0.254	0.017	4.55	0.36	0.128	0.012	0.61982	0.579	15.2	41.3
M16-34	M16-34 - 10	0.93	0.057	181	41	1.25	0.28	0.95469	0.46	1.28	-300
M16-34	M16-34 - 11	0.292	0.01	4.47	0.15	0.1094	0.0099	0.23974	48.9	31.7	0.794
M16-34	M16-34 - 12	0.578	0.031	15.53	0.77	0.1929	0.018	0.29843	4.67	7.51	1.899
M16-34	M16-34 - 13	0.86	0.035	61.1	2.8	0.504	0.05	0.65154	1.2	2.92	3.03
M16-34	M16-34 - 14	0.912	0.042	60.5	3.1	0.484	0.052	0.66603	0.485	2.576	7.05
M16-34	M16-34 - 15	0.909	0.037	88.3	7	0.671	0.077	0.83786	1.24	2.08	2.13
M16-34	M16-34 - 16	0.791	0.036	41.8	1.9	0.382	0.037	0.53198	1.091	3.77	4.29
M16-34	M16-34 - 17	0.885	0.038	79.2	3.7	0.638	0.063	0.59493	0.293	1.86	9.5
M16-34	M16-34 - 18	0.808	0.041	41.9	2.4	0.38	0.04	0.59787	0.761	2.65	4.47
M16-34	M16-34 - 19	0.76	0.045	35.7	3.4	0.327	0.033	0.74681	2.23	3.83	2.08
M16-34	M16-34 - 2	0.866	0.039	48.6	2.6	0.4	0.037	0.54487	0.858	3.54	5.11
M16-34	M16-34 - 20	0.954	0.041	93.3	6.7	0.71	0.082	0.82806	0.241	1.51	-160
M16-34	M16-34 - 21	0.954	0.045	138.4	9.1	1.039	0.12	0.75695	0.398	1.156	4.32
M16-34	M16-34 - 22	0.515	0.02	11.62	0.43	0.1607	0.015	0.314	8	12.01	1.799
M16-34	M16-34 - 23	0.719	0.033	30.1	1.6	0.296	0.03	0.57812	1.85	4.45	2.9
M16-34	M16-34 - 24	0.314	0.012	5.06	0.21	0.115	0.01	0.38389	21.2	34.3	1.881
M16-34	M16-34 - 25	0.933	0.038	207	57	1.48	0.4	0.99614	0.86	2.4	-60
M16-34	M16-34 - 26	0.433	0.015	8.47	0.26	0.1401	0.013	0.23415	25.34	19.57	0.902
M16-34	M16-34 - 27	0.78	0.03	37.2	1.4	0.344	0.033	0.48098	2.08	4.69	2.73
M16-34	M16-34 - 28	0.844	0.039	56.8	4	0.483	0.054	0.78405	1.52	3.21	2.62
M16-34	M16-34 - 29	0.4	0.014	7.36	0.28	0.1294	0.012	0.35944	44	22.37	0.597
M16-34	M16-34 - 3	0.772	0.041	36.3	5.8	0.305	0.043	0.89761	1.76	4.32	2.99
M16-34	M16-34 - 30	no value	NAN	no value	NAN	no value	NAN	NaN	Below LOD	Below LOD	no value
M16-34	M16-34 - 31	0.487	0.018	10.07	0.44	0.1475	0.014	0.53452	9.24	14.46	1.837
M16-34	M16-34 - 32	0.759	0.034	33	1.4	0.314	0.03	0.48069	1.067	4.74	5.67
M16-34	M16-34 - 33	0.409	0.014	7.62	0.23	0.1334	0.012	0.31011	8.23	19.93	2.878
M16-34	M16-34 - 34	0.378	0.013	6.57	0.25	0.1238	0.011	0.45948	20.37	27.7	1.621
M16-34	M16-34 - 35	0.927	0.039	104.3	6.3	0.806	0.087	0.76376	0.0032	1.373	-3260
M16-34	M16-34 - 36	0.898	0.055	83.4	8	0.67	0.081	0.79565	0.229	1.245	-19
M16-34	M16-34 - 37	no value	NAN	no value	NAN	no value	NAN	NaN	Below LOD	Below LOD	no value
M16-34	M16-34 - 38	0.278	0.011	4.17	0.17	0.1066	0.0095	0.36077	30.3	40.01	1.572

Apatite U–Pb thermochronology

Sample No.	Sample - spot	$^{207}Pb/^{206}Pb$	± 2SE	$^{207}Pb/^{235}U$	± 2SE	$^{206}Pb/^{238}U$	± 2SE	ErrorCorrelation 6/38 vs 7/35	Th (PPM)	U (PPM)	U/Th
M16-34	M16-34 - 39	0.525	0.026	11.46	0.94	0.1537	0.016	0.84379	4.02	11.49	3.6
M16-34	M16-34 - 4	0.779	0.037	43.8	5.5	0.402	0.055	0.92486	0.99	2.96	4.25
M16-34	M16-34 - 40	0.913	0.041	116.5	9.7	0.905	0.11	0.83074	0.5	1.25	5.1
M16-34	M16-34 - 5	0.921	0.051	78.2	6	0.624	0.07	0.75959	0.035	1.296	-1960
M16-34	M16-34 - 6	0.446	0.016	9.2	0.36	0.1444	0.014	0.43444	19.69	17.8	1.031
M16-34	M16-34 - 7	0.964	0.049	148	11	1.131	0.13	0.77139	0.0131	0.801	-1590
M16-34	M16-34 - 8	0.739	0.039	26	2.6	0.248	0.029	0.86755	1.88	4.75	3.02
M16-34	M16-34 - 9	0.806	0.032	41.1	1.7	0.364	0.035	0.54799	1.46	4.34	3.7
M16-35	M16-35 - 1	0.3488	0.0096	5.72	0.13	0.117	0.01	0.020918	158.8	51.3	0.3771
M16-35	M16-35 - 10	0.342	0.014	5.54	0.37	0.1119	0.01	0.81667	30.5	45.9	1.768
M16-35	M16-35 - 11	0.515	0.016	11.31	0.52	0.1549	0.015	0.69093	25.5	22.5	1.047
M16-35	M16-35 - 12	0.754	0.027	34.4	2.8	0.318	0.035	0.89672	7.6	8.07	1.245
M16-35	M16-35 - 13	0.646	0.021	18.3	0.78	0.2025	0.019	0.7283	48.8	14.02	0.349
M16-35	M16-35 - 14	0.919	0.032	79.9	5.4	0.618	0.066	0.87947	1.98	3.89	2.37
M16-35	M16-35 - 15	0.682	0.025	20.57	0.83	0.2125	0.019	0.54045	31.1	10.63	0.4015
M16-35	M16-35 - 16	0.578	0.049	22.6	5.5	0.233	0.044	0.98735	23.5	22.7	1.12
M16-35	M16-35 - 17	0.527	0.014	11.9	0.34	0.1613	0.015	0.42821	20.54	18.47	1.066
M16-35	M16-35 - 18	0.572	0.026	13.5	1	0.1661	0.016	0.82646	15.67	18.45	1.393
M16-35	M16-35 - 19	0.604	0.021	15.33	0.59	0.1819	0.017	0.52049	12.02	15.28	1.512
M16-35	M16-35 - 2	0.346	0.011	5.54	0.23	0.1138	0.01	0.67227	42.29	46.93	1.306
M16-35	M16-35 - 20	0.604	0.025	17	1.1	0.198	0.019	0.82511	16.92	12.67	0.891
M16-35	M16-35 - 21	0.906	0.034	68.1	2.5	0.546	0.053	0.64635	2.45	3.08	1.528
M16-35	M16-35 - 22	0.437	0.016	8.37	0.3	0.1369	0.012	0.29111	99.4	30.52	0.3634
M16-35	M16-35 - 23	0.329	0.012	5.31	0.25	0.1137	0.01	0.64091	24	52.4	2.637
M16-35	M16-35 - 24	0.807	0.032	44.5	4	0.378	0.044	0.89481	2.88	5.65	2.61
M16-35	M16-35 - 25	0.372	0.011	5.98	0.19	0.1144	0.01	0.43786	42.9	39.5	1.093
M16-35	M16-35 - 26	0.956	0.038	122	15	0.902	0.13	0.94339	1.57	2.34	1.95
M16-35	M16-35 - 27	0.3531	0.0096	5.68	0.14	0.1154	0.01	0.40926	24.88	44.3	2.113
M16-35	M16-35 - 28	0.377	0.011	6.5	0.16	0.1224	0.011	0.15644	15.72	39.4	2.985
M16-35	M16-35 - 29	0.2774	0.006	4.08	0.1	0.1044	0.0093	0.52154	50.2	73.2	1.764
M16-35	M16-35 - 3	0.27	0.008	4	0.13	0.1054	0.0093	0.40863	26.56	71.97	3.179
M16-35	M16-35 - 30	0.46	0.015	9.22	0.24	0.1434	0.013	0.15921	40.1	26.71	0.795

Apatite U–Pb thermochronology

Sample No.	Sample - spot	$^{207}Pb/^{206}Pb$	± 2SE	$^{207}Pb/^{235}U$	± 2SE	$^{206}Pb/^{238}U$	± 2SE	ErrorCorrelation 6/38 vs 7/35	Th (PPM)	U (PPM)	U/Th
M16-35	M16-35 - 31	0.825	0.026	50.3	2	0.436	0.041	0.62158	12.13	3.63	0.357
M16-35	M16-35 - 32	0.612	0.022	15.61	0.55	0.1825	0.017	0.43473	22.56	13.09	0.692
M16-35	M16-35 - 33	0.357	0.011	5.88	0.17	0.1172	0.01	0.16814	35.16	44.2	1.494
M16-35	M16-35 - 34	0.8	0.025	39.2	1.3	0.352	0.033	0.60563	1.25	6.33	6.65
M16-35	M16-35 - 35	0.278	0.0099	4.25	0.2	0.1073	0.0096	0.64586	65.1	68.6	1.308
M16-35	M16-35 - 36	0.926	0.041	136.8	9	1.043	0.11	0.76251	2.56	1.448	0.694
M16-35	M16-35 - 37	0.2866	0.007	4.21	0.1	0.1041	0.0093	0.23394	32.8	65.9	2.402
M16-35	M16-35 - 38	0.387	0.011	6.68	0.17	0.1238	0.011	0.31544	17.07	39.8	2.794
M16-35	M16-35 - 39	0.982	0.04	165	12	1.201	0.13	0.9277	0.386	1.42	5.77
M16-35	M16-35 - 4	0.655	0.023	20.11	0.89	0.2186	0.02	0.60493	32	11.25	0.4101
M16-35	M16-35 - 40	0.53	0.017	12.24	0.41	0.1647	0.015	0.51724	115.6	22.18	0.2303
M16-35	M16-35 - 5	0.772	0.03	36.5	1.3	0.343	0.033	0.49275	9.53	5.8	0.719
M16-35	M16-35 - 6	0.871	0.042	143	37	1.02	0.26	0.97266	2.41	4.63	2.43
M16-35	M16-35 - 7	no value	NAN	no value	NAN	no value	NAN	NaN	Below LOD	Below LOD	no value
M16-35	M16-35 - 8	0.417	0.031	7.72	0.91	0.1286	0.013	0.91308	35.2	36.7	1.204
M16-35	M16-35 - 9	0.527	0.05	20.1	6.8	0.203	0.046	0.99309	13.8	24	2.042
M16-45	M16-45 - 1	0.735	0.033	48.4	4.8	0.474	0.06	0.90387	150	4.87	0.0404
M16-45	M16-45 - 10	0.748	0.036	46.2	2.3	0.443	0.045	0.61997	102.8	3.08	0.0361
M16-45	M16-45 - 11	0.729	0.026	35.5	1.1	0.348	0.032	0.37208	201.4	7.05	0.0421
M16-45	M16-45 - 12	0.765	0.027	38.7	1.5	0.36	0.034	0.55522	151.7	5.46	0.0432
M16-45	M16-45 - 13	0.675	0.024	26.17	0.97	0.2789	0.026	0.45614	305	9.65	0.03821
M16-45	M16-45 - 14	0.767	0.027	42.2	1.9	0.393	0.038	0.65119	173.3	5.77	0.04
M16-45	M16-45 - 15	0.624	0.022	21.7	1	0.2446	0.023	0.59736	288	9.79	0.04116
M16-45	M16-45 - 16	0.741	0.031	36.3	2.3	0.353	0.038	0.77255	120.1	4.14	0.0413
M16-45	M16-45 - 17	0.732	0.024	40.2	2	0.39	0.038	0.76084	195.6	6.23	0.0385
M16-45	M16-45 - 18	0.766	0.025	42.5	1.3	0.396	0.037	0.566	157.1	5.31	0.0407
M16-45	M16-45 - 19	0.745	0.028	35.8	1.3	0.344	0.032	0.39372	211.9	6.83	0.0389
M16-45	M16-45 - 2	0.733	0.03	45.8	5.4	0.438	0.06	0.93087	166	5.44	0.0398
M16-45	M16-45 - 20	0.572	0.025	15.35	0.74	0.1918	0.018	0.56663	361.4	11.72	0.03924
M16-45	M16-45 - 21	0.786	0.025	58.4	3.2	0.534	0.054	0.8311	104.5	3.68	0.0427
M16-45	M16-45 - 22	0.729	0.024	37.1	1.6	0.363	0.035	0.68497	195.6	6.53	0.04036
M16-45	M16-45 - 23	0.615	0.024	17.36	0.69	0.2027	0.019	0.4594	238.4	8.71	0.04404

Apatite U–Pb thermochronology

Sample No.	Sample - spot	$^{207}Pb/^{206}Pb$	± 2SE	$^{207}Pb/^{235}U$	± 2SE	$^{206}Pb/^{238}U$	± 2SE	ErrorCorrelation 6/38 vs 7/35	Th (PPM)	U (PPM)	U/Th
M16-45	M16-45 - 24	0.774	0.03	47.8	1.9	0.447	0.043	0.57381	148.2	4.81	0.03928
M16-45	M16-45 - 25	0.826	0.035	57.6	2.9	0.5	0.049	0.65187	111	3.16	0.0344
M16-45	M16-45 - 26	0.738	0.032	29	1.6	0.285	0.028	0.67138	225	7.09	0.03848
M16-45	M16-45 - 27	0.734	0.026	36.3	1.5	0.355	0.034	0.59473	149.3	4.92	0.04
M16-45	M16-45 - 28	0.86	0.036	70.2	4.2	0.581	0.06	0.7627	67.7	2.31	0.0419
M16-45	M16-45 - 29	0.764	0.028	45.2	2.2	0.42	0.041	0.65503	166	5.76	0.0421
M16-45	M16-45 - 3	0.725	0.028	34.8	2.1	0.339	0.034	0.75456	203.9	6.47	0.0382
M16-45	M16-45 - 30	0.675	0.023	28.6	1.4	0.305	0.029	0.72182	257	8.44	0.03996
M16-45	M16-45 - 31	0.894	0.036	137.3	8	1.126	0.12	0.75244	38.6	1.518	0.0478
M16-45	M16-45 - 32	0.736	0.023	36.6	1.3	0.355	0.033	0.63312	194.4	6.17	0.03866
M16-45	M16-45 - 33	0.71	0.022	30.9	1.1	0.3109	0.029	0.56073	185	6.53	0.04293
M16-45	M16-45 - 34	0.771	0.03	47.4	2.3	0.44	0.042	0.61714	91.8	3.4	0.045
M16-45	M16-45 - 35	0.918	0.033	184	12	1.399	0.15	0.82925	35.26	1.111	0.0383
M16-45	M16-45 - 36	0.782	0.029	52.3	3.6	0.479	0.052	0.85036	143	4.56	0.0391
M16-45	M16-45 - 37	0.895	0.032	178	10	1.449	0.16	0.87449	27.8	1.186	0.0516
M16-45	M16-45 - 38	0.867	0.033	170	11	1.405	0.15	0.80644	30.5	1.165	0.0475
M16-45	M16-45 - 39	0.748	0.026	35.1	1.6	0.333	0.032	0.64646	201.1	6.5	0.03945
M16-45	M16-45 - 4	0.748	0.03	40.1	1.9	0.381	0.038	0.64223	159.9	5.27	0.03945
M16-45	M16-45 - 40	0.678	0.027	26.1	1.2	0.279	0.027	0.66701	223	7.4	0.04068
M16-45	M16-45 - 5	0.751	0.026	39.9	1.6	0.382	0.037	0.65474	157.5	5.26	0.04
M16-45	M16-45 - 6	0.826	0.032	104	12	0.876	0.12	0.94174	83	2.72	0.0431
M16-45	M16-45 - 7	0.736	0.028	32.5	1.4	0.318	0.03	0.61624	194.8	6.73	0.0415
M16-45	M16-45 - 8	0.708	0.024	30.6	1.2	0.3072	0.029	0.51133	220.8	7.29	0.03974
M16-45	M16-45 - 9	0.759	0.024	42.4	1.5	0.398	0.037	0.58943	167.2	5.59	0.04013
M16-46	M16-46 - 1	0.867	0.029	79	4.3	0.649	0.067	0.84753	1.82	3.14	2.11
M16-46	M16-46 - 10	0.89	0.028	102	6.7	0.818	0.088	0.84987	0.573	2.358	5.95
M16-46	M16-46 - 11	0.465	0.015	9.3	0.46	0.1417	0.013	0.73659	7.25	27.4	4.69
M16-46	M16-46 - 12	0.891	0.024	92.6	3.9	0.75	0.074	0.81956	1.253	3.78	4
M16-46	M16-46 - 13	0.91	0.031	119	7.3	0.941	0.1	0.81148	0.746	1.98	3.58
M16-46	M16-46 - 14	0.66	0.022	21.41	0.82	0.232	0.022	0.6081	1.795	12.77	9.06
M16-46	M16-46 - 15	0.6	0.017	15.95	0.48	0.1899	0.017	0.4886	4.53	17.49	4.78
M16-46	M16-46 - 16	0.715	0.027	27.8	1.3	0.276	0.026	0.60251	1.78	7.01	5.04

Apatite U–Pb thermochronology

Sample No.	Sample - spot	$^{207}Pb/^{206}Pb$	± 2SE	$^{207}Pb/^{235}U$	± 2SE	$^{206}Pb/^{238}U$	± 2SE	ErrorCorrelation 6/38 vs 7/35	Th (PPM)	U (PPM)	U/Th
M16-46	M16-46 - 17	0.724	0.019	28.03	0.77	0.2754	0.025	0.50491	3.64	11.79	4.05
M16-46	M16-46 - 18	0.683	0.022	23.46	0.67	0.2461	0.023	0.32934	2.69	13.76	6.51
M16-46	M16-46 - 19	0.654	0.044	31.8	6.5	0.3	0.054	0.98662	2.87	21.9	15.3
M16-46	M16-46 - 2	0.781	0.026	41.7	2.9	0.376	0.039	0.88216	113	8.25	5.2
M16-46	M16-46 - 20	0.86	0.021	75.3	2.6	0.619	0.058	0.77388	0.682	4.81	9.59
M16-46	M16-46 - 21	0.898	0.027	99.8	4	0.797	0.078	0.8034	0.955	2.89	4.11
M16-46	M16-46 - 22	0.777	0.019	41.6	1.4	0.382	0.036	0.70135	2.25	8.77	4.98
M16-46	M16-46 - 23	0.734	0.019	34.3	0.91	0.336	0.031	0.62493	2.09	9.59	5.84
M16-46	M16-46 - 24	0.822	0.025	60.3	4.7	0.518	0.056	0.90315	0.777	4.79	8.67
M16-46	M16-46 - 25	0.87	0.026	72.2	2.6	0.594	0.056	0.63196	1.195	3.92	4.18
M16-46	M16-46 - 26	0.882	0.024	105	3.6	0.852	0.081	0.72325	1.299	3.48	3.57
M16-46	M16-46 - 27	0.724	0.023	26.7	0.94	0.2636	0.024	0.56652	4.17	8.84	2.67
M16-46	M16-46 - 28	0.752	0.022	36	1.3	0.34	0.032	0.62725	2.126	9.39	5.51
M16-46	M16-46 - 29	0.874	0.025	86.7	2.8	0.7	0.064	0.60913	1.711	4.09	3.04
M16-46	M16-46 - 3	0.64	0.02	20.4	1.3	0.226	0.022	0.87482	12.6	17.2	1.717
M16-46	M16-46 - 30	0.897	0.036	86.8	3.6	0.691	0.067	0.63221	0.96	2.05	2.89
M16-46	M16-46 - 31	0.879	0.022	78.7	2.8	0.636	0.06	0.70467	0.516	4.51	12.4
M16-46	M16-46 - 32	0.903	0.031	121	5.1	0.953	0.092	0.71488	0.794	2.9	4.95
M16-46	M16-46 - 33	0.807	0.026	50.1	3.7	0.434	0.045	0.8909	0.666	4.84	10
M16-46	M16-46 - 34	0.79	0.019	47.9	1.8	0.432	0.041	0.77423	2.14	7.42	4.44
M16-46	M16-46 - 35	no value	NAN	no value	NAN	no value	NAN	NaN	Below LOD	Below LOD	no value
M16-46	M16-46 - 36	0.93	0.022	182	16	1.4	0.18	0.95665	1.72	2.26	1.7
M16-46	M16-46 - 37	0.736	0.028	33.7	4	0.317	0.041	0.94894	5.52	8.32	1.897
M16-46	M16-46 - 38	0.837	0.023	67.5	2.3	0.574	0.054	0.6434	0.814	4.84	7.94
M16-46	M16-46 - 39	0.794	0.039	58.3	7.1	0.506	0.071	0.93407	1.02	6.4	11.9
M16-46	M16-46 - 4	0.89	0.035	98.8	4.8	0.807	0.081	0.75061	1.14	2.27	2.63
M16-46	M16-46 - 40	0.777	0.018	39.8	1.2	0.3637	0.033	0.58925	0.677	8.2	16.5
M16-46	M16-46 - 5	0.834	0.032	71.8	2.8	0.62	0.06	0.59121	1.65	3.1	2.41
M16-46	M16-46 - 6	0.893	0.03	109.7	5.9	0.869	0.086	0.78685	0.506	2.268	6.32
M16-46	M16-46 - 7	0.759	0.025	34.8	1.2	0.328	0.031	0.56911	1.68	7.46	5.79
M16-46	M16-46 - 8	0.904	0.022	103.8	4	0.823	0.079	0.79098	1.07	3.6	4.42
M16-46	M16-46 - 9	0.685	0.023	24.69	0.88	0.2572	0.024	0.51815	1.169	10.83	11.99

Apatite U–Pb thermochronology

Sample No.	Sample - spot	$^{207}Pb/^{206}Pb$	± 2SE	$^{207}Pb/^{235}U$	± 2SE	$^{206}Pb/^{238}U$	± 2SE	ErrorCorrelation 6/38 vs 7/35	Th (PPM)	U (PPM)	U/Th
M16-52	M16-52 - 1	0.649	0.015	22.9	1.1	0.2496	0.024	0.88517	34.5	22.93	0.832
M16-52	M16-52 - 10	0.724	0.022	35.1	2.8	0.34	0.037	0.93198	25.2	16.78	0.84
M16-52	M16-52 - 11	0.657	0.026	26.1	3.5	0.27	0.036	0.97951	31.8	22	0.891
M16-52	M16-52 - 12	0.609	0.031	22.4	3.4	0.243	0.034	0.984	40.8	30.5	0.991
M16-52	M16-52 - 13	0.549	0.013	14.22	0.72	0.1821	0.017	0.88641	57	38.93	0.858
M16-52	M16-52 - 14	0.464	0.016	9.71	0.58	0.148	0.014	0.90506	92.5	57.9	0.7891
M16-52	M16-52 - 15	0.561	0.011	15.17	0.38	0.1917	0.017	0.66347	52.87	35.23	0.837
M16-52	M16-52 - 16	0.589	0.019	18.5	1.1	0.2205	0.022	0.87223	43.3	30.5	0.898
M16-52	M16-52 - 17	0.79	0.018	55.6	1.7	0.502	0.047	0.74401	9.98	8.85	1.131
M16-52	M16-52 - 18	0.675	0.016	26.9	1.3	0.2804	0.026	0.86914	27.56	19.83	0.903
M16-52	M16-52 - 19	0.64	0.019	23.7	1.8	0.258	0.027	0.95837	36.3	24.9	0.884
M16-52	M16-52 - 2	0.805	0.019	62.7	5.5	0.549	0.063	0.97644	13.51	10.73	0.987
M16-52	M16-52 - 20	0.776	0.02	49.9	1.3	0.46	0.042	0.5432	14.81	9.79	0.834
M16-52	M16-52 - 21	0.5343	0.0098	12.99	0.25	0.1731	0.015	0.45158	65.8	45.6	0.875
M16-52	M16-52 - 22	0.525	0.014	12.33	0.59	0.1661	0.015	0.86129	58.8	43.9	0.942
M16-52	M16-52 - 23	0.543	0.012	13.54	0.34	0.1776	0.016	0.49509	67.1	40.3	0.7588
M16-52	M16-52 - 24	0.778	0.017	48.2	1.6	0.439	0.041	0.76988	13.44	10.19	0.961
M16-52	M16-52 - 25	0.718	0.013	34.96	0.71	0.3467	0.031	0.60866	21.42	15.44	0.912
M16-52	M16-52 - 26	0.541	0.023	14	1.6	0.187	0.023	0.98045	51.2	41.8	1.063
M16-52	M16-52 - 27	0.691	0.019	30.1	2.9	0.304	0.035	0.96204	35.3	21.6	0.792
M16-52	M16-52 - 28	0.534	0.02	13.7	1.2	0.1757	0.018	0.96322	65.6	46.2	0.894
M16-52	M16-52 - 29	0.583	0.015	16.34	0.43	0.1989	0.018	0.4	47.1	26.63	0.714
M16-52	M16-52 - 3	0.645	0.019	23.2	1.4	0.253	0.025	0.9167	36	24.1	0.817
M16-52	M16-52 - 30	0.624	0.014	20.5	1.1	0.2313	0.022	0.91229	39.3	25.82	0.83
M16-52	M16-52 - 31	0.623	0.014	20.32	0.54	0.2314	0.021	0.55409	35.5	25.1	0.894
M16-52	M16-52 - 32	0.761	0.017	51	2.4	0.473	0.046	0.85866	12.14	10.07	1.051
M16-52	M16-52 - 33	0.578	0.013	15.8	0.37	0.1946	0.017	0.44237	56.1	32.52	0.7336
M16-52	M16-52 - 34	0.773	0.016	42.9	1.2	0.396	0.036	0.71202	12.7	11.47	1.134
M16-52	M16-52 - 35	0.689	0.019	29.2	2.1	0.296	0.03	0.95927	19.8	18.94	1.249
M16-52	M16-52 - 36	0.718	0.019	36.4	2.8	0.356	0.038	0.95083	20.4	14.51	0.907
M16-52	M16-52 - 37	0.746	0.021	35.1	1.7	0.333	0.031	0.8216	18.74	13.61	0.923
M16-52	M16-52 - 38	0.621	0.015	19.1	0.69	0.2196	0.02	0.7997	36.79	26.31	0.908

Apatite U–Pb thermochronology

Sample No.	Sample - spot	$^{207}Pb/^{206}Pb$	± 2SE	$^{207}Pb/^{235}U$	± 2SE	$^{206}Pb/^{238}U$	± 2SE	ErrorCorrelation 6/38 vs 7/35	Th (PPM)	U (PPM)	U/Th
M16-52	M16-52 - 39	0.55	0.014	13.88	0.52	0.181	0.017	0.8389	61.5	48.3	0.992
M16-52	M16-52 - 4	0.611	0.014	18.54	0.81	0.2149	0.02	0.87591	52.2	27.41	0.6557
M16-52	M16-52 - 40	0.514	0.022	13.1	1.4	0.17	0.018	0.96542	65.4	44.9	0.87
M16-52	M16-52 - 5	0.496	0.031	15.7	3.1	0.198	0.03	0.99043	91	60	0.853
M16-52	M16-52 - 6	0.492	0.014	10.4	0.54	0.1487	0.014	0.88445	88.5	57.8	0.822
M16-52	M16-52 - 7	0.501	0.02	12.04	0.99	0.1672	0.017	0.95057	60.4	49.5	1.029
M16-52	M16-52 - 8	0.524	0.011	12.69	0.4	0.172	0.016	0.75359	69.4	43.9	0.7912
M16-52	M16-52 - 9	0.699	0.026	43.7	5.1	0.425	0.057	0.98092	23.3	17.3	1.023
M16-53	M16-53 - 1	0.568	0.012	15.93	0.35	0.1999	0.018	0.48591	44.56	29.86	0.852
M16-53	M16-53 - 10	0.564	0.019	16.34	0.79	0.2044	0.019	0.79798	63.4	28.6	0.582
M16-53	M16-53 - 11	0.543	0.011	14.63	0.46	0.1913	0.017	0.78709	57.5	30.1	0.6688
M16-53	M16-53 - 12	0.481	0.019	11.59	0.91	0.168	0.017	0.91734	84	42.6	0.666
M16-53	M16-53 - 13	0.656	0.015	25.39	0.53	0.2761	0.025	0.37033	40.61	18.01	0.5674
M16-53	M16-53 - 14	0.402	0.032	9.4	1.2	0.153	0.017	0.96395	111	74	0.788
M16-53	M16-53 - 15	0.544	0.013	14.08	0.46	0.1839	0.017	0.67742	64.1	32.94	0.6605
M16-53	M16-53 - 16	0.517	0.014	12.35	0.78	0.1681	0.017	0.9256	64.4	39.7	0.789
M16-53	M16-53 - 17	0.492	0.033	13.2	1.7	0.176	0.021	0.97771	101	45.6	0.604
M16-53	M16-53 - 18	0.596	0.013	17.52	0.67	0.2085	0.019	0.82683	54.69	25.45	0.5966
M16-53	M16-53 - 19	0.599	0.014	18.09	0.62	0.2164	0.02	0.7668	55.6	23	0.528
M16-53	M16-53 - 2	0.603	0.016	19.08	0.42	0.2265	0.02	0.28844	50.8	23.53	0.589
M16-53	M16-53 - 20	0.602	0.016	17.47	0.37	0.2071	0.019	0.10886	51.4	24.2	0.6033
M16-53	M16-53 - 21	0.644	0.014	21.26	0.53	0.2341	0.021	0.59206	29.98	20.33	0.869
M16-53	M16-53 - 22	0.586	0.013	17.57	0.53	0.2123	0.019	0.6669	52.9	22.5	0.5458
M16-53	M16-53 - 23	0.607	0.013	12.85	0.54	0.1506	0.014	0.86849	71.9	35.23	0.6266
M16-53	M16-53 - 24	0.398	0.023	7.34	0.64	0.1268	0.012	0.91601	124	77	0.732
M16-53	M16-53 - 25	0.543	0.013	14.62	0.43	0.1913	0.017	0.60589	38.1	32.1	1.086
M16-53	M16-53 - 26	0.689	0.015	27.11	0.76	0.28	0.025	0.66642	26.04	15.05	0.74
M16-53	M16-53 - 27	0.4075	0.0092	7.81	0.16	0.1364	0.012	0.23449	54.6	57.8	1.359
M16-53	M16-53 - 28	0.524	0.018	14.17	0.92	0.1883	0.018	0.88294	74.9	32.8	0.573
M16-53	M16-53 - 29	0.681	0.018	25.96	0.93	0.2714	0.025	0.72198	30.07	15.22	0.652
M16-53	M16-53 - 3	0.778	0.016	47.2	1.5	0.433	0.04	0.70081	12.19	8.25	0.866
M16-53	M16-53 - 30	0.377	0.016	6.71	0.54	0.1239	0.012	0.91982	139.5	71.9	0.671

Apatite U–Pb thermochronology

Sample No.	Sample - spot	$^{207}Pb/^{206}Pb$	± 2SE	$^{207}Pb/^{235}U$	± 2SE	$^{206}Pb/^{238}U$	± 2SE	ErrorCorrelation 6/38 vs 7/35	Th (PPM)	U (PPM)	U/Th
M16-53	M16-53 - 31	0.524	0.019	14.41	0.97	0.1918	0.019	0.83861	34.9	29.8	1.113
M16-53	M16-53 - 32	0.629	0.013	22.92	0.82	0.2587	0.024	0.81701	49.6	20.88	0.539
M16-53	M16-53 - 33	0.623	0.012	20.25	0.44	0.2304	0.02	0.4556	34.68	20.24	0.752
M16-53	M16-53 - 34	0.676	0.013	25.15	0.51	0.2663	0.024	0.45378	46.01	19.23	0.5385
M16-53	M16-53 - 35	0.678	0.012	26.38	0.56	0.2779	0.025	0.63764	43.3	17.34	0.5144
M16-53	M16-53 - 4	0.518	0.011	12.51	0.33	0.1733	0.016	0.70093	63.3	35	0.7036
M16-53	M16-53 - 5	0.473	0.05	14	2.3	0.181	0.024	0.97659	65.5	100	1.57
M16-53	M16-53 - 6	0.663	0.016	24.44	0.9	0.2598	0.024	0.78589	35.4	16.73	0.603
M16-53	M16-53 - 7	0.37	0.011	6.65	0.31	0.1269	0.011	0.89558	152.3	71.1	0.5943
M16-53	M16-53 - 8	0.666	0.019	24.91	0.59	0.2688	0.025	0.38234	32.62	14.82	0.58
M16-53	M16-53 - 9	0.215	0.0049	2.975	0.073	0.0983	0.0087	0.41369	423	202	0.6083

Muscovite and biotite Rb–Sr thermochronology

Sample No.	Sample - spot	Mineral	Population	$^{87}Rb/^{86}Sr$	± 2SE	$^{87}Sr/^{86}Sr$	± 2SE
M16-15	M16-15-b1	biotite	Included	190.7	1.8	1.966	0.019
M16-15	M16-15-b2	biotite	Included	2497	98	18.07	0.71
M16-15	M16-15-b3	biotite	Included	3110	130	24.6	1
M16-15	M16-15-b4	biotite	Included	1418	24	10.83	0.19
M16-15	M16-15-b5	biotite	Included	2809	75	21.26	0.55
M16-15	M16-15-b6	biotite	Included	1859	44	14.37	0.39
M16-15	M16-15-b7	biotite	Included	2876	72	21.91	0.51
M16-15	M16-15-b8	biotite	Included	3280	130	25.07	0.82
M16-15	M16-15-b9	biotite	Included	2425	99	18.95	0.85
M16-15	M16-15-b10	biotite	Included	1903	67	15.08	0.64
M16-15	M16-15-m2	muscovite	Included	1.2721	0.0052	0.7363	0.0014
M16-15	M16-15-m3	muscovite	Included	1.1984	0.0091	0.7344	0.0016
M16-15	M16-15-m5	muscovite	Included	2.433	0.022	0.7448	0.0023
M16-15	M16-15-m6	muscovite	Included	2.002	0.016	0.7429	0.0021
M16-15	M16-15-m7	muscovite	Included	1.228	0.0076	0.7332	0.0015
M16-15	M16-15-m9	muscovite	Included	0.00142	0.00011	0.7234	0.0022
M16-15	M16-15-m10	muscovite	Included	0.00542	0.0003	0.7263	0.0029
M16-16	M16-16-b3	biotite	Included	3440	110	24	0.67
M16-16	M16-16-b4	biotite	Included	3358	73	24.8	0.55
M16-16	M16-16-b5	biotite	Included	3687	87	27.59	0.72
M16-16	M16-16-b6	biotite	Included	3500	100	25.48	0.77
M16-16	M16-16-b7	biotite	Included	3850	100	28.54	0.77
M16-16	M16-16-b8	biotite	Included	3035	80	23.12	0.67
M16-16	M16-16-b9	biotite	Included	4860	190	34.7	1.3
M16-16	M16-16-b10	biotite	Included	3192	78	23.38	0.62
M16-16	M16-16-m2	muscovite	Included	0.01078	0.00054	0.7243	0.0031
M16-16	M16-16-m3	muscovite	Included	2.684	0.024	0.7417	0.002
M16-16	M16-16-m5	muscovite	Included	2.431	0.013	0.7412	0.0017
M16-16	M16-16-m6	muscovite	Included	2.483	0.012	0.7417	0.0015
M16-16	M16-16-m8	muscovite	Included	2.959	0.019	0.7462	0.0017
M16-16	M16-16-m9	muscovite	Included	2.733	0.025	0.7425	0.0018
M16-16	M16-16-m10	muscovite	Included	2.565	0.014	0.7409	0.0017

Muscovite and biotite Rb–Sr thermochronology

Sample No.	Sample - spot	Mineral	Population	$^{87}Rb/^{86}Sr$	± 2SE	$^{87}Sr/^{86}Sr$	± 2SE
M16-16	M16-16-m4	muscovite	Excluded	0	3.3	2	1.3
M16-16	M16-16-m7	muscovite	Excluded	2.1	4	1.11	0.36
M16-17	M16-17-b1	biotite	Included	1718	86	12.68	0.77
M16-17	M16-17-b2	biotite	Included	2841	80	20.63	0.63
M16-17	M16-17-b6	biotite	Included	1999	45	15.4	0.36
M16-17	M16-17-b7	biotite	Included	1511	40	11.64	0.45
M16-17	M16-17-b8	biotite	Included	1904	88	15.27	0.75
M16-17	M16-17-b9	biotite	Included	1680	37	13.11	0.45
M16-17	M16-17-m1	muscovite	Included	0.00323	0.00022	0.7257	0.0015
M16-17	M16-17-m2	muscovite	Included	1.759	0.0086	0.7404	0.0015
M16-17	M16-17-m3	muscovite	Included	1.706	0.01	0.7381	0.0022
M16-17	M16-17-m5	muscovite	Included	2.1168	0.0091	0.742	0.0015
M16-17	M16-17-m6	muscovite	Included	2.076	0.025	0.742	0.0022
M16-17	M16-17-m7	muscovite	Included	2.483	0.011	0.7433	0.0014
M16-17	M16-17-m8	muscovite	Included	0.00781	0.00048	0.7256	0.0013
M16-17	M16-17-m9	muscovite	Included	2.442	0.017	0.7443	0.0018
M16-17	M16-17-m10	muscovite	Included	0.00479	0.00017	0.7277	0.0019
M16-17	M16-17-b3	biotite	Excluded	0.0823	0.0054	0.7305	0.0099
M16-17	M16-17-b4	biotite	Excluded	370.3	7	2.198	0.07
M16-17	M16-17-b5	biotite	Excluded	2117	82	14.93	0.6
M16-17	M16-17-b10	biotite	Excluded	421	11	2.464	0.084
M16-17	M16-17-m4	muscovite	Excluded	18	14	1.43	0.68
M16-24	M16-24-b1	biotite	Included	696	16	5.43	0.13
M16-24	M16-24-b2	biotite	Included	5550	460	38.9	3.6
M16-24	M16-24-b6	biotite	Included	770	110	6.2	1
M16-24	M16-24-b7	biotite	Included	745	34	6.37	0.33
M16-24	M16-24-b10	biotite	Included	1430	100	10.61	0.73
M16-24	M16-24-m1	muscovite	Included	12.24	0.18	0.813	0.0062
M16-24	M16-24-m2	muscovite	Included	12.31	0.11	0.8126	0.0066
M16-24	M16-24-m4	muscovite	Included	19.93	0.36	0.8708	0.0094
M16-24	M16-24-m5	muscovite	Included	11.41	0.23	0.8003	0.0086
M16-24	M16-24-m6	muscovite	Included	12.63	0.17	0.8182	0.0062

Muscovite and biotite Rb–Sr thermochronology

Sample No.	Sample - spot	Mineral	Population	$^{87}Rb/^{86}Sr$	± 2SE	$^{87}Sr/^{86}Sr$	± 2SE
M16-24	M16-24-m7	muscovite	Included	8.65	0.13	0.7879	0.0055
M16-24	M16-24-m8	muscovite	Included	13.13	0.14	0.807	0.012
M16-24	M16-24-m9	muscovite	Included	12.16	0.1	0.812	0.0071
M16-24	M16-24-m10	muscovite	Included	11.03	0.13	0.8065	0.0064
M16-24	M16-24-b3	biotite	Excluded	160	3.4	1.258	0.014
M16-24	M16-24-b4	biotite	Excluded	192.8	2.8	1.531	0.036
M16-24	M16-24-b5	biotite	Excluded	181	2.8	1.715	0.034
M16-24	M16-24-b8	biotite	Excluded	218	3.8	1.491	0.034
M16-24	M16-24-b9	biotite	Excluded	-2.1	4.9	-0.63	0.33
M16-24	M16-24-m3	muscovite	Excluded	1.31	0.71	0.95	0.16
M16-32	M16-32-b1	biotite	Included	592	14	4.64	0.12
M16-32	M16-32-b2	biotite	Included	103.3	6.6	1.392	0.06
M16-32	M16-32-b3	biotite	Included	650	12	5.28	0.11
M16-32	M16-32-b6	biotite	Included	678	17	5.35	0.14
M16-32	M16-32-b8	biotite	Included	204.2	5.5	2.054	0.04
M16-32	M16-32-b9	biotite	Included	609	15	4.99	0.12
M16-32	M16-32-b10	biotite	Included	176.7	5.9	1.865	0.04
M16-32	M16-32-m1	muscovite	Included	0.3526	0.0018	0.7162	0.0012
M16-32	M16-32-m2	muscovite	Included	0.2996	0.0018	0.71575	0.00095
M16-32	M16-32-m3	muscovite	Included	0.3351	0.0014	0.7154	0.0013
M16-32	M16-32-m4	muscovite	Included	0.00255	0.00017	0.7142	0.0011
M16-32	M16-32-m5	muscovite	Included	0.00048	0.000037	0.71361	0.00094
M16-32	M16-32-m6	muscovite	Included	0.3257	0.0017	0.7151	0.001
M16-32	M16-32-m7	muscovite	Included	0.297	0.0017	0.7164	0.0013
M16-32	M16-32-m8	muscovite	Included	0.000913	0.000066	0.71348	0.00092
M16-32	M16-32-m10	muscovite	Included	0.401	0.0052	0.7167	0.0028
M16-32	M16-32-b4	biotite	Excluded	0.2419	0.0025	0.7124	0.0028
M16-32	M16-32-b5	biotite	Excluded	0.000174	0.000028	0.71277	0.00096
M16-32	M16-32-b7	biotite	Excluded	248.1	5.9	2.203	0.046
M16-32	M16-32-m9	muscovite	Excluded	0.5056	0.0077	0.7141	0.0041
M16-34	M16-34-b1	biotite	Excluded	0.2304	0.0024	0.7139	0.0022
M16-34	M16-34-b2	biotite	Excluded	0.2164	0.0025	0.7143	0.0025

Muscovite and biotite Rb–Sr thermochronology

Sample No.	Sample - spot	Mineral	Population	$^{87}Rb/^{86}Sr$	± 2SE	$^{87}Sr/^{86}Sr$	± 2SE
M16-34	M16-34-b3	biotite	Excluded	4.3	8.3	1.5	0.88
M16-34	M16-34-b4	biotite	Excluded	0.2049	0.0021	0.7148	0.0024
M16-34	M16-34-b5	biotite	Excluded	0.2278	0.0021	0.7134	0.0023
M16-34	M16-34-b6	biotite	Excluded	0.000147	0.000019	0.71286	0.00091
M16-34	M16-34-b7	biotite	Excluded	-0.8	6.7	0.7	1.9
M16-34	M16-34-b8	biotite	Excluded	-12.2	8.6	-0.23	0.49
M16-34	M16-34-b9	biotite	Excluded	0.2589	0.0032	0.7174	0.0028
M16-34	M16-34-b10	biotite	Excluded	0.2317	0.0024	0.7158	0.0024
M16-35	M16-35-b4	biotite	Included	648.1	9.5	5.194	0.088
M16-35	M16-35-b5	biotite	Included	602.9	8.1	4.941	0.076
M16-35	M16-35-b6	biotite	Included	87.3	1.7	1.209	0.014
M16-35	M16-35-b1	biotite	Excluded	-5.4	7.5	0.6	1.5
M16-35	M16-35-b2	biotite	Excluded	-7.7	6.6	0.3	0.46
M16-35	M16-35-b3	biotite	Excluded	-6.6	5.1	-0.14	0.6
M16-35	M16-35-b7	biotite	Excluded	490	160	1.84	0.55
M16-35	M16-35-b8	biotite	Excluded	0.000687	0.00006	0.7144	0.001
M16-35	M16-35-b9	biotite	Excluded	-7.5	5	0.1	0.7
M16-35	M16-35-b10	biotite	Excluded	-13	6.8	-0.56	0.36
M16-45	M16-45-b1	biotite	Included	825	13	6.552	0.098
M16-45	M16-45-b2	biotite	Included	598.3	8.7	4.972	0.083
M16-45	M16-45-b3	biotite	Included	761	11	6.101	0.085
M16-45	M16-45-b4	biotite	Included	728	11	5.858	0.079
M16-45	M16-45-b5	biotite	Included	587.2	6.3	4.914	0.069
M16-45	M16-45-b6	biotite	Included	648	12	5.38	0.081
M16-45	M16-45-b7	biotite	Included	552	10	4.747	0.063
M16-45	M16-45-b8	biotite	Included	707.2	9.9	5.804	0.087
M16-45	M16-45-b9	biotite	Included	604	14	5.201	0.088
M16-45	M16-45-b10	biotite	Included	0.7859	0.0035	0.7192	0.0012
M16-46	M16-46-b2	biotite	Included	0.2751	0.0035	0.7105	0.0025
M16-46	M16-46-b3	biotite	Included	410.5	4.9	3.587	0.046
M16-46	M16-46-b4	biotite	Included	424.9	7	3.765	0.052
M16-46	M16-46-b6	biotite	Included	431.2	5.4	3.941	0.071

Muscovite and biotite Rb–Sr thermochronology

Sample No.	Sample - spot	Mineral	Population	$^{87}Rb/^{86}Sr$	± 2SE	$^{87}Sr/^{86}Sr$	± 2SE
M16-46	M16-46-b7	biotite	Included	376.8	4.9	3.351	0.046
M16-46	M16-46-b10	biotite	Included	433	11	3.89	0.12
M16-46	M16-46-m1	muscovite	Included	0.561	0.0057	0.7132	0.0018
M16-46	M16-46-m2	muscovite	Included	0.3109	0.0048	0.7108	0.0011
M16-46	M16-46-m3	muscovite	Included	0.3052	0.002	0.7114	0.001
M16-46	M16-46-m4	muscovite	Included	0.00024	0.00003	0.70846	0.0009
M16-46	M16-46-m9	muscovite	Included	0.3019	0.0031	0.7109	0.0012
M16-46	M16-46-m10	muscovite	Included	0.2791	0.0017	0.7107	0.0012
M16-46	M16-46-b1	biotite	Excluded	278.8	4	2.419	0.052
M16-46	M16-46-b5	biotite	Excluded	488.2	6	4.052	0.046
M16-46	M16-46-b8	biotite	Excluded	0.2527	0.0033	0.7051	0.0022
M16-46	M16-46-b9	biotite	Excluded	0.2659	0.003	0.7142	0.0029
M16-46	M16-46-m5	muscovite	Excluded	0.2841	0.0021	0.70974	0.00078
M16-46	M16-46-m6	muscovite	Excluded	0.000466	0.000033	0.70793	0.00091
M16-46	M16-46-m7	muscovite	Excluded	0.000341	0.000024	0.7099	0.001
M16-46	M16-46-m8	muscovite	Excluded	0.000565	0.000042	0.70989	0.00096
M16-47	M16-47-m1	muscovite	Included	0.391	0.002	0.71184	0.00099
M16-47	M16-47-m3	muscovite	Included	0.000592	0.000044	0.7075	0.0011
M16-47	M16-47-m4	muscovite	Included	0.001262	0.000046	0.70905	0.00081
M16-47	M16-47-m6	muscovite	Included	0.3511	0.0028	0.71154	0.0009
M16-47	M16-47-m7	muscovite	Included	1.0131	0.0073	0.7182	0.0015
M16-47	M16-47-m8	muscovite	Included	0.00634	0.00018	0.7084	0.0015
M16-47	M16-47-m9	muscovite	Included	0.000941	0.000042	0.70875	0.00082
M16-47	M16-47-b1	biotite	Excluded	0.752	0.086	0.7148	0.0052
M16-47	M16-47-b2	biotite	Excluded	0.00467	0.00017	0.70869	0.00095
M16-47	M16-47-b3	biotite	Excluded	0.444	0.0025	0.7137	0.0012
M16-47	M16-47-b4	biotite	Excluded	4.54	0.63	0.7109	0.0029
M16-47	M16-47-b5	biotite	Excluded	2.89	0.055	0.7103	0.003
M16-47	M16-47-b6	biotite	Excluded	0.047	0.0041	0.7133	0.0025
M16-47	M16-47-b7	biotite	Excluded	0.001636	0.000082	0.71073	0.00098
M16-47	M16-47-m2	muscovite	Excluded	-2.5	3.4	1.5	1.4
M16-47	M16-47-m5	muscovite	Excluded	0.3367	0.0026	0.7136	0.0015

Muscovite and biotite Rb–Sr thermochronology

Sample No.	Sample - spot	Mineral	Population	$^{87}Rb/^{86}Sr$	± 2SE	$^{87}Sr/^{86}Sr$	± 2SE
M16-47	M16-47-m10	muscovite	Excluded	-6.5	6.2	-0.5	0.35
M16-52	M16-52-b1	biotite	Included	3221	77	23.96	0.5
M16-52	M16-52-b2	biotite	Included	2875	73	21.32	0.47
M16-52	M16-52-b3	biotite	Included	0.105	0.026	0.714	0.015
M16-52	M16-52-b4	biotite	Included	4252	97	30.25	0.71
M16-52	M16-52-b5	biotite	Included	3510	110	26.33	0.81
M16-52	M16-52-b6	biotite	Included	4001	92	29.09	0.74
M16-52	M16-52-b7	biotite	Included	3456	60	26.07	0.43
M16-52	M16-52-b8	biotite	Included	3480	75	25.53	0.71
M16-52	M16-52-b9	biotite	Included	3492	77	25.3	0.52
M16-52	M16-52-b10	biotite	Included	3810	110	26.9	0.75
M16-52	M16-52-m2	muscovite	Included	0.0538	0.0085	0.7148	0.0015
M16-52	M16-52-m3	muscovite	Included	0.0124	0.0017	0.7143	0.0015
M16-52	M16-52-m4	muscovite	Included	3.578	0.036	0.7421	0.0016
M16-52	M16-52-m5	muscovite	Included	0.0487	0.003	0.7171	0.0021
M16-52	M16-52-m6	muscovite	Included	2.711	0.019	0.7352	0.0014
M16-52	M16-52-m7	muscovite	Included	2.635	0.017	0.7321	0.0019
M16-52	M16-52-m8	muscovite	Included	3.336	0.027	0.7387	0.0017
M16-52	M16-52-m9	muscovite	Included	2.761	0.019	0.7333	0.0019
M16-52	M16-52-m10	muscovite	Included	3.505	0.04	0.7416	0.0021
M16-52	M16-52-m1	muscovite	Excluded	2.589	0.03	0.7297	0.002
M16-53	M16-53-b1	biotite	Included	3690	410	28.4	2.7
M16-53	M16-53-b2	biotite	Included	4660	200	34.6	1.5
M16-53	M16-53-b3	biotite	Included	2750	130	21.1	1.1
M16-53	M16-53-b4	biotite	Included	4920	200	37.5	1.3
M16-53	M16-53-b5	biotite	Included	4.44	0.13	0.7313	0.0039
M16-53	M16-53-b6	biotite	Included	3072	76	24.01	0.62
M16-53	M16-53-b7	biotite	Included	4260	170	30.7	1.2
M16-53	M16-53-b8	biotite	Included	3213	81	23.38	0.61
M16-53	M16-53-b9	biotite	Included	0.021	0.031	0.692	0.022
M16-53	M16-53-b10	biotite	Included	2570	110	18.6	0.79
M16-53	M16-53-m4	muscovite	Included	0.3487	0.0059	0.7182	0.0024

Muscovite and biotite Rb–Sr thermochronology

Sample No.	Sample - spot	Mineral	Population	$^{87}Rb/^{86}Sr$	± 2SE	$^{87}Sr/^{86}Sr$	± 2SE
M16-53	M16-53-m5	muscovite	Included	3.761	0.036	0.7428	0.0024
M16-53	M16-53-m6	muscovite	Included	5.024	0.025	0.7537	0.0022
M16-53	M16-53-m7	muscovite	Included	0.00368	0.00023	0.7141	0.0018
M16-53	M16-53-m8	muscovite	Included	4.972	0.06	0.7488	0.0029
M16-53	M16-53-m10	muscovite	Included	4.99	0.11	0.7542	0.0065
M16-53	M16-53-m1	muscovite	Excluded	0.00174	0.00025	0.7173	0.0016
M16-53	M16-53-m2	muscovite	Excluded	0.676	0.014	0.7245	0.0026
M16-53	M16-53-m3	muscovite	Excluded	0.1756	0.0058	0.704	0.013
M16-53	M16-53-m9	muscovite	Excluded	4.3	5.5	1.55	0.79

Appendix 4.4 Structure and thermochronology of Madagascar: Landsat images and structural interpretation examples

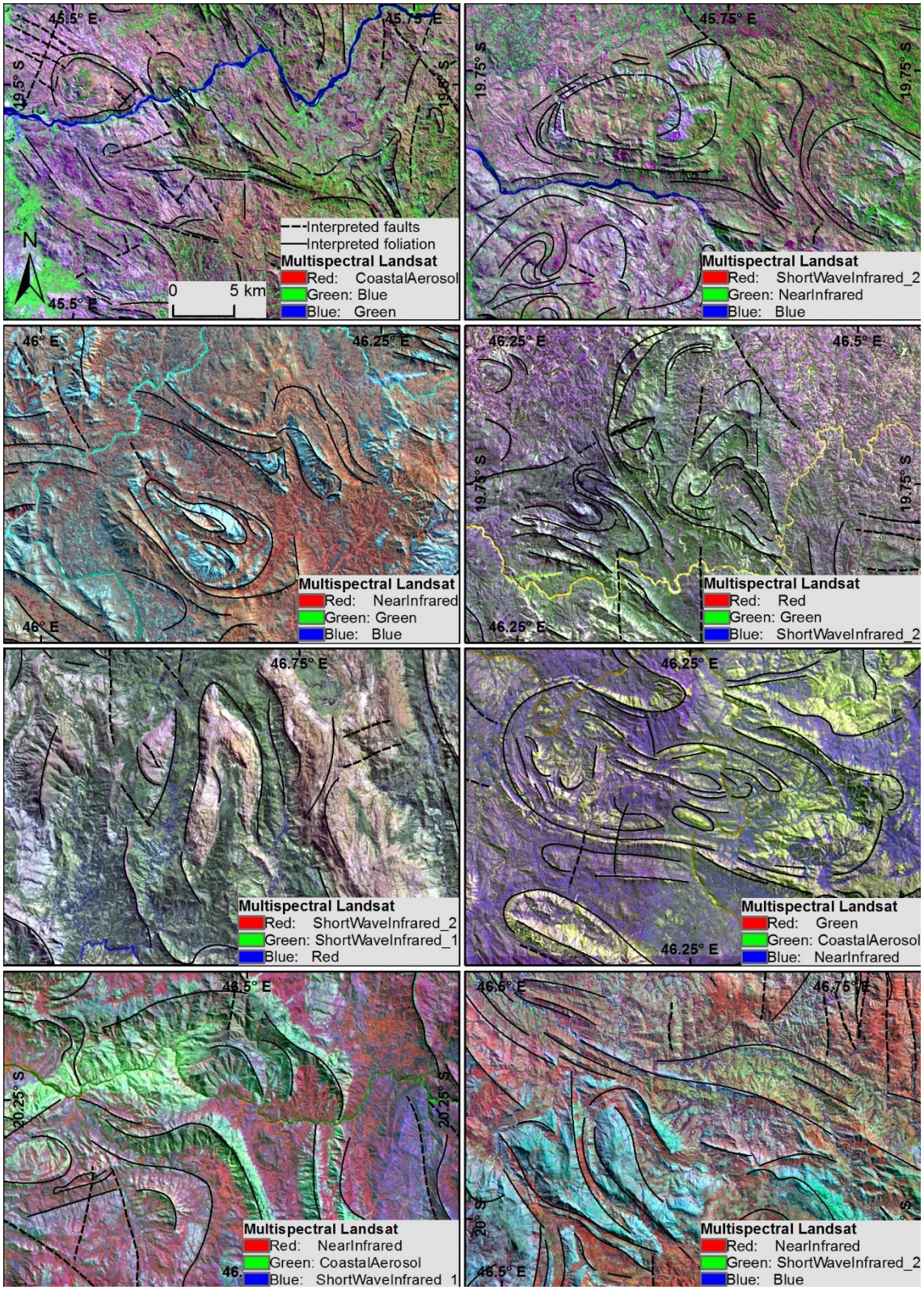

Appendix 5.1 Proterozoic basin evolution during Nuna: U–Pb zircon data

Sample No.	Sample - spot	$^{207}Pb/^{206}Pb$	± 2SE	$^{207}Pb/^{235}U$	± 2SE	$^{206}Pb/^{238}U$	± 2SE	Error Correlation 6/38 vs 7/35	Age $^{207}Pb/^{235}U$	± 2SE	Age $^{206}Pb/^{238}U$	± 2SE	Age $^{207}Pb/^{206}Pb$	± 2SE	Concordance 7/6 vs 6/38	Pb (PPM)	Th (PPM)	U (PPM)	U/Th
M16-10	M16-10 - 128.d	0.302	0.014	27.19	1.3	0.6355	0.017	0.68087	3389	46	3170	66	3478	74	91.14434	1910	101	185.4	1.831
M16-10	M16-10 - 133.d	0.2374	0.011	18.29	0.87	0.5478	0.014	0.5854	3004	46	2815	58	3100	74	90.80645	2479	160.4	336	2.043
M16-10	M16-10 - 117.d	0.2171	0.01	16.04	0.76	0.5283	0.014	0.53646	2878	45	2734	57	2957	78	92.45857	1761	111.2	175.2	1.55
M16-10	M16-10 - 105.d	0.2759	0.013	19.81	0.96	0.5201	0.014	0.71225	3080	46	2704	62	3337	75	81.03087	591	42.8	117.3	2.759
M16-10	M16-10 - 38.d	0.2352	0.012	16.65	1.1	0.517	0.026	0.93904	2894	74	2670	120	3087	74	86.49174	440	38.6	79.5	1.91
M16-10	M16-10 - 52.d	0.1762	0.0086	11.7	0.58	0.482	0.013	0.58799	2578	47	2535	57	2613	82	97.01493	583	55.4	104.6	1.895
M16-10	M16-10 - 147.d	0.1877	0.0098	12.57	0.67	0.4769	0.014	0.47582	2648	48	2512	63	2712	87	92.62537	140.7	14.07	50.2	3.73
M16-10	M16-10 - 45.d	0.1676	0.008	10.61	0.51	0.4592	0.012	0.55031	2488	45	2435	55	2534	84	96.09313	480	46.5	118.2	2.407
M16-10	M16-10 - 61.d	0.1568	0.0075	9.77	0.46	0.4578	0.012	0.47508	2412	44	2429	54	2418	81	100.4549	2360	134	177	1.332
M16-10	M16-10 - 14.d	0.187	0.0091	11.71	0.58	0.4551	0.012	0.71582	2579	48	2424	53	2712	79	89.38053	636	50.4	96.8	2.019
M16-10	M16-10 - 121.d	0.1604	0.0077	10.35	0.5	0.4556	0.012	0.61005	2465	45	2419	55	2456	81	98.49349	1557	117.2	169	1.425
M16-10	M16-10 - 96.d	0.168	0.008	10.57	0.51	0.4549	0.012	0.58656	2485	45	2416	54	2535	79	95.30572	2070	134.3	221.9	1.76
M16-10	M16-10 - 8.d	0.1691	0.0081	10.46	0.5	0.4536	0.012	0.35698	2475	44	2411	52	2545	80	94.73477	1261	94.3	189.7	2.216
M16-10	M16-10 - 79.d	0.1677	0.008	10.54	0.5	0.4523	0.012	0.48863	2482	45	2405	53	2531	81	95.02173	920	92.1	164.9	1.846
M16-10	M16-10 - 23.d	0.1766	0.0083	10.8	0.51	0.4462	0.012	0.63433	2507	47	2378	52	2619	80	90.79801	1012	76.3	235	3.223
M16-10	M16-10 - 13.d	0.1659	0.0079	10.08	0.48	0.4419	0.012	0.49852	2441	44	2359	52	2513	80	93.87187	1114	92.9	176.1	2.023
M16-10	M16-10 - 108.d	0.1623	0.0079	9.84	0.48	0.4382	0.012	0.50197	2418	45	2342	54	2475	82	94.62626	664	52.4	137.9	2.582
M16-10	M16-10 - 12.d	0.1697	0.0081	10.13	0.48	0.4351	0.011	0.36052	2446	44	2328	50	2552	80	91.22257	1783	145.9	251	1.865
M16-10	M16-10 - 87.d	0.1837	0.0088	10.97	0.53	0.4307	0.012	0.68485	2519	46	2307	56	2683	79	85.98584	666	56.1	132.7	2.462
M16-10	M16-10 - 115.d	0.1647	0.0079	9.86	0.48	0.429	0.011	0.568	2420	45	2301	52	2501	81	92.0032	1250	95.2	226	2.32
M16-10	M16-10 - 135.d	0.1762	0.0084	10.55	0.52	0.4272	0.012	0.64064	2482	46	2292	52	2613	81	87.71527	796	68.2	132.7	1.884
M16-10	M16-10 - 31.d	0.1828	0.0087	10.78	0.52	0.4268	0.011	0.52045	2503	45	2291	50	2675	79	85.64486	1251	128	153.3	1.136
M16-10	M16-10 - 102.d	0.254	0.012	14.9	0.72	0.4236	0.012	0.68588	2807	46	2276	52	3207	75	70.96975	2550	186	238	1.313
M16-10	M16-10 - 141.d	0.1641	0.008	9.79	0.51	0.4239	0.013	0.79126	2410	49	2276	59	2493	83	91.29563	615	74.8	151.4	2.106
M16-10	M16-10 - 30.d	0.1617	0.0079	9.47	0.47	0.4224	0.011	0.46244	2383	45	2275	54	2473	79	91.99353	1162	96.9	108.3	1.093
M16-10	M16-10 - 131.d	0.1547	0.0075	9.22	0.45	0.4234	0.012	0.64409	2361	48	2275	55	2394	81	95.02924	1021	73.9	123.1	1.632
M16-10	M16-10 - 92.d	0.1666	0.008	9.64	0.47	0.4211	0.012	0.60017	2399	44	2265	53	2520	81	89.88095	3030	181.5	186.5	1.1
M16-10	M16-10 - 156.d	0.1744	0.0083	10.17	0.5	0.4175	0.011	0.68828	2448	46	2249	51	2597	79	86.59992	1361	88.1	158.4	1.821
M16-10	M16-10 - 28.d	0.1592	0.0075	9.188	0.43	0.4169	0.011	0.45904	2356.1	44	2246	48	2448	84	91.74837	1816	146.5	253.1	1.709

Sample No.	Sample - spot	$^{207}Pb/^{206}Pb$	± 2SE	$^{207}Pb/^{235}U$	± 2SE	$^{206}Pb/^{238}U$	± 2SE	Error Correlation 6/38 vs 7/35	Age $^{207}Pb/^{235}U$	± 2SE	Age $^{206}Pb/^{238}U$	± 2SE	Age $^{207}Pb/^{206}Pb$	± 2SE	Concordance 7/6 vs 6/38	Pb (PPM)	Th (PPM)	U (PPM)	U/Th
M16-10	M16-10 - 15.d	0.1612	0.0077	9.11	0.43	0.4093	0.011	0.55452	2348	43	2211	49	2466	80	89.65937	1352	123.3	278	2.311
M16-10	M16-10 - 66.d	0.134	0.0065	7.51	0.37	0.4066	0.011	0.5155	2172	44	2198	51	2151	89	102.185	1431	128.6	149.2	1.222
M16-10	M16-10 - 155.d	0.1652	0.008	9.29	0.45	0.4025	0.011	0.55079	2366	44	2180	51	2506	81	86.99122	1105	74.6	137.5	1.881
M16-10	M16-10 - 35.d	0.1783	0.0084	9.68	0.47	0.3957	0.011	0.82395	2403	45	2148	51	2635	78	81.51803	920	112	260	2.214
M16-10	M16-10 - 153.d	0.1624	0.0082	8.97	0.5	0.3958	0.014	0.72787	2329	55	2148	67	2473	85	86.85807	404	30.47	78	2.597
M16-10	M16-10 - 75.d	0.1618	0.0081	8.86	0.45	0.3949	0.011	0.4911	2321	46	2145	50	2468	85	86.91248	613	63.5	95	1.514
M16-10	M16-10 - 116.d	0.1749	0.0087	9.6	0.58	0.395	0.018	0.91277	2386	59	2137	87	2600	84	82.19231	1210	79.4	146	1.739
M16-10	M16-10 - 142.d	0.1618	0.0078	8.93	0.44	0.3923	0.011	0.62089	2329	44	2133	50	2471	81	86.32133	748	96.2	196.6	2.135
M16-10	M16-10 - 149.d	0.1368	0.0065	7.26	0.35	0.3786	0.01	0.65948	2142	44	2069	47	2183	83	94.77783	620	80.7	254	3.228
M16-10	M16-10 - 136.d	0.1547	0.0073	8.14	0.4	0.3764	0.01	0.73758	2244	44	2059	49	2395	80	85.97077	1429	176.6	385	2.212
M16-10	M16-10 - 132.d	0.1531	0.0073	8.08	0.39	0.374	0.01	0.59606	2238	44	2047	48	2378	81	86.08074	1099	93.4	247	2.602
M16-10	M16-10 - 17.d	0.1529	0.0073	7.83	0.38	0.3715	0.0096	0.49368	2211	44	2036	45	2376	83	85.69024	1815	181.6	244	1.477
M16-10	M16-10 - 29.d	0.1562	0.0075	8	0.38	0.3711	0.0096	0.45797	2230	43	2034	45	2411	82	84.36333	2546	214	266	1.223
M16-10	M16-10 - 20.d	0.1518	0.0073	7.74	0.48	0.37	0.015	0.96107	2190	58	2022	73	2367	78	85.42459	1102	101.5	301	3.16
M16-10	M16-10 - 36.d	0.1514	0.0073	7.63	0.37	0.3679	0.01	0.53392	2186	43	2019	47	2357	82	85.65974	718	96.6	199.5	1.922
M16-10	M16-10 - 81.d	0.1451	0.0072	7.4	0.38	0.3676	0.011	0.52487	2158	45	2017	50	2282	85	88.38738	364	41.8	98.3	2.467
M16-10	M16-10 - 5.d	0.1588	0.0075	7.89	0.38	0.3649	0.0095	0.60039	2217	43	2005	45	2441	81	82.13847	1389	119.8	315	2.875
M16-10	M16-10 - 46.d	0.1692	0.0081	8.46	0.41	0.3641	0.01	0.6959	2283	47	2001	49	2546	81	78.59387	719	74.4	188.9	2.446
M16-10	M16-10 - 67.d	0.193	0.014	9.47	0.72	0.3558	0.01	0.23728	2360	67	1961	48	2715	120	72.22836	1540	68	146.6	2.242
M16-10	M16-10 - 126.d	0.1456	0.007	7.37	0.35	0.3548	0.0093	0.5775	2156	43	1957	44	2292	82	85.38394	1927	158.6	266	1.656
M16-10	M16-10 - 85.d	0.1558	0.0077	7.61	0.38	0.3523	0.01	0.51382	2183	45	1945	48	2404	85	80.90682	847	92	141.3	1.595
M16-10	M16-10 - 97.d	0.1634	0.0079	7.88	0.39	0.3486	0.0095	0.6244	2215	44	1927	45	2487	81	77.48291	1358	115.2	256.8	2.33
M16-10	M16-10 - 113.d	0.125	0.0061	5.98	0.29	0.3431	0.009	0.53608	1971	43	1901	43	2024	86	93.92292	2840	264.5	195.3	0.741
M16-10	M16-10 - 57.d	0.161	0.0077	7.42	0.39	0.3321	0.011	0.82997	2158	47	1847	51	2466	86	74.89862	1045	114.3	212	1.855
M16-10	M16-10 - 33.d	0.1628	0.0076	7.279	0.35	0.3257	0.0084	0.72329	2145	43	1817	41	2483	79	73.17761	2342	279	585	1.967
M16-10	M16-10 - 90.d	0.1802	0.009	8.11	0.42	0.324	0.012	0.73194	2239	47	1807	57	2653	85	68.11157	782	48.2	153.6	3.213
M16-10	M16-10 - 48.d	0.235	0.018	10.64	0.99	0.3219	0.011	0.88752	2442	87	1797	53	3020	130	59.50331	3450	168.4	317	1.847
M16-10	M16-10 - 3.d	0.1861	0.0088	8.13	0.4	0.3209	0.0087	0.801	2244	43	1793	42	2706	77	66.26016	3180	276	433	1.691
M16-10	M16-10 - 152.d	0.1142	0.006	5.09	0.27	0.3204	0.0089	0.37335	1831	44	1791	43	1855	94	96.54987	2550	237	120.5	0.519
M16-10	M16-10 - 42.d	0.1274	0.0061	5.54	0.27	0.3177	0.0086	0.48791	1906	42	1778	42	2058	86	86.39456	533	74.1	264.1	3.307
M16-10	M16-10 - 111.d	0.1124	0.0053	4.929	0.25	0.3161	0.0089	0.83404	1808	40	1770	44	1835	86	96.45777	1634	165.3	378	2.221
M16-10	M16-10 - 119.d	0.2105	0.01	9.24	0.5	0.3154	0.011	0.85224	2356	52	1765	56	2905	79	60.75731	1504	94.5	179.9	1.834

Sample No.	Sample - spot	$^{207}Pb/^{206}Pb$	± 2SE	$^{207}Pb/^{235}U$	± 2SE	$^{206}Pb/^{238}U$	± 2SE	Error Correlation 6/38 vs 7/35	Age $^{207}Pb/^{235}U$	± 2SE	Age $^{206}Pb/^{238}U$	± 2SE	Age $^{207}Pb/^{206}Pb$	± 2SE	Concordance 7/6 vs 6/38	Pb (PPM)	Th (PPM)	U (PPM)	U/Th
M16-10	M16-10 - 130.d	0.1528	0.0073	6.79	0.36	0.3137	0.011	0.76685	2081	52	1758	54	2373	84	74.08344	988	80	227	2.81
M16-10	M16-10 - 44.d	0.1803	0.011	7.8	0.49	0.3132	0.0099	0.76544	2203	52	1755	49	2658	84	66.02709	1680	180	250	1.304
M16-10	M16-10 - 32.d	0.1236	0.0059	5.313	0.25	0.3122	0.0079	0.4663	1870	41	1751	39	2006	84	87.28814	1504	213.3	426	1.889
M16-10	M16-10 - 24.d	0.1659	0.0079	7.04	0.4	0.31	0.014	0.9493	2108	53	1735	68	2513	80	69.04099	2020	151	261	1.754
M16-10	M16-10 - 89.d	0.1958	0.0094	8.31	0.44	0.3056	0.011	0.86556	2260	49	1717	53	2788	80	61.58537	1160	76.4	185	2.67
M16-10	M16-10 - 148.d	0.1208	0.0062	5.1	0.27	0.301	0.0085	0.42042	1832	45	1695	42	1957	95	86.61216	288	46.2	115.1	2.557
M16-10	M16-10 - 107.d	0.1247	0.0063	5.143	0.26	0.298	0.008	0.48215	1841	42	1681	40	2020	87	83.21782	726	81.8	191	2.286
M16-10	M16-10 - 7.d	0.1431	0.0072	5.76	0.36	0.296	0.014	0.88694	1930	54	1668	69	2258	84	73.87068	2750	246	175	0.77
M16-10	M16-10 - 150.d	0.1765	0.0093	7.19	0.45	0.296	0.017	0.89487	2122	60	1664	87	2608	87	63.80368	736	71.2	143.2	2.07
M16-10	M16-10 - 144.d	0.1178	0.0061	4.8	0.24	0.2882	0.0086	0.32391	1782	41	1632	45	1914	96	85.26646	284	43.2	108.9	2.607
M16-10	M16-10 - 82.d	0.1615	0.009	6.31	0.38	0.286	0.01	0.71	2022	49	1619	51	2464	90	65.70617	505	55.2	142.8	2.692
M16-10	M16-10 - 51.d	0.1564	0.0078	6.16	0.42	0.285	0.014	0.95211	1985	60	1612	71	2413	82	66.80481	791	96.2	176	1.776
M16-10	M16-10 - 50.d	0.1465	0.0072	5.73	0.3	0.2837	0.0084	0.77189	1932	45	1609	42	2300	85	69.95652	958	140.4	253	1.777
M16-10	M16-10 - 63.d	0.1451	0.0074	5.54	0.29	0.2816	0.0078	0.5995	1908	47	1599	39	2286	89	69.94751	812	60.8	137.3	2.354
M16-10	M16-10 - 109.d	0.1144	0.0055	4.442	0.22	0.2804	0.0081	0.63185	1721	38	1597	38	1866	89	85.58414	1486	164	416	2.474
M16-10	M16-10 - 9.d	0.1162	0.038	4.401	3.7	0.2772	0.033	0.61906	1711	200	1577	150	1894	240	83.26294	2139	227	319	1.55
M16-10	M16-10 - 68.d	0.1539	0.0076	5.81	0.31	0.2735	0.0085	0.74923	1944	47	1557	43	2384	83	65.3104	1081	123.4	227	1.942
M16-10	M16-10 - 84.d	0.1609	0.0077	5.922	0.29	0.2651	0.0076	0.63468	1963	44	1515	39	2462	81	61.53534	1066	161.8	368	2.349
M16-10	M16-10 - 100.d	0.1192	0.0062	4.34	0.32	0.263	0.014	0.89207	1682	61	1497	74	1933	95	77.44439	658	61.5	146	2.32
M16-10	M16-10 - 6.d	0.1495	0.0074	5.161	0.26	0.2543	0.0081	0.5774	1844	42	1459	41	2333	86	62.53751	3120	279	281	1.095
M16-10	M16-10 - 98.d	0.1397	0.0068	4.881	0.24	0.2528	0.0072	0.56383	1797	41	1452	37	2219	84	65.43488	1211	119.1	324	2.826
M16-10	M16-10 - 137.d	0.1505	0.0072	5.28	0.29	0.2496	0.0091	0.88955	1859	48	1435	47	2353	86	60.98598	1531	205.6	356.4	1.764
M16-10	M16-10 - 64.d	0.1583	0.0084	5.39	0.3	0.25	0.012	0.91161	1875	49	1434	63	2433	90	58.93958	1530	95	428	4.59
M16-10	M16-10 - 56.d	0.1156	0.0056	3.965	0.19	0.2486	0.0066	0.30018	1626	39	1431	34	1884	88	75.95541	326	49.7	319	6.55
M16-10	M16-10 - 76.d	0.2051	0.018	7.04	0.96	0.2454	0.013	0.90878	2106	88	1413	65	2861	110	49.38833	1900	129.5	265.6	2.072
M16-10	M16-10 - 103.d	0.1446	0.0069	4.916	0.24	0.2449	0.0066	0.56562	1804	41	1412	34	2283	86	61.84845	1041	129.7	398	3.076
M16-10	M16-10 - 18.d	0.128	0.0062	4.294	0.21	0.2441	0.0076	0.78232	1690	41	1407	40	2066	86	68.10261	1762	177.5	443	2.706
M16-10	M16-10 - 4.d	0.1789	0.0089	5.91	0.3	0.2429	0.0084	0.70421	1960	44	1400	44	2637	80	53.09063	2250	200	331	1.765
M16-10	M16-10 - 120.d	0.1282	0.0063	4.29	0.23	0.2401	0.008	0.85002	1685	46	1386	42	2067	88	67.0537	2210	216	286	1.49
M16-10	M16-10 - 59.d	0.1509	0.0074	4.97	0.28	0.2379	0.0089	0.86243	1808	47	1374	46	2351	85	58.44322	1188	138.1	280	2.021
M16-10	M16-10 - 134.d	0.1707	0.0081	5.571	0.27	0.2328	0.0062	0.61776	1910	41	1349	33	2562	81	52.65418	1990	215	590	2.663
M16-10	M16-10 - 91.d	0.1365	0.0066	4.392	0.22	0.2326	0.0064	0.65611	1709	41	1348	34	2179	84	61.86324	1748	130.2	367	3.004

Sample No.	Sample - spot	$^{207}Pb/^{206}Pb$	± 2SE	$^{207}Pb/^{235}U$	± 2SE	$^{206}Pb/^{238}U$	± 2SE	Error Correlation 6/38 vs 7/35	Age $^{207}Pb/^{235}U$	± 2SE	Age $^{206}Pb/^{238}U$	± 2SE	Age $^{207}Pb/^{206}Pb$	± 2SE	Concordance 7/6 vs 6/38	Pb (PPM)	Th (PPM)	U (PPM)	U/Th
M16-10	M16-10 - 145.d	0.1279	0.01	4.16	0.28	0.2317	0.0071	0.35948	1664	48	1343	38	2064	100	65.06783	1507	256.3	332.4	1.347
M16-10	M16-10 - 22.d	0.105	0.0051	3.349	0.16	0.2317	0.0061	0.54069	1491	38	1343	32	1709	90	78.58397	312	41.8	429	10.97
M16-10	M16-10 - 140.d	0.1495	0.0074	4.77	0.27	0.2268	0.0085	0.81801	1772	47	1316	45	2333	84	56.40806	2690	373	368	1.018
M16-10	M16-10 - 124.d	0.1107	0.0057	3.5	0.19	0.2218	0.009	0.88788	1520	45	1289	48	1804	90	71.45233	1231	112.1	373	3.284
M16-10	M16-10 - 151.d	0.1445	0.0072	4.37	0.25	0.2164	0.0077	0.82019	1700	47	1261	41	2282	89	55.25855	973	74.3	337	4.22
M16-10	M16-10 - 106.d	0.1128	0.0057	3.339	0.19	0.2144	0.0078	0.6703	1488	43	1251	41	1839	91	68.0261	252	32.7	242	7.36
M16-10	M16-10 - 99.d	0.1175	0.0065	3.44	0.21	0.2127	0.0093	0.67287	1505	48	1241	49	1899	100	65.35018	465	48.5	77.4	1.624
M16-10	M16-10 - 53.d	0.1692	0.0086	4.92	0.25	0.2121	0.0074	0.66858	1804	43	1239	39	2542	86	48.74115	1460	138.7	332	2.394
M16-10	M16-10 - 94.d	0.1116	0.0056	3.27	0.23	0.2097	0.0097	0.95079	1458	59	1224	52	1817	93	67.36379	659	70.4	428	6.23
M16-10	M16-10 - 37.d	0.1379	0.0071	3.79	0.2	0.2009	0.0068	0.6504	1586	44	1179	36	2192	86	53.7865	662	69.8	285	3.78
M16-10	M16-10 - 72.d	0.1612	0.013	4.34	0.21	0.1945	0.0089	0.31294	1699	40	1145	49	2461	110	46.5258	941	87	257.4	3.09
M16-10	M16-10 - 73.d	0.1736	0.0094	4.66	0.26	0.1934	0.0065	0.50225	1754	46	1139	35	2579	89	44.1644	668	67.9	108.5	1.688
M16-10	M16-10 - 125.d	0.1203	0.0059	3.28	0.19	0.1907	0.0066	0.91254	1469	45	1124	36	1956	87	57.46421	1910	222	454	1.989
M16-10	M16-10 - 54.d	0.1846	0.0088	4.761	0.24	0.1872	0.0058	0.81042	1776	42	1105	32	2696	75	40.98665	1340	137	463	3.384
M16-10	M16-10 - 27.d	0.1348	0.0065	3.469	0.17	0.187	0.0055	0.75904	1518	40	1105	30	2157	84	51.22856	2270	239	499	2.099
M16-10	M16-10 - 114.d	0.1584	0.0077	4.123	0.21	0.1868	0.0058	0.72758	1656	42	1104	31	2434	82	45.35744	1520	137.9	320	2.291
M16-10	M16-10 - 40.d	0.101	0.005	2.521	0.14	0.1818	0.0059	0.86499	1273	41	1076	32	1634	92	65.85067	1036	233	530	2.072
M16-10	M16-10 - 26.d	0.1269	0.0062	3.14	0.19	0.1793	0.0066	0.91429	1436	46	1062	36	2050	86	51.80488	336	42.5	504	12.46
M16-10	M16-10 - 157.d	0.1222	0.006	3.07	0.16	0.179	0.0053	0.84905	1422	40	1061	29	1985	86	53.45088	1319	168	569	3.48
M16-10	M16-10 - 138.d	0.1715	0.0086	4.263	0.21	0.1781	0.0061	0.66381	1684	42	1056	33	2566	83	41.15355	1562	199	398	2.047
M16-10	M16-10 - 118.d	0.1561	0.0075	3.773	0.19	0.1737	0.0061	0.86527	1584	41	1032	33	2410	81	42.82158	2270	181	563	3.04
M16-10	M16-10 - 160.d	0.1585	0.0077	3.82	0.21	0.1719	0.006	0.86698	1592	45	1022	33	2435	82	41.97125	2310	125.7	541	4.27
M16-10	M16-10 - 41.d	0.196	0.0095	4.457	0.22	0.1657	0.0045	0.60863	1721	42	988	25	2789	79	35.42488	1790	265	399	1.353
M16-10	M16-10 - 11.d	0.1219	0.0059	2.701	0.14	0.1616	0.0048	0.78146	1326	38	966	27	1979	86	48.81253	1228	170	546	3.503
M16-10	M16-10 - 2.d	0.1606	0.0079	3.355	0.18	0.1534	0.0053	0.81011	1489	43	919	30	2456	82	37.41857	1491	114.8	435	4.046
M16-10	M16-10 - 95.d	0.1663	0.0085	3.5	0.2	0.1524	0.0057	0.82695	1524	43	913	32	2515	84	36.30219	1600	126.1	321	2.718
M16-10	M16-10 - 43.d	0.1742	0.0088	3.592	0.19	0.1507	0.0052	0.69741	1544	42	904	29	2591	85	34.89	1094	63.5	442	6.57
M16-10	M16-10 - 86.d	0.2031	0.01	4.24	0.24	0.1504	0.0054	0.82663	1680	44	903	30	2847	80	31.7176	2143	191.1	403	2.182
M16-10	M16-10 - 69.d	0.1647	0.0086	3.43	0.22	0.1491	0.0062	0.80612	1501	52	895	35	2494	87	35.88613	2250	239	410	1.92
M16-10	M16-10 - 110.d	0.1167	0.006	2.398	0.11	0.1482	0.0043	0.37735	1241	36	891	24	1902	88	46.84543	1492	130.9	533	3.94
M16-10	M16-10 - 93.d	0.1653	0.013	3.36	0.17	0.1472	0.0071	0.86583	1491	42	884	41	2506	100	35.27534	2660	82.7	596	7.67
M16-10	M16-10 - 62.d	0.1579	0.0085	3.14	0.19	0.1465	0.0049	0.79293	1441	48	881	28	2420	89	36.40496	2300	105.8	485	4.565

Sample No.	Sample - spot	$^{207}Pb/^{206}Pb$	± 2SE	$^{207}Pb/^{235}U$	± 2SE	$^{206}Pb/^{238}U$	± 2SE	Error Correlation 6/38 vs 7/35	Age $^{207}Pb/^{235}U$	± 2SE	Age $^{206}Pb/^{238}U$	± 2SE	Age $^{207}Pb/^{206}Pb$	± 2SE	Concordance 7/6 vs 6/38	Pb (PPM)	Th (PPM)	U (PPM)	U/Th
M16-10	M16-10 - 19.d	0.1866	0.0091	3.7	0.2	0.1445	0.0049	0.80307	1567	43	869	27	2708	81	32.0901	1640	77.1	339	4.9
M16-10	M16-10 - 78.d	0.1504	0.0072	2.903	0.16	0.1388	0.0051	0.91506	1378	41	837	29	2347	82	35.66255	1670	107.9	575	5.38
M16-10	M16-10 - 58.d	0.1658	0.012	3.146	0.26	0.1373	0.0039	0.25554	1441	54	829	22	2504	100	33.10703	1720	161	576	3.623
M16-10	M16-10 - 123.d	0.2357	0.011	4.41	0.29	0.1316	0.0068	0.95723	1701	55	796	38	3087	77	25.78555	3270	181.7	621	3.316
M16-10	M16-10 - 70.d	0.1146	0.0057	2.066	0.15	0.13	0.0062	0.92529	1132	45	787	35	1869	87	42.10808	1163	156	814	5.81
M16-10	M16-10 - 65.d	0.2864	0.015	5.09	0.31	0.1291	0.0043	0.78804	1825	52	782	25	3387	83	23.08828	5270	165.9	643	4.003
M16-10	M16-10 - 49.d	0.0895	0.0043	1.566	0.083	0.1268	0.0039	0.85902	954	33	769	22	1409	93	54.57771	1175	250	963	3.709
M16-10	M16-10 - 77.d	0.195	0.011	3.43	0.21	0.1265	0.0048	0.72066	1503	48	767	28	2772	84	27.66955	2320	91	618	7.42
M16-10	M16-10 - 34.d	0.2238	0.012	3.479	0.19	0.1136	0.0046	0.75744	1520	45	693	27	3002	81	23.08461	2208	209.4	784	3.515
M16-10	M16-10 - 158.d	0.1937	0.01	3.001	0.17	0.1122	0.0058	0.81007	1403	43	684	34	2761	89	24.77363	1422	71.7	283	3.925
M16-10	M16-10 - 1.d	0.0763	0.0038	1.16	0.06	0.1109	0.0031	0.62319	780	28	678.1	18	1100	96	61.64545	546	119.4	872	7.64
M16-10	M16-10 - 60.d	0.0891	0.0044	1.264	0.063	0.1023	0.0028	0.5095	829	28	627.8	16	1399	97	44.87491	929	121.7	1037	8.7
M16-10	M16-10 - 139.d	0.0757	0.0038	1.055	0.054	0.0992	0.0026	0.50169	730	27	609.7	15	1078	100	56.55844	222	51.7	887	18.44
M16-10	M16-10 - 83.d	0.1603	0.0081	2.197	0.11	0.0988	0.0029	0.60416	1178	36	607	17	2451	86	24.7654	1780	88.6	703	8.44
M16-10	M16-10 - 16.d	0.0533	0.0036	0.726	0.056	0.0986	0.0046	0.61691	548	33	606	27	290	150	208.9655	0.5	Below LOD	86.2	########
M16-10	M16-10 - 25.d	0.2661	0.013	3.61	0.2	0.0985	0.0032	0.88707	1547	43	605	19	3279	77	18.45075	5140	54.6	788	14.78
M16-10	M16-10 - 112.d	0.1427	0.0095	1.912	0.11	0.0959	0.0031	0.75323	1082	39	590	18	2254	97	26.17569	1580	87.1	589	6.7
M16-10	M16-10 - 47.d	0.2055	0.01	2.698	0.15	0.0954	0.0038	0.88389	1323	41	587	22	2866	79	20.48151	2017	161.5	564	3.422
M16-10	M16-10 - 154.d	0.225	0.011	2.99	0.17	0.095	0.0033	0.88951	1400	44	585	19	3011	81	19.42876	3840	331	717	2.6
M16-10	M16-10 - 127.d	0.1745	0.0085	2.324	0.12	0.0939	0.0035	0.84769	1217	38	578	20	2596	82	22.26502	2710	79.7	746	8.88
M16-10	M16-10 - 55.d	0.2379	0.012	3.027	0.15	0.0928	0.0032	0.52771	1412	39	572	19	3097	82	18.46949	2040	46.9	557	12.35
M16-10	M16-10 - 101.d	0.0721	0.0038	0.929	0.047	0.0927	0.0025	0.1496	666	25	571.4	15	987	100	57.8926	549	73.1	1052	14.91
M16-10	M16-10 - 21.d	0.0776	0.0038	0.978	0.049	0.0916	0.0024	0.5377	692	25	564.9	14	1129	97	50.03543	894	49	1438	31.45
M16-10	M16-10 - 104.d	0.076	0.0053	0.966	0.071	0.0915	0.0027	0.66647	685	35	564.3	16	1084	110	52.0572	352	56.6	646	11.35
M16-10	M16-10 - 74.d	0.2575	0.014	3.29	0.2	0.0914	0.0033	0.82782	1469	48	563	20	3221	84	17.47904	1930	57.6	484	8.7
M16-10	M16-10 - 88.d	0.2008	0.011	2.54	0.16	0.0912	0.0043	0.81392	1273	46	562	25	2821	88	19.92201	1620	53.1	503	9.77
M16-10	M16-10 - 71.d	0.2632	0.013	3.27	0.18	0.0894	0.0028	0.79974	1470	43	552	17	3259	80	16.93771	3160	96.9	822	8.88
M16-10	M16-10 - 80.d	0.2523	0.014	3.066	0.17	0.0878	0.0031	0.5287	1420	42	542	18	3187	84	17.00659	2560	46.7	619	13.55
M16-10	M16-10 - 143.d	0.0998	0.0051	1.209	0.065	0.0862	0.003	0.69454	802	30	533	18	1609	96	33.12617	542	58.7	794	13.98
M16-10	M16-10 - 146.d	0.2076	0.011	2.461	0.15	0.0842	0.0032	0.78644	1257	42	521	19	2881	82	18.084	1126	58.5	482	8.66
M16-10	M16-10 - 122.d	0.1176	0.0073	1.294	0.093	0.0779	0.0036	0.57761	838	40	483	21	1907	110	25.32774	340	22.3	230.1	10.43
M16-10	M16-10 - 39.d	0.2798	0.016	2.73	0.2	0.0705	0.0029	0.90115	1321	55	439	17	3345	91	13.12407	1103	60.5	370	5.72

Sample No.	Sample - spot	$^{207}Pb/^{206}Pb$	± 2SE	$^{207}Pb/^{235}U$	± 2SE	$^{206}Pb/^{238}U$	± 2SE	Error Correlation 6/38 vs 7/35	Age $^{207}Pb/^{235}U$	± 2SE	Age $^{206}Pb/^{238}U$	± 2SE	Age $^{207}Pb/^{206}Pb$	± 2SE	Concordance 7/6 vs 6/38	Pb (PPM)	Th (PPM)	U (PPM)	U/Th
M16-10	M16-10 - 159.d	0.2941	0.014	2.722	0.14	0.0659	0.0022	0.91421	1331	39	411	13	3436	76	11.96158	6970	92.9	1156	12.6
M16-10	M16-10 - 10.d	0.2472	0.012	2.186	0.13	0.0645	0.0034	0.89196	1174	40	403	20	3164	78	12.73704	3148	118.8	985	9.11
M16-10	M16-10 - 129.d	0.2731	0.016	2.154	0.16	0.0564	0.0026	0.57745	1163	46	354	16	3320	86	10.66265	1260	61.1	313	5.18
M16-11	M16-11 - 70.d	no value	NAN	no value	NAN	no value	NAN	NaN	no value	NAN	no value	NAN	no value	NAN	#VALUE!	94.7	0.103	Below LOD	no value
M16-11	M16-11 - 95.d	no value	NAN	no value	NAN	no value	NAN	NaN	no value	NAN	no value	NAN	no value	NAN	#VALUE!	169	Below LOD	Below LOD	no value
M16-11	M16-11 - 73.d	0.2265	0.011	16.47	0.78	0.5326	0.014	0.6079	2903	45	2752	58	3026	76	90.94514	680	64.7	251.4	3.568
M16-11	M16-11 - 51.d	0.1835	0.0088	13.28	0.64	0.5224	0.014	0.58721	2704	46	2708	61	2685	84	100.8566	490	42	96.5	2.3
M16-11	M16-11 - 112.d	0.1709	0.0089	12.21	0.65	0.518	0.017	0.51477	2615	49	2688	72	2556	87	105.1643	366	30.2	38.4	1.219
M16-11	M16-11 - 108.d	0.1844	0.0089	13.22	0.63	0.5157	0.014	0.4989	2697	47	2680	57	2693	75	99.51727	2338	261.7	191	0.736
M16-11	M16-11 - 94.d	0.1958	0.01	13.86	0.72	0.513	0.015	0.43403	2740	51	2668	63	2781	85	95.93671	299	23.67	52.9	2.155
M16-11	M16-11 - 62.d	0.1901	0.0089	13.41	0.63	0.5063	0.013	0.64019	2708	45	2644	59	2741	77	96.46115	1131	94.9	408	4.257
M16-11	M16-11 - 9.d	0.1993	0.0096	13.92	0.67	0.5064	0.013	0.65491	2742	46	2640	57	2818	77	93.68346	933	109.7	207.3	1.915
M16-11	M16-11 - 80.d	0.1853	0.0089	12.85	0.62	0.4993	0.013	0.51795	2667	46	2610	57	2698	79	96.73832	496	42.7	135.8	3.11
M16-11	M16-11 - 114.d	0.1538	0.0078	10.47	0.52	0.4959	0.013	0.27025	2475	46	2595	58	2387	81	108.7139	837	76	90	1.125
M16-11	M16-11 - 91.d	0.1933	0.0092	13.21	0.63	0.495	0.013	0.61658	2694	45	2592	57	2768	77	93.64162	2131	161.3	299	1.741
M16-11	M16-11 - 124.d	0.1542	0.0077	10.32	0.52	0.485	0.013	0.43937	2461	47	2548	58	2386	86	106.7896	1282	126.9	80.7	0.625
M16-11	M16-11 - 47.d	0.1754	0.0087	11.93	0.66	0.484	0.016	0.81493	2593	50	2539	69	2604	83	97.50384	751	59.4	88.5	1.467
M16-11	M16-11 - 130.d	0.1855	0.009	12.12	0.6	0.4825	0.013	0.55244	2611	47	2537	58	2702	84	93.89341	705	80.3	127.8	1.611
M16-11	M16-11 - 109.d	0.1785	0.0086	11.98	0.63	0.482	0.015	0.89053	2598	49	2534	65	2636	79	96.1305	1249	170	296	1.92
M16-11	M16-11 - 8.d	0.1885	0.0092	12.43	0.61	0.4804	0.013	0.57962	2636	46	2528	58	2724	81	92.8047	352	38.3	107.3	2.867
M16-11	M16-11 - 56.d	0.1651	0.0078	10.95	0.53	0.4774	0.013	0.56475	2518	44	2515	55	2509	84	100.2391	930	86.2	184.1	2.127
M16-11	M16-11 - 58.d	0.1795	0.0085	11.79	0.58	0.4737	0.014	0.83029	2586	46	2498	60	2646	77	94.40665	3080	274	353	1.271
M16-11	M16-11 - 42.d	0.1757	0.0083	11.67	0.55	0.4732	0.012	0.55512	2577	44	2497	53	2613	75	95.56066	1334	99.4	240.8	2.338
M16-11	M16-11 - 72.d	0.1724	0.0083	10.95	0.52	0.4649	0.013	0.46685	2518	44	2460	55	2577	81	95.45984	1130	121	166.5	1.268
M16-11	M16-11 - 67.d	0.1672	0.0081	10.53	0.52	0.4645	0.013	0.655	2481	46	2458	56	2526	82	97.308	901	98.1	135.5	1.31
M16-11	M16-11 - 71.d	0.172	0.0085	10.73	0.54	0.4577	0.014	0.54567	2497	47	2428	60	2571	82	94.43796	944	101.2	68.6	0.626
M16-11	M16-11 - 46.d	0.1589	0.0077	10.06	0.49	0.4514	0.012	0.62395	2441	48	2401	54	2440	81	98.40164	863	69.7	100.4	1.39
M16-11	M16-11 - 84.d	0.1723	0.0084	10.68	0.52	0.451	0.012	0.43296	2494	46	2399	52	2575	82	93.16505	4510	303	175.3	0.5104
M16-11	M16-11 - 125.d	0.1584	0.0078	9.89	0.5	0.4499	0.013	0.60841	2421	47	2393	59	2433	86	98.35594	1144	114	133	1.162
M16-11	M16-11 - 102.d	0.158	0.0081	9.74	0.49	0.4472	0.013	0.29042	2407	46	2381	58	2425	88	98.18557	707	104.1	90.2	0.869
M16-11	M16-11 - 38.d	0.1597	0.0079	9.95	0.5	0.4452	0.012	0.56136	2427	46	2373	55	2446	83	97.01554	707	55.3	76.2	1.333
M16-11	M16-11 - 98.d	0.1568	0.0075	9.32	0.45	0.4335	0.012	0.51722	2368	44	2321	52	2418	82	95.98842	601	95.2	207.8	2.17

Sample No.	Sample - spot	$^{207}Pb/^{206}Pb$	± 2SE	$^{207}Pb/^{235}U$	± 2SE	$^{206}Pb/^{238}U$	± 2SE	Error Correlation 6/38 vs 7/35	Age $^{207}Pb/^{235}U$	± 2SE	Age $^{206}Pb/^{238}U$	± 2SE	Age $^{207}Pb/^{206}Pb$	± 2SE	Concordance 7/6 vs 6/38	Pb (PPM)	Th (PPM)	U (PPM)	U/Th
M16-11	M16-11 - 93.d	0.1917	0.0091	11.33	0.54	0.4275	0.011	0.53257	2550	44	2294	50	2757	73	83.20638	243	23.6	331	13.79
M16-11	M16-11 - 127.d	0.1625	0.0077	9.36	0.45	0.4253	0.011	0.55591	2373	44	2284	52	2483	85	91.9855	1176	149.8	283	1.959
M16-11	M16-11 - 132.d	0.168	0.0084	9.65	0.52	0.4252	0.014	0.71953	2397	50	2281	63	2531	84	90.12248	1240	142.5	121.2	0.839
M16-11	M16-11 - 131.d	0.1733	0.0084	9.69	0.46	0.4147	0.012	0.37834	2405	44	2235	53	2585	81	86.46035	1126	124.2	176	1.455
M16-11	M16-11 - 92.d	0.1674	0.0082	9.52	0.48	0.4116	0.011	0.70443	2386	47	2221	52	2527	82	87.89078	1395	144	156.2	1.048
M16-11	M16-11 - 76.d	0.1584	0.0076	8.93	0.43	0.4082	0.01	0.54605	2329	44	2206	48	2435	81	90.59548	472	52.4	303	5.36
M16-11	M16-11 - 74.d	0.1469	0.0075	8.02	0.41	0.3979	0.012	0.34082	2230	46	2158	53	2301	88	93.78531	397	45.8	77.9	1.559
M16-11	M16-11 - 19.d	0.2316	0.011	12.53	0.72	0.395	0.016	0.9235	2635	58	2142	78	3059	78	70.02288	959	121	166	1.4
M16-11	M16-11 - 121.d	0.1337	0.0064	7.27	0.35	0.3942	0.01	0.60609	2144	43	2142	48	2147	80	99.76712	1384	182.8	244.5	1.303
M16-11	M16-11 - 25.d	0.1368	0.0067	7.55	0.38	0.3925	0.011	0.49525	2176	44	2133	50	2182	86	97.75435	1559	151.6	145	1.011
M16-11	M16-11 - 53.d	0.1343	0.0068	7.32	0.37	0.3918	0.011	0.34048	2148	45	2130	52	2147	87	99.2082	674	74.5	122.1	1.626
M16-11	M16-11 - 103.d	0.1514	0.0072	8.156	0.39	0.3892	0.0099	0.41246	2249	41	2119	46	2358	82	89.86429	1681	291	384	1.316
M16-11	M16-11 - 83.d	0.1713	0.0082	9.03	0.45	0.3848	0.011	0.77372	2339	46	2098	50	2571	76	81.60249	1484	114	337	2.601
M16-11	M16-11 - 17.d	0.1537	0.0073	8.06	0.38	0.3838	0.0099	0.47459	2236	43	2094	46	2384	81	87.83557	786	83.2	316	3.863
M16-11	M16-11 - 29.d	0.1283	0.0063	6.76	0.34	0.3756	0.01	0.48911	2078	44	2055	48	2069	87	99.32334	741	75.8	146.8	2.035
M16-11	M16-11 - 90.d	0.1689	0.0097	9.01	0.8	0.377	0.02	0.98334	2293	89	2051	96	2526	100	81.19557	2965	279.2	401	1.34
M16-11	M16-11 - 44.d	0.1479	0.007	7.776	0.37	0.3735	0.01	0.62896	2205	42	2045	47	2320	81	88.14655	2616	246	363	1.415
M16-11	M16-11 - 20.d	0.1614	0.0076	8.28	0.4	0.3726	0.011	0.80015	2261	43	2040	50	2471	84	82.55767	1896	206	330	1.591
M16-11	M16-11 - 26.d	0.1346	0.0065	6.96	0.34	0.3676	0.01	0.59008	2104	44	2018	47	2155	85	93.64269	1347	139.3	268.9	2.042
M16-11	M16-11 - 40.d	0.1547	0.0074	7.96	0.39	0.366	0.01	0.73408	2224	45	2010	48	2395	81	83.92484	1400	117.8	270	2.185
M16-11	M16-11 - 16.d	0.1535	0.0073	7.58	0.37	0.3624	0.0097	0.58904	2181	43	1993	46	2381	81	83.70433	976	126.5	273	2.199
M16-11	M16-11 - 104.d	0.1556	0.0076	7.72	0.41	0.3588	0.011	0.73701	2194	47	1975	52	2403	81	82.18893	379	54.8	127.7	2.33
M16-11	M16-11 - 30.d	0.1408	0.007	7.02	0.35	0.3559	0.01	0.45723	2111	44	1962	49	2231	86	87.94263	1180	197	93.2	0.511
M16-11	M16-11 - 66.d	0.1257	0.0074	6.03	0.35	0.3557	0.012	0.26788	1973	50	1960	55	2012	110	97.41551	133	18	53.4	2.9
M16-11	M16-11 - 89.d	0.1852	0.0096	9.02	0.45	0.3545	0.011	0.37996	2341	49	1955	51	2690	86	72.67658	1970	124	173	1.288
M16-11	M16-11 - 115.d	0.1056	0.0051	5.116	0.25	0.3524	0.0095	0.54593	1840	43	1946	45	1721	88	113.0738	1104	143.4	278	1.854
M16-11	M16-11 - 116.d	0.105	0.0052	5.104	0.25	0.3518	0.0092	0.43372	1835	42	1943	44	1709	90	113.6922	686	89	247	2.71
M16-11	M16-11 - 65.d	0.1188	0.0064	5.71	0.3	0.3459	0.01	0.35343	1928	47	1914	50	1923	97	99.53198	372	39.4	73	1.828
M16-11	M16-11 - 87.d	0.1207	0.0059	5.67	0.28	0.3398	0.0093	0.53394	1924	44	1885	45	1966	93	95.87996	2078	204.2	145.7	0.649
M16-11	M16-11 - 126.d	0.1448	0.0075	6.8	0.63	0.34	0.023	0.97953	2039	87	1870	110	2274	91	82.23395	2390	304	319	1.15
M16-11	M16-11 - 78.d	0.1548	0.0075	7.19	0.44	0.3338	0.014	0.87564	2127	60	1855	69	2394	87	77.48538	1580	260	295	1.09
M16-11	M16-11 - 11.d	0.1504	0.0082	6.87	0.34	0.3334	0.013	0.47419	2093	46	1854	62	2344	87	79.09556	552	76.7	136.7	1.836

Sample No.	Sample - spot	$^{207}Pb/^{206}Pb$	± 2SE	$^{207}Pb/^{235}U$	± 2SE	$^{206}Pb/^{238}U$	± 2SE	Error Correlation 6/38 vs 7/35	Age $^{207}Pb/^{235}U$	± 2SE	Age $^{206}Pb/^{238}U$	± 2SE	Age $^{207}Pb/^{206}Pb$	± 2SE	Concordance 7/6 vs 6/38	Pb (PPM)	Th (PPM)	U (PPM)	U/Th
M16-11	M16-11 - 79.d	0.1191	0.0057	5.541	0.27	0.3333	0.0087	0.53985	1906	42	1854	42	1944	91	95.37037	3210	415	275	0.6243
M16-11	M16-11 - 41.d	0.1805	0.0096	8.41	0.44	0.3319	0.011	0.43246	2273	47	1853	55	2645	88	70.05671	659	54.3	73.3	1.342
M16-11	M16-11 - 75.d	0.1473	0.0071	6.7	0.36	0.3294	0.011	0.88277	2066	49	1834	52	2310	84	79.39394	1757	223.5	277	1.124
M16-11	M16-11 - 23.d	0.145	0.007	6.79	0.43	0.33	0.014	0.95934	2071	57	1834	67	2288	83	80.15734	2630	297	271	0.962
M16-11	M16-11 - 59.d	0.1149	0.0055	5.23	0.27	0.3292	0.0099	0.7726	1855	43	1834	48	1874	86	97.86553	1120	144.5	350	2.422
M16-11	M16-11 - 123.d	0.1455	0.007	6.6	0.33	0.3287	0.0092	0.74155	2057	43	1831	45	2290	83	79.95633	849	110.5	368	3.28
M16-11	M16-11 - 113.d	0.1247	0.0062	5.67	0.33	0.3289	0.013	0.86741	1919	50	1830	61	2017	88	90.72881	1600	196	223	1.066
M16-11	M16-11 - 111.d	0.1637	0.0083	7.4	0.42	0.328	0.014	0.7951	2154	51	1826	67	2492	84	73.27448	1178	160	144	0.872
M16-11	M16-11 - 77.d	0.1201	0.0059	5.435	0.26	0.3272	0.0084	0.06031	1891	43	1825	41	1956	92	93.30266	841	110.9	247.5	2.083
M16-11	M16-11 - 55.d	0.1305	0.0064	5.87	0.3	0.3244	0.0099	0.71719	1953	42	1810	48	2099	85	86.23154	702	76.4	205	2.62
M16-11	M16-11 - 18.d	0.1238	0.0063	5.48	0.27	0.3242	0.0086	0.093443	1895	42	1810	42	2002	90	90.40959	618	74.5	160.5	2.178
M16-11	M16-11 - 36.d	0.1109	0.0054	5.05	0.26	0.3243	0.009	0.57148	1824	45	1810	44	1821	95	99.39594	687	70.8	165.7	2.279
M16-11	M16-11 - 85.d	0.1188	0.0059	5.24	0.27	0.3206	0.0095	0.60521	1855	44	1792	46	1930	90	92.84974	851	81.9	139.9	1.518
M16-11	M16-11 - 69.d	0.1229	0.0063	5.34	0.28	0.3201	0.0092	0.44954	1872	44	1789	45	1989	90	89.9447	687	94.7	152.2	1.514
M16-11	M16-11 - 10.d	0.1627	0.0079	7.13	0.4	0.3186	0.011	0.88417	2120	52	1781	56	2479	83	71.84349	1146	162	290	1.838
M16-11	M16-11 - 15.d	0.1614	0.0077	7.03	0.38	0.3177	0.01	0.89229	2109	49	1777	52	2467	80	72.03081	1851	239	400	1.678
M16-11	M16-11 - 106.d	0.1203	0.0058	5.32	0.27	0.3169	0.0097	0.74411	1869	44	1773	47	1956	87	90.64417	358	67.6	274	4.06
M16-11	M16-11 - 7.d	0.1175	0.0057	5.111	0.26	0.3149	0.0088	0.62553	1836	42	1764	44	1914	87	92.16301	966	182	276	1.552
M16-11	M16-11 - 3.d	0.1187	0.0058	5.181	0.26	0.3135	0.0085	0.45765	1850	44	1757	41	1930	87	91.03627	1099	113.5	187.7	1.639
M16-11	M16-11 - 97.d	0.2011	0.01	8.58	0.59	0.312	0.017	0.88273	2277	61	1743	82	2827	83	61.65547	1004	147	146	0.98
M16-11	M16-11 - 54.d	0.111	0.0054	4.78	0.24	0.3104	0.009	0.68423	1778	44	1742	44	1809	90	96.2963	818	111.1	278	2.45
M16-11	M16-11 - 43.d	0.1089	0.0054	4.736	0.24	0.3091	0.0086	0.55594	1771	42	1735	42	1774	90	97.80158	984	117	196	1.703
M16-11	M16-11 - 22.d	0.1454	0.0072	6.25	0.31	0.305	0.0085	0.66145	2008	45	1716	42	2287	84	75.03279	3020	323	282	0.919
M16-11	M16-11 - 27.d	0.1206	0.0062	5.18	0.27	0.3042	0.0082	0.43946	1846	45	1712	41	1956	97	87.52556	1131	195.1	190.3	1.034
M16-11	M16-11 - 100.d	0.1672	0.0081	6.76	0.39	0.294	0.012	0.92895	2073	53	1658	61	2526	81	65.63737	737	187	225	1.145
M16-11	M16-11 - 39.d	0.1492	0.0071	6.07	0.31	0.2899	0.0093	0.85676	1983	46	1640	46	2333	82	70.29576	2000	182	397	2.074
M16-11	M16-11 - 50.d	0.1255	0.0066	5.12	0.31	0.2899	0.011	0.74306	1830	51	1639	53	2032	97	80.65945	473	55.7	125.6	2.137
M16-11	M16-11 - 57.d	0.138	0.0067	5.47	0.29	0.2852	0.01	0.85888	1890	46	1615	50	2198	87	73.47589	2210	292	294	1.007
M16-11	M16-11 - 4.d	0.1618	0.0078	6.37	0.33	0.2819	0.0096	0.86643	2024	45	1599	48	2471	81	64.71064	2660	328	372	1.146
M16-11	M16-11 - 88.d	0.1409	0.0068	5.36	0.3	0.2751	0.011	0.87144	1871	49	1564	53	2238	87	69.88382	2310	226	411	1.64
M16-11	M16-11 - 110.d	0.1118	0.0055	4.26	0.23	0.2729	0.0081	0.70365	1681	44	1555	41	1822	89	85.34577	615	84	229.5	3.57
M16-11	M16-11 - 129.d	0.124	0.0061	4.502	0.22	0.2692	0.0079	0.57916	1729	41	1536	40	2009	87	76.45595	900	144	376	2.661

Sample No.	Sample - spot	$^{207}Pb/^{206}Pb$	± 2SE	$^{207}Pb/^{235}U$	± 2SE	$^{206}Pb/^{238}U$	± 2SE	Error Correlation 6/38 vs 7/35	Age $^{207}Pb/^{235}U$	± 2SE	Age $^{206}Pb/^{238}U$	± 2SE	Age $^{207}Pb/^{206}Pb$	± 2SE	Concordance 7/6 vs 6/38	Pb (PPM)	Th (PPM)	U (PPM)	U/Th
M16-11	M16-11 - 31.d	0.1184	0.0058	4.48	0.25	0.269	0.0096	0.83132	1721	45	1534	48	1932	90	79.39959	721	126	333	2.68
M16-11	M16-11 - 24.d	0.1175	0.006	4.4	0.26	0.2657	0.0093	0.79626	1707	52	1518	48	1911	91	79.43485	800	102.5	156.2	1.632
M16-11	M16-11 - 2.d	0.1595	0.008	5.94	0.32	0.2654	0.0084	0.82876	1963	53	1516	43	2447	89	61.95341	3150	268	349	1.297
M16-11	M16-11 - 12.d	0.1276	0.006	4.534	0.22	0.2595	0.007	0.75307	1736	41	1487	36	2066	79	71.97483	948	151.5	495	3.359
M16-11	M16-11 - 68.d	0.1236	0.0059	4.335	0.22	0.2589	0.009	0.86667	1697	43	1482	46	2005	84	73.91521	727	150	432	2.756
M16-11	M16-11 - 45.d	0.1333	0.0065	4.77	0.27	0.2533	0.0092	0.91691	1772	48	1454	47	2137	84	68.03931	1303	174	344	1.877
M16-11	M16-11 - 21.d	0.1645	0.0083	5.56	0.34	0.2402	0.0098	0.87932	1900	55	1385	51	2495	86	55.51102	2410	359	279	0.851
M16-11	M16-11 - 99.d	0.1054	0.0051	3.424	0.17	0.2367	0.007	0.69178	1508	39	1369	37	1716	89	79.77855	1072	249	440	1.743
M16-11	M16-11 - 63.d	0.1285	0.0063	4.06	0.23	0.2271	0.0087	0.88872	1639	46	1317	45	2073	85	63.53111	1410	228	412	1.8
M16-11	M16-11 - 117.d	0.1224	0.0059	3.69	0.22	0.2193	0.0099	0.93088	1560	50	1275	53	1986	86	64.1994	1400	254	443	1.649
M16-11	M16-11 - 118.d	0.1579	0.008	4.58	0.27	0.2101	0.0087	0.82237	1737	48	1227	46	2432	90	50.4523	2780	492	391	0.775
M16-11	M16-11 - 82.d	0.122	0.0061	3.55	0.27	0.21	0.012	0.95878	1518	62	1225	63	1977	92	61.96257	2010	206	405	1.92
M16-11	M16-11 - 48.d	0.1342	0.0073	3.92	0.28	0.2077	0.011	0.86451	1600	60	1213	58	2138	96	56.73527	169	26.1	109.6	4.23
M16-11	M16-11 - 86.d	0.1009	0.005	2.87	0.18	0.2062	0.0088	0.90537	1366	47	1207	47	1640	90	73.59756	779	112	533	4.77
M16-11	M16-11 - 49.d	0.136	0.0068	3.92	0.23	0.2051	0.0077	0.85715	1609	47	1201	41	2170	86	55.34562	898	115	460	4.11
M16-11	M16-11 - 61.d	0.1116	0.0054	3.16	0.19	0.2041	0.0087	0.9317	1441	47	1195	46	1825	85	65.47945	466	88.8	484	5.37
M16-11	M16-11 - 107.d	0.1006	0.0053	2.844	0.15	0.2038	0.0076	0.78309	1364	39	1195	40	1627	96	73.44806	400	104.8	500	4.91
M16-11	M16-11 - 37.d	0.1373	0.0065	3.87	0.22	0.2004	0.0079	0.91297	1601	45	1176	42	2190	83	53.69863	2550	321	541	1.626
M16-11	M16-11 - 13.d	0.1177	0.0058	3.194	0.18	0.1975	0.0065	0.76582	1451	43	1161	35	1914	90	60.65831	807	162.8	446	2.762
M16-11	M16-11 - 35.d	0.1207	0.0097	3.34	0.38	0.1972	0.0091	0.82872	1485	69	1159	48	1959	110	59.16284	701	134.9	398	3.02
M16-11	M16-11 - 34.d	0.164	0.0089	4.42	0.37	0.196	0.015	0.94115	1688	70	1145	82	2493	85	45.9286	840	127	223	1.78
M16-11	M16-11 - 33.d	0.1341	0.0065	3.59	0.24	0.192	0.011	0.95649	1536	55	1131	58	2148	85	52.65363	1770	299	498	1.684
M16-11	M16-11 - 105.d	0.1114	0.006	2.92	0.18	0.192	0.011	0.86389	1379	48	1128	61	1806	98	62.45847	1024	179	838	5.31
M16-11	M16-11 - 28.d	0.0983	0.0055	2.53	0.2	0.1817	0.01	0.86145	1266	62	1074	55	1589	110	67.58968	328	53.4	359	7.03
M16-11	M16-11 - 96.d	0.1239	0.0061	3.05	0.19	0.1804	0.0091	0.90755	1411	46	1066	50	2007	88	53.1141	1116	222	494	2.21
M16-11	M16-11 - 81.d	0.1536	0.0075	3.69	0.24	0.1751	0.0092	0.9423	1557	51	1038	50	2381	85	43.59513	1550	148	501	2.913
M16-11	M16-11 - 32.d	0.1239	0.0076	2.93	0.19	0.1697	0.0058	0.74088	1387	44	1010	32	2005	100	50.37406	2260	247	878	4.13
M16-11	M16-11 - 122.d	0.1135	0.0056	2.62	0.16	0.1677	0.0074	0.88194	1299	45	998	41	1849	88	53.97512	832	74.1	585	7.67
M16-11	M16-11 - 119.d	0.1825	0.0088	4.17	0.26	0.1658	0.0076	0.94831	1658	51	987	42	2672	80	36.93862	2370	267	506	1.837
M16-11	M16-11 - 64.d	0.1232	0.0062	2.831	0.16	0.1657	0.0062	0.81587	1359	41	987	34	1996	88	49.4489	1072	132.5	617	4.62
M16-11	M16-11 - 6.d	0.1394	0.0068	3.16	0.19	0.1634	0.0072	0.93534	1439	47	974	40	2215	84	43.97291	1260	201	508	2.546
M16-11	M16-11 - 5.d	0.1171	0.0062	2.551	0.13	0.1577	0.0061	0.52624	1284	38	943	34	1898	95	49.68388	1614	111.3	690	6.07

Sample No.	Sample - spot	$^{207}Pb/^{206}Pb$	± 2SE	$^{207}Pb/^{235}U$	± 2SE	$^{206}Pb/^{238}U$	± 2SE	Error Correlation 6/38 vs 7/35	Age $^{207}Pb/^{235}U$	± 2SE	Age $^{206}Pb/^{238}U$	± 2SE	Age $^{207}Pb/^{206}Pb$	± 2SE	Concordance 7/6 vs 6/38	Pb (PPM)	Th (PPM)	U (PPM)	U/Th
M16-11	M16-11 - 60.d	0.0867	0.0043	1.729	0.092	0.1443	0.0053	0.7793	1017	34	868	30	1345	97	64.53532	369	84.4	619	7.26
M16-11	M16-11 - 120.d	0.0829	0.0042	1.631	0.097	0.1439	0.0069	0.8859	978	37	865	39	1257	99	68.81464	664	125	689	5.44
M16-11	M16-11 - 1.d	0.0896	0.0044	1.709	0.1	0.1363	0.0061	0.90746	1007	38	823	34	1411	94	58.32743	1016	84.1	795	9.31
M16-11	M16-11 - 14.d	0.1023	0.0069	1.663	0.093	0.1206	0.0039	0.042491	991	35	734	23	1637	110	44.83812	148	16.1	342	21.8
M16-11	M16-11 - 128.d	0.1422	0.0074	2.3	0.15	0.1191	0.0043	0.89916	1205	44	725	25	2244	91	32.30838	1440	82.7	774	9.48
M16-11	M16-11 - 52.d	0.183	0.01	2.925	0.16	0.1164	0.0048	0.52399	1385	42	709	28	2663	89	26.62411	2040	65.5	644	9.83
M16-11	M16-11 - 101.d	0.0756	0.0039	1.179	0.064	0.1132	0.0038	0.63523	788	31	691	22	1071	100	64.51914	209	45.5	636	14.53
M16-30	M16-30 - 2.d	0.1813	0.0088	13.14	0.66	0.533	0.015	0.64682	2687	47	2752	64	2660	82	103.4586	683	43.4	95.4	2.056
M16-30	M16-30 - 20.d	0.164	0.0086	11.19	0.61	0.4866	0.015	0.50561	2533	50	2562	60	2486	88	103.0571	993	101.5	52.9	0.539
M16-30	M16-30 - 18.d	0.1742	0.009	11.51	0.61	0.4747	0.014	0.5153	2560	49	2502	61	2589	88	96.63963	630	64.3	56.7	0.885
M16-30	M16-30 - 19.d	0.1593	0.0081	10.49	0.54	0.4712	0.014	0.49961	2480	46	2487	59	2446	83	101.6762	820	89.2	83.8	0.951
M16-30	M16-30 - 13.d	0.1609	0.0079	10.41	0.52	0.4695	0.013	0.51698	2469	47	2480	58	2459	83	100.854	836	75.5	106.6	1.391
M16-30	M16-30 - 12.d	0.1646	0.0083	10.63	0.55	0.469	0.013	0.5211	2487	48	2478	57	2496	84	99.27885	1003	87.8	102.6	1.138
M16-30	M16-30 - 8.d	0.1645	0.008	10.17	0.5	0.4558	0.012	0.57669	2451	48	2420	54	2498	82	96.8775	1920	141.7	127.9	0.833
M16-30	M16-30 - 11.d	0.1648	0.008	9.71	0.47	0.4311	0.012	0.59647	2406	44	2309	54	2501	81	92.32307	1830	159	172	1.018
M16-30	M16-30 - 14.d	0.148	0.0075	8.76	0.44	0.428	0.012	0.34997	2314	43	2300	55	2315	88	99.35205	773	76.3	127	1.764
M16-30	M16-30 - 5.d	0.1157	0.0058	5.59	0.28	0.3563	0.0097	0.41123	1912	44	1964	46	1883	92	104.3016	746	66.3	158.1	2.198
M16-30	M16-30 - 9.d	0.135	0.0068	6.35	0.39	0.343	0.014	0.86846	2014	58	1895	67	2156	88	87.89425	717	51.8	171	2.96
M16-30	M16-30 - 17.d	0.1138	0.0057	5.21	0.26	0.3288	0.0092	0.39651	1852	42	1832	45	1853	92	98.8667	566	80.7	185	2.299
M16-30	M16-30 - 6.d	0.1512	0.0074	6.7	0.35	0.326	0.0099	0.7802	2068	48	1818	48	2355	84	77.19745	1200	86.5	247	2.672
M16-30	M16-30 - 10.d	0.1121	0.0056	4.71	0.25	0.3071	0.0098	0.68388	1764	43	1725	48	1827	91	94.41708	1652	193	261	1.275
M16-30	M16-30 - 15.d	0.1348	0.0076	5.54	0.42	0.294	0.016	0.84595	1903	62	1655	80	2150	110	76.97674	280	28.6	102.4	3.65
M16-30	M16-30 - 16.d	0.1432	0.0074	5.58	0.41	0.278	0.014	0.94299	1889	70	1577	72	2263	86	69.68626	1910	630	217	0.85
M16-30	M16-30 - 3.d	0.1374	0.0072	4.74	0.27	0.2534	0.0075	0.67997	1768	50	1455	39	2182	94	66.68194	1520	113	281	2.381
M16-30	M16-30 - 4.d	0.1232	0.0071	3.52	0.3	0.2063	0.011	0.94099	1503	71	1205	57	1979	110	60.88934	5.20E+03	1200	505	0.727
M16-30	M16-30 - 21.d	0.1342	0.0068	3.72	0.22	0.1979	0.0076	0.85468	1568	49	1162	41	2145	89	54.17249	837	122	275	2.238
M16-30	M16-30 - 1.d	0.086	0.0046	1.87	0.15	0.1577	0.0086	0.88893	1056	52	942	48	1330	110	70.82707	469	33.9	268	7.4
M16-30	M16-30 - 7.d	0.0958	0.0065	1.86	0.22	0.1358	0.0098	0.97568	1021	79	817	55	1490	140	54.83221	285	25.4	431	27.3
MAD17-11-4A	MAD17-11-4A - 41.d	no value	NAN	no value	NAN	no value	NAN	NaN	no value	NAN	no value	NAN	no value	NAN	#VALUE!	0.7	Below LOD	Below LOD	no value
MAD17-11-4A	MAD17-11-4A - 54.d	no value	NAN	no value	NAN	no value	NAN	NaN	no value	NAN	no value	NAN	no value	NAN	#VALUE!	40	Below LOD	Below LOD	no value
MAD17-11-4A	MAD17-11-4A - 66.d	no value	NAN	no value	NAN	no value	NAN	NaN	no value	NAN	no value	NAN	no value	NAN	#VALUE!	2080	Below LOD	Below LOD	no value
MAD17-11-4A	MAD17-11-4A - 18.d	0.1605	0.0078	10.79	0.54	0.4785	0.014	0.61962	2502	47	2526	64	2456	82	102.8502	836	66.5	113.5	1.583

Sample No.	Sample - spot	$^{207}Pb/^{206}Pb$	± 2SE	$^{207}Pb/^{235}U$	± 2SE	$^{206}Pb/^{238}U$	± 2SE	Error Correlation 6/38 vs 7/35	Age $^{207}Pb/^{235}U$	± 2SE	Age $^{206}Pb/^{238}U$	± 2SE	Age $^{207}Pb/^{206}Pb$	± 2SE	Concordance 7/6 vs 6/38	Pb (PPM)	Th (PPM)	U (PPM)	U/Th
MAD17-11-4A	MAD17-11-4A - 17.d	0.1744	0.0087	11.47	0.57	0.4721	0.014	0.44807	2560	46	2491	60	2594	83	96.0293	1448	112.9	112.8	0.918
MAD17-11-4A	MAD17-11-4A - 6.d	0.1742	0.0084	11.27	0.54	0.4696	0.012	0.44789	2547	47	2481	55	2594	79	95.64379	1869	123.1	209	1.59
MAD17-11-4A	MAD17-11-4A - 42.d	0.1652	0.0082	10.36	0.52	0.4631	0.013	0.49718	2464	46	2452	55	2504	83	97.92332	1718	121.1	128.9	0.978
MAD17-11-4A	MAD17-11-4A - 12.d	0.1631	0.0079	10.36	0.51	0.4565	0.012	0.60202	2466	45	2423	55	2483	81	97.58357	2304	159.4	191.6	1.084
MAD17-11-4A	MAD17-11-4A - 65.d	0.1658	0.0079	10.43	0.52	0.4548	0.014	0.74132	2471	46	2415	60	2513	80	96.10028	1730	175	221	1.201
MAD17-11-4A	MAD17-11-4A - 10.d	0.1885	0.0091	11.84	0.64	0.452	0.015	0.88125	2585	53	2399	68	2725	79	88.0367	2372	133.6	200	1.354
MAD17-11-4A	MAD17-11-4A - 83.d	0.1643	0.008	10.2	0.5	0.4461	0.012	0.49316	2451	46	2377	54	2495	83	95.27054	3880	180	181	0.972
MAD17-11-4A	MAD17-11-4A - 14.d	0.1606	0.0078	9.89	0.49	0.4416	0.012	0.5626	2422	46	2357	56	2458	82	95.89097	1194	90.4	179.3	1.797
MAD17-11-4A	MAD17-11-4A - 1.d	0.1509	0.0072	9.23	0.44	0.4364	0.011	0.49442	2360	44	2334	51	2354	81	99.15038	1544	176	367	2.122
MAD17-11-4A	MAD17-11-4A - 21.d	0.178	0.0087	10.02	0.49	0.4114	0.011	0.46475	2434	46	2220	51	2629	83	84.44275	6160	83.1	189	2.161
MAD17-11-4A	MAD17-11-4A - 35.d	0.1608	0.0077	9.1	0.46	0.4113	0.012	0.81176	2345	46	2219	56	2460	81	90.20325	3720	276	202	0.723
MAD17-11-4A	MAD17-11-4A - 49.d	0.1799	0.0092	10.05	0.67	0.408	0.018	0.87807	2422	65	2200	84	2651	79	82.98755	1098	75.4	116	1.442
MAD17-11-4A	MAD17-11-4A - 43.d	0.1364	0.0074	7.49	0.41	0.4058	0.012	0.4464	2166	50	2194	57	2167	97	101.246	307	23.1	51.4	2.104
MAD17-11-4A	MAD17-11-4A - 68.d	0.1505	0.0083	8.38	0.46	0.4004	0.013	0.43002	2272	54	2169	58	2334	98	92.93059	3780	81.1	54.2	0.69
MAD17-11-4A	MAD17-11-4A - 9.d	0.1578	0.008	8.73	0.46	0.3993	0.012	0.64156	2310	50	2165	54	2424	86	89.31518	793	55.1	109.9	1.853
MAD17-11-4A	MAD17-11-4A - 80.d	0.2637	0.013	14.61	0.86	0.399	0.017	0.88384	2779	59	2160	79	3263	77	66.19675	2330	30.7	126	3.94
MAD17-11-4A	MAD17-11-4A - 52.d	0.1784	0.0085	9.72	0.47	0.3907	0.011	0.66975	2406	46	2126	49	2635	81	80.68311	1388	176	332	1.75
MAD17-11-4A	MAD17-11-4A - 19.d	0.1249	0.006	6.69	0.33	0.3855	0.011	0.55195	2069	43	2101	49	2024	85	103.8043	1204	119.7	231.5	1.802
MAD17-11-4A	MAD17-11-4A - 4.d	0.1779	0.0086	9.58	0.55	0.383	0.014	0.90803	2386	53	2087	66	2629	80	79.3838	1189	115.5	363	3.149
MAD17-11-4A	MAD17-11-4A - 8.d	0.1611	0.0078	8.34	0.45	0.373	0.013	0.87088	2262	51	2041	60	2464	81	82.83279	4250	309	321	0.95
MAD17-11-4A	MAD17-11-4A - 63.d	0.1293	0.0066	6.57	0.33	0.3667	0.011	0.4324	2052	45	2012	52	2078	91	96.82387	336	46.8	96.9	1.99
MAD17-11-4A	MAD17-11-4A - 11.d	0.1615	0.008	8.11	0.44	0.3609	0.012	0.80836	2237	50	1984	58	2466	83	80.45418	1570	96.6	236	2.164
MAD17-11-4A	MAD17-11-4A - 77.d	0.129	0.0074	6.3	0.35	0.3565	0.012	0.29558	2012	48	1963	59	2073	100	94.69368	22	0.412	41.5	########
MAD17-11-4A	MAD17-11-4A - 39.d	0.1166	0.0056	5.459	0.26	0.3426	0.0092	0.41683	1893	41	1899	44	1900	88	99.94737	1187	120.3	319	2.497
MAD17-11-4A	MAD17-11-4A - 37.d	0.1091	0.0056	5.07	0.27	0.3372	0.01	0.56815	1826	45	1872	48	1775	95	105.4648	683	72.3	114.5	1.51
MAD17-11-4A	MAD17-11-4A - 56.d	0.1721	0.0087	8.03	0.58	0.3348	0.018	0.73207	2233	96	1861	93	2575	100	72.27184	826	137.4	427	2.89
MAD17-11-4A	MAD17-11-4A - 67.d	0.1781	0.0089	8.17	0.49	0.329	0.014	0.88116	2240	55	1827	68	2634	80	69.36219	2220	49.6	149.6	3.27
MAD17-11-4A	MAD17-11-4A - 23.d	0.1397	0.007	6.18	0.31	0.3244	0.0089	0.39917	1999	45	1811	43	2215	90	81.76072	4460	41.9	130.1	2.967
MAD17-11-4A	MAD17-11-4A - 40.d	0.1094	0.0055	4.84	0.25	0.3246	0.0088	0.57565	1789	44	1811	43	1781	91	101.6844	1845	184.5	208.4	1.064
MAD17-11-4A	MAD17-11-4A - 25.d	0.126	0.0063	5.406	0.27	0.3158	0.0083	0.33441	1884	42	1769	41	2036	87	86.88605	5670	60.4	189.5	3.023
MAD17-11-4A	MAD17-11-4A - 36.d	0.106	0.0052	4.323	0.22	0.2938	0.0089	0.75772	1695	43	1660	44	1727	89	96.12044	570	66.3	324	4.68
MAD17-11-4A	MAD17-11-4A - 58.d	0.1108	0.0055	4.32	0.22	0.2796	0.0083	0.67804	1694	43	1588	42	1804	92	88.02661	228	41.8	319	7.24

Sample No.	Sample - spot	$^{207}Pb/^{206}Pb$	± 2SE	$^{207}Pb/^{235}U$	± 2SE	$^{206}Pb/^{238}U$	± 2SE	Error Correlation 6/38 vs 7/35	Age $^{207}Pb/^{235}U$	± 2SE	Age $^{206}Pb/^{238}U$	± 2SE	Age $^{207}Pb/^{206}Pb$	± 2SE	Concordance 7/6 vs 6/38	Pb (PPM)	Th (PPM)	U (PPM)	U/Th
MAD17-11-4A	MAD17-11-4A - 47.d	0.1895	0.0094	6.98	0.35	0.2734	0.0094	0.77255	2107	45	1557	48	2738	80	56.86633	286	21.6	429	18.34
MAD17-11-4A	MAD17-11-4A - 31.d	0.1174	0.006	4.37	0.24	0.2731	0.0088	0.72097	1701	46	1555	45	1907	91	81.54169	1651	87.3	174	1.927
MAD17-11-4A	MAD17-11-4A - 44.d	0.1111	0.0057	3.92	0.22	0.2637	0.0089	0.70327	1618	47	1507	45	1807	91	83.3979	655	67	240	3.23
MAD17-11-4A	MAD17-11-4A - 71.d	0.1195	0.0066	4.36	0.26	0.2619	0.0098	0.69883	1696	52	1498	50	1930	100	77.61658	9580	124.4	119.6	0.952
MAD17-11-4A	MAD17-11-4A - 81.d	0.1104	0.0054	3.83	0.21	0.2497	0.0082	0.81146	1595	45	1436	43	1800	90	79.77778	969	40.9	448	10.79
MAD17-11-4A	MAD17-11-4A - 78.d	0.1433	0.0072	4.93	0.31	0.246	0.0089	0.90466	1796	52	1416	46	2259	87	62.6826	1.55E+04	218	394	1.734
MAD17-11-4A	MAD17-11-4A - 55.d	0.12	0.0062	4.04	0.23	0.2427	0.012	0.78404	1638	52	1407	62	1950	90	72.15385	516	85.3	355	3.75
MAD17-11-4A	MAD17-11-4A - 15.d	0.1374	0.0068	4.66	0.26	0.2428	0.0088	0.8383	1753	47	1400	46	2188	85	63.98537	1520	130	467	3.181
MAD17-11-4A	MAD17-11-4A - 74.d	0.1343	0.0066	4.55	0.27	0.2425	0.0096	0.89979	1731	51	1398	50	2149	87	65.05351	2.72E+04	231	425	1.853
MAD17-11-4A	MAD17-11-4A - 32.d	0.1543	0.0075	4.98	0.32	0.2355	0.011	0.92789	1807	61	1362	57	2390	85	56.98745	2710	144	415	2.75
MAD17-11-4A	MAD17-11-4A - 79.d	0.2117	0.01	6.71	0.4	0.229	0.0095	0.9512	2065	59	1326	50	2915	85	45.48885	2.40E+04	289	477	1.54
MAD17-11-4A	MAD17-11-4A - 34.d	0.1151	0.0059	3.51	0.24	0.2208	0.01	0.92322	1515	54	1283	53	1872	92	68.53632	1460	135	342	2.523
MAD17-11-4A	MAD17-11-4A - 2.d	0.1244	0.0062	3.77	0.25	0.2157	0.01	0.88986	1579	60	1257	54	2014	93	62.41311	634	112	517	4.73
MAD17-11-4A	MAD17-11-4A - 50.d	0.1127	0.0057	3.32	0.2	0.215	0.0077	0.81351	1480	46	1254	41	1841	96	68.11515	409	44.2	285	6.29
MAD17-11-4A	MAD17-11-4A - 7.d	0.1645	0.0083	4.75	0.33	0.207	0.011	0.95843	1757	62	1211	58	2497	84	48.4982	2690	174	548	2.98
MAD17-11-4A	MAD17-11-4A - 75.d	0.1451	0.0076	4.05	0.23	0.1998	0.0063	0.77523	1635	46	1173	34	2278	86	51.49254	2.26E+04	147	374	2.45
MAD17-11-4A	MAD17-11-4A - 30.d	0.1176	0.0058	3.113	0.17	0.1947	0.007	0.78851	1432	41	1146	38	1914	89	59.87461	1027	53.2	417	7.56
MAD17-11-4A	MAD17-11-4A - 76.d	0.1494	0.0076	4.05	0.27	0.1942	0.0093	0.90691	1630	57	1142	50	2337	82	48.86607	2.22E+04	184	348	1.782
MAD17-11-4A	MAD17-11-4A - 33.d	0.1075	0.0054	2.83	0.17	0.1928	0.008	0.87398	1357	42	1135	43	1755	90	64.67236	850	39.7	268	6.66
MAD17-11-4A	MAD17-11-4A - 29.d	0.1219	0.0062	3.19	0.2	0.1927	0.0087	0.85559	1446	49	1134	47	1981	86	57.24382	3350	103.5	341	3.2
MAD17-11-4A	MAD17-11-4A - 26.d	0.1387	0.0075	3.66	0.31	0.1904	0.011	0.96034	1532	72	1120	59	2196	96	51.00182	7490	91	312	3.87
MAD17-11-4A	MAD17-11-4A - 57.d	0.1422	0.0071	3.62	0.29	0.184	0.013	0.95634	1530	66	1081	69	2247	86	48.10859	770	120	451	3.44
MAD17-11-4A	MAD17-11-4A - 62.d	0.1805	0.0091	4.56	0.35	0.183	0.013	0.95097	1720	65	1078	69	2656	86	40.58735	689	61.2	314	4.97
MAD17-11-4A	MAD17-11-4A - 72.d	0.1023	0.0052	2.553	0.14	0.1792	0.006	0.80644	1283	41	1062	33	1657	93	64.09173	1.56E+04	163	447	2.85
MAD17-11-4A	MAD17-11-4A - 45.d	0.1473	0.0076	3.44	0.19	0.1738	0.0071	0.78539	1507	44	1032	39	2306	89	44.75282	988	58.3	428	6.88
MAD17-11-4A	MAD17-11-4A - 38.d	0.1293	0.0064	3.03	0.19	0.1707	0.0076	0.90065	1407	48	1014	42	2081	86	48.72657	2190	179	516	2.708
MAD17-11-4A	MAD17-11-4A - 46.d	0.1374	0.0068	3.16	0.2	0.1702	0.0067	0.91174	1438	49	1012	37	2187	87	46.27343	272	32	587	17.13
MAD17-11-4A	MAD17-11-4A - 73.d	0.1247	0.0062	2.81	0.21	0.1626	0.0095	0.94588	1345	53	968	52	2017	89	47.99207	9.10E+03	106	562	5.25
MAD17-11-4A	MAD17-11-4A - 82.d	0.1093	0.0054	2.41	0.16	0.1588	0.008	0.92438	1236	46	948	44	1780	92	53.25843	1370	75.3	562	7.19
MAD17-11-4A	MAD17-11-4A - 16.d	0.0972	0.0049	2.001	0.13	0.1472	0.0074	0.92599	1106	47	883	42	1562	94	56.53009	776	96.9	491	4.73
MAD17-11-4A	MAD17-11-4A - 48.d	0.112	0.0055	2.161	0.13	0.1433	0.0057	0.88117	1163	40	863	32	1827	88	47.23591	2130	185	567	2.812
MAD17-11-4A	MAD17-11-4A - 3.d	0.0979	0.013	1.948	0.2	0.1427	0.0051	0.1262	1097	63	860	29	1580	140	54.43038	838	125	1030	8.5

Sample No.	Sample - spot	$^{207}Pb/^{206}Pb$	± 2SE	$^{207}Pb/^{235}U$	± 2SE	$^{206}Pb/^{238}U$	± 2SE	Error Correlation 6/38 vs 7/35	Age $^{207}Pb/^{235}U$	± 2SE	Age $^{206}Pb/^{238}U$	± 2SE	Age $^{207}Pb/^{206}Pb$	± 2SE	Concordance 7/6 vs 6/38	Pb (PPM)	Th (PPM)	U (PPM)	U/Th
MAD17-11-4A	MAD17-11-4A - 51.d	0.1963	0.011	3.79	0.23	0.1401	0.0065	0.74081	1588	48	844	37	2782	90	30.33789	540	129	177	1.22
MAD17-11-4A	MAD17-11-4A - 53.d	0.1361	0.0071	2.563	0.14	0.1367	0.0058	0.72611	1286	41	825	33	2167	92	38.07107	618	82.5	593	6.72
MAD17-11-4A	MAD17-11-4A - 69.d	0.0838	0.0042	1.592	0.1	0.1356	0.006	0.91492	960	40	819	34	1287	94	63.63636	4230	137	600	4.69
MAD17-11-4A	MAD17-11-4A - 61.d	0.0908	0.0046	1.659	0.098	0.1325	0.0061	0.85839	992	39	801	35	1439	99	55.66366	124	24.4	566	21.77
MAD17-11-4A	MAD17-11-4A - 64.d	0.0898	0.0062	1.576	0.12	0.126	0.0053	0.82651	953	45	764	30	1405	110	54.37722	551	68.8	805	11.35
MAD17-11-4A	MAD17-11-4A - 59.d	0.1512	0.0076	2.56	0.18	0.1213	0.006	0.92621	1277	49	737	34	2352	87	31.33503	607	65.6	638	8.79
MAD17-11-4A	MAD17-11-4A - 28.d	0.1294	0.0065	2.106	0.12	0.1189	0.0038	0.75119	1147	39	724	22	2082	91	34.77426	3870	120	565	4.46
MAD17-11-4A	MAD17-11-4A - 24.d	0.1236	0.0078	1.668	0.1	0.1045	0.0071	0.6938	997	39	639	41	1971	120	32.42009	1.37E+04	108.4	764	6.75
MAD17-11-4A	MAD17-11-4A - 60.d	0.061	0.015	0.72	0.15	0.1031	0.0084	-0.17435	513	99	630	49	110	410	572.7273	0.13	Below LOD	8.47	########
MAD17-11-4A	MAD17-11-4A - 5.d	0.2325	0.011	3.286	0.18	0.1012	0.004	0.89611	1474	41	621	23	3065	78	20.26101	2040	164	903	5.08
MAD17-11-4A	MAD17-11-4A - 22.d	0.0865	0.0045	1.191	0.071	0.1009	0.0037	0.56072	795	31	619	21	1337	98	46.29768	2850	35.8	683	19.2
MAD17-11-4A	MAD17-11-4A - 20.d	0.05877	0.0028	0.745	0.037	0.091	0.0026	0.6716	564.5	21	561.4	15	553	110	101.519	231	84.1	2540	29.02
MAD17-11-4A	MAD17-11-4A - 70.d	0.0579	0.0031	0.714	0.038	0.0888	0.0024	0.37198	546	23	548.3	14	507	120	108.146	394	21.1	763	37.4
MAD17-11-4A	MAD17-11-4A - 27.d	0.065	0.0033	0.705	0.036	0.0799	0.0022	0.35831	541.3	21	495.3	13	761	110	65.08541	457	43.6	901	21.7
MAD17-11-4A	MAD17-11-4A - 84.d	0.133	0.0078	0.868	0.057	0.048	0.0031	0.81765	630	30	302	19	2114	100	14.28571	2350	93	1540	16.31
MAD17-11-4A	MAD17-11-4A - 13.d	0.1818	0.014	0.2701	0.014	0.01075	0.00059	0.6337	242.5	12	68.9	3.8	2656	110	2.594127	1539	322	4420	12.18

Appendix 5.2 Proterozoic basin evolution during Nuna: REE zircon data

Grain_number	P_ppm_m31	Y_ppm_m89	Nb_ppm_m93	La_ppm_m139	Ce_ppm_m140	Pr_ppm_m141	Nd_ppm_m146	Sm_ppm_m147	Eu_ppm_m153	Gd_ppm_m157	Tb_ppm_m159	Dy_ppm_m163	Ho_ppm_m165	Er_ppm_m166	Tm_ppm_m169	Yb_ppm_m172	Lu_ppm_m175	Hf_ppm_m178	Ta_ppm_m181	Th_ppm_m232	U_ppm_m238
M16-10 - 1	371	707	4.48	1.43	12.8	0.73	3.6	2.9	1.5	11.3	4.4	56.7	23.43	116.9	27.57	280.6	59.5	12043	2.8	131.3	950
M16-10 - 2	1073	1384	1.98	31.3	142.8	20.7	110.7	52	12.93	81.7	18.6	160.7	44	156	29.6	264.1	50.1	11070	1.08	152.6	572.9
M16-10 - 3	888	1556	4.31	4.74	34.8	3.23	18.2	12.8	2.25	37.1	12.26	139.8	50.6	225.5	46.04	415.4	79.12	11713	2.64	292.3	454.1
M16-10 - 4	813	1820	4.97	14.1	66.1	8.5	49.4	33.5	7	74.6	22.3	223	62.7	244	44.7	371	62.3	11430	1.84	216.8	344.4
M16-10 - 5	202	370	3.94	2.73	39.5	1.79	9	4.13	1.19	9.1	2.83	30.1	11.26	54.6	12.86	136.2	28.7	10744	2.19	114.3	296.6
M16-10 - 6	571	1234	3.95	8.42	126.6	7.95	46.4	21.1	4.74	47.9	12.76	123.6	40.04	161.7	31.3	280.5	53.82	8838	1.325	296.2	290.3
M16-10 - 7	950	2590	2.19	5.6	35.7	4.78	28.7	20.4	3.08	77.2	21.8	247	89.7	384	73.5	644	121.7	8635	1.01	267	186
M16-10 - 8	177	1615	1.24	Below LOD	5.15	0.036	1.41	4.64	0.487	32.5	11.79	145	56.08	245.5	48.03	419.6	78.18	9317	0.571	89.8	177.6
M16-10 - 9	373	1277	3.22	4.5	24.3	1.47	9	10.7	0.71	35.2	11.74	126	44.8	188.3	36.78	315.3	59.5	9615	1.47	199	275.4
M16-10 - 10	3670	5290	4.01	123.9	665	103.6	574	253	48.2	385	80.6	615	147.7	446	70.8	577	107	9820	3.15	199.8	1641
M16-10 - 11	449	619	2.05	6.9	51.5	3.27	13.6	6.35	2.16	15.6	4.58	51	19.2	92.2	22.1	232.9	52.8	10714	1.32	194.4	622
M16-10 - 12	371	2154	1.71	0.069	10.3	0.386	5.85	10.47	1.11	55.2	17.57	196.7	71.9	302	58.4	503.7	97.5	7919	0.946	137.4	236.6
M16-10 - 13	550	1210	1.64	6.1	18.2	1.33	6.6	3.3	0.394	21.9	7.97	102.8	41.6	188.6	37.43	334.3	64.5	8110	0.637	87.3	166.8
M16-10 - 14	630	376.8	0.57	6.3	20.7	1.39	6.1	1.9	0.181	9.4	2.77	33.4	12.82	55.8	11.6	105.6	20.2	9569	0.239	44.4	86.7
M16-10 - 15	89	376.9	1.02	0.009	16.12	Below LOD	0.34	0.64	0.29	5.87	2.02	26.97	10.95	57.6	14.5	159.2	36.32	11552	0.979	112.8	259.4
M16-10 - 16	Below LOD	Below LOD	4.67E+06	Below LOD	Below LOD	Below LOD	Below LOD	Below LOD	Below LOD	Below LOD	Below LOD	Below LOD	Below LOD	Below LOD	Below LOD	Below LOD	4.5	19190	3.78E+05	Below LOD	59460
M16-10 - 17	143	322.4	0.721	0.026	10.76	0.051	0.86	1.66	0.421	6.91	2.62	27.37	10.22	47.6	10.14	101.6	20.46	8432	0.407	149.8	222.1
M16-10 - 18	1178	2140	2.72	12.83	63	9.24	52	27.6	5.84	64.4	19.08	204.3	69.9	289.7	57.67	494	91.9	11200	1	178.4	486.9
M16-10 - 19	1486	2293	2.22	26.6	276.2	19.39	102.3	50.9	15.46	91.5	26.21	259.6	77.6	309.8	60.4	547	96.7	10150	1.52	76.9	380.1
M16-10 - 20	182	666.4	2.21	2.22	12.37	0.74	3.54	2.51	0.739	10.79	3.95	50.5	21.56	107.2	24.36	241.8	50.9	10798	0.99	83.9	271
M16-10 - 21	630	873	3.67	14.4	51.3	5.33	25.3	10.9	3.66	18.9	5.31	63.9	26	139.2	36.26	402.9	89.3	11810	4.28	46.8	1499
M16-10 - 22	496	903	0.62	0.73	2.81	0.276	1.74	3.22	0.283	22	8.26	89.7	28.65	117.2	22.11	193	36.07	11530	0.345	36.73	412.4
M16-10 - 23	183	402.6	0.565	0.018	6.44	0.03	0.53	1.02	0.58	7.46	2.33	29.9	12.24	63.2	14.58	160.5	37.7	8986	0.337	65.5	219
M16-10 - 24	437	718	1.36	8.3	67.7	7.5	41.9	22.2	4.91	36.2	8.5	73.3	22.1	88.1	17.55	171.5	37.8	10282	0.569	141.5	260
M16-10 - 25	5450	5431	3.46	108.4	651	95.8	480	212.4	62.1	290.5	67.9	561	148.3	526.1	96.6	821	145.9	12330	3.08	71.3	1101
M16-10 - 26	328	595.6	2.74	2.62	7.78	1.29	6.09	4.07	1.65	19.2	6.86	69.3	18.67	65.1	11.3	93.8	16.81	11870	2.72	38.7	497
M16-10 - 27	735	1392	5.9	12.9	118.3	6.65	38.3	17.9	4.46	46.4	11.12	115.3	39.04	171.3	35.04	317.2	61.6	7483	1.72	264.8	589.4

Grain_number	P_ppm_m31	Y_ppm_m89	Nb_ppm_m93	La_ppm_m139	Ce_ppm_m140	Pr_ppm_m141	Nd_ppm_m146	Sm_ppm_m147	Eu_ppm_m153	Gd_ppm_m157	Tb_ppm_m159	Dy_ppm_m163	Ho_ppm_m165	Er_ppm_m166	Tm_ppm_m169	Yb_ppm_m172	Lu_ppm_m175	Hf_ppm_m178	Ta_ppm_m181	Th_ppm_m232	U_ppm_m238
M16-10 - 28	197	460.4	2.41	0.05	27.57	0.079	0.9	1.5	0.8	9.4	2.91	34.8	13.34	70.4	16.55	162.6	31.89	9039	0.838	127.3	231.8
M16-10 - 29	209	347.2	1.26	2.64	40.6	1.39	7.75	4.04	0.95	13.7	3.3	33.1	11.26	49.06	10.34	100.2	20.19	9424	0.42	202.2	262.9
M16-10 - 30	150	357.6	0.739	0.0047	17.14	0.04	1.21	2.55	0.527	9.5	2.86	32.4	11.47	51.3	11.04	103	21.64	8663	0.315	88.2	101.9
M16-10 - 31	305	715	1.58	0.77	59.8	0.65	5	6.21	1.44	21.6	6.26	66.8	23.46	101.1	21.87	198.7	39.35	8911	0.447	118.6	140.9
M16-10 - 32	143	592.6	2.2	0.069	12.01	0.077	1.4	2.9	0.113	17.8	5.49	59.8	20.5	87.7	16.55	150.9	29.39	10525	0.894	194.8	386.7
M16-10 - 33	559	4136	32.21	0.67	39.93	0.46	5.14	11.4	2.42	80.1	29.54	374	147.3	633.8	120.4	1007	183.4	9645	9.33	260.6	539.8
M16-10 - 34	2390	4570	85.4	65.6	393	58.4	350	191	40.4	295	70.1	566	140.2	463	79.1	658	117.1	11275	25.1	305	1125
M16-10 - 35	326	787	2.13	2.31	25.2	2.31	15.8	9.4	1.94	22.4	6.55	73	25.73	112.6	23.14	212.1	40.6	9469	0.964	103.1	241.2
M16-10 - 36	650	996	5.24	16.2	53.2	3.94	17.1	6.4	0.404	21.3	7.5	91.4	34.56	153	30.58	270.5	50.84	8642	1.78	89.2	183.4
M16-10 - 37	574	799	1.43	9.2	84.6	6.71	33	17.4	4.42	38.6	10.16	89.6	26.4	101.3	19.71	171.3	30.3	11560	1.16	74.3	301.3
M16-10 - 38	387	1254	1.76	1.83	9.56	1.02	5.7	7.8	0.93	34.1	10.42	119.6	43.3	184.2	35.97	321.4	61.2	8184	0.768	36.5	76.6
M16-10 - 39	4620	7570	6.69	85.5	472	71.5	400	226	45	393	100.2	890	223.4	739	125.1	969	159.4	11520	3.32	246	1525
M16-10 - 40	590	853	2.83	10.9	42.7	3.34	16.5	7.4	1.48	21.7	7.12	79.1	28.63	123.3	25.12	225.2	41.78	10741	1.83	239.9	543
M16-10 - 41	1890	2713	2.59	87.9	275.5	41.1	207.8	89.3	23.9	142.8	34.2	293.9	82.5	301.1	55.9	488	91.6	9260	2.7	383	564
M16-10 - 42	240	426.4	1.12	0.49	7.04	0.368	2.59	2.85	0.386	12.23	3.91	40.1	14.26	59.8	12.15	109.9	21.8	9794	0.643	68.2	244.6
M16-10 - 43	1584	1994	3.09	31.6	161.5	27.1	144.9	78.1	17.66	131.8	31.7	253	63.8	208.1	38.3	313	53.1	11900	1.44	80.9	573.5
M16-10 - 44	613	1075	3.91	11.9	124	10.15	51.9	28.2	6.2	51.1	12.74	116	34.1	132.2	25.03	224.3	40.53	9084	1.27	185.9	262.4
M16-10 - 45	154	703.3	1.25	0.401	4.74	0.044	0.59	1.39	0.285	11.6	4.48	57.5	24.07	112.9	23.5	212.5	41.36	8295	0.56	41.84	107.8
M16-10 - 46	183	478	1.14	2.04	25	1.53	7.4	4.92	1.37	11.82	3.88	43.2	15.42	68.2	14.77	142.4	28.87	9950	0.675	71.4	186.8
M16-10 - 47	4150	5893	4.94	95.9	1016	78.2	406	193	55.7	287.7	66.4	588.3	160.5	565.5	103.5	881	155.8	10250	2.54	282.8	1038
M16-10 - 48	2420	736	1.92	54	135	13.8	58	17.8	3	28.5	7.03	71.5	23.92	103.8	22.37	215.2	44.34	10211	0.745	155.2	309.5
M16-10 - 49	648	994	6.01	3.69	21	0.96	4.03	4.9	1.92	21.1	7.44	85.8	31.55	151.9	34.87	363.5	74.2	12620	6.35	250.1	996
M16-10 - 50	437	697.2	1.14	0.44	6.33	0.53	4.66	8.51	0.85	32	7.83	74.4	22.97	90.7	17.21	148.3	28.06	8284	0.359	123.3	234.4
M16-10 - 51	274	389	0.84	2.17	12.6	1.12	7.4	5.65	1.02	14.3	4.07	41.6	12.93	51.7	10.08	93	17.27	10280	0.419	83.1	156
M16-10 - 52	276	802	0.87	Below LOD	15.9	0.02	1.59	3.07	1.77	19.6	5.85	65.8	24.9	115.6	24.92	240.8	52.93	7801	0.236	47.5	95.9
M16-10 - 53	627	1215	1.73	16.7	99.4	11.4	61.4	32.9	7.72	60.4	15.8	142	38.7	137.9	25.2	209	36.7	9020	0.67	145.4	372.1
M16-10 - 54	1365	2145	2.28	33.9	178.1	22.7	129.3	64	16.08	111.5	27.4	245.6	67.7	242.7	45.3	387	70.4	10266	1.31	168.7	605
M16-10 - 55	4090	3860	3.36	71.3	432	57.8	316	150	38.9	211.8	46.8	399	103.3	362	64.9	561	102	12198	2.6	85.3	1096
M16-10 - 56	608	1075	0.88	0.59	4.37	0.209	1.05	1.78	0.225	14.2	6.41	87.4	35.84	167.4	37.63	359.3	71.8	11424	0.765	44.1	294.2
M16-10 - 57	423	831	1.56	5.03	53.5	3.53	21	13.9	3.56	28.4	8.43	84.4	26.5	111.6	22.8	216	45.3	9670	0.441	120.5	237
M16-10 - 58	1310	1626	2.43	34.7	256	24.6	118.9	55.6	15.5	78.7	20.6	185.5	52.1	198	40.3	371	69.6	10872	2.13	176.5	675

Grain_number	P_ppm_m31	Y_ppm_m89	Nb_ppm_m93	La_ppm_m139	Ce_ppm_m140	Pr_ppm_m141	Nd_ppm_m146	Sm_ppm_m147	Eu_ppm_m153	Gd_ppm_m157	Tb_ppm_m159	Dy_ppm_m163	Ho_ppm_m165	Er_ppm_m166	Tm_ppm_m169	Yb_ppm_m172	Lu_ppm_m175	Hf_ppm_m178	Ta_ppm_m181	Th_ppm_m232	U_ppm_m238
M16-10 - 59	532	786	1.47	8.82	75.8	6.04	30.7	15	4.41	28.5	7.77	76.7	23.9	99.9	21.7	209.7	43.1	9984	0.701	157.7	333
M16-10 - 60	522	844	3.39	6.55	43.5	4.35	18.3	9.8	2.81	15.1	5.24	63.8	26.62	145.8	38.27	427.5	92.8	11387	8.67	129.1	1173
M16-10 - 61	208	557	1.41	Below LOD	26.25	0.065	1.16	2.46	0.516	12.5	4.08	45.7	17.78	83.5	18.44	184.8	39.2	10021	0.666	125.7	160.6
M16-10 - 62	2070	3030	2.37	34.4	164.6	26.6	150.7	83.3	17.7	143	36.8	333	95.1	360.2	68.8	589	104.5	11120	1.29	144.7	628
M16-10 - 63	323	662	2.93	2.83	22	1.89	13.1	6.6	1.46	18.4	5.69	61.5	22.04	97.6	20.4	186.5	36.92	9431	1.16	62.2	137.2
M16-10 - 64	570	910	1.14	9.9	69.4	6.3	38.6	19.3	4.45	40.6	9.6	86	24.6	90.8	17.2	167	36.2	9880	0.265	97.8	421
M16-10 - 65	4380	5120	3.99	274	671	85.8	400	145.3	38.3	261	56.3	478	134.9	465	83	684	123.9	10464	1.81	266.5	976
M16-10 - 66	131	552.4	0.464	Below LOD	8.69	0.085	1.81	3.28	0.69	16.2	4.88	51.1	17.8	78.3	15.88	147.3	28.85	8553	0.227	122.5	136.4
M16-10 - 67	711	1743	8.37	28.1	83.2	7.9	40.3	20.1	4.89	56.3	16.67	173.6	59.2	246.2	47.2	421.5	77.4	7784	3.61	81	165.6
M16-10 - 68	4470	482.7	1.37	68.5	165	14.7	60.7	13.5	2.01	19.9	4.26	42.6	15.03	68.4	15.47	152.2	31.71	10285	0.668	133.1	233.8
M16-10 - 69	1630	2802	3.4	38.7	190.5	26.8	147.1	65.1	17.7	118.7	28.8	266	82.1	323.8	62	535	100	10220	3.52	292.3	501
M16-10 - 70	1077	1493	4.37	13.8	44.3	5.63	25	13.6	4.5	43.5	13.81	146.4	49.5	211.2	45.5	428	83.3	8413	2.59	222	1160
M16-10 - 71	4800	6530	5.85	103.8	483	79.9	436	226.5	49.7	379	89.5	754	199.3	675	118.2	979	167.3	10920	5.04	151.2	1225
M16-10 - 72	622	1194	4.12	8.42	53.5	7.07	43.4	24.5	6.63	51.6	14.06	128.6	39.7	155	29.8	270	51.1	7580	0.91	75	219
M16-10 - 73	586	1507	1.26	9.46	80.8	8	51.3	35.8	11.9	76.5	18.71	173.5	50.8	188	33.95	286.9	53.2	6590	0.879	78	122.3
M16-10 - 74	4310	4730	4.74	83.7	413	42.4	227	107.4	28.4	215	48.3	423	118.9	408	70	549	99.3	11720	4.74	121.1	1006
M16-10 - 75	162	285.5	0.71	0.103	23.57	0.052	1.07	2.27	0.82	9.33	2.68	25.74	8.95	38.2	8.1	82.4	17.13	8717	0.218	59.7	89.4
M16-10 - 76	1720	1208	0.97	75.7	188	25	127.2	45.9	13.5	72.9	15.3	128	35.2	137	27.8	262	53.8	9930	0.71	179.1	406
M16-10 - 77	2720	4290	3.17	55.2	250.5	36.3	198.2	108.9	24.5	185	48.3	461	133.6	501	97	870	161.4	11230	2.86	102.8	803.3
M16-10 - 78	2340	4005	3.32	41.5	183.2	25.12	145.8	80.9	16.56	160.9	43.5	407.8	119.7	442.3	79.7	651.2	114.4	10640	1.54	142	816
M16-10 - 79	238	1411	1.14	Below LOD	5.4	0.081	1.97	3.88	0.376	23.8	9.56	121.1	48.6	218	43.6	383.9	73.6	8859	0.604	77.3	150.7
M16-10 - 80	4800	5470	2.72	87.9	460	62.3	330	150	41.6	262	61.9	530	146.7	519	96.1	823	147.6	11950	2.22	74	1052
M16-10 - 81	193	536.9	3.06	0.01	5.23	0.031	0.49	1.51	0.092	9.63	3.61	44.9	18.18	83.5	17.22	158.4	30.73	10146	1.473	35.63	91.3
M16-10 - 82	184	551	0.74	1.87	11.49	1.15	8.1	4.42	1.63	14.1	4.08	45.1	16.87	77.5	18.06	186.4	42.1	8708	0.336	54.4	150.9
M16-10 - 83	1880	2996	2.16	48.5	257	32.1	175.5	86	20.8	152.2	37	323	88	317	60.7	534	103.1	11740	2.4	114.4	988
M16-10 - 84	410	938	2.44	5.12	33	3.4	17.2	10.3	2.77	25.3	7.44	85.8	30.36	135	27.41	255.8	49.6	10048	1.54	161.9	383.5
M16-10 - 85	284	500.6	1.62	0.005	6.24	0.074	1.12	3.05	0.252	14	4.46	47.3	16.39	68.2	13.64	121.6	23.51	9682	0.513	79.9	129.5
M16-10 - 86	2000	2868	3.31	58.5	322	42.2	228	117.9	24.7	178	42.8	354	92.2	309.8	56	472	84.5	10080	1.24	281.7	623.1
M16-10 - 87	251	924	4.67	0.07	7.03	0.132	1.23	2.79	0.501	18.4	6.21	79.9	31.72	141.8	28.83	264.2	50.4	9256	1.97	49	122.3
M16-10 - 88	2240	3960	4.31	58.9	339	59.1	332	181	34.5	287	62.7	489	117.1	382	62.7	479	83.4	11690	3.04	123.2	1215

Grain_number	P_ppm_m31	Y_ppm_m89	Nb_ppm_m93	La_ppm_m139	Ce_ppm_m140	Pr_ppm_m141	Nd_ppm_m146	Sm_ppm_m147	Eu_ppm_m153	Gd_ppm_m157	Tb_ppm_m159	Dy_ppm_m163	Ho_ppm_m165	Er_ppm_m166	Tm_ppm_m169	Yb_ppm_m172	Lu_ppm_m175	Hf_ppm_m178	Ta_ppm_m181	Th_ppm_m232	U_ppm_m238
M16-10 - 89	545	1335	1.96	10.71	78.3	9.2	51.4	31.6	6.87	58.3	16.23	152.2	45	171.4	33.1	289.5	54.9	9880	0.8	86.5	229.1
M16-10 - 90	580	1271	1.96	9.7	52.4	6.99	40.1	17.3	4.18	37.1	10.3	115.9	41.5	182	36.8	329.4	62.5	9160	0.923	52.4	173.5
M16-10 - 91	655	1357	3.48	8.35	56	5.38	29	15.8	4.04	38.1	11.32	126.9	45.1	193	39.8	356.4	69.8	9570	1.55	142.9	414.6
M16-10 - 92	284	878	6.98	1.18	23.6	0.67	4.44	4.35	0.44	18.6	6.35	76.8	29.02	127.7	26.89	240.6	45.79	10207	2.51	165	175.9
M16-10 - 93	1900	3011	1.89	30.2	173	22.7	130.2	73.9	13.18	126.5	34.1	326.1	95	351	62.8	521	92.1	11050	1.66	84.1	624
M16-10 - 94	977	1744	1.33	2.25	9.8	0.97	4.3	4.77	0.65	28.4	12.32	149.4	57.4	259	54.5	491	96.2	10750	0.76	67.2	415
M16-10 - 95	877	1986	2.45	19.9	124.3	12.95	81.1	44.6	10.09	90.9	24.1	225.2	60.1	212.7	38.3	320.6	59.5	10060	1.08	190.4	506.6
M16-10 - 96	272	1416	1.9	0.58	7.05	0.189	2.54	3.65	0.453	26.1	9.37	119.6	48.59	218.1	44.01	389.7	74.2	7690	0.693	116.5	200.4
M16-10 - 97	312	1177	3	0.62	11.11	0.296	1.96	2.64	0.435	18.9	7.07	93.8	39.28	183.5	38.75	349.3	68.4	9425	1.21	101.7	235
M16-10 - 98	478	893	1.4	4.73	23.9	2.78	17.1	11.1	2.32	32	8.62	86.4	29.23	120	24.03	219.5	43	8288	0.779	123.6	350.8
M16-10 - 99	223	522	0.89	1.71	14.1	1.56	9.8	6.5	1.23	18.9	5	55.1	18.1	72.2	14.31	124	22.22	9720	0.414	44.2	72
M16-10 - 100	282	347	0.77	3.27	31.1	2.87	15.8	9.8	1.31	25.2	5.5	45.9	12.28	47	9.33	75.9	12.1	11640	0.39	63.1	146.8
M16-10 - 101	498	864	4.33	9.45	107	9.6	49.8	20.9	3.57	28.8	8.26	88.2	28.4	132.7	30.59	300.9	60.2	11760	4.73	73.4	1122
M16-10 - 102	799	2063	4.84	4.95	69.5	3.74	20.1	14.4	5.11	52.8	16.62	190.2	68.6	300	63.6	594	117.5	8725	1.66	181.8	243.6
M16-10 - 103	351	671	1.92	4.76	40.5	2.59	16.1	9	2.46	21.9	5.64	57.3	20.09	91	21.44	232.3	54.1	10440	1.07	134.8	430.7
M16-10 - 104	494	1005	4.87	10.75	70	8.03	44.7	24.1	5.92	40.7	10.58	100.2	30.97	134.1	28.95	284.9	62.2	12009	5.55	105.8	1255
M16-10 - 105	218	405	2.94	1.16	13	0.95	6.4	3.76	0.76	9.5	3.2	35.5	13.03	59	12.36	113.5	21.92	9829	1.47	41.02	118.8
M16-10 - 106	222	281.4	0.52	0.93	4.65	0.43	2.27	3.65	0.349	17.6	4.91	39.2	9.08	28.79	4.92	42.8	7.56	12340	0.301	30.86	237.1
M16-10 - 107	259	650.6	2.68	0.034	5.54	0.047	1.07	2.22	0.103	13.8	4.83	57.4	22.57	103.6	21.88	200.3	39.26	10360	1.24	71.9	173.2
M16-10 - 108	162	738.3	1.33	Below LOD	4.34	0.0038	0.48	1.42	0.24	12.3	4.48	61	25.41	117.6	23.87	222.8	44.44	8520	0.608	47.22	128.7
M16-10 - 109	346	924	4.63	2.87	26	2.29	12.5	8.6	1.73	23.5	7.93	90.2	30.9	131.9	26.33	236.2	44.31	10608	2.42	168.8	441.6
M16-10 - 110	874	1944	5.25	21.5	87.4	12.9	71.9	38.9	7.62	79.8	19.96	190.9	56.7	218.6	40.4	341.9	63.8	10700	3.26	176.5	729.8
M16-10 - 111	203	675	3.55	0.31	10.7	0.35	2.32	2.79	0.29	12.1	4.73	58.6	23.11	104	21.77	199.9	39.07	9992	1.93	148.6	350.5
M16-10 - 112	1420	2308	4.29	49.1	207	36.7	219	97.8	18.4	171	33.1	252	63.8	206.9	37.3	313.8	58.6	11130	3.17	134.1	942
M16-10 - 113	283	880	1.77	0.037	21.7	0.234	4.05	9	0.87	34.4	9.52	93.1	30.2	116.6	21.31	173.9	30.83	10083	0.76	247	184.6
M16-10 - 114	987	1596	2.64	17.5	131	14.4	83.5	44.5	10.75	74.8	18.91	167.7	49.7	193.6	37.59	333.4	62.7	9778	0.732	164.3	396.2
M16-10 - 115	191	1035	2.45	Below LOD	6.99	0.034	0.72	2.57	0.197	18.3	6.42	85.9	35.26	164	33.86	305.4	59.4	9038	1.08	86.8	211.7
M16-10 - 116	317	616	1.58	1.68	24	1.42	8.9	5.3	1.29	15.1	4.88	53.7	19.7	90.5	18.74	174.1	35	8990	0.603	70	130
M16-10 - 117	242	695.3	0.84	Below LOD	11.79	0.048	1.31	2.75	0.676	15.7	4.98	59.6	23.7	108.4	22.97	221	45.97	8037	0.377	100.5	163
M16-10 - 118	1418	2462	5.39	23	138.3	15.9	93.6	57.2	9.88	118.7	31	284.4	79.5	285.9	52	424.5	76.1	10085	2.7	243.8	776

Grain_number	P_ppm_m31	Y_ppm_m89	Nb_ppm_m93	La_ppm_m139	Ce_ppm_m140	Pr_ppm_m141	Nd_ppm_m146	Sm_ppm_m147	Eu_ppm_m153	Gd_ppm_m157	Tb_ppm_m159	Dy_ppm_m163	Ho_ppm_m165	Er_ppm_m166	Tm_ppm_m169	Yb_ppm_m172	Lu_ppm_m175	Hf_ppm_m178	Ta_ppm_m181	Th_ppm_m232	U_ppm_m238
M16-10 - 119	643	1938	1.34	7.62	56.1	7.06	41.9	27.1	5.67	61	18.47	190.9	64.6	269.1	52.7	467	90.6	9224	0.82	127.8	247
M16-10 - 120	609	1287	1.45	12.33	65.2	8.75	48.5	29.6	4.68	59.5	14.5	136	40.4	149.6	27.6	229	39.9	9110	0.59	225	322.9
M16-10 - 121	97	371.9	0.83	Below LOD	14.28	0.049	1.03	1.45	0.432	8.55	2.79	32.3	11.45	52.2	11.13	108.9	22.8	10029	0.4	104.8	154
M16-10 - 122	1450	2810	3.44	32.2	162	23.4	136	68.9	14.9	131	32	290	78	295	55.9	505	101.9	10710	3.11	109.6	1149
M16-10 - 123	4210	4840	6	85.7	445	73.9	410	210	52.2	327	74.4	588	146.7	490	88	757	138.7	13040	4.42	271	919
M16-10 - 124	668	757	0.93	4.7	24.5	3.73	18.8	14.8	2.34	38.9	10.96	97.6	24.8	78.1	12.51	90.4	14.5	11040	0.291	122.6	419
M16-10 - 125	519	1041	1.99	7.23	52.5	3.33	17.7	12.1	3.55	32.4	10.05	101.7	33.3	149.7	33.5	330	70.2	8930	0.83	258.3	542
M16-10 - 126	438	821	1.81	1.99	19.6	0.5	2.87	4.03	0.81	20.1	5.98	73.4	27.73	123.9	26.32	241.4	48.26	8576	0.967	139.6	242.6
M16-10 - 127	2600	3720	4.24	68.6	219.1	41.2	229.3	110.4	21.8	200.7	48.7	419	111.9	383	69.1	603	111.4	10900	8.94	115.4	1078
M16-10 - 128	295	1114	3.76	0.011	7.79	0.091	1.32	3.04	0.438	24.4	8.09	99.1	38.1	169.4	33	293	56.4	9570	1.74	90.5	172.4
M16-10 - 129	4550	12530	8.1	118.7	770	118.4	672	390	91.5	637	186.4	1649	419	1309	202	1376	197.2	11430	3.81	269	1451
M16-10 - 130	277	849	2.5	3.46	27.7	2.47	12.7	4.67	1.32	17.5	5.86	72.8	28.65	132.9	27.76	255.2	52.1	9740	1.011	74.5	223
M16-10 - 131	480	275.4	0.71	4.5	28.3	1.2	5.7	2.18	0.645	7.39	1.99	21.83	8.29	40.3	9.45	100.8	23.59	9012	0.312	65	113.9
M16-10 - 132	188	555	2.95	1.08	15.74	0.56	3.89	2.66	0.54	11.5	3.99	46.6	17.83	81.6	17.37	162.1	31	10502	2.02	89.5	248.9
M16-10 - 133	211	618.5	4.91	0.019	8.25	0.049	0.65	1.7	0.091	10.05	3.65	48.7	19.67	93.4	19.74	183.5	36.06	9825	2.37	140.3	308
M16-10 - 134	664	1130	7.4	6.99	40.4	3.74	21.8	12.9	3.26	35.3	9.55	102.3	36.3	154.3	31.98	282.7	53.23	10480	4.11	239.7	685.6
M16-10 - 135	172	688.8	3.7	0.005	7.22	0.03	0.83	1.94	0.164	11.9	4.62	58.3	23.04	106	21.9	199.5	38.85	9304	1.47	60.3	122.6
M16-10 - 136	533	1228	2.1	0.71	16.63	0.75	4.15	3.79	0.91	21.5	8.1	101.2	39.91	192.6	42.7	404.4	82.6	11860	1.86	181.3	388.3
M16-10 - 137	900	1630	1.6	14	60.2	7.4	42.3	22.7	6.14	60	16.7	170	54.4	215	39.7	341	63	8139	0.867	259	442
M16-10 - 138	1340	1830	2.08	22.6	143.5	15.73	87	42.8	10.51	79.5	20.5	182.8	54.1	205.5	39.8	358	69	10210	0.94	260	515.4
M16-10 - 139	257	520	2.88	1.98	17.8	1.02	6.2	2.44	0.98	6.6	2.55	38.4	15.6	89.2	23.8	270.4	61.2	11670	6.36	63.8	1119
M16-10 - 140	1860	3630	16	28.7	161.2	16.34	89.1	50.4	10.87	105.3	33.23	349.5	117.3	483.2	92.1	765	133.2	10390	4.07	514.6	505.2
M16-10 - 141	403	942	1.5	4.4	15.1	0.98	5	2.78	0.276	17	6	80.3	32.21	148.6	30.57	272.1	52.59	8373	0.667	69.6	139.9
M16-10 - 142	282	1204	1.78	0.46	8.09	0.236	2.07	3.26	0.397	20.7	7.83	98.5	40.57	185.2	38.36	341	66.61	8665	0.798	89.2	183.3
M16-10 - 143	810	1582	4.88	32.5	196	28.1	148.5	47	12.04	72.3	16.51	152	46.2	196.1	43	421.2	87	11910	5.44	98.4	1311
M16-10 - 144	506	1047	1.64	0.79	6.28	0.46	2.89	4.34	0.32	23.9	8.24	98.4	35.44	146.7	26.7	219.7	41.21	10510	0.469	43.9	111.1
M16-10 - 145	798	1417	2.04	7.8	83.7	6.72	34.6	24	6.55	50.9	13.76	135.8	44.2	196.2	42.5	422	87.5	8940	0.78	231	304
M16-10 - 146	3270	4700	3.75	77.7	561	64.9	352	171.4	47	252	63.3	560	150.9	543	99	862	142.1	12190	4.64	122	1024
M16-10 - 147	218	525.7	0.231	Below LOD	3.16	0.062	1.2	2.34	1.03	13.4	4.06	46.1	17.68	80.1	17.52	172.7	36.76	7958	0.055	12.93	47.16
M16-10 - 148	138	230.3	0.544	Below LOD	6.53	0.0035	0.82	1.86	0.244	8.9	2.19	21.56	7.94	31.7	6.43	59.7	12.2	10563	0.277	42.16	106.7

Grain_number	P_ppm_m31	Y_ppm_m89	Nb_ppm_m93	La_ppm_m139	Ce_ppm_m140	Pr_ppm_m141	Nd_ppm_m146	Sm_ppm_m147	Eu_ppm_m153	Gd_ppm_m157	Tb_ppm_m159	Dy_ppm_m163	Ho_ppm_m165	Er_ppm_m166	Tm_ppm_m169	Yb_ppm_m172	Lu_ppm_m175	Hf_ppm_m178	Ta_ppm_m181	Th_ppm_m232	U_ppm_m238
M16-10 - 149	125	562	6.48	0.02	9.65	0.027	0.26	1.91	0.041	10.4	4.04	50	19.26	87.1	17.78	153.9	28.25	10800	2.93	72.1	234.1
M16-10 - 150	610	1199	1.51	9.2	86	7.4	44.1	19.5	6	42	12.3	126	40.7	165	31.8	280	50.1	8736	0.64	79.1	173
M16-10 - 151	519	952	1.43	6.5	62	5.5	28.8	15.1	4.58	33.5	8.99	87.8	29.7	122.8	24.97	236.4	49.9	10820	0.697	85.2	373
M16-10 - 152	59	412	0.78	Below LOD	29.8	0.21	3.57	5.71	2.47	19.9	4.86	42.7	12.95	50.2	9.94	89.6	16.96	9161	0.21	212	112.7
M16-10 - 153	215	259.8	0.428	0.56	5.54	0.17	0.75	0.56	0.197	4.85	1.611	19.7	8.26	40.3	9.11	96.7	21.21	10107	0.251	25.92	69.4
M16-10 - 154	4730	5820	4.48	59.1	479	51.6	267	129.3	41.3	222	60.7	622	176.4	677	129.8	1145	191.2	10700	3.3	422	1021
M16-10 - 155	181	437.9	0.85	Below LOD	8.12	0.029	0.94	1.32	0.268	9.6	2.88	36.6	13.86	66.5	15.3	147.6	30.53	9314	0.323	64.9	127.9
M16-10 - 156	148	312.2	1.04	Below LOD	5.39	Below LOD	0.57	1.22	0.072	6.13	2.15	26.5	10.1	47.1	9.58	89.7	17.98	9794	0.531	76.6	147.1
M16-10 - 157	630	1083	2.73	1.32	23.2	0.41	3.03	3.63	1.5	22.3	8.08	95.5	35.37	160.4	35.76	346.2	70.3	11670	1.42	161.7	592.1
M16-10 - 158	1052	2560	2.11	21.3	136	17.8	101.2	56.6	13.7	110.1	31.1	292	85.5	311	56.5	469	81.5	9391	0.72	86.7	363
M16-10 - 159	5480	7920	5.08	129.1	713	100.7	581	299	59.6	501	113.3	900	221.3	691	112.6	886	146.2	11980	3.62	135.1	1810
M16-10 - 160	876	1060	3.32	20.7	114.5	14	75.9	30.6	6.13	50.3	10.98	99.7	28.9	109.7	21.59	198.2	39.3	11490	2.61	137	624
M16-11 - 1	549	889	6.92	6.27	36.8	2.95	16.8	14.4	8.92	33	8.79	84.5	28.1	140.1	34.2	362	71.6	7675	3.34	127.2	1261
M16-11 - 2	537	1063	2.89	3.4	67.8	2.71	20.3	12	4.47	34.3	9.75	98.4	34.3	159.1	35.4	348.7	72.5	9039	0.96	307	425.3
M16-11 - 3	1225	2204	1.36	1.74	23.8	2.15	17.4	41.9	18.2	121.4	25.6	227.7	74.8	315.1	63.6	585.9	115.8	10900	0.713	104.4	183.7
M16-11 - 4	699	1305	2.82	9.35	158	10.28	63.3	35.6	10.81	71.8	17.71	150.4	45.5	183.8	37.2	333	64.6	9256	1.09	342	423.4
M16-11 - 5	2240	3228	6.13	23.1	294	25.8	132	50.9	16.8	89.1	26.2	286.4	104.3	513.4	116.5	1142	224.5	11820	3.93	151.6	993
M16-11 - 6	988	2477	3.85	23.3	223	18.4	100.1	62.1	20.7	134.6	35	302	85.9	334.1	66.7	596	111.8	8144	1.91	292	721
M16-11 - 7	807	1632	2.72	1.19	14.9	0.91	6.03	7.4	2.13	39	12.57	146.2	55.3	248.5	52.6	479.2	93.8	10490	1.46	191.7	280.8
M16-11 - 8	173	610	1.47	0.203	5.9	0.141	1.34	1.86	0.68	11.7	4.52	54.2	20.87	95.6	20.07	188.1	38.8	7622	0.634	36.6	98.3
M16-11 - 9	257	1072	3.1	12.8	38.3	3.55	14.6	7.7	2.13	26.8	8.52	99.1	37.3	165.6	33.02	294.2	56.6	8032	1.67	120.3	214.5
M16-11 - 10	353	674	2.13	4.9	118.2	6.35	32.8	17.7	5.06	32.7	8.37	75	22.42	96.8	21.05	200.1	39.3	9970	0.921	217.9	371.6
M16-11 - 11	515	1880	9.76	3.28	64.7	3.31	20.7	19.4	4.71	68	20.7	209	68.6	266	47.3	373	63.6	8197	3.39	106.9	181.5
M16-11 - 12	231	2709	54	1.97	80.2	2.18	15.3	13.6	2.44	53.8	20.26	253.5	94.8	412	79.5	647	107.1	8896	14.66	162.3	499
M16-11 - 13	469	1272	6.27	1.23	25.1	1.16	8.9	12.6	6.58	48.8	12.57	125.4	41	175.1	36	326.2	62	9089	1.87	212.8	542
M16-11 - 14	730	1018	11.1	2.83	31.5	2.87	13.6	11.2	3.76	21.8	7.57	84.3	32.3	162.7	43.3	481	106.8	11080	6.88	56.9	1051
M16-11 - 15	263	653	4.63	0.078	28.8	0.059	1.23	4.42	1.64	19.2	5.48	59.5	21.46	94.5	19.86	182.8	35.51	10900	1.84	281.1	435.3
M16-11 - 16	217	635	1.41	1.56	43.8	2.23	13.5	10	3.06	28.7	7.47	70.5	21.71	87.4	17.76	159.8	31.38	9446	0.75	139.8	285.2
M16-11 - 17	297	742	1.21	Below LOD	2.76	0.031	0.71	2.03	0.15	15.9	5.38	64.9	25.31	111.9	23.4	209	41.13	10403	0.693	79.8	289.4

Grain_number	P_ppm_m31	Y_ppm_m89	Nb_ppm_m93	La_ppm_m139	Ce_ppm_m140	Pr_ppm_m141	Nd_ppm_m146	Sm_ppm_m147	Eu_ppm_m153	Gd_ppm_m157	Tb_ppm_m159	Dy_ppm_m163	Ho_ppm_m165	Er_ppm_m166	Tm_ppm_m169	Yb_ppm_m172	Lu_ppm_m175	Hf_ppm_m178	Ta_ppm_m181	Th_ppm_m232	U_ppm_m238
M16-11 - 18	202	646	3.12	0.067	6.29	0.061	0.76	2.28	0.156	13.1	4.22	55.9	21.93	101.7	21.67	200.7	40.41	9863	1.3	77.5	161.3
M16-11 - 19	454	786	2.12	9	151	10.7	52.9	25	8.5	47.5	11.3	95.7	27.4	107.7	23.4	223	44.5	10810	0.601	144.8	195.5
M16-11 - 20	291	563	4.63	1.76	56.3	2.19	13.5	7.5	2.45	21.3	5.84	56.2	18.82	81.8	17.97	166.4	31.52	10346	1.96	227.9	360.1
M16-11 - 21	800	1613	4	14.1	242	17.9	105	54.8	16.9	107.3	25.1	208	55.8	209	40.3	350	62.1	9700	1.53	417	386
M16-11 - 22	526	1202	6.05	3.1	91.1	3.2	18.6	15.8	4.97	44.7	12.17	123.8	40.4	176.2	38	349.1	70.2	9113	2.19	332.2	339.3
M16-11 - 23	347	784	4.64	0.93	55.3	1.24	8.4	7	2.42	24.3	6.81	71.7	25.82	114.2	25.41	244.5	48.1	8548	1.79	265	283
M16-11 - 24	707	2050	0.96	5.24	16.1	2.83	21.9	17	4.46	70.3	19.8	193.8	65.1	260.1	48.8	413	78.1	9659	0.673	92.2	165.7
M16-11 - 25	160	288.2	1.17	0.34	19.31	0.18	1.77	2.61	0.589	8.55	2.52	26.3	9.27	39.8	8.32	78.7	14.71	8971	0.506	119	133.4
M16-11 - 26	124	236.7	1.69	Below LOD	17.26	0.029	0.64	1.6	0.326	5.95	1.82	20.14	7.37	33.5	7.54	77.5	16.74	9679	0.823	108.3	244.2
M16-11 - 27	707	1456	1.18	2.06	29.5	2.73	18.1	17.7	3.66	55.5	15.67	157.6	52.52	215.2	41.83	376.3	73.7	9250	0.344	162.3	183.4
M16-11 - 28	459	640	2.6	2.33	23.8	1.99	11	9.9	3.81	28.6	7.97	71.4	20.85	73.8	15.55	143.2	27.7	11450	1.28	76.5	593
M16-11 - 29	214	561.7	1.82	Below LOD	9.05	0.056	1.6	2.37	0.249	13.1	4.11	50	18.65	84.9	17.2	155.9	30.56	8966	0.824	62.8	139.1
M16-11 - 30	422	704	0.84	1.41	34.3	1.43	10.4	9.9	2.76	27.7	7.35	72.8	24.4	101.9	20.2	185	36.7	8505	0.361	165	90.1
M16-11 - 31	1080	1940	1.55	4.44	81.9	3	18.1	13.6	4.19	49.5	16.48	186.1	66.5	287.5	60.9	559	107.1	10850	0.957	135.4	393
M16-11 - 32	2880	3920	5.11	17.4	92	13.2	76.9	60.4	27.9	137.4	38.9	381.9	126.3	551.7	115.2	1055	195.1	10730	2.17	266	1097
M16-11 - 33	870	1160	2.49	12.9	145	9.2	47.6	30.7	13.2	75.3	18.9	157	40.4	154	29.3	265	49.4	8470	0.87	377	671
M16-11 - 34	810	1620	3.09	30.8	466	33.7	178	90	26.2	128	30.1	233	59	221	45.7	434	86.4	10142	1.37	239	458
M16-11 - 35	1100	2200	2.02	52.8	243	22.2	115.6	58.2	17.2	109.4	28.6	258	73.7	280	55.3	479	85.3	11220	1.32	207	660
M16-11 - 36	647	1180	0.7	Below LOD	1.01	0.113	1.46	3.52	0.065	25.6	8.63	104.1	39.39	173.9	35.18	315.3	61.02	10610	0.345	61.4	146.1
M16-11 - 37	892	3561	14.66	3.59	46.2	2.23	15.4	19.9	8.83	90.2	29	331.3	123.7	529.5	106.1	922	172.3	7974	5.3	534	912
M16-11 - 38	128	337.2	0.76	Below LOD	14.08	0.018	0.48	1.21	0.267	7.53	2.24	27.5	10.89	50.3	11.16	110.6	23.06	8774	0.358	51.1	71.2
M16-11 - 39	368	1424	6.6	5.66	70.9	5.28	28.8	15.8	4.13	46.9	12.15	131.5	47	211.5	44.72	423.7	87	6933	2.17	236.4	514.5
M16-11 - 40	122	561.7	2.55	0.254	20.21	0.29	2.57	4.71	0.412	16.8	5	52.8	18.94	83.6	17.65	168.7	33.7	8469	0.965	108.5	250.1
M16-11 - 41	530	1787	2.07	2.86	40.2	2.59	18.8	15.4	4.84	63.8	17.9	185	62.9	253	47.9	408	75	7970	0.97	50.9	70.1
M16-11 - 42	271	992	8.14	Below LOD	21.47	0.04	1.13	2.66	0.201	19	6.85	87.5	33.46	154	32.29	293.1	56.2	10830	4.01	90.3	222.7
M16-11 - 43	1040	2213	1.33	Below LOD	4.83	0.097	2.81	7.1	0.58	41.4	15.2	196.1	74.5	335	68.8	629	122.6	10550	0.792	104.6	180.5
M16-11 - 44	324	1230	3.17	0.028	13.81	0.28	3.86	6.5	0.71	35.2	11.32	121.5	41.56	171.8	32.78	279	51.73	9571	1.11	235.8	356
M16-11 - 45	176	371	2.35	0.48	33.7	0.377	2.69	4.54	2.84	14.8	3.5	32.1	11.42	53.7	12.23	138.3	30.12	10340	0.681	212.3	422.3

Grain_number	P_ppm_m31	Y_ppm_m89	Nb_ppm_m93	La_ppm_m139	Ce_ppm_m140	Pr_ppm_m141	Nd_ppm_m146	Sm_ppm_m147	Eu_ppm_m153	Gd_ppm_m157	Tb_ppm_m159	Dy_ppm_m163	Ho_ppm_m165	Er_ppm_m166	Tm_ppm_m169	Yb_ppm_m172	Lu_ppm_m175	Hf_ppm_m178	Ta_ppm_m181	Th_ppm_m232	U_ppm_m238
M16-11 - 46	134	282.4	0.68	Below LOD	15.54	Below LOD	0.42	1.41	0.298	7.22	2.01	23.6	9.01	41.1	9.04	85.2	17.9	9065	0.293	64.1	94.5
M16-11 - 47	147	562.4	1.16	0.72	13	0.3	2.74	3.7	1.18	15.6	4.25	51.1	18.94	85.9	18.03	169.4	35.8	7772	0.49	58.9	91.7
M16-11 - 48	380	550	2.59	5.24	60	5.29	33.2	16.3	4.64	23.7	6.79	63	18.6	83.7	20.2	208.9	44.5	12465	2.58	123.9	523
M16-11 - 49	595	914	4.79	5.6	70	3.99	24	14.6	5.89	34.3	8.95	88.2	30.3	137.1	32.4	327.9	69.7	10400	2.33	157.5	681
M16-11 - 50	293	734	1.47	0.34	15.95	0.51	4.1	4.44	1.29	18.8	5.85	65.7	24.64	111.8	23.87	225.9	48.05	8728	0.817	52.9	120
M16-11 - 51	194	558.3	2.13	Below LOD	5.42	0.032	0.45	1.63	0.139	9.8	3.54	45	18.63	86.2	18.45	173	33.64	9691	1.02	39	92.7
M16-11 - 52	2240	2649	7.1	79.6	1202	110.5	563	190	53.4	231	50.9	393	96.1	343	67.3	606	104.3	10980	2.83	112.4	1148
M16-11 - 53	299	913	1.9	0.037	25.4	0.092	1.38	3.04	1.11	16.3	5.59	72.1	28.93	147.8	33.96	344	75.2	9200	0.651	67.4	114.5
M16-11 - 54	770	1361	1.3	0.116	2.99	0.164	2.11	4.19	0.47	29.4	10.26	123.5	47.34	207.3	43.83	398.1	75.5	11200	0.821	111.4	287.3
M16-11 - 55	492	1379	7.06	5.2	68.5	4.67	28.6	19.1	4.65	52	15.19	151.8	51.6	203.4	39.5	346	63	10110	2.18	80.8	219
M16-11 - 56	135	927	2.54	Below LOD	9.56	0.03	1.18	2.5	0.431	16.6	6.37	79.1	32.04	145.1	30.07	267.9	53.55	7863	0.961	77.8	173.8
M16-11 - 57	432	1398	2.93	0.71	56.2	0.66	8.1	8	2.78	33.4	10.04	112.2	43.6	206.7	47.4	489	105.1	9020	1.02	390	411
M16-11 - 58	621	2426	5.24	3.55	66.7	4.33	28.9	23.2	7.9	89.9	25	250.9	85.1	352.3	69.3	596.7	108	9570	2.89	324.5	436.1
M16-11 - 59	1273	2224	2.04	0.106	3.72	0.31	3.27	10.7	1.03	52.5	17.87	201.9	75.7	326.9	66.7	605.3	119.9	9584	0.97	147.7	379.2
M16-11 - 60	593	598	6.46	6.93	98.2	7.49	37.5	23	6.73	35.1	8.76	76.3	21.1	79.7	16.25	162	29.1	11600	2.38	129	949
M16-11 - 61	340	669	5.86	0.045	29.1	0.035	1	4.05	2.93	24.2	6.64	65.5	21.84	98.4	22.68	219.9	43.1	12300	2.86	123.4	689.8
M16-11 - 62	1062	2456	10.97	Below LOD	8.89	0.075	1.61	5.06	0.215	39.8	17.25	222.2	82.6	341.4	64.58	536	96.2	11367	4.23	86	390.1
M16-11 - 63	521	972	5.11	1.07	29.2	0.54	3.84	7.6	4.51	30.9	8.28	88.1	31.5	141.9	32.14	311.1	61.7	10610	1.92	309	593
M16-11 - 64	828	979	6.56	15.7	209	11.1	58.2	36.5	16.9	61.6	14.8	119.3	33.6	134.4	30.9	321.1	65.5	12200	3.76	202	954
M16-11 - 65	129	508.6	1.67	Below LOD	4.14	0.04	0.82	2.16	0.192	12.5	3.98	47.5	17.58	78.5	16.12	147.2	29.07	8752	0.626	35.8	69.5
M16-11 - 66	215	413	0.69	0.084	2.42	0.071	0.73	1.44	0.261	11	3.18	37.6	14.2	59.7	12.57	111.2	22.05	10020	0.257	16.94	51.6
M16-11 - 67	159	378.2	0.84	Below LOD	17.61	0.042	0.7	1.63	0.295	11	2.99	33.4	12.4	54.5	11.36	103	20.27	9755	0.372	89.7	127.1
M16-11 - 68	1501	2460	2.31	12.7	158	14.3	80.8	44.5	15.6	89.5	23.9	229.5	83	380.5	85.2	840	163.1	12030	1.81	183.8	544
M16-11 - 69	804	1310	0.57	1.71	14.1	1.24	10.5	11.2	1.11	51	14.4	141	44.9	174	32	268	48.7	10440	0.344	105.8	173
M16-11 - 70	no value	no value	no value	no value	no value	no value	no value	no value	no value	no value	no value	no value	no value	no value	no value	no value	no value	no value	no value	no value	no value
M16-11 - 71	299	1144	1.72	0.126	33.8	0.72	12	14.7	4.13	50.7	13.91	131.7	40.8	154.3	28.31	231	41.29	7941	0.75	93.7	65.5

Grain_number	P_ppm_m31	Y_ppm_m89	Nb_ppm_m93	La_ppm_m139	Ce_ppm_m140	Pr_ppm_m141	Nd_ppm_m146	Sm_ppm_m147	Eu_ppm_m153	Gd_ppm_m157	Tb_ppm_m159	Dy_ppm_m163	Ho_ppm_m165	Er_ppm_m166	Tm_ppm_m169	Yb_ppm_m172	Lu_ppm_m175	Hf_ppm_m178	Ta_ppm_m181	Th_ppm_m232	U_ppm_m238
M16-11 - 72	230	703.8	1.38	Below LOD	24.56	0.1	1.79	3.4	0.7	17.3	5.26	61.3	22.87	106.3	22.99	222.3	46.73	8161	0.782	108.7	154.5
M16-11 - 73	129	461.5	1.22	Below LOD	7.09	Below LOD	0.19	1.19	0.444	9.09	3.07	39.5	14.89	69.2	14.99	146.4	31.04	10540	0.816	59.2	238.8
M16-11 - 74	142	231.8	0.66	Below LOD	5.42	0.027	0.45	1.35	0.167	5.87	1.63	19.3	7.15	34	7.04	69.2	14.37	8322	0.326	42.18	74.6
M16-11 - 75	209	501.6	1.33	0.45	21.7	0.7	5.67	6.57	2.22	22.8	5.62	54.2	16.36	65.4	12.64	117.1	22.24	7841	0.525	209.3	268.2
M16-11 - 76	294	417	1.52	Below LOD	4.75	0.15	2.71	7.39	0.72	27.9	7.32	57.6	13.82	40.47	6.23	42.2	6.46	11040	0.883	47.78	289.4
M16-11 - 77	552	1122	2.88	0.91	8.78	0.28	2.32	3.76	0.51	22.4	7.51	95.1	38.14	180.7	38.41	363.1	73.65	10980	1.63	100	234.9
M16-11 - 78	368	794	3.14	0.037	14.02	0.056	1.18	3.98	1.35	18.4	6.18	72.1	26.95	119.7	25.34	239.1	46.3	9510	1.59	271	327
M16-11 - 79	187	2190	4.46	0.064	17.22	0.45	8.88	15.1	0.51	67.9	20.66	226.4	78.6	316.3	58.46	470.3	79.2	10630	2.47	373.6	258.8
M16-11 - 80	338	1213	2.5	0.025	6.35	0.186	2.89	5.54	0.8	30.4	10.25	117	43.4	181.7	35.9	317.8	61.5	8782	1.1	38.4	129.1
M16-11 - 81	1280	1876	7.25	33.4	296	30.6	167	76.8	26.3	114.6	27.3	227.6	65.7	260	55	494	93.2	12730	4.37	252	851
M16-11 - 82	895	1732	3.15	7.31	61.1	6.71	38.8	28.9	8.59	73.3	19.32	186	58.9	247.7	51.4	479	92.9	9690	2.68	257	566
M16-11 - 83	134	226.5	1.07	1.19	14.8	0.82	4.8	2.78	1.03	5.8	1.76	18.4	7.28	36.8	9.07	101.4	22.97	9014	0.903	121.1	365.3
M16-11 - 84	338	1346	2.1	0.229	18.82	0.92	11.15	15.3	2.16	55.5	14.7	148.4	48	185.5	33.33	277.3	50.2	8503	1.02	276.3	163.5
M16-11 - 85	686	1350	1.81	Below LOD	7.33	0.067	2.02	3.73	0.545	24.6	9.14	114.5	45.4	209.9	45.9	425.3	85.5	10390	0.865	76.9	133.5
M16-11 - 86	1960	2687	5.4	0.79	9.82	0.79	6.2	19.9	11.72	77.1	21.4	234.3	89	425.3	100.3	980	194.9	12720	2.67	152.4	777
M16-11 - 87	696	2128	1.43	0.121	5.7	0.56	10.4	13.6	0.72	66.1	19.27	210.7	73.5	303.8	55.8	465.4	84.1	9580	1.014	192.5	139.9
M16-11 - 88	537	2068	5.24	0.38	79.1	0.4	5.5	9.5	4.66	48.9	14.3	166.1	61.1	270.4	57.4	558	111.4	8593	1.73	281.2	510
M16-11 - 89	537	498	1.55	3.15	56	2.46	15.6	8.7	3.15	21.8	5.39	50.5	15.83	70.8	15.15	149	30.42	9230	0.99	153.2	212.4
M16-11 - 90	400	1848	8	0.023	17.8	0.177	2.75	5.75	0.9	38	13.43	161.4	62.7	283	58.1	513	95.9	9300	3.34	325	472
M16-11 - 91	294	940	7.57	Below LOD	14.89	0.047	1.41	3.84	0.75	19.6	6.82	81.3	31.33	147.1	31.31	290	55.7	9861	3.61	154.6	285.3
M16-11 - 92	258	477	2.06	Below LOD	18.99	0.076	0.38	3.2	1.26	16.1	4.5	45.1	15.54	67.6	14.29	134.6	26.5	10431	1.003	143.1	151.1
M16-11 - 93	Below LOD	89.4	0.76	0.029	3.2	0.029	0.37	0.39	0.2	1.56	0.682	7.67	2.79	13.42	3	31.3	6.79	11030	0.363	22.63	318.3
M16-11 - 94	327	749	1.92	Below LOD	3.38	0.06	0.82	1.82	0.412	13.3	5.21	64.6	24.99	115	24.33	221	44.52	8769	0.817	22.83	50.56
M16-11 - 95	no value	no value	no value	no value	no value	no value	no value	no value	no value	no value	no value	no value	no value	no value	no value	no value	no value	no value	no value	no value	no value

Grain_number	P_ppm_m31	Y_ppm_m89	Nb_ppm_m93	La_ppm_m139	Ce_ppm_m140	Pr_ppm_m141	Nd_ppm_m146	Sm_ppm_m147	Eu_ppm_m153	Gd_ppm_m157	Tb_ppm_m159	Dy_ppm_m163	Ho_ppm_m165	Er_ppm_m166	Tm_ppm_m169	Yb_ppm_m172	Lu_ppm_m175	Hf_ppm_m178	Ta_ppm_m181	Th_ppm_m232	U_ppm_m238
M16-11 - 96	3040	6.40E+03	6.52	6.58	62.5	5	38.1	48.6	29.8	251	72	710	204	730	123	940	149	11110	3.58	301	693
M16-11 - 97	781	1265	3.47	10.4	177	12	63.5	31.3	8.7	53.5	13.79	136.4	44	186.1	39.5	362	70	9620	1.29	172	183
M16-11 - 98	150	404	0.78	0.46	14.2	0.319	2.29	1.98	0.66	8	2.52	29.2	11.88	61.7	14.87	165.2	39.35	9870	0.375	86.4	200.2
M16-11 - 99	538	1091	5.13	2.92	44.2	1.96	12.5	10.8	3.39	33.3	9.64	102.6	35.03	150.5	30.43	269.5	51.5	9891	2.1	296.1	552
M16-11 - 100	624	1249	2.15	9.82	156.4	11.1	63.5	39.1	13.12	76.5	19.1	161	43.6	167	32.2	291	53.4	8900	0.66	248	298
M16-11 - 101	790	945	6.85	6.69	85	6.18	33.3	26.7	13.76	56.7	11.69	101.5	30.64	150	36.5	412	86.8	11290	5.34	92.6	1379
M16-11 - 102	195	502.9	2.61	0.038	13.52	0.12	1.68	2.72	0.57	13.2	4.25	48.2	17.27	75.8	14.88	135.7	26.07	9214	1.084	93.2	85.1
M16-11 - 103	137	463.1	4.92	0.296	19.45	0.3	2.04	2.4	0.523	9.1	3.15	40.3	15.13	75.1	16.83	169.2	34.69	11458	2.74	288.3	399
M16-11 - 104	172	2465	2.59	0.155	6.47	0.213	3.89	7.5	1.4	52.2	17.65	222.3	87.4	378	73.7	647.8	124.8	8365	1.33	53.8	129.7
M16-11 - 105	2690	2700	3.99	27.9	164	15.1	73	57	23.1	154	40	348	91	323	60.9	514	85	11990	1.94	285	1300
M16-11 - 106	608	905	1.55	0.81	9.07	0.83	7.9	11	1.41	52.2	14.54	121.5	29.45	87.3	13.78	104.4	17.12	10650	0.594	85.4	352
M16-11 - 107	889	1210	3.29	6.23	97.1	9.35	47.9	30.3	10.27	69.1	17.5	150.2	42	157	30.3	262	45.4	12700	1.61	151.4	749
M16-11 - 108	585	1402	3.41	Below LOD	21.99	0.135	3.08	7.2	0.274	34.4	12.07	134.5	47.3	205.4	40.44	355.7	65.93	10631	1.33	242.8	184.9
M16-11 - 109	250	1146	3.8	Below LOD	8.19	0.059	1.3	3.36	1.08	21.6	7.55	96.8	38.6	182.5	38.3	360	73.2	8336	1.4	177	345
M16-11 - 110	655	1106	0.79	0.81	6.17	0.76	6.3	9.8	0.92	39.5	11.82	117.6	37.2	143.5	27.3	224	40.3	11350	0.452	81.7	257.6
M16-11 - 111	555	1080	1.73	5.05	87.3	5.06	30.9	25.6	8.79	66.3	15.23	134.6	37.8	147.5	28.15	255.1	48.7	8143	0.7	152.7	146.3
M16-11 - 112	212	1034	1.2	Below LOD	11.69	0.211	3.7	6.84	1.25	32.8	9.5	103.2	35.95	149.4	29.13	249.1	46.2	8834	0.555	28.33	38.1
M16-11 - 113	342	1005	5.07	0.88	52.3	0.85	5.8	6.4	1.89	26.4	8.41	92.2	33.31	146.6	30.23	276.4	53.9	9590	2.08	214.9	256.5
M16-11 - 114	334	416.3	1.47	4.2	26	0.9	5.7	3.74	0.69	12	3.63	39.5	13.67	58.6	12.43	113.5	21.98	8725	0.69	69.7	87.5
M16-11 - 115	714	1283	1.83	Below LOD	6.99	0.045	1.03	2.44	0.28	20	7.65	102.7	42.33	199.2	43.37	410	82.3	10650	1.232	139.4	289.1
M16-11 - 116	694	1264	0.64	Below LOD	1.58	0.127	2.07	6.02	0.085	34.9	11.23	122.6	43.1	176.7	34.3	297	57	10650	0.43	78.9	236.7
M16-11 - 117	1690	2830	2.81	31.1	307	28.8	150	73.1	25.8	162	37.8	330	96.9	367	69.8	585	99.6	10030	1.25	357	650
M16-11 - 118	1910	3630	7.07	37.5	589	47.6	265	124.8	41.1	254	56.7	457	123.7	452	88.4	762	136.9	8047	2.67	768	654
M16-11 - 119	1683	2162	9.06	58.5	814	75.3	384	145.9	43.8	193	42.7	322	77.8	281.9	57	524	92.2	10210	3.1	394	794
M16-11 - 120	2860	5971	10.16	5.7	36.7	3.22	21.1	19.1	5.97	104.2	38.1	483.5	194	927	200	1913	367.1	11090	4.69	216.2	1293
M16-11 - 121	216	416.9	5.23	1.16	49.5	1.27	6.1	3.02	1.06	10.8	3.11	35.8	13.3	66.2	14.88	157.6	32.22	10680	2.66	165.9	237.4
M16-11 - 122	1610	2012	4.71	35.2	981	34.9	180	83.2	27.2	106.1	26.9	235.5	70.6	309.7	70.9	675	129.3	12420	2.42	115	952
M16-11 - 123	358	679	3.91	2.9	65.1	2.85	16.7	9.6	3.04	23.1	6.58	68.2	23.05	99.8	21.75	197.8	37.71	9700	2.45	112.6	399.4

Grain_number	P_ppm_m31	Y_ppm_m89	Nb_ppm_m93	La_ppm_m139	Ce_ppm_m140	Pr_ppm_m141	Nd_ppm_m146	Sm_ppm_m147	Eu_ppm_m153	Gd_ppm_m157	Tb_ppm_m159	Dy_ppm_m163	Ho_ppm_m165	Er_ppm_m166	Tm_ppm_m169	Yb_ppm_m172	Lu_ppm_m175	Hf_ppm_m178	Ta_ppm_m181	Th_ppm_m232	U_ppm_m238
M16-11 - 124	349	1356	1.52	0.151	10.69	0.85	11.7	13.8	2.74	52.7	14.83	149.3	48.92	191.8	35.88	305.3	55.02	8725	0.703	116.4	78.2
M16-11 - 125	213	539	0.73	0.037	17.74	0.111	2.05	2.75	1.08	14.3	4.25	46.2	16.82	78.6	17.31	175.9	37.3	9599	0.386	110.8	135.9
M16-11 - 126	356	1480	4.52	0.33	26.4	0.52	5.05	8.2	2.73	43.1	12.74	137.7	50.7	214.8	42.7	378.9	72.8	8710	1.15	316	359
M16-11 - 127	138	482.8	1.44	0.162	19.2	0.288	1.65	2.47	0.68	11.2	3.34	40.4	15.54	73.1	16.57	168.7	35.83	10550	0.609	156.9	297.3
M16-11 - 128	1500	2904	11.4	37.2	361	27.1	157.3	104.6	49.6	194.9	45.7	365.4	92.8	337	68.9	632	114.1	11030	4.14	156.5	1440
M16-11 - 129	311	784	5.06	1.93	27	1.31	8.9	7.9	2.19	24.7	6.62	75.8	26.46	117.1	24.58	218.4	41.96	10100	1.87	173.6	451
M16-11 - 130	204	445	1.23	Below LOD	30.5	0.059	1.3	2.16	0.384	9.3	3.16	37.4	14.67	65.3	14.43	143.3	30.16	9340	0.468	77.7	123
M16-11 - 131	367	1072	1.87	0.086	34.9	0.416	4.63	6.8	1.68	30.7	8.56	98	35.73	159.6	33.89	320	64.7	8135	0.96	131.1	189.1
M16-11 - 132	314	1082	1.07	0.49	42.3	0.63	9	13.6	3.93	48	11.98	116.9	36.8	146.3	28.51	249.2	48	7829	0.394	163.5	135.9
M16-25 - 1	1098	3667	9.89	9.3	75.2	6.16	39.8	27.4	6.64	72.6	21.6	253.5	101.1	500.5	123.5	1366	313.4	9340	3.47	1168	1866
M16-25 - 2	1250	3463	15.65	5	91.4	5.5	35.5	19.4	5.1	61.5	18.48	236.6	97.6	497.1	128.3	1420	325.8	8904	4.13	1376	2235
M16-25 - 3	873	3290	11.32	2.83	69.4	2.85	19.1	16.2	3.01	53.2	17.55	222.8	90.8	483	121.4	1362	315	9090	6.53	965	1823
M16-25 - 4	800	2770	5.27	12.4	141	10.3	65.6	40.3	9.59	77.5	20.86	214.7	77.2	364	90.1	966	217	9510	1.97	698	1161
M16-25 - 5	584	2030	4.18	5.67	58.5	3.54	30.6	16.6	3.51	53.6	13.6	149	58	273	68.4	743	175	10870	3.54	471	901
M16-25 - 6	360	1470	2.84	11.9	83.9	9.5	64	41	12.1	57.4	14.2	129	41.3	179	44.1	537	105.2	10590	1.56	258	609
M16-25 - 7	810	2772	7.48	12.8	116.1	8.85	65.7	29.8	8	68.8	18.34	197.6	79.8	387.6	96.8	1077	248.6	9150	2.66	898	1466
M16-25 - 8	74	84.3	0.149	Below LOD	2.27	Below LOD	Below LOD	0.09	0.032	0.57	0.289	4.12	2.36	16.67	6.18	95.8	29.38	11690	0.065	13.81	86.1
M16-25 - 9	Below LOD	92.7	0.149	Below LOD	2.27	Below LOD	Below LOD	0.1	0.088	1.11	0.309	5.38	2.64	17.48	5.11	70.9	21.24	12170	0.048	10.26	63.2
M16-25 - 10	708	2039	8.27	4.72	76.1	4.85	31.5	17.4	5.08	40.2	11.22	133.4	54.8	302.7	82.6	965	233.3	9240	3.15	626	1436
M16-25 - 11	740	2687	9.36	9.6	102.9	7.72	54.8	29.4	8.03	59.1	16.14	189.9	73.2	373.3	93.3	1041	242	9244	3.96	901	1551
M16-25 - 12	530	2190	6.41	12.6	108.5	13.4	86.3	45	12.2	77.4	16.5	176	60.3	296	74.5	832	189	9830	2.81	607	1088
M16-25 - 13	930	2796	12.92	4.65	93.6	4.66	29.7	15.9	3.55	51.3	15.28	186.7	79.6	418	105.7	1178	279.5	8490	3.79	1903	2238
M16-25 - 14	117	252	0.133	1.06	5.62	0.85	5.8	4.42	1.13	7.7	1.59	17.2	6.75	36.8	11.41	158.9	46	12000	0.05	14.69	100.6
M16-25 - 15	no value	no value	no value	no value	no value	no value	no value	no value	no value	no value	no value	no value	no value	no value	no value	no value	no value	no value	no value	no value	no value
M16-25 - 16	660	3229	10.39	36	221	30.1	195	92	30.8	150.8	28.1	250.6	85.7	399	94.8	1085	245.7	9012	5.7	946	1636
M16-25 - 17	744	2400	7.35	8.1	105	9.2	64.6	33.5	7.4	61.6	16.14	175.2	66.9	326	83.4	964	223	9620	3.28	665	1409
M16-25 - 18	Below LOD	1260	3.9	13.2	54.8	7.6	41.9	20.2	7.5	35	10	108	36	155	40.4	565	101	10060	2.64	210	614
M16-25 - 19	Below LOD	78.2	0.096	Below LOD	2.05	Below LOD	0.059	Below LOD	0.083	0.74	0.314	4.16	2.14	15.1	5.2	72.8	24.43	11880	0.031	5.33	60.6

Grain_number	P_ppm_m31	Y_ppm_m89	Nb_ppm_m93	La_ppm_m139	Ce_ppm_m140	Pr_ppm_m141	Nd_ppm_m146	Sm_ppm_m147	Eu_ppm_m153	Gd_ppm_m157	Tb_ppm_m159	Dy_ppm_m163	Ho_ppm_m165	Er_ppm_m166	Tm_ppm_m169	Yb_ppm_m172	Lu_ppm_m175	Hf_ppm_m178	Ta_ppm_m181	Th_ppm_m232	U_ppm_m238
M16-25 - 20	500	1630	3.49	9.7	75.5	9.9	76	35.1	10.8	73	14.6	124	42.8	186	46.6	504	105.1	9400	1.45	455	682
M16-25 - 21	Below LOD	250	1.6	1.58	14.3	1.24	7.3	4.2	1.63	7.9	1.95	18.1	6.8	36.6	9.93	123	32.4	11843	1.9	60	197
M16-25 - 22	Below LOD	305	0.98	0.76	10.2	0.82	5.9	5	1.14	7.7	2	20.4	8.7	46	11.8	141	35.3	10660	0.25	50	162
M16-25 - 23	777	2756	7.1	6.23	89.3	4.6	30.5	16.4	3.83	51.5	15.99	191	78.8	391	100.5	1134	264	9300	2.33	802	1475
M16-25 - 24	136	399	0.34	5.1	142	4.66	31.1	18.8	4.4	28	5.11	39.2	10.67	45.2	11.68	143.4	39.7	12010	0.128	31.9	103.6
M16-25 - 25	no value	no value	no value	no value	no value	no value	no value	no value	no value	no value	no value	no value	no value	no value	no value	no value	no value	no value	no value	no value	no value
M16-25 - 26	3430	11260	176.4	242	1300	131	781	395	57.3	706	170	1450	387	1413	257	2250	379	8402	13.42	2600	2580
M16-25 - 27	290	922	10.81	9.9	209	9.7	75.3	43.5	5.13	64.6	15.2	125.1	33.7	119.5	21.5	172	30.4	10067	1.83	91.5	129.5
M16-30 - 1	452	537	1.32	1.83	15.9	1.47	11.2	8.7	3.61	25.8	6.9	62.3	17.9	75	18	195	40.6	11930	0.488	42.7	330
M16-30 - 2	198	780	2.8	Below LOD	11.06	0.079	1.34	2.91	0.216	18.6	5.92	69.6	27.53	118.1	23.58	205.8	38.31	7972	1.03	42.5	91.1
M16-30 - 3	498	561	1.48	1.34	27.6	0.54	3.98	3.04	2.28	10.5	3.68	45.9	17.3	88.8	22.54	248	54.2	10560	0.86	129	323.3
M16-30 - 4	3190	1150	1.93	2730	5.60E+03	640	2350	371	52	241	32.4	185	39.7	137	27	255.8	52.5	9790	0.99	1290	606
M16-30 - 5	546	839	0.48	Below LOD	1.19	0.123	2.29	5.35	0.103	25.7	7.68	80.9	28	115.8	22.24	196.3	36.1	10980	0.223	64.1	152.1
M16-30 - 6	300	696	2.13	3.4	22.5	1.14	5.5	3.83	1.1	16.5	4.82	57.9	22.1	101.9	22.4	212.1	43.7	10260	1.01	98	282.2
M16-30 - 7	720	834	0.94	0.92	9	0.51	2.59	2.16	2.27	8.1	3.53	54.6	26.3	155	46.9	573	132	11820	1.65	26.1	555
M16-30 - 8	200	500.5	0.93	0.117	27.53	0.54	7.75	6.87	1.04	24.4	5.74	53.4	16.65	63.7	12.38	105.5	20.03	8770	0.351	130.9	120
M16-30 - 9	414	1361	2.45	0.56	9.27	0.304	2.44	4.78	1.17	25.3	9.11	115.8	46.12	214.3	44.85	419.9	84.7	10290	1.36	56.3	181.1
M16-30 - 10	375	754	2.17	11.5	54	5	16.6	6.8	1.42	18.7	5.7	66.1	24.2	113	24	239	49	10500	1.34	189.3	263.8
M16-30 - 11	294	766	1.2	0.006	32.4	0.204	3.44	5.37	2.52	21.7	6.44	66.3	23.97	104.9	23.11	224.7	46.66	7544	0.463	151.4	167.4
M16-30 - 12	129	372.1	0.78	Below LOD	25.51	0.018	1.15	2.16	1.08	11.5	3.05	32.7	11.46	50.8	11.27	111.8	23.61	8563	0.373	80.4	96.4
M16-30 - 13	132	309.2	0.79	Below LOD	16.15	Below LOD	0.7	1.71	0.396	7.2	2.21	26.5	9.64	44.8	10.08	98.6	20.47	9122	0.349	70.6	103.2
M16-30 - 14	245	737	1.28	0.059	21.1	0.101	1.56	4.02	1.94	22.6	6.38	70.1	25.2	103	19.1	168	31.7	8810	0.445	68	119.1
M16-30 - 15	125	256	0.506	0.041	8.65	0.015	0.41	0.68	0.53	6.28	1.78	21.5	8.22	39	8.95	88.5	18.93	9570	0.359	25.85	98.1
M16-30 - 16	750	849	1.2	273	780	98	430	75	12.7	75	12	94	27.1	114.7	25.2	244	50	8430	0.358	610	256
M16-30 - 17	489	730	0.7	0.035	1.84	0.217	3.53	9	0.174	36.4	9.59	84.8	24.46	89.8	16.06	131.9	23.61	11260	0.326	75.2	178.2

Grain_number	P_ppm_m31	Y_ppm_m89	Nb_ppm_m93	La_ppm_m139	Ce_ppm_m140	Pr_ppm_m141	Nd_ppm_m146	Sm_ppm_m147	Eu_ppm_m153	Gd_ppm_m157	Tb_ppm_m159	Dy_ppm_m163	Ho_ppm_m165	Er_ppm_m166	Tm_ppm_m169	Yb_ppm_m172	Lu_ppm_m175	Hf_ppm_m178	Ta_ppm_m181	Th_ppm_m232	U_ppm_m238
M16-30 - 18	211	577	1.08	Below LOD	21.68	0.082	1.86	2.53	0.84	14.2	4.12	47.6	18.47	86.6	20.06	189.8	41.3	8322	0.412	60.5	54.8
M16-30 - 19	157	495.4	2.17	Below LOD	22.1	0.039	0.3	1.22	0.243	8.5	3	38.7	15.38	77.5	18.21	177.8	36.82	10913	1.51	82.5	80.3
M16-30 - 20	164	414	1.34	0.007	35.8	0.4	7.18	8.2	2.29	24.9	5.62	47.6	13.85	51.7	9.4	80.3	14.75	8378	0.316	92.4	50.1
M16-30 - 21	486	572	2.13	3.3	69.3	2.82	15.2	7.7	6.23	22.8	5.49	53.1	17.64	77.5	17.25	182.1	36.9	10324	0.86	172.6	397
MAD17-11-4A - 1	322	1443	9.65	Below LOD	18.17	0.054	1.57	3.81	0.238	24.8	9.95	124.4	49.8	226.6	45.41	393.3	71.6	9482	3.24	164	357.6
MAD17-11-4A - 2	777	1034	4.45	1.36	26	0.93	8.9	8.7	4.57	28.7	7.93	88.7	33.3	153.7	33.1	330.9	65.7	10860	3.01	155.7	755
MAD17-11-4A - 3	710	1199	6.14	2.38	32.9	3.78	28.2	22	11.4	52.2	12.8	115.6	38.3	167.2	40.1	428	86.5	12040	5.94	126.9	1096
MAD17-11-4A - 4	259	683	20.72	1.56	19.56	1.6	8.8	5.03	2.33	16.4	4.91	57.7	21.6	105.6	25.1	242	47.2	9990	10.08	128.6	418
MAD17-11-4A - 5	1210	2734	20.4	48.7	184.6	34.6	189	102.8	53.2	169.1	43.1	370	100.7	375	75.4	670	117.5	11340	2.89	290	1534
MAD17-11-4A - 6	230	608.9	1.13	Below LOD	25.93	0.027	0.58	1.5	0.98	13.5	4.51	51.9	19.98	90.9	19.53	193.3	42.22	10075	0.477	116.1	203
MAD17-11-4A - 7	590	1498	5.6	17.2	63.2	9.4	46.7	21.6	11.1	49.8	13.8	144	48.4	223	48.6	474	93.2	9930	2.95	235.1	781
MAD17-11-4A - 8	394	1000	4.43	0.29	62.1	0.369	4.8	7.39	1.63	27.8	8.73	91.8	32.73	143.8	30.82	288.2	57.8	8555	2.17	281.7	298.9
MAD17-11-4A - 9	212	492.3	1.74	Below LOD	8.36	0.086	1.34	2.98	0.459	12	4	45.7	16.89	71.7	15.06	142.4	27.73	8175	0.748	54.2	110.9
MAD17-11-4A - 10	354	1608	4.84	0.9	17.46	1.22	9.6	10.6	1.84	43	13.96	154.3	55.8	233.3	46.3	398	73	8591	1.69	140.8	212.1
MAD17-11-4A - 11	310	1068	2.63	1.4	22	1.22	10.2	9.1	2.73	34	9.2	102.1	36	154.1	31.5	280.7	55.4	8066	1.26	113	270.1
MAD17-11-4A - 12	190	400.2	3.7	Below LOD	22.25	0.039	1.3	2.33	0.31	12.2	3.35	37.4	13.74	56.8	11.33	103.9	19.99	9451	1.28	158.3	194.7
MAD17-11-4A - 13	5310	9210	795	135.3	914	152	865	523	148.5	722	176.7	1399	332	1142	220.8	1923	298	14860	13.93	682	9320
MAD17-11-4A - 14	244	558	1.46	Below LOD	14.63	0.025	0.91	2	0.56	12.4	4.06	48.9	18.65	86.2	18.45	175.2	35.08	10059	0.67	85.1	173.3
MAD17-11-4A - 15	364	705	4.78	1.78	22.1	1.53	7.9	5.9	2.74	15.4	5.15	60.9	22.91	111.5	26.35	281.2	57.1	10940	2.38	190.4	684
MAD17-11-4A - 16	664	1163	3.63	3.7	30.8	3.79	26.6	18.3	15.3	50.9	13.7	125	38.2	164	33.7	335	67.5	10370	3.11	139.2	749
MAD17-11-4A - 17	309	966	2.45	Below LOD	20	0.183	3.06	5.13	0.95	24.8	7.67	87.4	31.38	139.9	27.41	243.8	46.73	8623	0.927	103.2	106.7
MAD17-11-4A - 18	470	380	1.1	0.99	16.17	0.65	4.4	3.32	0.252	11	3.32	34.5	12.52	55.3	11.98	116.8	23.57	8044	0.349	63.1	111.6
MAD17-11-4A - 19	245	2036	18.73	0.024	22.9	0.219	4.47	11.1	1.54	57.9	19.42	217	76	297	54.2	438.2	75.8	8612	5.13	110.2	220.5
MAD17-11-4A - 20	780	1418	33.7	0.95	10.99	1.13	7.6	4.43	1.8	15.6	6.64	97.1	44.4	254.4	69.5	787	170.2	18420	32.8	91.6	2919
MAD17-11-4A - 21	168	484.5	2.07	Below LOD	24.63	0.05	0.69	1.63	0.341	9.2	3.36	40.7	15.06	71.7	15.53	146.5	28.42	9377	0.847	70.3	179.3

Grain_number	P_ppm_m31	Y_ppm_m89	Nb_ppm_m93	La_ppm_m139	Ce_ppm_m140	Pr_ppm_m141	Nd_ppm_m146	Sm_ppm_m147	Eu_ppm_m153	Gd_ppm_m157	Tb_ppm_m159	Dy_ppm_m163	Ho_ppm_m165	Er_ppm_m166	Tm_ppm_m169	Yb_ppm_m172	Lu_ppm_m175	Hf_ppm_m178	Ta_ppm_m181	Th_ppm_m232	U_ppm_m238
MAD17-11-4A - 22	1060	1643	273	96	176	20.1	85	25.7	5.65	44.1	12.74	136	50.7	247	60.6	640	137.2	11840	31.6	66.6	1391
MAD17-11-4A - 23	263	479	1.42	Below LOD	6.91	0.086	0.82	2.76	0.6	13.3	3.86	45.7	16.07	70.6	14.49	128.2	25.9	8820	0.708	37.9	131.6
MAD17-11-4A - 24	1910	1520	7.08	23.7	81	14.4	78	46.7	36.3	93	24.1	206	54.2	200	36.8	298	51.2	10190	3.64	171.8	1388
MAD17-11-4A - 25	779	1544	0.89	Below LOD	1.3	0.03	1.26	2.97	0.124	24	9.56	129.6	51.74	240.1	50.9	477.7	94.6	11060	0.474	50.8	180.5
MAD17-11-4A - 26	326	594	1.28	1.44	12.23	0.75	3.78	3.14	1.23	12.2	4.37	50.7	19.05	93.4	22.8	236	49.2	9600	1.29	96.2	419
MAD17-11-4A - 27	633	1087	4.74	2.52	22.4	5.44	34.3	21	16.2	30	8.52	96.9	35.4	182.6	49.5	579	125.2	12620	6.06	55.6	1333
MAD17-11-4A - 28	614	1544	8.47	16.3	76.9	13.85	91.5	52.5	25.5	89.1	21.45	183	51	197.2	41.2	388	74.5	11290	3.32	186	958
MAD17-11-4A - 29	440	1007	3.28	6.2	37.4	4.84	26.8	16	5.86	39.6	10.63	106.2	33.61	137.7	28.04	258.1	48.4	10470	1.05	132	487
MAD17-11-4A - 30	379	566	1.78	1.75	10.1	1.56	9.7	7.8	3.2	29.6	8.96	74.1	18.27	59.3	11.21	93	15.4	12180	1.03	65.1	556
MAD17-11-4A - 31	292	360.6	0.84	0.03	1.62	0.079	1.4	4.32	0.333	19.4	4.88	42.5	12.24	45	8.71	76.6	14.16	10170	0.32	82.6	179.8
MAD17-11-4A - 32	1040	1080	1.84	0.51	28	0.69	6.5	8.3	5.12	35.8	12.1	127	38	147	29.5	266	48.6	9750	0.73	164.1	506
MAD17-11-4A - 33	820	1102	1.65	0.25	3.61	0.59	4	5.3	2.03	29.7	9.19	105	36.9	157.5	32.9	309.4	59.8	10970	0.91	67.6	492
MAD17-11-4A - 34	408	1291	2.01	0.31	10.09	0.47	4.9	7.7	1.58	24.6	9.35	110.4	42.9	198.2	43.4	414	83.6	9300	1.04	167.2	469
MAD17-11-4A - 35	770	1447	3.67	3.1	26.4	1.39	12.6	13.5	1.61	52.5	14.57	153.7	51.8	207.5	41.4	350	63.6	9559	1.3	276.4	218.8
MAD17-11-4A - 36	437	566	0.82	0.49	2.16	0.36	4.11	6.5	0.65	32.5	8.26	68.8	18.89	68.5	12.9	112.7	19.63	11210	0.538	80.3	365.4
MAD17-11-4A - 37	1029	1786	1.13	0.03	5.1	0.113	1.81	4.87	0.56	33.7	11.95	152.8	59.8	274.4	57.6	535	108	10942	0.78	65.2	104.8
MAD17-11-4A - 38	840	1520	6.54	5.59	72.5	6.44	43.3	28.1	15	69.7	18.7	169	50.7	204	39.3	351	60.9	9750	2.52	260.7	766
MAD17-11-4A - 39	294	694	2.64	Below LOD	9.72	0.12	2.17	4.02	0.126	20.1	5.95	64.9	24.05	110.9	24.29	236.3	50.2	10300	1.066	116.7	316.4
MAD17-11-4A - 40	541	1360	1.22	0.019	4.01	0.193	3.16	7.2	0.153	36.3	11.73	133.4	46.93	197.7	38.34	331.3	60.3	10270	0.75	168.9	197.9
MAD17-11-4A - 41	no value	no value	no value	no value	no value	no value	no value	no value	no value	no value	no value	no value	no value	no value	no value	no value	no value	no value	no value	no value	no value
MAD17-11-4A - 42	124	349.5	1.07	Below LOD	24.41	0.094	1	2.89	0.66	12.7	3.44	33.5	11.22	46.9	9.81	93.2	19.11	8837	0.335	110.1	121.7
MAD17-11-4A - 43	152	199.4	0.57	Below LOD	9.73	0.036	0.37	0.45	0.186	4.66	1.57	16.63	6.33	27.4	5.96	57.5	11.64	10210	0.206	20.37	47.98
MAD17-11-4A - 44	348	277.3	0.388	0.05	1.01	0.102	1.51	3.62	0.297	15.6	3.76	32.1	9.28	35.1	6.64	61.9	11.77	11630	0.201	59	218.4
MAD17-11-4A - 45	415	1217	15.51	5.66	36.9	5.45	34.1	24.7	12.5	54.9	14.88	144.3	44.5	174.6	34.1	300.7	54.3	8040	6.64	81	638
MAD17-11-4A - 46	421	608	3.4	0.27	4.62	0.305	2.32	3.3	1.25	9.8	3.95	46.5	19.15	103.7	26.14	283.7	59.3	10890	4.94	39	747
MAD17-11-4A - 47	800	824	3.57	1.17	5.25	1.01	6	5.8	2.8	20.1	8.13	87.3	24.06	79.1	14.11	124	22	11040	2.12	33.7	698
MAD17-11-4A - 48	908	1516	4.58	10.5	75.2	6.56	35.5	18.8	10.15	46.9	13.61	141.8	49.4	230	52.8	544	112.3	8740	1.64	261	833
MAD17-11-4A - 49	225	436	1.84	0.013	12.11	0.084	0.51	1.29	0.42	8.1	2.77	35.4	13.69	67.6	15.73	158.5	33.21	9173	0.747	67.4	110.6

Grain_number	P_ppm_m31	Y_ppm_m89	Nb_ppm_m93	La_ppm_m139	Ce_ppm_m140	Pr_ppm_m141	Nd_ppm_m146	Sm_ppm_m147	Eu_ppm_m153	Gd_ppm_m157	Tb_ppm_m159	Dy_ppm_m163	Ho_ppm_m165	Er_ppm_m166	Tm_ppm_m169	Yb_ppm_m172	Lu_ppm_m175	Hf_ppm_m178	Ta_ppm_m181	Th_ppm_m232	U_ppm_m238
MAD17-11-4A - 50	727	1198	1.6	0.239	3.36	0.45	2.45	4.26	0.58	22.1	8.43	105.4	40.11	178.7	38.08	359.1	69.9	11090	1.88	47.6	334
MAD17-11-4A - 51	402	1269	4.88	5.7	93.6	4.75	24.2	16.9	7.58	43.8	12.1	124.6	43.4	187.8	39.99	368.2	74.5	9539	1.5	137.4	186
MAD17-11-4A - 52	505	1233	12.49	0.47	22.26	0.37	3.16	4.56	0.86	22.7	8.62	109.3	41.32	193.7	40.85	373.3	71.2	9800	4.79	166.4	329.7
MAD17-11-4A - 53	1250	1585	2.39	30.6	88.9	14.7	71.5	32.1	22.3	58.6	17.45	175.8	54.2	223.3	47	432.5	82.4	11330	1.28	109.6	834
MAD17-11-4A - 54	no value	no value	no value	no value	no value	no value	no value	no value	no value	no value	no value	no value	no value	no value	no value	no value	no value	no value	no value	no value	no value
MAD17-11-4A - 55	517	843	1.79	1.44	9.3	1.21	9	7	1.9	26.9	7.57	82.5	27.25	116.3	24.62	224.2	44.7	9800	1.15	117.2	508
MAD17-11-4A - 56	150	371.6	0.86	Below LOD	7.6	0.056	0.98	1.37	0.67	9.3	3.26	32.5	11.63	54.4	11.8	122.7	24.62	10390	0.463	99.4	333.2
MAD17-11-4A - 57	449	989	3.91	5.17	34.4	4.58	26.1	15.4	8.72	32.2	9.62	96.1	32.1	138.7	29.4	282.5	53.8	8960	1.42	178.6	731
MAD17-11-4A - 58	673	876	0.86	0.29	2.1	0.37	3.06	5	0.79	25.7	8.39	89.8	28.71	114.8	24	211.8	40.2	11060	0.518	43.5	363.3
MAD17-11-4A - 59	694	1479	4.64	15	71.8	14.02	79.6	45.2	29.9	83.1	21.1	181.1	50.1	189.4	38.9	351	61.5	10860	1.35	101.7	1040
MAD17-11-4A - 60	Below LOD	Below LOD	6.20E+07	Below LOD	Below LOD	Below LOD	Below LOD	Below LOD	Below LOD	Below LOD	Below LOD	Below LOD	Below LOD	Below LOD	Below LOD	Below LOD	Below LOD	1.92E+04	3.52E+06	Below LOD	9.82E+04
MAD17-11-4A - 61	687	937	1.83	2.55	16.6	3	20.8	12.5	6.24	23	8.44	87.6	29.1	131.7	30.52	313.6	64.5	12360	1.25	34.1	853
MAD17-11-4A - 62	517	1119	7.3	7.2	50.5	7.63	45	22.6	10.4	46.4	11.57	116.9	37.6	157.5	31.78	285.6	53	9550	2.41	78.6	453
MAD17-11-4A - 63	179	599	4.43	Below LOD	7.85	0.136	1.6	2.46	0.363	15.4	4.93	56.9	20.79	90.7	17.28	153.7	27.29	8204	1.67	43.3	98.7
MAD17-11-4A - 64	850	1083	3.22	3.76	24.9	3.73	24.6	15.5	9.7	39.6	11.58	120.7	35.8	135.6	28.2	266.9	47.2	11990	2.2	100.9	1285
MAD17-11-4A - 65	223	462.8	2.89	0.088	32.4	0.027	0.8	1.64	0.227	9.5	3.53	39.8	14.83	69.1	15.04	142.5	28.56	10122	1.05	170.4	231.3
MAD17-11-4A - 66	no value	no value	no value	no value	no value	no value	no value	no value	no value	no value	no value	no value	no value	no value	no value	no value	no value	no value	no value	no value	no value
MAD17-11-4A - 67	276	598	1.94	0.98	10.35	0.72	3.91	3.55	0.99	13.3	4.36	52.4	19.78	91.1	18.88	179.9	35.31	9154	0.95	44.9	151.6
MAD17-11-4A - 68	187	671	2.09	Below LOD	30	0.125	1.41	4.35	1.29	20	5.71	63.4	22.06	97.9	20.88	194.8	39.07	8653	0.648	71.6	52
MAD17-11-4A - 69	648	1400	29.7	24.2	280	22.9	78	25.4	8.44	60.2	17	172	56.5	242	56.3	546	94.9	9460	19.7	186.9	908
MAD17-11-4A - 70	771	1058	2.34	0.103	2.25	Below LOD	0.44	0.48	0.277	6.6	3.86	66.1	33.42	196.3	53.75	601.8	128.7	12130	3.74	21.03	827
MAD17-11-4A - 71	240	592	1.92	0.4	39.3	0.59	6.15	7.2	2.2	29.3	6.98	66.1	20.72	79.6	15.25	135.8	24.15	8610	0.567	120.5	123.6
MAD17-11-4A - 72	426	689	2.34	0.76	34.5	0.38	3.3	3.3	0.96	11.5	4.2	54.3	22.1	112.9	26.69	285.8	59.2	10950	1.19	152.3	470
MAD17-11-4A - 73	1080	2265	3.31	8.08	28.5	5.75	34.6	26.2	14.3	64.6	19.81	216.8	75.2	334.2	72.2	679	130.5	11370	1.35	137.2	795
MAD17-11-4A - 74	209	488	2.38	0.4	37.3	0.287	2.31	2.49	1.35	9.2	3.09	37	15.24	73.1	17.76	193.4	42.8	10020	1.05	263.9	549.3
MAD17-11-4A - 75	497	949	3.68	3.75	63.1	3.95	21.2	13.3	7.8	36.7	9.43	96	30.8	129.9	28.5	279	55.3	10070	1.14	130.5	368
MAD17-11-4A - 76	960	2170	4.25	9.47	62.8	6	35.1	25.1	13	93	26.3	238	71.1	269	50.1	442	75.3	8810	2.25	234.3	483

Grain_number	P_ppm_m31	Y_ppm_m89	Nb_ppm_m93	La_ppm_m139	Ce_ppm_m140	Pr_ppm_m141	Nd_ppm_m146	Sm_ppm_m147	Eu_ppm_m153	Gd_ppm_m157	Tb_ppm_m159	Dy_ppm_m163	Ho_ppm_m165	Er_ppm_m166	Tm_ppm_m169	Yb_ppm_m172	Lu_ppm_m175	Hf_ppm_m178	Ta_ppm_m181	Th_ppm_m232	U_ppm_m238
MAD17-11-4A - 77	Below LOD	12.37	0.16	Below LOD	0.189	Below LOD	Below LOD	Below LOD	0.087	0.33	0.138	1.46	0.344	1.31	0.199	1.29	0.254	19650	0.05	0.343	38.5
MAD17-11-4A - 78	271	653	1.99	0.45	49.1	0.86	7.6	8	3.9	26.4	6.6	64.3	20.92	86.5	19.05	191.3	36.9	8013	0.599	212.3	430
MAD17-11-4A - 79	528	1296	5.99	7.6	69.9	6.9	44.6	30.1	13.2	60.5	16.1	145.6	45.1	170	31.6	276	48.9	9070	2.63	254	464
MAD17-11-4A - 80	179	587	4.71	2.23	16.2	2.43	15	8.4	4.84	17.8	5.33	56	20.19	85.5	17.29	155.1	29.8	9950	2.2	30.6	141.4
MAD17-11-4A - 81	818	1190	0.85	0.48	4.86	0.73	4.4	6	1.39	30.8	10.54	120	39.9	171	33.87	303.4	58.7	11450	0.471	41.3	523
MAD17-11-4A - 82	698	1014	2.15	4.03	19.9	2.81	19	12.5	6.3	37.6	11.3	108.7	33.3	134.3	27.65	261	47.5	10750	1.18	103	861
MAD17-11-4A - 83	161	345.2	1.73	Below LOD	25.53	Below LOD	0.54	1.21	0.111	6.9	2.16	27.2	10.54	50.7	11.32	109.9	22.79	10730	0.83	158.3	179.4
MAD17-11-4A - 84	3210	5950	51.6	135.4	736	128.4	712	312	185.9	447	100.4	790	197.7	709	144.2	1357	251.9	16890	27.3	288	5320

Appendix 5.3 Proterozoic basin evolution during Nuna: CL images

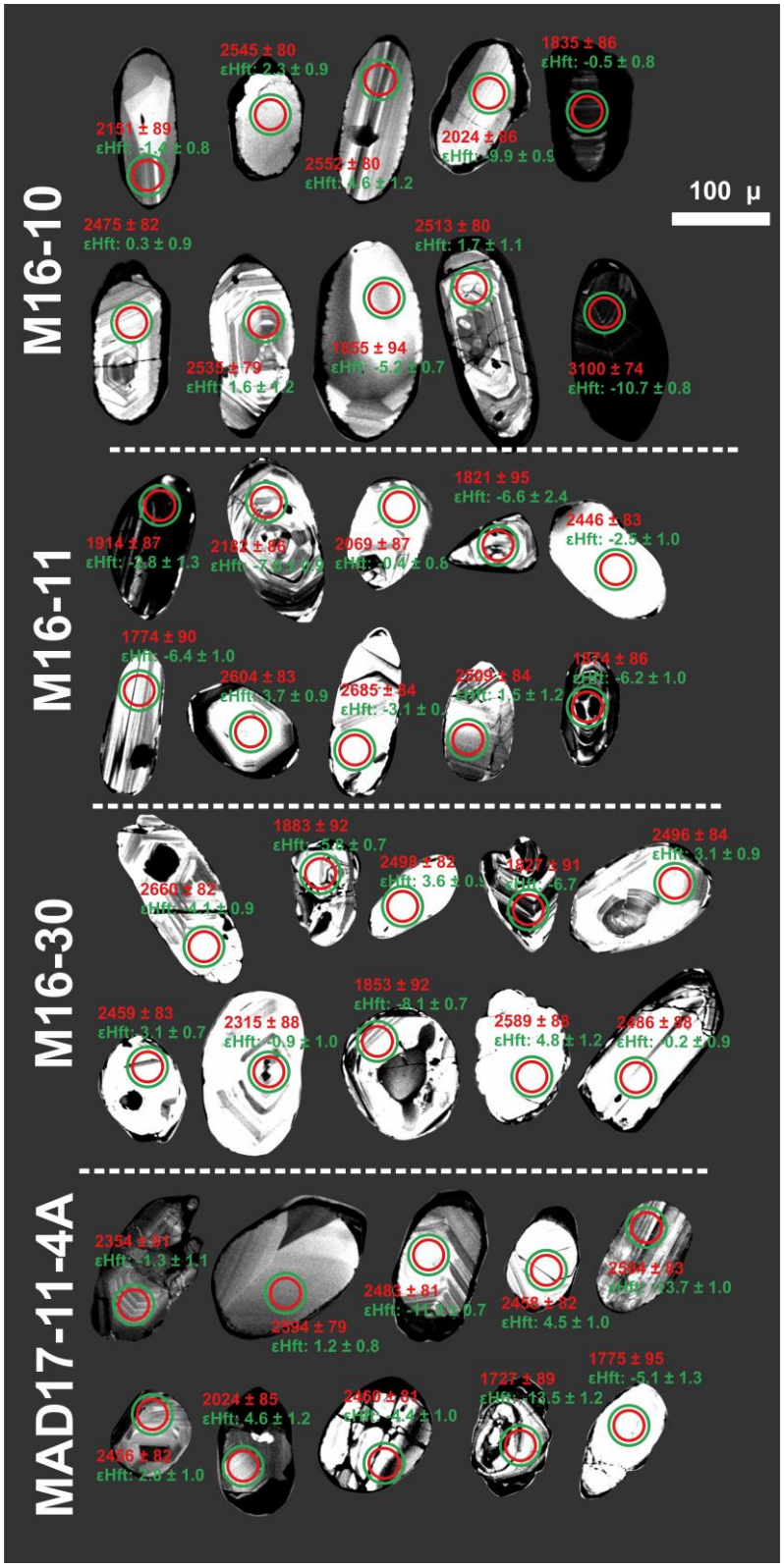

Appendix 5.4 Proterozoic basin evolution during Nuna: Hf isotope data

Sample N	Analysis N	$^{176}Hf/^{177}Hf$	2 S.E.	$^{176}Lu/^{177}Hf$	U/Pb AGE	2 S.E.	Hf Chur (t)	Hf DM (t)	Hf NC(t)	Hf_i	eHf	2SE	TDMc	TNCc	Above DM line?
CP183B	SA_CP183B_12	0.28156757	2.15164E-05	0.001856105	1878	18	0.281587	0.281881	0.281810	0.281501	-3.04	0.76087456	2.69	2.5430437	No
CP183B	SA_CP183B_11	0.281570613	2.21204E-05	0.001691903	1876	18	0.281588	0.281883	0.281812	0.281510	-2.77	0.782233126	2.68	2.525101919	No
CP183B	SA_CP183B_14	0.281465812	2.55938E-05	0.001191048	1850	18	0.281605	0.281902	0.281831	0.281424	-6.44	0.905061885	2.88	2.72451123	No
CP183B	SA_CP183B_13	0.281562369	2.32326E-05	0.001090651	1841	18	0.281611	0.281909	0.281838	0.281524	-3.09	0.821564455	2.67	2.51578075	No
CP183B	SA_CP183B_03	0.281535542	2.50854E-05	0.001280746	1855	18	0.281602	0.281898	0.281827	0.281490	-3.96	0.887085589	2.73	2.579840193	No
CP183B	SA_CP183B_05	0.281222342	2.09694E-05	0.000803873	2635	17	0.281093	0.281316	0.281254	0.281182	3.18	0.741529838	2.92	2.787458447	No
CP183B	SA_CP183B_07	0.281064395	2.24135E-05	0.000561318	2383	17	0.281258	0.281505	0.281440	0.281039	-7.79	0.79259975	3.37	3.231933023	No
CP183B	SA_CP183B_08	0.281272572	2.42304E-05	0.000898093	2483	17	0.281192	0.281430	0.281366	0.281230	1.33	0.856849137	2.91	2.772210812	No
CP183B	SA_CP183B_09	0.281648484	3.79822E-05	0.002204184	1891	18	0.281579	0.281872	0.281801	0.281569	-0.35	1.343148319	2.54	2.390381125	No
CP183B	SA_CP183B_06	0.281624007	3.30622E-05	0.001872124	1860	18	0.281599	0.281895	0.281824	0.281558	-1.46	1.169165314	2.58	2.432733732	No
CP183B	SA_CP183B_17	0.281617589	2.33048E-05	0.000599448	2494	17	0.281186	0.281422	0.281359	0.281589	14.35	0.82411668	2.14	2.001487953	Yes
CP183B	SA_CP183B_18	0.281597529	2.60628E-05	0.000543392	1852	28	0.281604	0.281901	0.281830	0.281578	-0.92	0.921645956	2.55	2.393525948	No
CP183B	SA_CP183B_15	0.281110424	1.98355E-05	0.000628814	2438	17	0.281222	0.281464	0.281400	0.281081	-5.01	0.701433875	3.25	3.111640477	No
CP183B	SA_CP183B_16	0.281056132	2.45615E-05	0.000804696	2301	38	0.281312	0.281567	0.281501	0.281021	-10.35	0.868555661	3.45	3.316937866	No
CP183B	SA_CP183B_19	0.281261696	3.66126E-05	0.001440059	2689	17	0.281057	0.281275	0.281214	0.281188	4.64	1.294714571	2.87	2.744868244	No
CP183B	SA_CP183B_20	0.281211861	2.38592E-05	0.000724006	2515	17	0.281172	0.281406	0.281343	0.281177	0.20	0.843721985	3.00	2.865818979	No
CP183B	SA_CP183B_01	0.281598649	2.75119E-05	0.000699888	2071	18	0.281462	0.281738	0.281670	0.281571	3.88	0.972889634	2.43	2.2823847	No
CP183B	SA_CP183B_02	0.281600484	3.15284E-05	0.001761837	1872	18	0.281591	0.281886	0.281815	0.281538	-1.89	1.114923143	2.62	2.468672851	No
CP183B	SA_CP183B_04	0.281517311	2.36908E-05	0.001088726	1941	18	0.281546	0.281834	0.281764	0.281477	-2.45	0.837767938	2.71	2.558311534	No
CP183B	SA_CP183B_10	0.281503829	2.21928E-05	0.00055398	1866	34	0.281595	0.281890	0.281819	0.281484	-3.94	0.784795684	2.74	2.587020154	No
BDW197	SA_BDW197_18	0.281559125	2.55277E-05	0.001027653	1758	18	0.281665	0.281970	0.281898	0.281525	-4.98	0.902723256	2.72	2.562866786	No
BDW197	SA_BDW197_19	0.281434479	2.42668E-05	0.000476084	1745	18	0.281674	0.281980	0.281908	0.281419	-9.06	0.85813524	2.95	2.797376664	No
BDW197	SA_BDW197_24	0.281385105	1.86284E-05	0.000233543	1814	18	0.281629	0.281929	0.281857	0.281377	-8.95	0.658748036	3.00	2.845762898	No
BDW197	SA_BDW197_27	0.281466459	1.80746E-05	0.000534444	1819	18	0.281626	0.281925	0.281854	0.281448	-6.31	0.639162445	2.84	2.69171087	No
BDW197	SA_BDW197_28	0.281446027	1.92467E-05	0.000906529	1811	18	0.281631	0.281931	0.281860	0.281415	-7.67	0.680613753	2.92	2.767016687	No
BDW197	SA_BDW197_33	0.281178109	2.46285E-05	0.000763931	2459	17	0.281208	0.281448	0.281384	0.281142	-2.34	0.870925702	3.11	2.970957312	No
BDW197	SA_BDW197_37	0.281141	2.07473E-05	0.000809856	2497	17	0.281183	0.281419	0.281356	0.281102	-2.87	0.733677972	3.17	3.033300905	No
BDW197	SA_BDW197_39	0.281368416	2.62003E-05	0.000984926	2234	17	0.281355	0.281616	0.281550	0.281327	-1.02	0.926508765	2.85	2.709957922	No
BDW197	SA_BDW197_44	0.281297713	2.38056E-05	0.000868706	2405	17	0.281243	0.281488	0.281424	0.281258	0.51	0.841827619	2.89	2.75762589	No
BDW197	SA_BDW197_45	0.281423297	2.21475E-05	0.00040328	2034	18	0.281486	0.281765	0.281697	0.281408	-2.78	0.783190604	2.80	2.652801171	No

Sample N	Analysis N	$^{176}Hf/^{177}Hf$	2 S.E.	$^{176}Lu/^{177}Hf$	U/Pb AGE	2 S.E.	Hf Chur (t)	Hf DM (t)	Hf NC(t)	Hf_i	eHf	2SE	TDMc	TNCc	Above DM line?
BDW197	SA_BDW197_46	0.281455601	2.30124E-05	0.00090805	1808	18	0.281632	0.281933	0.281861	0.281424	-7.39	0.813777312	2.90	2.747987832	No
BDW197	SA_BDW197_52	0.281347318	2.34024E-05	0.001544172	2621	17	0.281102	0.281326	0.281264	0.281270	5.98	0.827566904	2.74	2.609176362	No
BDW197	SA_BDW197_54	0.281455961	2.12197E-05	0.000638871	1853	18	0.281604	0.281900	0.281829	0.281434	-6.05	0.750381977	2.85	2.702962683	No
BDW197	SA_BDW197_58	0.280964077	2.17946E-05	0.000708442	2473	17	0.281199	0.281438	0.281374	0.280931	-9.55	0.770712363	3.54	3.407364934	No
BDW197	SA_BDW197_63	0.281488836	2.13902E-05	0.000811002	1821	18	0.281624	0.281924	0.281852	0.281461	-5.81	0.756410483	2.82	2.66317998	No
BDW197	SA_BDW197_64	0.281456773	2.30878E-05	0.000703395	1811	18	0.281631	0.281931	0.281859	0.281433	-7.03	0.816443372	2.88	2.728956965	No
BDW197	SA_BDW197_67	0.281181389	2.42184E-05	0.000861477	2498	17	0.281183	0.281419	0.281355	0.281140	-1.50	0.856424566	3.09	2.952965459	No
BDW197	SA_BDW197_75	0.281445212	2.14021E-05	0.00088051	1817	18	0.281627	0.281927	0.281855	0.281415	-7.53	0.756832811	2.92	2.763541707	No
BDW197	SA_BDW197_77	0.281458154	2.1806E-05	0.000692764	1823	18	0.281623	0.281922	0.281851	0.281434	-6.71	0.771115474	2.87	2.718841318	No
CP23	SA_CP23_03	0.281132727	2.05655E-05	0.000451184	2461	17	0.281207	0.281446	0.281382	0.281112	-3.39	0.727249044	3.17	3.034546857	No
CP23	SA_CP23_12	0.281249729	1.80084E-05	0.000347561	2515	17	0.281171	0.281406	0.281343	0.281233	2.19	0.636824229	2.88	2.747514048	No
CP23	SA_CP23_19	0.282108879	2.95673E-05	0.000884397	1084	24	0.282099	0.282466	0.282386	0.282091	-0.28	1.045576077	1.91	1.734537963	No
CP23	SA_CP23_23	0.281362885	1.89273E-05	0.000177068	1825	18	0.281622	0.281920	0.281849	0.281357	-9.40	0.669318516	3.03	2.882268975	No
CP23	SA_CP23_28	0.280977207	2.30315E-05	0.000390555	2499	17	0.281182	0.281418	0.281355	0.280959	-7.95	0.814452775	3.47	3.334056935	No
CP23	SA_CP23_29	0.281292617	2.8685E-05	0.000517271	2534	17	0.281159	0.281392	0.281329	0.281268	3.86	1.014375814	2.80	2.663741574	No
CP23	SA_CP23_31	0.281268496	2.39453E-05	0.00058345	2681	17	0.281062	0.281281	0.281220	0.281239	6.28	0.846768091	2.77	2.641488489	No
CP23	SA_CP23_33	0.281266234	2.25136E-05	0.000590166	2178	17	0.281392	0.281658	0.281591	0.281242	-5.34	0.796139711	3.06	2.92195595	No
CP23	SA_CP23_38	0.282164588	3.49777E-05	0.00093412	1080	20	0.282101	0.282469	0.282389	0.282146	1.57	1.236899866	1.79	1.616728504	No
CP23	SA_CP23_41	0.281413569	2.12641E-05	0.000178392	1997	18	0.281510	0.281793	0.281724	0.281407	-3.67	0.75195391	2.82	2.676169273	No
CP23	SA_CP23_50	0.282126072	2.02172E-05	0.000451509	1112	32	0.282081	0.282445	0.282366	0.282117	1.27	0.714931879	1.84	1.661395559	No
CP23	SA_CP23_51	0.281948751	1.74318E-05	0.00055014	1001	44	0.282152	0.282527	0.282446	0.281938	-7.57	0.616433245	2.29	2.117078881	No
CP23	SA_CP23_59	0.281256984	2.10446E-05	0.000389943	2503	17	0.281179	0.281415	0.281351	0.281238	2.11	0.744189381	2.88	2.742948129	No
CP23	SA_CP23_62	0.28217374	2.62799E-05	0.000712719	1112	20	0.282081	0.282445	0.282366	0.282159	2.76	0.92932505	1.74	1.568830505	No
CP23	SA_CP23_63	0.281246201	2.33892E-05	0.000568646	2540	17	0.281155	0.281387	0.281324	0.281219	2.26	0.82710024	2.90	2.76391752	No
CP23	SA_CP23_73	0.282145041	2.82429E-05	0.000850786	1167	30	0.282046	0.282405	0.282327	0.282126	2.85	0.998740035	1.78	1.607607832	No
M16-10	SA_M16-10_08	0.281261292	2.52214E-05	0.000926523	2545	80	0.281152	0.281383	0.281321	0.281216	2.29	0.891892916	2.90	2.765959445	No
M16-10	SA_M16-10_108	0.28124418	2.64446E-05	0.000793525	2475	82	0.281198	0.281436	0.281372	0.281207	0.32	0.935149863	2.96	2.826028374	No
M16-10	SA_M16-10_111	0.281619001	2.38423E-05	0.000540805	1835	86	0.281615	0.281913	0.281842	0.281600	-0.53	0.843124564	2.51	2.356613814	No
M16-10	SA_M16-10_113	0.281230624	2.55394E-05	0.000397738	2024	86	0.281492	0.281773	0.281704	0.281215	-9.84	0.903139621	3.21	3.066783854	No
M16-10	SA_M16-10_12	0.281348347	3.50882E-05	0.001470745	2552	80	0.281147	0.281378	0.281315	0.281277	4.61	1.240807539	2.77	2.634176705	No
M16-10	SA_M16-10_121	0.281253243	2.02207E-05	0.000420917	2456	81	0.281210	0.281450	0.281386	0.281234	0.83	0.715053847	2.92	2.780168897	No
M16-10	SA_M16-10_128	0.280717812	3.0076E-05	0.000861138	3478	74	0.280533	0.280677	0.280625	0.280660	4.52	1.063565548	3.51	3.405166535	Yes
M16-10	SA_M16-10_13	0.281269648	3.06777E-05	0.001010598	2513	80	0.281173	0.281407	0.281344	0.281221	1.72	1.084842542	2.91	2.77381167	No

Sample N	Analysis N	$^{176}Hf/^{177}Hf$	2 S.E.	$^{176}Lu/^{177}Hf$	U/Pb AGE	2 S.E.	Hf Chur (t)	Hf DM (t)	Hf NC(t)	Hf_i	eHf	2SE	TDMc	TNCc	Above DM line?
M16-10	SA_M16-10_133	0.280517081	2.35522E-05	0.00055028	3100	74	0.280785	0.280964	0.280908	0.280484	-10.71	0.832865334	4.09	3.977586902	No
M16-10	SA_M16-10_141	0.281273034	2.70396E-05	0.000866042	2493	83	0.281186	0.281422	0.281359	0.281232	1.63	0.956187676	2.90	2.762665684	No
M16-10	SA_M16-10_147	0.281160318	2.40215E-05	0.000744348	2712	87	0.281042	0.281258	0.281197	0.281122	2.84	0.849462995	3.00	2.870653858	No
M16-10	SA_M16-10_149	0.281264829	2.14213E-05	0.000510227	2183	83	0.281389	0.281654	0.281587	0.281244	-5.16	0.757510546	3.06	2.915191595	No
M16-10	SA_M16-10_152	0.281467616	2.03245E-05	0.000306378	1855	94	0.281602	0.281898	0.281827	0.281457	-5.16	0.718727657	2.80	2.651800429	No
M16-10	SA_M16-10_28	0.281283533	2.64216E-05	0.000530254	2448	84	0.281215	0.281456	0.281392	0.281259	1.54	0.93433506	2.87	2.731307613	No
M16-10	SA_M16-10_30	0.28121862	2.37126E-05	0.000398881	2473	79	0.281199	0.281437	0.281374	0.281200	0.03	0.83853757	2.98	2.841748603	No
M16-10	SA_M16-10_45	0.281255117	2.47758E-05	0.000817942	2534	84	0.281159	0.281392	0.281329	0.281216	2.01	0.876135222	2.91	2.773742389	No
M16-10	SA_M16-10_52	0.281165292	3.46088E-05	0.001274457	2613	82	0.281107	0.281332	0.281270	0.281102	-0.19	1.223853856	3.10	2.968980301	No
M16-10	SA_M16-10_61	0.281216963	2.20852E-05	0.000506655	2418	81	0.281235	0.281479	0.281414	0.281194	-1.48	0.780990847	3.02	2.886229513	No
M16-10	SA_M16-10_66	0.281390251	2.32536E-05	0.000515518	2151	89	0.281410	0.281678	0.281611	0.281369	-1.44	0.822305651	2.81	2.667338189	No
M16-10	SA_M16-10_79	0.281301046	3.58833E-05	0.001353831	2531	81	0.281161	0.281394	0.281331	0.281236	2.66	1.268926758	2.87	2.733006388	No
M16-10	SA_M16-10_96	0.28126917	3.32022E-05	0.001340438	2535	79	0.281158	0.281391	0.281328	0.281204	1.63	1.174116251	2.93	2.79696051	No
M16-11	SA_M16-11_007	0.281552498	3.62556E-05	0.001825479	1914	87	0.281564	0.281855	0.281784	0.281486	-2.76	1.282092276	2.70	2.554907369	No
M16-11	SA_M16-11_025	0.281190779	2.50858E-05	0.000337906	2182	86	0.281389	0.281655	0.281588	0.281177	-7.56	0.887096586	3.20	3.057109381	No
M16-11	SA_M16-11_029	0.281472591	2.35465E-05	0.000517232	2069	87	0.281463	0.281739	0.281671	0.281452	-0.39	0.832665925	2.68	2.537620432	No
M16-11	SA_M16-11_036	0.281472096	6.85308E-05	0.000999138	1821	95	0.281624	0.281923	0.281852	0.281438	-6.63	2.423422522	2.86	2.71264793	No
M16-11	SA_M16-11_038	0.281164688	2.88751E-05	0.000409019	2446	83	0.281217	0.281458	0.281394	0.281146	-2.53	1.021098518	3.11	2.97149484	No
M16-11	SA_M16-11_043	0.281528946	2.81943E-05	0.001624004	1774	90	0.281655	0.281958	0.281886	0.281474	-6.41	0.997021979	2.81	2.661611379	No
M16-11	SA_M16-11_047	0.281240645	2.58448E-05	0.000455077	2604	83	0.281113	0.281339	0.281277	0.281218	3.74	0.913939332	2.86	2.728742105	No
M16-11	SA_M16-11_051	0.280999003	2.33115E-05	0.000529045	2685	84	0.281060	0.281278	0.281217	0.280972	-3.12	0.82435438	3.33	3.200547572	No
M16-11	SA_M16-11_056	0.281267304	3.30061E-05	0.001057158	2509	84	0.281175	0.281410	0.281347	0.281217	1.47	1.16718125	2.92	2.785592702	No
M16-11	SA_M16-11_059	0.281465512	2.7385E-05	0.001399445	1874	86	0.281590	0.281884	0.281814	0.281416	-6.19	0.968402314	2.88	2.728396733	No
M16-11	SA_M16-11_062	0.280889109	5.06674E-05	0.001965355	2741	77	0.281023	0.281236	0.281175	0.280786	-8.42	1.791728678	3.68	3.556350117	No
M16-11	SA_M16-11_067	0.281236883	2.01713E-05	0.000279906	2526	82	0.281164	0.281398	0.281335	0.281223	2.10	0.713306986	2.89	2.76170796	No
M16-11	SA_M16-11_072	0.281223757	2.96834E-05	0.000983409	2577	81	0.281131	0.281359	0.281297	0.281175	1.59	1.049681232	2.97	2.834165564	No
M16-11	SA_M16-11_079	0.281457753	2.83291E-05	0.001056395	1944	91	0.281544	0.281832	0.281762	0.281419	-4.47	1.001790403	2.83	2.681353223	No
M16-11	SA_M16-11_080	0.280965569	3.26036E-05	0.000882609	2698	79	0.281051	0.281268	0.281207	0.280920	-4.66	1.152947609	3.43	3.301527025	No
M16-11	SA_M16-11_094	0.281066702	2.43161E-05	0.00101865	2781	85	0.280996	0.281206	0.281146	0.281012	0.57	0.85987945	3.19	3.061113126	No
M16-11	SA_M16-11_102	0.281002119	2.16614E-05	0.000397774	2425	88	0.281231	0.281473	0.281409	0.280984	-8.78	0.766003059	3.46	3.323593244	No
M16-11	SA_M16-11_106	0.281371214	2.156E-05	0.000274675	1956	87	0.281537	0.281823	0.281754	0.281361	-6.24	0.762418329	2.95	2.797302498	No
M16-11	SA_M16-11_108	0.281036493	2.901E-05	0.000962947	2693	75	0.281054	0.281272	0.281211	0.280987	-2.40	1.025867032	3.29	3.164487169	No
M16-11	SA_M16-11_109	0.281268128	3.46375E-05	0.001525051	2636	79	0.281092	0.281315	0.281253	0.281191	3.54	1.224872233	2.90	2.767020128	No

Sample N	Analysis N	$^{176}Hf/^{177}Hf$	2 S.E.	$^{176}Lu/^{177}Hf$	U/Pb AGE	2 S.E.	Hf Chur (t)	Hf DM (t)	Hf NC(t)	Hf_i	eHf	2SE	TDMc	TNCc	Above DM line?
M16-11	SA_M16-11_112	0.281050697	2.62067E-05	0.000672212	2556	87	0.281145	0.281375	0.281312	0.281018	-4.50	0.926735302	3.31	3.177325585	No
M16-11	SA_M16-11_125	0.281329473	3.274E-05	0.000698325	2433	86	0.281225	0.281467	0.281403	0.281297	2.55	1.157769178	2.79	2.658738054	No
M16-30	SA_M16-30_02	0.280993278	2.40718E-05	0.000620241	2660	82	0.281076	0.281297	0.281235	0.280962	-4.07	0.851239993	3.36	3.235861908	No
M16-30	SA_M16-30_05	0.281438502	2.11151E-05	0.000468438	1883	92	0.281584	0.281878	0.281807	0.281422	-5.76	0.74668485	2.86	2.710334816	No
M16-30	SA_M16-30_08	0.281304213	2.51618E-05	0.000450713	2498	82	0.281183	0.281419	0.281355	0.281283	3.56	0.889785051	2.79	2.652063294	No
M16-30	SA_M16-30_10	0.281454236	2.53692E-05	0.000680818	1827	91	0.281620	0.281919	0.281848	0.281431	-6.74	0.897119661	2.88	2.723960564	No
M16-30	SA_M16-30_12	0.281290873	2.52169E-05	0.000420766	2496	84	0.281184	0.281420	0.281357	0.281271	3.09	0.891733557	2.81	2.678404601	No
M16-30	SA_M16-30_13	0.281312014	1.85907E-05	0.000382578	2459	83	0.281208	0.281448	0.281384	0.281294	3.05	0.657412918	2.79	2.650256082	No
M16-30	SA_M16-30_14	0.281303202	2.69528E-05	0.000577241	2315	88	0.281303	0.281556	0.281490	0.281278	-0.88	0.953120953	2.91	2.767178647	No
M16-30	SA_M16-30_17	0.281384557	1.86128E-05	0.00028831	1853	92	0.281604	0.281900	0.281829	0.281374	-8.14	0.658194882	2.98	2.828571251	No
M16-30	SA_M16-30_18	0.281304153	3.39964E-05	0.000912235	2589	88	0.281123	0.281350	0.281288	0.281259	4.84	1.20219969	2.78	2.650481313	No
M16-30	SA_M16-30_20	0.281198243	2.4655E-05	0.000279178	2486	88	0.281190	0.281428	0.281364	0.281185	-0.20	0.871864412	3.00	2.865582355	No
MAD17-11-4A	SA_MAD17-11-4A_01	0.281296464	3.04718E-05	0.001222076	2354	81	0.281277	0.281527	0.281462	0.281242	-1.26	1.077561163	2.96	2.821311557	No
MAD17-11-4A	SA_MAD17-11-4A_06	0.28118353	2.38869E-05	0.000616663	2594	79	0.281120	0.281347	0.281284	0.281153	1.19	0.844701644	3.00	2.871698745	No
MAD17-11-4A	SA_MAD17-11-4A_12	0.280889807	2.02338E-05	0.000302652	2483	81	0.281192	0.281430	0.281366	0.280875	-11.27	0.715518567	3.65	3.516726842	No
MAD17-11-4A	SA_MAD17-11-4A_14	0.281358692	2.8574E-05	0.000510351	2458	82	0.281209	0.281449	0.281385	0.281335	4.48	1.010448052	2.70	2.5644884	No
MAD17-11-4A	SA_MAD17-11-4A_17	0.280765822	2.82751E-05	0.000618667	2594	83	0.281120	0.281347	0.281284	0.280735	-13.67	0.99987919	3.87	3.745326268	No
MAD17-11-4A	SA_MAD17-11-4A_18	0.281320209	2.75335E-05	0.000693277	2456	82	0.281210	0.281450	0.281386	0.281288	2.76	0.973655317	2.80	2.665416767	No
MAD17-11-4A	SA_MAD17-11-4A_19	0.281685113	3.42996E-05	0.001610072	2024	85	0.281492	0.281773	0.281704	0.281623	4.64	1.212921862	2.35	2.197640731	No
MAD17-11-4A	SA_MAD17-11-4A_35	0.281116444	2.88369E-05	0.000687864	2460	81	0.281208	0.281447	0.281383	0.281084	-4.39	1.019746703	3.23	3.092857239	No
MAD17-11-4A	SA_MAD17-11-4A_36	0.281331242	3.35609E-05	0.000816082	1727	89	0.281685	0.281993	0.281921	0.281305	-13.51	1.186798805	3.20	3.050459758	No
MAD17-11-4A	SA_MAD17-11-4A_37	0.281559298	3.60686E-05	0.001417425	1775	95	0.281654	0.281958	0.281886	0.281512	-5.06	1.275476563	2.73	2.581357369	No
MAD17-11-4A	SA_MAD17-11-4A_39	0.28147799	2.72473E-05	0.000675341	1900	88	0.281573	0.281865	0.281795	0.281454	-4.24	0.963532878	2.78	2.63249304	No
MAD17-11-4A	SA_MAD17-11-4A_40	0.28152778	3.2098E-05	0.001026728	1781	91	0.281650	0.281953	0.281881	0.281493	-5.58	1.13506597	2.77	2.617392233	No
MAD17-11-4A	SA_MAD17-11-4A_42	0.281320096	2.64214E-05	0.000436381	2504	83	0.281179	0.281414	0.281351	0.281299	4.29	0.934328904	2.75	2.613637926	No
MAD17-11-4A	SA_MAD17-11-4A_43	0.28135286	2.88211E-05	0.000520379	2167	97	0.281399	0.281666	0.281599	0.281331	-2.41	1.019186763	2.88	2.738348872	No
MAD17-11-4A	SA_MAD17-11-4A_63	0.281423918	2.25513E-05	0.000740482	2078	91	0.281457	0.281733	0.281664	0.281395	-2.22	0.797471231	2.80	2.65515493	No
MAD17-11-4A	SA_MAD17-11-4A_65	0.281163472	1.98957E-05	0.00042727	2513	80	0.281173	0.281407	0.281344	0.281143	-1.06	0.703563288	3.07	2.938833627	No
MAD17-11-4A	SA_MAD17-11-4A_68	0.281746997	3.13967E-05	0.001051595	2334	98	0.281290	0.281542	0.281476	0.281700	14.58	1.110268603	1.99	1.853612076	Yes
MAD17-11-4A	SA_MAD17-11-4A_77	0.28134703	1.44848E-05	7.00803E-06	2073	100	0.281461	0.281736	0.281668	0.281347	-4.04	0.512220043	2.90	2.759924193	No
MAD17-11-4A	SA_MAD17-11-4A_83	0.281135474	2.47521E-05	0.000332201	2495	83	0.281185	0.281421	0.281358	0.281120	-2.31	0.875296375	3.13	2.998207469	No
PP727B	SA_PP727B_03	0.281647887	2.16141E-05	0.000381971	1862	18	0.281597	0.281893	0.281822	0.281634	1.31	0.764330564	2.42	2.267155218	No
PP727B	SA_PP727B_05	0.281616428	3.16426E-05	0.001594079	1817	18	0.281627	0.281926	0.281855	0.281561	-2.32	1.118963862	2.60	2.450016935	No

Sample N	Analysis N	$^{176}Hf/^{177}Hf$	2 S.E.	$^{176}Lu/^{177}Hf$	U/Pb AGE	2 S.E.	Hf Chur (t)	Hf DM (t)	Hf NC(t)	Hf_i	eHf	2SE	TDMc	TNCc	Above DM line?
PP727B	SA_PP727B_12	0.281363245	1.78245E-05	0.000194378	1964	21	0.281532	0.281818	0.281748	0.281356	-6.24	0.630319029	2.95	2.803438931	No
PP727B	SA_PP727B_16	0.281352366	1.93572E-05	0.00054831	1843	18	0.281610	0.281907	0.281836	0.281333	-9.83	0.684520294	3.07	2.922086371	No
PP727B	SA_PP727B_20	0.281230424	1.63844E-05	0.000539358	2592	17	0.281121	0.281348	0.281286	0.281204	2.94	0.579394365	2.90	2.765927975	No
PP727B	SA_PP727B_21	0.281240145	2.38008E-05	0.000979357	2716	16	0.281039	0.281255	0.281194	0.281189	5.34	0.841655465	2.85	2.725921402	No
PP727B	SA_PP727B_33	0.280881976	2.07444E-05	0.000546638	2527	17	0.281163	0.281397	0.281334	0.280856	-10.95	0.733575617	3.66	3.532914312	No
PP727B	SA_PP727B_34	0.281518748	2.67377E-05	0.001408102	2163	17	0.281402	0.281670	0.281602	0.281461	2.08	0.945512511	2.61	2.465431601	No
PP727B	SA_PP727B_39	0.28123969	2.76862E-05	0.001080633	2511	17	0.281174	0.281409	0.281346	0.281188	0.49	0.979053294	2.98	2.845161971	No
PP727B	SA_PP727B_40	0.281439484	2.26452E-05	0.0009939	2166	17	0.281400	0.281667	0.281600	0.281399	-0.06	0.800791433	2.74	2.596424597	No
PP727B	SA_PP727B_45	0.281103934	2.35135E-05	0.000589816	2542	17	0.281154	0.281386	0.281323	0.281075	-2.80	0.831498178	3.20	3.064971142	No
PP727B	SA_PP727B_50	0.281387481	2.28896E-05	0.000508989	1840	18	0.281612	0.281909	0.281838	0.281370	-8.60	0.8094332	3.00	2.846124285	No
PP727B	SA_PP727B_51	0.281621141	1.9441E-05	0.000474987	1866	18	0.281595	0.281890	0.281819	0.281604	0.33	0.687483978	2.48	2.329515705	No
PP727B	SA_PP727B_60	0.281502126	1.99207E-05	0.000827233	1841	18	0.281612	0.281909	0.281838	0.281473	-4.91	0.704448605	2.78	2.625082299	No
PP727B	SA_PP727B_65	0.281287558	2.51511E-05	0.000880795	2490	17	0.281188	0.281425	0.281361	0.281246	2.05	0.889406578	2.87	2.735146763	No
PP727B	SA_PP727B_66	0.281389564	1.86984E-05	0.000411158	1797	18	0.281640	0.281941	0.281869	0.281376	-9.37	0.6612232	3.01	2.858520074	No
PP727B	SA_PP727B_71	0.281606316	2.57313E-05	0.001081054	1864	18	0.281597	0.281892	0.281821	0.281568	-1.02	0.909926014	2.56	2.40887051	No
PP727B	SA_PP727B_72	0.281257209	2.29302E-05	0.000774905	2493	17	0.281186	0.281422	0.281359	0.281220	1.23	0.810871715	2.92	2.786707598	No
PP727B	SA_PP727B_73	0.281270173	2.04525E-05	0.000759748	2470	17	0.281201	0.281440	0.281376	0.281234	1.19	0.723254033	2.90	2.770291711	No
PP727B	SA_PP727B_74	0.281648626	3.14672E-05	0.002428426	1844	18	0.281609	0.281906	0.281835	0.281564	-1.62	1.112760118	2.58	2.429562324	No
RK7207	SA_RK7207_03	0.282002557	3.60402E-05	0.00173079	772	27	0.282298	0.282693	0.282610	0.281977	-11.34	1.274471956	2.35	2.168891062	No
RK7207	SA_RK7207_06	0.281993871	3.81718E-05	0.001570266	767	30	0.282301	0.282697	0.282614	0.281971	-11.69	1.349851978	2.37	2.185771242	No
RK7207	SA_RK7207_10	0.281957527	4.4917E-05	0.001753219	773	28	0.282297	0.282693	0.282609	0.281932	-12.94	1.588380505	2.45	2.267491364	No
RK7207	SA_RK7207_11	0.281987959	3.82074E-05	0.001724846	776	28	0.282295	0.282690	0.282607	0.281963	-11.77	1.35111108	2.38	2.198463721	No
RK7207	SA_RK7207_15	0.282012249	3.30078E-05	0.001323066	773	28	0.282297	0.282692	0.282609	0.281993	-10.76	1.167241624	2.32	2.134188324	No
RK7207	SA_RK7207_18	0.282019008	4.32285E-05	0.001627486	791	25	0.282286	0.282680	0.282597	0.281995	-10.31	1.528670376	2.30	2.119905078	No
RK7207	SA_RK7207_23	0.282037617	3.01226E-05	0.001327143	530	59	0.282451	0.282869	0.282783	0.282024	-15.12	1.065213774	2.40	2.212718629	No
RK7207	SA_RK7207_24	0.281958942	3.77096E-05	0.001496581	785	27	0.282289	0.282683	0.282600	0.281937	-12.48	1.333508545	2.43	2.249426866	No
RK7207	SA_RK7207_25	0.281989556	3.7189E-05	0.001720563	726	34	0.282327	0.282727	0.282643	0.281966	-12.79	1.315097295	2.40	2.221569273	No
RK7207	SA_RK7207_28	0.281993025	3.03936E-05	0.001359451	794	27	0.282284	0.282677	0.282594	0.281973	-11.02	1.074794212	2.35	2.166026128	No
RK7207	SA_RK7207_29	0.28198234	3.64928E-05	0.001819814	808	24	0.282275	0.282667	0.282584	0.281955	-11.35	1.290480272	2.38	2.197192419	No
RS285	SA_RS285_01	0.280718849	2.26234E-05	0.000484351	3112	16	0.280777	0.280955	0.280899	0.280690	-3.11	0.800020456	3.66	3.547034346	No
RS285	SA_RS285_06	0.280770965	2.22087E-05	0.000514362	3148	16	0.280754	0.280928	0.280873	0.280740	-0.49	0.785355059	3.54	3.423580524	No
RS285	SA_RS285_12	0.280984529	4.15076E-05	0.002401725	2934	16	0.280895	0.281090	0.281032	0.280849	-1.64	1.467816222	3.44	3.315703579	No
RS285	SA_RS285_14	0.280753739	2.95622E-05	0.001616417	3177	16	0.280734	0.280906	0.280851	0.280655	-2.82	1.045393522	3.70	3.583007595	No

Sample N	Analysis N	$^{176}Hf/^{177}Hf$	2 S.E.	$^{176}Lu/^{177}Hf$	U/Pb AGE	2 S.E.	Hf Chur (t)	Hf DM (t)	Hf NC(t)	Hf_i	eHf	2SE	TDMc	TNCc	Above DM line?
RS285	SA_RS285_15	0.280923554	2.42842E-05	0.001022428	2550	17	0.281148	0.281380	0.281317	0.280874	-9.77	0.858752961	3.61	3.482105524	No
RS285	SA_RS285_19	0.282013311	2.58269E-05	0.001047648	783	21	0.282291	0.282685	0.282602	0.281998	-10.38	0.913304542	2.30	2.117811116	No
RS285	SA_RS285_27	0.280821339	2.74469E-05	0.001409775	3182	16	0.280731	0.280902	0.280847	0.280735	0.15	0.970593669	3.53	3.41433508	No
RS285	SA_RS285_30	0.281013124	1.85003E-05	0.000584624	2484	17	0.281192	0.281430	0.281366	0.280985	-7.35	0.654216385	3.42	3.286606089	No
RS285	SA_RS285_39	0.281145269	2.22261E-05	0.000398711	2678	17	0.281064	0.281284	0.281222	0.281125	2.15	0.785970475	3.01	2.883416418	No
RS285	SA_RS285_40	0.282018389	2.36532E-05	0.000740324	829	21	0.282262	0.282652	0.282569	0.282007	-9.02	0.836436744	2.25	2.070704217	No
RS285	SA_RS285_42	0.281056501	2.21551E-05	0.000485584	2469	17	0.281202	0.281440	0.281377	0.281034	-5.97	0.783461041	3.33	3.193768683	No
RS285	SA_RS285_47	0.281576023	1.85952E-05	0.000379986	1809	18	0.281632	0.281932	0.281861	0.281563	-2.45	0.657575302	2.60	2.451554587	No
RS285	SA_RS285_52	0.281950192	3.23267E-05	0.001727778	807	21	0.282276	0.282668	0.282585	0.281924	-12.45	1.143153534	2.44	2.264455562	No
RS285	SA_RS285_53	0.280987298	2.35564E-05	0.000992956	2705	17	0.281046	0.281263	0.281202	0.280936	-3.93	0.833016138	3.39	3.264287157	No
RS285	SA_RS285_54	0.280846534	1.91451E-05	0.000385312	2473	17	0.281199	0.281437	0.281374	0.280828	-13.18	0.677019705	3.75	3.620463532	No
RS285	SA_RS285_57	0.280825957	2.05879E-05	0.000687457	2984	16	0.280862	0.281053	0.280995	0.280787	-2.69	0.728039048	3.54	3.418266942	No
RS285	SA_RS285_66	0.280968903	2.2275E-05	0.000773425	2506	17	0.281177	0.281413	0.281349	0.280932	-8.73	0.787701857	3.52	3.385718522	No
RS285	SA_RS285_68	0.280807541	2.40252E-05	0.000642796	3274	16	0.280669	0.280832	0.280778	0.280767	3.48	0.849593815	3.41	3.296650815	No
RS285	SA_RS285_69	0.281978725	1.7885E-05	0.000531511	809	30	0.282274	0.282666	0.282583	0.281971	-10.74	0.632460484	2.34	2.161325187	No
RS285	SA_RS285_79	0.280743409	2.7409E-05	0.001365756	3413	16	0.280577	0.280727	0.280674	0.280654	2.73	0.969252167	3.56	3.454718898	No
RT06431	SA_RT06431_26	0.28129797	2.67027E-05	0.000738492	2236	17	0.281354	0.281615	0.281549	0.281267	-3.12	0.944274356	2.98	2.836362465	No
RT06431	SA_RT06431_27	0.281491675	2.77831E-05	0.00088708	2078	18	0.281457	0.281732	0.281664	0.281457	-0.02	0.982482247	2.67	2.522926628	No
RT06431	SA_RT06431_30	0.281454835	2.18931E-05	0.000711359	1848	18	0.281607	0.281903	0.281832	0.281430	-6.28	0.774195424	2.86	2.713261409	No
RT06431	SA_RT06431_31	0.281469444	2.1807E-05	0.000807276	1840	18	0.281612	0.281910	0.281838	0.281441	-6.07	0.771152338	2.85	2.693850325	No
RT06431	SA_RT06431_32	0.281418979	2.10428E-05	0.000422012	1845	18	0.281608	0.281905	0.281834	0.281404	-7.25	0.744127046	2.92	2.769591736	No
RT06431	SA_RT06431_35	0.281504698	1.72471E-05	0.000506846	1827	18	0.281620	0.281919	0.281848	0.281487	-4.73	0.609900851	2.76	2.603267001	No
RT06431	SA_RT06431_37	0.281397868	1.86672E-05	0.000525617	1818	18	0.281627	0.281926	0.281855	0.281380	-8.76	0.660119388	2.99	2.837854598	No
RT06431	SA_RT06431_46	0.28157247	1.87702E-05	0.001000918	1815	18	0.281628	0.281928	0.281857	0.281538	-3.21	0.663763078	2.65	2.501757074	No
RT06431	SA_RT06431_50	0.281503486	2.11007E-05	0.001073774	1802	18	0.281637	0.281938	0.281866	0.281467	-6.03	0.746175244	2.81	2.661425364	No
RT06431	SA_RT06431_52	0.281566092	2.60325E-05	0.001359644	1817	18	0.281627	0.281926	0.281855	0.281519	-3.82	0.920575544	2.69	2.540468194	No
RT06431	SA_RT06431_57	0.281527971	2.32974E-05	0.000467888	1911	18	0.281566	0.281857	0.281786	0.281511	-1.95	0.823853913	2.65	2.50354358	No
RT06431	SA_RT06431_58	0.281011973	2.1588E-05	0.000905526	2439	17	0.281221	0.281463	0.281399	0.280970	-8.95	0.763406487	3.48	3.344790887	No
RT06431	SA_RT06431_67	0.281398085	1.84363E-05	0.000355083	1800	18	0.281638	0.281939	0.281867	0.281386	-8.94	0.651953188	2.99	2.834800072	No
RT06431	SA_RT06431_76	0.281487525	1.87411E-05	0.000611113	1806	18	0.281634	0.281935	0.281863	0.281467	-5.95	0.662732336	2.81	2.659643923	No
RT06431	SA_RT06431_81	0.280938782	2.55076E-05	0.000640594	2685	17	0.281060	0.281278	0.281217	0.280906	-5.47	0.902015226	3.47	3.338313699	No

Appendix 5.5 Proterozoic basin evolution during Nuna: Itremo Group REE plots

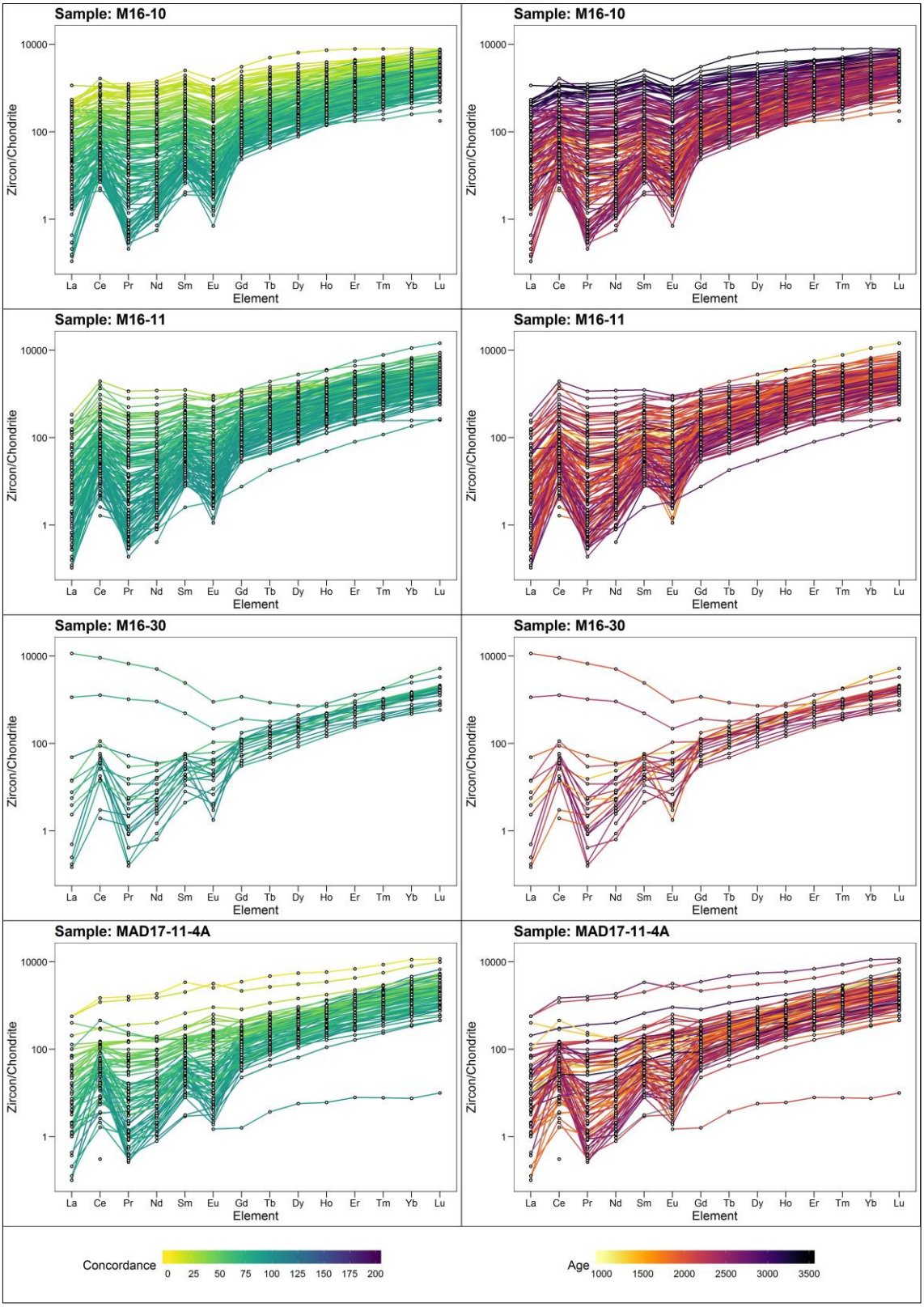

Appendix 5.7 Proterozoic basin evolution during Nuna: Detrital zircon U–Pb and Hf plots for all data